Otfried Madelung (Ed.)

Semiconductors – Basic Data

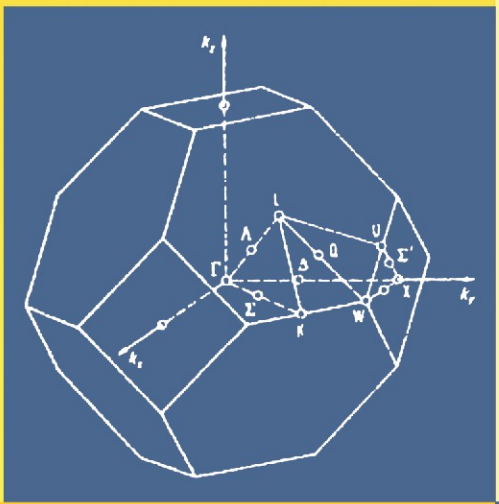

2nd revised Edition

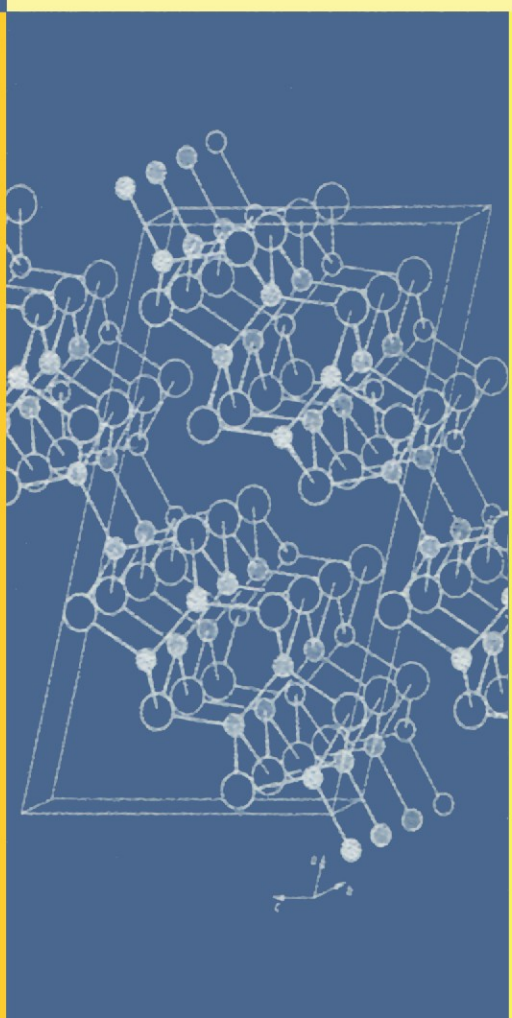

Springer

Otfried Madelung (Editor)
Semiconductors - Basic Data

Springer

Berlin
Heidelberg
New York
Barcelona
Budapest
Hong Kong
London
Milan
Paris
Santa Clara
Singapore
Tokyo

Otfried Madelung (Editor)

Semiconductors - Basic Data

2nd revised Edition

With 359 Figures

Springer

Prof. Dr. Otfried Madelung
Am Kornacker 18
D-35041 Marburg

The 1st ed. was published in 2 volumes in the series "Data in Science and Technology" under title *Semiconductors.*

Cataloging-in-Publication Data applied for

Die Deutsche Bibliothek - CIP-Einheitsaufnahme
Semiconductors - Basic Data / ed.: Otfried Madelung. 2.,rev. ed.
Berlin; Heidelberg; New York; Barcelona; Budapest; Hong Kong;
London; Milan; Paris; Santa Clara; Singapore; Tokyo: Springer, 1996
Früher mehrb. begrenztesWerk u.d.T.: Semiconductors
NE: Madelung,Otfried [Hrsg.]

ISBN-13: 978-3-642-97677-3 e-ISBN-13: 978-3-642-97675-9
DOI: 10.1007/978-3-642-97675-9

This work is subject to copyright. All rights are reserved, whether the whole or part of the material is concerned, specifically the rights of translation, reprinting, reuse of illustrations, recitation, broadcasting, reproduction on microfilm or in other ways, and storage in data banks. Duplication of this publication or parts thereof is permitted only under the provisions of the German Copyright Law of September 9, 1965, in its current version, and permission for use must always be obtained from Springer-Verlag. Violations are liable for prosecution act under German Copyright Law.

© Springer-Verlag Berlin Heidelberg 1991, 1992, and 1996
Softcover reprint of the hardcover 3rd edition 1996

The use of general descriptive names, registered names, trademarks, etc. in this publication does not imply, even in the absence of a specific statement, that such names are exempt from the relevant protective laws and regulations and therefore free for general use.

Production: PRODUSERV Springer Produktions-Gesellschaft, Berlin
Cover layout: Lewis & Leins, Berlin
Typesetting: Camera ready copy from editor

SPIN: 10532384 63/3020 - 5 4 3 2 1 0 - Printed of acid-free paper

Preface

The frequent use of well known critical data handbooks like Beilstein, Gmelin and Landolt-Börnstein is impeded by the fact that merely larger libraries - often far away from the scientist's working place - can afford such precious collections. To satisfy an urgent need of many scientists working in the field of semiconductor physics for having at their working place a comprehensive, high quality, but cheap collection of at least the basic data of their field of interest this volume contains the most important data of semiconductors. All data were compiled from information on semiconductors presented on more than 6 000 pages in various volumes of the New Series of Landolt-Börnstein.

We hope to meet the needs of the community of semiconductor physicists with this volume, forming a bridge between the laboratory and additional information sources in the libraries.

Marburg, January 1996 **The Editor**

Table of contents

A Introduction

1 General remarks 1
2 The corresponding Landolt-Börnstein volumes 2
3 Physical quantities tabulated in this volume 3

B Physical data

1 Elements of the IVth group and IV-IV compounds
- 1.1 Diamond (C) 5
- 1.2 Silicon (Si) 11
- 1.3 Germanium (Ge) 28
- 1.4 Grey tin (a-Sn) 42
- 1.5 Silicon carbide (SiC) 47
- 1.6 Silicon germanium alloys (Si_xGe_{1-x}) 57

2 III-V compounds
- 2.1 Boron nitride (BN) 60
- 2.2 Boron phosphide (BP) 65
- 2.3 Boron arsenide (BAs) 68
- 2.4 Aluminium nitride (AlN) 69
- 2.5 Aluminium phosphide (AlP) 72
- 2.6 Aluminium arsenide (AlAs) 75
- 2.7 Aluminium antimonide (AlSb) 80
- 2.8 Gallium nitride (GaN) 86
- 2.9 Gallium phosphide (GaP) 91
- 2.10 Gallium arsenide (GaAs) 101
- 2.11 Gallium antimonide (GaSb) 114
- 2.12 Indium nitride (InN) 122
- 2.13 Indium phosphide (InP) 124
- 2.14 Indium arsenide (InAs) 133
- 2.15 Indium antimonide (InSb) 141
- 2.16 Ternary and quaternary alloys between III-V compounds 155

3 Elements (other than group IV elements)
- 3.1 Group III elements 160
- 3.2 Group IV elements ..... see chapter 1
- 3.3 Group V elements 161
- 3.4 Group VI elements 162

4 Binary compounds (other than III-V compounds)
- 4.1 IA-IB compounds 164
- 4.2 I_x-V_y compounds 164
  - 4.2.1 I-V compounds 164
  - 4.2.2 I_3-V compounds 165
  - 4.2.3 I_2-I-V compounds 166
- 4.3 I_x-VI_y compounds 167
- 4.4 I-VII compounds 170
- 4.5 II_x-IV_y compounds 173
  - 4.5.1 II_2-IV compounds 173
  - 4.5.2 II-IV_2 compounds 175
- 4.6 II_X-V_y compounds 175
  - 4.6.1 II_3-V_2 compounds 175

4.6.2 II_4-V_3 compounds ... 177
4.6.3 II-V compounds ... 177
4.6.4 II-V_2 compounds ... 178
4.6.5 II-V_4 compounds ... 179
4.6.6 Further II-V compounds ... 179
4.7 II-VI compounds ... 180
4.7.1 IIA-VIB compounds ... 180
4.7.2 Zinc chalcogenides ... 182
4.7.3 Cadmium chalcogenides ... 184
4.7.4 Mercury chalcogenides ... 186
4.8 II-VII_2 compounds ... 188
4.9 III-V compounds ... see chapter 2
4.10 III_x-VI_y compounds ... 190
4.10.1 III-VI compounds ... 190
4.10.2 III_2-VI_3 compounds ... 192
4.10.3 Further III_x-VI_y compounds ... 192
4.10.4 III-III-VI compounds ... 193
4.11 III-VII compounds ... 194
4.12 IV_x-V_y compounds ... 196
4.12.1 IV-V compounds ... 196
4.12.2 IV-V_2 compounds ... 197
4.13 IV_x-VI_y compounds ... 197
4.13.1 IV-VI compounds ... 197
4.13.2 IV-VI_2 compounds ... 200
4.13.3 IV_2-VI_3 compounds ... 202
4.14 IV-VII_2 compounds ... 203
4.15 V_x-VI_y compounds ... 204
4.16 V-VII_3 compounds ... 207

5 Ternary compounds
5.1 Tetrahedrally bonded ternary and quasi-binary compounds ... 209
5.1.1 III_2-VI_3 compounds ... 209
5.1.2 I-III-VI_2 compounds ... 211
5.1.3 II-IV-V_2 compounds ... 216
5.1.4 I_2-IV-V_3 compounds ... 219
5.1.5 I_2-V-VI_4 compounds ... 220
5.1.6 II-III_2-VI_4 compounds ... 221
5.1.7 Other ordered vacancy compounds ... 224
5.1.8 Quaternary compounds ... 225
5.2 Further ternary compounds ... 226
5.2.1 I_x-IV_y-VI_z compounds ... 226
5.2.2 I_x-V_y-VI_z compounds ... 227
5.2.3 II_x-III_y-VI_z compounds ... 230
5.2.4 III_x-V_y-VI_z compounds ... 231
5.2.5 IV_x-V_y-VI_z compounds ... 232
5.2.6 V-VI-VII compounds ... 233
5.2.7 Other ternary compounds ... 235

6 Further compounds with semiconducting properties
6.1 Boron compounds ... 237
6.2 Binary transition metal compounds ... 238
6.2.1 Compounds with elements of the IVth group ... 238
6.2.2 Compounds with elements of the Vth group ... 238
6.2.3 Oxides ... 239
6.2.4 Chalcogenides ... 240
6.3 Binary rare earth compounds ... 241

6.4 Ternary transition metal compounds 242
6.4.1 Pnigochalcogenides 242
6.4.2 Spinels and related compounds 242
6.4.3 Oxides 243
6.4.4 Further chalcogenides 243
6.5 Ternary rare earth compounds 243

7 Figures to chapters 3, 4 and 5 247

Appendix

1 Index of Substances 299
2 Synopsis of the sections of this book and the corresponding sections of volumes III/17, III/22 and III/23a of the New Series of Landolt-Börnstein 307
3 Contents of the volumes of the New Series of Landolt-Börnstein dealing with semiconductors 311

A Introduction

1 General remarks

This volume contains basic data of semiconductors. All data were compiled from volumes of the New Series of the Landolt-Börnstein data handbook. They comprise the information a scientist working on semiconductors is needing in his every-day work.
The volume consists of three parts: A. Introduction, B. Physical data, C. Appendix.
In part B the chapters 1 and 2 cover data on the most important semiconductors, the elements of the IVth group and the III-V compounds. Here detailed information is given on all physical properties of these substance groups. Chapters 3 to 7 present basic data on more than 600 other substances with semiconducting properties. The scope and the arrangement of data is as follows:

Chapters 1 and 2 on group IV elements and III-V compounds

The data presented in these chapters are ordered under the following headings:
- Electronic properties:
  band structure / energies at symmetry points of the band structure / energy gaps (direct energy gap, indirect energy gap) / exciton energies / intra conduction band energies / intra valence band energies / critical point energies / spin-orbit splitting energies / camel's back structure of the conduction band edge / structure of the top of the valence band / effective masses (effective masses, electrons; effective masses, holes) / g-factor of electrons / valence band parameters.
- Lattice properties:
  structure / high pressure phases / transition temperature (pressure) or decomposition temperature / lattice parameters / linear thermal expansion coefficient / density / melting point / phonon dispersion relations / phonon frequencies (wavenumbers) / second order elastic moduli / third order elastic moduli.
- Transport properties:
  electrical conductivity (intrinsic conductivity) / (intrinsic) carrier concentration / carrier mobilities (electron mobility, hole mobility) / thermal conductivity (resistivity).
- Optical properties:
  optical constants / absorption coefficient / reflectance / extinction coefficient / refractive index / dielectric constants.
- Impurities and defects:
  solubility of impurities / diffusion coefficient (self-diffusion, impurity diffusion) / binding energies of (shallow) impurities / energy levels of impurities, defects and complexes or of deep centers.
  For alloys bowing parameters and crossover concentrations are also given.

Chapters 3 to 7 on further semiconducting elements and compounds

To cover the properties of more than 600 semiconductors several restrictions were necessary:
- Only diagrams showing lattice structures and band structures have been included. Thus, no temperature or pressure dependence of parameters, no optical spectra etc. could be presented. Most data are values at room temperature and normal pressure.
- No references have been given. For all references as well as for all supplementary information (experimental conditions, experimental method, further data, errors etc.) the reader has to consult the respective subvolumes of volumes NS III/17 and 22 of Landolt-Börnstein (see below).
- For technical reasons the figures to chapters 3 ... 5 are presented in chapter 7.

In Chapters 3, 4 and 5 all data have been grouped into eight colums:
- Substance: The name of the semiconducting substance.
- Structure: symmetry type of the lattice and space group for normal conditions.
  Further information about the locations of atoms in the unit cell, about high temperature phases or high pressure phases have been omitted.
- Static and dynamical lattice parameters:

Lattice constants. Density, melting temperature (in some cases peritectic temperature). Data on second order elastic constants have been added in simple cases only where the elastic properties are determined by a small number of tensor components. Dielectric constants. Phonon frequencies are given only if the phonon spectrum is characterized by a small number of frequencies e.g. TO and LO modes at the center of the Brillouin zone or some infrared active or Raman-active modes. For complicated phonon spectra no data are given.
- Band structure parameters: Energy gaps. Data were given here mostly for room temperature, but characteristic data at other temperatures were added if necessary. If possible the type of the transition (optical, thermal, direct, indirect etc.) has been indicated. Effective masses of electrons and holes, polaron masses.
- Transport properties: In most cases only the mobilities are listed. Since such data represent upper limits or are accidentally measured values carrier densities or conductivities (resistivities) have been added when necessary. Activation energies for conductivity have been included in some cases.

In Chapter 6 data on compounds are listed, for which the information on semiconducting properties is scarce, or for which semiconductivity is only of minor importance. In this chapter the tables have been restricted to six colums giving information on structure, optical and thermal energy gaps and carrier mobilities. Here activation energies for conductivity have been indicated, if this was stated explicitely in the original paper. In many cases the references do not differentiate between thermal energy gaps and activation energies.

The following restrictions should be taken in mind when using these tables:
- If not stated otherwise all data are room temperature values. Only for parameters which do not depend strongly on temperature (e.g. effective masses) data measured at other temperatures were included without mentioning it.
- Physical data can be judged confidentally only by added information about measuring and evaluation methods, about the reference the value has been taken from etc. All this valuable information is lacking here because of the restriction of the number of pages for this data collection. The reader has to go back to the corresponding Landolt-Börnstein volumes for such information. Adding such informations in the present text - and the references to the original papers too - had surpassed the frame of this volume.
- The data presented here had often to be chosen from several values, given in the Landolt-Börnstein volumes, if no unique choice had been possible for the author of the respective chapter. In such cases the "most reliable one" - according to the judgement of the editor - or the "newest" one has been listed.

Appendices

To facilitate the use of this book three Appendices have been added: 1. Index of Substances, 2. Synopsis of the sections of this book and the corresponding sections of volumes III/17 and III/22 of the New Series of Landolt-Börnstein, 3. Lists of Contents of the volumes of the New Series of Landolt-Börnstein dealing with semiconductors.

2 The corresponding Landolt-Börnstein volumes

Although the most relevant data have been summarized here the respective volumes of the New Series of Landolt-Börnstein contain much more information about these topics. In addition data on other properties can be found on the more than 6 000 pages of volumes 17a ... i, 22a,b and 23a of Group III of the New Series:
Volume III/17a (and its supplement and extension III/22a) present data on group IV elements and III-V compounds. Additional information is given on topics as temperature and pressure dependence of energy band parameters, critical point energies, Kane and Luttinger band structure parameters, exciton parameters and deformation potentials; temperature and pressure dependence of lattice parameters, Debye temperatures, sound velocities, bulk modulus, Grüneisen parameters; carrier concentrations, drift velocities, galvanomagnetic, thermomagnetic and thermoelectric coefficients; optical constants and spectra, elasto- and piezooptic coefficients, Raman spectra; magnetic susceptibility, heat capacity, thermodynamical data and many other topics.
Volume III/22b is devoted to an extensive representation of all relevant data on impurities and defects in group IV and III-V semiconductors as solubilities and segregation constants, diffusion coefficients, shallow defect levels, deep defects and impurities, luminescence data, ESR and ENDOR data, local vibrational modes.
In addition to these physical data the volumes III/17c and d concentrate on technological data of the group IV, III-V and some other semiconductors. The volumes III/17b, e ...h present data on elements other than group IV elements and on binary, ternary and polynary semiconductors. Volume III/17i adds data on amorphous and organic semiconductors as well as on some special topics.
Chapter 2.1 of volume III/23a presents photoemission spectra and related band structure and core level data of tetrahedrally bonded semiconductors.
The organization and tables of contents of these volumes are described in the Appendix.

3 Physical quantities tabulated in this volume

Data on the following physical quantities are given in the tables and figures of Part B:

Electronic structure

energies (unit eV):

$E(\boldsymbol{k})$ energy of a band state at wave vector $\boldsymbol{k}$.
Instead of the value of $\boldsymbol{k}$ often the respective symmetry point in the Brillouin zone is given (Γ, X, L, Σ ... for the meaning of the symbols see Fig. 2 in section 1.1 for the diamond and zincblende structure, Fig. 5 in section 2.1 for the wurtzite structure). Subscripts to these letters designate the irreducible representation of the energy state (1, 1', 2, 12, 25'...). Indices c or v differentiate between states lying in the conduction or valence band, respectively.

E_c, E_v energies of the edges of conduction and valence bands, respectively.

E_g energy gap between conduction and valence band. Further subscripts refer to: dir: direct gap, ind: indirect gap, opt: optical gap (threshold energy for optical transitions), pseu: pseudodirect energy gap, th: thermal gap (energy gap extrapolated to 0K from transport measurements), x: excitonic gap (energy gap minus exciton binding energy), ||, ⊥ electric field parallel or perpendicular to a crystal axis;
L(T) superscripts for longitudinal (transverse) exciton energies.

E_b binding energy of the exciton.

Δ mostly spin-orbit splittings of energy levels (subscripts 0, so, 1, 2 and dashes (') refer to the location of the level as explained in the tables),
also other splittings of energy levels (cf: crystal-field splitting, ex: exciton exchange interaction energy, L-T: longitudinal-transverse exciton splitting energy)

E_0... the letter E with other subscripts refers to intra- and interband transitions as explained in the tables (E_0, E_1, E_2 ...).

effective masses (in units of the electron mass m_0):

m_n, m_p effective mass of electrons (holes); other subscripts refer to: c: conductivity effective mass, cr: cyclotron resonance effective mass, ds: density of states mass, p,h: heavy holes, p,l: light holes, so: effective mass in the spin-orbit split band, (X ...): effective mass at symmetry point X ..., ||, ⊥: effective mass parallel or perpendicular to a principal axis

ellipsoidal energy surfaces as occuring in the conduction band of group IV and III-V semiconductors are characterized by the longitudinal and transverse effective masses

$m_{||}$, $m_\perp$ defined by the equation

where $\kappa = \boldsymbol{k} - \boldsymbol{k}_0$ and $\kappa_x \parallel \boldsymbol{k}_0$, κ_y, $\kappa_z \perp \boldsymbol{k}_0$.

camel's back structure occurs at the conduction band edge in several III-V compounds. The relevant parameters Δ, Δ_0, ΔE, $m_{||}$ etc. are explained in Fig. 2 and the accompanying equation in the tables of section 2.9.

warped energy surfaces as occuring in the valence band of group IV and III-V semiconductors are characterized by valence band parameters

A, B, C defined by the equation

***g*-factor** of electrons: g_c

Lattice parameters

crystal lattice, phase transitions:

a, b, c lattice parameters (unit Å or nm)

α, β, γ angles

u ratio of lattice parameters

α coefficient of linear thermal expansion (unit K^{-1})

d density (unit g cm^{-3}) (d_X: density determined from X-ray data)

T_m melting temperature (unit K)
T_{tr} transition temperature (unit K)
T_{perit} peritectic temperature (unit K)
p_{tr} transition pressure for phase transitions (unit Pa)

phonon parameters:

ν phonon frequency (unit s^{-1})
wavenumber
$\nu(\boldsymbol{k})$ phonon dispersion relation (dependence of phonon frequency on wave vector), instead of $\boldsymbol{k}$ often the reduced wave vector $\zeta = k/k_{max}$ is used.
Subscripts to the frequencies (wavenumbers) refer to transverse and longitudinal optical and acoustic branches (TO, LO, TA, LA) and to the symmetry points in the Brillouin zone as for the band structure energies. Further subscripts refer to Raman active (R) and infrared active (ir) modes.

elastic moduli:

c_{lm}, c_{lmn} second (third) order elastic moduli (unit dyn cm^{-2})

Transport properties

R resistance (unit Ω)
R_H Hall coefficient (unit cm^3C^{-1})
σ, (σ_i) (intrinsic) electrical conductivity (unit $\Omega^{-1}cm^{-1}$)
ρ electrical resistivity (unit Ωcm)
κ thermal conductivity (subscript L: lattice contribution) (unit $Wcm^{-1}K^{-1}$)
E_A activation energy (mostly for temperature dependence of conductivity) (unit eV)

carrier concentrations (unit cm^{-3}) and **carrier mobilities** (unit cm^2/Vs):

n electron concentration
p hole concentration
n_i intrinsic carrier concentration
μ_n, μ_p electron and hole mobilities, respectively. Further subscripts refer to: dr: drift mobility, c: conductivity mobility, H: Hall mobility, $\|$, $\perp$: parallel (perpendicular to a principal axis)

Optical properties

K absorption coefficient (unit cm^{-1})
R reflectance (dimensionless)
n (real) refractive index (dimensionless)
k extinction coefficient (dimensionless)

ε, ε_{ik} **dielectric constant** (component of the dielectric tensor); subscripts and brackets refer to: 1: real part of the complex dielectric constant, 2: imaginary part of the complex dielectric constant, 0: low frequency limit, ∞: high frequency limit, $\|$, $\perp$: parallel or perpendicular to a crystal axis

Impurities and defects
(Substitutional impurities are designated by (s), interstitial ones by (i))

c^{eq} solubility of an impurity (maximum concentration incorporated in the solid in equilibrium without inducing a phase transition) (unit cm^{-3})
c_0, ΔH parameters of the Arrhenius equation $c^{eq} = c_0 \exp[-\Delta H/k_B T]$
For a retrograde solubility a maximum solubility C^{eq}_{max} is observed at a temperature $T_{max} < T_m$.
D diffusion coefficient (unit cm^2s^{-1})
D_0, Q parameters occurring in the equation $D = D_0 \exp[Q/k_B T]$
E_b binding energy of donors ($E_c - E_d$) or acceptors ($E_a - E_v$)
E for deep levels the type (d, a) is given; positive values refer to the valence band edge, negative values to the conduction band edge.

B Physical data

1 Elements of the IVth group and IV–IV compounds

Physical property	Numerical value	Experimental conditions	Experimental method, remarks	Ref.

1.1 Diamond (C)

Electronic properties

band structure: Fig. 1 [84C] (Brillouin zone: Fig. 2)

Diamond is an indirect gap semiconductor, the lowest minima of the conduction band being located along the Δ-axes. The valence band has the structure common to all group IV semiconductors: three at Γ degenerate bands (spin neglected, symmetry $\Gamma_{25'}$). The spin orbit splitting of these bands is neglegible.

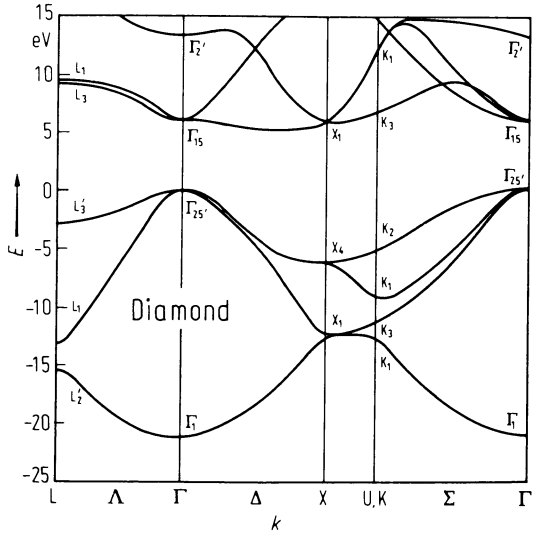

Fig. 1. Diamond. Band structure calculated by an ab intio LCAO method [84C].

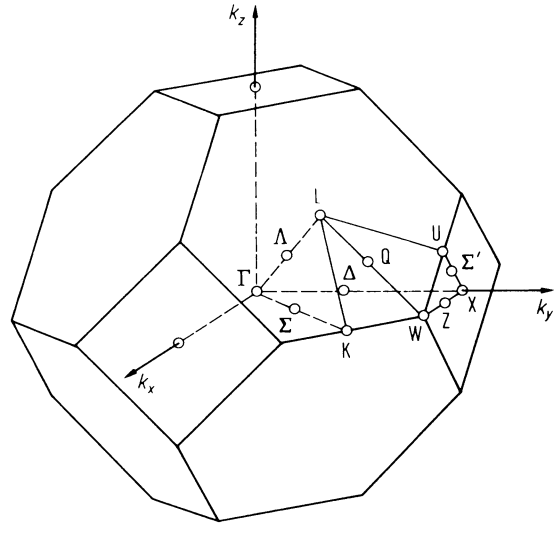

Fig. 2. Brillouin zone of the face centered cubic lattice, the Bravais lattice of the diamond and zincblende structures.

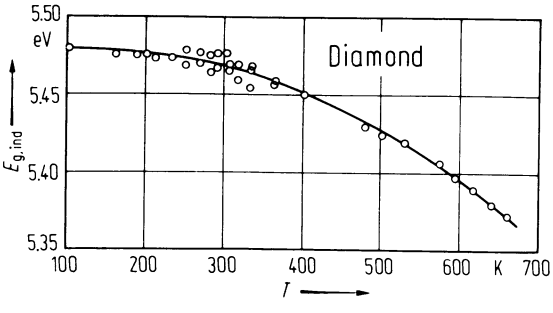

Fig. 3. Diamond. Indirect gap vs. temperature [64C].

Physical property	Numerical value	Experimental conditions	Experimental method, remarks	Ref.
energies of symmetry points of the band structure (relative to the top of the valence band) (in eV):				
$E(\Gamma_{1v})$	-21.03 ($-21(1)$)		theoretical data:	
$E(\Gamma_{25'v})$	0.00		ab initio LCAO calculations	
$E(\Gamma_{15c})$	6.02 (6.0(2))		[84C], see Fig. 1	
$E(\Gamma_{2'c})$	13.41 (15.3(5))		experimental data	
$E(X_{1v})$	-12.43		(in brackets):	
$E(X_{4v})$	-6.27		photon energy dependent	
$E(X_{1c})$	5.91		photoemission [80H]	
$E(L_{1v})$	-13.09 ($-12.8(3)$)			
$E(L_{3'v})$	-2.82			
$E(L_{3c})$	9.23			
$E(L_{1c})$	9.58			
indirect energy gap:				
$E_{g,ind}$ ($\Gamma_{25'v} - \Delta_{1c}$)	5.50(5) eV	RT	quantum photoyield	79H
$dE_{g,ind}/dT$	$-5 \cdot 10^{-5}$ eV/K	135 ··· 300 K	see Fig. 3	64C
Position of the minima of the conduction band along the Δ-axis: $\boldsymbol{k} = (0.76(1), 0, 0)$ [65D].				
direct energy gap:				
$E_{g,dir}$ ($\Gamma_{25'v} - \Gamma_{15c}$)	6.5 eV		angular dependent electron energy loss spectroscopy	82A
$dE_{g,dir}/dT$	-6.10^{-4} eV/K	135 ··· 300 K	absorption	64C
exciton binding energy:				
E_b	0.080(5) eV		recombination radiation	65D
spin-orbit splitting energy:				
$\Delta(\Gamma_{25'v})$	0.006(1) eV		cyclotron resonance	62R
effective masses, electrons (in units of m_0):				
$m_{n\parallel}$	1.4		field dependence of	80N
$m_{n\perp}$	0.36		electron drift velocity	
effective masses, holes (in units of m_0):				
$m_{p,h}$	1.08		calculated density of states	83R
$m_{p,l}$	0.36		from best set of valence	
m_{so}	0.15		band parameters	
valence band parameters:				
$\|A\|$	3.61		most probable set of para-	83R
$\|B\|$	0.18		meters out of six sets	
$\|C\|$	3.67		published by various authors,	

Physical property	Numerical value	Experimental conditions	Experimental method, remarks	Ref.

Lattice properties

Structure

The element carbon usually crystallizes in two modifications: diamond (cubic) and graphite (hexagonal) (Fig. 4). Under normal conditions (RT, atmospheric pressure) graphite is stable, diamond is metastable. According to their extrinsic properties diamonds are classified in several types (Ia, Ib, IIa, IIb).

High-pressure phases are not known.
Space group: O_h^7–Fd3m

lattice parameter:

a	3.56683(1) Å	298 K	X-ray diffraction	59K

For temperature dependence, see Fig. 5a.

linear thermal expansion coefficient: Fig. 5b.

density:

d	3.51525 g cm^{-3}		calculated from lattice constant	79F

melting point:

T_m	4100 K	$p = 12.5$ GPa	diamond-graphite-liquid eutectic	63B

phonon dispersion relations: Fig. 6.

phonon frequencies (in THz):

$\nu_{TO/LO}(\Gamma_{25'})$	39.9	300 K	Raman spectroscopy	70S
$\nu_{TA}(L_3)$	16.9			
$\nu_{LA}(L_1)$	30.2			
$\nu_{LO}(L_{2'})$	37.5			
$\nu_{TO}(L_{3'})$	36.2			
$\nu_{TA}(X_3)$	24.2			
$\nu_{LA/LO}(X_1)$	35.5			
$\nu_{TO}(X_4)$	32.0			

second order elastic moduli (in 10^{12} dyn cm^{-2}):

c_{11}	10.764(2)	296 K	Brillouin scattering	75G
c_{12}	1.252(23)			
c_{44}	5.774(14)			

Transport and optical properties

Most electrical and optical properties of diamond are *extrinsic*, i.e. strongly dependent on the impurity content. The most common impurity being nitrogen. Substitutional boron generates p-conductivity.

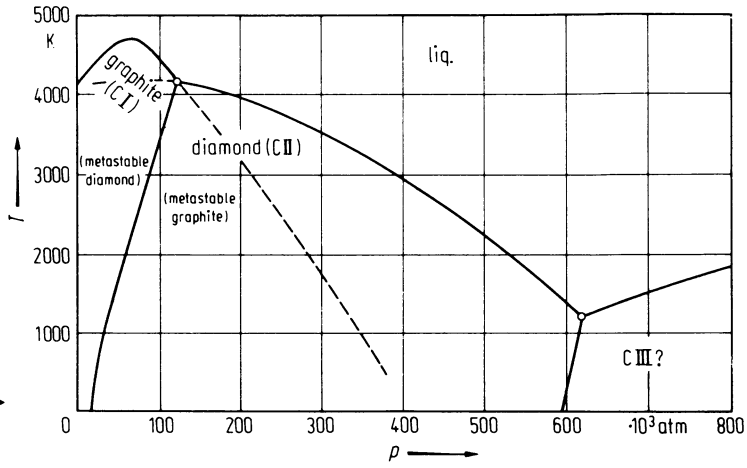

Fig. 4. C. $p - T$ diagram [62B]. ▶

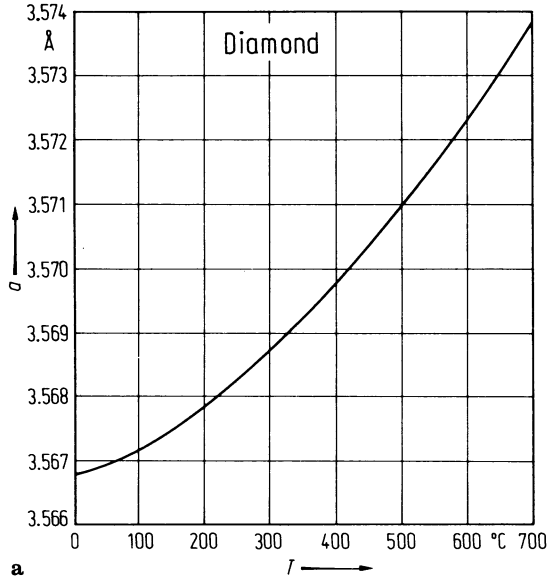

a

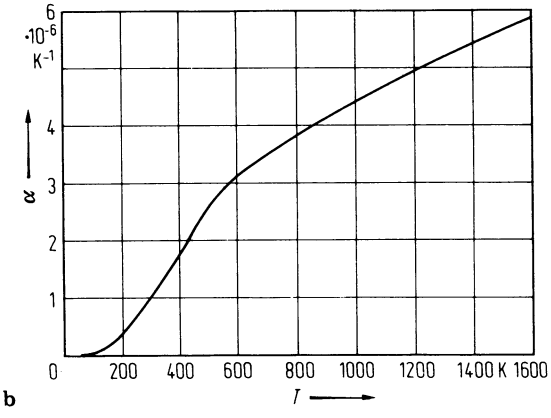

b

Fig. 5. Diamond. (a) Lattice parameter vs. temperature [57S], (b) linear thermal expansion coefficient vs. temperature [75S].

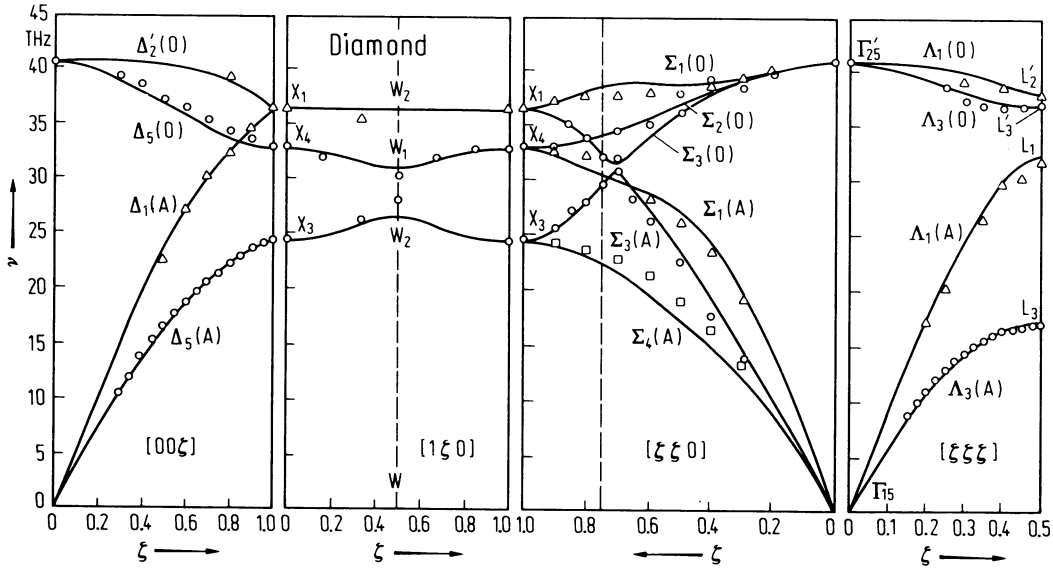

Fig. 6. Diamond. Phonon dispersion relations. Experimental data from neutron scattering, full curves: shell model calculation [67W].

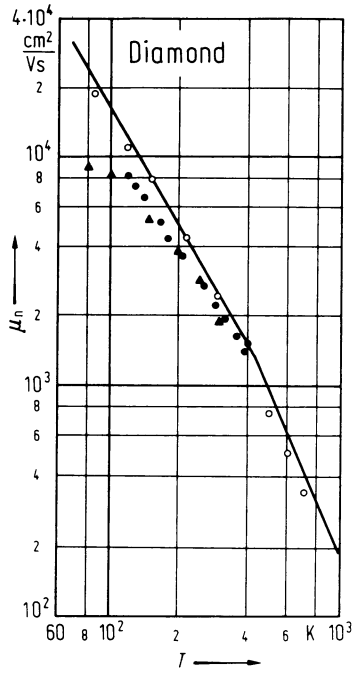

Fig. 7. Diamond. Electron mobility vs. temperature. Open circles: drift mobility data of [80N], full triangles and circles: Hall mobility data of [54R] and [67K], respectively. Continuous curve: theoretical drift mobility [80N].

◀

Fig. 8. Diamond. Hole mobility vs. temperature. Open circles: drift mobility data from [81R], full circles and triangles: Hall mobility data of [67K] and [65D], respectively. Solid and dashed curves: calculated drift and Hall mobilities, respectively [83R].

▶

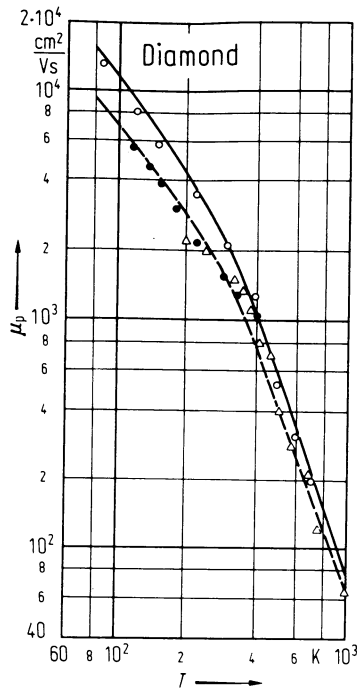

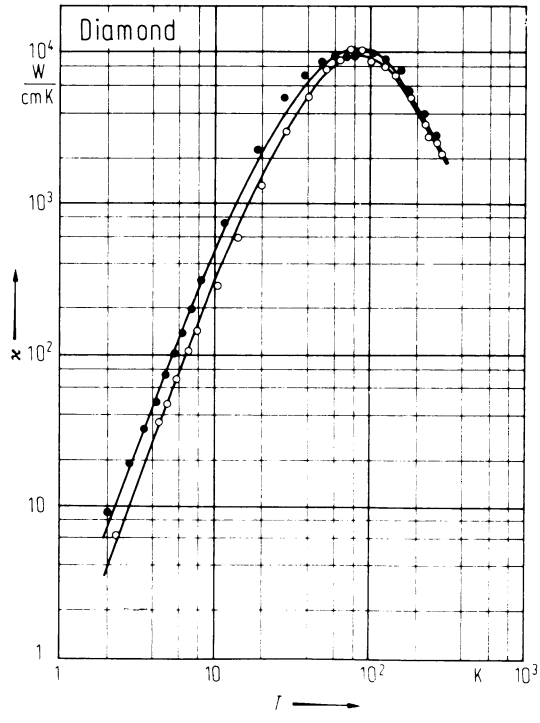

Fig. 9. Diamond. Thermal conductivity vs. temperature for two type IIa diamonds [76B].

Physical property	Numerical value	Experimental conditions	Experimental method, remarks	Ref.
electron mobility:				
μ_n	$\approx 2000\,cm^2/Vs$	RT	for temperature dependence of Hall and drift mobility, see Fig. 7	80N
hole mobility:				
μ_p	$2100\,cm^2/Vs$	RT	for temperature dependence of Hall and drift mobility, see Fig. 8	81R
	$\propto T^{-1.5}$	below 400 K		
	$\propto T^{-2.8}$	above 400 K		

thermal conductivity: mostly defect induced, see Fig. 9.

refractive index:

n	3.5	$\lambda = 177.0\,nm$		62P

n fits the empirical formula

$$n^2 - 1 = \frac{a\lambda^2}{\lambda^2 - \lambda_1^2} + \frac{b\lambda^2}{\lambda^2 - \lambda_2^2}: \quad a = 0.3306, \quad b = 4.3356, \quad \lambda_1 = 175.0\,nm, \quad \lambda_2 = 106.0\,nm$$

dielectric constant:

ε	5.70(5)	300 K	capacitance measurement at $10^3 \cdots 10^4$ Hz	77F

Temperature dependence: $\varepsilon = 5.70 - 5.35 \cdot 10^{-5}\,T + 1.66 \cdot 10^{-7}\,T^2$ (T in K) [77F].

Impurities and defects

Most electrical, optical and thermal properties of diamond are extrinsic, i.e. strongly dependent on the impurity content, the most important impurities being nitrogen and boron.

binding energies of impurities

Impurity	E_b[eV]	T[K]	Remarks	Ref.
Donors				
N	2	300	substitutional nitrogen; photoconductivity threshold	75V
	4	300	nitrogen aggregates;	67D
	(1.45 eV above valence band)		photoconductivity threshold, pair recombination	74C
Li	0.103(15)	300 ··· 600	ion implantation; conductivity measurements	79V
Acceptors				
B	0.370(10)	200 ··· 400	$n_a = 2 \cdot 10^{16}\,cm^{-3}$; conductivity measurements	78M
	0.3685(15)	150 ··· 1250	$n_a \approx 5 \cdot 10^{16}\,cm^{-3}$; Hall measurements	79C
	0.370	300 ··· 1000	synthetic diamond; $n_a = 2 \cdot 10^{16}\,cm^{-3}$; conductivity measurements	79B

References for 1.1

54R Redfield, A.G.: Phys. Rev. **94** (1954) 526.
57S Skinner, B.J.: Am. Mineral. **42** (1957) 39.
59K Kaiser, W., Bond, W.L.: Phys. Rev. **115** (1959) 857.
62B Bundy, F.P.: Science **137** (1962) 1055.
62P Philipp, H.R., Taft, E.A.: Phys. Rev. **127** (1962) 159.
62R Rauch, C.J.: Proc. Int. Conf. Phys. Semicond., Exeter **1962** (A.C. Strickland ed.), The Inst. of Phys. and the Phys. Soc., London, p. 276.
63B Bundy, F.P.: J. Chem. Phys. **38** (1963) 631.
64C Clark, C.D., Dean, P.J., Harris, P.V.: Proc. Roy. Soc. London **A277** (1964) 312.
65D Dean, P.J., Lightowlers, E.C., Wright, D.R.: Phys. Rev. **A140** (1965) 352.
67D Denham, P., Lightowlers, E.C., Dean, P.J.: Phys. Rev. **161** (1967) 762.
67K Konorova, E.A., Shevchenko, S.A.: Sov. Phys. Semicond. (English Transl.) **1** (1967) 299; Fiz. Tekh. Poluprovodn. **1** (1967) 364.
67W Warren, J.L., Yarnell, J.L., Dolling, G., Cowley, R.A.: Phys. Rev. **158** (1967) 805.
70S Solin, S.A., Ramdas, A.K.: Phys. Rev. **B1** (1970) 1687.
74C Collins, A.T.: Ind. Diamond Rev. **34** (1974) 131.
75G Grimsditch, M.H., Ramdas, A.K.: Phys. Rev. **B11** (1975) 3139.
75S Slack, G.A., Bartram, S.F.: J. Appl. Phys. **46** (1975) 89.
75V Vermeulen, L.A., Farrer, R.G.: Diamond Research 1975 (Suppl. to Ind. Diamond Rev.) 18.
76B Berman, R., Martinez, M.: Diamond Research 1976 (Suppl. Ind. Diamond. Rev.) 7.
77F Fontanella, J., Johnston, R.L., Colwell, J.H., Andeen, C.: Appl. Opt. **16** (1977) 2949.
78M Massarani, B., Bourgoin, J.C., Chrenko, R.M.: Phys. Rev. **B17** (1978) 1764.
79F Field, J.E. (ed.): The Properties of Diamond, Academic Press, London, New York, San Francisco **1979**.
79H Himpsel, F.J., Knapp, J.A., van Vechten, J.A., Eastman, D.E.: Phys. Rev. **B20** (1979) 624.
79B Bourgoin, J.C., Krynicki, J., Blanchard, B.: Phys. Status Solidi **(a)52** (1979) 293.
79C Collins, A.T., Lightowlers, E.C.: The Properties of Diamond, Field, J.E. (ed.), London, New York, San Francisco: Academic Press **1979**, p. 79.
79V Vavilov, V.S., Konorova, E.A., Stepanova, E.B., Trukhan, E.M.: Sov. Phys.-Semicond. **13** (1979) 635.
80H Himpsel, F.J., van der Veen, J.F., Eastman, D.E.: Phys. Rev. **B22** (1980) 1967.
80N Nava, F., Canali, C., Jacoboni, C., Reggiani, L.: Solid State Commun. **33** (1980) 475.
81R Reggiani, L., Bosi, S., Canali, C., Nava, F.: Phys. Rev. **B23** (1981) 3050.
82A Armon, H., Sellschop, J.P.F.: Phys. Rev. **B26** (1982) 3289.
83R Reggiani, L., Waechter, D., Zukotynski, S.: Phys. Rev. **B28** (1983) 3550.
84C Chelikowsky, J.R., Louie, S.G.: Phys. Rev. **B29** (1984) 3470.

Physical property	Numerical value	Experimental conditions	Experimental method, remarks	Ref.

1.2 Silicon (Si)

Electronic properties

band structure: Fig. 1 (Brillouin zone, see Fig. 2 of section 1.1)

The *conduction band* is characterized by six equivalent minima along the [100] axes of the Brillouin zone located at about $k_0 = 0.85\ (2\pi/a)$ (symmetry Δ_1). The surfaces of constant energy are ellipsoids of revolution with major axes along [100]. Higher minima are located at Γ and along the [111] axes about 1 eV above the [100] minima.

The *valence band* has its maximum at the Γ point (symmetry Γ_8), the (warped) light and heavy hole bands being degenerate at this point. The third spin-orbit split-off band has Γ_7-symmetry. The spin-orbit splitting energy at Γ is small compared to most interband energy differences. Thus, spin-orbit interaction is mostly neglected and the symmetry notation of the single group of the diamond lattice is used in the following tables.

energies of symmetry points of the band structure (relative to the top of the valence band) (in eV):

$E(\Gamma_{1v})$	-12.34 ($-12.5(6)$)	theoretical data:
$E(\Gamma_{25'v})$	0.00	localized atomic orbital
$E(\Gamma_{15c})$	3.50 (3.34 ··· 3.36)	calculation [85S], see Fig. 1
$E(\Gamma_{2'c})$	4.09 (4.15(5))	
$E(X_{1v})$	-7.75	

Physical property	Numerical value	Experimental conditions	Experimental method, remarks	Ref.
$E(X_{4v})$	−2.89 (−2.9)		experimental data (in brackets):	
$E(X_{1c})$	1.12 (1.13)		from a compilation in	
$E(L_{2'v})$	−9.62 (−9.3(4))		[83M], mostly photoemission	
$E(L_{1v})$	−7.01 (−6.8(2))		data	
$E(L_{3'v})$	−1.25 (−1.2(2))			
$E(L_{1c})$	2.29 (2.04(6))			
$E(L_{3c})$	4.34 (3.9(1))			
indirect energy gaps (in eV):				
$E_{g,ind}$	1.1700	0 K (extrapol.)	wavelength modulated	74B
$(\Gamma_{25'v} - \Delta_{1c})$	1.1242	300 K	transmission	
$E_{g,th}$	1.205	0 K (extrapol.)	linear extrapolation from temperature dependence of conductivity above 200 K	67B
Temperature dependence $E_g(T) = A + BT + CT^2$ with $A = 1.170$ eV, $B = 1.059 \cdot 10^{-5}$ eV K^{-1}, $C = -6.05 \cdot 10^{-7}$ eV K^{-2} up to 300 K [74B]; see also Fig. 2 [85L].				
$E_{g,ind}$	1.650(10) eV		optical absorption	74F
$(\Gamma_{25'v} - L_{1c})$	2.04(6) eV		cf. table above ("energies of symmetry points")	83M

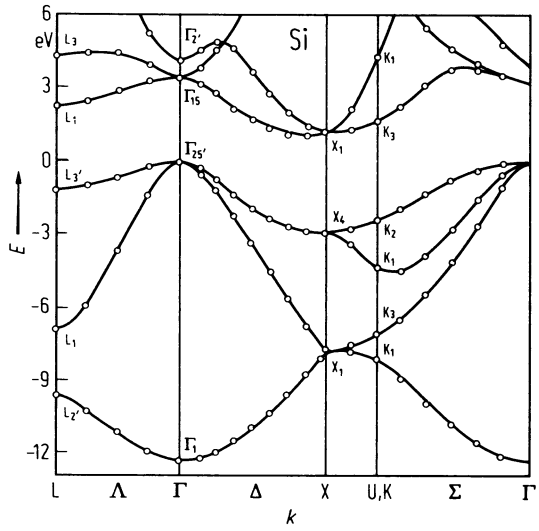

Fig. 1. Si. Band structure. Solid line: non-local, energy-dependent pseudopotential calculation, circles: localized atomic orbital method [85S].

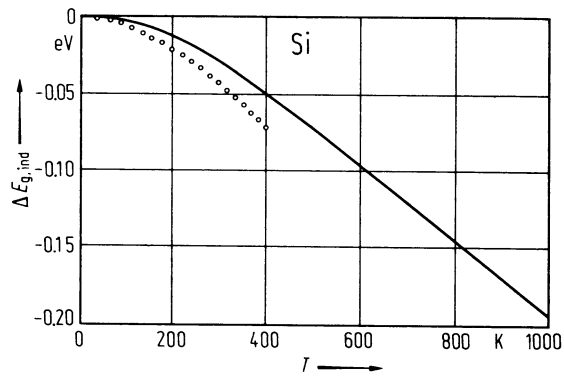

Fig. 2. Si. Temperature dependence of the indirect energy gap. Solid line: calculated, circles: experimental [85L]; $\Delta E_{g,ind} = E_{g,ind}(T) - E_{g,ind}(0)$.

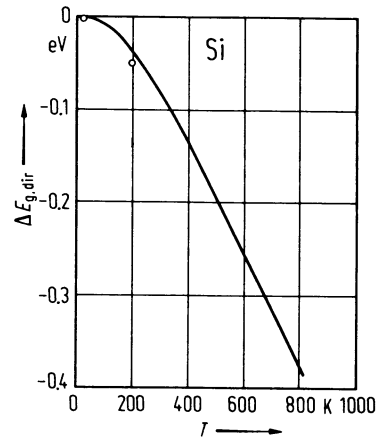

Fig. 3. Si. Temperature dependence of the direct band gap ($\Delta E_{g,dir} = E_{g,dir}(T) - E_{g,dir}(0)$). Solid line: calculated [85L], circles: experimental [72A].

Physical property	Numerical value	Experimental conditions	Experimental method, remarks	Ref.
exciton energies (in eV):				
$E(1S)$	1.15454(7)	1.6 K	photoluminescence emission	80S
E_b	0.0143(5)	1.8 K	exciton binding energy	77L2
direct energy gap (in eV):				
$E_{g,dir}$	4.185(10)	4.2 K	electroreflection	72A
$(\Gamma_{25'v} - \Gamma_{2'c})$	4.135	190 K		
$= E_0$	4.15···4.21		cf. table above ("energies of symmetry points")	83M
At higher temperatures E_0 cannot be optically resolved from the dominating E_2 critical point. Temperature dependence, see Fig. 3				
spin-orbit splitting energy:				
$\Delta_0(\Gamma_{25'v})$	0.0441(3) eV	1.8 K	wavelength modulated absorption	74N
	0.045 eV	10 K	electroreflectance	78D
critical point energies (in eV):				
E_0'	3.378	10 K	ellipsometry	83J1
Direct transitions at Γ to higher conduction band. Nearly degenerate with the E_1 critical point, but different temperature shift. E_0' and E_1 cannot clearly be resolved by experiment.				
E_1	3.46(15)	10 K	electroreflectance	78D
Contributions mainly from transitions along the Λ-axes and at L.				
E_1'	5.45	10 K	electroreflectance	78D
Transitions between $\Lambda_{3v} - \Lambda_{3c}$.				
E_2	4.330	10 K	ellipsometry	83J
Contributions to E_2 from various transitions along the Σ and Δ axes.				
effective masses, electrons (in units of m_0):				
$m_{n\parallel}$	0.1905(1)	1.26 K	cyclotron resonance, temperature dependence of transverse mass, see Fig. 4	65H
$m_{n\perp}$	0.9163(4)			
$m_{n,ds}$	1.026	4.2 K	cyclotron resonance, temperature dependence of density of states mass, see Fig. 5a	67B
***g*-factor of electrons:**				
g_c	1.99893(28)		esr	66K
effective masses, holes (in units of m_0):				
$m_{p,h}$	0.537	4.2 K	cyclotron resonance	67B
$m_{p,l}$	0.153			
m_{so}	0.234			
$m_{p,ds}$	0.591	4.2 K	temperature dependence of density of states mass, see Fig. 5b	
In non-parabolic bands the density of states mass obtained through a calculation of the carrier concentration becomes temperature dependent, whereas the mass obtained directly from a calculation of the density of states				

Fig. 4. Si. Transverse electron mass determined by cyclotron resonance vs. temperature [76O]. ▶

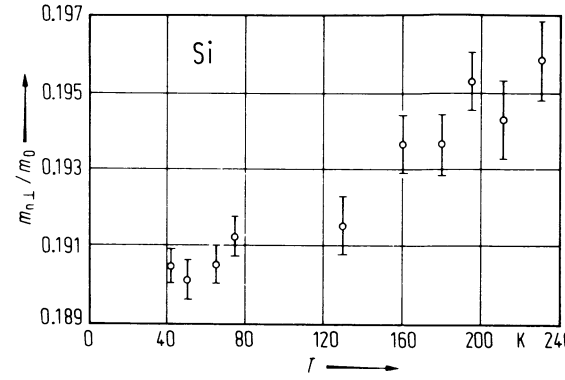

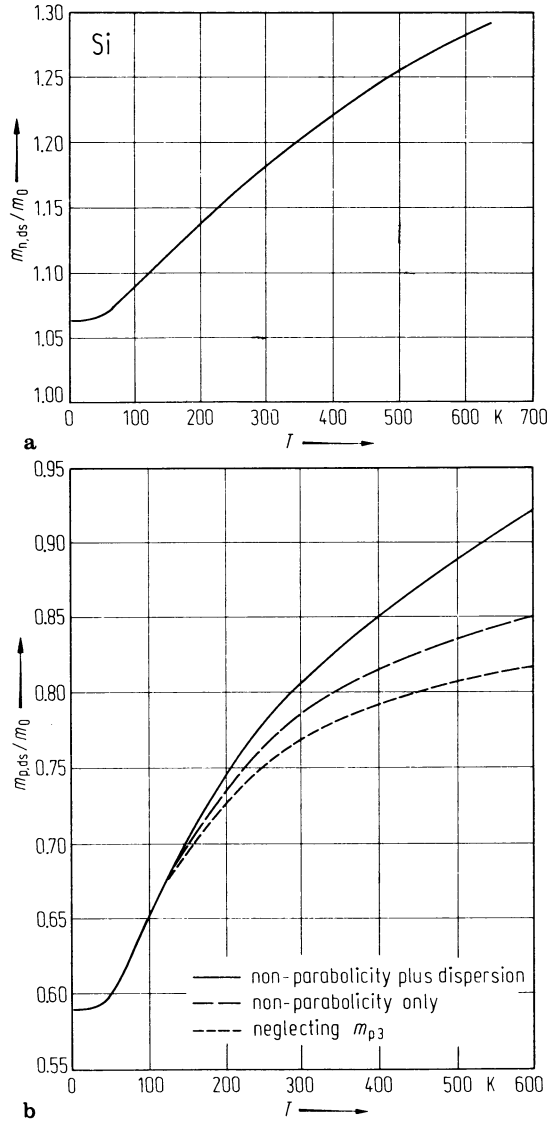

Fig. 5. Si. (a) Conduction band density of states mass vs. temperature for a sample with donor concentration below $5 \cdot 10^{17}\,cm^{-3}$. (b) Valence band density of states mass vs. temperature as calculated from the experimentally determined valence band parameters [67B].

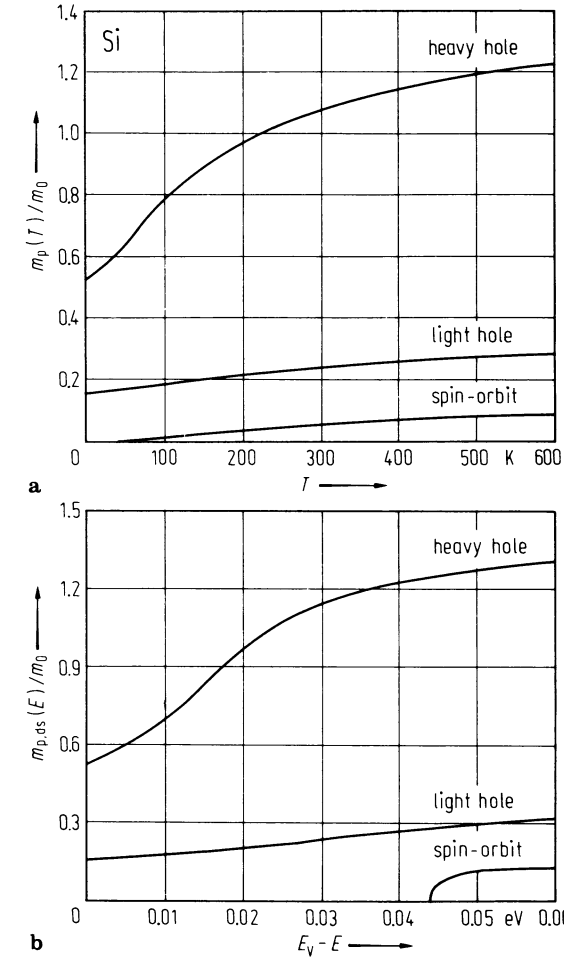

Fig. 6. Si. (a) Density of states mass obtained from carrier concentration vs. temperature for the three valence bands, (b) density of states mass obtained from the calculated density of states vs. energy measured from the top of the valence band. Both masses are related to each other by $m_p^{3/2}(T) = \langle m_{ds}^{3/2}(E) \rangle$, where $\langle \cdots \rangle$ means a weighted thermal average [83L].

Physical property	Numerical value	Experimental conditions	Experimental method, remarks	Ref.

becomes energy dependent. The former is the weighted thermal average of the latter: $m_p^{3/2}(T) = \langle m_{p,ds}^{3/2}(E) \rangle$. For the temperature and energy dependences of both masses, see Fig. 6.

valence band parameters:

A	−4.27(2)		cyclotron resonance	65B
B	−0.63(8)			
$\|C\|$	4.93(15)			

Lattice properties

Structure

Si I	space group O_h^7–Fd3m (diamond lattice)		stable at normal pressure	
Si II	space group D_{4h}^{19}–$I4_1/amd$		grey tin structure	
Si III	space group T_h^7–Ia3		metastable	84O1
Si IV	space group D_{6h}^4–$P6_3/mmc$			
Si V	space group D_{6h}^1–P6/mmm		simple hexagonal	84O1
Si VI			unidentified; stable above 34 GPa	84O1
Si VII			hexagonal close packed structure; stable above ≈ 45 GPa	84O1

transition pressures (in GPa):

p_{tr}	11.2(2)···12.5(2)		Si I → Si II	84H,
	13.2(2)···16.4(5)		Si II → Si V	85M1
	14.5···11.0		Si V → Si II	
	10.8···8.5		Si II → Si III	

lattice parameter (in nm):

a	0.543102018(34)	295.7 K	high purity single crystal measured in vacuum	82B1

temperature dependence of the lattice parameter: $a(T)$ in high-purity material can be approximated in the range 20···800 °C by $a(T) = 5.4304 + 1.8138 \cdot 10^{-5}(T - 298.15\,\text{K}) + 1.542 \cdot 10^{-9}(T - 298.15\,\text{K})^2$ [73Y2], see also Fig. 7.

linear thermal expansion coefficient:

α	$2.59(5) \cdot 10^{-6}\,\text{K}^{-1}$	298.2 K	84O2

Temperature dependence: Fig. 8 [84O2]. The data of Fig. 8 can be approximated in the temperature range 120···1500 K by the formula:
$\alpha(T) = (3.725\,[1 - \exp(-5.88 \cdot 10^{-3}\,[T - 124])] + 5.548 \cdot 10^{-4}\,T) \cdot 10^{-6}\,\text{K}^{-1}$ (T in K).

density:

d	2.329002 g cm^{-3}	25 °C	hydrostatic weighing, high purity crystal	64H

melting point:

T_m	1685(2) K	73H

phonon dispersion relations: Fig. 9.

Physical property	Numerical value	Experimental conditions	Experimental method, remarks	Ref.
phonon frequencies (in THz):				
$\nu_{LTO}(\Gamma_{25'})$	15.53(23)	296 K	from inelastic neutron scattering	63D
$\nu_{TA}(X_3)$	4.49(6)			
$\nu_{LAO}(X_1)$	12.32(20)			
$\nu_{TO}(X_4)$	13.90(30)			
$\nu_{TA}(L_3)$	3.43(5)			
$\nu_{LA}(L_{2'})$	11.35(30)			
$\nu_{LO}(L_1)$	12.60(32)			
$\nu_{TO}(L_{3'})$	14.68(30)			

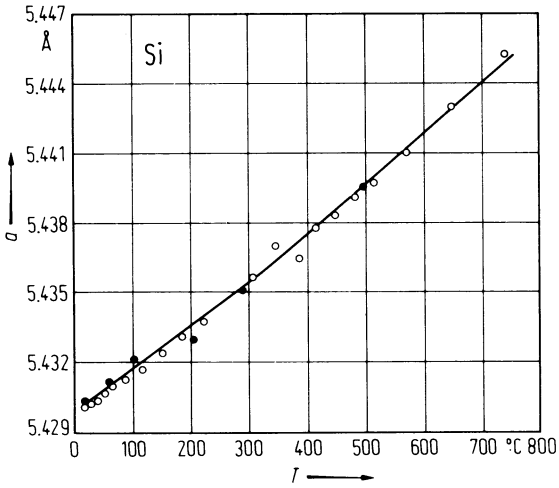

Fig. 7. Si. Lattice parameter vs. temperature in the range 20···740 °C, measurements on various samples [61H].

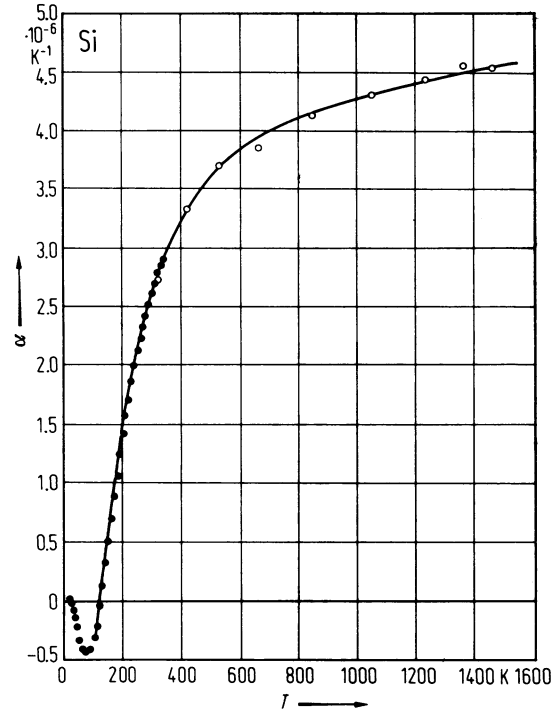

Fig. 8. Si. Linear thermal expansion coefficient vs. temperature. Experimental data from [77L1] (full circles) and [84O2] (open circles).

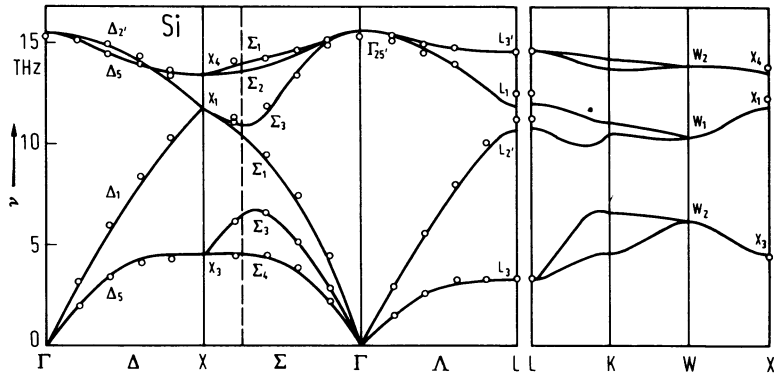

Fig. 9. Si. Phonon dispersion relation. Solid lines: theoretical [77W1], data points from [63D] and [72N].

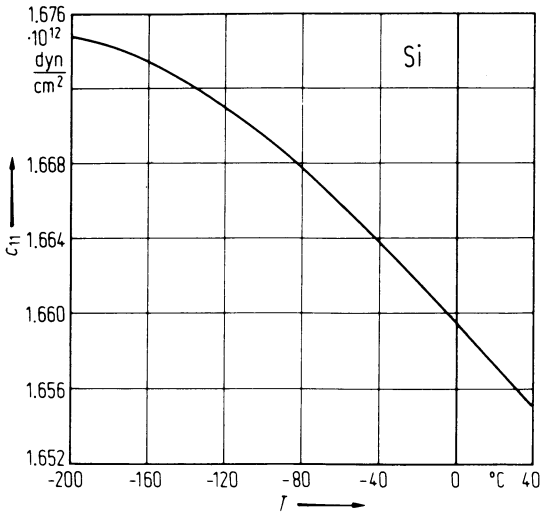

Fig. 10. Si. Second-order elastic modulus c_{11} vs. temperature [53M].

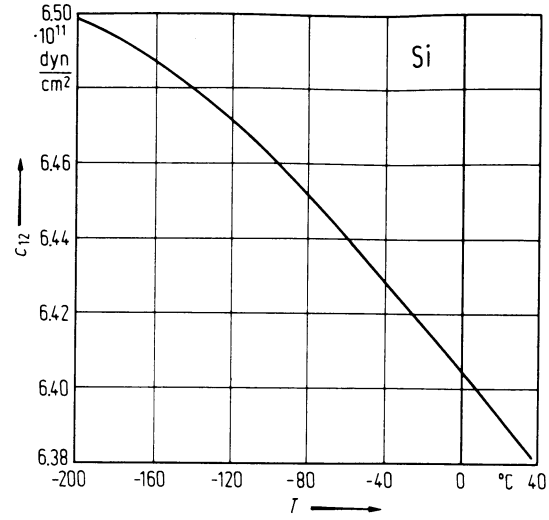

Fig. 11. Si. Second-order elastic modulus c_{12} vs. temperature [53M].

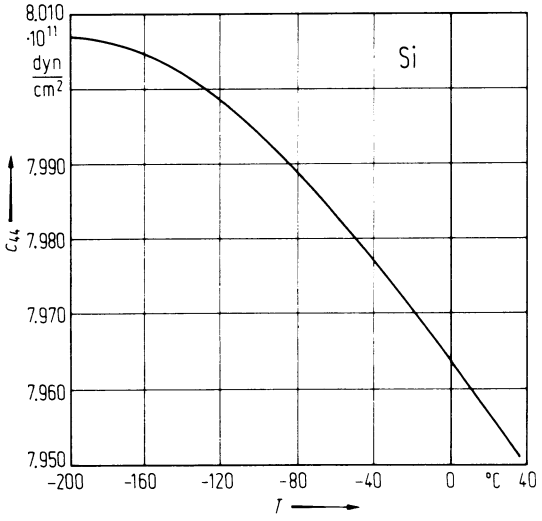

Fig. 12. Si. Second-order elastic modulus c_{44} vs. temperature [53M].

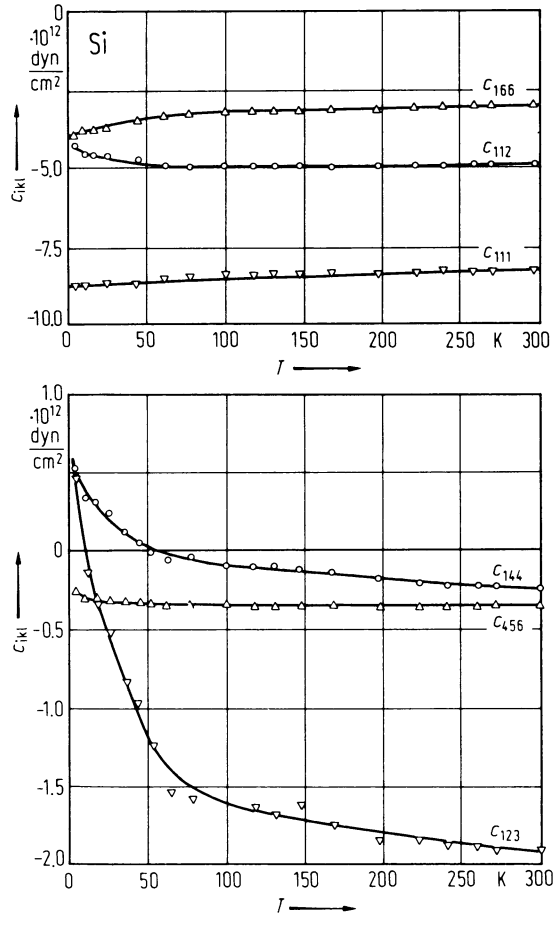

Fig. 13. Si. Third-order elastic moduli vs. temperature. Solid lines: best fit to the data [83P].

Physical property	Numerical value	Experimental conditions	Experimental method, remarks	Ref.
second order elastic moduli (in 10^{11} dyn cm^{-2}):				
c_{11}	16.577	298 K	p-type sample, from ultrasound	64M
c_{12}	6.393	$\varrho = 410\,\Omega$cm	sound measurements	
c_{44}	7.962		for temperature dependence, see Figs. 10···12	
third order elastic moduli (in 10^{12} dyn cm^{-2}):				
c_{111}	−8.34(11)	298 K	ultrasonic harmonic generation	81P
c_{112}	−5.31(32)		combined with pressure	
c_{144}	−0.95(24)		derivative of elastic constants	
c_{123}	−0.02(18)		for full temperature	
c_{166}	−2.96(12)		dependence, see Fig. 13	
c_{456}	−0.074(22)			

Transport properties

Contributions to the electric transport are exclusively made by electrons in the [100]-conduction band minima and (heavy and light) holes in the two uppermost valence bands. In samples with impurity concentrations below 10^{12} cm^{-3} the mobilities are determined by pure lattice scattering down to temperatures of about 10 K (n-type) or 50 K (p-type), respectively. For electrons the lattice mobility below 50 K is dominated by deformation potential coupling to acoustic phonons. At higher temperatures, intervalley scattering between the equivalent minima of the conduction band is added to the intravalley process, modifying the familiar $T^{-1.5}$ dependence to $T^{-2.42}$. At temperatures below 100 K, the lattice mobility of holes is dominated by acoustic scattering, but does not follow the $T^{-1.5}$ law due to the non-parabolicity of the valence bands. The proportionality of μ_p to $T^{-2.2}$ around RT is a consequence of optical phonon scattering.

intrinsic conductivity:

σ_i	$3.16 \cdot 10^{-6}\,\Omega^{-1}$ cm^{-1}	300 K	54M

The intrinsic conductivity up to 1273 K is given by the phenomenological expression $\log_{10} \sigma_i = 4.247 - 2.924 \cdot 10^3\, T^{-1}$ (σ_i in Ω^{-1} cm^{-1}, T in K).

intrinsic carrier concentration:

n_i	$1.02 \cdot 10^{10}$ cm^{-3}	300 K	see Fig. 14 for temperature dependence	77W2

n_i can be expressed in the range 200···500 K by $n_i(T) = 5.71 \cdot 10^{19} (T/300)^{2.365} \cdot \exp(-6733/T)$ cm^{-3} [77W2], in the range 450···700 K by $n_i(T) = 3.87 \cdot 10^{16}\, T^{3/2} \cdot \exp(-1.21/2\,kT)$ cm^{-3} (T in K, kT in eV).

electron mobility:

μ_n	1450 cm^2/Vs	300 K	lattice scattering mobility	54M

Around RT μ_n can be expressed by $\mu_n = 1.43 \cdot 10^9\, T^{-2.42}$ cm^2/Vs (T in K). For temperature dependence, see Fig. 15.

hole mobility (μ in cm^2/Vs):

$\mu_{H,p}$	370	300 K	ultrapure sample	82H,
	2.10^5	20 K	see Fig. 16 (b)	83S1,
				83S2,
$\mu_{c,p}$	505	300 K	see Fig. 16 (a)	83S3
	$1.6 \cdot 10^5$	20 K		

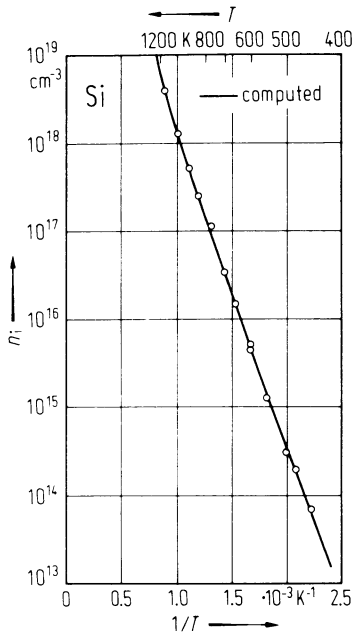

Fig. 14. Si. Carrier concentration in the intrinsic range vs. reciprocal temperature [54M].

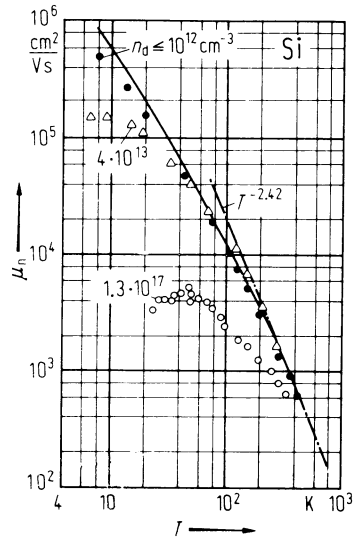

Fig. 15. Si. Electron mobility vs. temperature; data points from three authors, solid line: theoretical lattice scattering mobility, dash-dotted line: $T^{-2.42}$ dependence of μ_n around RT [77J].

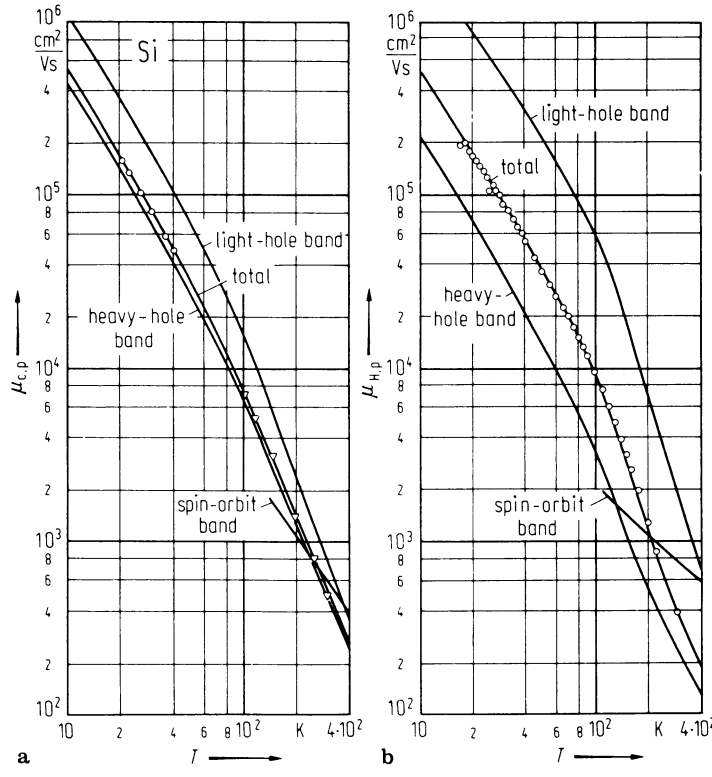

Fig. 16. Si. (a) Conductivity hole mobility vs. temperature (circles from [82M], triangles from [56L]). Solid lines: calculated contributions from the three valence bands. (b) Hall hole mobility vs. temperature (circles from [82M]). Solid lines as in (a) [83S1, 83S2].

Physical property	Numerical value	Experimental conditions	Experimental method, remarks	Ref.
thermal resistivity (in cm K W^{-1}):				
κ_L^{-1}	$0.1598 + 1.532 \cdot 10^{-3} T + 1.583 \cdot 10^{-6} T^2$		100 K < T < 1200 K, lattice contribution	68F

Optical properties

dielectric constant:

		T[K], ν[MHz]		
ε	12.1	4.2,	750	capacitance bridge
	11.9	300	750	

reflectance: in the temperature range 1100···1400 °C the reflectance can be approximated by $R = 30.37 + 1 \cdot 10^{-2} T - 1.3 \cdot 10^{-5} T^2 + 9.19 \cdot 10^{-10} T^3 + 5.65 \cdot 10^{-12} T^4$ (R in %, T in °C) [81L].
For the dependence of the absorption coefficient, extinction coefficient and refractive index on photon energy see Fig. 17.

refractive index: in the range 2.4···25 μm n can be approximated by the dispersion formula $n = A + BL + CL^2 + D\lambda^2 + E\lambda^4$ (λ in μm) with $L = (\lambda - 0.28)^{-1} \mu m^{-1}$, $A = 3.41983$, $B = 0.159906$ μm, $C = -0.123109\ \mu m^2$, $D = 1.26878 \cdot 10^{-6}\ \mu m^{-2}$, $E = -1.95104 \cdot 10^{-9}\ \mu m^{-4}$ [80E].

optical constants:

real and imaginary parts of the dielectric constant measured by spectroscopical ellipsometry; n, k, R, K calculated from these data [83A]; see also Fig. 18.

$\hbar\omega$[eV]	ε_1	ε_2	n	k	R	$K[10^3\ cm^{-1}]$
1.5	13.488	0.038	3.673	0.005	0.327	0.78
2.0	15.254	0.172	3.906	0.022	0.351	4.47
2.5	18.661	0.630	4.320	0.073	0.390	18.48
3.0	27.197	2.807	5.222	0.269	0.461	81.73
3.5	22.394	33.818	5.610	3.014	0.575	1069.19
4.0	12.240	35.939	5.010	3.586	0.591	1454.11
4.5	−19.815	24.919	2.452	5.082	0.740	2317.99
5.0	−10.242	11.195	1.570	3.565	0.675	1806.67
5.5	−9.106	8.846	1.340	3.302	0.673	1840.59
6.0	−7.443	5.877	1.010	2.909	0.677	1769.27

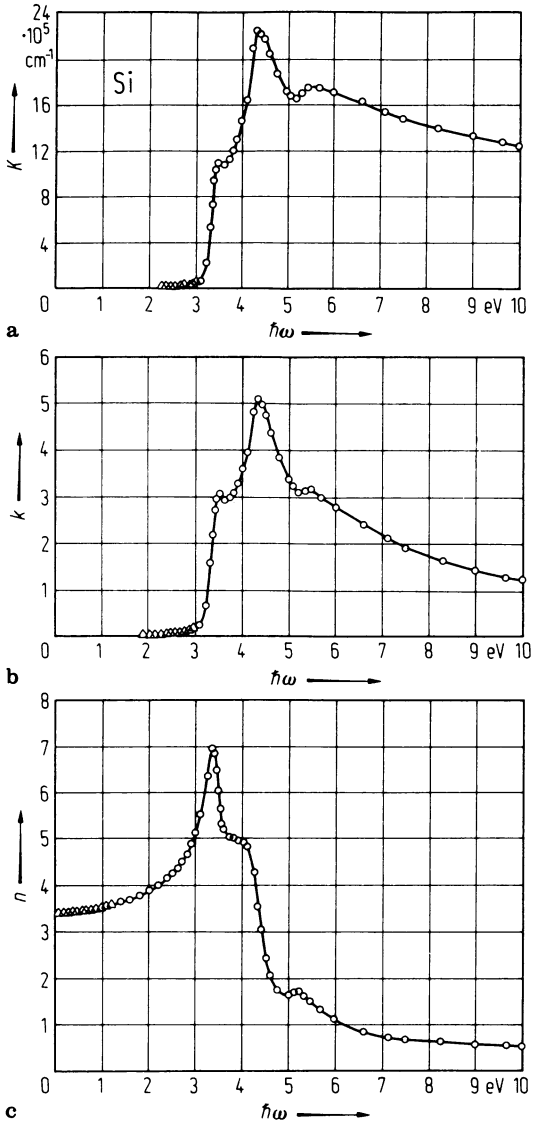

Fig. 17. Si. Optical constants below 10 eV vs. photon energy. (a) Absorption coefficient, (b) extinction coefficient, (c) refractive index [57C, 60P].

◀

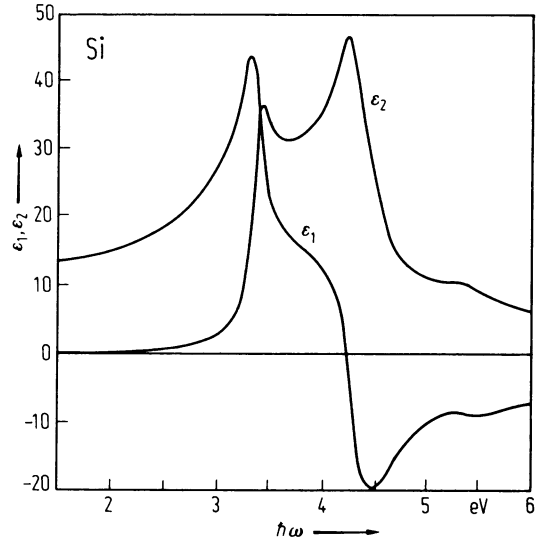

Fig. 18. Si. Real and imaginary parts of the dielectric constant vs. photon energy [83A].

Impurities and defects

The following tables on solubilities, diffusion coefficients and energy levels contain a representative selection of data and references from more than 50 pages on these topics in volume **NS III/22b**.

solubility of impurities in Si

Impurity	c_{max}^{eq} [cm^{-3}]	T_{max} [°C]	c_0 [cm^{-3}]	ΔH [eV]	T-Range [°C]	Ref.
Ag	10^{16}	1300	107	2.78	1024···1325	87R
Al	$2 \cdot 10^{19}$	1150				69W
As			$2.2 \cdot 10^{22}$	0.47	700··· 900	87A1
	$2.5 \cdot 10^{20}$	1000				83N
Au (s)	10^{17}	1300				88J
(i)	$1.5 \cdot 10^{15}$	1050	$8.2 \cdot 10^{24}$	2.56	700···1100	86G1
B			$3.2 \cdot 10^{22}$	0.43	870···1200	86D
	$8 \cdot 10^{20}$	1410				83W2
Bi	$8 \cdot 10^{17}$	1300				69W
C	$4 \cdot 10^{17}$	1400	$4 \cdot 10^{24}$	2.30	1000···1400	83K
Co	$3.5 \cdot 10^{6}$	1300	10^{26}	2.83	700···1250	83W1
Cr	10^{16}	1350	$5.5 \cdot 10^{24}$	2.79	800···1400	83W1
Cu	$1.5 \cdot 10^{18}$	1300	$5.5 \cdot 10^{23}$	1.49	500···1250	83W1
Fe	$2 \cdot 10^{16}$	1200	$1.8 \cdot 10^{16}$	2.94	900···1200	85W1
Ga	$6 \cdot 10^{20}$	1100				82B2
H	$7 \cdot 10^{15}$	1410				83W2
			$1.6 \cdot 10^{20}$	1.46	400··· 600	68I
In	$4 \cdot 10^{18}$	1100				82B2
Li	$6.5 \cdot 10^{19}$	1200				83W2
Mn	$1.5 \cdot 10^{16}$	1200	$5 \cdot 10^{25}$	2.78	900···1150	86G2
N	$4.5 \cdot 10^{15}$	1400				73Y1
Ni	$3 \cdot 10^{17}$	1100	$2.6 \cdot 10^{22}$	1.34	900···1200	86G1
O	$2 \cdot 10^{18}$	1400	$8.9 \cdot 10^{27}$	2.19	1350···1400	86C1
Os	$3.2 \cdot 10^{16}$	1260	$9 \cdot 10^{25}$	2.69	800···1000	87A2
P	$4 \cdot 10^{20}$	1100				83N
Pd	$4 \cdot 10^{15}$	1200	$1.8 \cdot 10^{20}$	1.34	900···1200	78S
Pt (s)	10^{17}	1250	$1.1 \cdot 10^{27}$	2.71	800···1000	75L
S	$2.5 \cdot 10^{17}$	1200				84W1
Sb	$5.3 \cdot 10^{19}$	1300	$3.81 \cdot 10^{21}$	0.56	850···1300	89N
Se	$7 \cdot 10^{16}$	1200	$5.5 \cdot 10^{27}$	2.84	800···1200	78V
Si	10^{18}	1400	10^{8}	4.40	700···1400	85T
Sn	$6 \cdot 10^{19}$	1100				69W
Ti	$2.3 \cdot 10^{13}$	1100	$6.6 \cdot 10^{23}$	2.85	1000···1250	86G1
Tl	$4 \cdot 10^{17}$	900				81K1
Vacancy	$6 \cdot 10^{17}$	1400	$8 \cdot 10^{23}$	2.0	800···1400	85T
Zn	$2.3 \cdot 10^{16}$	1100	$7.3 \cdot 10^{21}$	1.50	900···1360	86G1

(s): substitutional, (i): interstitial

diffusion coefficients of impurities in Si

Impurity	D_0 [$cm^2 s^{-1}$]	Q [eV]	T-Range [°C]	Ref.
Ag (i)	$6 \cdot 10^{-5}$	1.15	1024 ··· 1325	87R
Al	8.69	3.39	1060 ··· 1240	86S3
As	0.38	3.58	900 ··· 1400	77F2
Au (i)	$2.4 \cdot 10^{-4}$	0.39	300 ··· 1100	83G2
(s)	2.75	2.04	1100 ··· 1200	83G2
B	5.1	3.70	700 ··· 1200	83W1
Bi	3.96	4.12	1000 ··· 1200	77F1
C	1.9	3.10	1070 ··· 1400	83G1
Co	$9 \cdot 10^{-4}$	0.37	760 ··· 1100	88U
Cu (i)	$4.7 \cdot 10^{-3}$	0.43	400 ··· 900	86G1
(s)	$4 \cdot 10^{-3}$	1.0	800 ··· 1100	86G1
Fe	$1.3 \cdot 10^{-3}$	0.68	30 ··· 1300	83W1
Ga	6.3	3.48	1200 ··· 1250	85D
H	$4.2 \cdot 10^{-5}$	0.56	27 ··· 700	87P1
In	752	4.38	1000 ··· 1200	83C
K	$1.1 \cdot 10^{-8}$	0.80	500 ··· 800	72Z
Li	$2.5 \cdot 10^{-3}$	0.66	25 ··· 1350	83W1
N	0.87	3.29	1100 ··· 1200	76P
Na	0.01	1.27	500 ··· 850	76B
Ni (i)	$2 \cdot 10^{-3}$	0.47	800 ··· 1300	86G1
(s)	0.1	1.92	450 ··· 800	86G1
O	0.13	2.53	500 ··· 1400	86M2
P	10.5	3.69	1050 ··· 1350	83W1
S	0.22	2.10	1000 ··· 1230	88S2
Sb	30	4.08	1000 ··· 1200	87T
Se	0.3	2.60	1000 ··· 1310	88S1
Si	640	4.80	800 ··· 1200	86S1
Sn	0.054	3.50	1100 ··· 1200	74A
Te	0.9	3.30	1000 ··· 1310	88S1
Ti	0.015	1.8	950 ··· 1200	88M
Tl	351	4.26	1100 ··· 1338	77F1
Vac	0.6	4.03	700 ··· 1100	85T
Zn (i)	$3 \cdot 10^{-6}$	0.40	1100 ··· 1300	86G1

(s): substitutional, (i): interstitial

energy levels and structural information
on impurities, defects, and complexes in silicon. Negative energy refers to conduction band edge, positive energy refers to valence band edge.

Impurity, defect	E [eV]	Type	Remarks	Ref.
Al	+0.06903	a	T_d-symmetry, substitutional	83S4
	+0.17	d	interstitial Al after irradiation,	79T1
Al-C	+0.0563	a	aluminum-carbon pair, (X-center)	83S4
Al-Fe	+0.19	d	Fe(interstitial)-Al(substitutional) donor-acceptor pair, T_2-symmetry	88W
Al-H			passivation of Al substitutional acceptor	87S
As-Vac	−0.47	d	E-center, irradiation, anneals out at $T > 450$ K	79T2
Au	+0.346	d	substitutional	82W
	+0.632			
	(−0.545)			
B	+0.04439	a	substitutional acceptor	83F
B-C	+0.0371	a	boron-carbon pair, X-center	83S4
B-Fe	+0.100	d	B(substitutional)-Fe(interstitial)	86G1
	−0.23	a	donor-acceptor pair	
B-H			hydrogenation of B acceptor, atomic hydrogen	87S
Bi	−0.0710	d	substitutional, 1s(A_1) ground state,	85H1
Cd	+0.55	a	double substitutional acceptor Cd(0/−), single charge state	81D
	−0.45	a	double substitutional acceptor Cd(−/− −), double charge state	
Cr	−0.22	d	interstitial, Cr(0/+), $3d^6/3d^5$	86G1
	+0.128	d	double donor, interstitial?	81K2
Cu			many levels reported, uncertain identification	86G1
			inactive at $T < 850$ °C, several irradiation defects at $T > 850$ °C	86C2
			triple acceptor most likely	85F2
	+0.222		Cu-related, frequently reported values	86C2
	+0.411		passivated by hydrogen	85W2
Fe	+0.385	d	interstitial after quenching	86G1
Ga	+0.07273	a	substitutional acceptor	82S
Ga-C	+0.0572	a	Ga(substitutional)-C(substitutional) pair (X-center)	85F1
Ga-Fe	+0.14	d	Fe(interstitial)-Ga(substitutional)	86G1
	+0.23	d	donor-acceptor pair, configuration bistability	
Ga-H			passivation by atomic H	87S
In	+0.15558	a	substitutional acceptor,	83S4
In-C	+0.1128		In(substitutional)-C(substitutional), (X-center)	82S
In-Fe	+0.160	d	Fe(interstitial)-In(substitutional)	86G1
	+0.27	d	donor-acceptor pair	
In-H			passivation by atomic H,	87P1
Li	−0.03381	d	interstitial	81S
Li-Al			Li(interstitial)-Al(substitutional) donor-acceptor pair	65W1

(*Continued*)

Impurity, defect	E [eV]	Type	Remarks	Ref.
Li-B			Li(interstitial)-B(substitutional) donor-acceptor pair	65W2
Mg	−0.1075	d	interstitial Mg(0)	72H
	−0.2565	d	interstitial Mg(+), T_d-symmetry	
Mn	+0.26	d	$Mn^{++/+}$ $3d^5$ interstitial,	86G1
	−0.42	d	$Mn^{+/0}$ $3d^6$	
	−0.12	a	$Mn^{0/-}$ $3d^7$	
	+0.34	d	$Mn^{+/0}$ $3d^2$ substitutional,	86G1
	−0.43	a	$Mn^{0/-}$ $3d^5$	
N			N-N pairs main incorporation	86S4
	−0.19	d	off-center substitutional partial	86S4
Ni			uncertain identification,	86G1
			15Ni-related complexes	87L
O			Si-O-Si bridging, displaced [111]-axis, electrically inactive	87P2
	−0.061	d	"thermal donor" TD, double donor (0/+), formation at 350···500 °C	87P2
	−0.132	d	"thermal donor" TD, double donor (+/++), formation at 350···500 °C, structure uncertain, C_{2v}-symmetry	87P2
O-Vac	−0.17	a	A-center, after irradiation C_{2v}-symmetry, (100)-orientation	87P2
P	−0.04558	d	substitutional, single donor	82G
	−0.0037	a	D^--center, binding of a second electron at 4 K	82N
P-Vac	−0.45	a	E-center, irradiation damage,	77K
Pd	−0.23	a	Pd(−/0) predominant incorporation, $T = 900 \cdots 1200$ °C annealing and quenching	86S2
	+0.33	d	Pd(+/0) predominant incorporation, $T = 900 \cdots 1200$ °C annealing and quenching	84L
Pd-H			passivation by atomic H	87P1
Pt	+0.32···+0.36	d	substitutional Pt(+/0)	87N
	−0.23···−0.26	a	substitutional Pt(0/−)	86S2
S	−0.3182	d	substitutional S(+/0)double donor, T_d-symmetry	86P
	−0.6132	d	substitutional S(++/+)double donor, T_d-symmetry	86P
S-S	−0.1875	d	sulfur pair S_2(+/0) C_{3v}-symmetry	86P
	−0.3700	d	sulfur pair S_2(++/0)	86P
Sb-Vac	−0.44	a	E-center, irradiation, anneals at $T = 460$ K	79T2
Sb	−0.04277	d	substitutional single donor	84S
Se	−0.3065	d	substitutional double donor Se(+/0), T_d-symmetry, 1s(A1)	86P
	−0.5932	d	substitutional double donor Se(++/+), T_d-symmetry 1s(A1)	86P
Se-Se	−0.2064	d	Se-pair, double donor, Se_2(+/0), D_{3D}-symmetry	86P
	−0.3892	d	Se-pair, double donor, Se_2(++/+), D_{3D}-symmetry	86P

(*Continued*)

Impurity, defect	E [eV]	Type	Remarks	Ref.
Ta	−0.21			77B
Te	−0.1987	d	substitutional double donor Te(+/0), T_d-symmetry	86P
	−0.4112	d	substitutional double donor Te(++/+), T_d-symmetry	86P
Te-Te	−0.1580	d	double donor pair Te_2(+/0), D_{3D}-symmetry	84W2
Ti	+0.25 ··· +0.28	d	double donor $3d^3 - 3d^2$, interstitial	83W1
	−0.28	d	single donor $3d^4 - 3d^3$, interstitial	83W1
	−0.08	a	single acceptor $3d^5 - 3d^4$, interstitial	83W1
Tl	+0.2460	a	substitutional acceptor	83S4
Tl-C	+0.1800	a	X-center	83S4
Tl-H			passivation by atomic H	87P1
V	+0.32	d	double donor V(++/+), interstitial $3d^4 - 3d^3$,	86G1
	−0.45	d	single donor V(+/0), interstitial $3d^5 - 3d^4$,	86G1
Vac	+0.05	d	metastable center, single charge	84W3
Vac-Vac	+0.20	d	divacancy,	85H2
	−0.23	a	stable at $T \leqq 300\,°C$	
Zn	+0.32	a	double acceptor Zn(0/−), substitutional	86G1
	−0.47 (+0.66)	a	double acceptor Zn(−/− −), substitutional	86G1

Reference for 1.2

53M McSkimin, H.J.: J. Appl. Phys. **24** (1963) 988.
54M Morin, F.J., Maita, J.P.: Phys. Rev. **96** (1954) 28.
56L Ludwig, G.W., Watters, R.L.: Phys. Rev. **101** (1956) 1699.
57C Carlson, R.O.: Phys. Rev. **108** (1957) 1390.
60P Philipp, H.R., Taft, E.A.: Phys. Rev. **120** (1960) 37.
61H Hall, R.O.A.: Acta Crystallogr. **14** (1961) 1004.
63D Dolling, G.: in "Inelastic Scattering of Neutrons in Solids and Liquids", IAEA, Vienna **1963**, Vol. II, p. 37.
64H Hennis, J.: J. Res. Nat. Bur. Stand. **68A** (1964) 529.
64M McSkimin, H.J., Andreatch jr., P.: J. Appl. Phys. **35** (1964) 2161.
65B Balslev, I., Lawaetz, P.: Phys. Lett. **19** (1965) 6.
65H Hensel, J.C., Hasegawa, H., Nakayama, M.: Phys. Rev. **138** (1965) A225.
65W1 Weltzin, R.D., Swalin, R.A., Hutchinson, T.E.: Acta Metall. **13** (1965) 115.
65W2 Waldner, M., Hiller, M.A., Spitzer, W.G.: Phys. Rev. **A140** (1965) 172.
66K Kodera, H.: J. Phys. Soc. Jpn. **21** Suppl. (1966) 578.
67B Barber, H.D.: Solid State Electron. **10** (1967) 1039.
68F Fulkerson, W., Moore, J.P., Williams, R.K., Graves, R.S., McElroy, D.L.: Phys. Rev. **167** (1968) 765.
68I Ichimiya, T., Furuichi, T.: Int. J. Appl. Radiat. Isot. **19** (1968) 573.
69W Wolf, H.F.: Semiconductors, New York: Wiley-Interscience **1971**.
72A Aspnes, D.E., Studna, A.A.: Solid State Commun. **11** (1972) 1375.
72H Ho, L.T., Ramdas, A.K.: Phys. Rev. **B5** (1972) 462.
72N Nilsson, G., Nelin, G.: Phys. Rev. **B6** (1972) 3777.
72Z Zorin, E.I., Pavlov, P.V., Tetelbaum, D.I., Khokhlov, A.F.: Fiz. Tekh. Poluprovodn. **6** (1972) 28.
73H Hultgren, R., Desai, P.D., Hawkins, D. T., Gleiser, M., Kelly, K.K., Wagman, D.D.: The Thermodynamic Properties of the Elements, American Society for Metals, Metals Park, Ohio **1973**.
73Y1 Yatsurugi, Y., Akiyama, N., Endo, Y., Nozaki, T.: J. Electrochem. Soc. **120** (1973) 975.
73Y2 Yin, W.M., Paff. R.J.: J. Appl. Phys. **45** (1973) 1456.
74A Akasaka, Y., Horie, K., Nakamura, G.: Jpn. J. Appl. Phys. **13** (1974) 1533.
74B Bludau, W., Onton, A., Heinke, W.: J. Appl. Phys. **45** (1974) 1846.
74F Foreman, R.A., Aspnes, D.E.: Solid State Commun. **14** (1974) 100.
75L Lisiak, K.P., Milnes, A.G.: Solid State Electron. **18** (1975) 533.
74N Nishino, T., Takeda, M., Hamakawa, Y.: Solid State Commun. **14** (1974) 627.

76B Belikova, M.N., Zastavnyi, A.V., Korol, V.M.: Fiz. Tekh. Poluprovodn. **10** (1976) 535.
76H Hensel, J.C.: unpublished.
76O Ousset, J.C., Leotin, J., Askenasy, S., Skolnick, M.S., Stradling, R.A.: J. Phys. **C9** (1976) 2802.
76P Pavlov, P.V., Zorin, E.I., Tetelbaum, D.I., Khokhlov, A.F.: Phys. Status Solidi (a) **35** (1976) 11.
77B Busta, H.H., Waggener, H.A.: J. Electrochem. Soc. **124** (1977) 1424.
77F1 Fair, R.B.: Semiconductor Silicon 1977, Huff. H.R., Sirtl, E. (eds.), The Electrochem Soc. **1977** p. 968.
77F2 Fair, R.B., Tsai, J.C.C.: J. Electrochem. Soc. **124** (1977) 1107.
77J Jacoboni, C., Canali, C., Ottaviani, G., Alberigi Quaranta, A.: Solid State Electron. **20** (1977) 77.
77K Kimerling, L.C.: Radiation Effects in Semiconductors 1976, in: Inst. Phys. Conf. Ser. **31** (1977) 221.
77L1 Lyon, K.G., Salinger, G.L., Swenson, C.A., White, G.K.: J. Appl. Phys. **48** (1977) 865.
77L2 Lipari, N.O., Altarelli, M.: Phys. Rev. **B15** (1977) 4883.
77W1 Weber, W.: Phys. Rev. **B15** (1977) 4793.
77W2 Wasserrab, Th.: Z. Naturforsch. **32a** (1977) 746.
78D Daunois, A., Aspnes, D.E.: Phys. Rev. **B18** (1978) 1824.
78S So, L., Whiteley, J.S., Ghandi, S.K., Baliga, B.J.: Solid State Electron. **21** (1978) 887.
78V Vydianath, H.R., Lorenzo, J.S., Kröger, F.A.: J. Appl. Phys. **49** (1978) 5928.
79T1 Troxel, J.R., Chatterjee, A.P., Watkins, G.D.: Phys. Rev. **B19** (1979) 5336.
79T2 Troxel, J.R.: Ph.D. Thesis, Lehigh University, U.S.A. **1979**.
80E Edwards, D.F., Ochoa, E.: Appl. Opt. **19** (1980) 4130.
80S Schmid, W.: Phys. Rev. Lett. **45** (1980) 1726.
81D Dyunaidov, S.S., Urmanov, N.A., Gafurova, M.V.: Phys. Status Solidi (a) **66** (1981) K79.
81K1 Keller, W.: Diplomarbeit Univ. Erlangen **1981**.
81K2 Kunio, T., Nishino, T., Ohta, E., Sakata, M.: Solid State Electron. **24** (1981) 1087.
81L Lampert, M.O., Koebel, J.M., Siffert, P.: J. Appl. Phys. **52** (1981) 4975.
81P Philip, J., Breazeale, M.A.: J. Appl. Phys. **52** (1981) 3383.
81S Szablak, B., Altarelli, M.: Solid State Commun. **37** (1981) 341.
82B1 Becker, P., Seyfried, P., Siegert, H.: Z. Physik **B48** (1982) 17.
82B2 Budzak, Ya.S., Mavrin, O.I.: Phys. Status Solidi (a) **69** (1982) K61.
82G Grimmeiss, H.G., Janzén, E., Larsson, K.: Phys. Rev. **B25** (1982) 2627.
82H Haug, A., Schmid, W.: Solid State Electron. **25** (1982) 665.
82M Mitchel, W.C., Hemenger, P.M.: J. Appl. Phys. **53** (1982) 6880.
82N Narita, S., Shinbashi, T., Kobayashi, M.: J. Phys. Soc. Jpn. **51** (1982) 2186.
82S Searle, C.W., Ohmer, M.C., Hemenger, P.M.: Solid State Commun. **44** (1982) 1597.
82W Wu, R.H., Peaker, A.R.: Solid State Electron. **25** (1982) 463.
83A Aspnes, D.E., Studna, A.A.: Phys. Rev. **B27** (1983) 985.
83C Cerofolini, G.F., Pignatel, G.U., Riva, F.: Thin Solid Films **10** (1983) 275.
83F Fischer, D.W., Rome, J.J.: Phys. Rev. **B27** (1983) 4826.
83G1 Gösele, U., Tan, T.Y.: Aggregation Phenomena of Point Defects in Si, Sirtl, E. (ed.), The Electrochem. Soc. **1983**, p. 17.
83G2 Graff, K.: Aggregation Phenomena of Point Defects in Si, Sirtl, E. (ed.), The Electrochem. Soc. **1983**, p. 121.
83J Jellison, G.E., Modine, F.A.: Phys. Rev. **B27** (1983) 7466.
83K Kolbesen, B.O.: Aggregation Phenomena of Point Defects in Si, Sirtl, E. (ed.), The Electrochem. Soc. **1983**, p. 155.
83L Lang, J.E., Madarasz, F.L., Hemenger, P.M.: J. Appl. Phys. **54** (1983) 3612.
83M Mašović, D.R., Vukajlović, F.R., Zeković, S.: J. Phys. **C16** (1983) 6731.
83N Nobili, D.: Aggregation Phenomena of Point Defects in Si, Sirtl, E. (ed.), The Electrochem Soc. **1983**, p. 189.
83P Philip, J., Breazeale, M.A.: J. Appl. Phys. **54** (1983) 752.
83S1 Szmulowicz, F.: Appl. Phys. Lett. **43** (1983) 485.
83S2 Szmulowicz, F.: Phys. Rev. **B28** (1983) 5943.
83S3 Szmulowicz, F., Madarasz, F.L.: Phys. Rev. **B27** (1983) 2605.
83S4 Searle, C.W., Hemenger, P.M., Ohmer, M.C.: Solid State Commun. **48** (1983) 995.
83W1 Weber, E.: Appl. Phys. **A30** (1983) 1.
83W2 Wacker Chemitronics Co.: Silicon calculator **1983**.
84H Hu, J.Z., Spain, I.L.: Solid State Commun. **44** (1984) 263.
84L Lemke, H.: Phys. Status Solidi (a) **86** (1984) K39.
84O1 Olijnuk, H., Sikka, S.K., Holzapfel, W.B.: Phys. Lett. **A103** (1984) 137.
84O2 Okada, Y., Tokumaru, Y.: J. Appl. Phys. **56** (1984) 314.
84S Scalar, N.: Appl. Phys. **55** (1984) 2972.
84W1 Wagner, P., Holm, C., Sirtl, E., Oeder, R., Zulehner, W.: Festkörperprobleme **XXIV** (1984) 191.
84W2 Wagner, P., Holm, C.: 13th Int. Conf. on Defects in Semiconductors **1984**.
84W3 Watkins, G.D.: Festkörperprobleme XXIV, Grosse, P. (ed.), Braunschweig: Vieweg **1984**, p. 163.
85D Danilicheva, T.A., Markvicheva, V.S., Nisnevich, J.D.: Izv. Akad. Nauk SSSR Neorg. Mater. **21** (1985) 525.
85F1 Fischer, D.W., Mitchel, W.C.: J. Appl. Phys. **58** (1985) 3118.
85F2 Fazzio, A., Caldas, M.J., Zunger, A.: Phys. Rev. **B32** (1985) 934.
85H1 Hertel, N., Materlik, G., Zegenhagen, J.: Z. Phys. **B58** (1985) 199.
85H2 Harris, R.D., Watkins, G.D.: Proc. Defect. Conf. Coronado, Kimmerling, L.C., (ed.), The Met. Soc. of AIME **1985**, p. 799.
85L Lautenschlager, P., Allen, P.B., Cardona, M.: Phys. Rev. **B31** (1985) 2163.
85S Sieh, K.S., Smith, P.V.: Phys. Status Solidi (b) **129** (1985) 259.
85T Tan, T.Y., Gösele, U.: Appl. Phys. **A37** (1985) 1.
85W1 Weber, E.R.: Proc. SPIE (Proc. Soc. Photo-Opt. Instrum. Eng.) **524** (1985) 160.
85W2 Wang, Z., Chen, K., Qin, G.: Chin. J. Semicond. **6** (1985) 437.

86C1 Carlberg, T.: J. Electrochem. Soc. **133** (1986) 1941.
86C2 Chen, K.-M., Qin, G.-G.: Proc. 14th Int. Conf. on Defects in Semiconductors, Paris **1986**.
86D Dominguez, E., Jaraiz, M.: J. Electrochem. Soc. **133** (1986) 1895.
86G1 Graff, K.: Semiconductor Silicon 1986, H.R. Huff et al. (eds.), The Electrochem. Soc. **1986**, p. 751.
86G2 Gilles, D., Bergholz, W., Schröter, W.: J. Appl. Phys. **59** (1986) 3590.
86M1 Mononi, C.S., Hu, J.Z., Spain, I.L.: Phys. Rev. **B34** (1986) 362.
86M2 Mikkelsen jr., J.C.: Mater. Res. Soc. Symp. Proc. **59** (1986) 19.
86P Pensl, G., Roos, G., Holm, C., Wagner, P.: Proc. 14th Int. Conf. on Defects in Semiconductors, Paris **1986**.
86S1 Stolwijk, N.A., Hölzl, J., Frank, W., Weber, E.R., Mchrer, H.: Appl. Phys **A39** (1986) 37.
86S2 Stöffler, W., Weber, J.: Proc 14th Int. Conf. on Defects in Semiconductors, Paris **1986**.
86S3 Schulz, H.J.: European Semiconductor Device Research Conference (ESSDERC) **1986**.
86S4 Stein, H.J.: Proc. MRS Meeting Boston 1986, Mikkelsen, J. (ed.) MRS Pittsburgh, Pa. **1986**, p. 523.
87A1 Angelucci, R., Armigliato, A., Landi, E., Nobili, D., Solmi, S.: ESSDERC Conference Bologna **1987**.
87A2 Azomov, S.A., Yunusov, M.S., Nurkuziev, G.: Fiz. Tekh. Poluprovodn. **21** (1987) 1555; Sov. Phys. Semicond. (English Transl.) **21** (1987) 944.
87L Lemke, H.: Phys. Status Solidi (a) **99** (1987) 205.
87N Nolte, D.D., Walukiewicz, W., Haller, E.E.: Phys. Rev. **B36** (1987) 9392.
87P1 Pearton, S.J., Corbett, J.W., Shi, T.S.: Appl. Phys. **A43** (1987) 153.
87P2 Pensl, G.: Proc. 5th Int. School ISPPME **1987**.
87R Rollert, F., Stolwijk, N.A., Mehrer, H.: J. Phys. **D20** (1987) 1148.
87S Stavola, M., Pearton, S.J., Lopata, J., Dautremont-Smith, W.C.: Appl. Phys. Lett. **50** (1987) 1086.
87T Tsai, J.C.C., Schimmel, D.G., Fair, R.B., Maszara, W.: J. Electrochem. Soc. **134** (1987) 1508.
88J Jäntsch, O.: private communication.
88M Mathiot, D., Hocine, S.: 15. Int. Conf. Defects in Semiconductors Budapest 1988.
88S1 Stuempel, H., Vorderwuelbecke, M., Mimkes, J.: Appl. Phys. **A46** (1988) 159.
88S2 Stolwijk, N.A., Grünebaum, D., Perret, M., Brohl, M.: Proc. 15th Int. Conf. on Defects in Semiconductors, Budapest 1988, Trans. Tech. Publ. **1988**.
88U Utzig, J., Gilles, D.: Proc. 15th Int. Conf. on Defects in Semiconductors, Budapest 1988, Ferency, G. (ed.), Trans. Tech. Publ. **1988**.
88W Watkins, G.D.: Proc. 15th Int. Conf. on Defects in Semiconductors, Budapest 1988, Ferency, G. (ed.), Trans. Tech. Publ. **1988**.
89N Nobili, D., Angelucci, R., Armigliato, A., Landi, E., Solmi, S.: J. Electrochem. Soc. **136** (1989) 1142.

Physical property	Numerical value	Experimental conditions	Experimental method, remarks	Ref.

1.3 Germanium (Ge)

Electronic properties

band structure: Fig. 1 (Brillouin zone, see Fig. 2 of section 1.1).

The *conduction band* is characterized by eight equivalent minima at the end points of the [111]-axes of the Brillouin zone (symmetry L_6). The surfaces of constant energy are ellipsoids of revolution with major axes along [111]. Higher minima are located at the Γ-point and (above this) on the [100]-axes.

The *valence band* has its maximum at the Γ-point (symmetry Γ_8), the (warped) light and heavy hole bands being degenerate at this point. The third spin-orbit split-off band has Γ_7-symmetry. The spin-orbit splitting is considerable. Thus, the symmetry notation of the double group of the diamond lattice is used in the following tables.

energies of symmetry points of the band structure (relative to the top of the valence band) (in eV):

$E(\Gamma_{6v})$	−12.66	theoretical data (Fig. 1)	76C
$E(\Gamma_{7v})$	−0.29		
$E(\Gamma_{8v})$	0.00		
$E(\Gamma_{7c})$	0.90		
$E(\Gamma_{6c})$	3.01		
$E(\Gamma_{8c})$	3.22		
$E(X_{5v})$	−8.65	for experimental data from angular resolved photo-emission, see [85W2] and [84H, 85N]	
$E(X_{5v})$	−3.29		
$E(X_{5c})$	1.16		
$E(L_{6v})$	−10.39		

Physical property	Numerical value	Experimental conditions	Experimental method, remarks	Ref.
$E(L_{6v})$	−7.61			
$E(L_{6v})$	1.63			
$E(L_{4,5v})$	−1.43			
$E(L_{6c})$	0.76			
$E(L_{6c})$	4.16			
$E(L_{4,5c})$	4.25			
indirect energy gap (in eV):				
$E_{g,ind}(\Gamma_{8v} - L_{6c})$	0.744(1)	1.5 K	magnetotransmission	59Z
	0.664	291 K	optical absorption	57M
$E_{g,th}$	0.785	0 K (extrapol.)	temperature dependence of intrinsic conductivity	54M1
Temperature dependence, see Fig. 2.				
direct energy gap:				
$E_{g,dir}(\Gamma_{8v} - \Gamma_{7c})$	0.898(1) eV	1.5 K	magnetoabsorption	59Z
	0.805(1) eV	293 K		
Temperature dependence, see Fig. 3.				

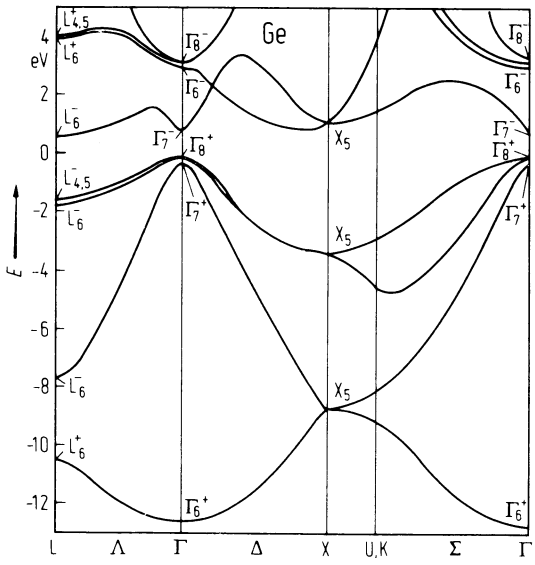

Fig. 1. Ge. Band structure obtained by a non-local pseudopotential calculation including spin-orbit splitting [76C].

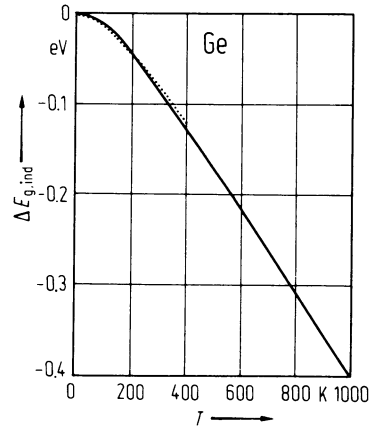

Fig. 2. Ge. Indirect gap vs. temperature. Solid line: calculated, dots: experimental ($\Delta E_{g,ind} = E_{g,ind}(T) - E_{g,ind}(0)$) [85L].

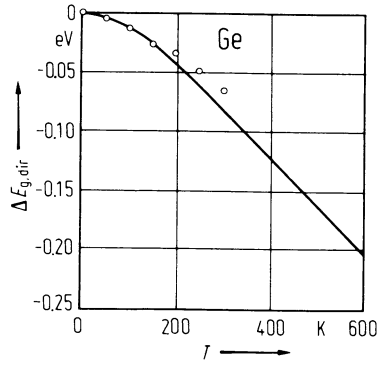

Fig. 3. Ge. Direct gap vs. temperature ($\Delta E_{g,dir} = E_g(T) - E_g(0)$). Solid line: theoretical calculations, circles: experimental [83A2].

Physical property	Numerical value	Experimental conditions	Experimental method, remarks	Ref.
exciton energies (in meV):				
$E(1S^{3/2}_{3/2}(L_4+L_5))$	740.46(3)	2.1 K, 5.1 K	absorption (at 2.1 K) and luminescence (at 5.1 K), the energy of the assisting LA (L) phonon is subtracted	79M
$E(1S^{3/2}_{1/2}(L_6))$	741.58(3)			
E_b	4.18		$1S^{3/2}_{3/2}(L_4+L_5)$	76A
	3.17		$1S^{3/2}_{1/2}(L_6)$	
critical point and spin-orbit splitting energies (in eV):				
E_1	2.111(3)	RT	from ellipsometric data by a two-dimensional critical point analysis (2D CP)	84V
$E_1+\Delta_1$	2.298(3)	RT	2D CP	
Δ_1	0.187(3)	RT	2D CP	
E'_0	3.123(19)	100 K	3D CP	
$E'_0+\Delta'_0$	3.309(19)	100 K	3D CP	
$\bar{E}'_0$	3.110	RT	2D CP; mean value of E'_0 and $E'_0+\Delta'_0$	
E_2	4.368(4)	RT	2D CP	
	4.346(3)	RT	1D CP	
effective masses, electrons (in units of m_0):				
$m_{n\perp}(L_6)$	0.0807(8)	30···100 K	cyclotron resonance	76F
	0.0823	120 K	magnetophonon resonance	82H2
$m_{n\parallel}(L_6)$	1.57(3)	30···100 K	cyclotron resonance	76F
	1.59	120 K	magnetophonon resonance	82H2
$m_n(\Gamma_7)$	0.0380(5)	30 K	piezomagnetoreflectance	70A

For the dependence of the transverse electron mass in the L_6-minima on the energy above the bottom of the band, see Fig. 4a.

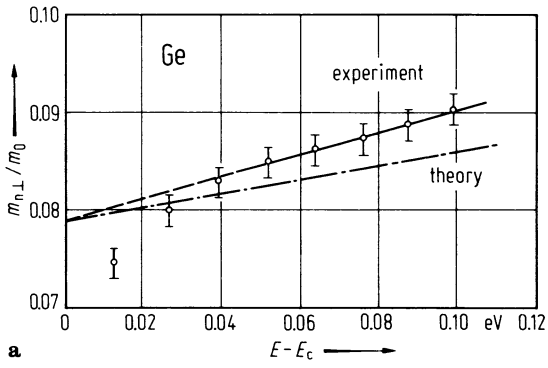

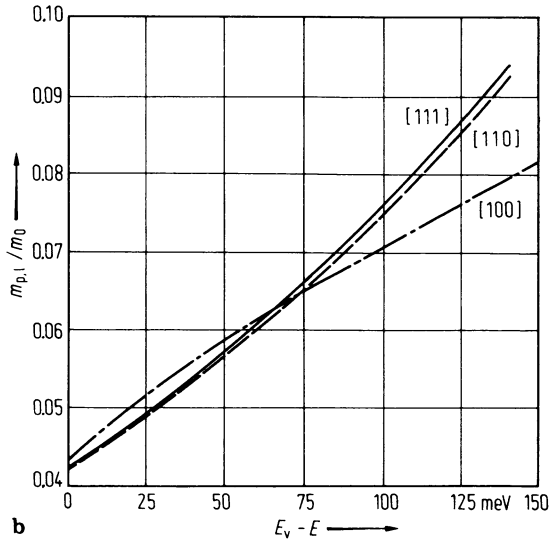

Fig. 4. Ge. (a) Dependence of the transverse electron mass in the L_6 minima on energy above the bottom of the conduction band measured by magnetopiezotransmission [69A], (b) cyclotron mass of light holes vs. energy below the top of the valence band ($B\parallel$[111], [110] and [100]) [80Z].

Physical property	Numerical value	Experimental conditions	Experimental method, remarks	Ref.
g-factor of electrons:				
g_c	−3.0(2)	30 K	piezomagnetoabsorption	70A
effective masses holes (in units of m_0):				
$m_{p,l}$	0.0438(3)	4 K	cyclotron resonance	56D
	0.0426(2)			
	0.0430(3)		values for B parallel [100], [111], [110], respectively	
$m_{p,h}$	0.284(1)			
	0.376(1)			
	0.352(4)			
m_{so}	0.095(7)	30 K	piezomagnetoabsorption	70A
For the dependence of the light hole mass on the energy below the top of the band, see Fig. 4b.				
valence band parameters:				
A	−13.3		extrapolated using a five level $k \cdot p$ scheme	75W
B	−8.57			
$\|C\|$	12.78			

Lattice properties

Structure

Ge I	space group O_h^7–Fd3m (diamond lattice)	low pressure phase	
G II	space group D_{4h}^{19}–$I4_1/amd$ (β-tin lattice)	from energy dispersive X-ray diffraction	83Q
Ge III	space group D_4^8–$P4_32_12$	obtained by quenching of Ge II to lower pressure	83Q
Ge IV	space group T_h^7–Ia3 (body centered cubic)	obtained by quenching of Ge II to 1 atm at 200 K	83L
transition pressure:			
p_{tr}(Ge I–Ge II)	10.7(5) GPa	diamond anvil, energy dispersive X-ray diffraction	82W
lattice parameter:			
a	5.6579060 Å	298.15 K	single crystal, for temperature dependence see Fig. 5	75B
linear thermal expansion coefficient: Fig. 6.				
density:				
d	5.3234 g cm^{-3}	298 K	hydrostatic weighing	52S
melting point:				
T_m	1210.4 K			73H

phonon dispersion relations: Fig. 7.

Physical property	Numerical value	Experimental conditions	Experimental method, remarks	Ref.
phonon frequencies (in THz):				
$\nu_{LTO}(\Gamma_{25'})$	9.02(2)	300 K	coherent inelastic neutron scattering	72N2
$\nu_{TA}(X_3)$	2.38(2)			
$\nu_{LAO}(X_1)$	7.14(2)			
$\nu_{TO}(X_4)$	8.17(3)			
$\nu_{TA}(L_3)$	1.87(2)			
$\nu_{LA}(L_{2'})$	6.63(4)			
$\nu_{TO}(L_{3'})$	8.55(3)			
$\nu_{TO}(L_1)$	7.27(2)			
second order elastic moduli (in 10^{11} dyn cm^{-2}):				
c_{11}	12.40	$T = 298$ K	ultrasound measurements for temperature dependence, see Fig. 8	71B
c_{12}	4.13			
c_{44}	6.83			

third order elastic moduli: Fig. 9.

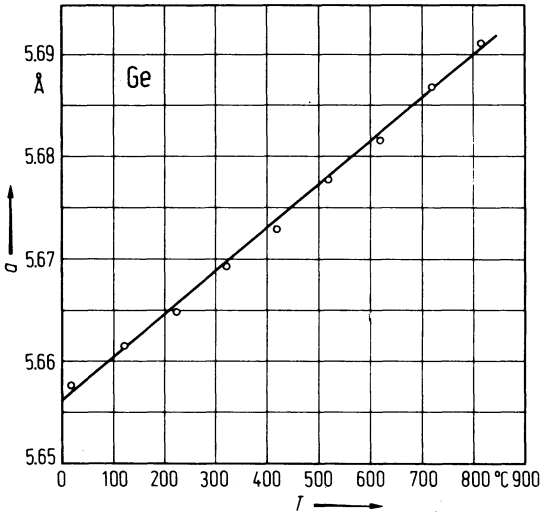

Fig. 5. Ge. Lattice parameter vs. temperature [68S].

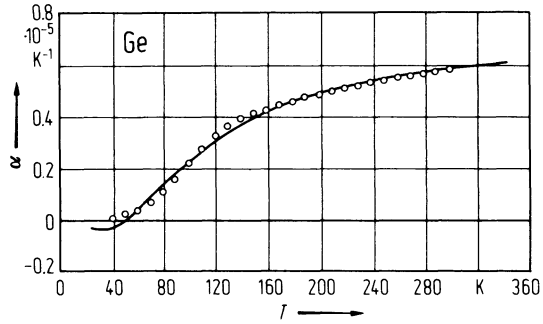

Fig. 6. Ge. Coefficient of linear thermal expansion vs. temperature in the range 40 to 360 K, single crystal [60N].

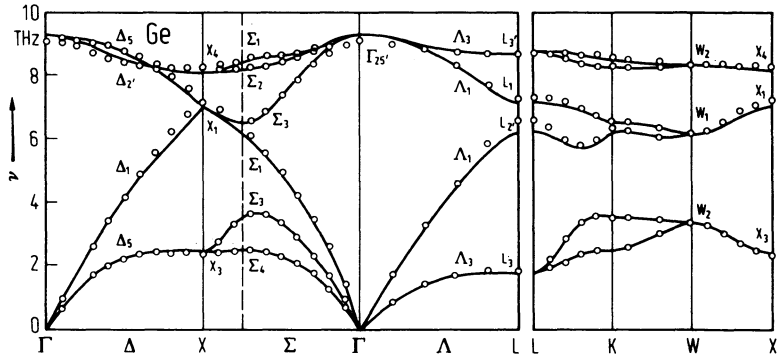

Fig. 7. Ge. Phonon dispersion relations. Experimental points from [71N, 72N1], solid lines: theory [77W].

Physical property	Numerical value	Experimental conditions	Experimental method, remarks	Ref.

Transport properties

Low field transport is maintained by electrons in the L_6 minima of the conduction band and holes near the point Γ_8 in the valence bands. At RT the mobility of samples with impurity concentrations below $10^{15}\,cm^{-3}$ is limited essentially by lattice scattering. At 77 K, even for doping concentrations below $10^{13}\,cm^{-3}$ the mobilities depend on the impurity concentration.

intrinsic conductivity:

σ_i	$2.1 \cdot 10^{-2}\,\Omega^{-1}\,cm^{-1}$	300 K	for temperature dependence, see Fig. 10	54M1

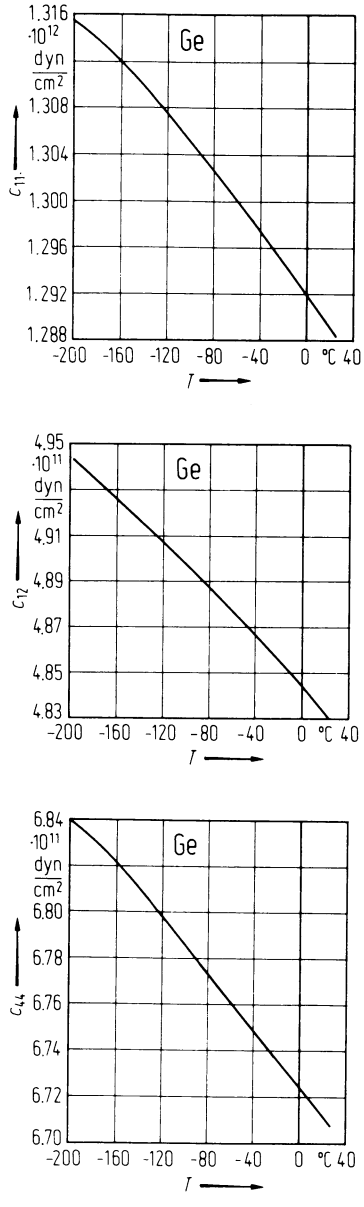

Fig. 8. Ge. Second order elastic moduli vs. temperature [53M].

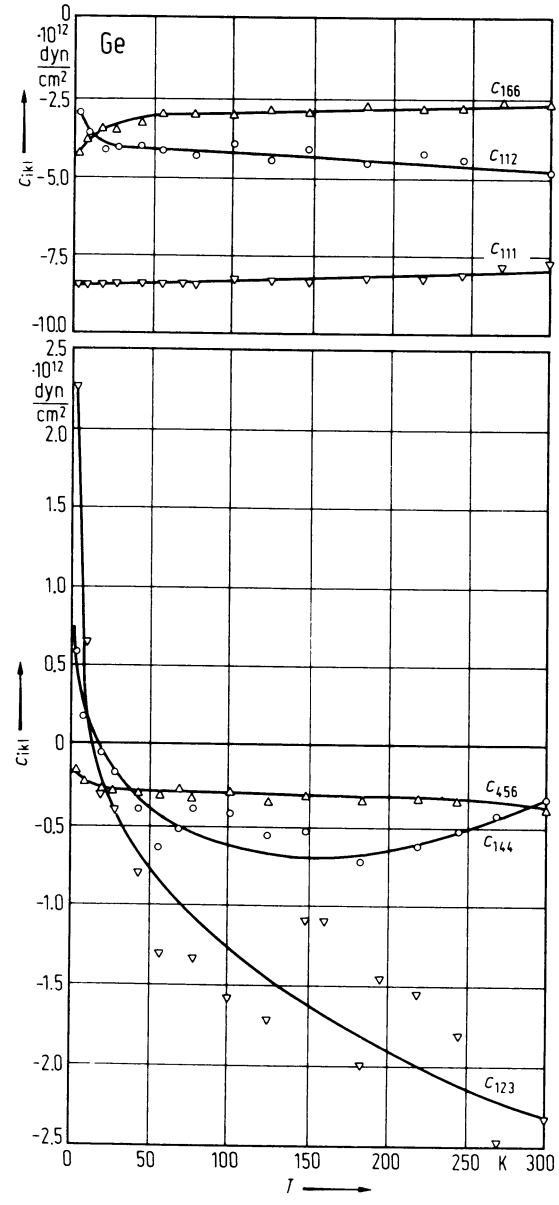

Fig. 9. Ge. Third-order elastic moduli vs. temperature. Solid lines: best fit to the data [83P].

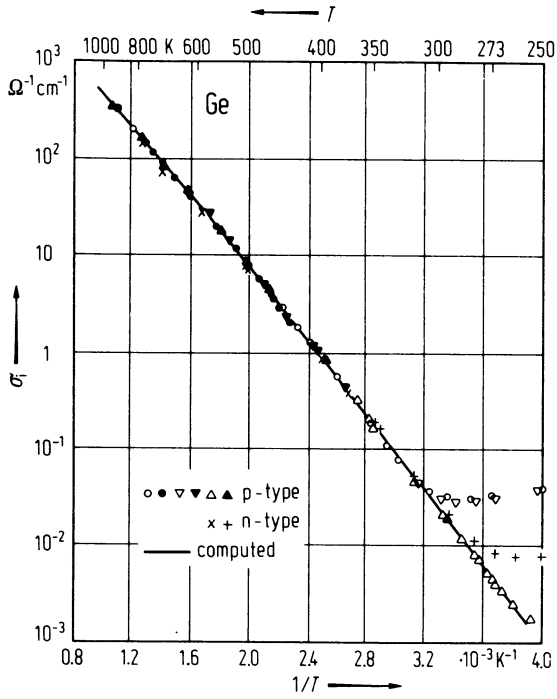

Fig. 10. Ge. Electrical conductivity vs. reciprocal temperature for six p-type and two n-type samples, solid line from empirical expressions for n_i and the mobilities as given in the tables [54M1].

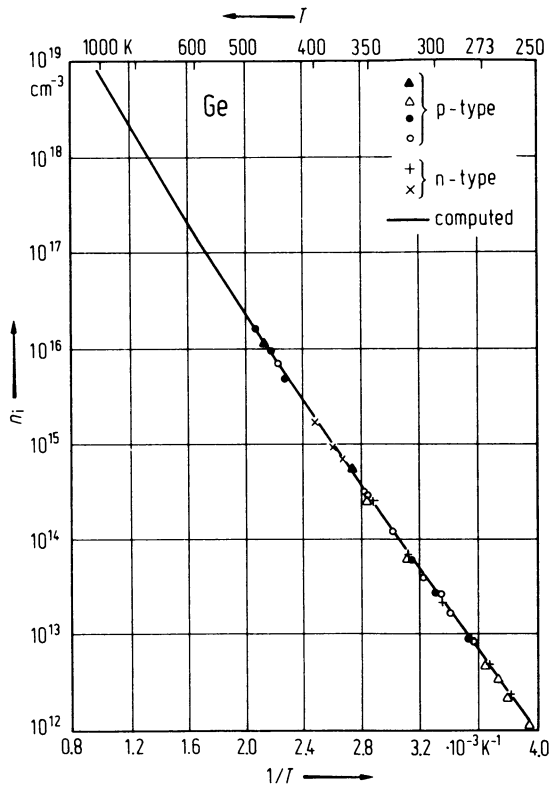

Fig. 11. Ge. Intrinsic carrier concentration vs. reciprocal temperature. Experimental data on four p-type and two n-type samples; solid line from empirical expression given in the tables [54M1].

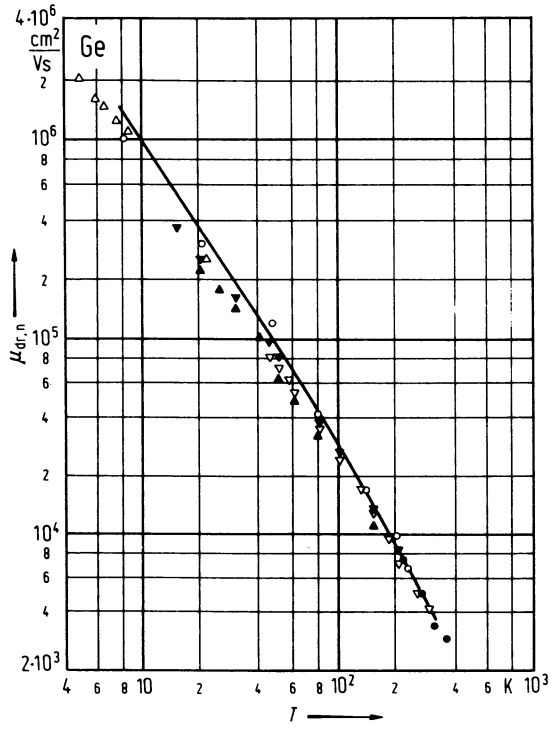

Fig. 12. Ge. (Ohmic) drift mobility of electrons vs. temperature obtained with a time-of-flight technique in hyperpure material (open circles); other symbols: data from five references; solid line: theory [81J].

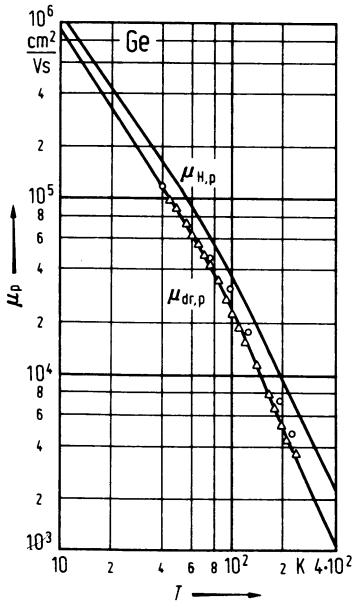

Fig. 13. Ge. Drift and Hall mobility of holes vs. temperature in the phonon-limited regime. Circles and triangles: experimental data, solid curves: theoretical analysis [83S].

Physical property	Numerical value	Experimental conditions	Experimental method, remarks	Ref.
intrinsic carrier concentration (in cm^{-3}):				
n_i	$2.33 \cdot 10^{13}$	300 K	for temperature dependence, see Fig. 11	54M1
	$1.76 \cdot 10^{16} T^{3/2} \exp(-0.785/2kT)$		best fit to experimental data (kT in eV, T in K)	
electron mobility (in cm^2/Vs):				
μ_n	3900	300 K	lattice mobility ($n_d \approx 10^{14} cm^{-3}$) determined by drift experiments with injected minority carriers	53P
	$4.90 \cdot 10^7 T^{-1.66}$		best fit to experimental data in the range 77···300 K	54M1
For temperature dependence, see Fig. 12.				
$\mu_n(\Delta_6)$	$800\,cm^2/Vs$	300 K	Hall measurements under a pressure of 70 kbar at a sample with $n_d = 4.7 \cdot 10^{13} cm^{-3}$	79A
hole mobility (in cm^2/Vs):				
μ_p	1800	300 K	lattice mobility in high purity samples	54M
	$1.05 \cdot 10^9 T^{-2.33}$		best fit to experimental data in the range 100···300 K	
For temperature dependence, see Fig. 13.				
thermal conductivity:				
Temperature dependence: Fig. 14.				

Optical properties

refractive index, spectral dependence at RT:				
n	4.00541 (11)	$\lambda = 8\,\mu m$	mean values for ten samples from various suppliers measured at 20.0 °C	82E1
	4.00412 (12)	9 μm		
	4.00319 (11)	10 μm		
	4.00248 (10)	11 μm		
	4.00194 (11)	12 μm	temperature coefficient between 20 °C and 25 °C: $4.0 \cdot 10^{-4}\,°C^{-1}$	
	4.00151 (10)	13 μm		
dielectric constant:				
		T[K], ν[MHz]		
ε	16.5	4.2, 750	capacitance bridge	66R
	16.0	4.2, 9200	microwave measurement	56A
	16.2	300 9200		

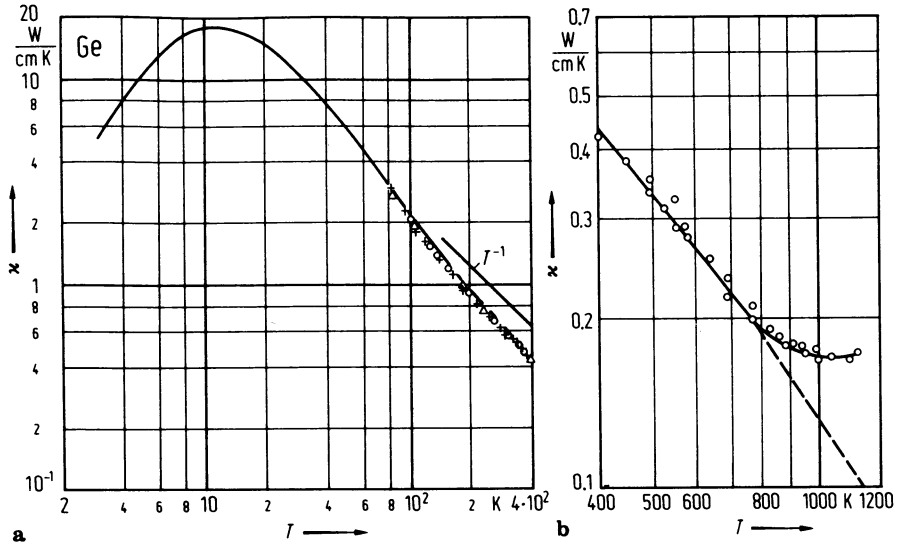

Fig. 14. Ge. Thermal conductivity vs. temperature. (a) 3···400 K, (b) 400···1200 K. Solid curve in (a) and data in (b) from [64G], experimental data in (a) from [84B]. Dashed line in (b): extrapolated lattice component.

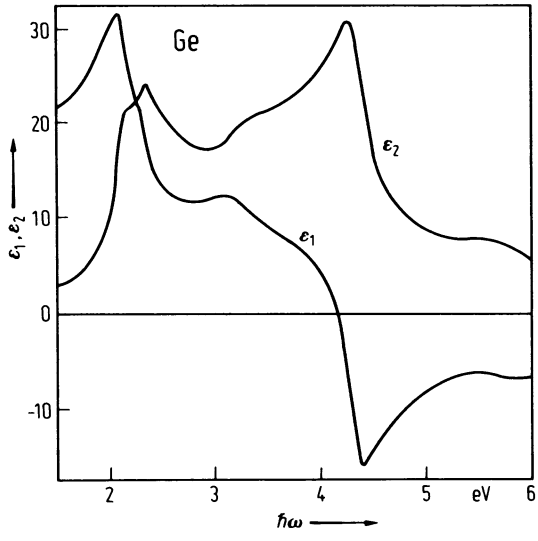

Fig. 15. Ge. Real and imaginary parts of the dielectric constant vs. photon energy [83A1].

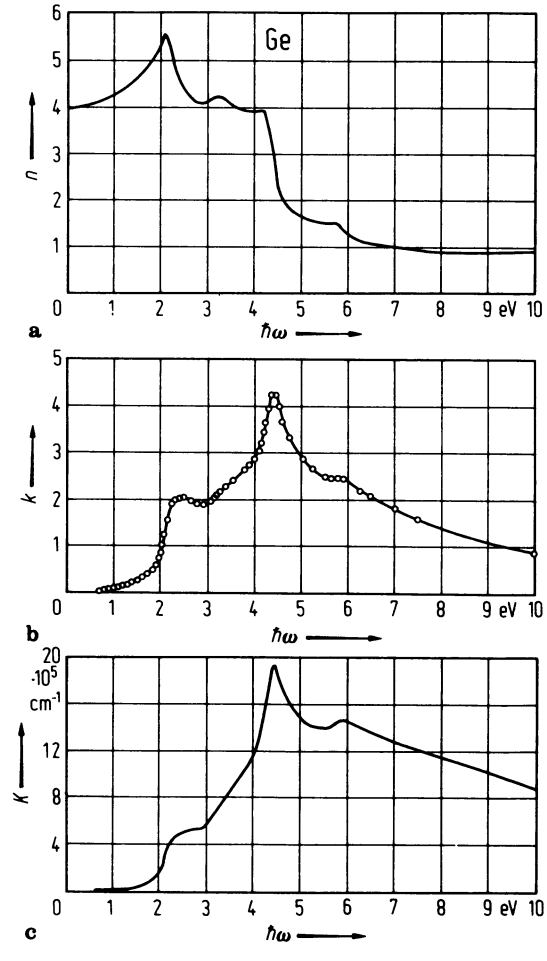

Fig. 16. Ge. Spectral dependence of (a) the refractive index, (b) the extinction coefficient and (c) the absorption coefficient [59P].

optical constants

real and imaginary parts of the dielectric constant measured by spectroscopical ellipso metry; n, k, R, K calculated from these data 83A1; see also Fig. 15.

$\hbar\omega$[eV]	ε_1	ε_2	n	k	R	K [10^3 cm^{-1}]
1.5	21.560	2.772	4.653	0.298	0.419	45.30
2.0	30.361	10.427	5.588	0.933	0.495	189.12
2.5	13.153	20.695	4.340	2.384	0.492	604.15
3.0	12.065	17.514	4.082	2.145	0.463	652.25
3.5	9.052	21.442	4.020	2.667	0.502	946.01
4.0	4.123	26.056	3.905	3.336	0.556	1352.55
4.5	−14.655	16.782	1.953	4.297	0.713	1960.14
5.0	−8.277	8.911	1.394	3.197	0.650	1620.15
5.5	−6.176	7.842	1.380	2.842	0.598	1584.57
6.0	−6.648	5.672	1.023	2.774	0.653	1686.84

The spectral dependence of n, k, and K below 10 eV is shown in Fig. 16.

Impurities and defects

solubility of impurities in Ge

Element	c_{max}^{eq} cm^{-3}	T_{max} °C	T-range °C	Ref.
Al	$4.3 \cdot 10^{20}$	675	496···937	59T2
Ag	$4 \cdot 10^{18}$	850	770···930	62K2
As	$8.1 \cdot 10^{19}$	800	740···937	62T1
Au	$4.1 \cdot 10^{16}$	≈885	700···870	64K
Be	$4 \cdot 10^{16}$	937	720···920	61B
Bi	$6 \cdot 10^{16}$	910	867···937	62T1
Cd	$2 \cdot 10^{18}$	840	760···910	60K
Cu	$3.6 \cdot 10^{16}$	878	577···927	85S2
Fe	$1.5 \cdot 10^{15}$	850	750···940	57B
Ga	$4.9 \cdot 10^{20}$	670	303···937	59T2
H	$2 \cdot 10^{15}$	937		82H1
He	$6.5 \cdot 10^{12}$	937	795···872	56W
In	$4 \cdot 10^{18}$	800	300···937	60T
Li	$7.5 \cdot 10^{18}$	800	593···899	57P
Ni	$8.0 \cdot 10^{15}$	890	800···937	59T1
O	$1.3 \cdot 10^{18}$	≈937		56T1
P	$2 \cdot 10^{20}$	600	500···900	62A
Pb	$5.6 \cdot 10^{17}$	870		60T
Sb	$1.2 \cdot 10^{19}$	800	708···937	62T1
Sn	$5 \cdot 10^{20}$	≈300	400···937	60T
Te	$6.3 \cdot 10^{18}$	840	770···900	62I
Tl	$9.5 \cdot 10^{18}$	917	800···930	62T2
Zn	$2.5 \cdot 10^{18}$	770	420···760	60T

diffusion coefficients of impurities and self-atoms in Ge

Element	D_0 $cm^2 s^{-1}$	Q eV	T-range °C	D (800 °C) $cm^2 s^{-1}$	Ref.
Al	$1.0 \cdot 10^3$	3.45	554···905	$6.2 \cdot 10^{-14}$	82D1
Ag	$4 \cdot 10^{-2}$	2.23	770···920	$1.3 \cdot 10^{-12}$	62K2
As	10.3	2.49	700···790	$2.1 \cdot 10^{-11}$	68I
Au	$2.5 \cdot 10^2$	2.3	600···750	$3.9 \cdot 10^{-9}$	68G
B	$9.5 \cdot 10^6$	4.5	760···850	$6.9 \cdot 10^{-15}$	67M
Be	0.5	2.5	720···920	$9.1 \cdot 10^{-13}$	61B
Bi	3.3	2.5		$6.0 \cdot 10^{-12}$	59R
Cd	$1.75 \cdot 10^9$	4.42	760···915	$3.0 \cdot 10^{-12}$	60K
Co	0.16	1.12	750···850	$8.8 \cdot 10^{-7}$	61W
Cu	5.5	1.55	577···927	$2.9 \cdot 10^{-7}$	85S2
Fe	0.13	1.1	775···930	$8.9 \cdot 10^{-7}$	57B
Ga	$1.4 \cdot 10^2$	3.31	554···916	$4.0 \cdot 10^{-14}$	86S
Ge	13.2	3.09	535···904	$4.2 \cdot 10^{-14}$	85W1
H	$2.72 \cdot 10^{-3}$	0.38	800···910	$4.5 \cdot 10^{-5}$	60F
In	$1.8 \cdot 10^4$	3.63	554···919	$1.6 \cdot 10^{-13}$	82D2
Li	$1 \cdot 10^{-6}$	0.43	50···150	$9.6 \cdot 10^{-9}$	76H
Na	0.029	1.55	660···830	$1.5 \cdot 10^{-9}$	77S
Ni	0.8	0.91	700···875	$4.3 \cdot 10^{-5}$	54M2
O	0.40	2.08	285···760	$6.8 \cdot 10^{-11}$	64C
P	$3.3 \cdot 10^2$	3.1	600···780	$9.1 \cdot 10^{-13}$	78M
Pb	$1.6 \cdot 10^3$	3.6	800	$2.0 \cdot 10^{-14}$	63B
Sb	21	2.08	650···850	$3.6 \cdot 10^{-9}$	70D
Sn	70	3.05	798···846	$5.7 \cdot 10^{-13}$	58V
Si	0.24	2.9	650···900	$5.7 \cdot 10^{-15}$	81R
Te	2.0	2.82	770···880	$2.1 \cdot 10^{-13}$	62I
Tl	$1.7 \cdot 10^3$	3.4	800···930	$1.8 \cdot 10^{-13}$	62T2
Zn	0.65	2.55	825···918	$6.9 \cdot 10^{-13}$	56K

binding energies of shallow impurities

Impurity	E_b[meV]	T[K]	Experimental method, remarks	Ref.
Group V substitutional donors				
Theory	9.81		donor effective mass calculation	69F
Sb	10.29	10, 4	optical absorption (photothermal ionization)	75S
Bi	12.81	10	optical absorption	64R
P	12.89	10	photoconductivity, absorption	74S
As	14.17	10	absorption	64R
Other shallow single donors				
Li	10.02	4	photoconductivity, absorption	72S
O-Li	10.47	6	piezophotoconductivity. Li tunnels between 4⟨111⟩ directions of molecular complex	78H
O-H	12.46	4	photoconductivity, labelled C in early work; obtained on quenching from 400 °C; isotope shift of 0.051 meV to lower energy on deuteration; tunnelling H center	80J
Group III substitutional acceptors				
Theory	11.2		acceptor EMT calculation	76B
B	10.82	4, 8	photoconductivity, optical absorption	74H

Impurity	E_b[meV]	T[K]	Experimental method, remarks	Ref.
Al	11.15		full series of EMT	
Ga	11.32		like excited states	
In	11.99		observed	
Tl	13.45		optical absorption	65J
Neutral double acceptors				
Be^0	24.80	2, 8	optical absorption and/or photoconductivity	83C
Zn^0	32.98	2, 8	optical absorption and/or photoconductivity	71M
Mg^0	35.85		optical absorption and/or photoconductivity	85M
Cd^0	54.96		optical absorption and/or photoconductivity	71M
Hg^0	91.65	6···20	optical absorption and/or photoconductivity	71M
Mn^0	55		optical absorption and/or photoconductivity	85M
Singly ionized double acceptors				
Be^-	58.02		optical absorption	83C
Zn^-	86.51	8···10	optical absorption, excited states observed	83C
Cd^-	160	20	Hall effect, photoconductivity	59T1
Hg^-	230	10	optical absorption	67C
Mn^-	100			85M
Group VI substitutional donors				
Se	286.2	19	photoconductivity	85G
	140, 280	10···300	Hall effect	59T1
Te	110	10···300	Hall effect	59N
	300			59T1
S	180, 280	10···300	Hall effect	59T1
	210, 250	60···160	DLTS	82P
O	17		Hall effect, photoconductivity	62K1
	40			82C
	200			
	60··· 80			78E
	160···180			
	16··· 17.3	7··· 40	absorption, D^0 state of oxygen-related thermal double donor	84C

energy levels of deep centers

Negative energy refers to conduction band edge, positive energy refers to valence band edge.

Impurity	E[meV]	T[K]	Remarks	Ref.
Group I impurities				
Cu^0	+43.25	20···300	Hall effect, photoconductivity	85S1
Cu^-	+330	20···300		84P
Cu^{2-}	−260, +410	20···300		84P
Au^0 acceptor	+160	20···300	Hall effect, photoconductivity	55D
Au^- acceptor	−200	20···300		57W
Au^{2-} acceptor	−40			65O
Au donor	+50		interstitial Au	
Ag^0	+130		Hall effect	59N
Ag^-	−280			
Ag^{2-}	−90			
Transition metal impurities				
Cr	+70, +120		resistivity	59N
Mn	+160, −370	30···400	resistivity, photoconductivity	59T1

Impurity	E[meV]	T[K]	Remarks	Ref.
Fe	+350, −270	30···400	resistivity, photoconductivity	59T1
Co	+250, −300	77···300	resistivity, Hall effect and photoconductivity	59T1
Pt	+40		resistivity, three acceptor levels, interpretation not clear	59N
Pd	+0.03, −0.18		resistivity, Hall effect	80G

energy levels of defect centers

Defect	E[meV]	Generation	Remarks	Ref.
Di-vacancy (V_2)-donor			E_v + 100, 120, 160 meV levels are interpreted as di-vacancy-donor complexes and are double acceptors	77M
	+100	1 MeV	P, As doped Ge	
	+120	γ-irr. at 280 K	Sb doped Ge	
	+160		Bi doped Ge	
Acceptors labeled by annealing		γ-irr. at 42 K	(a) double acceptors, anneal at 65 K, interpreted as vacancy-interstitial (Frenkel) pair "65 K" defects.	77M
			(b) acceptors, anneal at 160···200 K, arise from interstitial defects observed in dislocation	
Di-vacancy (V_2)-H	+80		free, high purity Ge grown in H-atmosphere;	77H
	+200		also produced by γ-irradiation of dislocated material. Attributed to di-vacancy-hydrogen complexes (c.f. di-vacancy-donor complexes above). E_v + 71 meV obtained if degeneracy factor of 4 assumed.	82E2
Di-vacancy (V_2)-Li	+100	γ-irr. at 280 K	Li doped, high purity Ge; resistivity, Hall effect	77H

References for 1.3

52S Straumanis, M.E., Aka, A.Z.: J. Appl. Phys. **23** (1952) 330.
53P Prince, M.B.: Phys. Rev. **92** (1953) 681.
54M1 Morin, F.J., Maita, J.P.: Phys. Rev. **94** (1954) 1525.
54M2 van der Maesen, F., Brenkman, J.A.: Philips Res. Rep. **9** (1954) 225.
55D Dunlap, W.C.: Phys. Rev. **97** (1955) 664.
56D Dexter, R.N., Zeiger, H.J., Lax, B.: Phys. Rev. **104** (1956) 637.
56K Kosenko, V.E.: Proc. Acad. Sci. USSR, Phys. Ser. (English Transl.) **20** (1956) 1399.
56T Thurmond, C.D., Guldner W.G., Beach, A.L.: J. Electrochem. Soc. **103** (1956) 603.
56W van Wieringen, A., Warmolitz, N.: Physica **22** (1956) 849.
57B Bugai, A.A., Kosenko, V.E., Miselyuk, E.G.: Sov. Phys. Tech. Phys. (English Transl.) **2** (1957) 183.
57M MacFarlane, G.G., McLean, T.P., Quarrington, J.E., Roberts, V.: Phys. Rev. **108** (1957) 1377.
57P Pell, E.M.: J. Phys. Chem. Solids **3** (1957) 74.
57W Woodbury, H.H., Tyler, W.W.: Phys. Rev. **105** (1957) 84.
58V Valenta, M.W.: Ph. D. Thesis, Univ. Illinois **1958** (Univ. Microfilm 58-5509); Bull. Am. Phys. Soc. **2** (1958) 102.
59N Newman, R., Tyler, W.W.: Solid State Physics, Vol. 8, Seitz, F., Turnbull, D. (eds.) New York: Academic Press **1959**, p. 49.
59P Philipp, H.P., Taft, E.A.: Phys. Rev. **113** (1959) 1002.
59R Reiss, H., Fuller, C.S.: Semiconductors, Hannay, N.B. (ed.), New York: Reinhold Publ. Corp., **1959**.
59T1 Tyler, W.W.: J. Phys. Chem. Solids **8** (1959) 59.
59T2 Trumbore, F.A., Probansky, E.M., Tartaglia, A.A.: J. Phys. Chem. Solids **11** (1959) 239.
59Z Zwerdling, S., Lax, B., Roth, L.M., Button, K.J.: Phys. Rev. **114** (1959) 80.
60F Frank, R.C., Thomas jr., J.E.: J. Phys. Chem. Solids **16** (1960) 144.
60K Kosenko, V.E.: Sov. Phys. Solid State (English Transl.) **1** (1960) 1481.
60T Trumbore, F.A.: Bell. Syst. Tech. J. **39** (1960) 205.
61B Belyaev, Yu.I., Zhidkov, V.A.: Sov. Phys. Solid State (English Transl.) **3** (1961) 133.
61W Wei, L.Y.: J. Phys. Chem. Solids **18** (1961) 162.
62A Abrikosov, N. Kh., Glasov, V.M., Lin Chên-Yüan: Russ. J. Inorg. Chem. (English Transl.) **7** (1962) 429.

62K1 Kaiser, W.: J. Phys. Chem. Solids **23** (1962) 225.
62K2 Kosenko, V.E.: Sov. Phys. Solid State (English Transl.) **4** (1962) 42.
62I Ignatkov, V.D., Kosenko, V.E.: Sov. Phys. Solid State (English Transl.) **4** (1962) 1193.
62T1 Trumbore, F.A., Spitzer, W.G., Logan, R.A., Luke, C.L.: J. Electrochem. Soc. **109** (1962) 734.
62T2 Tagirov, V.I., Kuliev, A.A.: Sov. Phys. Solid State (English Transl.) **4** (1962) 196.
63B Boltaks, B.I.: Diffusion in Semiconductors, London: Infosearch Ltd., **1963**.
64C Corbett, J.W., McDonald, R.S., Watkins, G.D.: J. Phys. Chem. Solids **25** (1964) 873.
64G Glassbrenner, C.J., Slack G.A.: Phys. Rev. **134A** (1964) 1058.
64K Kodera, H.: Jpn. J. Appl. Phys. **3** (1964) 369.
64R Reuszer, J.H., Fisher, P.: Phys. Rev. **135** (1964) A1125.
65J Jones, R.L., Fisher, P.: J. Phys. Chem. Solids **26** (1965) 1125.
65O Ostroborodova, V.V.: Fiz. Tverd. Tela **7** (1965) 610; Sov. Phys.-Solid State (English Transl.) **7** (1965) 484.
67C Chapman, R.A., Hutchinson, W.G.: Phys. Rev. **157** (1967) 615.
67M Meer, W., Pommerrenig, D.: Z. Angew. Phys. **23** (1967) 369.
68G Gromova, O.N., Khodunova, K.M.: Fiz. Khim. Obrab. Mater. **5** (1968) 150; Diffusion and Defect Data **3** (1969) 142.
68I Isawa, N.: Jpn. J. Appl. Phys. **7** (1968) 81.
68S Singh, H.P.: Acta Crystallogr. **24a** (1968) 469.
69A Aggarwal, R.L., Zuteck, M.D., Lax, B.: Phys. Rev. **180** (1969) 800.
69F Faulkner, R.A.: Phys. Rev. **184** (1969) 713.
70A Aggarwal, R.L.: Phys. Rev. **B2** (1970) 446.
70D Dudko, G.V., Marunina, N.I., Sukhov, G.V., Cherednichenko, D.I.: Sov. Phys. Solid State (English Transl.) **12** (1970) 1016.
71B Burenkov, Yu.A., Nikanorov, S.P., Stepanov, A.V.: Sov. Phys. Solid State (English Transl.) **12** (1971) 1940; Fiz. Tverd. Tela **12** (1970) 2428.
71M Moore, W.J.: J. Phys. Chem. Solids **32** (1971) 93.
71N Nilsson, G., Nelin, G.: Phys. Rev. **B3** (1971) 364.
72N1 Nelin, G., Nilsson, G.: Phys. Rev. **B5** (1972) 3151.
72N2 Nilsson, G., Nelin, G.: Phys. Rev. **B6** (1972) 3777.
72S Seccombe, S.D., Korn, D.: Solid State Commun. **11** (1972) 1539.
74H1 Haller, E.E., Hansen, W.L.: Solid State Commun. **15** (1974) 687.
74H2 Hensel, J.C., Suzuki, K.: Phys. Rev. **B9** (1974) 4219.
74S Skolnick, M.S., Eaves, L., Stradling, R.A., Portal, J.C., Askenazy, S.: Solid State Commun. **125** (1974) 1403.
75B Baker, J.F.C., Hart, M.: Acta Crystallogr. **31a** (1975) 2297.
75W Wiley, J.D.: in "Semiconductors and Semimetals", Vol. 10, R.K. Willardson, A.C. Beer eds., Academic Press, New York **1975**.
75S Skolnick, M.S., Eaves, L., unpublished.
76A Altarelli, M., Lipari, N.O.: Phys. Rev. Lett. **36** (1976) 619.
76B Baldereschi, A., Lipari, N.O.: Proc. 13th Int. Conf. on the Physics of Semicond., Rome 1976, Fumi, F.G. (ed.) Marves **1976**, p. 595.
76C Chelikowsky, J.R., Cohen, M.L.: Phys. Rev. **B30** (1976) 556.
76F Fink, D., Braunstein, R.: Phys. Status Solidi (b) **73** (1976) 361.
76H Hufschmidt, M., Möller, W., Pfeiffer, T.: Vak.-Tech. **25** (1976) 206.
77H Haller, E.E., Hubbard, G.S., Hansen, W.L.: IEEE Trans. Nucl. Sci. **NS24** (1977) 48.
77M Mashovets, T.M.: Int. Conf. on Radiation Effects in Semiconductors, Dubrovnik 1976, Institute of Physics Conf. Ser. No. **31 1977**, p. 30.
77S Stojić, M., Spirić, V., Kostoski, D.: Inst. Phys. Conf. Ser. **31** (1977) 304.
77W Weber, W.: Phys. Rev. **B15** (1977) 4789.
78E Emstev, V.V., Goncharev, L.A., Dostkhodzhoev, T.N.: Fiz. Tekh. Poluprovodn. **12** (1978) 139; Sov. Phys. Semicond. (English Transl.) **12** (1978) 78.
78H Haller, E.E., Falicov, L.M.: Phys. Rev. Lett. **41** (1978) 1192.
78M Matsumoto, S., Niimi, T.: J. Electrochem. Soc. **125** (1978) 1307.
79A Ahmad, C.N., Adams, A.R., Pitt, G.D.: J. Phys. **C12** (1979) L379.
79M Martin, T.P., Schaber, H.: Z. Physik **B35** (1979) 61.
80G Golubev, N.F., Latyshev, A.V.: Sov. Phys. Semicond. (English Transl.) **14** (1980) 1074.
80J Joos, B., Haller, E.E., Falicov, L.M.: Phys. Rev. **B22** (1980) 832.
80Z Zverev, V.N.: Sov. Phys. Solid State (English Transl.) **22** (1980) 1921; Fiz. Tverd. Tela **22** (1980).
81J Jacoboni, C., Nava, F., Canali, C., Ottaviani, G.: Phys. Rev. **B24** (1981) 1014.
81R Räisänen, J., Hirvonen, J., Anttila, A.: Solid-State Electron. **24** (1981) 333.
82C Clauws, P., Broeckx, J., Simeon, E., Vennik, J.: Solid State Commun. **44** (1982) 1011.
82D1 Dorner, P., Gust, W., Lodding, A., Odelius, H., Predel, B.: Acta Metall. **30** (1982) 941.
82D2 Dorner, P., Gust, W., Lodding, A., Odelius, H., Predel, B., Roll, U.: Z. Metallkd. **73** (1982) 325.
82E1 Edwin, R.P., Dudermel, M.T., Lamare, M.: Appl. Optics **21** (1982) 878.
82E2 Emstev, V.V., Mashovets, T.V., Nazaryan, E.K., Haller, E.E.: Sov. Phys. Semicond. (English Transl.) **16** (1982) 182.
82H1 Hansen, W.L., Haller, E.E., Luke, P.N.: IEEE Trans. Nucl. Sci. NS-**29** (1982) 738.
82H2 Hirose, Y., Shimomae, K., Hamaguchi, C.: J. Phys. Soc. Jpn. **51** (1982) 2226.
82P Pearton, S.J.: Aust. J. Phys. **35** (1982) 53.
82W Werner, A., Sanjorjo, J.A., Cardona, M.: Solid State Commun. **44** (1982) 155.
83A1 Aspnes, D.E., Studna, A.A.: Phys. Rev. **B27** (1983) 985.
83A2 Allen, P.B., Cardona, M.: Phys. Rev. **B27** (1983) 4760.

83C Cross, J.W., Holt, L.T., Ramdas, A.K., Sauer, R., Haller, E.E.: Phys. Rev. **B28** (1983) 6953.
83L López-Cruz, E., Cardona, M.: Solid State Commun. **45** (1983) 787.
83P Philip, J., Breazeale, M.A.: J. Appl. Phys. **54** (1983) 752.
83Q Qadri, S.B., Skelton, E.F., Webb, A.W.: J. Appl. Phys. **54** (1983) 3609.
83S Szmulowicz, F.: Phys. Rev. **B28** (1983) 5943.
84B Bakhchieva, S.R., Kekelidse, N.P., Kekua, M.G.: Phys. Status Solidi (a) **83** (1984) 139.
84C Clauws, P., Vennik, J.: Phys. Rev. **B30** (1984) 4837.
84H Hsieh, T.C., Miller, T., Chiang, T.C.: Phys. Rev. **B30** (1984) 7005.
84P Pearton, S.J., Haller, E.E., Kahn, J.M.: J. Phys. **C17** (1984) 2375.
84V Viña, L., Logothetidis, S., Cardona, M.: Phys. Rev. **B30** (1984) 1979.
85G Grimmeiss, H.G., Larsson, K., Montelius, L.: Solid State Commun. **54** (1985) 863.
85L Lautenschlager, P., Allen, P.B., Cardona, M.: Phys. Rev. **B31** (1985) 2163.
85M McMurray, R.E.: Solid State Commun. **53** (1985) 1127.
85N Nichols, J.M., Hansson, G.V., Karlsson, U.O., Persson, P.E.S., Uhrberg, R.I.G., Engelhard, R., Flodström, S.A., Koch, E.E.: Phys. Rev. **B32** (1985) 6663.
85S1 Salib, E.H., Fisher, P., Simmonds, P.E.: Phys. Rev. **B32** (1985) 2424.
85S2 Stolwijk, N.A., Frank, W., Hölzl, J., Pearton, S.J., Haller, E.E.: J. Appl. Phys. **57** (1985) 5211.
85W1 Werner, M., Mehrer, H., Hochheimer, H.D.: Phys. Rev. **B32** (1985) 3930.
85W2 Wachs, A.L., Miller, T., Hsieh, T.C., Shapiro, A.P., Chiang, T.C.: Phys. Rev. **B32** (1985) 2326.
86S Sodervall, U., Odelius, H., Lodding, A., Roll. U., Predel, B., Gust. W., Dorner, P.: Philos. Mag. **A54** (1986) 539.

Physical property	Numerical value	Experimental conditions	Experimental method, remarks	Ref.

1.4 Grey tin (α-Sn)

Electronic properties

band structure: Fig. 1 (Brillouin zone, see Fig. 2 of section 1.1).

α-Sn is a *zero-gap semiconductor* with its lowest conduction band and its highest valence band being degenerate at Γ (symmetry Γ_8). A second conduction band with L_6-minima follows at a slightly higher energy. It determines the properties of n-type samples for $n > 10^{17}\,cm^{-3}$ ($T > 77\,K$ in intrinsic samples). Two further bands with Γ_7-symmetry, respectively, are situated below the Γ_8 valence band.

energies of symmetry points of the band structure (relative to the top of the valence band) (in eV):

$E(\Gamma_{6v})$	−11.34	non-local pseudopotential calculation (see Fig. 1)	76C
$E(\Gamma_{7v})$	−0.80		
$E(\Gamma_{7c})$	−0.42		

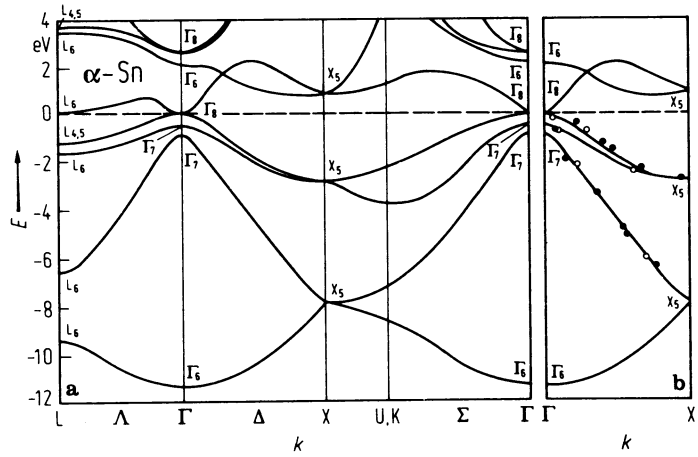

Fig. 1. α-Sn. (a) Band structure calculated by a non-local pseudopotential method [76C], (b) comparison with data from angular resolved photoemission along the Γ – X axis [83H].

Physical property	Numerical value	Experimental conditions	Experimental method, remarks	Ref.
$E(\Gamma_{8v,c})$	0.00		note that the Γ_{7c} conduction band has shifted *below* the Γ_{8v} band! Thus $E(\Gamma_{7c})$ is negative.	
$E(\Gamma_{6c})$	2.08			
$E(\Gamma_{8c})$	2.66			
$E(X_{5v})$	−7.88			
$E(X_{5v})$	−2.75			
$E(X_{5c})$	0.90			
$E(L_{6v})$	−9.44			
$E(L_{6v})$	−6.60			
$E(L_{6v})$	−1.68			
$E(L_{4,5v})$	−1.20			
$E(L_{6c})$	0.14			
$E(L_{6c})$	3.48			
$E(L_{4,5c})$	3.77			
energy differences above $\Gamma_{8v,c}$:				
$E(L_{6c}-\Gamma_{8c})$	0.094 eV	0 K (extrapol.)	conductivity and Hall coefficient in the range 70···270 K, Fig. 2	56K
	0.12 eV		"optical band gap"	81F
energy differences below $\Gamma_{8v,c}$:				
$E(\Gamma_{8v,c}-\Gamma_{7c})$	0.413 eV	1.5···85 K	interband magnetoreflection	70G
$\Delta_0(\Gamma_{8v,c}-\Gamma_{7v})$	0.8 eV			
critical point energies (in eV): (measured by ellipsometry on InSb substrate stabilized layers)				
E_1	1.316(5)	200 K	$\Lambda_{4,5v}-\Lambda_{6c}$	85V
$E_1+\Delta_1$	1.798(6)		$\Lambda_{6v}-\Lambda_{6c}$	
E_0'	2.42(3)		at or near $\Gamma_{8v}-\Gamma_{6c}$	
$E_0'+\Delta_0'$	2.72(3)		$\Gamma_{8v}-\Gamma_{8c}$	
E_1'	4.28(4)		$L_{4,5v}-L_{6c}$	
$E_1'+\Delta_1'$	4.51(4)		$L_{4,5v}-L_{4,5c}$	
effective masses, electrons and holes (in units of m_0):				
$m_{n,l}$	0.0236(2)	1.3 K	density of states mass	68B
$m_{n,h}$	0.21	4.2 K	$n(n_d)$-dependence	71L
$m_p(\Gamma_{8v})$	0.195		interband magnetoreflection	70G
$m_p(\Gamma_{7v})$	0.058			
valence band parameters:				
A	15.0	1.3 K	Γ_{8c}-band	75L
B	22.9			
C^2	−696			

Lattice properties

Grey tin crystallizes in the diamond structure, space group O_h^7–Fd3m (α-modification). Slightly below RT it transforms into the metallic high-temperature β-modification (white tin). This transformation can be inhibited by alloying Ge or Si or by stabilizing grey tin as a heteroepitaxial layer on a substrate with a nearly equal lattice constant.

Physical property	Numerical value	Experimental conditions	Experimental method, remarks	Ref.
lattice parameter:				
a	6.4892(1) Å	20 °C	X-ray	59T
da/dT	$3.1 \cdot 10^{-5}$ Å K^{-1}	−130 ··· 25 °C		
transition temperature:				
T_{tr}	13.2(1) °C		equilibrium value	84V
	32.0(2) °C		hysteresis for the transformation in pure Sn	
linear thermal expansion coefficient: Fig. 3.				
density:				
d	7.285 g cm^{-3}	18 °C		60B
phonon dispersion relations: Fig. 4.				

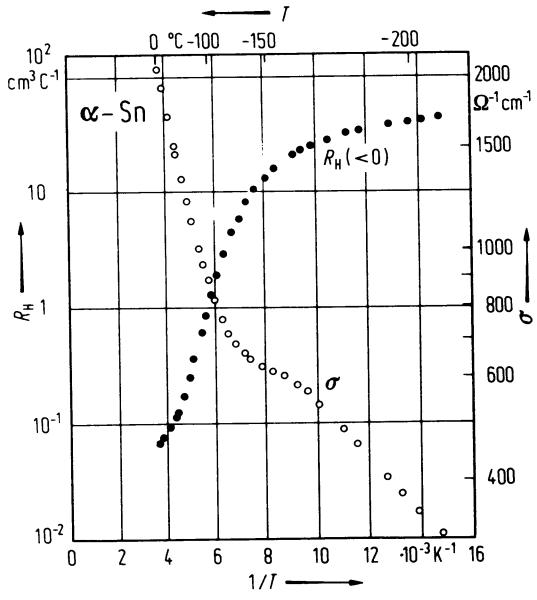

Fig. 2. α-Sn. Hall coefficient and conductivity vs. temperature of a sample containing about 10^{17} impurities/cm^3 [56K].

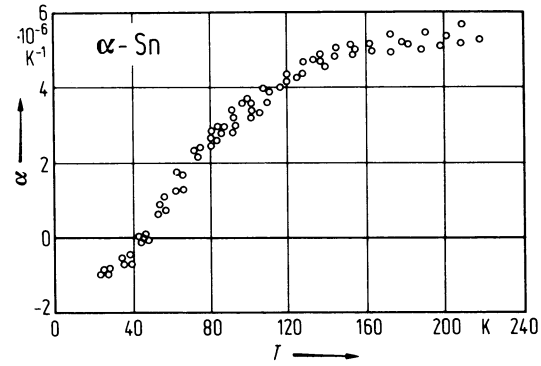

Fig. 3. α-Sn. Coefficient of linear thermal expansion vs. temperature [61N].

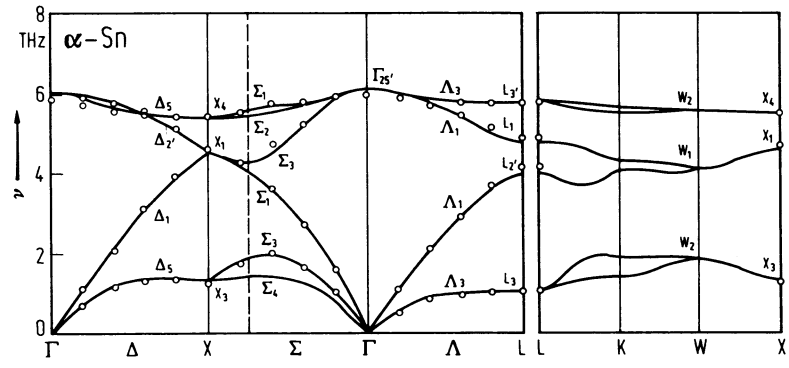

Fig. 4. α-Sn. Phonon dispersion curves. Experimental values from [71P], solid lines calculated with an adiabatic charge bond model [77W].

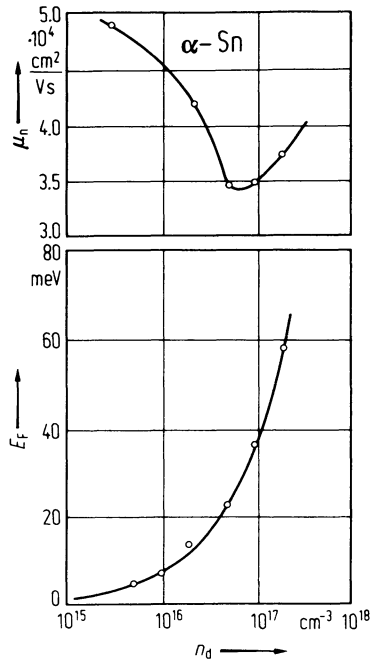

Fig. 5. α-Sn. Electron mobility at 5 K and Fermi energy vs. donor concentration. E_F measured from zero gap energy. An acceptor resonance level at 30 meV is suggested by the mobility minimum [82M].

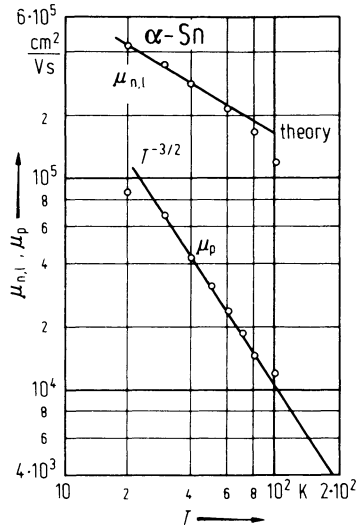

Fig. 6. α-Sn. Light electron mobility and hole mobility vs. temperature [71L].

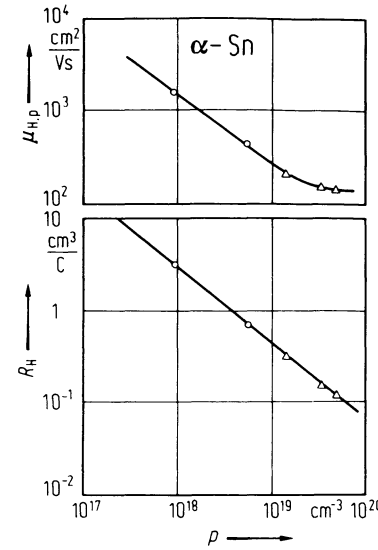

Fig. 7. α-Sn. Hall mobility (above) and Hall coefficient (below) vs. hole concentration at 77K. Data on bulk samples (open circles, [61T]) and substrate-stabilized metastable films [81F].

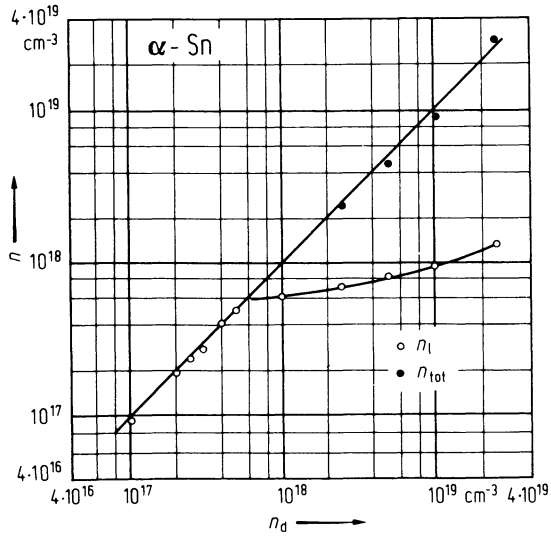

Fig. 8. α-Sn. Electron concentration at 4.2 K vs. donor concentration; n_l (light electron concentration) from oscillatory magnetoresistance, n_{tot} (total electron concentration) from Hall coefficient [71L].

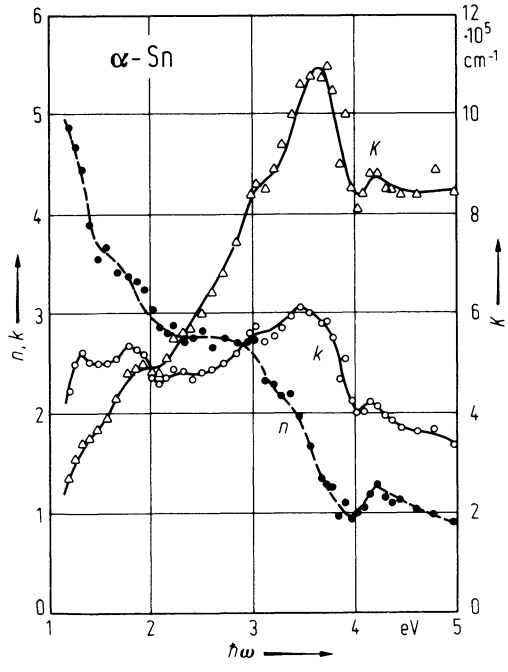

Fig. 9. α-Sn. Index of refraction n, extinction coefficient k and absorption coefficient K vs. photon energy [71H].

Physical property	Numerical value	Experimental conditions	Experimental method, remarks	Ref.
phonon frequencies (in THz):				
$\nu_{TO/LO}(\Gamma_{25'})$	6.00(6)	90 K	inelastic neutron scattering	71P
$\nu_{TA}(L_3)$	1.00(4)			
$\nu_{LA}(L_{2'})$	4.15(4)			
$\nu_{LO}(L_1)$	4.89(8)			
$\nu_{TO}(L_{3'})$	5.74(12)			
$\nu_{TA}(X_3)$	1.25(6)			
$\nu_{LA/LO}(X_1)$	4.67(6)			
$\nu_{TO}(X_4)$	5.51(8)			
second order elastic moduli (in 10^{12} dyn cm^{-2}):				
c_{11}	0.690		calculated from an eleven-parameter shell model fitted to experimental data	71P
c_{12}	0.293			
c_{44}	0.362			

Transport properties

In intrinsic samples light electrons and holes in the Γ_8-bands determine the transport properties. In heavily doped n-type samples the electrons in the L_6-minima dominate and grey tin behaves as an indirect gap semiconductor with E_g of about 0.09 eV (Fig. 2).

electron concentration: Fig. 8.

electron and hole mobilities (in cm^2/Vs):

$\mu_n(\Gamma_8)$	$1.2 \cdot 10^5$	100 K	from Hall data	71L
$\mu_n(L_6)$	$\approx 10^3$	4.2 K		
μ_p	$1 \cdot 10^4$	100 K	magnetoresistance for μ_n, μ_p, see also Figs. 5···7.	71L

Optical properties

Refractive index, extinction coefficient and absorption coefficient: Fig. 9.

dielectric constant:

ε	24	$T = 300$ K	background dielectric constant in the free carrier absorption region (from infrared reflectance measurements)	64L

References for 1.4

56K Kohnke, E.E., Ewald, A.W.: Phys. Rev. **102** (1956) 1481.
59T Thewlis, J., Davey, A.R.: Nature (London) **174** (1959) 1011.
60B Busch, G.A., Kern, R.: Solid State Physics, F. Seitz, D. Turnbull eds., Academic Press, New York, Vol. 11, **1960**, p. 1.
61N Novikova, S.I.: Sov. Phys. Solid State (English Transl.) **2** (1961) 2087; Fiz. Tverd. Tela **2** (1960) 2341.
61T Tufte, O.N., Ewald, A.W.: Phys. Rev. **122** (1961) 1431.
64L Lindquist, R.E., Ewald, A.W.: Phys. Rev. **135** (1964) A191.
68B Booth, B.L., Ewald, A.W.: Phys. Rev. **168** (1968) 805.
70G Groves, S.H., Pidgeon, C.R., Ewald, A.W., Wagner, R.J.: J. Phys. Chem. Solids **31** (1970) 2031.
71H Hanyu, T.: J. Phys. Soc. Jpn. **31** (1971) 1738.
71L Lavine, C.F., Ewald, A.W.: J. Phys. Chem. Solids **32** (1971) 1121.
71P Price, D.L., Rowe, J.M., Nicklow, R.M.: Phys. Rev. **B3** (1971) 1268.
75L Liu, L., Leung, W.: Phys. Rev. **B12** (1975) 2336.
76C Chelikowsky, J.R., Cohen, M.L.: Phys. Rev. **B14** (1976) 556.
77W Weber, W.: Phys. Rev. **B15** (1977) 4789.

81F Farrow, R.F.C., Robertson, D.S., Williams, G.M., Cullis, A.G., Jones, G.R., Young, I.M., Dennis, P.N.J.,: J. Crystal Growth **54** (1981) 507.
82M Myhra, S.: Phys. Status Solidi (b) **110** (1982) 97.
83H Höchst, H., Hernández-Calderón, I.: Surf. Sci. **126** (1983) 25.
84V Vnuk, F., DeMonte, A., Smith, R.W.: J. Appl. Phys. **55** (1984) 4171.
85V Viña, L., Höchst, H., Cardona, M.: Phys. Rev. **B31** (1985) 958.

Physical property	Numerical value	Experimental conditions	Experimental method, remarks	Ref.

1.5 Silicon carbide (SiC)

Silicon carbide crystallizes in numerous (more than two hundred) different modifications (polytypes). The most important are:

cubic unit cell:

3C-SiC	space group: T_d^2–F$\bar{4}$3m	lattice: zincblende

hexagonal unit cell:

2H-SiC	space group: C_{6v}^4–P6$_3$mc	lattice: wurtzite

rhombohedral unit cell:

15R-SiC	space group: C_{3v}^5–R3m

Other polytypes with rhombohedral unit cell: 21R-SiC, 24R-SiC, 27R-SiC etc.

In all polytypes except 3C- and 2H-SiC atomic layers with cubic (c) and hexagonal (h) symmetry follow in a regular alternation in the direction of the c axis. This can be thought of as a natural one-dimensional superlattice imposed on the "pure" – i.e. h-layer free – 3C-SiC [77D1], the period of the superlattice being different for different modifications.

Electronic properties

3C-SiC:

band structure: Fig. 1 (Brillouin zone, see section 1.1, Fig. 2).

energy gaps (in eV):

$E_{g,ind}$ ($\Gamma_{15v} - X_{1c}$)	2.416(1)	2 K	wavelength modulated absorption	81B
$E_{g,dir}$ ($\Gamma_{15v} - \Gamma_{1c}$)	6.0	300 K	optical absorption	65D
E_{gx}	2.38807(3)	1.4 K	excitonic energy gap, wavelength modulated absorption	84G

According to [79R] the temperature dependence of E_{gx} can be described by the empirical formula $E_{gx} = 3.024 - 0.3055 \cdot 10^{-4}\, T^2/(311\,\mathrm{K} - T)\,\mathrm{eV}$. See also Fig. 5.

effective masses, electrons (in units of m_0):

$m_{n\parallel}$	0.677(15)	45 K	cyclotron resonance	85K
$m_{n\perp}$	0.247(11)			

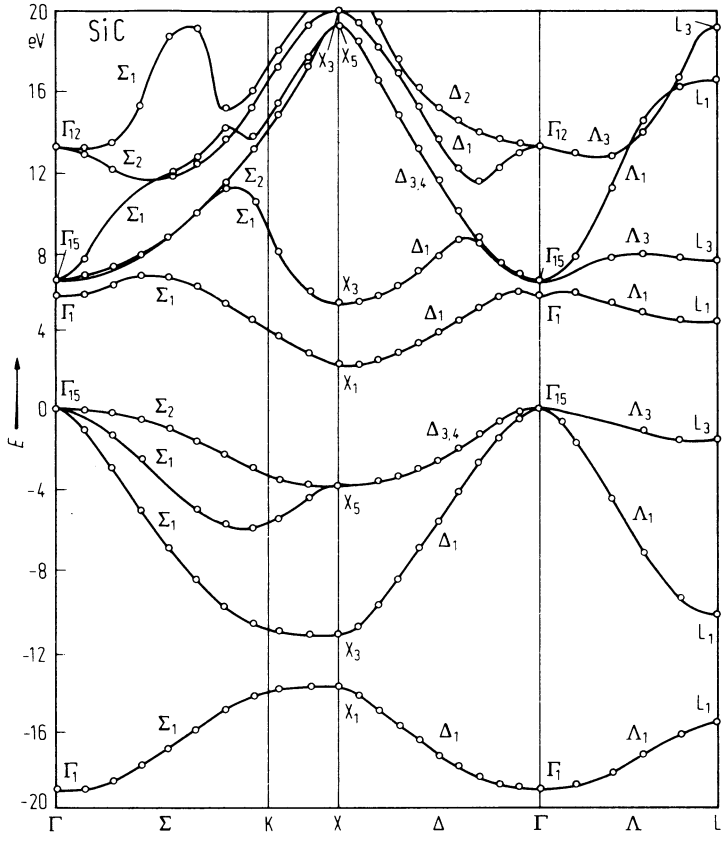

Fig. 1. SiC (3C). Band structure [74H].

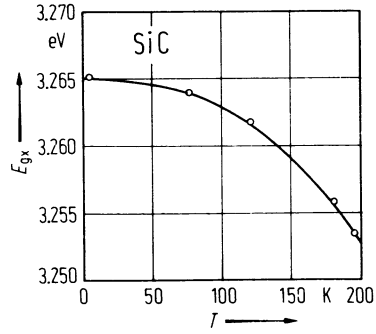

Fig. 3. SiC (4H). Excitonic energy gap vs. temperature [64C].

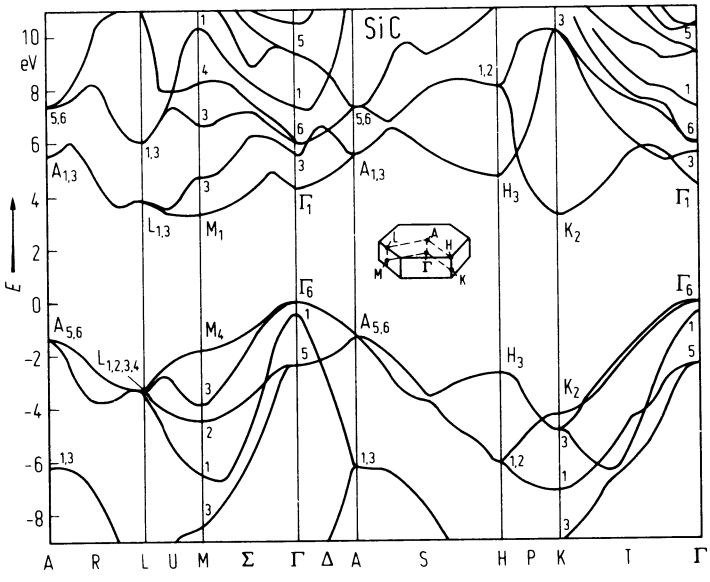

Fig. 2. SiC (2H). Band structure [74H].

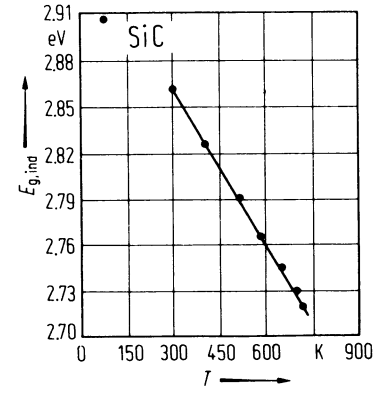

Fig. 4. SiC (6H). Energy gap $E_{g,ind}$ vs. temperature [60P].

Physical property	Numerical value	Experimental conditions	Experimental method, remarks	Ref.
effective masses, holes:				
Due to the small spin-orbit splitting the valence bands are highly non-parabolic, i.e. effective hole masses become strongly k-dependent.				
2H-SiC:				
band structure: Fig. 2.				
E_{gx}	3.330 eV		optical absorption, Fig. 5	66P
4H-SiC:				
E_{gx}	3.20 eV		see Figs. 3, 5	77D2
6H-SiC:				
$E_{g,ind}$	2.86 eV	300 K	optical absorption, Figs. 4, 5	60P
E_{gx}	3.0230 eV		wavelength modulated absorption	81H
$m_{n\parallel}$	$1.5(2)m_0$	300 K	Faraday rotation	67E
$m_{n\perp}$	$0.25m_0$			
$m_{p,ds}$	$1.0m_0$			
8H-SiC:				
E_{gx}	2.86 eV		see Fig. 5	77D2
15R-SiC:				
E_{gx}	2.9863 eV		see Figs. 5, 6	81H
$m_{n\parallel}$	$0.53m_0$		Faraday rotation	67E
$m_{n\perp}$	$0.28(2)m_0$			
21R-SiC:				
E_{gx}	2.92 eV		see Fig. 5	77D2
24R-SiC:				
E_{gx}	2.80 eV		see Fig. 7	77D2
Lattice properties				
3C-SiC:				
lattice parameter:				
a	4.3596 Å	297 K	Debye-Scherrer; for temperature dependence, see Fig. 8.	60T
linear thermal expansion coefficient:				
α	$2.77(42)\cdot 10^{-6}\,K^{-1}$	300 K	recommended value	75S
melting point:				
T_m	3103(40) K	$p = 35$ bar	peritectic decomposition temperature	60S
density:				
d	$3.166\,g\,cm^{-3}$	293 K		69K

Physical property	Numerical value	Experimental conditions	Experimental method, remarks	Ref.
phonon dispersion relations: Fig. 9.				
phonon wavenumbers (in cm^{-1}):				
$\bar{\nu}_{TO}(\Gamma)$	796.2(3)	RT	Raman spectroscopy	82O1
$\bar{\nu}_{LO}(\Gamma)$	972.2(3)			
$\bar{\nu}_{TA}(L)$	266	RT	discussion of Raman spectra including data from previous publications	82O2
$\bar{\nu}_{LA}(L)$	610			
$\bar{\nu}_{TO}(L)$	766			
$\bar{\nu}_{LO}(L)$	838			
$\bar{\nu}_{TA}(X)$	373			
$\bar{\nu}_{LA}(X)$	640			
$\bar{\nu}_{TO}(X)$	761			
$\bar{\nu}_{LO}(X)$	829			
second order elastic moduli (in 10^{12} dyn cm^{-2}):				
c_{11}	3.523			75K1
c_{12}	1.404			
c_{44}	2.329			

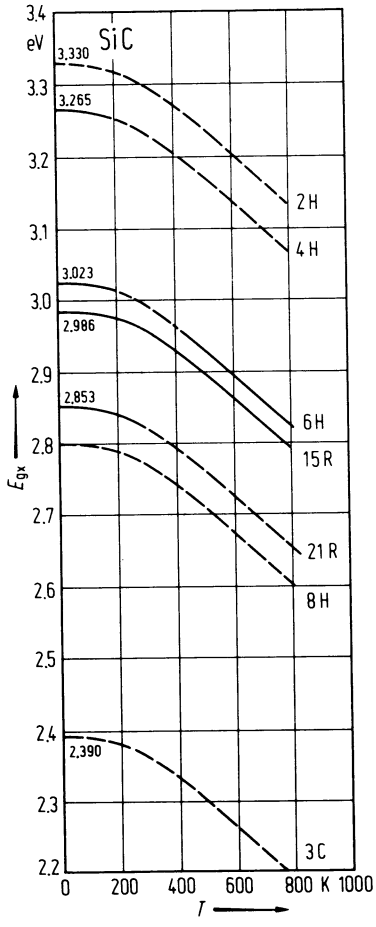

◀ Fig. 5. SiC. Excitonic energy gap of several polytypes vs. temperature [68C].

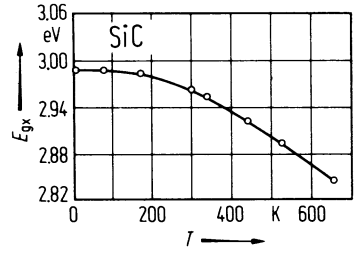

Fig. 6. SiC (15 R). Excitonic energy gap vs. temperature [63P].

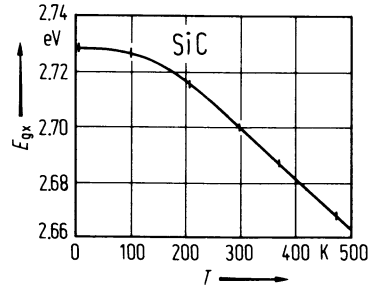

Fig. 7. SiC (24 R). Excitonic energy gap vs. temperature [64Z].

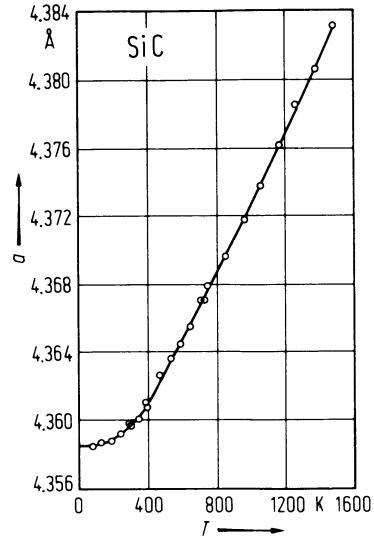

Fig. 8. SiC (3 C). Lattice constant vs. temperature [60T].

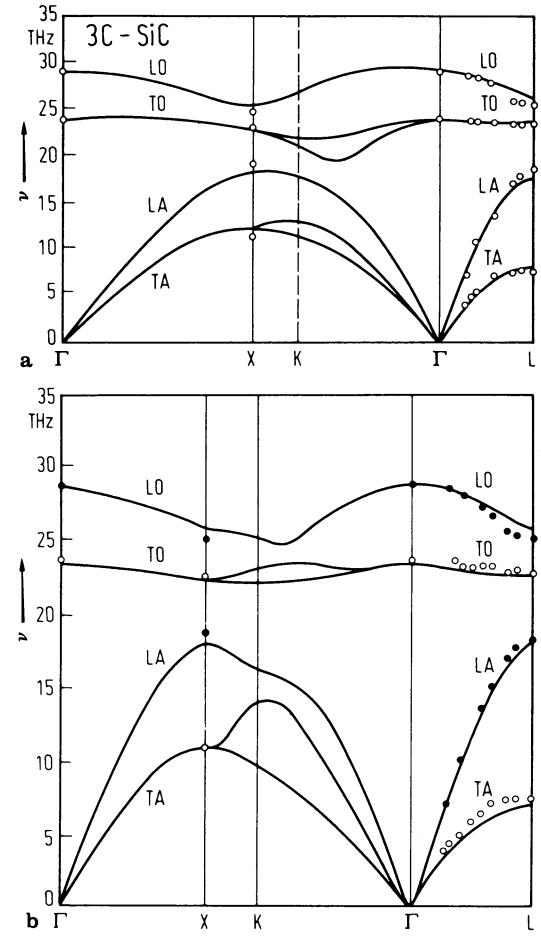

Fig. 9. 3C-SiC. Phonon dispersion relations, (a) derived from an eight-parameter bond-bending force model [82K], (b) derived from a real-space formalism based on scattering theory. Circles experimental [82L].

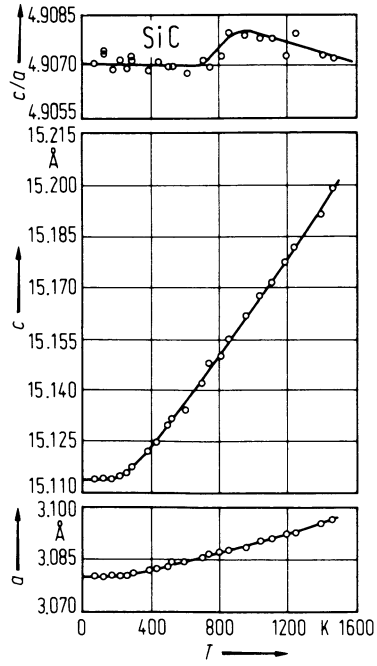

Fig. 10. SiC (6 H). Lattice constants vs. temperature [60T].

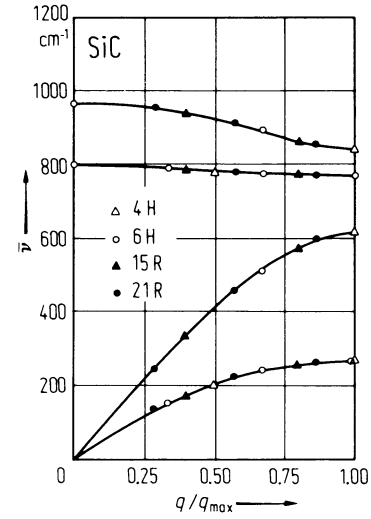

Fig. 11. SiC. Phonon dispersion relations for 4H, 6H, 15R and 21R polytypes along the axial direction vs. reduced wavevector [68F].

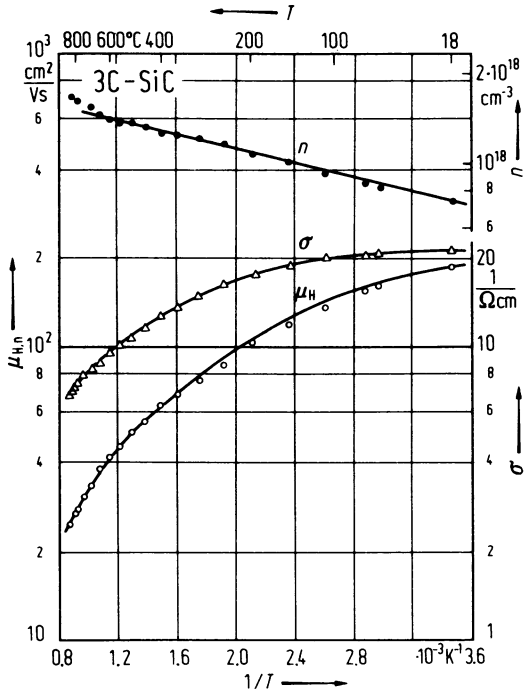

Fig. 12. 3C-SiC. Conductivity, carrier concentration and electron Hall mobility of an epitaxial layer on Si vs. temperature [84S].

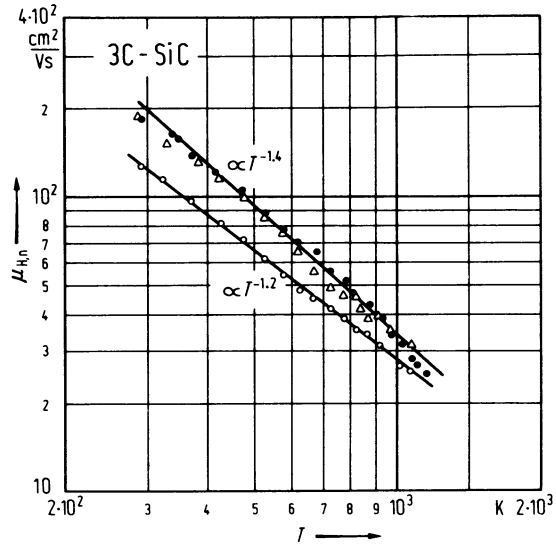

Fig. 13. 3C-SiC. Electron Hall mobility of three expitaxial layers on Si vs. temperature [84S].

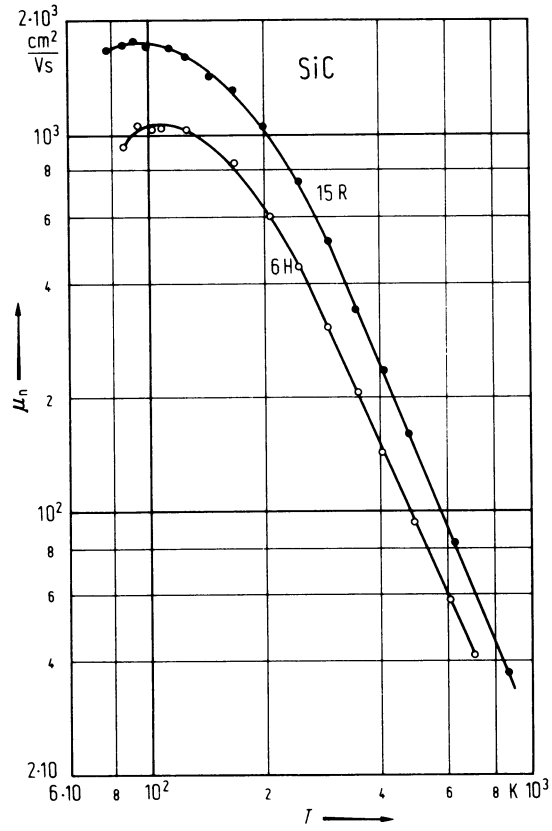

Fig. 14. SiC. Electron mobility vs. temperature in 6 H and 15 R samples [67B].

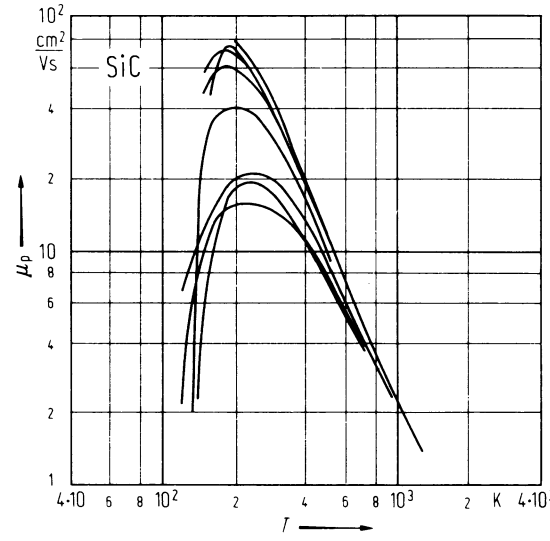

Fig. 15. SiC (6 H). Hole mobility of different samples vs. temperature [63V].

Physical property	Numerical value	Experimental conditions	Experimental method, remarks	Ref.
Hexagonal polytypes				
6H-SiC:				
lattice parameters:				
a	3.0806 Å	297 K	Debye-Scherrer; for temperature dependence, see Fig. 10	60T
c	15.1173 Å			
density:				
d	3.211 g cm^{-3}	300 K		67G
phonon dispersion relations (also for 4H-, 15R-, and 21R-SiC): Fig. 11.				
phonon energies (in meV):				
$h\nu_{TA}$	36.3		discussion of free exciton replica in wavelength modulated absorption	81H
	46.3			
$h\nu_{LA}$	53.3			
	77.0			
$h\nu_{TO}$	95.6			
$h\nu_{LO}$	104.2			
	107.0			

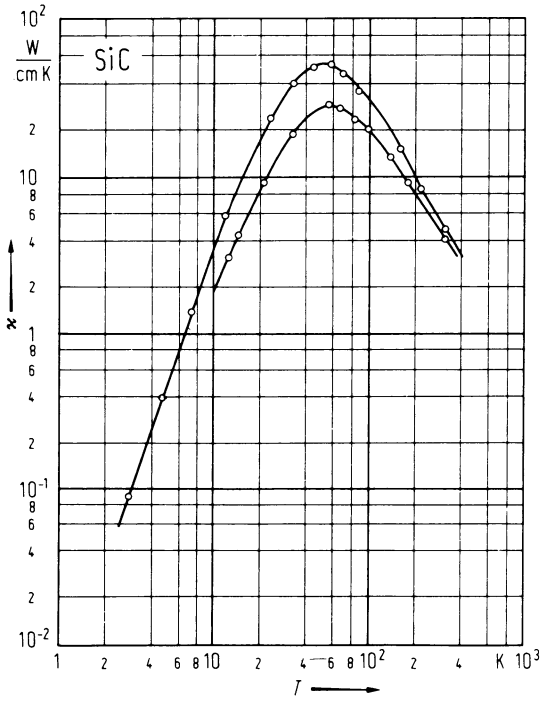

Fig. 16. SiC (6H). Thermal conductivity ($\perp c$-axis) vs. temperature for two different samples [64S].

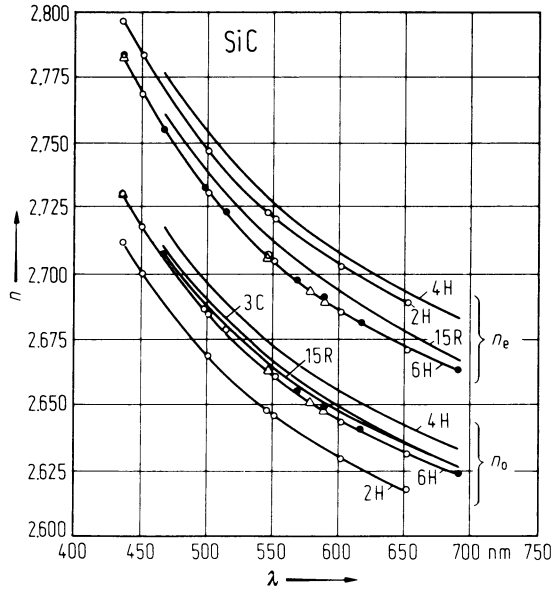

Fig. 17. SiC. Dispersion of refractive indices of several polytypes [72P].

Physical property	Numerical value	Experimental conditions	Experimental method, remarks	Ref.
second order elastic moduli (in 10^{12} dyn cm^{-2}):				
c_{11}	5.00(20)	300 K	ultrasonic resonance	65A
c_{12}	0.92(28)			
c_{33}	5.64(2)			
c_{44}	1.68(2)			

Transport and optical properties

electron and hole mobilities of 3C-SiC (in cm^2/Vs):

μ_n	900	300 K	crystalline	66N
	380	RT		83N
μ_p	15···21			83N

For Hall mobility in epitaxial layers on Si, see Figs. 12 and 13.
Mobilities in other polytypes are of the same order of magnitude, see Figs. 14 and 15.

thermal conductivity of 6H-SiC: Fig. 16.

refractive index:
Empirical formula for 3C-SiC: $n(\lambda) = 2.55378 + 3.417 \cdot 10^4 \lambda^{-2} (\lambda = 467 \cdots 691\,\text{nm})$ [69S]. For other polytypes see Fig. 17.

dielectric constants:

$\varepsilon(0)$	9.72	300 K	3C-SiC	70P
$\varepsilon(\infty)$	6.52			
$\varepsilon_\perp(0)$	9.66		6H-SiC	
$\varepsilon_\parallel(0)$	10.03			
$\varepsilon_\perp(\infty)$	6.52			
$\varepsilon_\parallel(\infty)$	6.70			

Impurities and defects

solubility of impurities in SiC

Impurity	c_{max}^{eq} [cm^{-3}]	T[°C]	Remarks	Ref.
N	$2.6 \cdot 10^{20}$	2450	crystal growth; nitrogen pressure 35 atm	65S
Be	$7 \cdot 10^{17}$	1800	diffusion experiments	68M
	$5 \cdot 10^{19}$	2300		
B	$2 \cdot 10^{19}$	1800	epitaxial growth;	77T
	$1.5 \cdot 10^{20}$	2300	(0001) face	
	$4 \cdot 10^{19}$	1800	epitaxial growth;	77T
	$2.5 \cdot 10^{20}$	2300	(000$\bar{1}$) face	
Al	$1.1 \cdot 10^{21}$	2300	epitaxial growth; (0001) face	77T
	$7 \cdot 10^{20}$	2300	epitaxial growth; (000$\bar{1}$) face	77T
Ga	$1.2 \cdot 10^{19}$	1800	epitaxial growth;	77T
	$1.2 \cdot 10^{19}$	2300	(0001) face	
	$2.8 \cdot 10^{18}$	1800	epitaxial growth	77T
	$7 \cdot 10^{18}$	2300	(000$\bar{1}$) face	

diffusion constants of impurities in 6H SiC

Dopant	D_0 $cm^2 s^{-1}$	Q eV	T °C	Remarks	Ref.
N	$4.6 \cdots 8.7 \cdot 10^{-4}$	7.6···9.3	2000···2550	pn-junction	66K
Be	32	5.2	1950···2250	pn-junction, probably substitutional diffusion	68M
	0.3	3.1	1700···2100	pn-junction, probably interstitial diffusion	68M
B	$1.6 \cdot 10^2$	5.6	1800···2250	pn-junction	66V
	3.2	5.1	1600···2550	pn-junction	74V
Al	1.8	4.9	1700···2000	pn-junction	60C
	0.2	4.9	1800···2250	pn-junction	66V
	8.0	6.1	1900···2300	pn-junction	69M
	$1.3 \cdot 10^{-8}$	2.4	1350···1800	Ion implantation; SIMS measurements	82T
Ga	0.17	5.5	2050···2300	pn-junction	74V

binding energy of impurities in SiC

Due to the existence of inequivalent lattice sites in silicon carbide (except for the 3C and 2H polytypes), there are several site-dependent energy levels for each donor or acceptor, respectively. Under most experimental conditions, however, one can only distinguish between energy levels assigned to impurity atoms at c-sites and energy levels caused by impurity atoms at h-sites. Impurity atoms at c-sites generally exhibit deeper levels than those at h-sites.

A. Donor levels

Impurity	E_b [meV]	T [K]	Remarks	Ref.
N	53.6(5)	6	3C, photoluminescence	77D1
	56.5	4	3C, photoluminescence	76K
	66	4	4H, h-site, luminescence of donor-acceptor pairs	80I
	124	4	4H, c-site, luminescence of donor-acceptor pairs	80I
	55(7)	77	4H, photoluminescence	77S
	95	60···1000	6H, $n_d = 5 \cdot 10^{16} cm^{-3}$; evaluation of Hall data; $n(T)$	70H
	100	4	6H, h-site, luminescence of donor-acceptor pairs	80I
	155	4	6H, c-site, luminescence of donor-acceptor pairs	80I
	52	60···1000	15R, $n_d = 3 \cdot 10^{16} cm^{-3}$; evaluation of Hall data; $n(T)$	70H
	64	4	15R, h-site, luminescence of donor-acceptor pairs	80I
	112	4	15R, c-site, luminescence of donor acceptor pairs	80I

B. Acceptor levels

Impurity	E_b [meV]	T [K]	Remarks	Ref.
Be	320	280···420	6H, photoluminescence	67K
	420	300···1000	6H, temperature dependence of Hall data	68M
	600			
B	735	4	3C, photoluminescence	75K2
	647	77	4H, photoluminescence	80I
	698	77	6H, h-site, photoluminescence	80I
	723	77	6H, c-site, photoluminescence	80I
	666	77	15R, h-site, photoluminescence	80I
	700	77	15R, c-site, photoluminescence	80I

Impurity	E_b[meV]	T[K]	Remarks	Ref.
Al	216	1.8	3C, luminescence of donor-acceptor pairs	70C
	260	77	3C, photoluminescence	68Z
	254	4	3C, luminescence of donor-acceptor pairs	80I
	191	4	4H, luminescence of donor-acceptor pairs	80I
	239	4	6H, h-site, luminescence of donor-acceptor pairs	80I
	249	4	6H, c-site, luminescence of donor-acceptor pairs	80I
	280	160	6H, DLTS	85A
	315	300···1300	6H, $n_a = 5 \cdot 10^{18}\,cm^{-3}$; evaluation of Hall data; $p(T)$	63V
	220	300···1300	6H, $n_a = 2 \cdot 10^{19}\,cm^{-3}$; evaluation of Hall data; $p(T)$	63V
	206	4	15R, h-sites, luminescence of donor-acceptor pairs	80I
	221			
	223	4	15R, c-sites, luminescence of donor-acceptor pairs	80I
	230			
	236			
Ga	343	4	3C, photoluminescence	76K
	267	4	4H, luminescence of donor-acceptor pairs	80I
	317	4	6H, h-site, luminescence of donor-acceptor pairs	80I
	333	4	6H, c-site, luminescence of donor-acceptor pairs	80I
	282	4	15R, h-sites, luminescence of donor-acceptor pairs	80I
	300			
	305	4	15R, c-sites, luminescence of donor-acceptor pairs	80I
	311			
	320			

References for 1.5

60C Chang, H.C., Le May, Ch.Z., Wallace, L.F.: Silicon carbide – a high temperature semiconductor, O'Connor, J.R., Smiltens, J. (eds.), Oxford, London, New York, Paris: Pergamon Press **1960**, p. 496.
60P Philipp, H.R., Taft, E.A.: Silicon Carbide – A High Temperature Semiconductor, J.R. O'Connor and J. Smiltens eds., Pergamon Press, Oxford, London, New York, Paris **1960**, p. 366.
60S Scace, R.I., Slack, G.A.: Silicon Carbide – A High Temperature Semiconductor, J.R. O'Connor and J. Smiltens eds., Pergamon Press, Oxford, London, New York, Paris **1960**, p. 24.
60T Taylor, A., Jones, R.M.: Silicon Carbide – A High Temperature Semiconductor, J.R. O'Connor and J. Smiltjens eds., Pergamon Press, Oxford, London, New York, Paris **1960**, p. 147.
63P Patrick, L., Hamilton, D.R., Choyke, W.J.: Phys. Rev. **132** (1963) 2023.
63V Van Daal, H.J., Knippenberg, W.F., Wasscher, J.D.: J. Phys. Chem. Solids **24** (1983) 109.
64C Choyke, W.J., Patrick, L., Hamilton, D.R.: Proc. 7th Int. Conf. Semicond., Paris 1964, M. Hulin ed., Dunod, Paris **1964**, p. 751.
64S Slack, G.A.: J. Appl. Phys. **35** (1964) 3460.
64Z Zanmarchi, G.: Proc. 7th Int. Conf. Semicond., Paris 1964, M. Hulin ed., Dunod, Paris **1964**, p. 57.
65A Arlt, G., Schodder, G.R.: J. Acoust. Soc. Am. **37** (1965) 384.
65D Dalven, R.: J. Phys. Chem. Solids **26** (1965) 439.
65S Scace, R.I., Slack, G.A.: J. Chem. Phys. **42** (1965) 805.
66K Kroko, L.J., Milnes, A.G.: Solid-State Electron. **9** (1966) 1125.
66N Nelson, W.E., Holder, F.A., Rosenbloom, A.: J. Appl. Phys. **37** (1966) 333.
66P Patrick, L., Hamilton, D.R., Choyke, W.J.: Phys. Rev. **143** (1966) 526.
66V Vodakov, Yu.A., Mokhov, E.N., Reifman, M.B.: Sov. Phys.-Solid State **8** (1966) 1040.
67B Barrett, D.L., Campbell, R.B.: J. Appl. Phys. **38** (1967) 53.
67E Ellis, B., Moss, T.S.: Proc. Royal Soc. (London) **A299** (1967) 383, 393.
67G Gomes de Mesquita, A.H.: Acta Crystallogr. **23** (1967) 610.
67K Kalnin, A.A., Pasynkov, V.V., Tairov, Y.M., Yaskov, D.A.: Sov. Phys.-Solid State **8** (1967) 2381.
68C Choyke, W.J.: Mater. Res. Bull. **4** (1969) S 141.
68F Feldman, D.W., Parker, J.H., Choyke, W.J., Patrick, L.: Phys. Rev. **173** (1968) 787.
68M Maslakovets, Yu.P., Mokhov, E.N., Vodakov, Yu.A., Lomakina, G.A.: Sov. Phys.-Solid State **10** (1968) 634.
68Z Zanmarchi, G.: J. Phys. Chem. Solids **29** (1968) 1727.
69K Kern, E.L., Hamill, D.W., Deem, H.W., Sheets, H.D.: Mater. Res. Bull. **4** (1969) 25.
69M Mokhov, E.N., Vodakov, Yu.A., Lomakina, G.A.: Sov. Phys. Solid-State **11** (1969) 415.

69S Shaffer, P.T.B., Naum, R.G.: J. Opt. Soc. Am. **59** (1969) 1498.
70C Choyke, W.J., Patrick, L.: Phys. Rev. **B2** (1970) 4959.
70H Hagen, S.H., Kapteyns, C.J.: Philips Res. Repts. **25** (1970) 1.
70P Patrick, L., Choyke, W.J.: Phys. Rev. **B2** (1970) 2255.
72P Powell, J.A.: J. Opt. Soc. Am. **62** (1972) 341.
74H Hemstreet, L.A., Fong, C.Y.: Silicon Carbide – 1973, R.C. Marshall, J.W. Faust, C.E. Ryan eds., Univ. of South Carolina Press, Columbia, S.C. **1974**, p. 284.
74V Vodakov, Yu.A., Mokhov, E.N.: Silicon Carbide, 1973, Marshall, R.C., Faust, J.W., Ryan, C.E. (eds.), Columbia, S.C.: University of South Carolina Press **1974**, p. 508.
75K1 Kunc, K., Balkanski, M., Nusimovici, M.A.: Phys. Status Solidi (b) **72** (1975) 229.
75K2 Kuwabara, H., Yamada, S.: Phys. Status Solidi **A30** (1975) 739.
75S Slack, G.A., Bartram, S.F.: J. Appl. Phys. **46** (1975) 89.
76K Kuwabara, H., Yamanaka, K., Yamada, S.: Phys. Status Solidi **A37** (1976) K 157.
77D1 Dean, P.J., Choyke, W.J., Patrick, L.: J. Lumin. **15** (1977) 299.
77D2 Dubrovskii, G.B., Lepneva, A.A.: Sov. Phys. Solid State (English Transl.) **19** (1977) 729; Fiz. Tverd. Tela **19** (1977) 1252.
77S Suzuki, A., Matsunami, H., Tanaka, T.: J. Electrochem. Soc. **124** (1977) 241.
77T Tairov, Y.M., Vodakov, Y.A.: Topics in Applied Physics, vol. 17: Electroluminescence, Pankove, J.I. (ed.), Berlin, Heidelberg, New York: Springer-Verlag **1977**, p. 31.
79R Ravindra, N.M., Srivastava, V.K.: Phys. Chem. Solids **40** (1979) 791.
80I Ikeda, M., Matsunami, H., Tanaka, T.: Phys. Rev. **B22** (1980) 2842.
81B Bimberg, D., Altarelli, M., Lipari, N.O.: Solid State Commun. **40** (1981) 437.
81H Humphreys, R.G., Bimberg, D., Choyke, W.J.: Solid State Commun. **39** (1981) 163.
82K Kushawa, M.S.: Phys. Status Solidi (b) **111** (1982) 337.
82L Lee, D.H., Joannopoulos, J.D.: Phys. Rev. Lett. **48** (1982) 1846.
82O1 Olego, D., Cardona, M., Vogl, P.: Phys. Rev. **B25** (1982) 3878.
82O2 Olego, D., Cardona, M.: Phys. Rev. **B25** (1982) 1151.
82T Tajima, Y., Kijima, K., Kingery, W.D.: J. Chem. Phys. **77** (1982) 2592.
83N Nishino, S., Powell, J.A., Will, H.A.: Appl. Phys. Lett. **42** (1983) 460.
84G Gorban', I.S., Gubanov, V.A., Lysenko, V.G., Pletyushkin, A.A., Timofeev, V.B.: Sov. Phys. Solid State (English Transl.) **26** (1984) 1385; Fiz. Tverd. Tela **26** (1984) 2282.
84S Sasaki, K., Sakuma, E., Misawa, S., Yoshida, S., Gonda, S.: Appl. Phys. Lett. **45** (1984) 72.
85A Anikin, M.M., Lebedev, A.A., Syrkin, A.L., Suvorov, A.V.: Sov. Phys.-Semicond. **19** (1985) 69.
85K Kaplan, R., Wagner, R.J., Kim, H.J., Davis, R.F.: Solid State Commun. **55** (1985) 67.

Physical property	Numerical value	Experimental conditions	Experimental method, remarks	Ref.

1.6 Silicon germanium alloys (Si_xGe_{1-x})

Silicon and germanium form a continuous series of solid solutions with gradually varying parameters.

The *band structure* shows a cross-over in the lowest conduction band edge from Ge-like [111] symmetry to Si-like [100] symmetry at $x \approx 0.15$ (Fig. 1). According to [83K] this value should lie a little bit higher ($x \cong 0.25$).

Compositional dependence of band gaps (calculated):

$E_g(\Gamma - X)$	$0.8941 + 0.0421\,x + 0.1691\,x^2$	85K
$E_g(\Gamma - L)$	$0.7596 + 1.0860\,x + 0.3306\,x^2$	

Transport properties have been mostly investigated on single crystals. The mobility is influenced by alloy scattering which contributes according to $\mu_{alloy} \propto T^{0.8}\,x^{-1}(1-x)^{-1}$. Near the band crossover ($x \approx 0.15$) intervalley scattering has to be taken into account.

Figures on transport properties: Figs. 2 ··· 5.

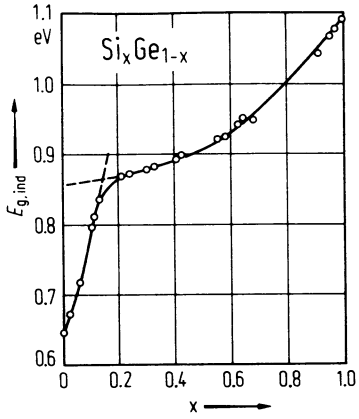

Fig. 1. Si_xGe_{1-x}. Compositional dependence of the indirect energy gap at 296 K based on a one-phonon analysis of the absorption edge. At about x = 0.15 a crossover occurs of the Ge-like [111] conduction band minima and the Si-like [100] conduction band minima [58B].

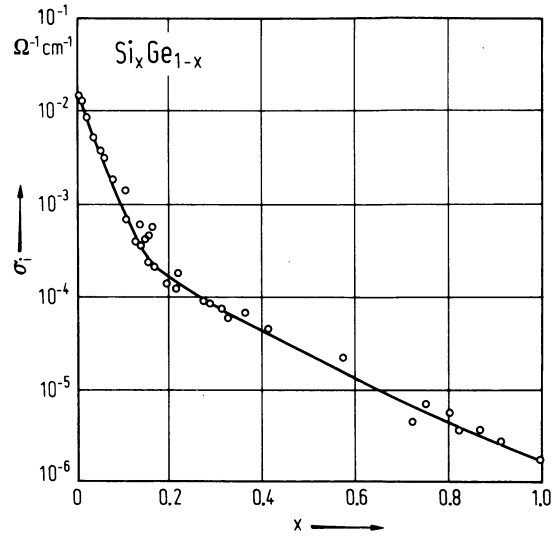

Fig. 2. Si_xGe_{1-x}. Composition dependence of the intrinsic conductivity at room temperature [60B].

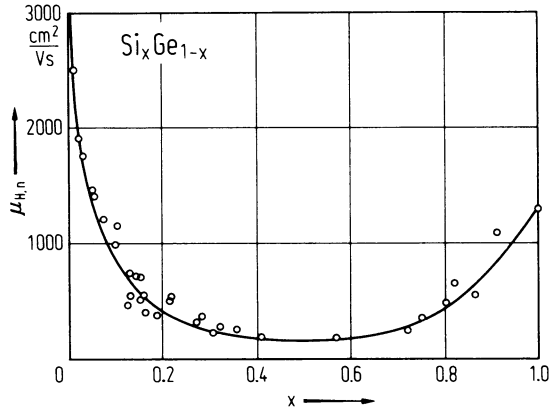

Fig. 3. Si_xGe_{1-x}. Composition dependence of the electron Hall mobility at room temperature [60B].

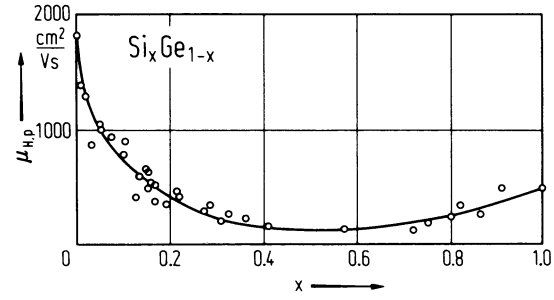

Fig. 5. Si_xGe_{1-x}. Composition dependence of the hole Hall mobility at room temperature [60B].

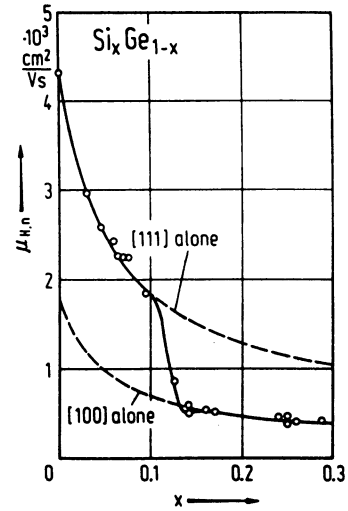

Fig. 4. Si_xGe_{1-x}. Composition dependence of the electron Hall mobility for $x < 0.3$. The dashed curves show the calculated mobilities for electrons in [100]- and [111]-valleys. The solid curve takes both types of valleys into account and includes an arbitrary form of intervalley scattering [58G].

References for 1.6

58B Braunstein, R., Moore, A.R., Herman, F.: Phys. Rev. **109** (1958) 695.
58G Glicksman, M.: Phys. Rev. **111** (1958) 125.
60B Busch, G., Vogt, O.: Helv. Phys. Acta **33** (1960) 437.
83K Kustov, E.F., Mel'nikov, E.A., Sutchenkov, A.A., Levadnii, A.I., Filikov, V.A.: Sov. Phys. Semicond. (English Transl.) **17** (1983) 481; Fiz. Tekh. Poluprovodn. **17** (1983) 769.
85K Krishnamurti, S., Sher, A., Chen, A.: Appl. Phys. Lett. **47** (1985) 160.

2 III–V compounds

Physical property	Numerical value	Experimental conditions	Experimental method, remarks	Ref.

2.1 Boron nitride (BN)

Boron nitride crystallizes in three modifications: BN_{cub} (cubic BN, zincblende structure), BN_{hex} (hexagonal BN) and BN_w (wurtzite structure). BN_{hex} is stable under normal conditions, BN_{cub} is metastable under normal conditions. The BN_w phase is metastable under all conditions.

2.1.A Cubic boron nitride

Electronic properties

All **band structure** calculations lead to an indirect gap structure, the conduction band minima being situated at X. Fig. 1 shows two recent calculations. (Brillouin zone: Fig. 2 of section 1.1.)

energy gaps (in eV):

$E_{g,ind}$ ($\Gamma_{15v} - X_{1c}$)	6.4(5)	RT	ultraviolet absorption; other literature data lie in the range 6···8 eV	74C
	6.99		calculated, Fig. 1b	85H
	8.6		calculated, Fig. 1a	84P
$E_{g,dir}$	14.5	RT	reflectivity	62P
($\Gamma_{15v} - \Gamma_{1c}$)	10.86		calculated, Fig. 1a	84P
	9.94		calculated, Fig. 1b	85H

effective masses (in units of m_0):

m_n	0.752		calculated from band structure data	85H
$m_{p,h}$	0.375	∥[100]		
	0.926	∥[111]		
$m_{p,l}$	0.150	∥[100]		
	0.108	∥[111]		

Lattice properties

lattice parameter:

a	3.6157(10) Å		X-ray	74S

melting point:

T_m	2973 °C			57W

density:

d	3.4870 g cm^{-3}		X-ray	74S

phonon wavenumbers:

$\bar{\nu}_{LO}$	1305(1) cm^{-1}	RT	Raman scattering	83S1
$\bar{\nu}_{TO}$	1054.7(6) cm^{-1}			

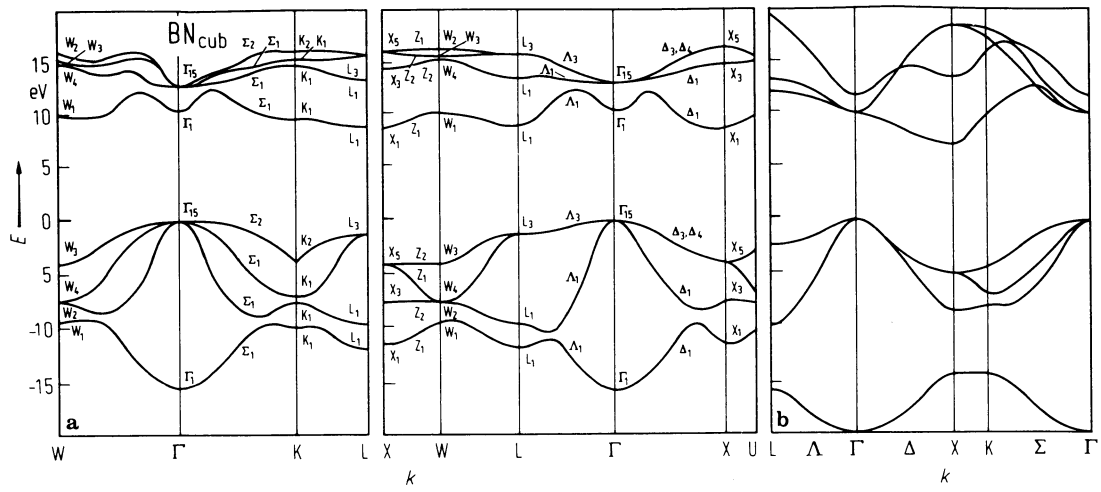

Fig. 1. BN, cubic. Band structure calculated with the LCAO-method, (a) including ionicity and fitting of APW results at high symmetry points [84P], (b) ab intitio calculation [84H].

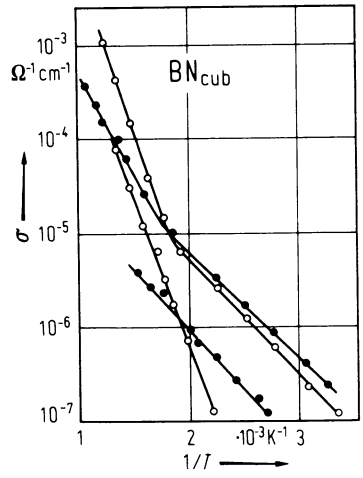

Fig. 2. BN_{cub}. Electrical conductivity vs. reciprocal temperature for different polycrystalline samples above RT [76B].

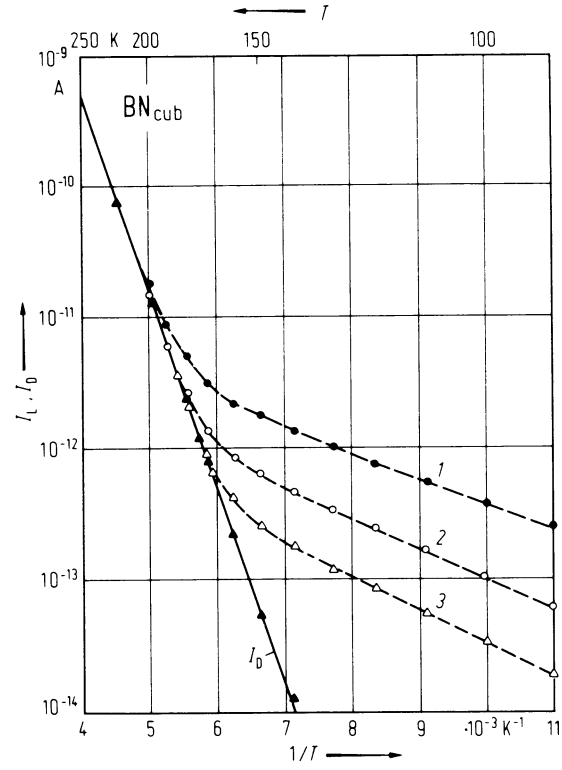

Fig. 3. BN_{cub}. Dark current (I_D) and photocurrent (I_L) at various illuminations (curve 1: $I = I_0$, 2: $I = 0.13\ I_0$, 3: $I = 0.01\ I_0$) vs. temperature for a small undoped single crystal [75H].

Physical property	Numerical value	Experimental conditions	Experimental method, remarks	Ref.
second order elastic moduli:				
c_{11}	7.120 $\cdot 10^{12}$ dyn cm^{-2}	$T = 300$ K	interpolated from measured values of other III–V compounds	63S

Transport and optical properties

Owing to the large gap all literature data refer to extrinsic conduction. For the temperature dependence of dark conductivity and photoconductivity, see Figs. 2 and 3.

carrier concentration and mobility:				
n	10^{15} cm^{-3}	$T = 500$ K	polycrystalline material, type of carrier not determined	76B
μ	0.2 cm^2/Vs			
n	10^{14} cm^{-3}	900 K	mobility increases exponentially with rising temperature between 500 K and 900 K	
μ	4 cm^2/Vs			
dielectric constants:				
$\varepsilon(0)$	7.1	300 K	infrared reflectivity	67G
$\varepsilon(\infty)$	4.5			
refractive index:				
n	2.117	300 K, $\lambda = 0.589$ μm		67G

2.1.B Hexagonal boron nitride

Electronic properties

band structure: Fig. 4, Brillouin zone: Fig. 5.

A recent band structure calculation taking into account interlayer interaction proposes an indirect gap of 3.9 eV between a valence band maximum at H and a conduction band minimum at M as well as additional interlayer conduction bands with minimum at the zone center [85C].

energy gaps (in eV):				
E_g	5.2 (2)	RT	reflectance, Fig. 4	84H
	3.2 ··· 5.8		range of experimental data discussed in [84H]	
$E_{g,th}$	7.1 (1)		temperature dependence of resistivity	82C

Lattice properties

lattice parameters:				
a	6.6612 Å	297 K		66L
c	2.5040 Å			
decomposition temperature:				
T_{dec}	2600 (100) K			65J
density:				
d	2.18 g cm^{-3}			

phonon dispersion relations: Fig. 6.

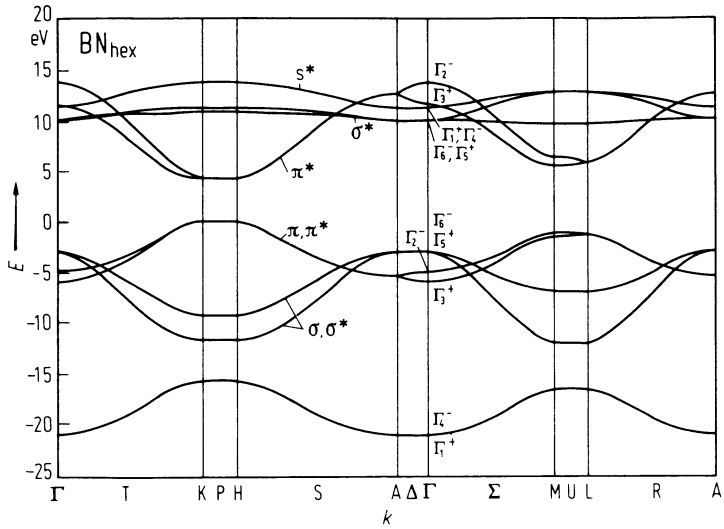

Fig. 4. BN, hexagonal. Band structure calculated with the tight binding method [84R].

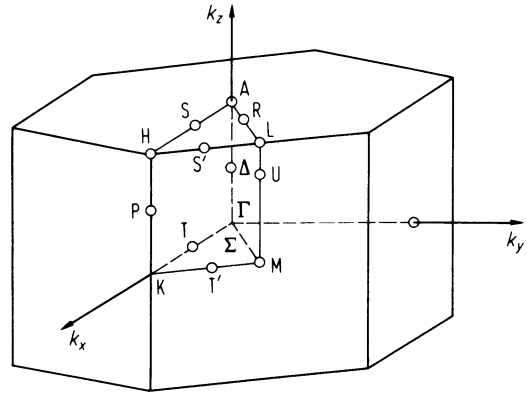

Fig. 5. Brillouin zone of the hexagonal lattice.

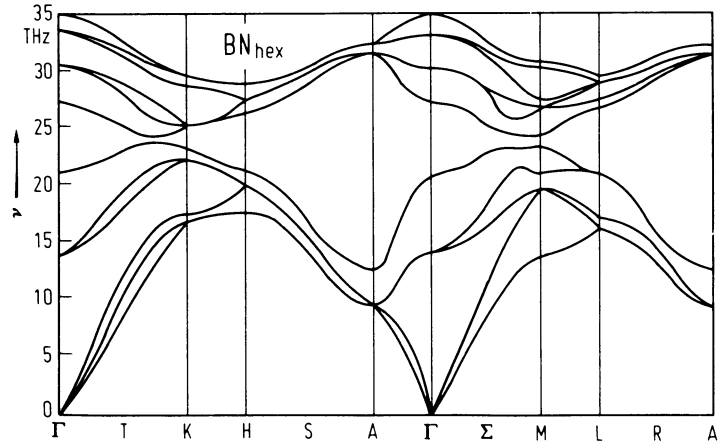

Fig. 6. BN, hexagonal. Phonon dispersion relations calculated with the rigid ion model [83S2].

Physical property	Numerical value	Experimental conditions	Experimental method, remarks	Ref.
phonon wavenumbers (in cm^{-1}):				
$\bar{\nu}$	49	E_{2g}	zone center Raman mode	84H
	770	A_{2u}	infrared active mode	
	1367	E_{2g}	zone center Raman mode	
	1383	E_{1u}	infrared active mode	

Transport and optical properties

Figure 7 shows the temperature dependence of the resistivity at high temperatures and a comparison with earlier literature data.

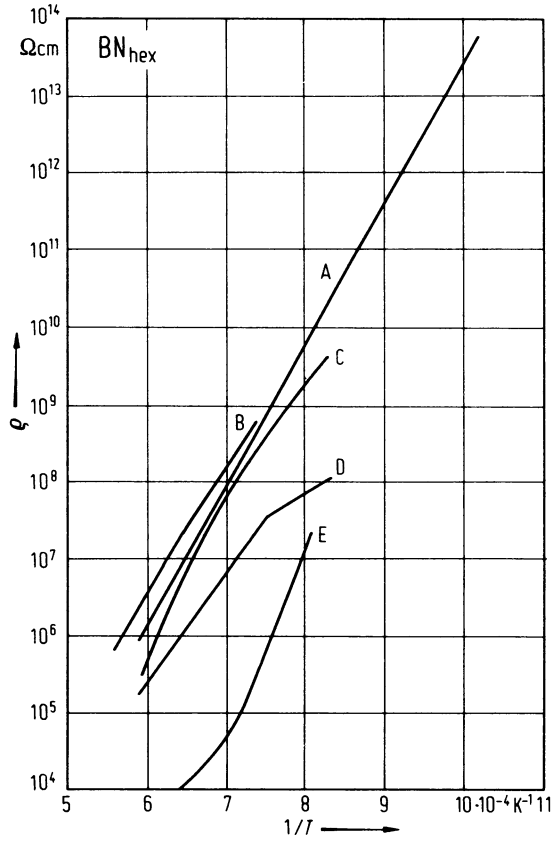

Fig. 7. BN, hexagonal. Resistivity vs. temperature above 700 °C. A: from bulk resistance of a disk measured in c direction. B ··· E: earlier literature data for comparison [82C].

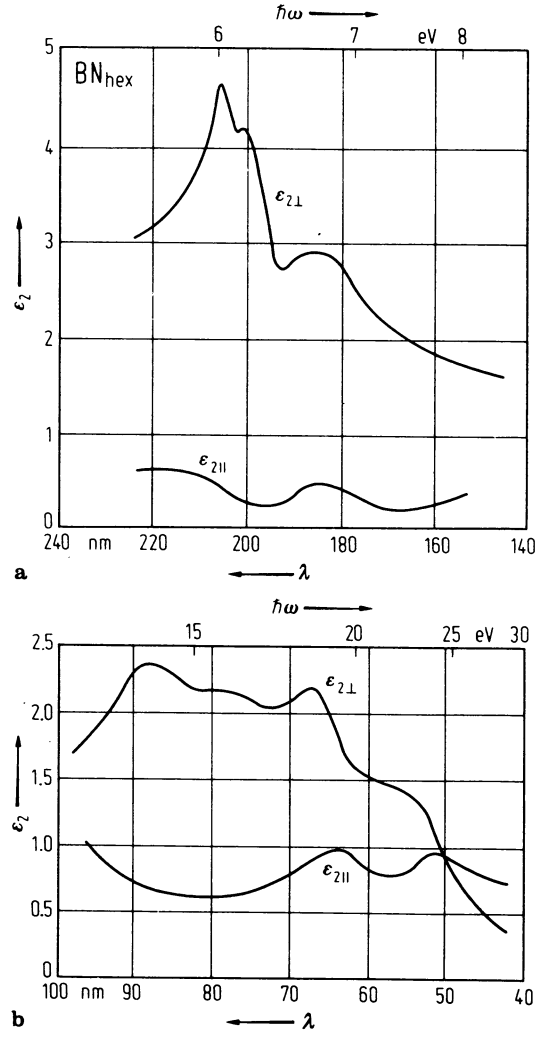

Fig. 8. BN, hexagonal. Ordinary and extraordinary dielectric functions ε_2 vs. wavelength and photon energy in the range 5 ··· 9 eV (a) and 13 ··· 30 eV (b) [81M].

Physical property	Numerical value	Experimental conditions	Experimental method, remarks	Ref.
refractive index:				
n	1.65	BN-film		81T
	1.65		perpendicular to c axis	83I
	2.13		parallel to c axis	
dielectric constants:				
$\varepsilon(0)$	5.06	300K	parallel to c axis	66G
	6.85		perpendicular to c axis	
$\varepsilon(\infty)$	4.10		parallel to c axis	
	4.95		perpendicular to c axis see also Fig. 8	

References for 2.1

57W Wentorf, R.H.: J. Chem. Phys. **26** (1957) 956.
62P Philipp, H.R., Taft, E.A.: Phys. Rev. **127** (1982) 159.
63S Steigmeier, E.F.: Appl. Phys. Lett. **3** (1963) 6.
65J Janaf Thermochemical Tables, US Dept. of Commerce NBS PB 16384 **(1965)**.
66G Geick, R., Perry, C.H., Rupprecht, G.: Phys. Rev. **146** (1966) 543.
66L Lynch, R.W., Drickamer, H.G.: J. Chem. Phys. **44** (1966) 181.
67G Gielisse, P.J., Mitra, S.S., Plendl, J.N., Griffis, R.D., Mansur, L.C., Marshall, R., Pascoe, E.A.: Phys. Rev. **155** (1967) 1039.
74C Chrenko, R.M.: Solid State Commun. **14** (1974) 511.
74S Soma, T., Sawaoka, S., Saito, S.: Mater. Res. Bull. **9** (1974) 755.
75H Halperin, A., Katzir, A.: J. Phys. Chem. Solids **36** (1975) 89.
76B Bam, I.S., Davidenko, V.M., Sidorov, V.G., Fel'dgun, L.I., Skagalov, M.D., Shalabutov, Y.K.: Sov. Phys. Semicond. (English Transl.) **10** (1976) 331; Fiz. Tekh. Poluprov. **10** (1976) 554.
81M Mamy, R., Thomas, J., Jezequel, G., Lemonnier, J.C.: J. Phys. (Paris) Lett. **42** (1981) L-473.
81T Takahashi, T., Itoh, H., Kuroda, M.: J. Cryst. Growth **53** (1981) 418.
82C Carpenter, L.G., Kirby, P.J.: J. Phys. **D15** (1982) 1143.
83I Ishii, T., Sato, T.: J. Cryst. Growth **61** (1983) 689.
83S1 Sanjurjo, J.A., López-Cruz, E., Vogl, P., Cardona, M.: Phys. Rev. **B28** (1983) 4579.
83S2 Sokolovskii, T.D.: Phys. Status Solidi (b) **118** (1983) 493.
84H Hoffmann, D.M., Doll, G.L., Eklund, P.C.: Phys. Rev. **B30** (1984) 6051.
84P Prasad, C., Dubey, J.D.: Phys. Status Solidi (b) **125** (1984) 625.
84R Robertson, J.: Phys. Rev. **B29** (1984) 2131.
85C Catellani, A., Posternak, M., Baldereschi, A., Jansen, H.J.F., Freeman, A.J.: Phys. Rev. **B32** (1985) 6997.
85H Huang, M., Ching, W.Y.: J. Phys. Chem. Solids **46** (1985) 977.

2.2 Boron phosphide (BP)

Electronic properties

band structure: Fig. 1 (Brillouin zone: Fig. 2 of section 1.1)

BP seems to be an indirect gap semiconductor. The maximum of the valence band is situated at the Γ point of the Brillouin zone. The conduction band minima are according to [72H] at the X points. According to [85H] minima at Γ, L and along the Δ axes occur within an energy range of 0.04 eV.

energy gap (in eV):

E_g	2.4	RT	analysis of diffuse reflection coefficient	83K
	2.2	Γ–X	calculated, Fig. 1	72H
	1.98	Γ–L	calculated, followed by minima along Δ (1.99 eV) and at Γ (2.02 eV)	85H

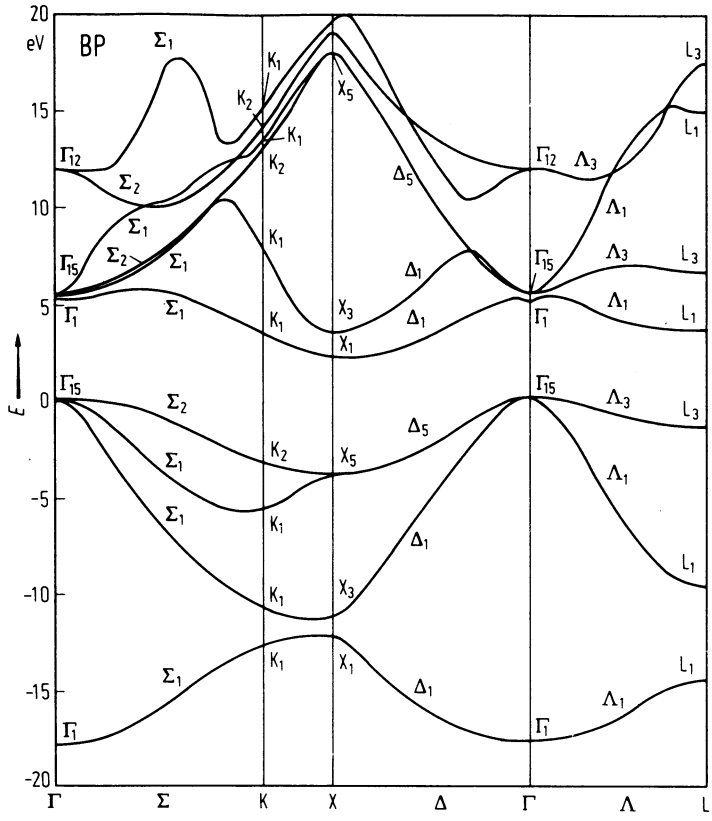

Fig. 1. BP. Band structure calculated by a non-local empirical pseudopotential method [72H].

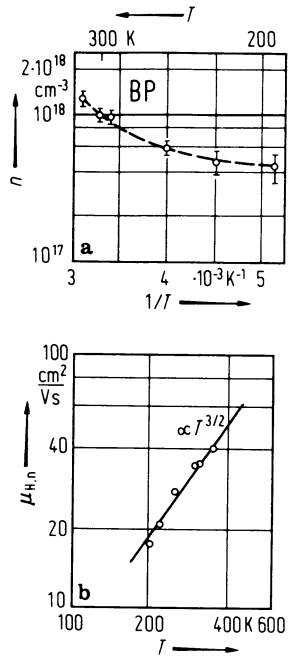

Fig. 2. BP. Electrical conductivity vs. temperature for five n-type samples [80Y].

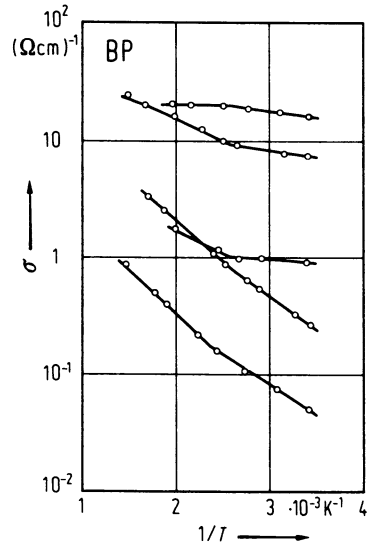

Fig. 3. BP. Electron concentration (a) and electron Hall mobility (b) vs. temperature for a single crystal [77K].

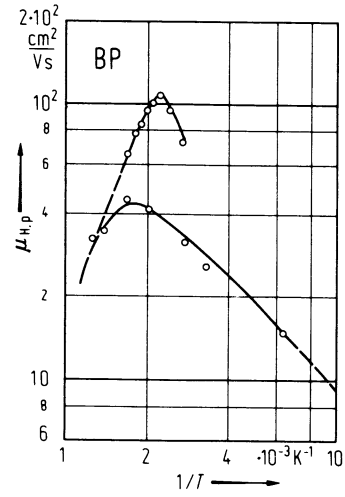

Fig. 4. BP. Hole Hall mobility vs. reciprocal temperature of two p-type single crystals with $p = 1 \cdots 5 \cdot 10^{18}\,cm^{-3}$ [60S].

Physical property	Numerical value	Experimental conditions	Experimental method, remarks	Ref.
Lattice properties				
structure: zincblende, space group T_d^2-F$\bar{4}$3m				
lattice parameter:				
a	4.5383(4) Å	297 K		75S
linear thermal expansion coefficient:				
α	$3.65 \cdot 10^{-6}\,K^{-1}$	400 K		75S
melting point: BP decomposes at 1400 K				
phonon wavenumbers:				
$\bar{\nu}_{LO}$	828.9(6) cm^{-1}	RT	Raman scattering	83S
$\bar{\nu}_{TO}$	799(1) cm^{-1}			
second order elastic moduli (in 10^{12} dyn cm^{-2}):				
c_{11}	5.15(1)	RT	Brillouin scattering	84W
c_{12}	1.0(1)			
c_{44}	1.60(5)			
Transport and optical properties				
BP is extrinsic at RT, the transport limited by impurity scattering. Fig. 2 shows typical conductivity vs. temperature curves.				
mobilities (in cm^2/Vs):				
μ_n	30 ··· 40	$T = 300$ K	single crystals, $n = 10^{18}\,cm^{-3}$	75I, 77K
	70 ··· 120		epitaxial films on Si, $n = 6 \cdot 10^{18} \cdots 2 \cdot 10^{21}\,cm^{-3}$ temperature dependence of electron mobility: Fig. 3	74S
μ_p	500	$T = 300$ K	single crystal, $p = 10^{18}\,cm^{-3}$	64W
	285 ··· 350		epitaxial layers on Si, $p = 5 \cdots 8 \cdot 10^{19}\,cm^{-3}$; temperature dependence of hole mobility: Fig. 4	74S
refractive index:				
n	3.34(5)	$\lambda = 454.5$ nm, RT	Brewster angle method	84W
	3.34(5)	458 nm		
	3.32(5)	488 nm		
	3.30(5)	496 nm		
	3.26(5)	514.5 nm		
	3.00(5)	632.8 nm		
	3.1	589.3 nm	reflectance	76T
dielectric constant:				
$\varepsilon(0)$	11	300 K	Schottky barrier reflectance	76T

References for 2.2

60S Stone, B., Hill, D.: Phys. Rev. Lett. **4** (1960) 282.
64W Wang, C.C., Cardona, M., Fischer, A.G.: RCA Review **25** (1964) 159.
71I Iwami, M., Fujita, N., Kawabe, K.: Jpn. J. Appl. Phys. **10** (1971) 1746.
72H Hemstreet, L.A., Fong, C.Y.: Phys. Rev. **B6** (1972) 1464.
74S Sohno, K., Takigawa, M., Nakada, T.: J. Cryst. Growth **24/25** (1974) 193.
75S Slack, G.A., Bartram, S.F.: J. Appl. Phys. **46** (1975) 89.
76T Takenaka, T., Takigawa, M., Sohno, K.: Jpn. J. Appl. Phys. **15** (1976) 2021.
77K Kato, N., Kamura, W., Iwami, M., Kawabe, K.: Jpn. J. Appl. Phys. **16** (1977) 1623.
80Y Yugo, S., Kimura, T.: Phys. Status Solidi (a) **59** (1980) 363.
83K Kurbatov, G.A., Sidorin, V.K., Sidorin, K.K., Sheludchenko, A.M.: Sov. Phys. Semicond. (English Transl.) **17** (1983) 746; Fiz. Tekh. Poluprovodn. **17** (1983) 1180.
83S Sanjurjo, J.A., López-Cruz, E., Vogl, P., Cardona, M.: Phys. Rev. **B28** (1983) 4579.
84W Wettling, W., Windsøhleif, J.: Solid State Commun. **50** (1984) 33.
85H Huang, M., Ching, W.Y.: J. Phys. Chem. Solids **46** (1985) 977.

Physical property	Numerical value	Experimental conditions	Experimental method, remarks	Ref.

2.3 Boron arsenide (BAs)

In the presence of As vapor the phase is stable up to 920 °C [65E], then decomposes into an orthorhombic subarsenide (B_6As).

band structure: Fig. 1 (Brillouin zone, see Fig. 2 of section 1.1). The calculated band structure shows an indirect (Γ–X) gap of a few eV. Experiments on this layers [74C] can be interpreted by a very small indirect gap (0.67 eV) or more probably by a direct gap of 1.46 eV. This latter result is consistent with earlier measurements [58P].

There is almost no further information about semiconducting properties of BAs.

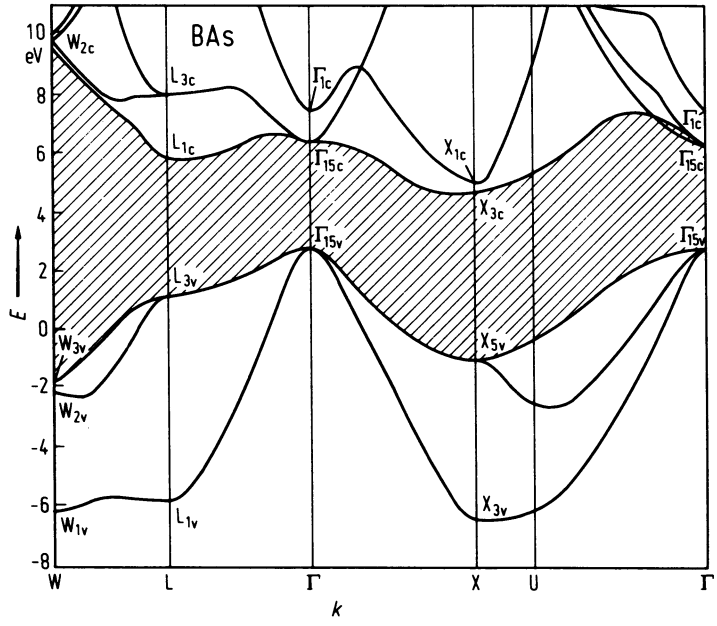

Fig. 1. BAs. Band structure calculated with a combined self-consistent OPW and pseudopotential method [70S].

Physical property	Numerical value	Experimental conditions	Experimental method, remarks	Ref.
lattice parameter:				
a	4.777 Å			77M
density:				
d	5.22 g cm^{-3}			77M

References for 2.3

58P Perri, A., LaPlaca, S., Post, B.: Acta Crystallogr. **11** (1958) 310.
65E Elliott, R.P.: Constitution of binary alloys, first suppl., McGraw Hill, New York 1965.
70S Stuckel, D.J.: Phys. Rev. **B1** (1970) 3458.
77M Merrill, L.: J. Phys. Chem. Ref. Data **6** (1977) 1205.

2.4 Aluminum nitride (AlN)

Electronic properties

band structure: Fig. 1 (Brillouin zone: Fig. 5 of section 2.1)

AlN is a semiconductor with a large direct gap. Since it crystallizes in the wurtzite lattice the band structure differs from that of the most other III–V compounds.

energies of symmetry points of the band structure (relative to the top of the valence band) (in eV):

$E(\Gamma_{1v})$	−18.40 (−14.43)	calculated, see Fig. 1 (data in brackets: [85H])	83K
$E(\Gamma_{3v})$	−7.10 (−4.68)		
$E(\Gamma_{5v})$	−1.22 (−0.60)		
$E(\Gamma_{6v}, \Gamma_{1'v})$	0.00		
$E(\Gamma_{1c})$	6.2 (6.25)		
$E(\Gamma_{3c})$	8.92 (9.38)		
$E(\Gamma_{6c}, \Gamma_{1'c})$	13.0		
$E(L_{1'3'v})$	−7.52 (−4.26)		
$E(L_{24v})$	−1.97 (−1.06)		
$E(L_{13v})$	−1.87 (−1.03)		
$E(L_{13c})$	9.99 (9.40)		
$E(L_{1'3'c})$	13.53		

energy gap (in eV):

$E_{g,dir}$	6.2	300 K	absorption (excitonic contribution near direct edge)	79Y
	6.23	77 K		
	6.28	300 K	from excitonic edge assuming exciton binding energy of 75 meV	80R

From the dichroism of the absorption edge follows that the $\Gamma_{1'}$ state (see Fig. 1) lies slightly higher than the Γ_6 state (transition $E \| c$ ($\Gamma_{1'v} - \Gamma_{1c}$) at lower energy than transition $E \perp c$ ($\Gamma_{6v} - \Gamma_{1c}$)), both states being split by crystal field interaction [79Y].

Lattice properties

AlN crystallizes at normal pressure in the wurtzite structure (space group $C_{6v}^4 - P6_3mc$). A phase transition at 21(1) GPa (tentatively to a NaCl phase) has been measured by shock compression [81K].

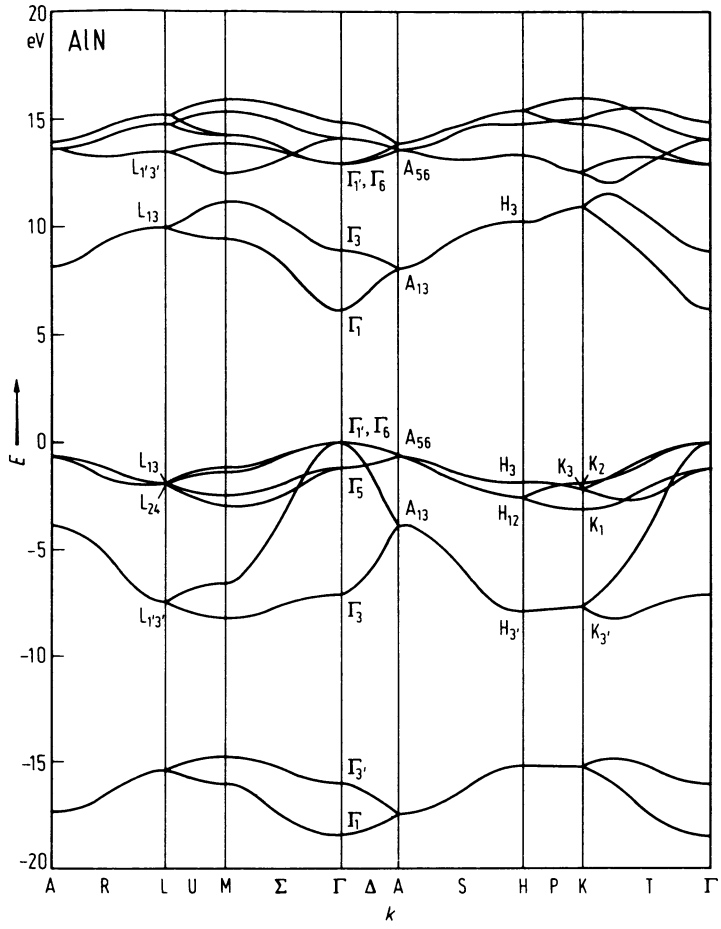

Fig. 1. AlN. Band structure calculated with a semi-empirical tight binding method [83K].

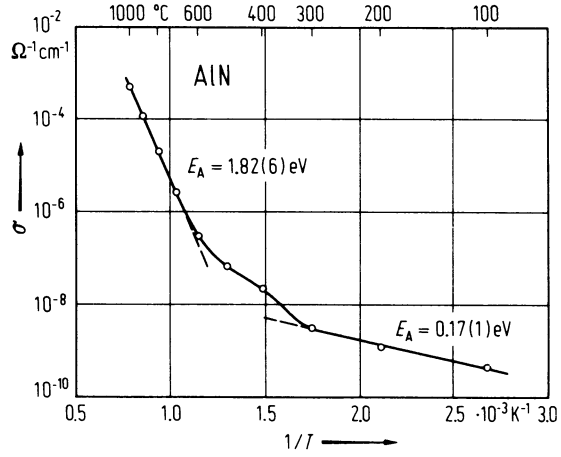

Fig. 2. AlN. Conductivity vs. reciprocal temperature for hot-pressed material [76F]. E_A: activation energy for conductivity.

Physical property	Numerical value	Experimental conditions	Experimental method, remarks	Ref.
lattice parameters:				
a	3.11(1) Å	RT	X-ray diffraction on ultrafine powder	82I
c	4.98(1) Å			
linear thermal expansion coefficient:				
$\alpha_\perp$	$5.27 \cdot 10^{-6}\,K^{-1}$	$T = 20 \cdots 800\,°C$	X-ray, epitaxial layers	74S
$\alpha_\parallel$	$4.15 \cdot 10^{-6}\,K^{-1}$			
melting point:				
T_m	3273 K			70M
density:				
d	$3.255\,g\,cm^{-3}$		X-ray	73S
phonon wavenumbers (in cm^{-1}):				
$\bar{\nu}_{LO}(E_1)$	895(2)	RT	Raman scattering	83S
$\bar{\nu}_{TO}(E_1)$	671.6(8)			
$\bar{\nu}_{LO}(A_1)$	888(2)			
$\bar{\nu}_{TO}(A_1)$	659.3(6)			
$\bar{\nu}(E_2)$	303		Raman scattering, tentative assignment	84C
$\bar{\nu}(E_2)$	426			
$\bar{\nu}_{TO}(A_1)$	514			
$\bar{\nu}_{TO}(E_1)$	614			
$\bar{\nu}_{LO}(A_1)$	663			
$\bar{\nu}_{LO}(E_1)$	821			

Transport and optical properties

Owing to the large energy gap, transport is always extrinsic.

conductivity (in $\Omega^{-1}\,cm^{-1}$):				
σ	$10^{-3} \cdots 10^{-5}$	$T = 290$ K	doped (Al_2OC) single p-type crystals (blue)	65E
	$10^{-11} \cdots 10^{-13}$	300 K	undoped single crystals (colorless or pale yellow) see also Fig. 2	
hole mobility:				
μ_p	$14\,cm^2/Vs$	$T = 290$ K	doped single crystal, the authors point out that this result must be viewed with some caution	65E
dielectric constants:				
$\varepsilon(0)$	9.14	300 K	reflectivity	67C
$\varepsilon(\infty)$	4.84			

References for 2.4

65E Edwards, J., Kawabe, K., Stevens, G., Tredgold, R.H.: Solid State Commun. **3** (1965) 99.
67C Collins, A.T., Lightowlers, E.C., Dean, P.J.: Phys. Rev. **158** (1967) 833.

70M MacChesney, J.B., Bridenbaugh, P.M., O'Connor, P.B.: Mater. Res. Bull. **5** (1970) 783.
73S Slack, G.A.: J. Phys. Chem. Solids **34** (1973) 321.
74S Sirota, N.N., Golodushko, V.Z.: Tezisy Dokl., Vses Konf. Khi., Svyazi Poluprovdn. Polumetallakh 5th (1974) 98.
76F Francis, R.W., Worrell, W.L.: J. Electrochem. Soc. **123** (1976) 430.
79Y Yamashita, H., Fukui, K., Misawa, S., Yoshida, S.: J. Appl. Phys. **50** (1979) 896.
80R Roskovcova, L., Pastrnak, J.: Czech. J. Phys. **B30** (1980) 586.
82I Iwama, S., Hayakawa, K., Arizumi, T.: J. Cryst. Growth **56** (1982) 265.
83K Kobayashi, A., Sankey, O.F., Volz, S.M., Dow, J.D.: Phys. Rev. **B28** (1983) 935.
83S Sanjurjo, J.A., López-Cruz, E., Vogl, P., Cardona, M.: Phys. Rev. **B28** (1983) 4579.
84C Carlone, C., Lakin, K.M., Shanks, H.R.: J. Appl. Phys. **55** (1984) 4010.
85H Huang, M.Z., Ching, W.Y.: J. Phys. Chem. Solids **46** (1985) 977.

Physical property	Numerical value	Experimental conditions	Experimental method, remarks	Ref.

2.5 Aluminum phosphide (AlP)

Electronic properties

band structure: Fig. 1 (Brillouin zone: see Fig. 2 of section 1.1)

AlP is an indirect gap semiconductor, the minima of the conduction bands are situated at the X points of the Brillouin zone (no camel's back structure! [85K2]). The top of the valence band has the structure common to all zincblende semiconductors.

energies of symmetry points of the band structure (relative to the top of the valence band) (in eV):

$E(\Gamma_{1v})$	−11.82		calculated, see Fig. 1	85H
$E(\Gamma_{15v})$	0.00			
$E(\Gamma_{1c})$	3.74			
$E(\Gamma_{15c})$	5.09			
$E(X_{5v})$	−2.27			
$E(X_{1c})$	2.51			
$E(X_{3c})$	4.30			
$E(L_{3v})$	−0.80			
$E(L_{1c})$	3.57			

energy gaps (in eV):

$E_{g,ind}$ $(\Gamma_{15v}-X_{1c})$	2.505(10)	4K	excitonic gap, photoluminescence; temperature dependence, see Fig. 2	73M
$E_{g,dir}$ $(\Gamma_{15v}-\Gamma_{1c})$	3.63(2) 3.62(2)	4K 300K	excitonic gap, photoluminescence	73M

effective masses (in units of m_0):

$m_{n\parallel}$	3.67		calculated from band structure of Fig. 1	85H
$m_{n\perp}$	0.212			
$m_{p,h}$	0.513	∥[100]		
	1.372	∥[111]		
$m_{p,l}$	0.211	∥[100]		
	0.145	∥[111]		

Lattice properties

structure:

AlP I	space group $T_d^2-F\bar{4}3m$ (zincblende lattice)	normal pressure phase
AlP II	NaCl structure	high pressure phase

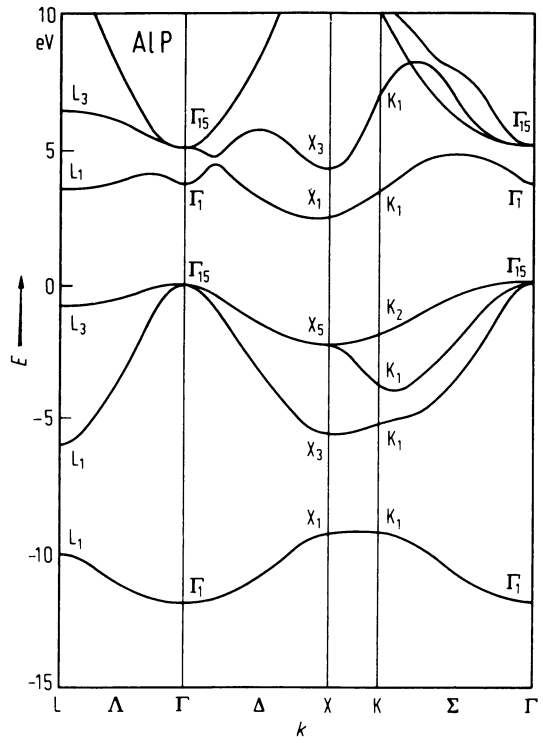

Fig. 1. AlP. Band structure calculated with an orthogonalized LCAO method [85H].

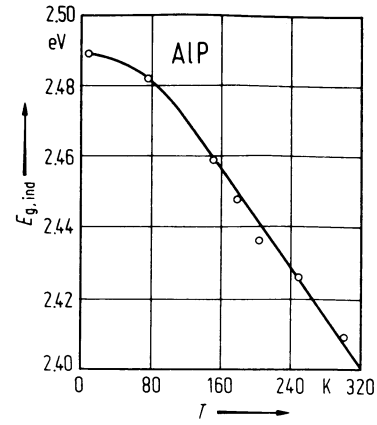

Fig. 2. AlP. Indirect energy gap vs. temperature [70M].

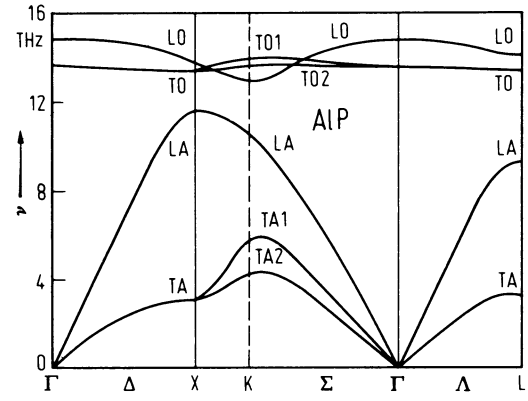

Fig. 3. AlP. Phonon dispersion relations [85K1].

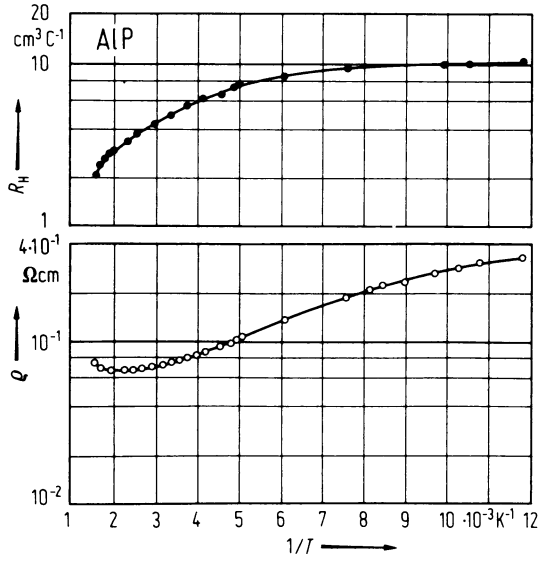

Fig. 4. AlP. Hall coefficient and resistivity vs. reciprocal temperature for an n-type sample [67R].

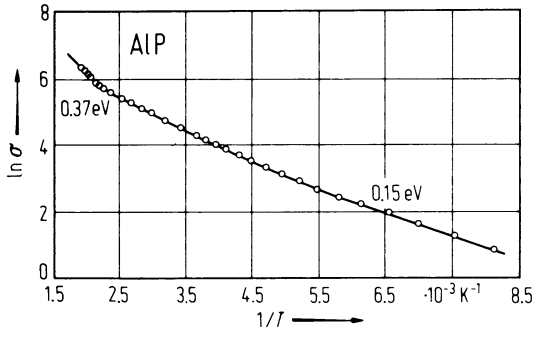

Fig. 5. AlP. Natural logarithm of conductivity vs. reciprocal temperature in an undoped sample [60G]. σ in $\Omega^{-1}\,cm^{-1}$. Activation energies are also shown.

Physical property	Numerical value	Experimental conditions	Experimental method, remarks	Ref.
transition pressure (in kbar):				
p_{tr}	140 ··· 170			78Y
lattice parameter:				
a	5.4635(4) Å	25 °C	epitaxial film on GaP	82B
density:				
d	2.40(1) g cm^{-3}			68C
melting point:				
T_m	2823 K			75O
phonon dispersion relations: Fig. 3.				
phonon wavenumbers:				
$\bar{\nu}_{LO}(\Gamma)$	501.0(2) cm^{-1}	300 K	Raman spectroscopy	70O
$\bar{\nu}_{TO}(\Gamma)$	439.4(2) cm^{-1}			
second order elastic moduli (in 10^{11} dyn cm^{-2}):				
c_{11}	18.83 ··· 14.59		theoretical estimates	85K1
c_{12}	6.71 ··· 8.44			
c_{44}	3.69 ··· 4.24			

Transport and optical properties

electron mobility:				
μ_n	60 cm^2/Vs	$T = 300$ K	thin films	66R
	10 ··· 80 cm^2/Vs	298 K	single crystals, $n = 1.3 \cdot 10^{18} \cdots 5.5 \cdot 10^{19}$ cm^{-3}	67R

The lattice mobility of holes has been estimated to 450 cm^2/Vs [75W]. See Figs. 4 and 5 for further data on transport properties.

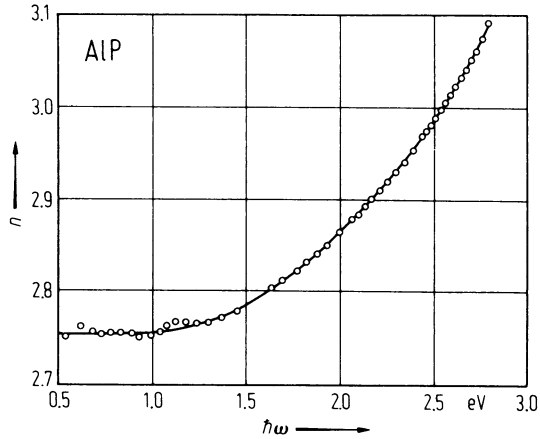

Fig. 6. AlP. Refractive index vs. photon energy at RT [70M].

Physical property	Numerical value	Experimental conditions	Experimental method, remarks	Ref.
thermal conductivity:				
κ	0.9 W cm^{-1} K^{-1}	$T = 300$ K		63S
dielectric constants:				
$\varepsilon(0)$	9.8		from refractive index	70M
$\varepsilon(0)/\varepsilon(\infty)$	1.3		from phonon frequencies	

refractive index: Fig. 6.

Impurities and defects

impurity levels: due to the great instability of AlP in moisture little work on defects has been reported. p-type conduction was found to arise from two acceptor species at $E_v + 0.15$ eV and $E_v + 0.37$ eV [60G]. These defects also seem to be involved in photoluminescence and optical absorption at energies below the band gap.

References for 2.5

60G Grimmeiss, H.G., Kischio, W., Rabenau, A.: Phys. Chem. Solids **16** (1960) 302.
63S Steigmeier, E.F.: Appl. Phys. Lett. **3** (1963) 6.
66R Reid, F.J., Miller, S.E., Goering, H.L.: J. Electrochem. Soc. **113** (1966) 467.
67R Reid, F.J., e.a.: Batelle Memoral. Inst. Ohio, High-Temperature Material Study, NASA CR-86021, June 1967, Contract No. NAS 12-107 N68-14557.
68C Caveney, R.J.: Philos. Mag. **17** (1968) 943.
70M Monemar, B.: Solid State Commun. **8** (1970) 1295.
70O Onton, A.: Proc. 10th Int. Conf. Phys. Semicond., Cambridge/Mass. 1970, USAC, Oak Ridge **1970**.
71L Lawaetz, P.: Phys. Rev. **B4** (1971) 3460.
73M Monemar, B.: Phys. Rev. **B8** (1973) 5711.
75O Osamura, K., Murakami, Y.: J. Phys. Chem. Solids **36** (1975) 1354.
75W Wiley, J.D.: in "Semiconductors and Semimetals", Vol. 10, R.K. Willardson, A.C. Beer eds., Academic Press, New York **1975**.
78Y Yu, S.C., Spain, I.L., Skelton, E.F.: Solid State Commun. **25** (1978) 49.
82B Bessolov, V.N., Konnikov, S.G., Umanskii, V.I. Yakovlev, Yu.P.: Sov. Phys. Solid State (English Transl.) **24** (1982) 875; Fiz. Tverd. Tela **24** (1982) 1528.
85H Huang, M., Ching, W.Y.: J. Phys. Chem. Solids **46** (1985) 977.
85K1 Kagaya, H.-M., Soma, T.: Phys. Status Solidi (b) **127** (1985) 89.
85K2 Kopylov, A.A.: Solid State Commun. **56** (1985) 1.

2.6 Aluminum arsenide (AlAs)

Electronic properties

band structure: Fig. 1 (Brillouin zone: see section 1.1, Fig. 2)

AlAs has a band structure similar to those of AlP or GaP. The minima of the conduction band are situated near the X points of the Brillouin zone.

energies of symmetry points of the band structure (relative to the top of the valence band) (in eV):

$E(\Gamma_{1v})$	-11.95 (-11.87)	calculated: [85H], Fig. 1, (in brackets: [80C])
$E(\Gamma_{15v})$	0.00	
$E(\Gamma_{1c})$	2.79 (2.81)	
$E(\Gamma_{15c})$	4.48 (4.21)	
$E(X_{1v})$	-9.63 (-9.80)	
$E(X_{3v})$	-5.69 (-5.52)	
$E(X_{5v})$	-2.38 (-2.32)	
$E(X_{1c})$	2.37 (2.21)	

Physical property	Numerical value	Experimental conditions	Experimental method, remarks	Ref.
$E(X_{3c})$	3.84 (2.89)			
$E(L_{1v})$	−5.95 (−6.41)			
$E(L_{3v})$	−0.88 (−0.97)			
$E(L_{1c})$	2.81 (2.48)			
$E(L_{3c})$	5.86 (4.87)			
energy gaps (in eV):				
$E_{g,ind}$	2.229(1)	4 K	excitonic gap, photoluminescence	73M
$(\Gamma_{15v} - X_{1c})$	2.223(1)	77 K		
	2.153(2)	300 K		
$E_{g,ind}$	2.363	295 K	transport	80L
$(\Gamma_{15v} - L_{1c})$				
$E_{g,dir}$	3.13(1)	4 K	excitonic gap, photoluminescence	73M
$(\Gamma_{15v} - \Gamma_{1c})$	3.03(1)	300 K		
exciton binding energy:				
E_b	0.0258 eV		calculation including camel's back structure	81B

For the temperature dependence of the indirect and direct energy gap, see Fig. 2.

critical point energies and spin-orbit splitting energies (in eV):

E_0	3.02	300 K	direct gap, see also tables above
$E_0 + \Delta_0$	3.32		data from [70O], assignment
$E_1(1)$	3.83		corrected by [71B] (from a
$E_1(2)$	3.96		compilation in [85A])
$E_1(1) + \Delta_1$	4.03		
$E_1(2) + \Delta_1$	4.16		
E_0'	4.54		
$E_0' + \Delta_0'$	4.69		
E_2	4.89		

camel's back structure of conduction band edge:
A camel's back structure of the bottom of the conduction band near X (see respective table and Fig. 2 of section 2.9) has been proved experimentally [81B].

Δ	411 meV	extrapolated using GaP data	85K
ΔE	0.2 meV		
k_m	$0.042(2\pi/a)$		
m_t	$0.227 m_0$		
$m_\parallel$	$10.7 m_0$		
m_l	$1.56 m_0$	longitudinal mass far above the band minimum (polaron correction included)	

effective masses, electrons (in units of m_0):
from a compilation and discussion of literature data in [85A]

$m_{n\perp}(X)$	0.19	effective masses at X neglecting
$m_{n\parallel}(X)$	1.1	camel's back structure
$m_{n,ds}(X)$	0.71	density of states masses obtained
$m_{n,c}(X)$	0.26	from $m_{ds} = N^{2/3} m_\perp^{2/3} m_\parallel^{1/3}$ with
$m_{n\perp}(L)$	0.0964	N = number of eq. minima

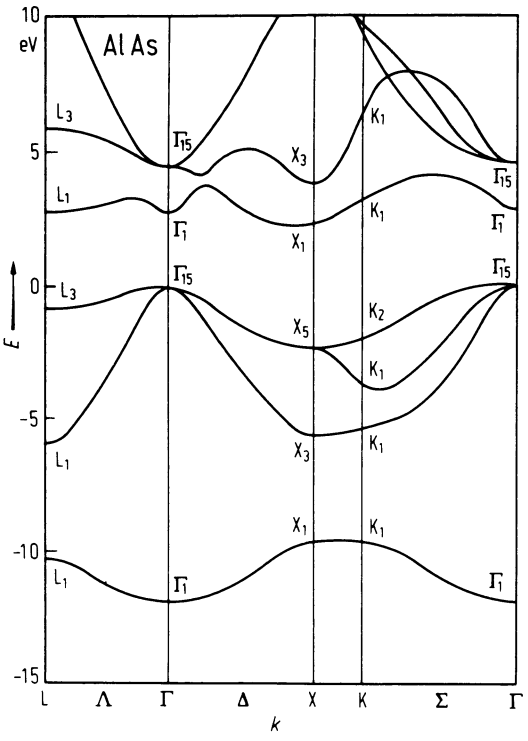

Fig. 1. AlAs. Band structure calculated with an orthogonalized LCAO method [85H].

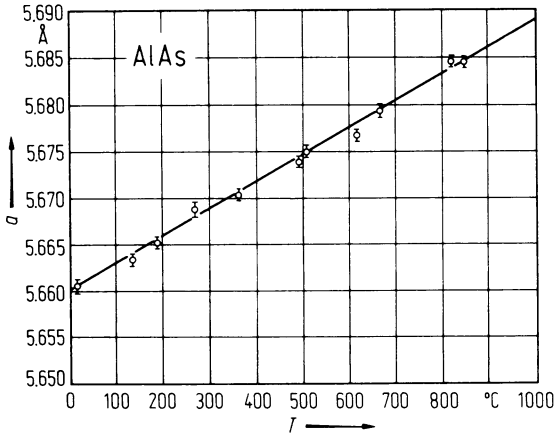

Fig. 3. AlAs. Lattice parameter vs. temperature [70E].

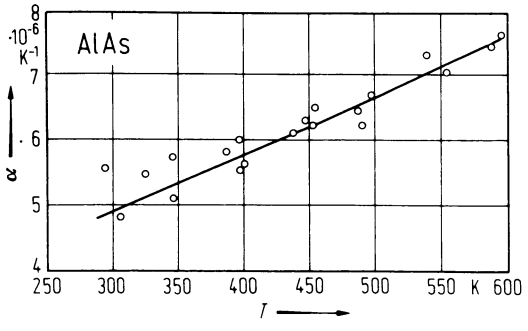

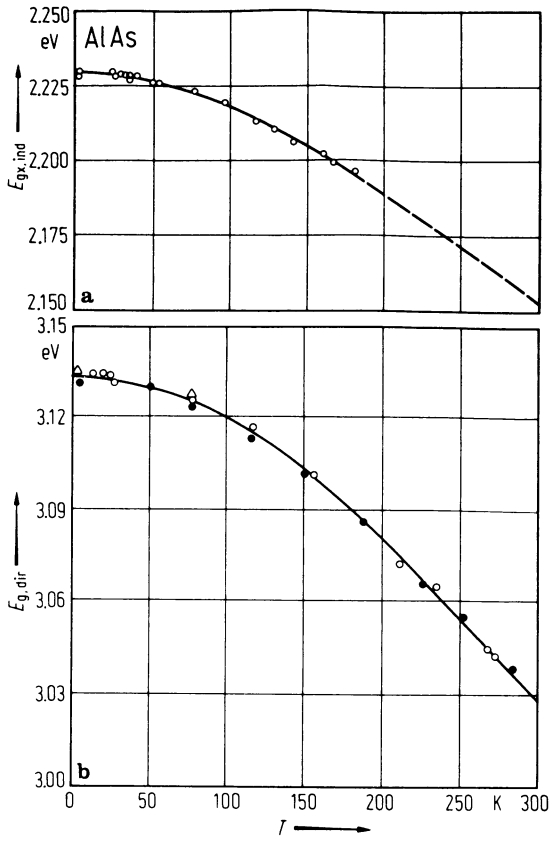

Fig. 2. AlAs. (a). Indirect excitonic gap and (b) direct gap vs. temperature. Due to a high impurity content the curve in (b) is believed to represent an energy a few meV above the excition edge in pure AlAs [73M].

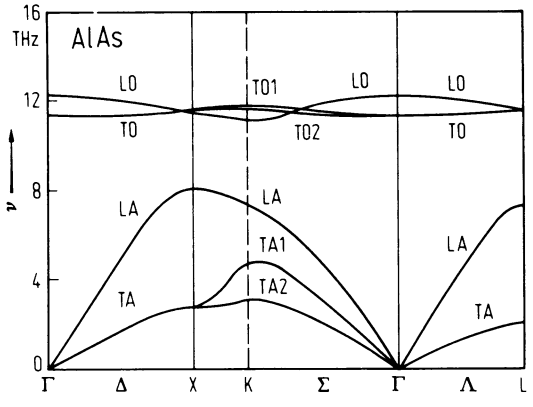

Fig. 5. AlAs. Phonon dispersion relations [83K].

◀

Fig. 4. AlAs. Coefficient of linear thermal expansion vs. temperature above RT [59P].

Physical property	Numerical value	Experimental conditions	Experimental method, remarks	Ref.
$m_{n\perp}(L)$	1.9		conductivity effective mass obtained from $m_c = (2/m_\perp + 1/m_\parallel)^{-1}$	
$m_{n,ds}(L)$	0.66			
$m_{n,c}(L)$	0.14			
$m_n(\Gamma)$	0.150		same values for m_{ds} and m_c	
effective masses, holes (in units of m_0):				
$m_{p,h}$	0.409	∥[100]	calculated from band structure data (see above)	85H
	1.022	∥[111]		
$m_{p,l}$	0.153	∥[100]		
	0.109	∥[111]		
valence band parameters:				
A	−4.03			75W
B	−2.09			
$\|C\|$	4.63			

Lattice properties

structure:
AlAs crystallizes in the zincblende structure (space group T_d^2–F$\bar{4}$3m). A high-pressure phase has not been observed.

lattice parameter:				
a	5.660 Å	291.15 K	for temperature dependence, see Fig. 3 [70E]	67P

coefficient of linear thermal expansion: see Fig. 4.

density:				
d	3.760 g cm^{-3}		calculated from lattice parameter	85A

melting point:				
T_m	2013(20) K			64K

phonon dispersion curves: Fig. 5.

phonon wavenumbers (energies) (in cm^{-1} and meV, respectively):

$\bar{\nu}_{LO}(\Gamma)$	403.7(50.09)
$\bar{\nu}_{TO}(\Gamma)$	361.7(44.88)

second order elastic moduli (in 10^{11} dyn cm^{-2}):

c_{11}	12.02	calculated with an empirical interpolation formula using data from other III–V compounds	85A
c_{12}	5.70		
c_{44}	5.89		

Transport and optical properties

Only few reliable data exist on the transport and optical properties of AlAs. Most results are extrapolations from data obtained on the technologically more important solid solutions of the type $Al_xGa_{1-x}As$.

Electron mobilities have been reported up to 300 cm^2/Vs at RT, hole mobilities should be about 200 cm^2/Vs for pure lattice scattering [75W].

Physical property	Numerical value	Experimental conditions	Experimental method, remarks	Ref.
electron mobility:				
μ_n	$294 \cdots 75\,cm^2/Vs$ $18\,cm^2/Vs$	$T = 300\,K$ $77\,K$	single crystal layers	71E

For temperature dependence of resistivity, carrier concentration and Hall mobility, see Figs. 6 and 7.

dielectric constants:				
$\varepsilon(0)$	10.06(4)			71F
$\varepsilon(\infty)$	8.16(2)			

refractive index: Fig. 8.

Impurities and defects

binding energy of donors (in eV):				
E_b	0.07	$T = 300\,K$	Si-doped sample	70K
	0.06		Zn-doped sample	
	0.05		Mg-doped sample	

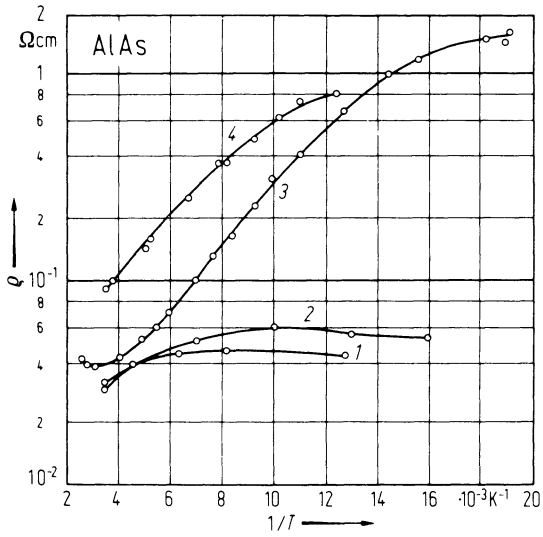

Fig. 6. AlAs. Resistivity vs. reciprocal temperature for four samples [65W].

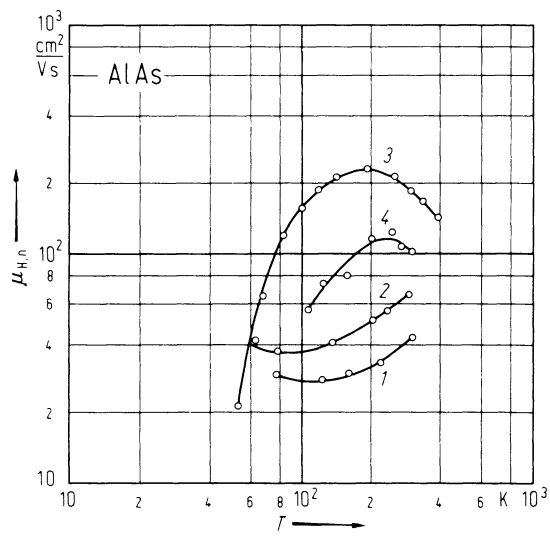

Fig. 7. AlAs. Electron Hall mobilities vs. temperature for the samples of Fig. 6 [65W].

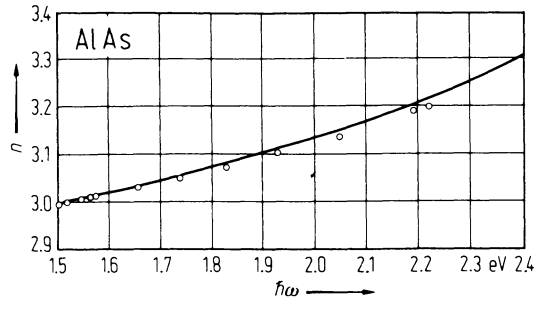

Fig. 8. AlAs. Refractive index vs. photon energy for the range 1.5 ··· 2.4 eV. Data from [71F], solid curve calculated by [85C].

References for 2.6

59P Pashintsev, I.I., Sirota, N.N.: Dokl. Akad. Nauk SSSR **3** (1959) 38.
64K Kischio, W.: Z. Anorg. Allg. Chem. **328** (1964) 187.
65W Whitaker, J.: Solid State Electron. **8** (1965) 649.
67P Pearson, W.B.: A Handbook of Lattice Spacing and Structure of Metals and Alloys, Pergamon Press, Oxford-Landon **1967**.
70E Ettenberg, M., Pfaff, R.J.: J. Appl. Phys. **41** (1970) 3926.
70K Kressel, H., Nicoll, F.H., Ettenberg, M., Yim, W.M., Sigai, A.G.: Solid State Commun. **8** (1970) 1407.
70O Onton, A.: Proc. 10th Int. Conf. Phys. Semicond., Cambridge/Mass. 1970, USAEC, New York **1970**, p. 107.
71B Berninger, W.H., Rediker, R.H.: Bull. Am. Phys. Soc. **16** (1971) 305.
71E Ettenberg, M., Sigai, A.G., Dreeben, A., Gilbert, S.L.: J. Electrochem. Soc. **119** (1971) 1355.
71F Fern, R.E., Onton, A.: J. Appl. Phys. **42** (1971) 3499.
73M Monemar, B.: Phys. Rev. **B8** (1973) 5711.
75W Wiley, J.D.: in "Semiconductors and Semimetals", Vol. 10, R.K. Willardson and A.C. Beer eds., Academic Press, New York and London **1975**.
80C Chen, A., Sher, A.: Phys. Rev. **B22** (1980) 3886.
80L Lee, H.J., Juravel, L.Y., Woolley, J.C., SpringThorpe, A.J.: Phys. Rev. **B21** (1980) 659.
81B Bimberg, D., Bludau, W., Linnebach, R., Bauser, E.: Solid State Commun. **37** (1981) 987.
83K Kagaya, H.-M., Soma, T.: Solid State Commun. **48** (1983) 785.
85A Adachi, S.: J. Appl. Phys. **58** (1985) R1.
85C Campi, D., Papuzza, C.: J. Appl. Phys. **57** (1985) 1305.
85H Huang, M., Ching, W.Y.: J. Phys. Chem. Solids **46** (1985) 977.
85K Kopylov, A.A.: Solid State Commun. **56** (1985) 1.

Physical property	Numerical value	Experimental conditions	Experimental method, remarks	Ref.

2.7 Aluminum antimonide (AlSb)

Electronic properties

band structure: Fig. 1 (Brillouin zone: see section 1.1, Fig. 2)

AlSb is an indirect gap semiconductor with conduction band minima near X. The valence band shows the structure common to all zincblende semiconductors.

energies of symmetry points of the band structure (relative to the top of the valence band) (in eV):

calculated, see Fig. 1				85H
$E(\Gamma_{15v})$	0.00			
$E(\Gamma_{1c})$	2.05			
$E(\Gamma_{15c})$	3.50			
$E(X_{5v})$	−2.31			
$E(X_{1c})$	2.08			
$E(X_{3c})$	3.02			
$E(L_{3v})$	−0.90			
$E(L_{1c})$	1.94			

energy gaps (in eV):
(single group symmetry notation; taking the spin-orbit splitting of the valence band into account, the Γ_{15v}-band corresponds to the upper spin-orbit split Γ_{8v}-band)

$E_{g,ind}$	1.615(3)	300 K	excitonic gap (see Fig. 2),	83A
$(\Gamma_{15v} - \Delta_{1c})$	1.686(1)	27 K	modulation spectroscopy	
$E_{g,ind}$	2.211	295 K	electroreflectance, see Fig. 3	
$(\Gamma_{15v} - L_{1c})$	2.327	35 K	for temperature dependence (critical point E_L)	
$E_{g,dir}$	2.300	295 K	electroreflectance, see Fig. 3	82J
$(\Gamma_{15v} - \Gamma_{1c})$	2.384	25 K	for temperature dependence (critical point E_0)	

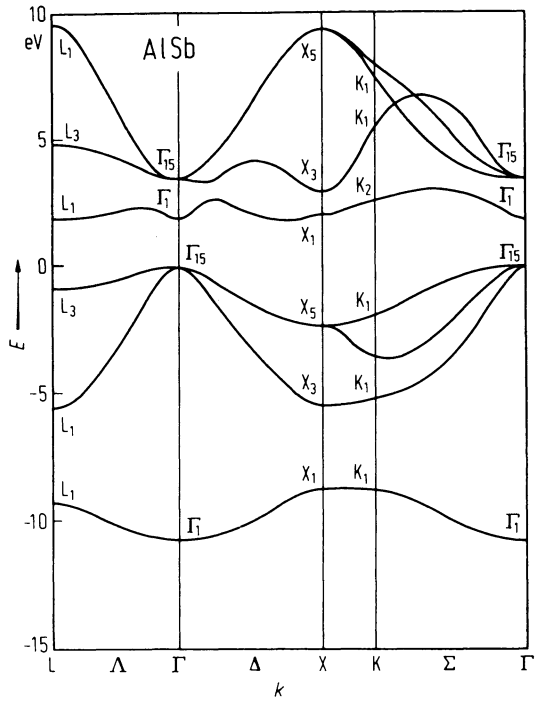

Fig. 1. AlSb. Band structure calculated with an orthogonalized LCAO method [85H].

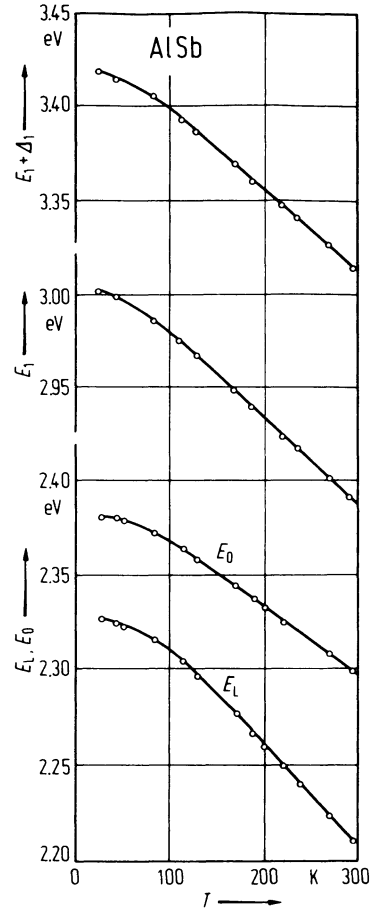

Fig. 3. AlSb. Critical point energies vs. temperature [82J].

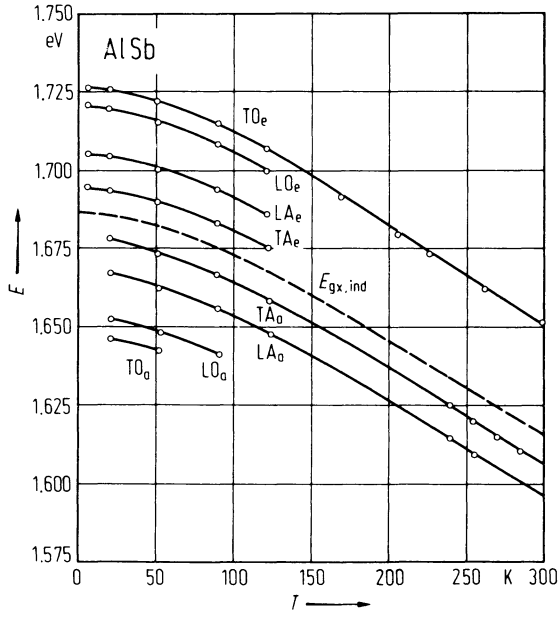

Fig. 2. AlSb. Indirect excitonic energy gap and energies of phonon assisted indirect transitions vs. temperature [83A]. Subscripts e and a stand for transitions involving emission and absotption of phonons.

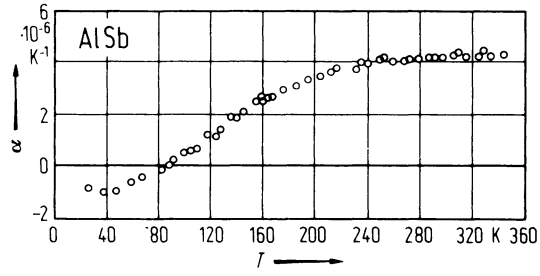

Fig. 4. AlSb. Coefficient of linear thermal expansion vs. temperature [63N].

Physical property	Numerical value	Experimental conditions	Experimental method, remarks	Ref.
spin-orbit splitting energies:				
$\Delta_0(\Gamma_{8v}-\Gamma_{7v})$	673 meV	295 K	splitting of Γ_{15v}	82J
$\Delta_1(L_{4,5v}-L_{6v})$	426 meV	295 K	splitting of L_{3v}	
camel's back structure of conduction band edge: (see respective table and Fig. 2 of section 2.9 for meaning of symbols)				
Δ	261 meV		estimates using $k\cdot p$ theory and GaP data	85K2
ΔE	7.4 meV			85K2
k_m	$0.101\,(2\pi/a)$			
m_t	$0.259 m_0$			
$m_\parallel$	$1.8 m_0$			
effective masses, holes (in units of m_0):				
$m_{p,h}$	0.336	$\parallel$[100]	theoretical estimates	85H
	0.872	$\parallel$[111]		
$m_{p,l}$	0.123	$\parallel$[100]		
	0.091	$\parallel$[111]		
valence band parameters:				
A	−4.12		calculation using $k\cdot p$ theory	75W
B	−2.09			
$\lvert C\rvert$	4.71			

Lattice properties

structure:				
AlSb I	space group T_d^2–$F\bar{4}3m$ (zincblende structure)		stable at normal pressure	
AlSb II	orthorhombic distortion of NaCl structure, space group D_{2h}^{23}–Fmmm?		high-pressure phase	82B
transition pressure:				
p_{tr}	77 (5) kbar		beginning of phase transition	82B
lattice parameter:				
a	6.1355 (1) Å	291.5 K	powder, X-ray measurement	58G
linear thermal expansion coefficient: Fig. 4.				
density:				
d	4.26 g cm^{-3}	293.15 K	slightly temperature dependent	69G
melting point:				
T_m	1338 K			75O

phonon dispersion relations: Fig. 5.

Physical property	Numerical value	Experimental conditions	Experimental method, remarks	Ref.
phonon wavenumbers (in cm^{-1}):				
$\bar{\nu}_{LO}(\Gamma)$	340.0(7)		first order Raman scattering	86V
$\bar{\nu}_{TO}(\Gamma)$	318.7(7)			

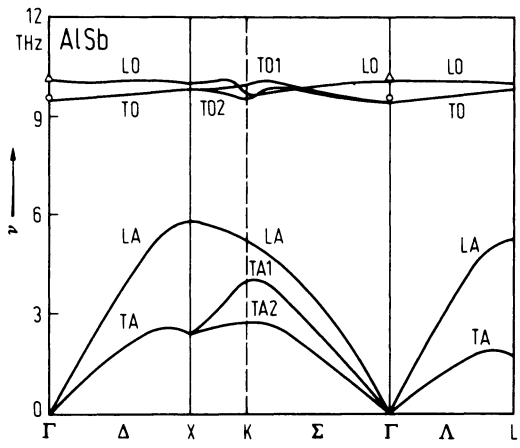

Fig. 5. AlSb. Phonon dispersion relations. Circle and triangle: experimental values for the zone center phonons [85K1].

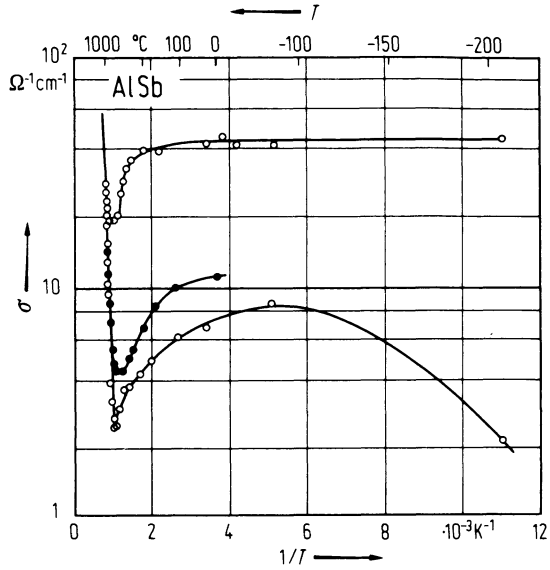

Fig. 6. AlSb. Conductivity vs. reciprocal temperature for three different polycrystalline p-type samples [53W].

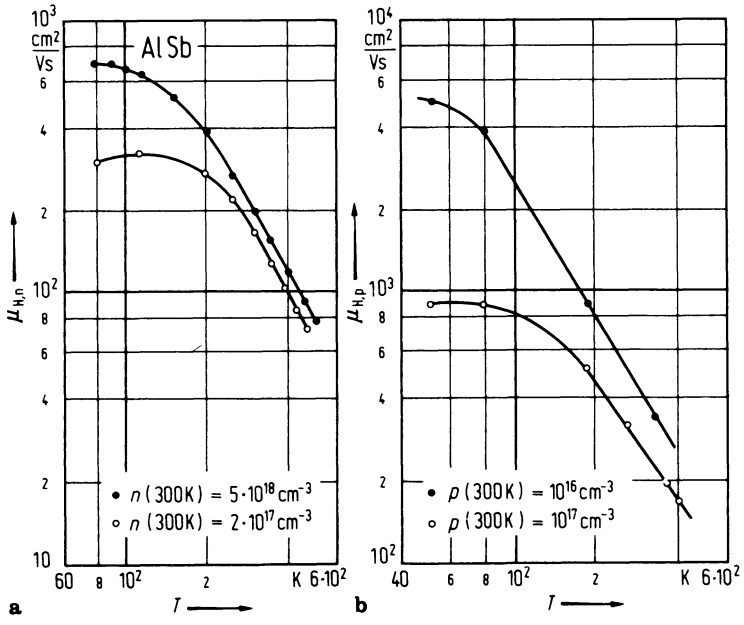

Fig. 7. AlSb. (a) Electron Hall mobility vs. temperature [66S], (b) hole Hall mobility vs. temperature [58R].

Physical property	Numerical value	Experimental conditions.	Experimental method, remarks	Ref.
second order elastic moduli (in 10^{11} dyn cm^{-2}):				
c_{11}	8.769 (20)	300 K	ultrasound, values reevaluated	60B
c_{12}	4.341 (20)		by [72W] using the correct	
c_{44}	4.076 (8)		density	

Transport properties

AlSb grown without intentionally doping becomes intrinsic at about 1000 K. At high temperatures acoustic-mode scattering dominates for the holes and polar optical-mode scattering for the electrons.

intrinsic conductivity $\sigma_i = \sigma_0 \exp(-E_{g,th}/2kT)$:				
σ_0	$1.12 \cdot 10^4\ \Omega^{-1}$ cm^{-1}		see also Fig. 6.	58N
$E_{g,th}$	1.57 eV			

electron mobility:				
μ_n	200 cm^2/Vs	295 K	single crystal, Te-doped	66S
	700 cm^2/Vs	77 K	$n = 4.7 \cdot 10^{16}$ cm^{-3}	

See Fig. 7a [66S] for temperature dependence ($T^{-1.8}$-dependence above 200 K).

hole mobility:				
μ_p	400 cm^2/Vs	300 K	single crystal,	58R
	2000 cm^2/Vs	77 K	p (300 K) $\approx 10^{16}$ vm^{-3}	66S

See Fig. 7b [58R] for temperature dependence ($T^{-2.2}$-dependence above 100 K).

thermal conductivity: Fig. 8

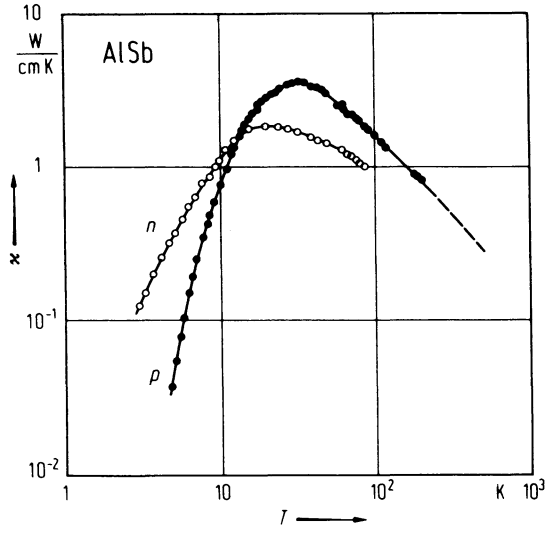

Fig. 8. AlSb. Thermal conductivity vs. temperature for an n-type and a p-type sample, low temperature range [69M].

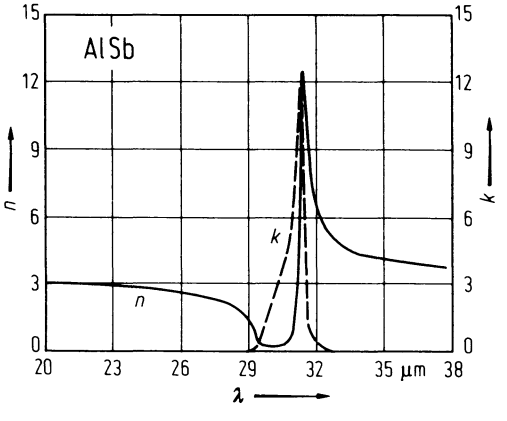

Fig. 9. AlSb. Refractive index n and extinction coefficient k vs. wavelength in the region of lattice absorption [62T].

Physical property	Numerical value	Experimental conditions	Experimental method, remarks	Ref.
Optical properties				
refractive index:				
		T[K], λ[μm]		
n	3.652	300 40	transmission and reflectance,	62T
	2.995	20	Fig. 9	
	2.080	15		
	3.100	10	transmission and reflectance	54O
	3.182	4		
	3.300	2		
	3.445	1.1		
absorption index:				
k	0.0006	300, 40	transmission and reflectance,	62T
	11.73	31.3	Fig. 9	
	0.001	20		
dielectric constants:				
$\varepsilon(0)$	12.04	300 K	ir reflectance, oscillator fit	62H
$\varepsilon(\infty)$	10.24			
Impurities and defects				
energy levels of donors and acceptors (in meV): No detailed analysis of donor states has yet been reported since the camel's back structure of the conduction band minimum leads to a strongly non-parabolic longitudinal effective mass.				
$E_c - E_d$	147		Se-doped, photoexcitation spectrum	68A
	160		Hall data (thermal activation energy)	60T
	68		Te-doped, Hall data	
$E_a - E_v$	42.5		effective mass estimate	
	40.4		unidentified species, from photoexcitation	68A
	41.9		spectra under uniaxial stress	
	102.7			

References for 2.7

53W Welker, H.: Z. Naturforsch, **8a** (1953) 248.
54O Oswald, F., Schade, R.: Z. Naturforsch. **9a** (1954) 611.
58G Giesecke, G., Pfister, H.: Acta Crystallogr. **11** (1958) 369.
58N Nasledov, D.N., Slobodchikov, S.V.: Sov. Phys. Techn. Phys. **3** (1958) 669.
58R Reid, F.J., Willardson, R.K.: J. Electron. Control **5** (1958) 54.
60B Bolef, D.I., Menes, M.: J. Appl. Phys. **31** (1960) 1426.
60T Turner, W.J., Reese, W.E.: Phys. Rev. **117** (1960) 1003.
62H Hass, M., Henvis, B.W.: J. Phys. Chem. Solids **23** (1962) 1099.
62T Turner, W.J., Reese, W.E.: Phys. Rev. **127** (1962) 126.
63N Novikova, S.I., Abrikhosov, N.Kh.: Sov. Phys. Solid State (English Transl.) **5** (1963) 1558; Fiz. Tverd. Tela **5** (1963) 2138.
66S Stirn, R.J., Becker, W.M.: Phys. Rev. **141** (1966) 621, **148** (1966) 907.
68A Ahlburn, B.T., Ramdas, A.K.: Phys. Rev. **167** (1968) 717.
69G Glazov, V.M., Chizhevskaya, S.N., Evgen'ev, S.B.: Zh. Fiz. Khim. **43** (1969) 373.
69M Muzhdaba, V.M.; Nashel'skii, A.Ya., Tamarin, P.V., Shalyt, S.S.: Sov. Phys. Solid State (English Transl.) **10** (1969) 2265; Fiz. Tverd. Tela **10** (1968) 2866.
71L Lawaetz, P.: Phys. Rev. **B4** (1971) 3460
72W Weil, R.: J. Appl. Phys. **43** (1972) 4271.

75O Osamura, K., Murakami, Y.: J. Phys. Chem. Solids **36** (1975) 931.
75W Wiley, D.J.: in "Semiconductors and Semimetals", vol. 10 Willardson, R.K., Beer, A.C. eds., Academic Press, New York 1975.
82B Baublitz, M., Ruoff, A.L.: J. Appl. Phys. **54** (1980) 2109.
82J Joullié, A., Girault, B., Joullié, A.M., Zien-Eddine, A.: Phys. Rev. **B25** (1982) 7830.
83A Alibert, C., Joullié, A., Joullié, A.M., Ance, C.: Phys. Rev. **B27** (1983) 4946.
85H Huang, M., Ching, W.Y.: J. Phys. Chem. Solids **46** (1985) 977.
85K1 Kagaya, H.M., Soma, T.: Phys. Status Solidi (b) **127** (1985) 89.
85K2 Kopylov, A.A.: Solid State Commun. **56** (1985) 1.
86V Ves, S., Strössner, K., Cardona, M.: Solid State Commun. **57** (1986) 483.

Physical property	Numerical value	Experimental conditions	Experimental method, remarks	Ref.

2.8 Gallium nitride (GaN)

Electronic properties

band structure: Fig. 1 (Brillouin zone: Fig. 5 of section 2.1).

The band structure given in Fig. 1 differs only slightly from other spin-neglecting calculations. Introduction of spin-orbit interaction leads to a splitting of the uppermost valence band at Γ from $\Gamma_1 + \Gamma_6$ into $\Gamma_9 + \Gamma_7 + \Gamma_7$. The energy differences between these terms can be described by two parameters – the spin-orbit splitting energy Δ_{so} and the crystal field splitting energy Δ_{cr}.

energy gap (in eV):

$E_{g,dir}$	3.503(2)	$T = 1.6$ K	photoluminescence, from excitonic gap adding the exciton binding energy	74M
	3.4751(5)		A-exciton (transition from Γ_{9v})	
	3.4815(10)		B-exciton (transition from upper Γ_{7v})	
	3.493(5)		C-exciton (transition from lower Γ_{7v})	
	3.44	300 K	temperature dependence below 295 K given by: $E_g(T) - E_g(0) = -5.08 \cdot 10^{-4} T^2/(996 - T)$, see Fig. 2 ($T$ in K)	

intra valence band energies:
The energy separations between the Γ_9 state and the two Γ_7 states can be calculated from the energy separations of the A-, B-, C-excitons.

Δ_{cr}	22(2) meV	calculated from the values given above	71D
Δ_{so}	11(+5, −2) meV		

effective masses (in m_0):

m_n	0.27(6)	$T = 300$ K	Faraday rotation	74R
$m_{n\perp}$	0.20(2)		fit of reflectance spectrum	73B
$m_{n\parallel}$	0.20(6)			
m_p	0.8(2)			75P

Lattice properties

structure:
GaN crystallizes in the wurtzite structure, space group $P6_3mc$.

lattice parameter:

a	3.160···3.190 Å	79L
c	5.125···5.190 Å	

temperature dependence of lattice parameter: Fig. 3.

Physical property	Numerical value	Experimental conditions	Experimental method, remarks	Ref.

linear thermal expansion coefficient: Fig. 4.

phonon dispersion relations: not yet determined. Nine optical branches.

phonon wavenumbers (in cm^{-1}):

$\bar{\nu}_{A1}(TO\parallel)$	533	$T = 300\,K$	Raman spectroscopy	70M
$\bar{\nu}_{E1}(TO\perp)$	559		Raman spectroscopy	72L
$\bar{\nu}_{E1}(LO\perp)$	746		Kramers-Kronig analysis of infrared reflectivity	73B
$\bar{\nu}_{A1}(LO)$	744			

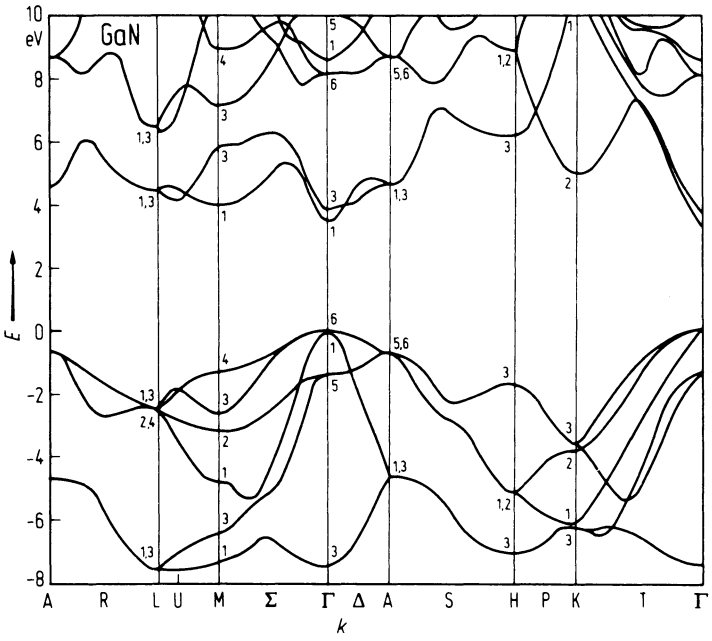

Fig. 1. GaN. Band structure calculated with an empirical pseudopotential method [74B].

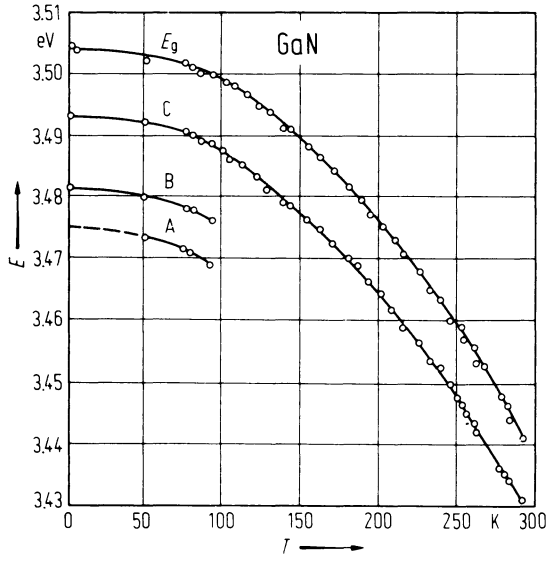

Fig. 2. GaN. Band gap energy and exciton energies vs. temperature [74M].

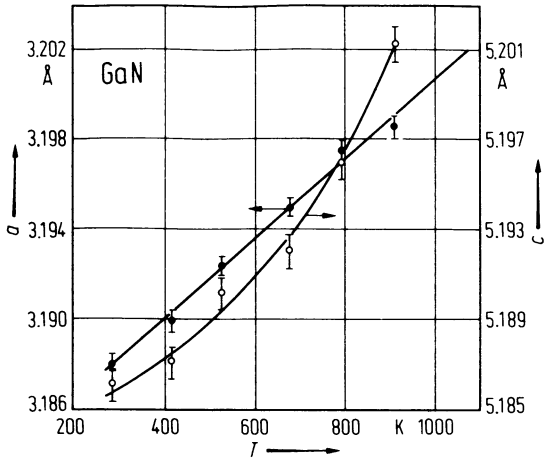

Fig. 3. GaN. Lattice parameters a and c vs. temperature for a single crystal layer [69M].

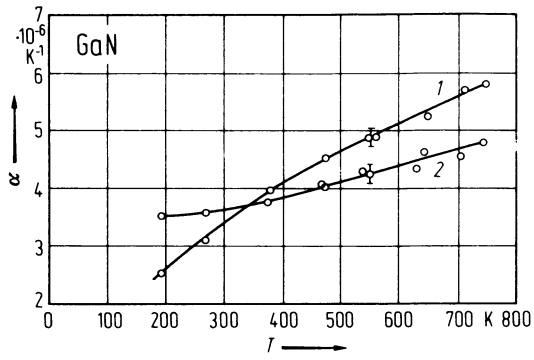

Fig. 4. GaN. Coefficient of linear thermal expansion vs. temperature; curve *1*: $\alpha_\perp$, *2*: $\alpha_\parallel$ [76S].

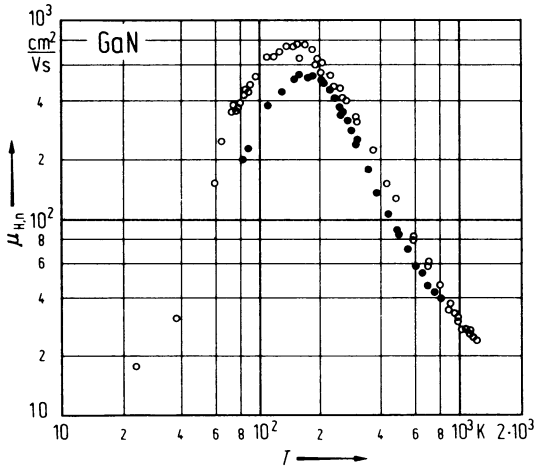

Fig. 5. GaN. Electron Hall mobility vs. temperature for two samples [73I2].

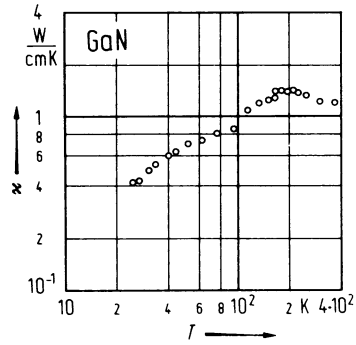

Fig. 6. GaN. Thermal conductivity along the c-axis vs. temperature [77S].

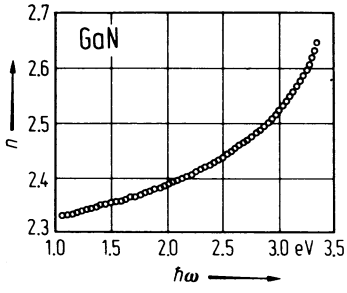

Fig. 7. GaN. Refractive index vs. photon energy at 300 K; $E \perp c$ [71E].

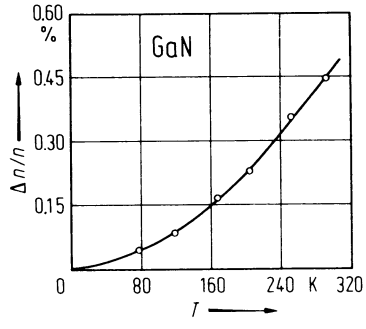

Fig. 8. GaN. Long-wavelength refractive index normalized to the 0 K value vs. temperature [71E].

Physical property	Numerical value	Experimental conditions	Experimental method, remarks	Ref.
second order elastic moduli (in 10^{11} dyn cm^{-2}):				
c_{11}	29.6 (1.8)		calculated from the mean square displacement of the lattice atoms measured by X-ray diffraction	
c_{12}	13.0 (1.1)			
c_{13}	15.8 (0.6)			
c_{33}	26.7 (1.8)			
c_{44}	2.41 (20)			

Transport properties

GaN is an extrinsic n-type semiconductor, p-type material does not seem achievable. Above room temperature transport is predominantly determined by polar-optical scattering and at lower temperatures by impurity scattering. Crystals with n larger than $8 \cdot 10^{18}$ cm^{-3} show metallic conduction with no appreciable variation in n or μ_n between 10 and 300 K.

conductivity:				
σ	$6 \cdots 12\,(\Omega\,\mathrm{cm})^{-1}$	$T = 300$ K	purest material, $n \approx 10^{17}$ cm^{-3}, undoped layers grown by vaporphase technique on sapphire	72I, 73I1, 78C
electron mobility:				
μ_n	$\leqq 440$ cm^2/Vs	$T = 300$ K	purest material, $n \approx 10^{17}$ cm^{-3}	72I, 72I1, 78C

For temperature dependence, see Fig. 5.

thermal conductivity: Fig. 6.

Optical properties

refractive index:				
n	2.29 (5)	$T = 300$ K (extrapolated to 0 eV), $E \perp c$	interference method (the value for $E \parallel c$ is 1.5 (2)% lower at 500 nm); for energy dependence, see Fig. 7, for long wavelength value, see Fig. 8.	71E
dielectric constants:				
$\varepsilon(0)$	10.4 (3)	$E \parallel c$	$\varepsilon(\infty)$ assumed to be isotropic	73B
	9.5 (3)	$E \perp c$		
$\varepsilon(\infty)$	5.8 (4)	$T = 300$ K, $E \parallel c$		70M
	5.35 (20)	$E \perp c$		73B

Impurities and defects

donors

Undoped GaN is n-type with electron concentrations $n \geqq 10^{17}$ cm^{-3}. The dominant donor is believed to be the nitrogen vacancy [75P]. The binding energy of this donor is subject to large controversy. Values given range from 42 (1) meV [71D1] over 29 (6) meV [74L] to 17 meV [79V]. A deep donor level with $E_d = 110$ meV is also postulated [79V]. No detailed information exists about the identity of these donors.

acceptors

Most data have been derived from photoluminescence peaks which are caused by the recombination of free or bound electrons with bound holes.

luminescence peak energies E_{peak}.

Impurity	E_{peak} [eV]	T [K]	Remarks	Ref.
Li	2.23	77	photoluminescence	73P
Be or V_{Ga}	3.264	4.2		73I1
Be-complex or Be_{Ga}	2.36			80M1
Mg or V_{Ga}	3.264			73I1
Mg-complex	2.95			73I1
or Mg_{Ga}				80M1
Dy	3.15	77		73P
Cd or V_{Ga}	3.268	4.2		80M1
	3.263	1.6		74L,
Cd-complex or Cd_{Ga}	2.7			80M1
Zn or V_{Ga}	3.268	4.2		80M1
Zn-complex or Zn_{Ga}	2.9			74L,
(A-band)				80M1
Zn_N(?) (B-band)	2.6			80M1
Zn_N^- (?) (C-band)	2.2			
Zn_N^{2-} (?) (D-band)	1.8			

deep defect states

Undoped GaN is invariably n-type usually with a high free electron concentration ($10^{17} \cdots 10^{18}\,cm^{-3}$) at room temperature. Although the dominant donor has not been unambiguously identified there is a consensus that it is an intrinsic defect and most probably the nitrogen vacancy [75P]. Energies are reported ranging from 17 meV [79V] to 42 meV [71D]. The resistivity of the material can be increased dramatically by the addition of group II atoms; these elements introduce deep acceptors which compensate the native donors. The same binding energy of 225 meV is reported [74L] for the addition of Zn, Cd, Mg, and Be, however it seems unlikely that these four dissimilar species would be identical and consequently it has been proposed that the acceptor is actually V_{Ga} [80M1]. The vacancy concentration is believed to be increased by the presence of the group II element.

binding energies of acceptors

Impurity	E_b [meV]	T [K]	Remarks	Ref.
V_{Ga}	225	4.2	photoluminescence	80M2
Hg	410	78	infrared quenching of luminescence	74E
Li	750			
Zn_{Ga}(A-band)	480	4.2		
	370(40)	4.2	photoluminescence	80M2
Zn_N(B-band)	650(80)			
Zn_N^-(C-band)	1020(50)			
Zn_N^{2-}(D-band)	1420(80)			

References for 2.8

69M Maruska, H.P., Tietjen, J.J.: Appl. Phys. Lett. **15** (1969) 327.
70M Manchon, D.D., Barker, A.S., Dean, J.P., Zetterstrom, R.B.: Solid State Commun. **8** (1970) 1227.
71D Dingle, R., Ilegems, M.: Solid State Commun. **9** (1971) 175.
71E Ejder, E.: Phys. Status Solidi (a) **6** (1971) K39.
72I Ilegems, M.: J. Cryst. Growth **13/14** (1972) 360.
72L Lemos, V., Argüello, C.A., Leite, R.C.C.: Solid State Commun. **11** (1972) 1351.
73B Barker, A.S., Ilegems, M.: Phys. Rev. **B7** (1973) 743.
73I1 Ilegems, M., Dingle, R.: J. Appl. Phys. **44** (1973) 4234.
73I2 Ilegems, M., Montgomery, H.C.: J. Phys. Chem. Solids **34** (1972) 885.
73P Pankove, J.I., Duffy, M.T., Miller, E.A., Berkeyheiser, J.E.: J. Lumin. **8** (1973) 89.
74B Bloom, S., Harbeke, G., Meier, E., Ortenburger, I.B.: Phys. Status Solidi (b) **66** (1974) 161.
74L Lagerstedt, O., Monemar, B.: J. Appl. Phys. **45** (1974) 2266.
74M Monemar, B.: Phys. Rev. **B10** (1974) 676.
74R Rheinländer, B., Neumann, H.: Phys. Status Solidi (b) **64** (1974) K123.
75P Pankove J.I., Bloom, S., Harbeke, G.: RCA Rev. **36** (1975) 163.
76S Sheleg, A.U., Savastenko, V.A.: Vesti Akad. Nauk BSSR, Ser. Fiz. Mat. Nauk **3** (1976) 126.
77S Sichel, E.K., Pankove, J.I.: J. Phys. Chem. Solids **38** (1977) 330.
78C Crouch, R.K., Debnam, W.J., Fripp, A.L.: J. Mater. Sci. **13** (1978) 2358.
78S Savastenko, V.A., Sheleg, A.U.: Phys. Status Solidi (a) **48** (1978) K135.
79L Lagerstedt, O., Monemar, B.: Phys. Rev. **B19** (1979) 3064.
79V Vavilov, V.S., Makarov, S.I., Chukichev, M.V., Chetverikova, I.F.: Sov. Phys. Semicond. (English Transl.) **13** (1979) 1259; Fiz. Tekh. Poluprov. **13** (1979) 2153.
80M1 Monemar, B., Lagerstedt, O., Gislason, H.P.: J. Appl. Phys. **51** (1980) 625.
80M2 Monemar, B., Gislason, H.P., Lagerstedt, O.: J. Appl. Phys. **51** (1980) 640.

Physical property	Numerical value	Experimental conditions	Experimental method, remarks	Ref.

2.9 Gallium phosphide (GaP)

Electronic properties

band structure: Fig. 1 (Brillouin zone: see section 1.1, Fig. 2)

GaP is an indirect gap semiconductor. The lowest set of *conduction bands* shows a camel's back structure (Fig. 2); the band minima are situated at the Δ-axes near the zone boundary. The *valence bands* show the usual structure characteristic for all zincblende semiconductors.

The spin-orbit splitting of the top of the valence band is negligible compared with most other energy separations in the band structure. Thus, Fig. 1 shows the band structure calculated without inclusion of the spin-orbit interaction using the single group notation for the high symmetry band states.

energies of symmetry points of the band structure (relative to the top of the valence band) (in eV):

$E(\Gamma_{1v})$	−12.99	−12.3	−13.2	symmetry symbols in single group notation
$E(\Gamma_{15v})$	0.00			
$E(\Gamma_{1c})$	2.88			first row: theoretical data according to [76C]
$E(\Gamma_{15c})$	5.24			
$E(X_{1v})$	−9.46		−9.6	second row: experimental data from angle resolved photoemission [84S1] see also Fig. 1
$E(X_{3v})$	−7.07	−6.8		
$E(X_{5v})$	−2.73	−3.0	−2.7	
$E(X_{1c})$	2.16			
$E(X_{3c})$	2.71			third row: XPS data [74L]
$E(L_{1v})$	−10.60	−10.8	−10.6	
$E(L_{2v})$	−6.84	−6.8	−6.9	
$E(L_{3v})$	−1.10	−0.9	−1.2	
$E(L_{1c})$	2.79			
$E(L_{3c})$	5.74			
$E(\Sigma_1^{min})$	−4.3	−3.8	−4.0	

Physical property	Numerical value	Experimental conditions	Experimental method, remarks	Ref.
indirect energy gap (in eV):				
$E_{g,ind}$ $(\Gamma_{15v} - \Delta_{1c})$	2.350(1)	0K, extrapolated	from exciton data obtained by wavelength modulated transmission	78H
	2.272	300 K		
Temperature dependence: Fig. 3. The curve in Fig. 3 can be approximated by the formula $E_{g,ind}(eV) = 2.338 - 6.2 \cdot 10^{-4} T^2/(T + 460)$ (T in K).				
$E_{gx}(1S, X_7)$	2.3284	4.2 K	excitonic gap, this value corresponds to the dip of the camel's back (see below)	78H

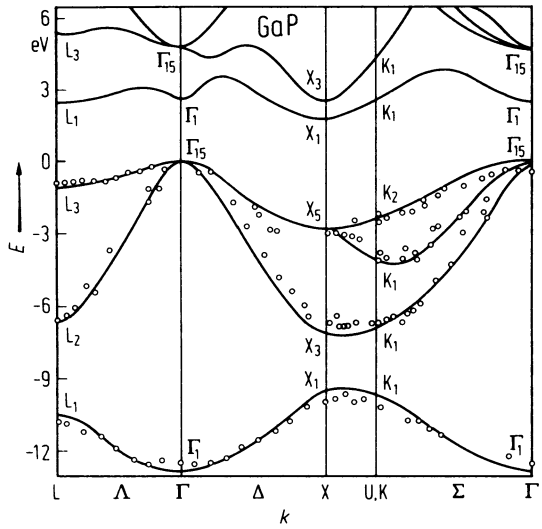

Fig. 1. GaP. Band structure calculated by a pseudopotential method neglecting spin-orbit interaction [76C]; circles: data from angle resolved photoemission [84S1].

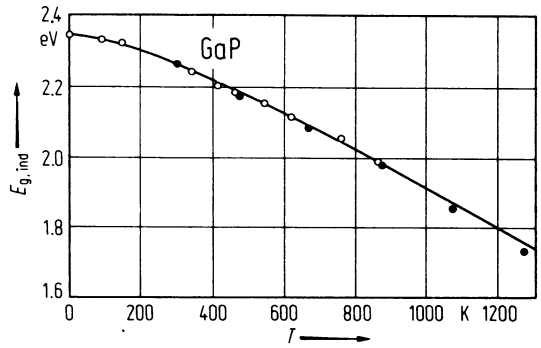

Fig. 3. GaP. Indirect energy gap vs. temperature from various authors. The solid curve was calculated by the formula given in the tables [69P].

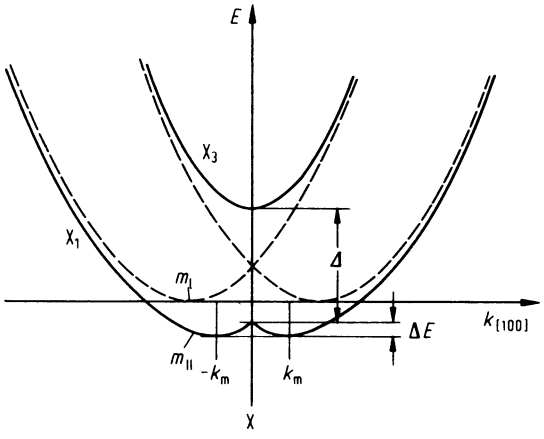

Fig. 2. GaP. Camel's back structure of the conduction band minima at the Δ-axes near the zone boundary X. Dashed curves: diamond structure, solid curves: zincblende structure. The higher band has X_3 (X_7) symmetry, the lower band X_1 (X_6) symmetry at the zone boundary.

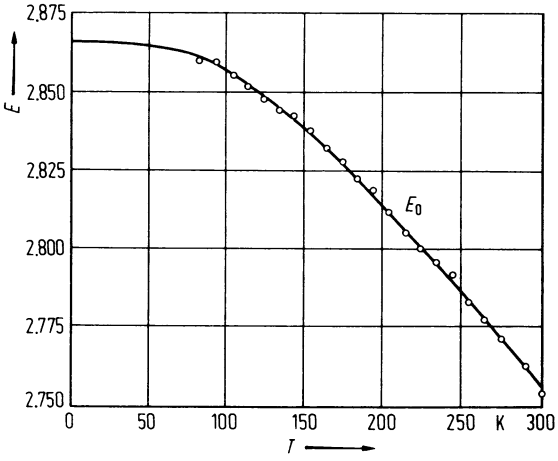

Fig. 4. GaP. Direct exciton edge E_0 and spin-orbit split edge $E_0 + \Delta_0$ vs. temperature measured with wavelength modulated reflectivity [83T].

Physical property	Numerical value	Experimental conditions	Experimental method, remarks	Ref.
$E_{g,ind}$ ($\Gamma_{15v} - L_{1c}$)	2.637(10) eV	78 K	electroabsorption	78K
direct energy gap (in eV):				
$E_{g,dir}$ ($\Gamma_{15v} - \Gamma_{1c}$)	2.895(4)	0K, extrapolated	photoconductivity	64N
	2.780(2)	300 K		
$E_{gx,dir}$	2.866	0K, extrapolated	excitonic gap, wavelength modulated reflectance	83T
Temperature dependence: Fig. 4; the curve in Fig. 4 can be approximated by $E_0(T) = E_0(0) - 0.1081 \cdot (\coth(164/T) - 1)$ (E in eV, T in K).				
spin-orbit splitting energy (in eV): (splitting of Γ_{15v} into Γ_{8v} (upper level) and Γ_{7v} (lower level))				
Δ_0	0.080(3)	100 ··· 200 K	wavelength modulated reflectivity	83T
camel's back structure of conduction band edge: The camel's back structure near the minimum can be described by the formula: $E(k) = \hbar^2 k^2/2m_l + \hbar^2 k_\perp^2/2m_t - ((\Delta/2)^2 + \Delta_0 \hbar^2 k^2/2m_l)^{1/2}$ with k and $k_\perp$: components of the wave vector parallel and perpendicular to the [100]-direction, respectively, m_t: effective mass perpendicular to the [100]-direction; Δ_0: parameter describing the non-parabolicity; all other parameters are explained in Fig. 2.				
Δ	355 meV		fitting of cyclotron resonance data obtained in very high magnetic fields	83M1, 83M2
Δ_0	433 meV			
m_t	$0.25\, m_0$			
m_l	$0.91\, m_0$			
ΔE	3.5 meV		from $\Delta E = (\Delta_0/4)(1 - \Delta/\Delta_0)^2$	
m	$10.9\, m_0$		from $m = m_l(1 - (\Delta/\Delta_0)^2)^{-1}$	
k_m	$0.025(2\pi/a)$		from $k_m = (2m_l \Delta E/\hbar^2)^{1/2}$	
effective mass, electrons (in units of m_0):				
m_n^*	0.254(4)		apparent effective masses from cyclotron resonance data at 119 μm (337 μm) assuming ellipsoidal energy surfaces at X_1 neglecting camel's back structure	83M1
$m_{n\perp}^*$	4.8(5)			
effective masses, holes (in units of m_0):				
$m_{p,h}$	0.67(4)	∥[111]	cyclotron resonance at 1.6 K	72S
$m_{p,l}$	0.17(1)	∥[111]		
$m_{p,so}$	0.4649		calculated from $k \cdot p$ model	83S1
valence band parameters:				
A	−4.20		calculated using $k \cdot p$ theory	75W
B	−1.97			
$\lvert C \rvert$	4.60			

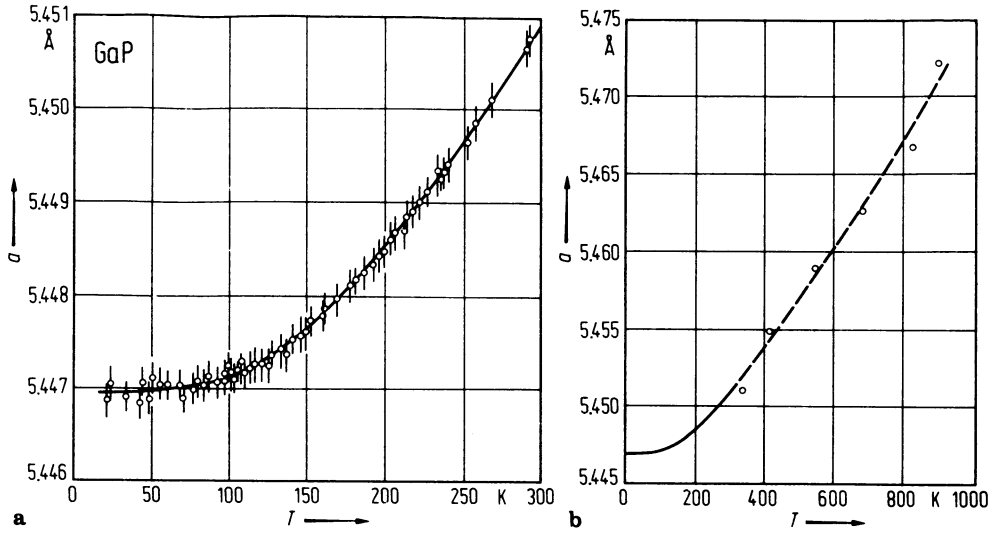

Fig. 5. GaP. Lattice parameter vs. temperature. (a) below RT [83D], (b) above RT, circles and broken line: [72K], solid line: data from (a).

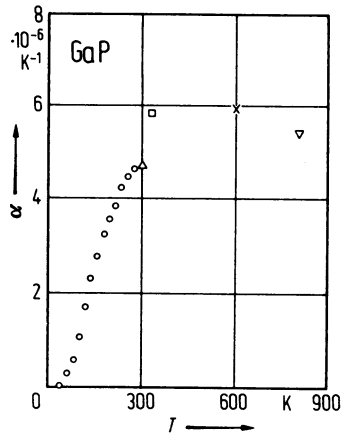

Fig. 6. GaP. Linear thermal expansion coefficient vs. temperature; circles: [83D], other symbols: data taken from literature.

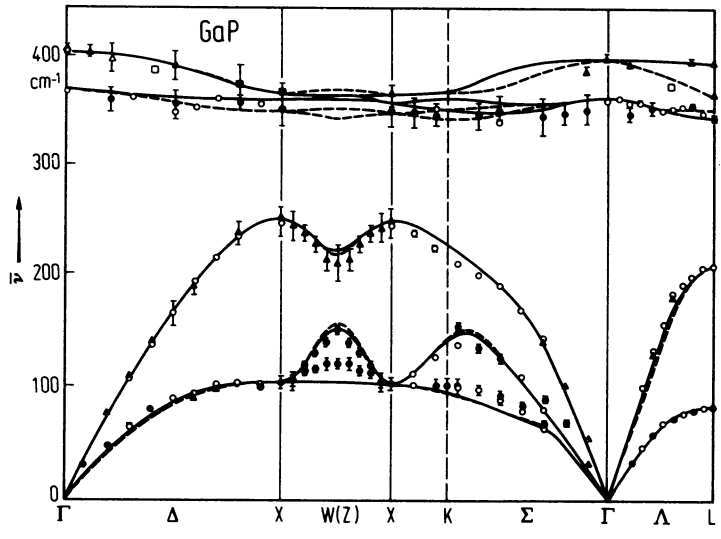

Fig. 7. GaP. Phonon dispersion relations calculated with an eleven parameter rigid ion model. Solid lines calculated to fit neutron diffraction data from [79B] (full symbols), dashed lines calculated to fit data from [68Y] (open symbols [82P]).

Physical property	Numerical value	Experimental conditions	Experimental method, remarks	Ref.
Lattice properties				
Structure				
GaP I	space group $T_d^2 - F\bar{4}3m$ (zincblende structure)		stable at normal pressure	
GaP II	tetragonal $D_{4h}^{19} - I4_1/amd$ (β-tin structure)		high-pressure phase	82B1
transition pressure:				
p_{tr}	215(8) kbar		beginning of phase transition	82B1
lattice parameter:				
a	5.4505(2) Å	RT, single crystal		80B

For temperature dependence, see Fig. 5.

linear thermal expansion coefficient: Fig. 6.

density:

d	4.138 g cm^{-3}	300 K		77M

melting point:

T_m	1730(5) K			84T

phonon dispersion relations: Fig. 7.

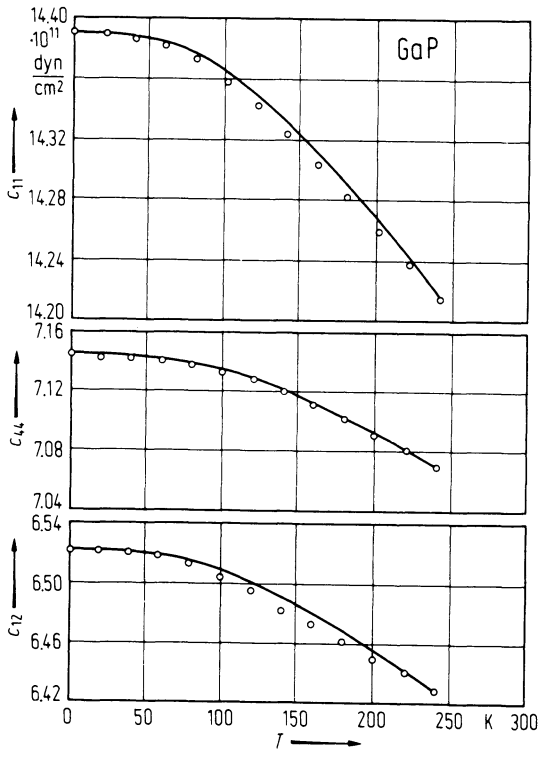

Fig. 8. GaP. Second order elastic moduli vs. temperature [75B].

Physical property	Numerical value	Experimental conditions	Experimental method, remarks	Ref.
phonon frequencies (in THz):				
$\nu(\Gamma)$	12.25(5)	LO	inelastic neutron scattering,	79B
$\nu(X)$	3.13(15)	TA	see also [68Y] and Fig. 7	
	7.5(4)	LA		
	10.65(50)	TO		
	11.0(3)	LO		
$\nu(L)$	2.50(5)	TA		
	10.6(2)	TO		
	12.16(5)	LO		
$\nu(W)$	3.70(10)	A_I		
	4.60(10)	A_{II}		
	6.4(5)	A_{III}		
	10.8(5)	O_I		
second order elastic moduli (in 10^{11} dyn cm^{-2}):				
c_{11}	14.050(28)	300 K	ultrasound ($f = 10/30$ MHz),	81Y
c_{12}	6.203(24)		temperature dependence,	
c_{44}	7.033(7)		Fig. 8	
third order elastic moduli (in 10^{12} dyn cm^{-2}):				
c_{111}	−7.37	300 K	ultrasound ($f = 10/30$ MHz);	81Y
c_{112}	−4.74		hydrostatic pressure up to	
c_{123}	−1.31		1.5 kbar, uniaxial pressure	
c_{144}	−1.07		up to 30 bar	
c_{155}	−2.34			
c_{456}	−0.62			

Transport properties

Intrinsic conductivity in GaP occurs even in high purity samples only above 500 °C. Thus, the transport properties are in general determined by the properties of impurities and lattice defects.

As in GaAs (see section 2.10) *semi-insulating GaP* can be obtained by doping with shallow donors and acceptors as well as deep centers. Resistivities at RT are of the order of $10^8 \cdots 10^{11}$ Ω cm.

carrier mobilities:

$\mu_{H,n}$	160 cm^2/Vs	RT, LPE grown layers	maximum mobility, temperature dependence $\propto T^{-1.7}$	83K2
$\mu_{H,p}$	135 cm^2/Vs		maximum mobility, temperature dependence $\propto T^{-2.3}$	

Temperature dependence (LPE grown layers): Fig. 9.

thermal conductivity: Fig. 10.

Optical properties

dielectric constants:

$\varepsilon(0)$	11.11	300 K	$\varepsilon(0)$: low-frequency capacitance measurements	83S2
	10.86	75.7 K		
$\varepsilon(\infty)$	9.11	300 K	$\varepsilon(\infty)$: derived from refractive index data	

refractive index (see also below): range 1.5 ··· 2.7 eV: Fig. 11.

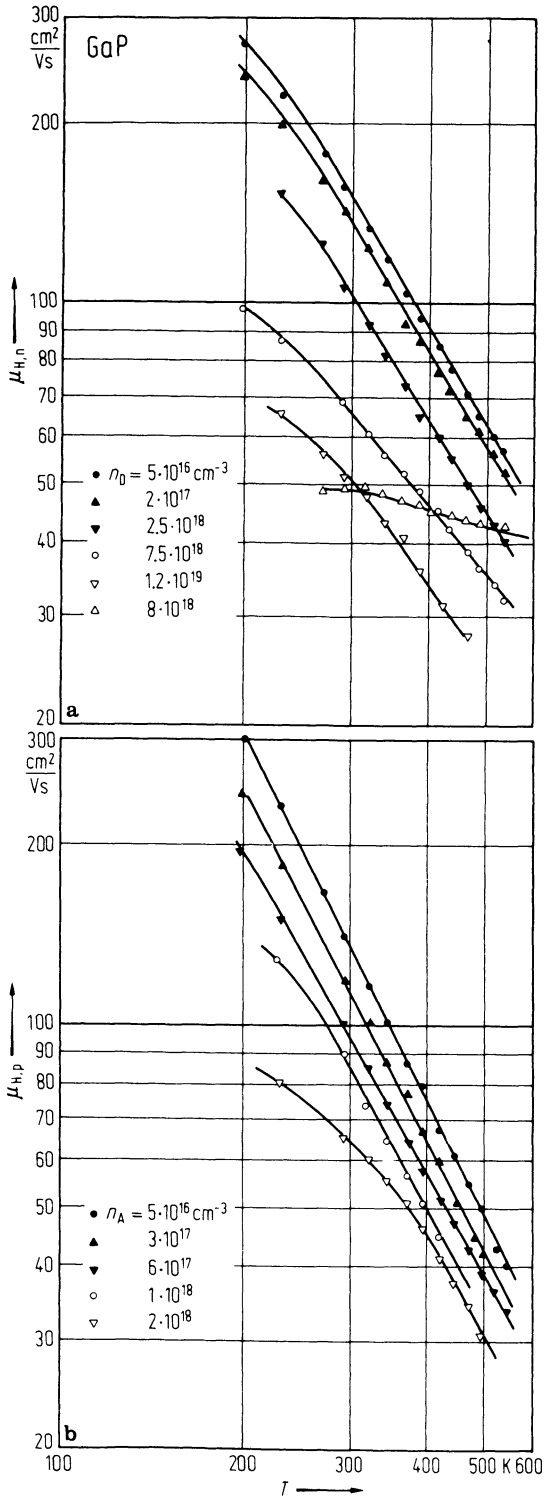

Fig. 9. GaP. Hall mobility in n-type (a) and p-type (b) LPE-grown layers vs. temperature [83K2].

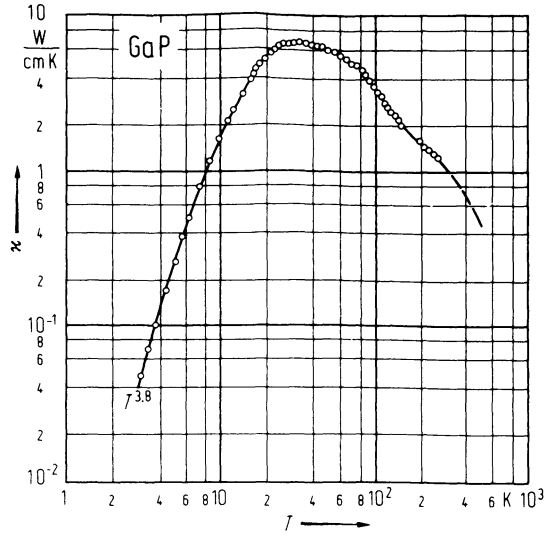

Fig. 10. GaP. Thermal conductivity vs. temperature for a p-type sample [69M3].

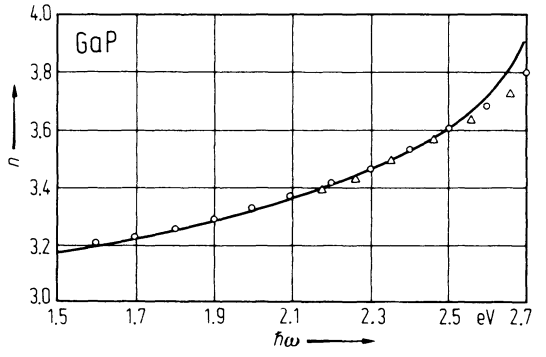

Fig. 11. GaP. Refractive index vs. photon energy in the range 1.5···2.7 eV. Circles and solid curve: calculated, triangles from [82B3][85C].

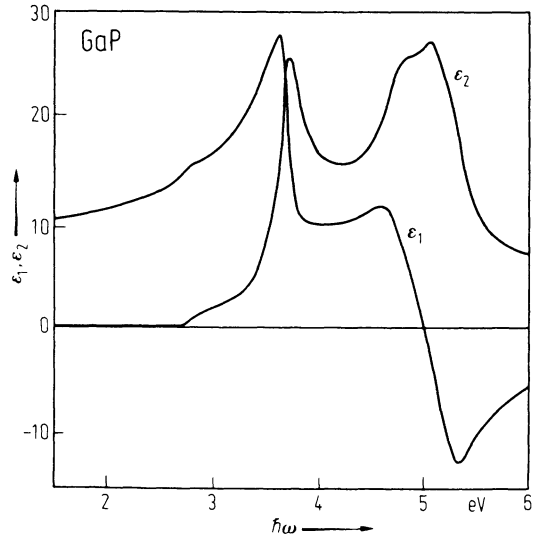

Fig. 12. GaP. Real and imaginary parts of the dielectric constant vs. photon energy [83A].

optical constants

real and imaginary parts of the dielectric constant measured by spectroscopical ellipsometry; n, k, R, K calculated from these data [83A]; see also Fig. 12.

$\hbar\omega$ [eV]	ε_1	ε_2	n	k	R	$K[10^3\,cm^{-1}]$
1.5	10.102	0.000	3.178	0.000	0.272	0.00
2.0	11.114	0.000	3.334	0.000	0.290	0.00
2.5	12.996	0.046	3.605	0.006	0.320	1.63
3.0	16.601	1.832	4.081	0.224	0.369	68.26
3.5	24.833	8.268	5.050	0.819	0.458	290.40
4.0	9.652	16.454	3.790	2.171	0.452	880.10
4.5	11.073	17.343	3.978	2.180	0.461	994.27
5.0	0.218	26.580	3.661	3.631	0.580	1839.99
5.5	−10.266	10.974	1.543	3.556	0.677	1982.53
6.0	−5.521	7.041	1.309	2.690	0.583	1635.71

Impurities and defects

diffusion coefficients of impurities in GaP

Impurity	D_0 [$cm^2\,s^{-1}$]	Q [eV]	Remarks	Ref.
Au	8	2.5 ± 0.3	from A face, $c^{eq} = 10^{16}\,cm^{-3}$ (1250 °C)	78D
Au	20	2.4 ± 0.2	from B face, $c^{eq} = 10^{16}\,cm^{-3}$ (1300 °C)	78D
Be			concentration dependent profiles	72I
S	$3.2 \cdot 10^3$	4.7	radiotracer	70Y
Zn			chemical diffusion profiles complex,	64C

shallow impurities

The effect of deviations from the ellipsoidal form of the conduction band (camel's back structure) on the donor states becomes serious since $E_{min}(\Delta) - E(X)$ is comparable to the binding energies of the donor excited states. Each state splits into two subcomponents involving a symmetric and antisymmetric contribution from the individual sub-minima [77K]. There is still some uncertainty over the exact classification of certain excited states of P-site donors and their magnetic properties which deviate significantly from the simple form of ellipsoidal minima [77C1].

Binding energies of donors

Impurity	E_b [meV]	T [K]	Remarks	Ref.
Theory	59(2)		effective mass theory	77K
O_P	897(1)	2	infrared photoluminescence (consistent with threshold of photo-neutralization spectra [78B, 78M1])	68D
S_P	107(1)	20	infrared absorption	78K
Se_P	105(1)	2	donor-acceptor pair spectra	73D2
Te_P	92.6(1.0)	20	infrared absorption	78K
Si_{Ga}	85(1)	20	infrared absorption	78K
Ge_{Ga}	204(1)	2	donor-acceptor spectra	73D3
Sn_{Ga}	72(1)		donor-acceptor spectra	73D3
Li_P	91(1)	2	bound exciton 'two-electron' replicas	73D1
Li_{Ga}	61(2)	2	unresolved donor acceptor pair spectra	

binding energies of acceptors

Impurity	E_b [meV]	T [K]	Remarks	Ref.
Theory	45.3 or 56.3		effective mass theory according to [74B], re-evaluated for $\varepsilon = 11.02$	78K
C_P	54.3(5)	2	donor-acceptor pair spectra (all data from [73D3] revised upward by 77.9 meV because of the increase in E_q discussed in [78K] and [78B], see also [78S] where an increase of 8.3 meV is preferred)	73D2
Si_P	210(1)			
Ge_P	265(1)			
Cu_P	530(30)	4		73G
	580	77	photoconductivity, absorption (the complex and ill-understood behavior of GaP:Cu in thermally stimulated current measurements has been noted by [78R])	71O, 74K
	650			
Be_{Ga}	56.6(5)	2	photoconductivity, absorption	73D2
Mg_{Ga}	59.9(5)			
Zn_{Ga}	69.7(5)	20	infrared absorption	78K
Cd_{Ga}	102.2(5)			
X	52(1)	2	donor-acceptor pair spectra	73D2

transition metal impurities

Energy levels related to isolated, substitutional transition metal impurities. ("+" above valence band edge, "−" below conduction band edge).

Impurity	E[eV]	Type	Remarks	T[K]	Ref.
Ti	−0.50(2)	a	DLTS and DLOS	77···350	87R
	+1.0(2)	d			
V	−0.58	a	Temperature dependent Hall effect		86U
	+0.20(5)	d	Electrical + optical measurements		89U
Cr	−1.2	1st a	Reinterpretation of		81C
	−0.5	2nd a	photo-ESR data [78K1]		81C
Mn	+(0.4···0.43)	a	Temperature dependent Hall effect		76E
Fe	+0.82	1st a	DLTS		85B
	−0.26	2nd a	DLTS		85B
Co	+0.41	1st a	Temperature dependent Hall and resistivity measurements		66L
	−0.33	2nd a			83J
Ni	+0.51	1st a	DLTS, σ_p^0 photocapacitance and photo-ESR		84P
	−0.82	2nd a	DLTS and transient capacitance		84Y

References for 2.9

64C Chang, L.L., Pearson, G.L.: J. Appl. Phys. **35** (1964) 374.
64N Nelson, D.F., Johnson, L.F., Gershenzon, M.: Phys. Rev. **135** (1964) A1399.
66L Loescher, D.H., Allen, J.W., Pearson, G.L.: J. Phys. Soc. Jpn. **21** Suppl. (1966) 239.
68D Dean, P.J., Henry, C.H.: Phys. Rev. **176** (1968) 928.

68Y Yarnell, J.L., Warren, J.L., Wenzel, R.G., Dean, P.J.: in "Neutron Inelastic Scattering Symposion", Copenhagen 1968, vol. 1, IAEA, Vienna **1968**, p. 301.

69M Muzhdaba, V.M., Nashel'skii, A.Ya., Tamarin, P.V., Shalyt, S.S.: Sov. Phys. Solid State (English Transl.) **10** (1969) 2265; Fiz. Tverd. Tela **10** (1968) 2866.

69P Panish, M.B., Casey, H.C.: J. Appl. Phys. **40** (1969) 163.

70Y Young, A.B.Y., Pearson, G.L.: J. Phys. Chem. Solids **31** (1970) 517.

71O Olsson, R.: Phys. Status Solidi (b) **46** (1971) 163.

72I Ilegems, M., O'Mara, W.C.: J. Appl. Phys. **43** (1972) 1190.

72K Kudman, I., Pfaff, R.J.: J. Appl. Phys. **43** (1972) 3760.

72S Schwerdtfeger, C.P.: Solid State Commun. **11** (1972) 779.

73D1 Dean, P.J.: Luminescence of Crystals, Molecules and Solutions, Williams, F.E. (ed.), New York: Plenum Press **1973**, p. 538.

73D2 Dean, P.J.: Progress in Solid State Chemistry, Vol. 8, McCaldin, J.O., Somorjai, G. (eds.), New York: Pergamon Press **1973**, p. 1.

73G Grimmeiss, H.G., Monemar, B.: Phys. Status Solidi (a) **19** (1973) 505.

74K Kopylov, A.A., Pikhtin, A.N.: Sov. Phys. Solid State (English Transl.) **16** (1974) 1837; Fiz. Tverd. Tela **16** (1974) 1837.

74L Ley, L., Pollak, R.A., McFeely, R.R., Kowalczyk, S.P.: Phys. Rev. **B9** (1974) 600.

75B Boyle, W.F., Sladek, R.J.: Phys. Rev. **B11** (1975) 2933.

75W Wiley, J.D.: in "Semiconductors and Semimetals", Vol. 10, R.K. Willardson and A.C. Beer eds., Academic Press, New York and London **1975**.

76C Chelikowsky, J.R., Cohen, M.L.: Phys. Rev. **B14** (1976) 556.

76E Evwaraye, A.O., Woodbury, H.H.: J. Appl. Phys. **47** (1976) 1595.

76S Street, R.A., Senske, W.: Phys. Rev. Lett. **37** (1976) 1292.

77K Kopylov, A.A., Pikhtin A.N.: Sov. Phys. Semicond. (English Transl.) **11** (1977) 510; Fiz. Tekh. Poluprovodn. **11** (1977) 867.

78D Dzhafarov, T.D., Litvin, A.A., Khudyakov, S.V.: Sov. Phys. Solid State **20** (1978) 152.

77M Merrill, L.: J. Phys. Chem. Ref. Data **6** (1977) 1205.

78H Humphreys, R.G., Rössler, U., Cardona, M.: Phys. Rev. **B18** (1978) 5590.

78K Kopylov, A.A., Pikhtin, A.N.: Solid State Commun. **26** (1978) 735.

79B Borcherds, P.H., Kung, K., Alfreys, G.F., Hall, R.L.: J. Phys. **C12** (1979) 4699.

80B Bessolov, V.N., Dedegkaev, T.T., Efimov, A.N., Kartenko, N.F., Yakovlev, Yu.P.: Sov. Phys. Solid State (English Transl.) **22** (1980) 1652; Fiz. Tverd. Tela **22** (1980) 2834.

81C Clerjaud, B., Gendron, F., Porte, C.: Appl. Phys. Lett. **38** (1981) 212.

81Y Yogurtcu, Y.K., Miller, A.J., Saunders, G.A.: J. Phys. Chem. Solids **42** (1981) 49.

82B1 Baublitz, M., Ruoff, A.L.: J. Appl. Phys. **53** (1982) 6179.

82B2 Burkhard, H., Dinges, H.W., Kuphal, E.: J. Appl. Phys. **53** (1982) 655.

82P Patel, C., Sherman, W.F., Wilkinson, G.R.: Phys. Status Solidi (b) **111** (1982) 649.

83A Aspnes, D.E., Studna, A.A: Phys. Rev. **B27** (1983) 985.

83D Deus, P., Voland, U., Schneider, H.A.: Phys. Status Solidi (a) **80** (1983) K29.

83J Jezewski, M., Baranowski, J.M.: 4th "Lund" Int. Conf. on Deep Level Impurities in Semicond., Eger Hungary, **1983**, unpublished.

83K Kao, Y.C., Eknoyan, O.: J. Appl. Phys. **54** (1983) 2468.

83M1 Miura, N., Kido, G., Suekane, M., Chikazumi, S.: J. Phys. Soc. Jpn. **52** (1983) 2838.

83M2 Miura, N., Kido, G., Suekane, M., Chikazumi, S.: Physica **117B&118B** (1983) 66.

83S1 Sharma, A.C., Ravindra, N.M., Auluck, S., Srivastava, V.K.: Phys. Status Solidi (b) **120** (1983) 715.

83S2 Samara, G.A.: Phys. Rev. **B27** (1983) 3494.

83T Takizawa, T.: J. Phys. Soc. Jpn. **52** (1983) 1057.

84P Peaker, A.R., Kaufmann, U., Zhan-Guo Wang, Wörner, R., Hamilton, B., Grimmeiss, H.G.: J. Phys. **C17** (1984) 6161.

84S Solal, F., Jezequel, G., Houzay, F., Barski, A., Pinchaux, R.: Solid State commun. **52** (1984) 37 and private communication from G. Jezequel.

84T Tmar, M., Gabriel, A., Chatillon, C., Ansara, I.: J. Crystal Growth **68** (1984) 557.

84Y Yang, X.Z., Samuelson, L., Grimmeiss, H.G.: J. Phys. **C17** (1984) 6521.

85B Brehme, S.: J. Phys. **C18** (1985) L319.

85C Campi, D., Papuzza, C.: J. Appl. Phys. **57** (1985) 1305.

86U Ulrici, W., Eaves, L., Friedland, K., Halliday, D.P., Kreissl, J.: Defects in Semiconductors, Proc. 14th Internat. Conf. Defects in Semicond., Paris (1986), von Bardeleben, H.J. (ed.), Materials Science Forum, Vol. 10···12, Trans. Tech. Publications, Switzerland, **1986**, p. 639.

87R Roura, P., Bremond, G., Nouailhat, A., Guillot, G., Ulrici, W.: Appl. Phys. Lett. **51** (1987) 1696.

89U Ulrici, W., Kreissl, J., Hayes, D.G., Eaves, L., Friedland, K.: Materials Science Forum, Vol. 38···41, Trans. Tech. Publications, Switzerland, **1989**, p 875.

Physical property	Numerical value	Experimental conditions	Experimental method, remarks	Ref.

2.10 Gallium arsenide (GaAs)

Electronic properties

band structure: Fig. 1 (Brillouin zone: section 1.1, Fig. 2).
GaAs is a direct gap semiconductor. The *conduction band* minimum is situated at Γ (symmetry Γ_8). Higher sets of minima at L and near X are important for optical as well as transport properties. The X-minimum has most probably a camel's back structure. The *valence bands* show the topology characteristic for all zincblende semiconductors.

energies of symmetry points of the band structure (relative to the top of the valence band) (in eV):

$E(\Gamma_{6v})$	−12.55	$E(\Gamma_{1v})$	−13.1	first row: designation of symmetry point in double group notation, data according to a nonlocal pseudopotential calculation [76C] (see Fig. 1)
$E(\Gamma_{7v})$	−0.35	$E(\Gamma_{15v})$	0.00	
$E(\Gamma_{8v})$	0.00			
$E(\Gamma_{6c})$	1.51	$E(\Gamma_{1c})$	1.632	
$E(\Gamma_{7c})$	4.55	$E(\Gamma_{15c})$	4.716	
$E(\Gamma_{8c})$	4.71			
$E(\Gamma_{6c})$	—	$E(\Gamma_{1c})$	8.33	
$E(X_{6v})$	−9.83	$E(X_{1v})$	−10.75	second row: designation of symmetry point in single group notation, data from angle resolved photoemission [80C] and photoelectron spectroscopy [85S]
$E(X_{6v})$	−6.88	$E(X_{3v})$	−6.70	
$E(X_{6v})$	−2.99	$E(X_{5v})$	−2.80	
$E(X_{7v})$	−2.89			
$E(X_{6c})$	2.03	$E(X_{1c})$	2.18	
$E(X_{7c})$	2.38	$E(X_{3c})$	2.58	
$E(L_{6v})$	−10.60	$E(L_{1v})$	−11.24	
$E(L_{6v})$	−6.83	$E(L_{1v})$	6.70	
$E(L_{6v})$	−1.42	$E(L_{3v})$	1.30	
$E(L_{4,5v})$	−1.20			
$E(L_{6c})$	1.82	$E(L_{1c})$	1.85	
$E(L_{6c})$	5.47	$E(L_{3c})$	—	
$E(L_{45c})$	5.52			

direct gap (in eV):

$E_{g,dir}$ $(\Gamma_{8v}-\Gamma_{6c})$	1.51914	0 K (extrapol.)	fitting of photoluminescence data	84S
	1.424(1)	300 K	differentiated reflectivity	74S1
$E_{g,th}$	1.604	0 K, extrapol.	intrinsic carrier concentration	82B3

temperature dependence of $E_{g,dir}$:
Empirical relation: $E_{g,dir}(T) = 1.519 - 5.408 \cdot 10^{-4} T^2/(T + 204)$ eV (T in K) according to [82B1]. See also Fig. 2.

exciton energies (in eV):

$E(1S, \Gamma_{5T})$	1.5150	1.8 K	reflectance	83S1
$E(1S, \Gamma_{5L})$	1.51544	10 K	resonant Brillouin scattering	83S2

higher conduction band minima (energy above Γ_{6c} minimum) (in eV):

$\Delta E_{\Gamma L}(\Gamma_{6c} - L_{6c})$	0.300(20)	120 K	photoemission	85D
$\Delta E_{\Gamma X}(\Gamma_{6c} - X_{6c})$	0.460(20)			

spin-orbit splitting energy:

$\Delta_0(\Gamma_{7v} - \Gamma_{8v})$	0.341(1) eV	4.2 K	electroreflectance	73A

Physical property	Numerical value	Experimental conditions	Experimental method, remarks	Ref.
critical point energies (in eV):				
$E_0 + \Delta_0$	1.859(1)	4.2 K	electroreflectance; assigned transition:	73A
			$\Gamma_{7v} - \Gamma_{6c}$	
E'_0	4.488(10)		$\Gamma_{8v} - \Gamma_{7c}$	
E'_0	4.529(10)		$\Delta_{5v} - \Delta_{5c}$	
$E'_0 + \Delta'_0$	4.659(10)		$\Gamma_{8v} - \Gamma_{8c}$	
$E'_0 + \Delta''_0$	4.712(10)		$\Delta_{5v} - \Delta_{5c}$	
$E'_0 + \Delta'_0 + \Delta_0$	5.014(15)		$\Gamma_{7v} - \Gamma_{8c}$	
E_1	3.043(9)		$\Lambda_{4,5v} - \Lambda_{6c}$	
$E_1 + \Delta_1$	3.2636(1)		$\Lambda_{6v} - \Lambda_{6c}$	
E_2	5.137(10)		at Σ	
	4.937(10)		$X_{7v} - X_{6c}$	
	5.014(10)		$X_{6v} - X_{6c}$	
	5.339(10)		$X_{7v} - X_{7c}$	
	5.415(15)		$X_{6v} - X_{7c}$	

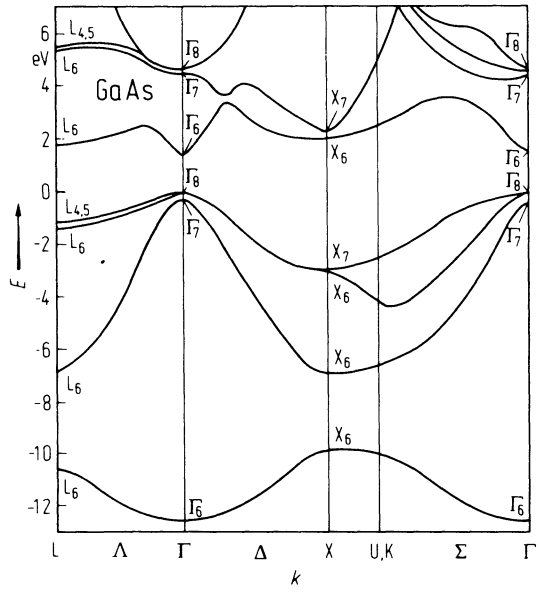

Fig.1. GaAs. Band structure obtained by a non-local pseudopotential calculation [76C].

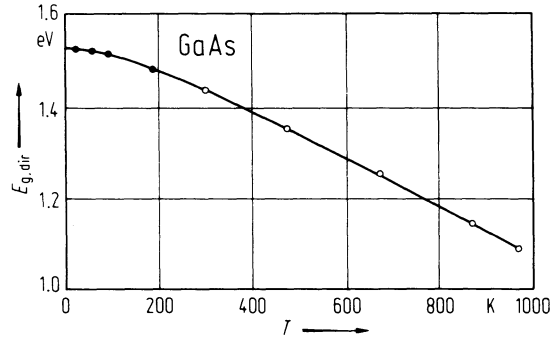

Fig. 2. GaAs. Direct energy gap vs. temperature. Data from two authors [69P].

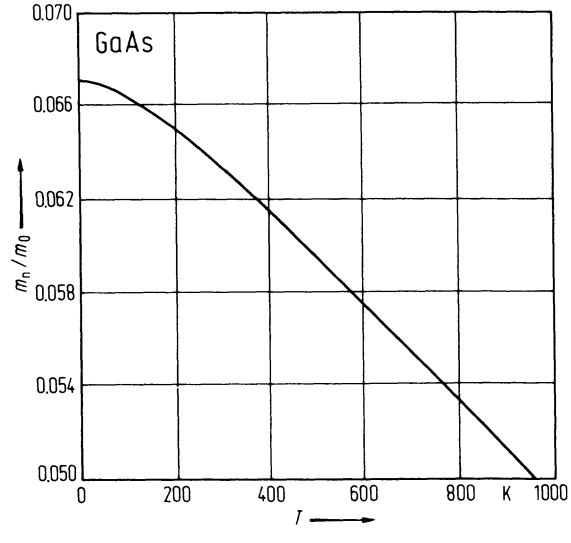

Fig. 3. GaAs. Effective electron mass vs. temperature obtained by a $k \cdot p$ calculation using experimental values for the input parameters [82B1].

Physical property	Numerical value	Experimental conditions	Experimental method, remarks	Ref.
effective mass, electrons (in units of m_0):				
$m_n(\Gamma)$	0.067	0 K	recommended band edge density of states mass	82B1
	0.063	300 K		
	0.0650(5)		deduced from cyclotron resonance corrected for polaron effects	83L1
For temperature dependence of m_n, see Fig. 3.				
camel's back structure of conduction band edge:				
ΔE	9.3 meV		for definition of the parameters, see Fig. 2 of section 2.9; values extrapolated from GaP using a $k \cdot p$ model	85K
Δ	304 meV			
k_m	$0.102(2\pi/a)$			
m_l	$1.8 m_0$			
m_t	$0.257 m_0$			
$m_{X,ds}$	$0.85 m_0$		density of states mass at X neglecting camel's back structure	82B1
***g*-factor of electrons:**				
g_c	−0.44(5)	4 K	piezospectroscopy	76S2
effective masses, holes (in units of m_0):				
$m_{p,h}$	0.51(2)	$T < 100$ K	recommended density of states mass values from discussion of various literature data	82B1
	0.50	300 K		
$m_{p,l}$	0.082(4)	$T < 100$ K		
	0.076	300 K		
m_{so}	0.154	$T < 100$ K		
	0.145	300 K		
$m_{p,ds}$	0.53		combined for heavy and light hole bands	
valence band parameters:				
A	−6.98(45)	77 K	cyclotron resonance	76S2
B	−4.5(2)			
$\lvert C \rvert$	6.2(10)			

Lattice properties

Structure

GaAs I	space group T_d^2–$F\bar{4}3m$ (zincblende structure)	stable at normal pressure	
GaAs II	orthorhombic distortion of NaCl structure space group probably D_{2h}^1–Pmmm	high-pressure phase	82B2
transition pressure:			
p_{tr}	172(7) kbar	beginning of phase transition	82B2

Physical property	Numerical value	Experimental conditions	Experimental method, remarks	Ref.
lattice parameter:				
a	5.65325(2) Å	300 K	X-ray, single crystal	75M2
For temperature dependence, see Fig. 4.				
linear thermal expansion coefficient: Fig. 5.				
density:				
d	5.3176(3) g cm^{-3}	298.15 K	Archimedean	65S2

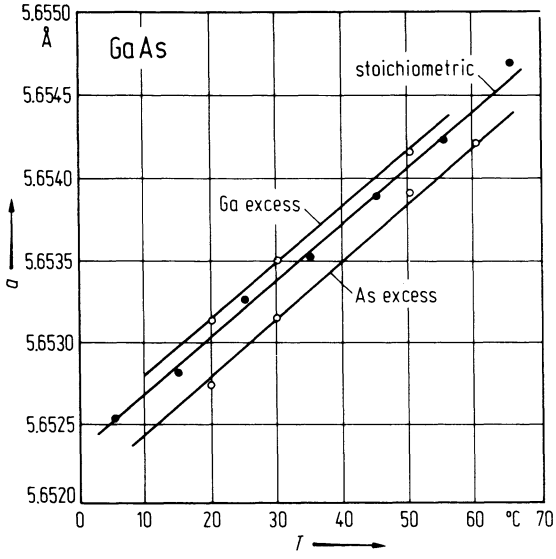

Fig. 4. GaAs. Lattice parameter vs. temperature for stoichiometric crystals and crystals with Ga and As excess, respectively [65S2].

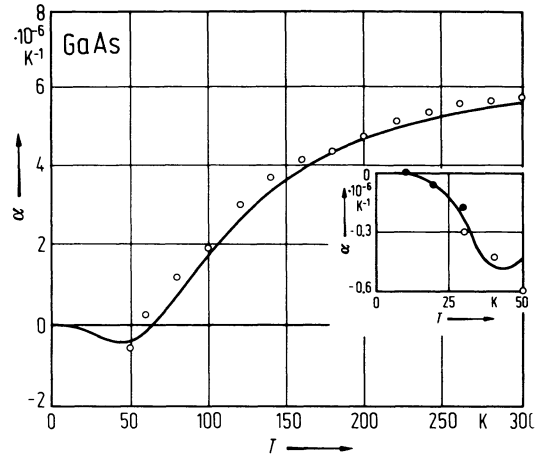

Fig. 5. GaAs. Coefficient of linear thermal expansion vs. temperature. Theoretical curve compared with experimental data [82S1].

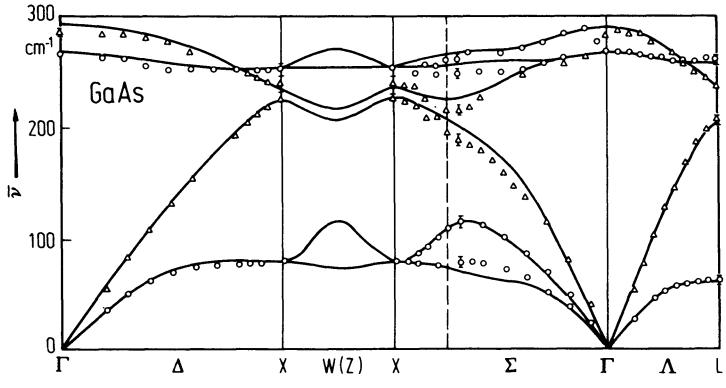

Fig. 6. GaAs. Phonon dispersion relations calculated with an eleven-parameter rigid-ion model. Experimental points from neutron diffraction [84P2].

Physical property	Numerical value	Experimental conditions	Experimental method, remarks	Ref.
melting point:				
T_m	1513 K			
phonon dispersion relations: Fig. 6.				
phonon wavenumbers (in cm^{-1}):				
$\bar{\nu}_{LO}(\Gamma)$	285.0 (67)		neutron scattering	84P
$\bar{\nu}_{TO}(\Gamma)$	267.3 (27)			
$\bar{\nu}_{LO}(X)$	240.7 (50)			
$\bar{\nu}_{LA}(X)$	226.7 (20)			
$\bar{\nu}_{TO}(X)$	252.0 (30)			
$\bar{\nu}_{TA}(X)$	78.7 (5)			
$\bar{\nu}_{LO}(L)$	238.3 (23)			
$\bar{\nu}_{LA}(L)$	208.7 (33)			
$\bar{\nu}_{TO}(L)$	261.3 (40)			
$\bar{\nu}_{TA}(L)$	62.0 (7)			
second order elastic moduli (in 10^{11} dyn cm^{-2}):				
c_{11}	11.9 (1)	300 K	recommended values from a discussion of several published data	82B1
	12.21 (3)	77 K		
	11.26	0 K		
c_{12}	5.38 (1)	300 K	$T = 0$ K data: extrapolated	
	5.66 (3)	77 K		
	5.71	0 K		
c_{44}	5.95 (1)	300 K		
	5.99 (1)	77 K		
	6.00	0 K		
third order elastic moduli (in 10^{12} dyn cm^{-2}):				
c_{111}	−6.75 (20)	RT, $n < 10^{17}$ cm^{-3}	ultrasound	66D
c_{112}	−4.02 (10)			
c_{123}	−0.04 (10)			
c_{144}	−0.70 (10)			
c_{166}	−3.20 (20)			
c_{456}	−0.69 (3)			

Transport properties

At low fields, the electrons occupy the Γ_6 minima at the zone center. The dominating scattering process at RT is polar optical scattering, while below 60 K the most important contribution to the lattice mobility is made by piezoelectric scattering. At RT, the hole mobility of samples with $p < 5 \cdot 10^{15}$ cm^{-3} is governed by lattice scattering alone.

intrinsic carrier concentration (in cm^{-3}):				
n_i	$2.1 \cdot 10^6$	300 K		82B3

The temperature dependence can be expressed by

$$n_i(T) = 1.05 \cdot 10^{16} T^{3/2} \exp(-1.604/2kT)$$

(T in K; kT in eV) for the range 33 K $< T <$ 475 K. For the range 250 K $< T <$ 1500 K and for comparison of various literature data, see Fig. 7.

Physical property	Numerical value	Experimental conditions	Experimental method, remarks	Ref.

At RT a fraction of about $4 \cdot 10^{-4}$ of the conduction electrons fills the L_6-bands; the fraction of the conduction electrons in the X_6-bands is negligible ($< 10^{-6}$). At 400 K the L_6-bands begin to hold an appreciable fraction of carriers and at 800 K the X_6-bands also take over parts of the electron population. At 100 K only 30% of all conduction electrons reside in the Γ_6-band. Thus, above RT the "one-band" approximation $n = 1/|R_H e|$ is of limited accuracy [80N].

electrical conductivity:

Since n_i (300 K) $= 2.1 \cdot 10^6\,cm^{-3}$ the electrical conductivity in GaAs is in general determined by charge carriers provided by impurities. Only by certain doping conditions (e.g. compensation of shallow acceptor levels by donor impurities and overcompensation by deep Cr levels) the Fermi level can be pinned in the middle of the energy gap and nearly intrinsic conduction can be achieved (*semi-insulating GaAs*, $\varrho = 10^5 \cdots 10^9\,\Omega cm$).

typical data for semi-insulating GaAs:

σ	$2.38 \cdot 10^{-9}\,\Omega^{-1}\,cm^{-1}$	RT, undoped sample	n and μ_n obtained from R_H and σ by a mixed conduction analysis	83W
n	$3.73 \cdot 10^6\,cm^{-3}$			
$\mu_{H,n}$	$3970\,cm^2/Vs$			
electron mobility (in cm^2/Vs):				
$\mu_{H,n}$	9200	300 K	epitaxial layer	82L1
	$2 \cdot 10^5$	77 K	$n(77\,K) = n(300\,K)$	
	$3.76 \cdot 10^5$	41 K	$= 1.3 \cdot 10^{13}\,cm^{-3}$	
	$9400\,(300/T)^{2.3}$		(T in K) in weak fields	83B1
$\mu_{dr,n}$	$8000\,(300/T)^{2.3}$		fairly close to RT	

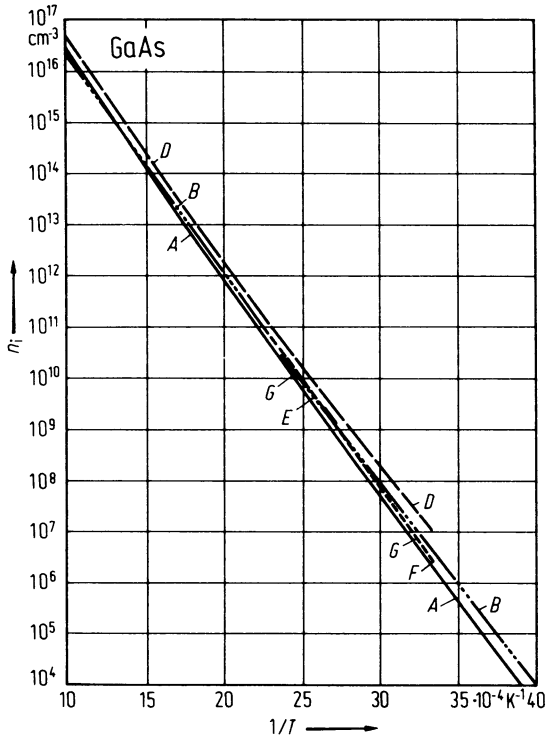

Fig. 7. GaAs. Intrinsic carrier concentration vs. reciprocal temperature for the range 250 ··· 1000 K. The solid curve (*A*) is the result of a critical discussion of the literature data.- Curves (*B*) ··· (*G*) represent data from other sources [82B].

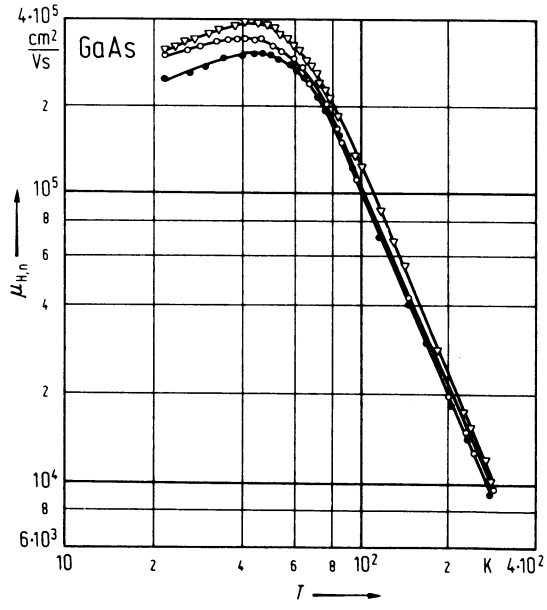

Fig. 8. GaAs. Electron Hall mobility vs. temperature for three high purity epitaxial layers ($n(300\,K) \simeq 3 \cdot 10^{13}\,cm^{-3}$). Solid curves: theoretical [82L1].

Physical property	Numerical value	Experimental conditions	Experimental method, remarks	Ref.

For temperature dependence in the range 20 K ··· 300 K, see Fig. 8. Separation of the mobility into contributions of several bands: Fig. 9.

hole mobility (in cm^2/Vs):

$\mu_{H,p}$	$400(300/T)^{2.3}$	near 300 K	(T in K)	75W
	402	300 K	theoretical, see Fig. 10	83L2
$\mu_{dr,p}$	$320(300/T)^{2.3}$			75W
heavy holes:	130	300 K	theoretical, see Fig. 10	83L2
light holes:	1060			

thermal conductivity: Fig. 11.

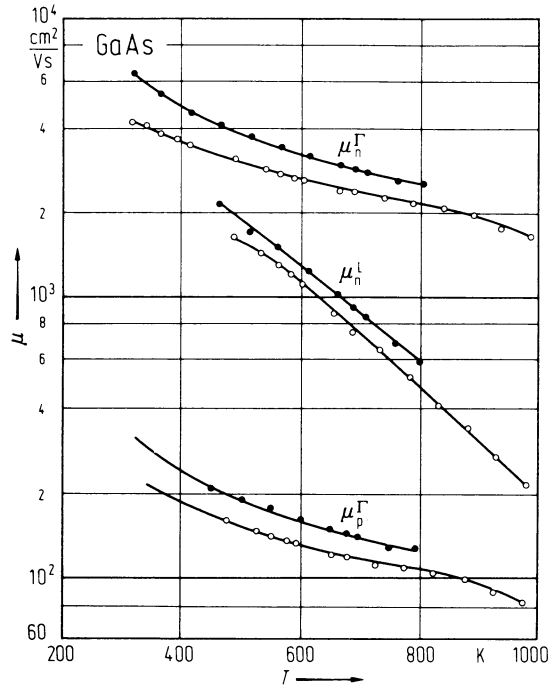

Fig. 9. GaAs. Carrier mobilities in the Γ- and L-minima of the conduction bands and in the Γ_8 valence bands for two samples [80N].

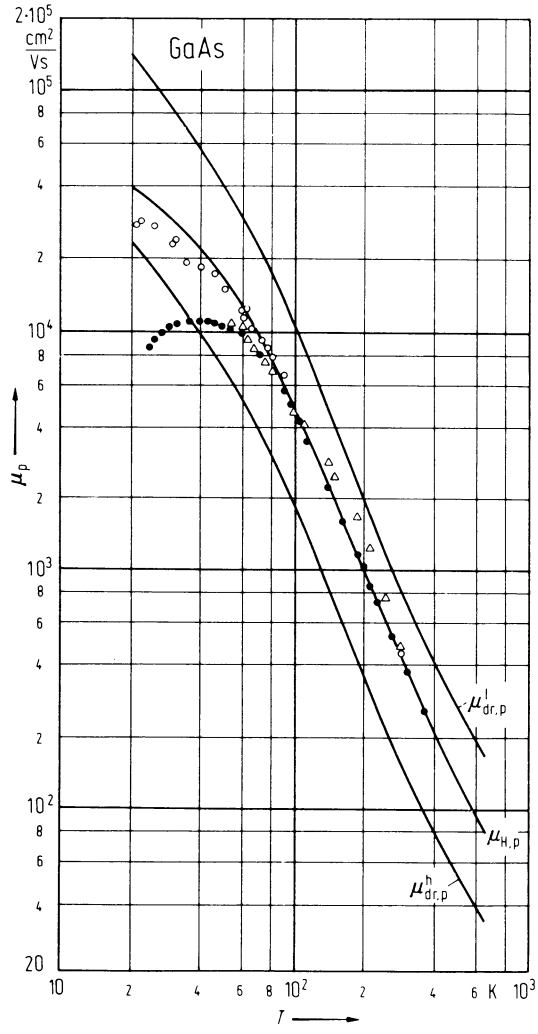

Fig. 10. GaAs. Theoretical lattice scattering limited hole mobility ($\mu_{H,p}$) vs. temperature and comparison with experimental data. Theoretical curves for the drift mobility of heavy and light holes are included [83L2].

Physical property	Numerical value	Experimental conditions	Experimental method, remarks	Ref.

Optical properties

dielectric constants:

$\varepsilon(0)$	$12.40\cdot(1 + 1.2\cdot10^{-4}T)$ (T in K)	recommended value and linearized temperature dependence below 600 K	82B1
$\varepsilon(\infty)$	$10.60\cdot(1 + 9.0\cdot10^{-5}T)$		

refractive index (see also below):

n	$3.255\cdot(1 + 4.5\cdot10^{-5}T)$	(T in K)	82B1

Dependence on photon energy: range 1 ··· 1.7 eV: Fig. 12.
In the range 0.3 ··· 1.4 eV various published data can be fitted by

$$n^2 = 7.10 + 3.78/(1 - 0.18(\hbar\omega)^2) \quad (\hbar\omega \text{ in eV}) \qquad \text{82B1}$$

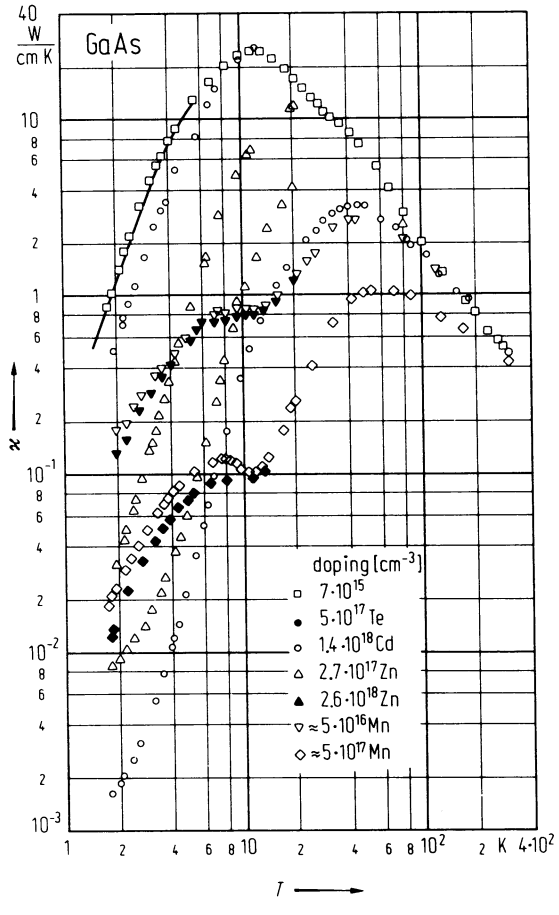

Fig. 11. GaAs. Thermal conductivity vs. temperature for seven samples with impurity concentrations between $7\cdot10^{15}$ cm^{-3} and $2.6\cdot10^{18}$ cm^{-3} [64H2].

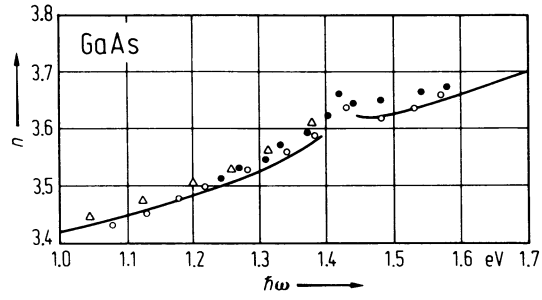

Fig. 12. GaAs. Refractive index vs. photon energy in the range 1.0 ··· 1.7 eV [85C], solid line: calculated, symbols: experimental data from three sources.

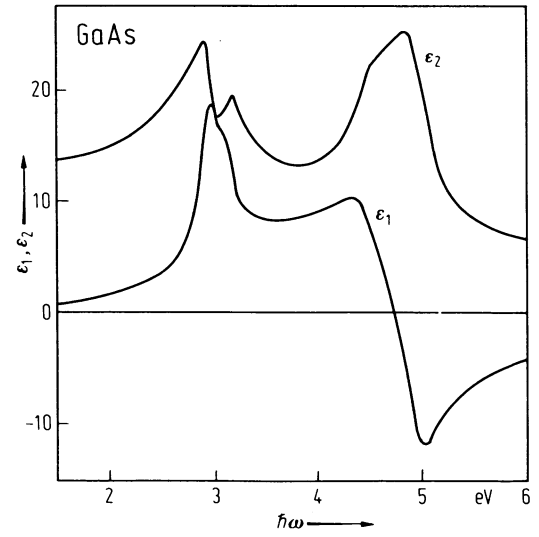

Fig. 13. GaAs. Real and imaginary parts of the dielectric constant vs. photon energy [83A].

optical constants:

real and imaginary parts of the dielectric constant measured by spectroscopical ellipsometry; n, k, R, K calculated from these data [83A]; see also Fig. 13.

$\hbar\omega$[eV]	ε_1	ε_2	n	k	R	K [10^3 cm^{-1}]
1.5	13.435	0.589	3.666	0.080	0.327	12.21
2.0	14.991	1.637	3.878	0.211	0.349	42.79
2.5	18.579	3.821	4.333	0.441	0.395	111.74
3.0	16.536	17.571	4.509	1.948	0.472	592.48
3.5	8.413	14.216	3.531	2.013	0.425	714.20
4.0	9.279	13.832	3.601	1.920	0.421	778.65
4.5	6.797	22.845	3.913	2.919	0.521	1331.28
5.0	−11.515	18.563	2.273	4.084	0.668	2069.81
5.5	−6.705	8.123	1.383	2.936	0.613	1636.68
6.0	−4.511	6.250	1.264	2.472	0.550	1503.20

Impurities and defects

solubility of impurities in GaAs

Impurity	c^{eq} [cm^{-3}]	T [°C]	Remarks	Ref.
Ag	$5\cdot10^{20}$	1000	radiotracer	64B
Au	$1.5\cdot10^{17}$	835	radiatracer	68K
C	$1.9\cdot10^{19}$	1100	^{14}C, mass spectrometry	78B
Cd	$\approx 2\cdot10^{18}$	1000	sheet resistance	64K2
Cr	$\approx 5\cdot10^{16}$	1100	radiotracer, possible As and interstitial sites	79T
Cu	$7\cdot10^{18}$ (max)	1100	radiotracer	64H
	$1.5\cdot10^{16}$	<700		
Ge	$>2\cdot10^{18}$	melt growth	lattice parameter, electrical activity	75M1
Hg	$5\cdot10^{17}$	1000		68K
Mn	$10^{18}\cdots10^{19}$	825	radiotracer	66L
O	$4\cdot10^{19}$ (max)	1100	mass spectrometer retrograde solubility	77B
Pb	$4\cdot10^{18}$	melt growth	lattice parameter, electrical activity	75M1
S	$1.6\cdot10^{18}$	900		60R
	$4\cdot10^{18}$	melt growth	lattice parameter, electrical activity	75M1
Se	$c_{Se}^{eq} = 9.5\cdot10^{23}\exp(-1.23(2)\,\mathrm{eV}/kT)\,\mathrm{cm}^{-3}$			78L
	$2\cdot10^{18}$	melt growth		75M1
Si	$>4.7\cdot10^{18}$	melt growth	n-type (Si_{Ga}?)	80F
	$>3\cdot10^{18}$	melt growth	p-type (Si_{As}?)	80F
	$6\cdot10^{18}$	LPE growth 856···750	p-type (both Si_{As} and Si_{Ga}?)	80F
Sn	$>1\cdot10^{19}$	LPE growth 856···750		75M1
Tc	$1\cdot10^{19}$	melt growth	lattice parameter, electrical activity	75M1
	$4.5\cdot10^{18}$	880	electrical activity, lattice parameter after anneal	79D
Zn	$4\cdot10^{20}$	1000	radiotracer	64C2
	$3.8\cdot10^{20}$	1000	radiotracer	76T

diffusion coefficients

Element	$D_0[cm^2 s^{-1}]$	Q[eV]	Remarks	Ref.
Self-diffusion coefficients				
Ga	$4 \cdot 10^{-5}$	2.6	radiotracer	83P
As	$5.5 \cdot 10^{-4}$	3.0	radiotracer, arsenic pressure dependence	83P
Impurity diffusion coefficients				
Ag	$4.0 \cdot 10^{-4}$	0.80	radiotracer	64B
	$2.5 \cdot 10^{1}$	2.27	radiotracer	73C
	complex profiles		radiotracer ($\sqrt{Dt} \simeq$ slice thickness)	81T
Au	$1.0 \cdot 10^{-3}$	1.0	radiotracer	64S
	$2.9 \cdot 10^{1}$	2.64	radiotracer	73C
Be	$7.3 \cdot 10^{-6}$	1.2	incremental sheet resistance	66P
Cd	$5.0 \cdot 10^{-2}$	2.43	radiotracer	60G
	concentration dependent		radiotracer	69S
Cr	$4.3 \cdot 10^{3}$	3.4	radiotracer	73C
	complex profiles dependent on As pressure		radiotracer ($\sqrt{Dt} \simeq$ slice thickness)	79T
	$6.3 \cdot 10^{5}$	3.4	outdiffusion	80K1
	$D(800\,°C) = 6.7 \cdot 10^{-12}$		SIMS	80W
	$8.53 \cdot 10^{4}$	3.53	outdiffusion, SIMS	82M
Cu	$3.0 \cdot 10^{-2}$	0.53	radiotracer	64H
Hg	$D(1000\,°C) = 5 \cdot 10^{-14}$			73C
In	$D(1000\,°C) = 7 \cdot 10^{-11}$			64K
Mg	$2.6 \cdot 10^{-2}$	2.7	pn-junction, SIMS	65M
				82S2
Mn	$6.5 \cdot 10^{-1}$	2.49	radiotracer, dependent on As pressure	65S1
O	$2.0 \cdot 10^{-3}$	1.1	outdiffusion	69R
S	$1.2 \cdot 10^{-4}$	1.8	pn-junction	61V
	dependence on As pressure		radiotracer	81T
Se	$3.0 \cdot 10^{3}$	4.16	radiotracer, Ga_2Se_3 layer formed	61G
Si	0.11	2.5	SIMS and differential Hall effect	84G
			SIMS, defect model	87K
Sn	$3.5 \cdot 10^{-2}$	2.7	radiotracer	63F
	3.2	3.3	radiotracer, undoped material, excess As pressure	78T
	$9.43 \cdot 10^{-8}$	1.9	radiotracer, n-type material $n \approx 2 \cdot 10^{18}\,cm^{-3}$	78T
Te	$D(1000\,°C) = 10^{-13}$			73C
	$D(1100\,°C) = 2 \cdot 10^{-12}$			
Tm	$2.3 \cdot 10^{-16}$	(−)1.0		64C1

Zinc diffusion data in GaAs

By far the most attention has been paid to the diffusion of zinc in gallium arsenide, because of its importance as a p-type dopant. The complex nature of the dependence of zinc diffusivity on the zinc concentration, the arsenic pressure, and the temperature has shown that it is absolutely vital to consider the ternary nature of the system in the interpretation and characterization of this dopant, and we cannot consider the compound as one element in a binary system.

shallow impurities

Impurity	E_b[meV]	T[K]	Remarks	Ref.
shallow donors, binding energies (in meV)				
The binding energies in the following table are calculated from the energetic positions of the 1S–2P transitions as observed in photoconductivity plus the binding energy of the 2P-state of 1.429 meV as calculated in [71S4]. The energy positions of the 1S–2P transitions without magnetic field are extrapolated from magnetic field experiments				
Theory	5.715		donor effective mass calculation	71S2
Pb, 'A' = ?	5.752	4.2	far infrared photoconductivity	76S1,
V_{Ga}, Pb	5.777			78C
Se	5.789			
Si	5.839			
S	6.870			
Ge	5.882			
C	5.913			
shallow acceptors, binding energies				
(F–B: free to bound transition, DAP: donor- acceptor-pair)				
$1S_{3/2}$ calculation	25.82		Effective mass theory using valence band parameters of [76S2] for the calculation	74B 78K
Be	28.0	5	F–B Photoluminescence	75A
C	26.9	≈20	Far infrared photoconductivity	78K
	26.0	5	F–B Photoluminescence	75A
Cd	34.7	5	F–B Photoluminescence	75A
Ge	40.4	5	F–B Photoluminescence	75A
Mg	28.7	≈20	Far infrared photoconductivity	78K
	28.4	5	F–B Photoluminescence	75A
Mn	113.1	28	F–B Photoluminescence	74S2
Si	34.8	≈20	Far infrared photoconductivity	78K
	34.5	5	F–B Photoluminescence	75A
	35.2	5	F–B Photoluminescence	80K2
Sn	170.5	5	F–B Photoluminescence	75A
	167.2	1.8	DAP Photoluminescence	76S2
Zn	30.6	≈20	Far infrared photoconductivity	78K
	30.7	5	F–B Photoluminescence	75A

Copper complexes

Copper is a potentially important contaminant in GaAs. It has been known for many years that copper introduces electrically active centers producing, for example, double compensation [64H, 84B]. These levels of n-type GaAs exhibit thermal activation energies measured from the valence band of 0.156 eV and 0.45 eV. There are also several photoluminescence lines which have been associated with copper or copper-related complexes.

Since copper occupying a substitutional gallium site, Cu_{Ga}, would be expected to act as a double acceptor, many of the electrical and optical signatures of copper-contaminated GaAs have been related to Cu_{Ga} or complexes involving Cu_{Ga} and native defects.

energy levels related to isolated, substitutional transition metal impurities

Impurity	E[eV]	Type	Remarks	T[K]	Ref.
Ti	0.23(1)	a	DLTS and capacitance transient measurements		86H
	−1.00(3)	d	DLTS and capacitance transient measurements		86B1
	+0.60(2)	d	DLTS		86G
V	−0.14	a	DLTS		80M1
Cr	+0.750(20)	a	DLTS (capture cross-section)	320	80M2
	+0.40(3)	d	σ_p^0 absorption photoionization		82U
Mn	+0.1130(5)	a	Luminescence	4	74S2
Fe	+0.49	a	Excitation of luminescence	4.2	83S3
	+0.6	a	σ_p^0 obtained from DLOS	218	82L2
	−0.85	a	σ_n^0 obtained from DLOS	218	82L2
Co	+0.14	a	σ_p^0 photoluminescence excitation photoionization	4.2	86D
Ni	+0.20	1st a	Temperature dependent Hall effect		72B
	−0.40(4)	2nd a	DLTS	0	86B2
	+1.03(3)	2nd a	σ_p^0 photoionization from ODLTS	202	86B2
Ag	+0.230	a	DLTS		82Y
Au	+0.397	a	DLTS		82Y

References for 2.10

60G Goldstein, B.: Phys. Rev. **118** (1960) 1024.
60R Reiss, H., Fuller, C.S.: Semiconductors, Hannay, N.B. (ed.), New York: Reinhold **1960**, p. 230.
61G Goldstein, B.: Phys. Rev. **121** (1961) 1305.
61V Vieland, L.J.: J. Phys. Chem. Solids **21** (1961) 318.
63F Fane, R.W., Goss, A.J.: Solid State Electron. **6** (1963) 383.
64B Boltaks, B.I., Shishiyanu, F.S.: Sov. Phys. Solid State **5** (1964) 1680.
64C1 Casey, H.C., Pearson, G.L.: J. Appl. Phys. **35** (1964) 3401.
64C2 Chang, L.L., Pearson, G.L.: J. Appl. Phys. **35** (1964) 1960.
64H1 Hall, R.N., Racette, J.H.: J. Appl. Phys. **35** (1964) 379.
64H2 Holland, M.G.: Proc. 7th Int. Conf. Phys. Semicond., Paris 1964, Dunod, Paris 1964.
64K1 Kendall, D.L.: Appl. Phys. Lett. **4** (1964) 67.
64K2 Kogan, L.M., Meskin, S.S., Ya Goikhmann, A.: Sov. Phys. Solid State **6** (1964) 882.
64S Sokolov, V.I., Shishiyanu, F.S.: Sov. Phys. Solid State **6** (1964) 265.
65M Moore, R.G.: Bull. Am. Phys. Soc. **10** (1965) 731.
65S1 Seltzer, M.S.: J. Phys. Chem. Solids **26** (1965) 243.
65S2 Straumanis, M.E., Kim. C.D.: Acta. Crystallogr. **19** (1965) 256.
66D Drabble, J.R., Brammer, A.J.: Solid State Commun. **4** (1966) 467.
66L Larrabee, G.B., Osborne, J.F.: J. Electrochem. Soc. **113** (1966) 564.
66P Poltoratskii, E.A., Stuckelbnikov, V.M.: Sov. Phys. Solid State **8** (1966) 770.
68K Kendall, D.L.: Semiconductors and Semimetals, Vol. 4, Willardson, Beer (eds.), New York, London: Academic Press **1968**, p. 163.
69P Panish, M.B., Casey, H.C.: J. Appl. Phys. **40** (1969) 163.
69R Rachmann, J., Biermann, R.: Solid State Commun. **7** (1969) 1771.
69S Showan, S.R., Shaw, D.: Phys. Status Solidi **35** (1969) K79.
71S1 Stringfellow, G.B.: Mater. Res. Bull. **6** (1971) 371.
71S2 Stillman, G.E., Larsen, D.M., Wolfe, C.M., Brandt, R.C.: Solid State Commun. **9** (1971) 2245.
72B Brown, W.J., Blakemore, J.S.: J. Appl. Phys. **43** (1972) 2242.
73A Aspnes, D.E., Studna, A.A.: Phys. Rev. **B7** (1973) 4605.
73C Casey, H.C.: Atomic Diffusion in Semiconductors, Shaw, D. (ed.), New York: Plenum Press **1973**, p. 351.
74B Baldereschi, A., Lipari, N.O.: Phys. Rev. **B9** (1974) 1525.
74S1 Sell, D.D., Casey, H.C., Wecht, K.W.: J. Appl. Phys. **45** (1974) 2650.
74S2 Schairer, W., Schmidt, M.: Phys. Rev. **B10** (1974) 2501.
75A Ashen, D.J., Dean, P.J., Hurle, D.T.J., Mullin, J.B., White, A.M.: J. Phys. Chem. Solids **36** (1975) 1041.
75M1 Mullin, J.B., Straughan, B.W., Driscoll, C.M.H., Willoughby, A.F.W.: CRC Critical Reviews in Solid State Sciences, **1975**, p. 441.

75M2 Mullin, J.B., Straughan, B.W., Driscoll, C.M.H., Willoughby, A.F.W.: Inst. Phys. Conf. Ser. **24** (1975) 275.
75W Wiley, J.D.: in "Semiconductors and Semimetals", Vol. 10, R.K. Willardson, A.C. Beer eds., Academic Press, New York **1975**.
76C Chelikowsky, J.R., Cohen, M.L.: Phys. Rev. **B14** (1976) 556.
76H Hess, K., Bimberg, D., Lipari, N.O., Fischbach, J.K., Altarelli, M.: Proc. 13th Int. Conf. Phys. Semicond., F.G. Fumi ed., Rome **1976**, p. 142.
76S1 Schairer, W., Bimberg, D., Kottler, W., Cho, K., Schmidt, M.: Phys. Rev. **B13** (1976) 3452.
76S2 Skolnick, M.S., Jain, A.K., Stradling, R.A., Leotin, L., Ousset, J.C., Ashkennazy, S.J.: J. Phys. **C9** (1976) 2809.
76T Tuck, B.: J. Phys. **D9** (1976) 2061.
77B Borisova, L.A., Akkerman, Z.L., Dorokhov, A.N.: Izv. Akad. Nauk SSSR Neorg. Mater. **13** (1977) 908.
78B Borisova, L.A., Arkymkhin, P.I., Akkerman, Z.L.: Izv. Akad. Nauk SSSR Neorg. Mater. **14** (1978) 1790.
78C Cooke, R.A., Hoult, R.A., Kirkman, R.F., Stradling, R.A.: J. Phys. **C11** (1978) 345.
78K Kirkman, R.F., Stradling, R.A., Lin-Chung, P.J.: J. Phys. **C11** (1978) 419.
78L Lidow, A., Gibbons, J.F., Deline, V.R., Evans, C.A.: Appl. Phys. Lett. **32** (1978) 572.
78T Tuck, B., Badawi, M.H.: J. Phys. **D11** (1978) 2541.
79D Dobson, P.S., Fewster, P.F., Hurle, D.T.J., Hutchinson, P.W., Mullin, J.B., Straughan, B.W., Willoughby, A.F.W.: Inst. Phys. Conf. Ser. **45** (1979) 163.
79T Tuck, B., Adegboyega, G.A.: J. Phys. **D12** (1979) 1895.
80C Chiang, T.C., Knapp, J.A., Aano, M., Eastman, D.E.: Phys. Rev. **B21** (1980) 3513.
80F Fewster, P.F., Willoughby, A.F.W.: J. Cryst. Growth **50** (1980) 648.
80K1 Kasahara, J., Watanabe, N.: Jpn. J. Appl. Phys. **19** (1980) L151.
80K2 Kunzel, H., Ploog, K.: Appl. Phys. Lett. **37** (1980) 416.
80M1 Martin, G.M.: Thesis Univ. P. et M. Curie, **1980**, unpublished.
80M2 Martin, G.M., Mitonneau, A., Pons, D., Mircea, A., Woodard, D.W.: J. Phys. **C13** (1980) 3855.
80N Nichols, K.H., Yee, C.M.L., Wolfe, C.M.: Solid State Electron. **23** (1980) 109.
80T Tuck, B., Adegboyega, G.A.: J. Phys. **D13** (1980) 433.
80W Wilson, R.G., Yasudev, P.K., Jamba, D.M., Evans, C.A., Deline, V.R.: Appl. Phys. Lett. **36** (1980) 215.
81T Tuck, B., Powell, R.G.: J. Phys. **D14** (1981) 317.
82B1 Blakemore, J.S.: J. Appl. Phys. **53** (1982) R123.
82B2 Baublitz, M., Ruoff, A.L.: J. Appl. Phys. **53** (1982) 6179.
82B3 Blakemore, J.S.: J. Appl. Phys. **53** (1982) 520.
82L1 Lin, L., Lin, Y., Zhong, X., Zhang, Y., Li, H.: J. Cryst. Growth **56** (1982) 344.
82L2 Leyral, P., Litty, F., Bremond, G., Nouailhat, A., Guillot, G.: Semi-Insulating III-V Materials, Evian 1982, Makram-Ebeid, S., Tuck, B. (eds.). Nantwich: Shiva Publishing, **1982**, p. 192.
82M Mizutami, T., Honda, T., Ishida, S., Kawasaki, Y.: Solid-State Electron. **25** (1982) 885.
82S1 Soma, T., Satoh, J., Matsuo, H.: Solid State Commun. **42** (1982) 889.
82S2 Small, M.B., Potemski, R.M., Reuter, W., Ghez, R.: Appl. Phys. Lett. **41** (1982) 1068.
82U Ulrici, W.: Phys. Status Solidi (b) **114** (1982) K87.
82Y Yan, Z.X., Milnes, A.G.: J. Electrochem. Soc. **129** (1982) 1353.
83A Aśpnes, D.E., Studna, A.A.: Phys. Rev. **B27** (1983) 985.
83B Büttner, H., Pollmann, J.: Physica **177&118** (1983) 278.
83L1 Lindemann, G., Lassnig, R., Seidenbusch, W., Gornik, E.: Phys. Rev. **B28** (1983) 4693.
83L2 Lee, H.J., Look, D.C.: J. Appl. Phys. **54** (1983) 4446.
83P Palfrey, H.D., Brown, M., Willoughby, A.F.W.: J. Electron. Mater. **12** (1983) 863.
83S1 Sharma, A.C., Ravindra, N.M., Auluck, S., Srivastava, V.K.: Phys. Status Solidi (b) **120** (1983) 715.
83S2 Soma, T., Kagaya, H.-M.: Phys. Status Solidi (b) **118** (1983) 245.
83S3 Shanabrook, B.V., Klein, P.B., Bishop, S.G.: Physica **B116** (1983) 444.
83W2 Winter, J.J., Leupold, H.A., Ross, R.L., Ballato, A.: J. Appl. Phys. **54** (1983) 5176.
84B Blakemore, J.S., Rahimi, S.: Semicond. Semimet. **20** (1984).
84G Greiner, M.E., Gibbons, J.F.: Appl. Phys. Lett. **44** (1984) 750.
84P Patel, C., Parker, T.J., Jamshidi, H., Sherman, W.F.: Phys. Status Solidi (b) **122** (1984) 461.
84S Skromme, B.J., Stillman, G.E.: Phys. Rev. **B29** (1984) 1982.
85C Campi, D., Papuzza, C.: J. Appl. Phys. **57** (1985) 1305.
85D Drouhin, H.-J., Hermann, C., Lampel, G.: Phys. Rev. **B31** (1985) 3859.
85K Kopylov, A.A.: Solid State Commun. **56** (1985) 1.
85S Straub, D., Skibowski, M., Himpsel, F.J.: Phys. Rev. **B32** (1985) 5237.
86B1 Brandt, C.D., Hennel, A.M., Pawlowicz, L.M., Wu, Y.T., Bryskiewicz, T., Lagowski, J., Gatos, H.C.: Appl. Phys. Lett. **48** (1986) 1162.
86B2 Brehme, S., Pickenhain, R.: Solid State Commun. **59** (1986) 469.
86D Deveaud, B., Lambert, B., Auvray, P., Hennel, A.M., Clerjaud, B., Naud, C.: J. Phys. **C19** (1986) 1251.
86G Guillot, G., Bremond, G., Bencherifa, A., Nouailhat, A., Ulrici, W.: Semi-Insulating III-V Materials, Hakone 1986, Kukimoto, H., Miyazawa, S. (eds.) Ohmsha, Tokyo, **1986**, p. 483.
86H Hennel, A.M., Brandt, C.D., Wu, Y.T., Bryskiewicz, T., Ko, K., Lagowski, J., Gatos, H.C.: Phys. Rev. **B33** (1986) 7353.
87K Kavanagh, K.L.: Ph.D. Thesis, University of Cornell **1987**.

Physical property	Numerical value	Experimental conditions	Experimental method, remarks	Ref.

2.11 Gallium antimonide (GaSb)

Electronic properties

band structure: Fig. 1 (Brillouin zone: see section 1.1, Fig. 2)
The *conduction band* is characterized by three sets of minima, the lowest minimum at Γ, slightly higher minima at the L-points at the surface of the Brillouin zone and even higher minima at the X-points. The *valence band* has the structure common to all zincblende semiconductors.

energies of symmetry points of the band structure (relative to the top of the valence band) (in eV):

$E(\Gamma_{6v})$	−12.00	−11.64(10)		symmetry symbols in double group notation
$E(\Gamma_{7v})$	−0.76	−0.82(7)	−0.756(15)	first row: theoretical [76C], see also Fig. 1
$E(\Gamma_{8v})$	0			second row: angular resolved photoelectron spectroscopy [80C]
$E(\Gamma_{6c})$	0.86		0.822(5)	third row: electroreflectance data at 10 K [76A]
$E(\Gamma_{7c})$	3.44		3.191(5)	
$E(\Gamma_{8c})$	3.77		3.404(10)	
$E(\Gamma_{8c})$			7.9(1)	
$E(L_{6v})$	−10.17	−10.06(10)		
$E(L_{6v})$	−6.25	−6.60(10)		
$E(L_{6v})$	−1.45	−1.55(10)	−1.530(10)	
$E(L_{4,5v})$	−1.00	−1.10(7)		
$E(L_{6c})$	1.22		1.095(10)	
$E(L_{4,5c})$	4.43		4.36(2)	
$E(L_{6c})$	4.59		4.49(2)	
$E(X_{6v})$	−9.33	−9.62(10)		
$E(X_{6v})$	−6.76	−6.90(10)		
$E(X_{6v})$	−2.61	−3.10(7)		
$E(X_{7v})$	−2.37	−2.86		
$E(X_{6c})$	1.72			
$E(X_{7c})$	1.79			
$E(\Sigma^{min}_{3,4v})$		−3.64(15)		
		−3.90(15)		

direct energy gap (in eV):

E_{gx}	0.8099(1)	2 K	photoluminescence, excitonic gap	73R
$E_{g,dir}(\Gamma_{8v}-\Gamma_{6c})$	0.8113(2)	2 K	from value above, assuming an exciton binding energy of 1.4 meV	
	0.822	0 K, extrapol.	electroreflectance, see Fig. 2	81J
	0.75	300 K		

critical point and spin orbit splitting energies (in eV):

$E_0+\Delta_0$ $(\Gamma_{7v}-\Gamma_{6c})$	1.569	27 K	modulation spectroscopy	83A2
$E_1(L_{4,5v}-L_{6c})$	2.185			
$E_1+\Delta_1$ $(L_{6v}-L_{6c})$	2.622			
$E_L(\Gamma_{8v}-L_{6c})$	0.871			

Physical property	Numerical value	Experimental conditions	Experimental method, remarks	Ref.
intra conduction band energies:				
L conduction band minima, energy difference to lowest minimum (in meV): (see also E_L above)				
$\Delta E = E(L_{6c}) - E(\Gamma_{6c})$	61 82	300 K	Hall effect, magnetoresistance; first value assuming $m_n(L) = 0.226\,m_0$, second value $m_n(L) = 0.43\,m_0$	84K
X conduction band minima, energy difference to lowest minimum (in meV):				
$E(X_{6c}) - E(\Gamma_{6c})$	430(2)	10 K	electroreflectance	76A
camel's back structure of conduction band edge: (see Fig. 2 of section 2.9 for the meaning of the symbols)				
Δ	178 meV		estimate from $k \cdot p$ theory	85 K
ΔE	25.1 meV		using GaP data	
k_m	$0.127\,(2\pi/a)$			
m_t	$0.250\,m_0$			
m_l	$1.2\,m_0$			

structure of top of valence band:
By the linear $E(k)$-term in the structure of the valence band of semiconductors with zincblende lattice the spin-degeneracy is lifted. The maxima of the heavy hole bands are shifted in [111]-direction, that of the light

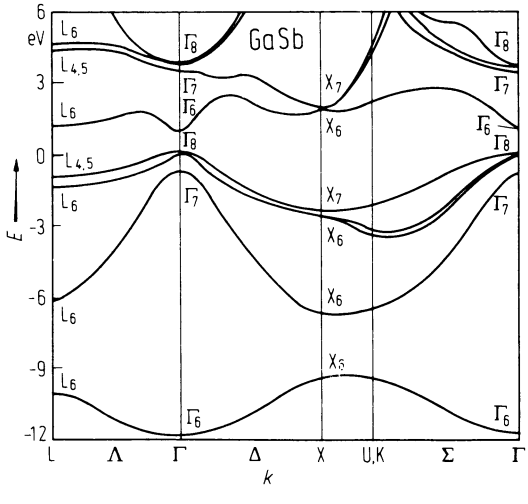

Fig. 1. GaSb. Band structure obtained with a non-local pseudopotential calculation [76C].

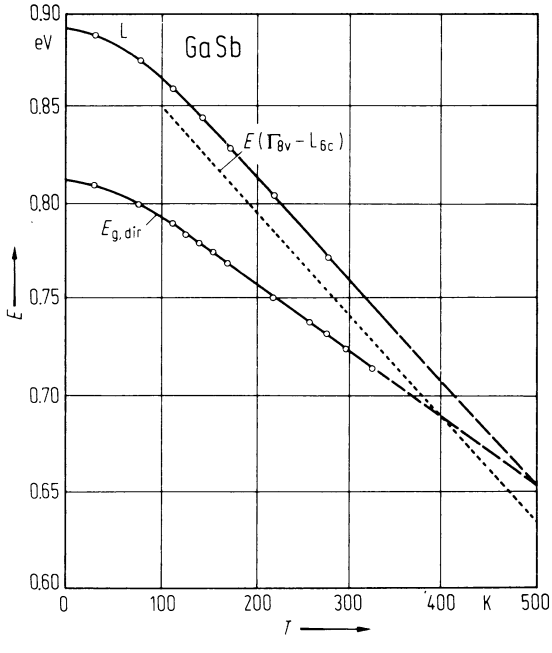

Fig. 2. GaSb. Energies of electroreflectance peaks vs. temperature. $E_{g,dir}$: direct $\Gamma_{8v} - \Gamma_{6c}$ transition, L: indirect $\Gamma_{8v} - L_{6c}$ transition, dotted line: $\Gamma_{8v} - L_{6c}$ gap obtained from L by subtracting the LA phonon energy of 17 meV [81J].

Physical property	Numerical value	Experimental conditions	Experimental method, remarks	Ref.
hole bands in [100]-direction. From an analysis of transport data the following values for the difference of energies at the top of the bands and at $k = 0$ have been found:				
$\Delta E[111]$	20 meV			79M
$\Delta E[100]$	5 meV			
$\Delta E[111] - \Delta E[100]$	7.5 meV			85H
effective masses (in units of m_0):				
$m_n(\Gamma_{6c})$	0.0412(12)	1 ··· 30 K	cyclotron resonance of hot electrons; taking into account non-parabolicity and polaron effect a bare effective mass of 0.0396(21) m_0 results	74H
$m_n(L_{6c})$	0.11		transverse	81L
	0.95		longitudinal	
	0.226		density of states analysis of transport data	
$m_n(X_{6c})$	0.22		transverse	81L
	1.51		longitudinal; analysis of transport data	
$m_{p,h}$	0.28(13)		conductivity and density of state masses from an analysis of transport data	85H
$m_{p,l}$	0.050(5)			
$m_{p,ds}$	0.82			
electron g-factor:				
g_c	−7.8(8)	30 K	stress modulated magneto-reflectance	72R2
valence band parameters:				
A	−11.7		calculated using $k \cdot p$ theory	75W
B	−8.19			
$\|C\|$	11.07			
Lattice properties				
Structure				
GaSb I	space group $T_d^2 - F\bar{4}3m$ (zincblende structure)		stable at normal pressure	
GaSb II	white tin structure space group $D_{4h}^{19} - I4_1/amd$		high-pressure phase	
transition pressure:				
p_{tr}	7.65(10) GPa	RT	first order Raman scattering	84A
lattice parameter:				
a	6.09593(4) Å	298.15 K	powder, X-ray	65S
temperature dependence: $a = a_0 + a_1 T + a_2 T^2 + a_3 T^3 + a_4 T^4$ with				
a_0	6.095882 Å	T in °C	up to 680 °C	
a_1	$3.4963 \cdot 10^{-5}$ Å °C^{-1}			

Physical property	Numerical value	Experimental conditions	Experimental method, remarks	Ref.
a_2	$3.3456 \cdot 10^{-8}$ Å °C^{-2}			
a_3	$-4.6309 \cdot 10^{-11}$ Å °C^{-3}			
a_4	$2.6369 \cdot 10^{-14}$ Å °C^{-4}			
thermal expansion: Fig. 3.				
density:				
d	5.6137(4) g cm^{-3}	300 K	small variation with temperature (5.60 g cm^{-3} at 900 K)	65S
melting point:				
T_m	985 K			69G
phonon dispersion relations: Fig. 4				
phonon wavenumbers (in cm^{-1}): For phonon frequencies obtained from inelastic neutron scattering, see Fig. 4.				
$\bar{\nu}_{TO}(\Gamma)$	223.6(3)	RT	first order Raman scattering	84A
$\bar{\nu}_{LO}(\Gamma)$	232.6(3)			

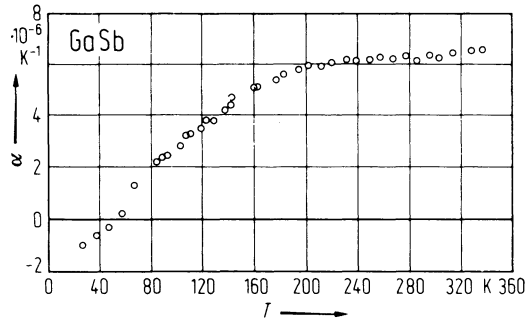

Fig. 3. GaSb. Linear thermal expansion coefficient vs. temperature measured with a quartz dilatometer. High temperature range [63N].

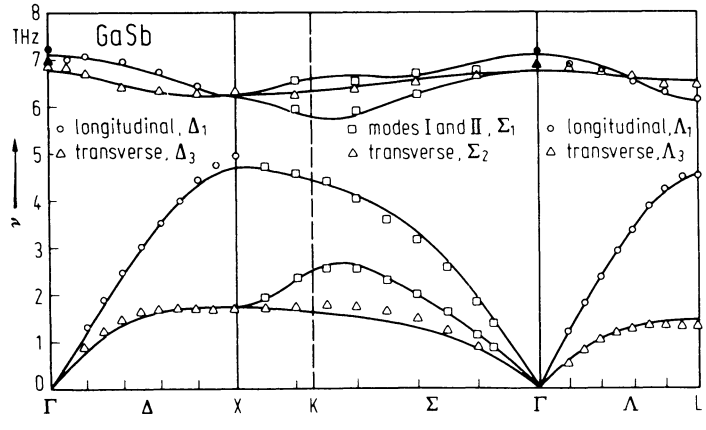

Fig. 4. GaSb. Phonon dispersion relations. Symbols: experimental results from inelastic neutron scattering; full lines: 14 parameter shell model calculation [75F].

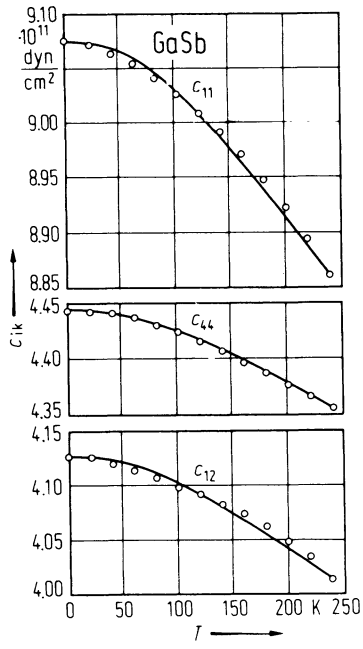

Fig. 5. GaSb. Second order elastic moduli vs. temperature [75B].

Physical property	Numerical value	Experimental conditions	Experimental method, remarks	Ref.
$\bar{\nu}_{TA}(L)$	46	300 K	second order Raman effect	76K
$\bar{\nu}_{TA}(X)$	56			
$\bar{\nu}_{TA}(W)$	75			
$\bar{\nu}_{LA}(L)$	155			
$\bar{\nu}_{LO}(L)$	204			
$\bar{\nu}_{LO}(X)$	210			
$\bar{\nu}_{TO}(L, X, \Sigma)$	218			
elastic moduli (in 10^{11} dyn cm^{-2}):				
c_{11}	8.834	296 K	ultrasound	75B
c_{12}	4.023			
c_{44}	4.322			

Transport properties

Transport in *n-type* GaSb is complicated by the contribution of three sets of conduction bands with minima situated at Γ, L and X. Data on transport coefficients can be consistently explained by a three band model [81L], the X-bands contributing to transport above 180 °C.

In *p-type* GaSb a multiellipsoidal model has to be used at *low temperatures* taking into account the shift of the heavy and light hole band away from $k = 0$. At *high temperatures* a warped sphere model (as in Si and Ge) is adequate. Analyses of transport data between 77 K and RT have to take into account the intermediate region between the two limiting cases.

electron mobility (in cm^2/Vs):				
μ_n	3750	Γ-minimum	typical RT values for the contributions of the three bands, obtained from a sample with $n = 1.49 \cdot 10^{18}$ cm^{-3}	81L
	482	L-minima		
	107	X-minima		

Further data for the L-band: 500 ··· 800 cm^2/Vs at RT, 800 ··· 1600 cm^2/Vs at 120 K [84K1].

For temperature dependence and the contributions of various scattering mechanisms to the mobility, see Fig. 6.

hole mobility:				
μ_p	680 cm^2/Vs	300 K	typical values for Hall mobilities with hole concentrations of 10^{17} cm^{-3}	85H
	2500 cm^2/Vs	77 K		

For temperature dependence and the contributions of heavy and light holes, see Fig. 7.

thermal conductivity: Fig. 8.

Optical properties

dielectric constants:				
$\varepsilon(0)$	15.69	300 K	reflectance and oscillator fit	62H
$\varepsilon(\infty)$	14.44			

Fig. 7. GaSb. Hall mobility vs. temperature for two samples with acceptor concentrations of $8 \cdot 10^{17}\,cm^{-3}$ (*1*) and $3 \cdot 10^{18}\,cm^{-3}$ (*2*). (above) Total Hall mobility, (below) contributions from heavy (h) and light (l) holes [79M].

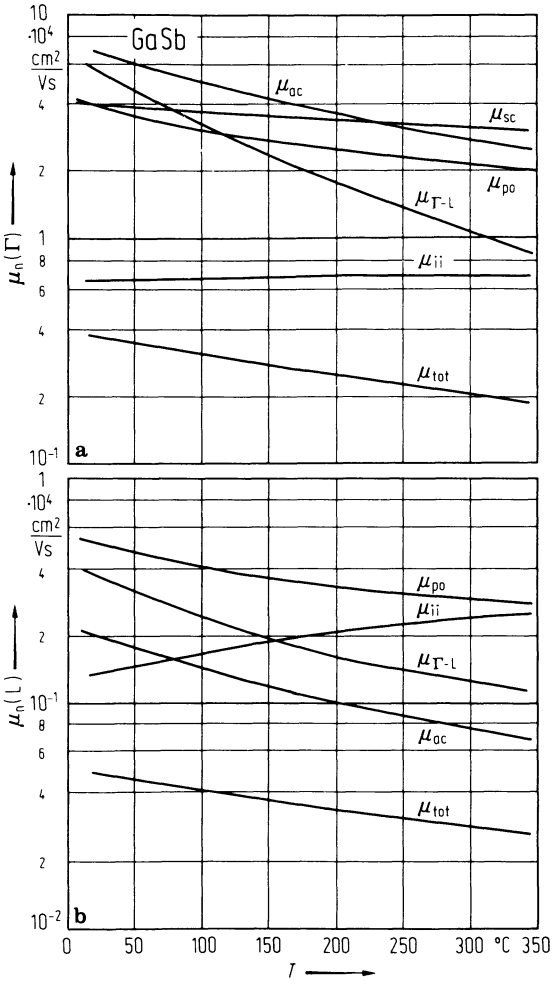

Fig. 6. GaSb. Electron mobility in (a) the Γ-band and (b) the L-band vs. temperature for a sample with $n = 1.49 \cdot 10^{18}$ cm^{-3} (μ_{tot}) and the contributions from various scattering mechanisms (ac – longitudinal acoustic phonon scattering, po – polar optical mode scattering, ii – ionized impurity scattering, sc – space charge scattering, Γ – L – intervalley scattering) [81L].

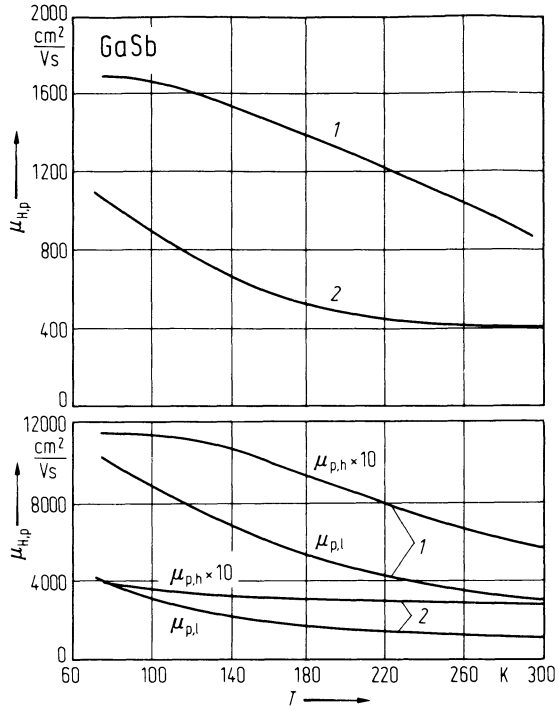

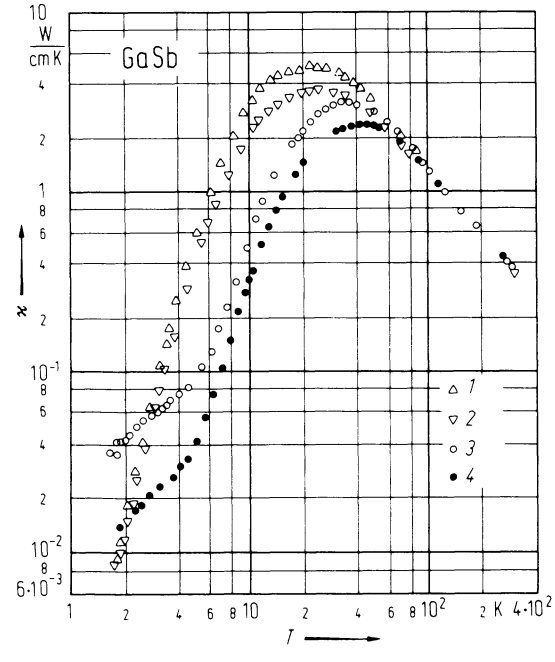

Fig. 8. GaSb. Thermal conductivity of two n-type samples with impurity content of $4 \cdot 10^{18}\,cm^{-3}$ (*1*) and $1.4 \cdot 10^{18}\,cm^{-3}$ (*2*) and of two p-type samples with $1 \cdot 10^{17}\,cm^{-3}$ (*3*) and $2 \cdot 10^{17}\,cm^{-3}$ (*4*) [64H].

optical constants

real and imaginary parts of the dielectric constant measured by spectroscopical ellipsometry; n, k, R, K calculated from these data [83A1]; see also Fig. 9.

$\hbar\omega$[eV]	ε_1	ε_2	n	k	R	$K[10^3\,cm^{-1}]$
1.5	19.135	3.023	4.388	0.344	0.398	52.37
2.0	25.545	14.442	5.239	1.378	0.487	279.43
2.5	13.367	19.705	4.312	2.285	0.484	579.07
3.0	9.479	15.738	3.832	2.109	0.444	641.20
3.5	7.852	19.267	3.785	2.545	0.485	902.86
4.0	−1.374	25.138	3.450	3.643	0.583	1477.21
4.5	−8.989	10.763	1.586	3.392	0.651	1547.17
5.0	−5.693	7.529	1.369	2.751	0.585	1394.02
5.5	−5.527	6.410	1.212	2.645	0.592	1474.51
6.0	−4.962	4.520	0.935	2.416	0.610	1469.28

Impurities and defects

diffusion coefficients

Element	$D_0[cm^2\,s^{-1}]$	Q[eV]	T[°C]	Remarks	Ref.
Self-diffusion coefficients					
Ga	$3.2\cdot10^3$	3.15	680···700	radiotracer	57E
Sb	$3.4\cdot10^4$	3.45	680···700	radiotracer	57E
Impurity diffusion coefficients					
In	$1.2\cdot10^{-7}$	0.53		radiotracer	60B
In	dependence on stoichiometry			SIMS	80M
Sn	$2.4\cdot10^{-5}$	0.80		radiotracer	60B
Sn	dependent on carrier density			radiotracer	75U
Te	$3.8\cdot10^{-4}$	1.20		radiotracer	60B
Cd	$1.5\cdot10^{-6}$	0.72		pn-junction depth measurement	68B
Zn	isoconcentration $D = 1.8\cdot10^{-11}\,cm^2\,s^{-1}$ at 560 °C			radiotracer (isoconcentration and chemical diffusion)	74D
Zn	$4.0\cdot10^{-2}$	1.6		pn-junction	81K

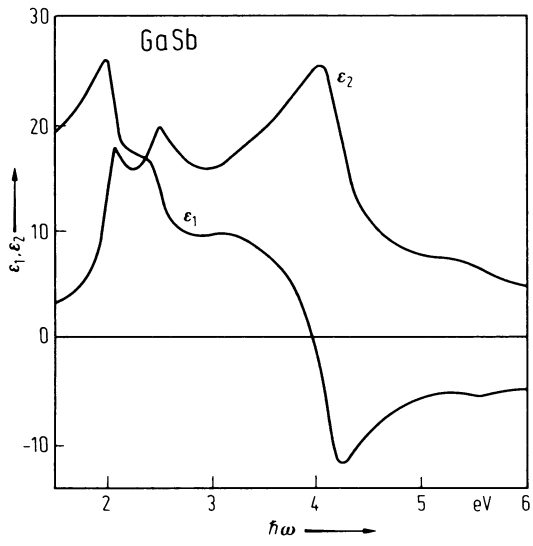

Fig. 9. GaSb. Real and imaginary parts of the dielectric constants vs. photon energy [83A1].

donors

Undoped, relatively pure GaSb is usually p-type. Thus, neutral donor states are not populated in equilibrium. No observations of inter-donor transitions have been reported. Conductivity and Hall coefficient relaxation experiments give evidence of a trap which is related to the S donor [79D].

binding energies of donors

Impurity	E_b [meV]	T [K]	Remarks	Ref.
Te(L)	20(5)	230	pressure dependence of Hall coefficient	69P
Te(X)	<80			71V
Se(L)	85	77	pressure dependence of conductivity	66K
Se(L)*(?)	30	4.2	Shybnikov-de Haas effect	76H
Se(X)	200	290		71V
S(L)	140···150			69P, 71V
S(X)	≈ 300			71V

acceptors

The dominant acceptor of undoped GaSb seems to be a native defect. Hall measurements show that this acceptor is doubly ionizable [65B, 72J]. The model of a $V_{Ga}Ga_{Sb}$ complex is in agreement with the results of thermodynamical investigations.

binding energies of acceptors

Impurity	E_b [meV]	T [K]	Remarks	Ref.
Si	9.4(5)	1.8	photoluminescence	76J
	13···15	4.2	photoluminescence	71B
Ge	9.5(5)	1.8	photoluminescence	76J
A	34.5	2	unknown impurities, photoluminescence of	72R1
B	54		pair-band. The C-acceptor binds a second	
C	102		hole. For this hole binding energies	72J
D	8		of 34.5 meV and 12 meV are reported.	72R1
E	12			
F	70(5)	12	The E-line is probably caused by an A^+-state	72K
G	130		of the B-acceptor	

References for 2.11

57E Eisen, F.H., Birchenall, C.E.: Acta Metall. **5** (1957) 265.
60B Boltaks, B.I., Gutorov, Yu.A.: Sov. Phys. Solid State **1** (1960) 930.
63N Novikova, S.I., Abrikosov, N.Kh.: Sov. Phys. Solid State (English Transl.) **5** (1963) 1558; Fiz. Tverd. Tela **5** (1963) 2138.
64H Holland, M.G.: Proc. Int. Conf. Phys. Semicond., Paris 1964, Dunod, Paris 1964 p. 713.
65B Baxter, R.D., Bate, R.T., Reid, F.J.: J. Phys. Chem. Solids **26** (1965) 14.
65S Straumanis, M.E., Kim, C.D.: J. Appl. Phys. **36** (1965) 3822.
66K Kosicki, B.B., Paul. W.: Phys. Rev. Lett. **17** (1966) 246.
68B Bougnot, J., Szepessy, L., Du Cunha, S.F.: Phys. Status Solidi **26** (1968) K127.
69G Glazov, V.M., Chizhevskaya, S.N., Evgen'ev, S.B.: Zh. Fiz. Khim. **43** (1969) 373.
69P Pitt, G.D.: High Temp. – High Pressures **7** (1969) 111.
71B Burdiyan, I.I., Mal'tsev, S.B., Mironov, I.F., Shreter, Yu.G.: Sov. Phys. Semicond. (English Transl.) **5** (1972) 1734; Fiz. Tekh. Poluprovodn. **5** (1971) 1996.
71V Vul, A.Ya., Bir, G.L., Shmartsev, Y.V.: Sov. Phys. Semicond. (English Transl.) **4** (1971) 2005; Fiz. Tekh. Poluprovodn. **4** (1970) 2331.
72J Jakowetz, W., Rühle, W., Breuninger, K., Pilkuhn, M.H.: Phys. Status Solidi (a) **12** (1972) 169.
72K Kyuregyan, A.S., Lazareva, I.K., Stuchebnikov, V.M., Yunovich, A.E.: Sov. Phys. Semicond. (English Transl.) **6** (1972) 208; Fiz Tekh. Poluprovodn. **6** (1971) 242.
72R1 Rühle, W., Jakowetz, W., Pilkuhn, M.H.: Proc. Int. Conf. Luminescence, Leningrad **1972**, p. 444.

72R2 Reine, M., Aggarwal, R.L., Lax, B.: Phys. Rev. **B5** (1972) 3033.
73R Rühle, W., Jakowetz, W., Wölk, C., Linnebach, R., Pilkuhn, M.: Phys. Status Solidi (b) **73** (1973) 225.
74H Hill, D.A., Schwerdtfeger, C.F.: J. Phys. Chem. Solids **35** (1974) 1533.
74D Du Cunha, S.F., Bougnot, J.: Phys. Status Solidi (a) **22** (1974) 205.
75B Boyle, W.F., Sladek, R.J.: Phys. Rev. **B11** (1975) 2933.
75F Farr, M.K., Taylor, J.G., Sinha, S.K.: Phys. Rev. **B11** (1975) 1587.
75U Uskov, V.A.: Sov. Phys. Semicond. **8** (1975) 1573.
75W Wiley, J.D.: in "Semiconductors and Semimetals", Vol. 10, R.K. Willardson and A.C. Beer eds., Academic Press, New York and London **1975**.
76A Aspnes, D.E., Olson, C.G., Lynch, D.W.: Phys. Rev. **B14** (1976) 4450.
76C Chelikowsky, J.R., Cohen, M.L.: Phys. Rev. **B14** (1976) 556.
76H Hoo, K., Becker, W.M., Sun, R.-Y.: Solid State Commun. **18** (1976) 313.
76J Jakowetz, W., Barthruff, D., Benz, K.W.: Proc. 6th Int. Symp. on GaAs and related compounds, Hilsum, C. (ed.), London: Inst. Phys. **1976**, p. 41.
76K Klein, P.B., Chang, R.K.: Phys. Rev. **B14** (1976) 2498.
79D Dmoski, L., Baj, M., Kubalski, M., Piotrzkowski, R., Porowski, S.: Inst. Phys. Conf. Ser. **43** (1979) 417.
79M Mathur, P.C., Jain, S.: Phys. Rev. **B19** (1979) 3152.
80C Chiang, T.C., Eastman, D.E.: Phys. Rev. **B22** (1980) 2940.
80M Mathiot, D., Edelin, G.: Philos. Mag. **A41** (1980) 447.
81J Joullié, A., Zein Eddine, A., Girault, B.: Phys. Rev. **B23** (1981) 928.
81K Kagawa, T., Motosugi, G.: Jpn. J. Appl. Phys. **20** (1981) 597.
81L Lee, H.J., Woolley, J.C.: Can. J. Phys. **59** (1981) 1844.
83A1 Aspnes, D.E., Studna, A.A.: Phys. Rev. **B27** (1983) 985.
83A2 Alibert, C., Joullié, A., Joullié, A.M., Ance, C.: Phys. Rev. **B27** (1983) 4946.
84A Aoki, K., Anastassakis, E., Cardona, M.: Phys. Rev. **B30** (1984) 681.
84K Kourkoutas, C.D., Bekris, P.D., Papaioannou, G.J., Euthymiou, P.C.: Solid State Commun. **49** (1984) 1071.
85H Heller, M.W., Hamerly, R.G.: J. Appl. Phys. **57** (1985) 4626.
85K Kopylov, A.A.: Solid State Commun. **56** (1985) 1.

Physical property	Numerical value	Experimental conditions	Experimental method, remarks	Ref.

2.12 Indium nitride (InN)

Electronic properties

The band structure (Fig. 1, Brillouin zone: Fig. 3 of section 2.1) shows a direct gap at Γ, closely similar to that of GaN.

energy gap (in eV):

$E_{g,dir}$	2.05 (1)	300 K	absorption edge,	77T
	2.11	78 K		75O
	1.89	RT		86F

effective mass:

m_{opt}	$0.11 m_0$	$T = 300$ K	plasma edge	77T

Calculated effective masses of $m_n = 0.12 m_0, m_{p,h} = 0.5 m_0, m_{p,l} = 0.17 m_0$ are reported [86F].

Lattice properties

lattice parameter:

a	3.5446 Å		epitaxial layers, X-ray	78P
c	5.7034 Å			

density:

d	6.81 g cm^{-3}	298.15 K	X-ray	67P

Physical property	Numerical value	Experimental conditions	Experimental method, remarks	Ref.
melting point:				
T_m	1373 K			70M
phonon wavenumbers:				
$\bar{\nu}_{TO}(\Gamma)$	478 cm^{-1}	$T = 300$ K	reflectivity, Kramers–Kronig analysis	75O
$\bar{\nu}_{LO}(\Gamma)$	694 cm^{-1}			
Transport properties				
electrical conductivity:				
σ	$2 \cdots 3 \cdot 10^2 \Omega^{-1} cm^{-1}$	$T = 300$ K	temperature coefficient of resistivity $3.7 \cdot 10^{-3} K^{-1}$ at $200 \cdots 300$ K for pressed powder	56J, 72H, 74T

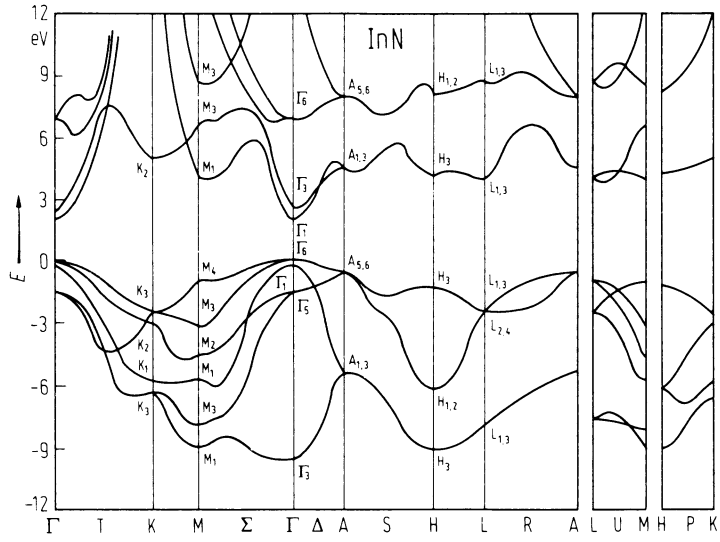

Fig. 1. InN. Band structure calculated by a pseudopotential method [86F].

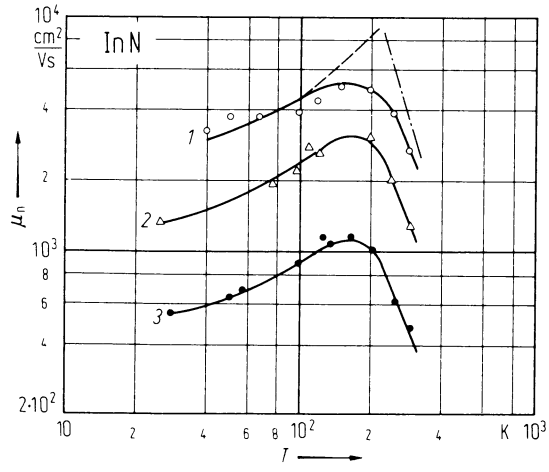

Fig. 2. InN. Electron mobility vs. temperature for three samples with RT carrier concentrations of $5.3 \cdot 10^{16}$ (*1*), $7.5 \cdot 10^{16}$ (*2*) and $1.8 \cdot 10^{17} cm^{-3}$ (*3*). Broken line: calculated ionized impurity scattering mobility, dot-dashed line: empirical high-temperature mobility ($\mu \propto T^{-3}$) for sample *1*. Solid lines: total mobility calculated for each sample [84T].

Physical property	Numerical value	Experimental conditions	Experimental method, remarks	Ref.
electron mobility:				
μ_n	250(50) cm^2/Vs	$T = 300$ K	see also Fig. 2	72H
	20 cm^2/Vs	300 K		74T
	35 ··· 50 cm^2/Vs	300 K		77M
Optical properties				
refractive index:				
n	2.56	$T = 300$ K, $n = 3 \cdot 10^{20}$ cm^{-3} $\lambda = 1.0$ µm	interference method	77T
	2.93	0.82 µm		
	3.12	0.66 µm		
dielectric constant:				
$\varepsilon(\infty)$	9.3	heavily doped film	infrared reflectivity	77T

References for 2.12

56J Juza, R., Rabenau, A.: Z. Anorg. Allg. Chem. **285** (1956) 212.
67P Pearson, W.B.: A Handbook of Lattice Spacings and Structures of Metals and Alloys, Pergamon Press, Oxford-London 1967.
70M MacChesney, J.B., Bridenbaugh, P.M., O'Connor, P.B.: Mater. Res. Bull. **5** (1970) 783.
72H Hovel, H.J., Cuomo, J.J.: Appl. Phys. Lett. **20** (1972) 71.
74T Trainor, J.W., Rose, K.: J. Electron. Mater. **3** (1974) 821.
75O Osamura, K., Naka, S., Murakami, Y.: J. Appl. Phys. **46** (1975) 3432.
77M Marasina, L.A., Pichugin, E.G., Tlaczala, M.: Krist. Techn. **12** (1977) 541.
77T Tyagai, V.A., Evstigneev, A.M., Krasiko, A.N., Adreeva, A.F., Malakhov, V.Ya.: Sov. Phys. Semicond. (English Transl.) **11** (1977) 1257; Fiz. Tekh. Poluprovodn. **11** (1977) 2142.
78P Pichugin, I.G., Tlachala, M.: Izv. Akad. Nauk SSSR, Neorg. Mater. **14** (1978) 175.
84T Tansley, T.L., Foley, C.P.: Electron. Lett. **20** (1984) 1087.
86F Foley, C.P., Tansley, T.L.: Phys. Rev. **B33** (1986) 1430.

2.13 Indium phosphide (InP)

Electronic properties

band structure: Fig. 1 (Brillouin zone: see section 1.1, Fig. 2)
InP is a direct semiconductor. The *conduction band* minimum is situated at Γ. Higher conduction band minima at L and X have been detected in optical experiments. The X band minima show no camel's back structure, in contrast to most other III–V compounds with zincblende structure [85K]. The *valence band* has the structure common to all zincblende type semiconductors.

energies at symmetry points of the band structure (relative to the top of the valence band) (in eV):

$E(\Gamma_{6v})$	−11.42	−0.108 (e)	symmetry symbols in double group notation
$E(\Gamma_{7v})$	−0.21		
$E(\Gamma_{8v})$	0		first row:
$E(\Gamma_{6c})$	1.50	1.42 (e)	calculated data from [76C],
$E(\Gamma_{7c})$	4.64	4.8 (b)	see Fig. 1
$E(\Gamma_{8c})$	4.92	4.87 (a)	
$E(X_{6v})$	−8.91		
$E(X_{6v})$	−6.01	−5.9 (f)	

Physical property	Numerical value	Experimental conditions	Experimental method, remarks	Ref.
$E(E_{6v})$	−2.09		second row:	
$E(X_{7v})$	−2.06	−2.2 (f)	comparison with experiment	
$E(X_{6c})$	2.44	2.38 (d, e)	using data on critical points	
$E(X_{7c})$	2.97		(a:[66S], b:[68M], c:[70J],	
$E(L_{6v})$	−9.67		d:[72O], e:[80C2], f:[83W])	
$E(L_{6v})$	−5.84			
$E(L_{6v})$	−1.09	−1.23 (b)		
$E(L_{4,5v})$	−0.94	−1.12 (b)		
$E(L_{6c})$	2.19	2.03 (c, e)		
$E(L_{6c})$	5.58			
$E(L_{4,5c})$	5.70			
direct energy gap:				
$E_{g,dir}$ $(\Gamma_{8v}-\Gamma_{6c})$	1.4236 (1) eV	1.6 K	from excitonic gap (below)	85M
	1.344 eV	300 K	absorption, photoluminescence	85B

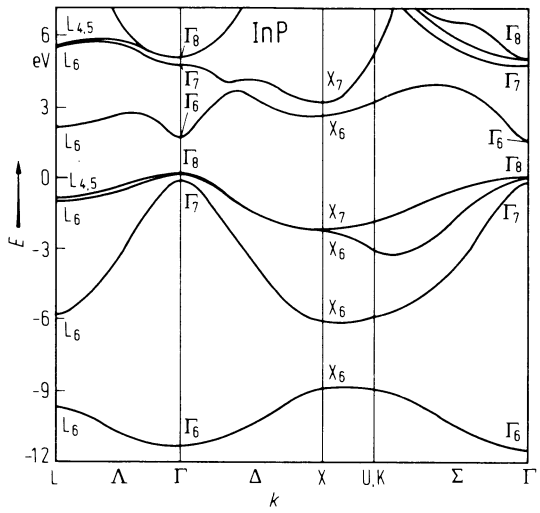

Fig. 1. InP. Band structure obtained with a non-local pseudopotential method [76C].

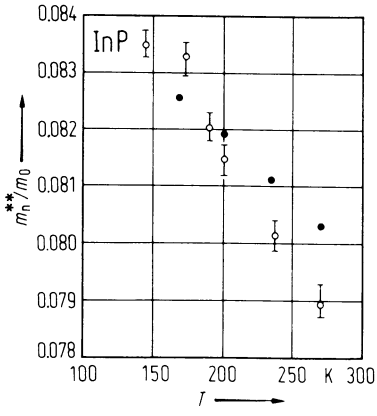

◀ Fig. 3. InP. Polaronic effective mass vs. temperature. Full circles: [71E], open circles: [84M].

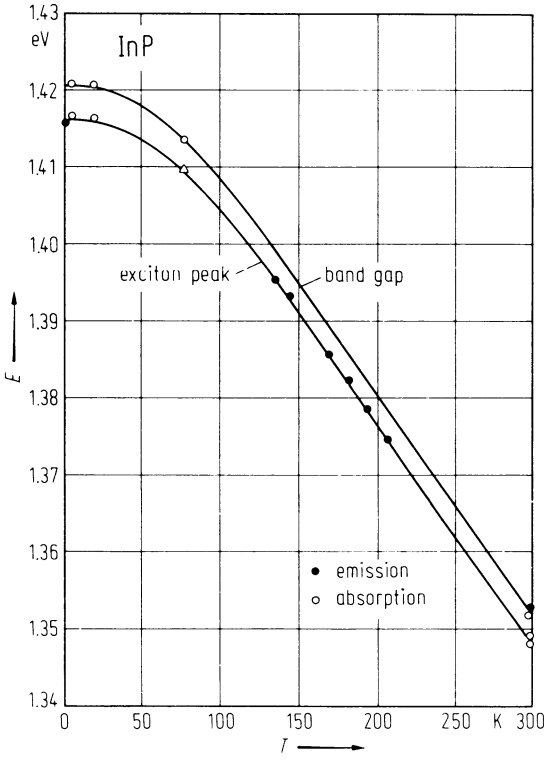

Fig. 2. InP. Energy gap and exciton peak energy vs. temperature below RT from absorption and emission data [64T].

Physical property	Numerical value	Experimental conditions	Experimental method, remarks	Ref.
temperature dependence of direct energy gap (in 10^{-4} eV K^{-1}):				
$dE_{g,dir}/dT$	−2.9	below RT	absorption, Fig. 2	64T
	−5.1	above RT	luminescence	83K
exciton energies (obtained from fitting of exciton fine structure in reflectivity at $T = 1.6$ K [85M]):				
$E(1S, T)$	1.41850(5) eV	1.6 K	transverse exciton, ground state	85M
$E(1S, L)$	1.41867(7) eV		longitudinal exciton, ground state	
E_b	5.1(1) meV	1.6 K	exciton binding energy	
Δ_{ex}	0.04(2) meV		exchange interaction energy	
intra conduction band energies (in eV):				
$E(X_{6c} - \Gamma_{6c})$	0.960(5)	8 K	wavelength derivative transmission	72O
$E(L_{6c} - \Gamma_{6c})$	0.39	RT	capacitance	80W1
	0.61	0···300 K	photoemission	70J
$\Delta'_0(\Gamma_{8c} - \Gamma_{7c})$	0.07	300 K	electroreflectance	66S
intra valence band energies (in eV):				
$\Delta_0(\Gamma_{8v} - \Gamma_{7v})$	0.108(1)	5 K	wavelength modulated reflectivity	80C
$\Delta_1(\Lambda_{4,5v} - \Lambda_{6c})$	0.133(4)	300 K	ellipsometry	82K
structure of top of valence band: By the linear term in $E(k)$ the maxima of the heavy hole valence band are shifted on the [111] axes, the energy of the band maximum relative to the energy at $k = 0$ being:				
$\Delta E[111]$	6 meV	78 K	electroabsorption	77V
	38 meV	298 K		
effective masses, electrons (in units of m_0):				
m_n	0.0765(5)	4.2 K	bare band edge mass obtained from polaron cyclotron resonance converted from polaron mass using a Fröhlich coupling constant $\alpha = 0.15(1)$	85H
m_n^{**}	0.079(0.075)	270 K	polaron (bare) band edge mass from magnetophonon resonance, see Fig. 3 for temperature dependence	84M
	0.084(0.080)	143 K		
electron *g*-factor:				
g_c	1.48(5)	4.2K	modulated photovoltaic effect	75R
effective masses, holes (in units of m_0):				
$m_{p,h}$	0.60(2)	110 K, $B \parallel [111]$	cyclotron resonance	74L
	0.56(2)	$B \parallel [100]$		
$m_{p,l}$	0.12(1)			
m_{so}	0.121(1)			

Physical property	Numerical value	Experimental conditions	Experimental method, remarks	Ref.
valence band parameters:				
A	−6.28		calculated using $k \cdot p$ theory	75W
B	−4.17			
$\|C\|$	6.24			
Lattice properties				
Structure				
InP I	space group $T_d^2 - F\bar{4}3m$ (zincblende structure)		stable at normal pressure	
InP II	space group $O_h^5 - Fm3m$ $a = 5.514$ Å		high-pressure phase	63J
transition pressure:				
p_{tr}	133 kbar			63J
lattice parameter:				
a	5.8687(10) Å	291.15 K	powder, X-ray	58G
	5.8871(6) Å	912 K		72K
linear thermal expansion coefficient: Fig. 4.				
density:				
d	4.81 g cm^{-3}			77M
melting point:				
T_m	1335(5) K		from a critical analysis of literature data	84T

phonon dispersion relations: Fig. 5.

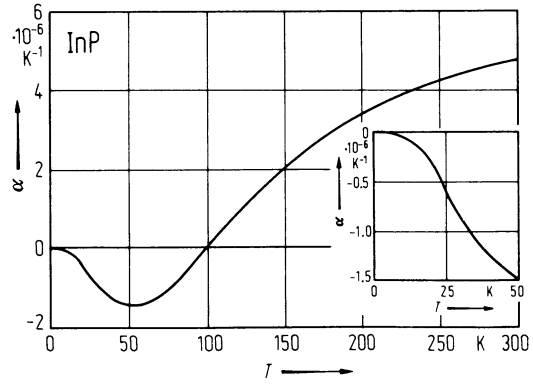

Fig. 4. InP. Linear thermal expansion coefficient vs. temperature calculated using experimental pressure derivatives of elastic moduli and phonon wavenumbers [82S2].

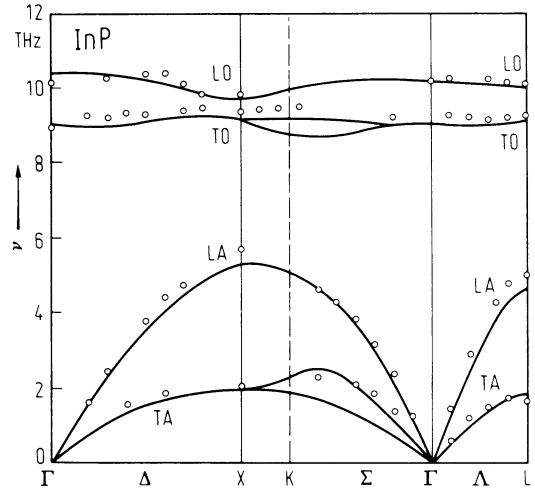

Fig. 5. InP. Phonon dispersion relations calculated by an eight parameter bond-bending force model (solid lines) [80 K] and experimental data from inelastic neutron scattering [75B].

Physical property	Numerical value	Experimental conditions	Experimental method, remarks	Ref.
phonon frequencies (in THz):				
$\nu_{LO}(111)(0.05)$	10.3(3)	RT, $n = 10^{12}\,cm^{-3}$	coherent inelastic neutron scattering	78B
$\nu_{TO}(\Gamma_{15})$	9.2(2)			
$\nu_{TA}(X_5)$	2.05(10)			
$\nu_{LA}(X_3)$	5.8(3)			
$\nu_{TO}(X_5)$	9.70(10)			
$\nu_{LO}(X_1)$	9.95(20)			
$\nu_{TA}(L_3)$	1.65(2)			
$\nu_{LA}(L_1)$	5.00(10)			
$\nu_{TO}(L_3)$	9.50(15)			
$\nu_{LO}(L_1)$	10.2(3)			
$\nu_{LO}(\Gamma)$	10.32(344.5 cm^{-1})		Raman scattering, zone center phonons	80T
$\nu_{TO}(\Gamma)$	9.093(303.3 cm^{-1})			
second order elastic moduli (in $10^{11}\,dyn\,cm^{-2}$):				
c_{11}	10.11	RT	ultrasonic wave transit times	80N
c_{12}	5.61			
c_{44}	4.56			
third order elastic moduli (in $10^{12}\,dyn\,cm^{-2}$):				
c_{111}	−8.6		calculated from elastic moduli, their pressure dependence and other literature parameters	80N
c_{112}	−1.85			
c_{123}	−5.1			
c_{144}	−6.5			
c_{166}	+1.6			
c_{456}	−0.042			

Transport properties

The transport in n-type samples is determined up to 800 K by the electrons in the Γ_{6c}-minimum. Only at very high temperatures L_{6c}-electrons contribute to the conductivity. In high purity samples polar scattering dominates at room temperature.

intrinsic carrier concentration (in cm^{-3}):				
n_i	$1.2 \cdot 10^8$	293 K	from an analysis of transport data	56W
	$8.4 \cdot 10^{15}\,T^{3/2} \exp(-1.34/2\,kT)$		for the range 700···920 K (T in K, kT eV) see Fig. 6	55F
electron mobility (typical data from the literature, in cm^2/Vs):				
$\mu_{H,n}$	131 600	77 K, VPE layer, $n = 2.5 \cdot 10^{14}\,cm^{-3}$		85Z
	5370	300 K		
	5900	300 K	theoretical upper limit	80W2

Mobility values for single crystal and polycrystalline samples are mostly lower. Best values at 300 K are around 4000 cm^2/Vs. At 77 K values up to 130 000 cm^2/Vs have been reported in [82A].

Physical property	Numerical value	Experimental conditions	Experimental method, remarks	Ref.
Temperature dependence of electron mobility: Fig. 7.				
hole mobility:				
$\mu_{H,p}$	$150(T/300\,K)^{-2.2}\,cm^2/Vs$		above 200 K; temperature dependence, see Fig. 8	75W
thermal conductivity: Fig. 9.				

Optical properties

dielectric constants:				
$\varepsilon(0)$	12.5(1)		fit of transport data	80L
	12.56(20)	300 K	capacitance measurements	86M
	11.93(20)	77 K		
	12.61		oscillator fit of infrared reflectance	62H
$\varepsilon(\infty)$	9.61			

According to [86M] the temperature dependence of $\varepsilon(0)$ below 220 K is given by $\varepsilon(0) = 11.76(1 + 2.26 \cdot 10^{-4} T)$ (T in K).

refractive index: in addition to the data above, see Fig. 10.

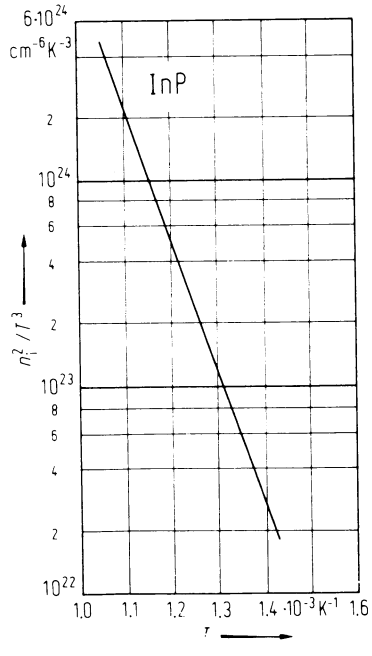

Fig. 6. InP. n_i^2/T^3 vs. reciprocal temperature [55F]. n_i: intrinsic concentration.

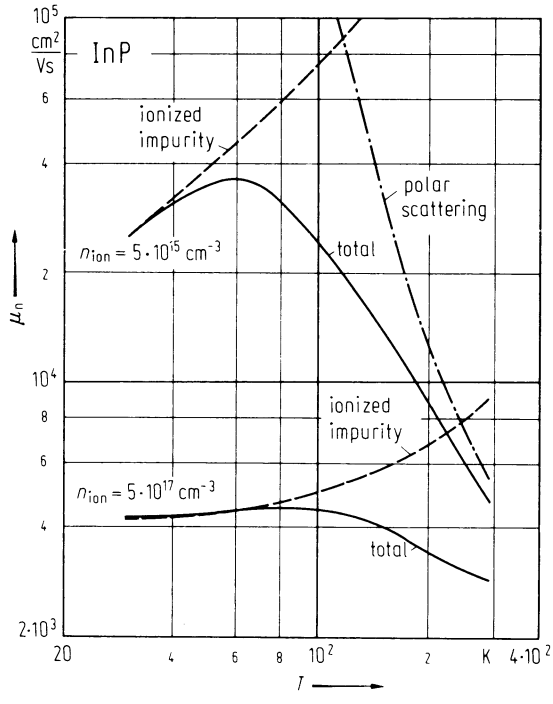

Fig. 7. InP. Electron mobility vs. temperature calculated for two concentrations of ionized impurities. Contributions from scattering mechanisms are indicated (dashed lines) [80W2].

optical constants:

real and imaginary parts of the dielectric constant measured by spectroscopical ellipsometry; n, k, R, K calculated from these data [83A]; see also Fig. 11.

$\hbar\omega$ [eV]	ε_1	ε_2	n	k	R	$K[10^3\,\mathrm{cm}^{-1}]$
1.5	11.904	1.400	3.456	0.203	0.305	30.79
2.0	12.493	2.252	3.549	0.317	0.317	64.32
2.5	14.313	3.904	3.818	0.511	0.349	129.56
3.0	17.759	10.962	4.395	1.247	0.427	379.23
3.5	6.400	12.443	3.193	1.948	0.403	691.21
4.0	6.874	10.871	3.141	1.730	0.376	701.54
4.5	8.891	16.161	3.697	2.186	0.449	996.95
5.0	−7.678	14.896	2.131	3.495	0.613	1771.52
5.5	−4.528	7.308	1.426	2.562	0.542	1428.14
6.0	−2.681	5.644	1.336	2.113	0.461	1285.10

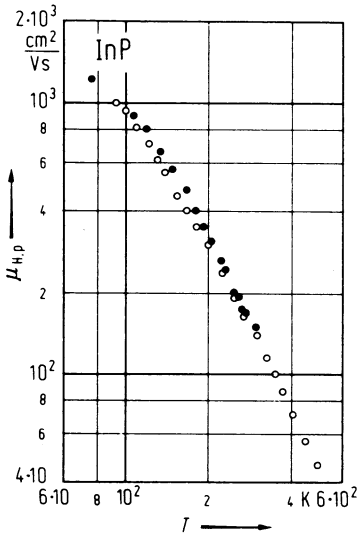

Fig. 8. InP. Hole Hall mobility vs. temperature for pure p-type samples, after [75W].

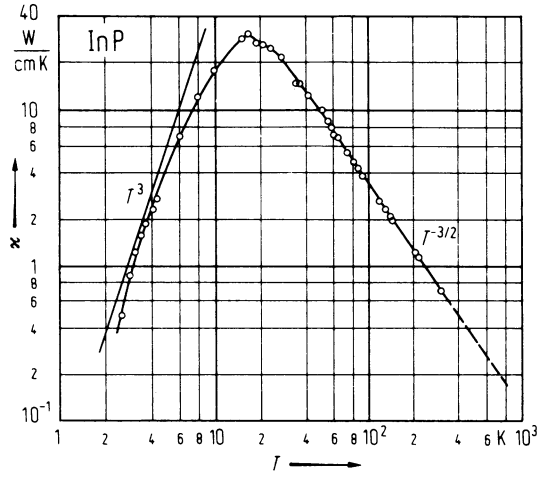

Fig. 9. InP. Thermal conductivity vs. temperature [65A].

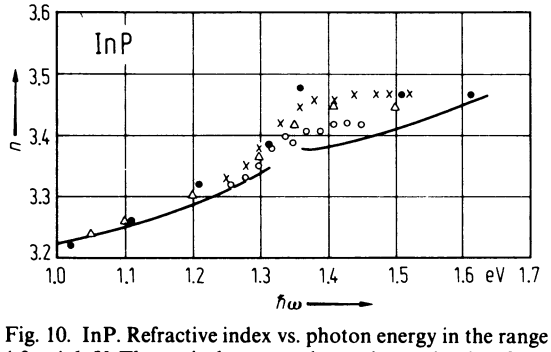

Fig. 10. InP. Refractive index vs. photon energy in the range 1.0 ··· 1.6 eV. Theoretical curve and experimental points from [82B] (triangles), [82S1] (full circles) and [85C] (open circles: p-type, crosses: n-type samples).

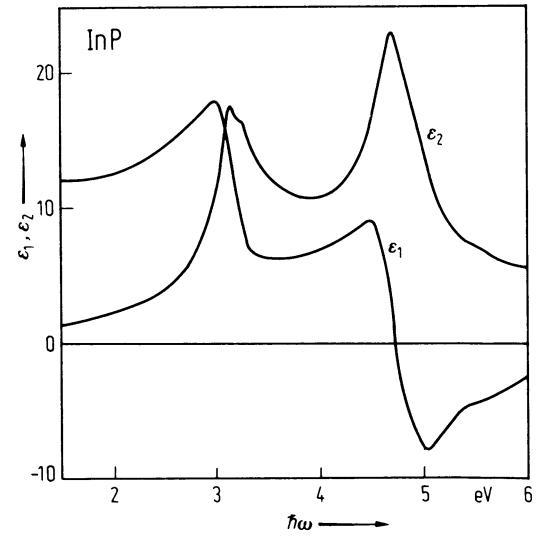

Fig. 11. InP. Real and imaginary parts of the dielectric constant vs. photon energy [83A].

Impurities and defects

diffusion coefficients

Element	D_0 [$cm^2 s^{-1}$]	Q [eV]	T [°C]	Remarks	Ref.
Self-diffusion coefficients					
In	$1 \cdot 10^5$	3.85	838 ··· 980	radiotracer	61G
P	$7 \cdot 10^{10}$	5.65	903 ··· 1010	radiotracer	61G
Impurity diffusion coefficients					
Ag	$3.6 \cdot 10^{-4}$	0.59		radiotracer	69A1
Au	$1.32 \cdot 10^{-5}$	0.48		radiotracer	69R
Cd	1.8	1.9		radiotracer	67A
Cu	$3.8 \cdot 10^{-3}$	0.69		radiotracer	69A2
Zn	complex profiles				64C

donors: Discrimination of donor chemical species is made difficult because of the small electron effective mass ($m_c^* < 0.1\, m_0$) and large dielectric constant ($\varepsilon_s \approx 12$). This leads to small values of electron binding energy at donor states. The effective mass donor Rydberg for InP is 7.31 meV [74H1]. The large extend of the electron wave function makes the central cell corrections small ($\psi^2(r=0)$), typically ≈ 0.1 meV. Random electric fields, strain and other effects can produce line widths for donor-related optical transitions which are larger than the central cell corrections, especially at zero magnetic field.

acceptors: Zinc and carbon are often common residual acceptors in InP. The group IV elements, except for C and Ge, do not substitute for P, and so show no amphoteric behavior.

binding energy of acceptors

Element	E_b [meV]	T [K]	Remarks	Ref.
Zn	48	4.2	Free-bound photoluminescence.	79D
	46.4(10)	10		76H
Cd	57.0(10)	1.8	No lineshape fits of emission lines were	72W
Hg	98(2)	6	attempted introducing some uncertainty	73W
C_p	41.3(5)	1.8	for the binding energies thus determined.	74H2
	41.5	4.2		79D
Ge_p	210(20)	2		76W
Mn	270(10)	6		73W
Cu	60 ··· 73	6	Probably Cu-vacancy complex	73W
Mg	31	77	Crystal grown by molecular beam epitaxy	77B
	108		Crystal grown by LEC	
Be	31		Crystal grown by molecular beam epitaxy	77B
	143		Crystal grown by gradient free growth	

transition metal impurities

Energy levels related to isolated, substitutional transition metal impurities. ("+" above valence band, "−" below conduction band.)

Impurity	E [eV]	Type	Remarks	T [K]	Ref.
Ti	−0.63(3)	d	DLTS		86B
V	+0.21	d	DLTS + σ_p^0 photoluminescence excitation photoionization	4	86D
Cr	−0.39(1)	a	Temperature dependent resistivity and Hall effect measurements		79I
	+0.96(1)	a	PICTS		82R
	+0.56	d	Temperature dependent Hall measurements		86L
Mn	+0.21	a	Temperature dependent resistivity and Hall measurements		84K
Fe	−0.65	a	Photoconductivity		81E
	+0.7850	a	σ_p^0 absorption photoionization; $^5T_2$ excited state located at +1.1379	1.3	86J
Co	+0.24	a	DLTS and ODLTS		84R
Ni	+0.48(4)	1st a	DLTS		90K
	−0.27(2)	2nd a	DLTS		89K
Au	−0.55	d	DLTS		87P

References for 2.13

55F Folberth, O.G., Weiss, H.: Z. Naturforsch. **10a** (1955) 615.
56W Weiss, H.: Z. Naturforsch. **11a** (1956) 430.
58G Giesecke, G., Pfister, H.: Acta Crystallogr. **11** (1958) 369.
62H Hass, M., Henvis, B.W.: J. Phys. Chem. Solids **23** (1962) 1099.
63J Jamieson, J.C.: Science **139** (1983) 845.
61G Goldstein, B.: Phys. Rev. **121** (1961) 1305.
64C Chang, L.L., Casey, H.C.: Solid State Electron. **7** (1964) 481.
64T Turner, W.J., Reese, W.E., Pettit, G.D.: Phys. Rev. **136** (1964) A1467.
65A Aliev, S.A., Nashelskii, A.Ya., Shalyt, S.S.: Sov. Phys. Solid State (English Transl.) **7** (1965) 1287; Fiz. Tverd. Tela **7** (1965) 1590.
66S Shaklee, K.L., Cardona, M., Pollak, F.H.: Phys. Rev. Lett. **16** (1966) 48.
67A Arseni, K.A., Boltaks, B.I., Gordin, V.L., Ugai, Ya.A.: Inorg. Mater. (USSR) **3** (1967) 1465.
68M Matatagui, E., Thompson, A.E., Cardona, M.: Phys. Rev. **176** (1968) 950.
69A1 Arseni, K.A., Boltaks, B.I.: Sov. Phys. Solid State **10** (1969) 2190.
69A2 Arseni, K.A.: Sov. Phys. Solid State **10** (1969) 2263.
69R Rembeza, S.I.: Sov. Phys. Semicond. **3** (1969) 519.
70J James, L.W., van Dyke, J.P., Herman, F., Chang, D.M.: Phys. Rev. **B1** (1970) 3998.
71E Eaves, L., Stradling, R.A., Askenazy, S., Leotin, J., Portal, J.C., Ulmet, J.P.: J. Phys. **C4** (1971) L42.
72K Kudman, I., Pfaff, R.J.: J. Appl. Phys. **43** (1972) 3760.
72O Onton, A., Chicotka, R.J., Yacoby, Y.: Proc. 11th Int. Conf. Phys. Semi,cond., Warsaw 1972, Polish Scientific Publishers, Warsaw **1972**, p. 1023.
72W White, A.M., Dean, P.J., Taylor, L.L., Clarke, R.C., Ashen, D.J., Mullin, J.B.: J. Phys. **C5** (1972) 1727.
73W Williams, E.W., Elder, W., Astles, M.G., Webb, M., Mullin, J.B., Straughan, B., Tulton, P.J.: J. Electrochem. Soc. **120** (1973) 1741.
74H1 Hoult, R.A., Stradling, R.A., Bradley, C.C.: J. Phys. **C7** (1974) 1164.
74H2 Hess, K., Stath, N., Benz, K.W.: J. Electrochem. Soc. **121** (1974) 1208.
74L Leotin, J., Barbaste, R., Askenazy, S., Skolnick, M.S., Stradling, R.A., Tuchendler, J.: Solid State Commun. **15** (1974) 693.
75B Borcherds, P.H., Alfrey, G.F., Saunderson, D.H., Woods, A.D.B.: J. Phys. **C8** (1975) 2022.
75R Rochon, P., Fortin, E.: Phys. Rev. **B12** (1975) 5803.
75W Wiley, J.D.: in "Semiconductors and Semimetals", Vol. 10, R.K. Willardson, A.C. Beer eds., Academic Press, New York **1975**.
76C Chelikowski, J.R., Cohen, M.L.: Phys. Rev. **B14** (1976) 556.
76H Hess, K.: Dissertation, Stuttgart **1976**.
76W White, A.M., Dean, P.J., Day, B.: Proc. XIIIth Int. Conf. on Physics of Semiconductors, Fumi, F.G. (ed.), Rome: Tipografia Marves **1976**, p. 1037.
77B Bimberg, D., Hess, K., Lipari, N.O., Fischebach, J.U., Altarelli, M.: Physica **B89** (1977) 139.
77M Merrill, L.: J. Phys. Chem. Ref. Data **6** (1977) 1205.
77V Vorobeev, L.E., Shturbin, A.V., Osokin, F.I.: Sov. Phys. Semicond. (English Transl.) **11** (1977) 879; Fiz. Tekh. Poluprovodn. **11** (1977) 1497.

79D Dean, P.J., Robbins, D.J., Bishop, S.G.: J. Phys. **C12** (1979) 5567.
79I Iseler, G.W.: Inst. Phys. Conf. Ser. **45** (1979) 144.
80C Camassel, J., Merle, P., Bayo, L., Mathieu, H.: Phys. Rev. **B22** (1980) 2020.
80K Kushwaha, M.S., Kushwaha, S.S.: Canad. J. Phys. **58** (1980) 351.
80L Lee, H.J., Basinski, J., Juravel, L.Y., Woolley, J.C.: Canad. J. Phys. **58** (1980) 923.
80N Nichols, D.N., Rimai, D.S., Sladek, R.J.: Solid State Commun. **36** (1980) 667.
80T Trommer, R., Müller, H., Cardona, M.: Phys. Rev. **B21** (1980) 4869.
80W1 Wada, O., Majerfeld, A., Choudhury, A.N.M.M.: J. Appl. Phys. **51** (1980) 423.
80W2 Walukiewicz, W., Lagowski, J., Jastrzebski, L., Rava, P., Lichtensteiger, M., Gatos, C.H., Gatos, H.C.: J. Appl. Phys. **51** (1980) 2659.
81E Eaves, L., Smith A.W., Williams, P.J., Cockayne, B., MacEwan, W.R.: J. Phys. **C14** (1981) 5063.
82A Adamski, J.A.: J. Cryst. Growth **60** (1982) 141.
82B Burkhard, H., Dinges, H.W., Kuphal, E.: J. Appl. Phys. **53** (1982) 655.
82K Kelso, S.M., Aspnes, D.E., Pollack, M.A., Nahory, R.E.: Phys. Rev. **B26** (1982) 6669.
82R Rhee, J.K., Battacharya, P.K.: J. Appl. Phys. **53** (1982) 4247.
82S1 Skolnick, M.S., Dean, P.J.: J. Phys. **C15** (1982) 5863.
82S2 Soma, T., Satoh, J., Matsuo, H.: Solid State Commun. **42** (1982) 889.
83A Aspnes, D.E., Studna, A.A.: Phys. Rev. **B27** (1983) 985.
83K Kirillov, D., Merz, J.L.: J. Appl. Phys. **54** (1983) 4104.
83W Williams, G.P., Cerrina, F., Anderson, J., Lapeyre, G.J., Smith, R.J., Hermanson, J., Knapp, J.A.: Physica **117B & 118B** (1983) 350.
84M Maeda, Y., Taki, H., Sakata, M., Ohta, E., Yamada, S., Fukui, T., Miura, N.: J. Phys. Soc. Jpn. **53** (1984) 3553.
84K Kuznetsov, V.P., Messerer, M.A., Omel'yanovskii, E.M.: Fiz. Tekh. Poluprovodn. **18** (1984) 446; Sov. Phys. Semicond. (English Transl.) **18** (1984) 278.
84R Rojo, P., Leyral, P., Nouailhat, A., Guillot, G., Lambert, B., Deveaud, B., Coquille, R.: J. Appl. Phys. **55** (1984) 395.
84T Tmar, M., Gabriel, A., Chatillon, C., Ansara, I.: J. Cryst. Growth **68** (1984) 557.
85B Bugajski, M., Lewandowski, W.: J. Appl. Phys. **57** (1985) 521.
85C Campi, D., Papuzza, C.: J. Appl. Phys. **57** (1985) 1305.
85H Helm, M., Knap, W., Seidenbusch, W., Lassnig, R., Gornik, E.: Solid State Commun. **53** (1985) 547.
85K Kopylov, A.A.: Solid State Commun. **56** (1985) 1.
85M Mathieu, H., Chen, Y., Camassel, J., Allegre, J., Robertson, D.S.: Phys. Rev. **B32** (1985) 4042.
85Z Zhu, L.D., Chan, K.T., Ballantyne, J.M.: Appl. Phys. Lett. **47** (1985) 47.
86B Brandt, C.D., Hennel, A.M., Pawlowicz, L.M., Wu, Y.T., Bryskiewicz, T., Lagowski, J., Gatos, H.C.: Appl. Phys. Lett. **48** (1986) 1162.
86D Deveaud, B., Plot, B., Lambert, B., Bremond, G., Guillot, G., Nouailhat, A., Clerjaud, B., Naud, C.: J. Appl. Phys. **59** (1986) 3126.
86J Juhl, A., Bimberg, D.: Semi-Insulating III–V Materials, Hakone 1986, Kukimoto, H., Miyazawa, S. (eds.), OHM, North-Holland, **1986**, p. 477.
86L Lambert, B., Toudic, Y., Coquille, R., Grandpierre, G., Gauneau, M.: Defects in Semiconductors, Proc. 14th Internat. Conf. Defects in Semicond., Paris (1986), von Bardeleben, H.J. (ed.), Materials Science Forum 10···12, Trans. Tech. Publications, Switzerland, **1986**, p. 651.
86M Meiners, L.G.: J. Appl. Phys. **59** (1986) 1611.
87P Parguel, V., Favennec, P.N., Gauneau, M., Rihet, Y., Chaplain, R., L'Haridon, H., Vaudry, C.: J. Appl. Phys. **62** (1987) 824.
89K Korona, K., Hennel, A.M.: Appl. Phys. Lett. **55** (1989) 1085.
90K Korona, K., Karpinska, K., Babinski, A., Hennel, A.M.: Acta Phys. Pol. **A77** (1990) 71.

Physical property	Numerical value	Experimental conditions	Experimental method, remarks	Ref.

2.14 Indium arsenide (InAs)

Electronic properties

band structure: Fig. 1 (Brillouin zone: see section 1.1, Fig. 2)
InAs resembles in its band structure InSb, having only a slightly larger energy gap and a smaller spin-orbit splitting of the top of the valence band.

energies of symmetry points of the band structure (relative to the top of the valence band) (in eV):

$E(\Gamma_{6v})$	−12.69	−12.3 (4)	symmetry symbols in double group notation
$E(\Gamma_{7v})$	−0.43		

Physical property	Numerical value	Experimental conditions	Experimental method, remarks	Ref.
$E(\Gamma_{8v})$	0.00		first row: theoretical [76C]	
$E(\Gamma_{6c})$	0.37		second row: XPS [74L] and	
$E(\Gamma_{7c})$	4.39		angular resolved photo-	
$E(\Gamma_{8c})$	4.63		emission [83W] data (spin-	
$E(X_{6v})$	−10.20	−9.8(3)	splitting not resolved)	
$E(X_{6v})$	−6.64	−6.3(2)		
$E(X_{6v})$	−2.47	−2.4(3)		
$E(X_{7v})$	−2.37			
$E(X_{6c})$	2.28			
$E(X_{7c})$	2.66			
$E(L_{6v})$	−10.92	−10.6(3)		
$E(L_{6v})$	−6.23			
$E(L_{6v})$	−1.26			
$E(L_{4,5v})$	−1.00	−0.9(3)		
$E(L_{6c})$	1.53			
$E(L_{6c})$	5.42			
$E(L_{4,5c})$	5.55			
$E(\Sigma^{min})$		−3.3(2)		
direct energy gap:				
$E_{g,dir}(\Gamma_{8v}-\Gamma_{6c})$	0.4180 eV	4.2 K	magnetotransmission	75V
	0.354(3) eV	295 K	electroreflectance	77L
For temperature dependence of energy gaps, see Fig. 2.				
spin-orbit splitting energies (in eV):				
$\Delta_0(\Gamma_{8v}-\Gamma_{7v})$	0.38(1)	1.5 K	magneto-electroreflectance	67P
$\Delta_1(L_{4,5v}-L_{6v})$	0.267	5 K	wavelength modulated reflectance	70Z
effective mass, electrons (in units of m_0):				
m_n	0.0239		calculated from valence band parameters below	83K
	0.0231	150 K	magnetophonon resonance	81T
	0.0219(5)	250 K		
For dependence on electron concentration, see Fig. 3.				
electron *g*-factor:				
g_c	−15.0		esr	82P
For the camel's back structure at the conduction band X-minima, see [85K].				
effective masses, holes (in units of m_0):				
$m_{p,h}$	0.43	along [111]	calculated from valence band	83K
	0.35	along [100]	parameters below	
$m_{p,l}$	0.026(2)	20 K	magnetoabsorption	67P
valence band parameters:				
A	−19.7		calculated using $k\cdot p$ theory	75W
B	−16.8			
$\lvert C\rvert$	13.66			

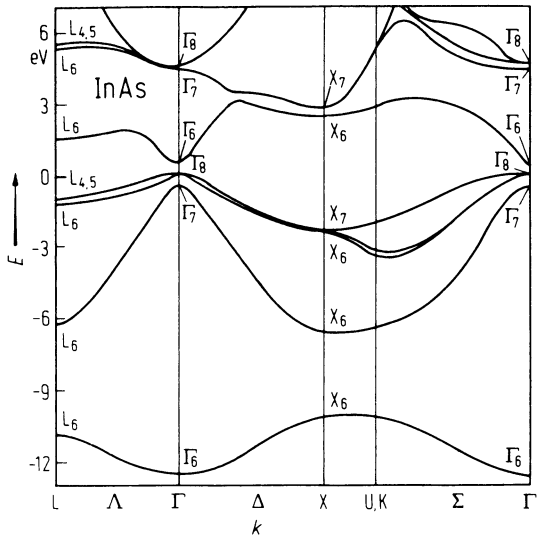

Fig. 1. InAs. Band structure obtained with a non-local pseudopotential calculation [76C].

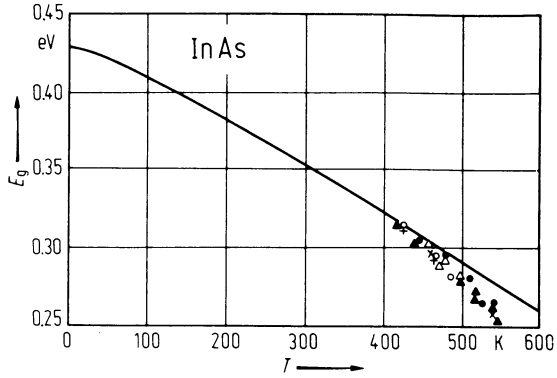

Fig. 2. InAs. Band gap vs. temperature. Solid line: optical band gap calculated from parameters used for fitting various transport data; symbols: thermal band gap of six samples obtained from conductivity and Hall coefficient [82Y].

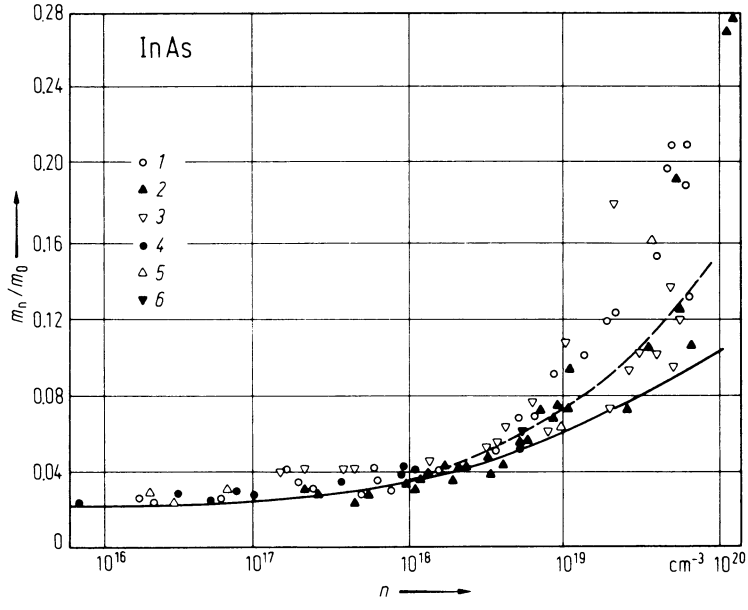

Fig. 3. InAs. Electron effective mass vs. electron concentration. Experimental data obtained by (*1*) Seebeck effect, (*2*) infrared reflectivity, (*3*) magnetic susceptibility, (*4*) Faraday effect, (*5*) recombination radiation, (*6*) cyclotron resonance [78S].

Physical property	Numerical value	Experimental conditions	Experimental method, remarks	Ref.
Lattice properties				
Structure				
InAs I	space group $T_d^2 - F\bar{4}3m$ (zincblende structure)		stable at normal pressure	
InAs II	space group $O_h^5 - Fm3m$ (rocksalt structure)		high pressure phase	85V
InAs III	space group $D_{4h}^{19} - I4_1/amd$ (β-tin structure)			85V
transition pressures (in kbar):				
p_{tr}(I–II)	70(2)	RT	X-ray diffraction	85V
p_{tr}(II–III)	170(4)			
No further phase transition observed up to 270 kbar [85V].				
lattice parameter:				
a	6.0583 Å	298.15 K		63O
linear thermal expansion coefficient:				
α	$4.52 \cdot 10^{-6}\,K^{-1}$	20···250 K	Figs. 4, 5	58S
density:				
d	$5.667\,g\,cm^{-3}$	300 K	X-ray	69R
melting point:				
T_m	1215 K			69G

phonon dispersion relations: Fig. 6.

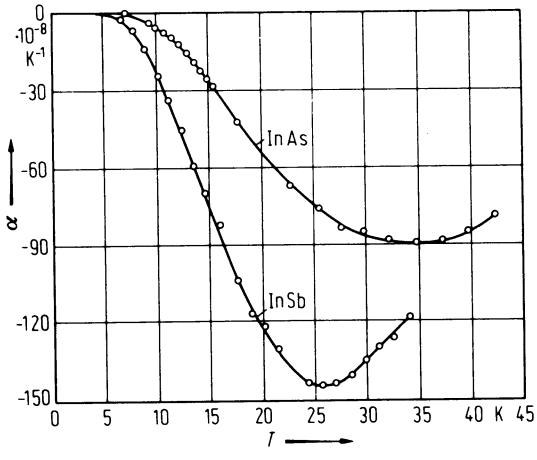

Fig. 4. InAs, InSb. Linear thermal expansion coefficient vs. temperature measured with a variable transformer dilatometer [67S].

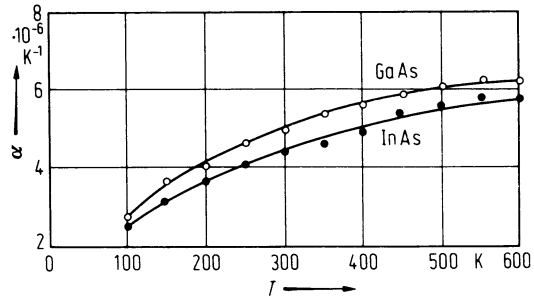

Fig. 5. GaAs, InAs. Temperature dependence of the coefficient of linear thermal expansion between 100 K and 600 K [58S].

Physical property	Numerical value	Experimental conditions	Experimental method, remarks	Ref.
phonon wavenumbers (in cm^{-1}):				
$\bar{\nu}_{TO}(\Gamma)$	217.3	300 K	Raman scattering	80C
$\bar{\nu}_{LO}(\Gamma)$	238.6			
$\bar{\nu}_{TA}(X)$	53			
$\bar{\nu}_{LA}(X)$	160			
$\bar{\nu}_{TO}(X)$	216			
$\bar{\nu}_{LO}(X)$	203	100 K		
$\bar{\nu}_{TA}(L)$	44	300 K		
$\bar{\nu}_{LA}(L)$	139.5			
$\bar{\nu}_{TO}(L)$	216			
$\bar{\nu}_{LO}(L)$	203	100 K		
elastic moduli (in 10^{11} dyn cm^{-2}):				
c_{11}	8.329	RT, n-type	ultrasound	63G
c_{12}	4.526			
c_{44}	3.959			

Transport properties

The transport properties are similar to those of InSb, i.e. the high electron mobility and the high mobility ratio determines the behavior of n-type and near-intrinsic samples.

intrinsic carrier concentration:
n_i can be expressed in the range 350···900 K by: $2.14 \cdot 10^{15}\, T^{3/2} \exp(-0.47/2kT)$ (kT in eV, T in K, n_i in cm^{-3}) (Fig. 7 [54F]). The extrapolated RT value then is:

n_i	$1.3 \cdot 10^{15}\, cm^{-3}$	300 K

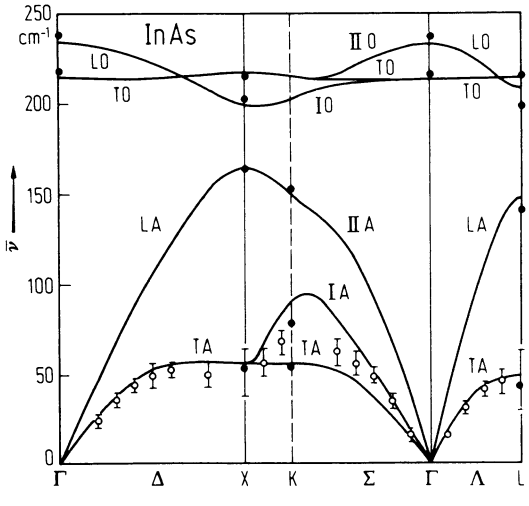

Fig. 6. InAs. Phonon dispersion relations. Solid lines: calculated, open circles: neutron data, full circles: Raman data [80C].

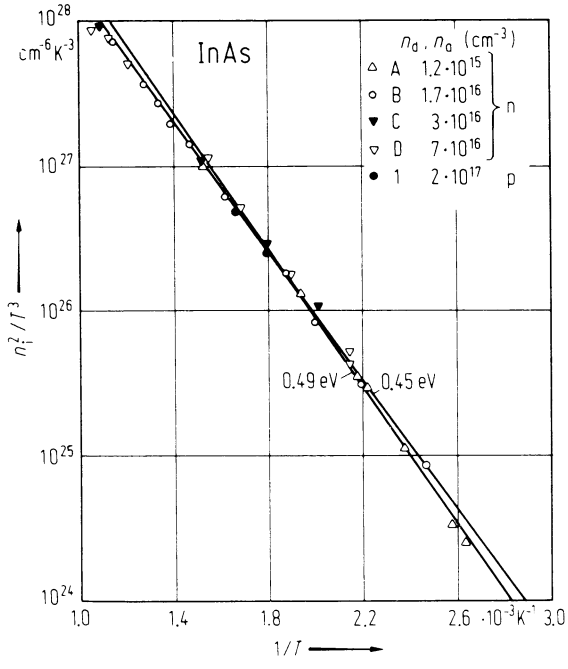

Fig. 7. InAs. Square of the intrinsic carrier concentration over T^3 vs. reciprocal temperature for different samples [54F].

Physical property	Numerical value	Experimental conditions	Experimental method, remarks	Ref.
electron and hole mobility (in cm^2/Vs):				
μ_n	$0.8 \cdots 1 \cdot 10^5$ $2 \cdots 3.3 \cdot 10^4$	77 K 300 K	pure material ($n \approx 10^{16}\,cm^{-3}$)	75R
For temperature dependence, see Fig. 8.				
μ_p	$100 \cdots 450$	300 K	temperature dependence $\propto T^m$ with $m \approx 1$ for low temperatures and > 2 for high temperatures (Fig. 9)	54F, 63M

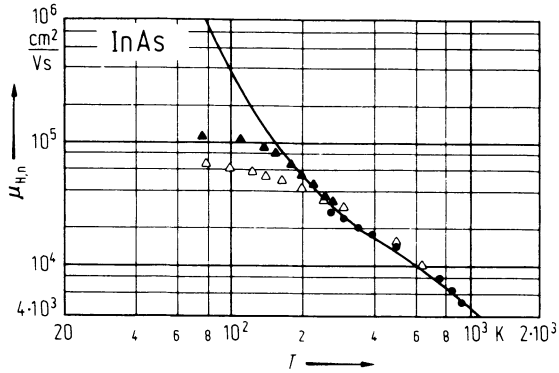

Fig. 8. InAs. Electron Hall mobility of pure material vs. temperature [75R]. Open triangles: $n = 1.7 \cdot 10^{16}\,cm^{-3}$, circles: $n = 4 \cdot 10^{16}\,cm^{-3}$, full triangles: $4 \cdot 10^{15}\,cm^{-3}$.

thermal conductivity: Fig. 10.

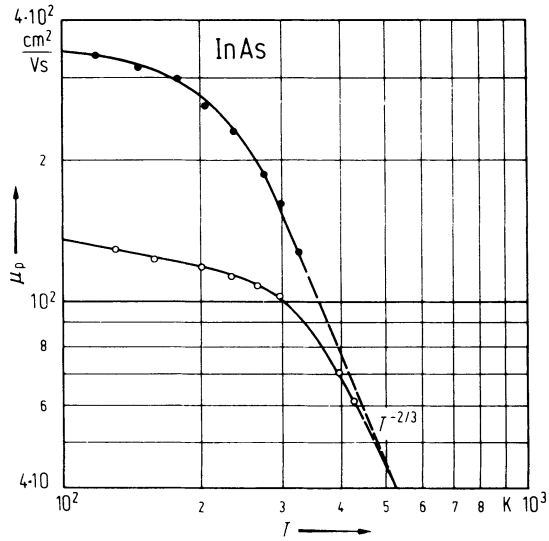

Fig. 9. InAs. Hole mobility ($8\sigma R_H/3\pi$) vs. temperature for two samples [54F].

Optical properties

dielectric constants:

$\varepsilon(0)$	15.15	300 K	infrared reflectance and oscillator fit	62H
$\varepsilon(\infty)$	12.25			

optical constants:
real and imaginary parts of the dielectric constant measured by spectroscopical ellipsometry; n, k, R, K calculated from these data [83A]; see also Fig. 11.

$\hbar\omega$ [eV]	ε_1	ε_2	n	k	R	$K[10^3\,cm^{-1}]$
1.5	13.605	3.209	3.714	0.432	0.337	65.69
2.0	15.558	5.062	3.995	0.634	0.370	128.43
2.5	15.856	15.592	4.364	1.786	0.454	452.64
3.0	6.083	13.003	3.197	2.034	0.412	618.46
3.5	5.973	10.550	3.008	1.754	0.371	622.13
4.0	7.744	11.919	3.313	1.799	0.393	729.23
4.5	−1.663	22.006	3.194	3.445	0.566	1571.19
5.0	−5.923	8.752	1.524	2.871	0.583	1455.26
5.5	−3.851	6.008	1.282	2.344	0.521	1306.62
6.0	−2.403	6.005	1.434	2.112	0.448	1284.15

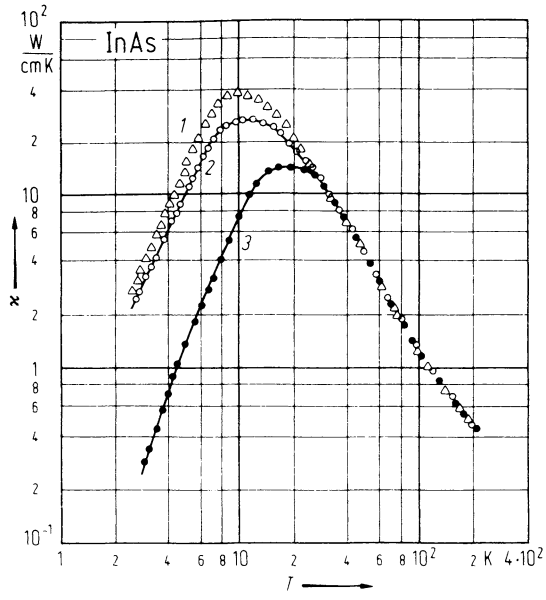

Fig. 10. InAs. Thermal conductivity below 200 K for three samples with *1*: $n = 1.6 \cdot 10^{16}\,cm^{-3}$, *2*: $n = 2 \cdot 10^{17}\,cm^{-3}$, *3*: $p = 2 \cdot 10^{17}\,cm^{-3}$ [71T].

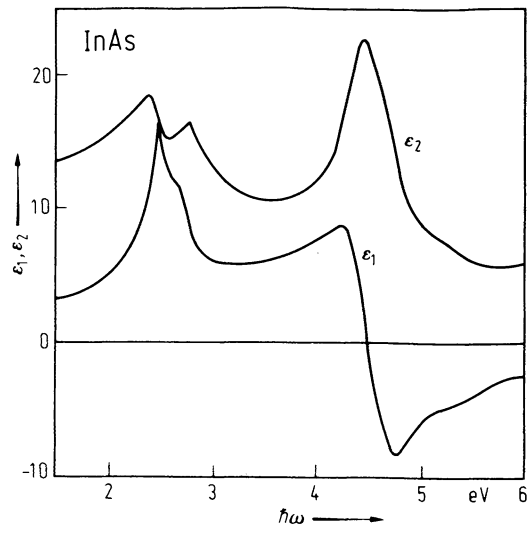

Fig. 11. InAs. Real and imaginary parts of the dielectric constant vs. photon energy [83A].

Impurities and defects

solubility of impurities in InAs

Impurity	c^{eq} [cm^{-3}]	T [°C]	Remarks	Ref.
Cd	$3.5 \cdot 10^{19}$ (max)	800	radiotracer	67A
S, Se, Te	full curves determined		microhardness and Hall effect studies	76G
Zn	$> 3 \cdot 10^{19}$ (max)	800		67B2

diffusion coefficients

Element	D_0 [$cm^2\,s^{-1}$]	Q [eV]	Remarks	Ref.
Self-diffusion coefficients				
In	$6.0 \cdot 10^{5}$	4.0	radiotracer	69K
As	$3.0 \cdot 10^{7}$	4.45	radiotracer	69K
Impurity diffusion-coefficients				
Ag	$7.3 \cdot 10^{-4}$	0.26	radiotracer	67B1
Au	$5.8 \cdot 10^{-4}$	0.65	radiotracer	67R
Cd	$7.4 \cdot 10^{-4}$	1.15	radiotracer	67A
Cd		2.4	pn-junction	81H
Cu	$3.6 \cdot 10^{-3}$	0.52	radiotracer	67F
Ge	$3.74 \cdot 10^{-6}$	1.17	pn-junction	62S
Mg	$1.98 \cdot 10^{-6}$	1.17	pn-junction	62S
S	6.78	2.20	pn-junction	62S
Sn	$1.49 \cdot 10^{-6}$	1.17	pn-junction	62S
Se	12.6	2.20	pn-junction	62S
Te	$3.43 \cdot 10^{-5}$	1.28	pn-junction	62S
Hg	$1.45 \cdot 10^{-5}$	1.32	radiotracer	71S
Zn	$4.2 \cdot 10^{-3}$	0.96 ± 0.02	isoconcentration	67B2
Zn	complex profiles		technique not known	73C

shallow impurities

Little is known about impurities in this material. The binding energies of some acceptors and donors are determined from photoluminescence experiments. It is, however, not known whether these impurities are point defects or complexes.

acceptor binding energies

Impurity	E_b [meV]	T [K]	Remarks	Ref.
Sn	10	77	photoluminescence of implanted material	75G
Ge	14		photoluminescence	74G
Si	20			
(?)	20		photoluminescence of Sn-doped material	76Z
structure defect	35	4.2		

References for 2.14

54F Folberth, O.G., Madelung, O., Weiss, H.: Z. Naturforsch. **9a** (1954) 954.
58S Sirota, N.N., Pashintsev, Yu.I.: Inzh. Fiz. Zh. Akad. Nauk BSSR **1** (1958) 38.
62H Hass, M., Henvis, B.W.: J. Phys. Chem. Solids **23** (1962) 1099.
62S Schillmann, E.: Compound Semiconductors – Preparation of III–V Compounds, Vol. 1, Willardson, R.K., Goering, H.L. (eds.), New York: Reinhold **1962**, p. 358.
63G Gerlich, D.: J. Appl. Phys. **34** (1963) 2915.
63M Mikhailova, M.P., Nasledov, D.N., Slobodchikov, S.V.: Sov. Phys. Solid State (English Transl.) **5** (1964) 1685; Fiz. Tverd. Tela **5** (1963) 2317.
63O Ozolin'sh, J.V., Averkieva, G.K., Ilvin'sh, A.F., Goryunova, N.A.: Sov. Phys. Cryst. (English Transl.) **7** (1963) 691.
67A Arseni, K.A., Boltaks, B.I., Rembeza, S.I.: Sov. Phys. Solid State **8** (1967) 2248.
67B1 Boltaks, B.I., Rembeza, S.I., Sharma, B.L.: Sov. Phys. Solid State **1** (1967) 196.
67B2 Boltaks, B.I., Rembeza, S.I.: Sov. Phys. Solid State **8** (1967) 2117.
67P Pidgeon, C.R., Groves, S.H., Feinleib, J.: Solid State Commun. **5** (1967) 677.
67R Rembeza, S.I.: Sov. Phys. Solid State **1** (1967) 516.
67S Sparks, P.W., Swenson, C.A.: Phys. Rev. **163** (1967) 779.
69G Glazov, V.M., Chizhevskaya, S.N., Evgen'ev, S.B.: Zh. Fiz. Khim. **43** (1969) 373.
69K Kato, H., Yokozawa, M., Kohara, R., Okabayashi, Y., Takayanagi, S.: Solid-State Electron. **12** (1969) 137.
69R Reifenberger, B., Keck, M.J., Trivisoono, J.: J. Appl. Phys. **40** (1969) 5403.
70Z Zucca, R.R.L., Shen, Y.R.: Phys. Rev. **155** (1970) 2668.
71S Sharma, B.L., Purohit, R.K., Mukerjee, S.N.: J. Phys. Chem. Solids **32** (1971) 1397.
71T Tamarin, P.V., Shalyt, S.S.: Sov. Phys. Semicond. (English Transl.) **5** (1971) 1097; Fiz. Tekh. Poluprovodn. **5** (1971) 1245.
73C Casey, H.C.: Quoted unpublished measurements of M.G. Buehler and G.L. Pearson, in "Atomic Diffusion in Semiconductors", Shaw, D. (ed.), New York: Plenum Press **1973**, p. 351.
74G Guseva, M.I., Zotova, N.V., Koval, A.V., Nasledov, D.N.: Sov. Phys. Semicond. (English Transl.) **8** (1974) 34; Fiz. Tekh. Poluprovodn. **8** (1974) 59.
74L Ley, L., Pollak, R.A., McFeely, F.R., Kowalczyk, S.P., Shirley, D.A.: Phys. Rev. **B9** (1974) 600.
75G Guseva, M.I., Zotova, N.V., Koval, A.V., Nasledov, D.N.: Sov. Phys. Semicond. (English Transl.) **8** (1975) 1323; Fiz. Tekh. Poluprovodn. **8** (1974) 2034.
75R Rode, D.L.: in "Semiconductors and Semimetals", Vol. 10, R.K. Willardson, A.C. Beer eds., Academic Press, New York **1975**.
75V Varfolomeev, A.V., Seisyan, R.P., Yakimova, R.N.: Sov. Phys. Semicond. (English Transl.) **9** (1975) 530; Fiz. Tekh. Poluprovodn. **9** (1975) 804.
75W1 Wiley, J.D.: in "Semiconductors and Semimetals", Vol. **10**, R.K. Willardson, A.C. Beer eds., Academic Press, New York 1975.
76C Chelikowsky, J.R., Cohen, M.L.: Phys. Rev. **B14** (1976) 556.
76G Glazov, V.M., Akopyan, R.A., Shvedkov, E.I.: Sov. Phys.-Semicond. **10** (1976) 378.
76Z Zotova, N.V., Karataev, V.V., Koval, A.V.: Sov. Phys. Semicond. (English Transl.) **9** (1976) 1275; Fiz. Tekh. Poluprovodn. **9** (1975) 1944.
77L Lukeš, F.: Phys. Status Solidi (b) **84** (1977) K113.
78S Semikolenova, N.A., Nesmelowa, I.M., Khabarov, E.N.: Sov. Phys. Semicond. (English Transl.) **12** (1978) 1139; Fiz. Tekh. Poluprovodn. **12** (1978) 1915.
80C Carles, R., Saint-Cricq, N., Renucci, J.B., Renucci, M.A., Zwick, A.: Phys. Rev. **B22** (1980) 4804.
81H Horikoshi, Y., Saito, H., Takanashi, Y.: Jpn. J. Appl. Phys. **20** (1981) 437.
81T Takayama, J., Shimomae, K., Hamaguchi, C.: Jpn. J. Appl. Phys. **20** (1981) 1265.
82P Pascher, H.: Opt. Commun. **41** (1982) 106.
82Y Yang June Jung, Byung Ho Kim, Hyung Jae Lee, Wolley, J.C.: Phys. Rev. **26** (1982) 3151.
83A Aspnes, D.E., Studna, A.A.: Phys. Rev. **B27** (1983) 985.

83K Kanskaya, L.M., Kokhanovskii, S.I., Seisyan, R.P., Efros, Al.L., Yukish, V.A.: Sov. Phys. Semicond. (English Transl.) **17** (1983) 449; Fiz. Tekh. Poluprovodn. **17** (1983) 718.
83W Williams, G.P., Cerrina, F., Anderson, J., Lapeyre, G.J., Smith, R.J., Hermanson, J., Knapp, J.A.: Physica **117B & 118B** (1983) 350.
85V Vohra, Y.K., Weir, S.T., Ruoff, A.L.: Phys. Rev. **B31** (1985) 7344.

Physical property	Numerical value	Experimental conditions	Experimental method, remarks	Ref.

2.15 Indium antimonide (InSb)

Electronic properties

band structure: Fig. 1 (Brillouin zone: see Fig. 2 of section 1.1)
InSb is a direct semiconductor. The minimum of the conduction band (Γ_6) is situated in the center of the Brillouin zone. Near the minimum, $E(k)$ is isotropic but non-parabolic. Thus the effective mass of the electrons is scalar and depends strongly on the electron concentration. Higher band minima (about 0.63 eV above the lowest minimum) seem to be established by transport measurements in heavily doped n-InSb [75F]. The valence band shows the structure common to all zincblende semiconductors i.e. two subbands degenerate at Γ_8 and one spin-split band (Γ_7). A small crystal field splitting of the heavy hole band is negligible for most phenomena.

energies of symmetry points of the band structure (relative to the top of the valence band) (in eV):

$E(\Gamma_{6v})$	−11.71	−11.7 (d)	symmetry symbols in double group notation
$E(\Gamma_{7v})$	−0.82	−0.850 (a)	first row: theoretical data of [76C, 85C], see Fig. 1
$E(\Gamma_{8v})$	0.00		second row: experimental data deduced from (a): [85L1], (b): [83L], (c): [81M]), (d): [74L]
$E(\Gamma_{6c})$	0.25	0.235 (b)	
$E(\Gamma_{7c})$	3.16	3.141 (a)	
$E(\Gamma_{8c})$	3.59	3.533 (a, c)	
$E(X_{6v})$	−9.20	−9.5 (d)	
$E(X_{6v})$	−6.43	−6.4 (d)	
$E(X_{6v})$	−2.45	−2.4 (d)	
$E(X_{7v})$	−2.24		
$E(X_{6c})$	1.71	1.79 (a, d)	
$E(X_{7c})$	1.83		
$E(L_{6v})$	−9.95	−10.5 (d)	
$E(L_{6v})$	−5.92		

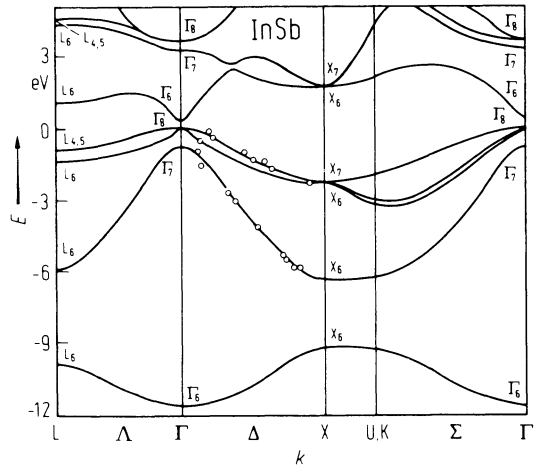

Fig. 1. InSb. Band structure obtained with a non-local pseudopotential calculation [76C], corrected in [84C] (Fig. from [84C]). Experimental data from angular resolved photoemission from a InSb (001) surface [83H] have been included (circles).

Physical property	Numerical value	Experimental conditions	Experimental method, remarks	Ref.
$E(L_{6v})$	−1.44	−1.4 (d)		
$E(L_{4,5v})$	−0.96	−0.9 (a, d)		
$E(L_{6c})$	1.03			
$E(L_{6c})$	4.30	4.32 (a, d)		
$E(L_{4,5c})$	4.53	4.47 (a, d)		
energy gaps (in eV):				
$E(1S)$	0.2363 (2)	2 K, $n_{77K} = 6 \cdot 10^{13}$ cm^{-3}	exciton ground state, from luminescence and absorption	79K2
$E_{g,dir}$	0.2368 (2)		calculated from $E(1S)$	79K2
	0.2352	1.8 K	resonant two-photon photo-Hall effect,	85L2,
	0.230	77 K	two-photon magnetoabsorption	82G
temperature dependence of energy gap:				
$E_g(T)$	$E_g(0) - aT^2/(b+T)$ with $a = 0.6$ meV K^{-1}, $b = 500$ K, Fig. 2			85L2
For camel's back structure of the conduction band X-minima, see [85K].				
spin-orbit splitting energies (in eV):				
$\Delta_0(\Gamma_{8v} - \Gamma_{7v})$	0.850	100 K	ellipsometry	85L1
$\Delta_1(\Lambda_{4,5v} - \Lambda_{6v})$	0.498 (4)			
$\Delta'_0(\Gamma_{7c} - \Gamma_{8c})$	0.392 (12)		ellipsometry	81M
critical point energies (in eV):				
$E_1(\Lambda_{4,5v} - \Lambda_{6c})$	1.968 (1)	100 K	ellipsometry	85L1
	1.872 (2)	RT		81M
$E'_0(\Gamma_{8v} - \Gamma_{7c})$	3.141 (12)			85L1
$E_2(X_{6,7v} - X_{6c})$	4.186 (2)			
$E'_1(L_{4,5v} - L_{6c})$	5.22 (3)			
effective masses, electrons (in units of m_0):				
$m_n(\Gamma_{6c})$	0.01359 (3)	4.2 K, $n = 4.6 \cdot 10^{13}$ cm^{-3}	Faraday effect	83Z
Dependence of electron effective mass on carrier concentration: see Fig. 3; energy dependence caused by the non-parabolicity of the conduction band: see Fig. 4.				
$m_n(L_{6c})$	$0.09 m_0$		electroreflection	79Z
electron g-factor:				
g_c	−50.6		intra conduction band magnetoabsorption	83G
effective masses, holes (in units of m_0):				
$m_{p,h}$	0.45 (3)	$T = 4 \cdots 77$ K, ∥ [111]	cyclotron resonance	63B2
	0.42 (3)	∥ [110]		
	0.34 (3)	∥ [100]		
$m_{p,l}$	0.0158 (5)	77 K, p-type	magnetoplasma resonance (decreases to 0.0147 at 150 K)	80S

Physical property	Numerical value	Experimental conditions	Experimental method, remarks	Ref.
valence band parameters:				
A	−35		calculated using $k \cdot p$ theory	75W
B	−31.4			
$\|C\|$	20.92			

Lattice properties

Structure

InSb I	space group T_d^2–F$\bar{4}$3m (zincblende structure)	stable at normal pressure

Data on high-pressure phases are conflicting [78Y].

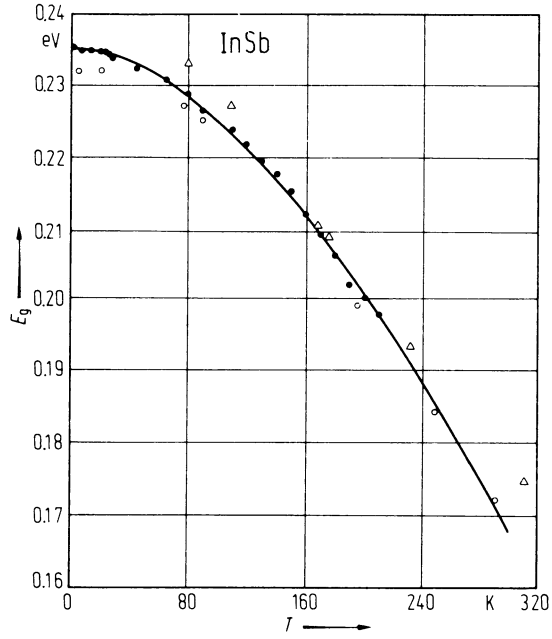

Fig. 2. InSb. Energy gap vs. temperature below RT measured by resonant two-photon photo-Hall effect (full circles); open circles and triangles: earlier literature data for comparison. Solid curve: fit by Varshni's formula as given in the tables [85L2].

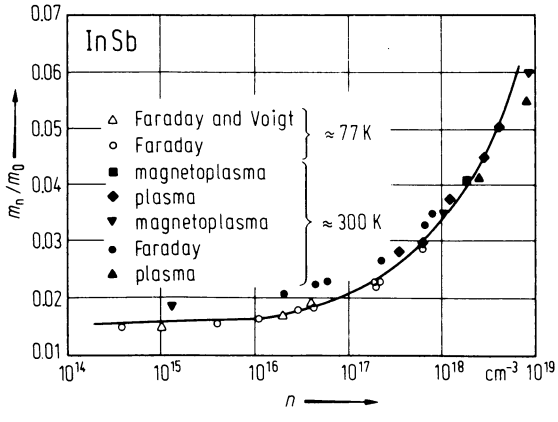

Fig. 3. InSb. Electron effective mass vs. carrier concentration. Comparison of results of several experimental measurements. Solid line: Kane's theory [77S].

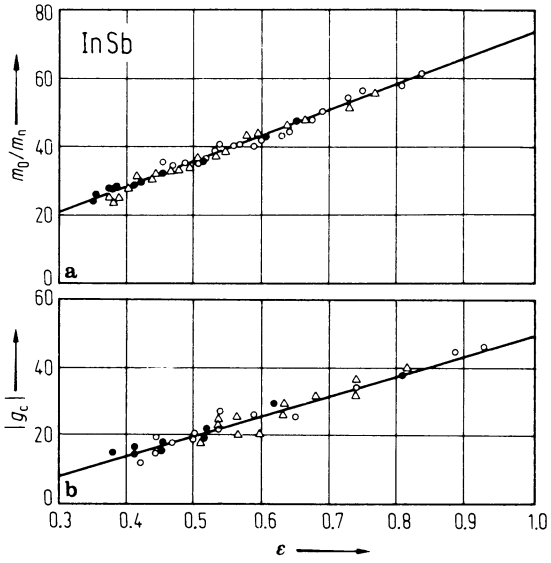

Fig. 4. InSb. Dependence of electron effective mass and g-factor on energy in the conduction band $\Delta E = E - E_c$. (a) reciprocal mass and (b) g-factor vs. $\varepsilon = E_g/(E_g + 2\Delta E)$ [83K].

Physical property	Numerical value	Experimental conditions	Experimental method, remarks	Ref.
lattice parameter:				
a	6.47937 Å	298.15 K	X-ray	65S
Temperature dependence in the range 10 ··· 60 °C and coefficient of linear thermal expansion, see Figs. 5 and 6.				
density:				
d	5.7747 (4) g cm^{-3}		X-ray	65S
melting point:				
T_m	800 (3) K			73H

phonon dispersion relations: Fig. 7.

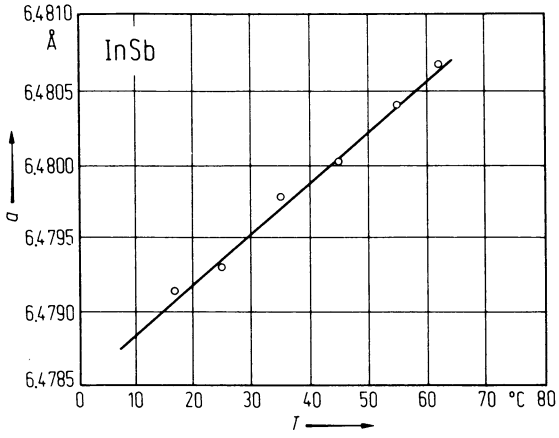

Fig. 5. InSb. Lattice parameter vs. temperature [65S].

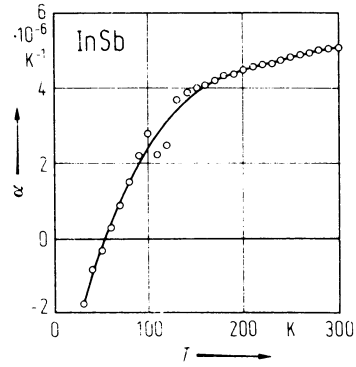

Fig. 6. InSb. Linear thermal expansion coefficient vs. temperature measured with an interferometer [58G]. High temperature range.

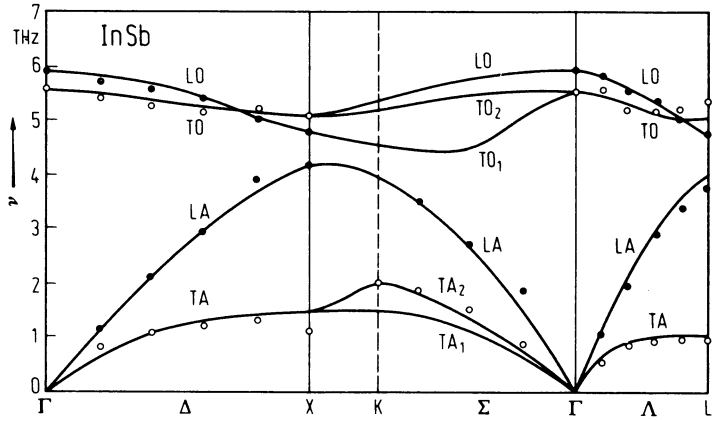

Fig. 7. InSb. Phonon dispersion relations calculated with a six parameter dynamic model [85R]. Experimental points from [71P].

Physical property	Numerical value	Experimental conditions	Experimental method, remarks	Ref.
phonon frequencies (in THz):				
$\nu_{LO}(\Gamma_{15})$	5.90(25)	300 K, $n =$ $8\cdot10^{13}$ cm^{-3}	coherent inelastic neutron scattering	71P
$\nu_{TO}(\Gamma_{15})$	5.54(5)			
$\nu_{TA}(X_5)$	1.12(5)			
$\nu_{LA}(X_3)$	4.30(10)			
$\nu_{LO}(X_1)$	4.75(20)			
$\nu_{TO}(X_5)$	5.38(17)			
$\nu_{TA}(L_3)$	0.98(5)			
$\nu_{LA}(L_1)$	3.81(6)			
$\nu_{LO}(L_1)$	4.82(10)			
$\nu_{TO}(L_3)$	5.31(6)			
$\nu_{TO}(\Gamma)$	5.49	0 K, extrapol.	zone center phonons, Raman spectroscopy	84L
	5.39	RT		
$\nu_{LO}(\Gamma)$	5.83	0 K, extrapol.		
	5.72	RT		

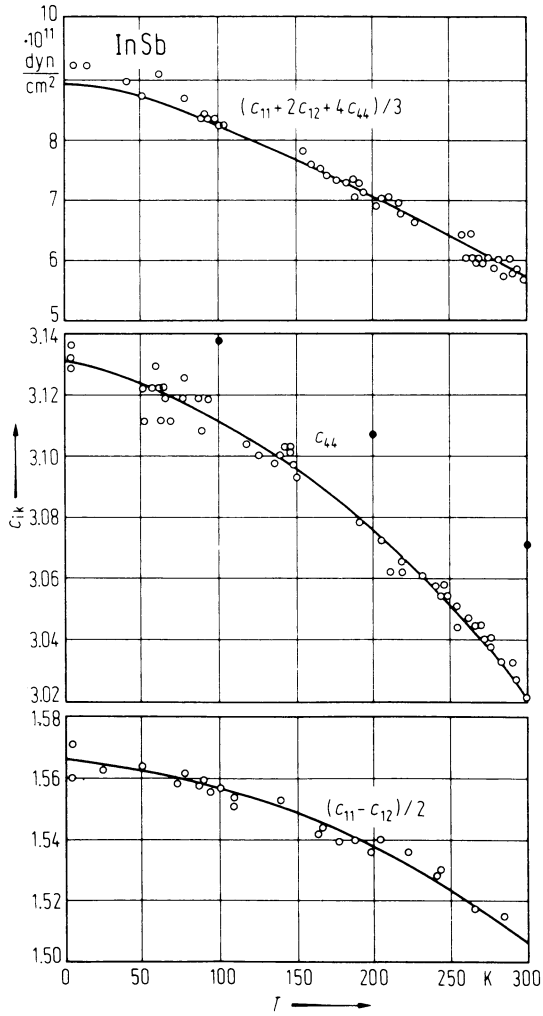

Fig. 8. InSb. Second order elastic moduli vs. temperature [59S].

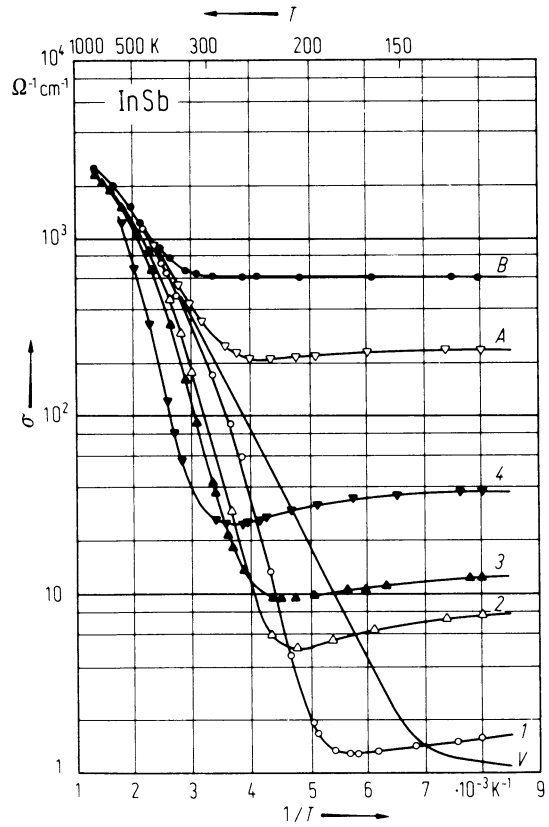

Fig. 9. InSb. Conductivity vs. reciprocal temperature. Curve V: $n \approx 10^{13}$ cm^{-3} [59V], A: $n = 1.3\cdot10^{16}$ cm^{-3}, B: $n = 1\cdot10^{16}$ cm^{-3}, 1: $p = 4\cdot10^{15}$ cm^{-3}, 2: $p = 2.2\cdot10^{16}$ cm^{-3}, 3: $p = 6\cdot10^{16}$ cm^{-3}, 4: $p = 2\cdot10^{17}$ cm^{-3} [54M].

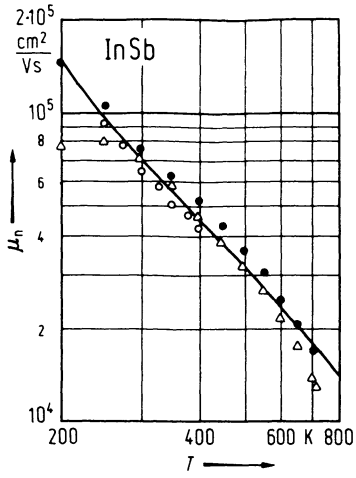

Fig. 10. InSb. Electron mobility vs. temperature. Experimental data are Hall mobilities from various sources. Solid line: calculated drift mobility [71R].

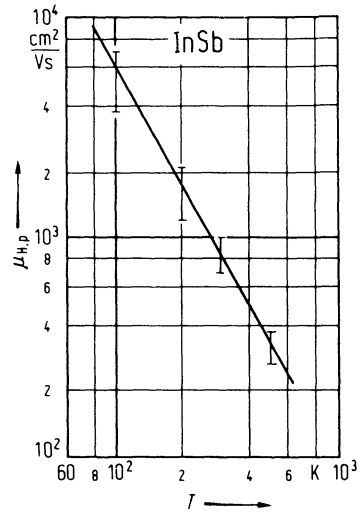

Fig. 11. InSb. Hole Hall mobility vs. temperature. The vertical bars indicate the ranges for the experimental values. The solid line has the slope − 1.8 [75W].

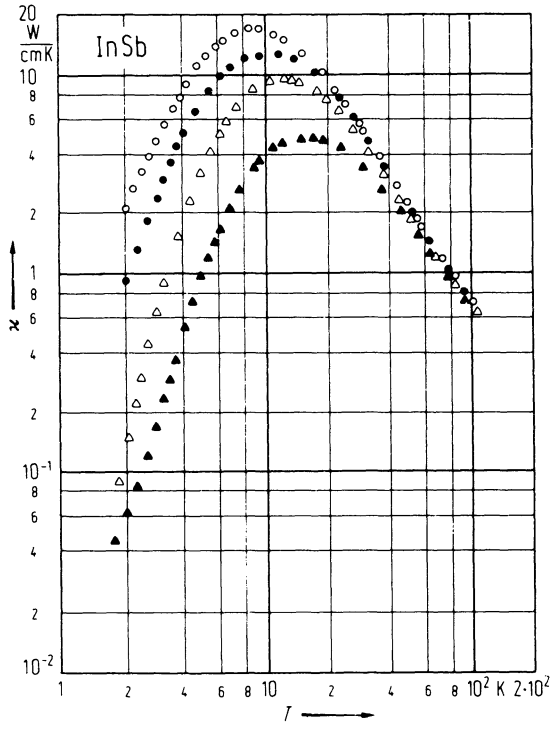

Fig. 12. InSb. Thermal conductivity vs. temperature of several p-type samples [71K].

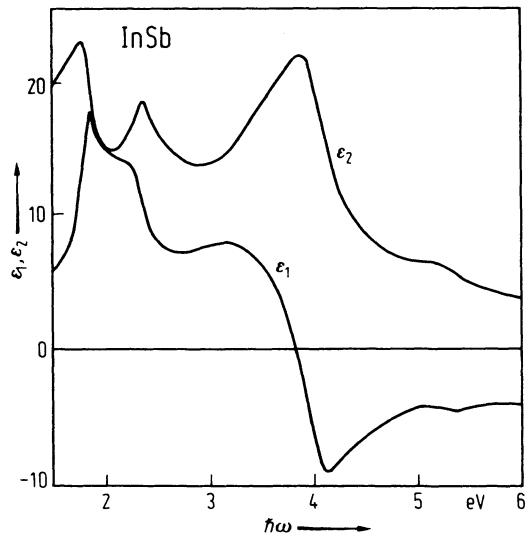

Fig. 13. InSb. Real and imaginary parts of the dielectric constant vs. photon energy [83A].

Physical property	Numerical value	Experimental conditions	Experimental method, remarks	Ref.
second order elastic moduli (in 10^{11} dyn cm^{-2}):				
c_{11}	6.918	0 K, extrapol.	ultrasound	59S
	6.669	300 K	for temperature dependence,	
c_{12}	3.788	0 K, extrapol.	see Fig. 8.	
	3.645	300 K		
c_{44}	3.132	0 K, extrapol.		
	3.020	300 K		

Transport properties

The transport properties in n-type material are mainly determined by the extremely high mobility of the electrons in the lowest conduction band minimum. Pure material with intrinsic conduction down to 200 K is available. At low temperatures and in doped material ionized-impurity scattering limits the electron mobility. In pure material below RT polar optical mode scattering is dominant. Above 400 K electron-hole scattering contributes significantly. Above 700 K multivalley conduction seems to occur.

electrical conductivity: Fig. 9.

intrinsic carrier concentration:

n_i	$2.04(55)\cdot10^{16}$ cm^{-3}	300 K	Hall effect	70C

The temperature dependence can be described in the range 150 ··· 300 K by the relation:

$$n_i = 5.76\cdot10^{14}\,T^{3/2}\exp(-0.26/2\,kT)\,\text{cm}^{-3}\,(T \text{ in K, } kT \text{ in eV})[70C]$$

electron mobility (in cm^2/Vs):

$\mu_{H,n}$	$7.7\cdot10^4\cdot(T/300\,\text{K})^{-1.66}$		see also Fig. 10	64M
	$6\cdot10^5$	$n_d = 5\cdot10^{14}$ cm^{-3}, 77 K		85W
$\mu_{dr,n}$	$5.25\cdot10^5$			

hole mobility (in cm^2/Vs):

$\mu_{p,h}$	$850\,(T/300\,\text{K})^{-b}$		b is 1.8 ··· 2.1 for the range 60 ··· 500 K, see Fig. 11.	75W
$\mu_{p,l}$	$3\cdot10^4$	295 K	from analysis of transport data	64S

thermal conductivity: Fig. 12.

Optical properties

dielectric constants:

$\varepsilon(0)$	16.8 (2)	gyroscopic sphere resonance	80D
	17.3 ··· 18.0	range of results obtained by infrared reflectivity (from compilation of data in [80D])	
$\varepsilon(\infty)$	15.68	infrared reflectance and oscillator fit	62H

optical constants

real and imaginary parts of the dielectric constant measured by spectroscopical ellipsometry; n, k, R, K calculated from these data [83A]; see also Fig. 13.

$\hbar\omega$[eV]	ε_1	ε_2	n	k	R	K[10^3 cm^{-1}]
1.5	19.105	5.683	4.418	0.643	0.406	97.79
2.0	14.448	14.875	4.194	1.773	0.443	359.46
2.5	7.811	15.856	3.570	2.221	0.447	562.77
3.0	7.354	13.421	3.366	1.994	0.416	606.27
3.5	5.995	17.673	3.511	2.517	0.474	892.82
4.0	−6.722	19.443	2.632	3.694	0.608	1497.79
4.5	−6.297	8.351	1.443	2.894	0.598	1320.24
5.0	−4.250	6.378	1.307	2.441	0.537	1237.01
5.5	−4.325	4.931	1.057	2.333	0.563	1300.55
6.0	−3.835	3.681	0.861	2.139	0.572	1300.85

Impurities and defects

diffusion coefficients

Element	D_0[cm^2 s^{-1}]	Q[eV]	T[K]	Remarks	Ref.
Self-diffusion coefficients in InSb.					
In	$5.0\cdot10^{-2}$	1.82	480···520	radiotracer (residual activity)	57E
In	$1.8\cdot10^{13}$	4.3	475···517	radiotracer	68K
Sb	$5.0\cdot10^{-2}$	1.94	480···520	radiotracer (residual activity)	57E
Sb	$3.1\cdot10^{13}$	4.3	475···517	radiotracer	68K
Impurity diffusion coefficients					
Ag	$\approx1.0\cdot10^{-7}$	≈0.25		radiotracer	62W
Au	$7.0\cdot10^{-4}$	0.32		radiotracer	64B
Co	$\approx1.0\cdot10^{-7}$	0.25		radiotracer	62W
Cd	$1.0\cdot10^{-5}$	1.1		radiotracer	63B1
Cu	$9.0\cdot10^{-4}$	1.08		radiotracer	63S
Fe	$\approx1.0\cdot10^{-7}$	≈0.25		radiotracer	62W
F	22	1.0		ion analyzer	79B
Hg	$4.0\cdot10^{-6}$	1.17		radiotracer	64G
Li	$7.0\cdot10^{-4}$	0.28		electrical profile	66T
Se	1.6	1.87		CV profiling	69R
Sn	$5.5\cdot10^{-8}$	0.75		radiotracer	61S
Te	$1.7\cdot10^{-7}$	0.57		radiotracer	57B
Zn	non-ideal profiles			radiotracer	73C

donors

Shallow, effective-mass like donors are always present in concentrations of at least 10^{13} cm^{-3}. Their influence on the semiconductor properties is strong due to their small binding energy of ≈0.7 meV. No detailed investigations exist.

acceptors

acceptor binding energies

Impurity	E_b [meV]	T [K]	Remarks	Ref.
Theory	8.5		$1S_{3/2}$, acceptor effective mass calculation	73L
Cd	9.86	4.5	Fourier transform spectroscopy	73K
Zn	9.86			
	9.1	1.5	infrared absorption	72M

Impurity	E_b [meV]	T [K]	Remarks	Ref.
Ge	9.25			
Cr	70	14···140	Hall effect, unknown charge; state acts as acceptor	80P
Mn	9.5	4.2···77	Hall effect	71D
Fe	13	10···200	Hall effect	73V1
Co	8	4.2···200	Hall effect	73V2
Cu^0	28	4.2···300	Hall effect	79K1
Cu^-	56			
Ag^0	29.8	4.5	Fourier transform spectroscopy, weakly bound hole	73K
Ag^-	56	4.2···300	Hall effect	79K1

References for 2.15

54M Madelung, O., Weiss, H.: Z. Naturforsch. **9a** (1954) 527.
57B Boltaks, B.I., Kulikov, G.S.: Sov. Phys. Tech. Phys. **2** (1957) 67.
57E Eisen, F.H., Birchenall, C.E.: Acta Metall. **5** (1957) 265.
58G Gibbons, D.F.: Phys. Rev. **112** (1958) 779.
59P Putley, E.H.: Proc. Phys. Soc. **73** (1959) 128.
59S Slutsky, L.J., Garland, C.W.: Phys. Rev. **113** (1959) 167.
59V Volokobinskaya, N.I., Galavanov, V.V., Nasledov, D.N.: Sov. Phys. Solid State (English Transl.) **1** (1959) 687; Fiz. Tverd. Tela **1** (1959) 756.
61S Sze, S.M., Wei, L.Y.: Phys. Rev. **124** (1961) 84.
62H Hass, M., Henvis, B.W.: J. Phys. Chem. Solids **23** (1962) 1099.
62W Watt, L.A.K., Chen, W.S.: Bull. Am. Phys. Soc. **7** (1962) 89.
63B1 Boltaks, B.I., Sokolov, V.I.: Sov. Phys. Solid State **5** (1963) 785.
63B2 Bagguley, D.M.S., Robinson, M.L.A., Stradling, R.A.: Phys. Lett. **6** (1963) 143.
63S Stocker, H.J.: Phys. Rev. **130** (1963) 2160.
64B Boltaks, B.I., Sokolov, V.I.: Sov. Phys. solid State **6** (1964) 600.
64G Gusev, I.A., Murin, A.N.: Sov. Phys. Solid State **6** (1964) 1229.
64M Madelung, O.: Physics of III-V Compounds, J. Wiley & Sons, New York **1964**.
64S Schönwald, H., Z. Naturforsch. **19a** (1964) 1276.
65S Straumanis, M.E., Kim, C.D.: J. Appl. Phys. **36** (1965) 3822.
66T Takobutake, T., Ikari, H., Uyeda, Y.: Jpn. J. Appl. Phys. **5** (1966) 839.
68K Kendall, D.L.: Semiconductors and Semimetals, Vol. 4, Willardson, R.K., Beer, A.C. (eds.), New York, London: Academic Press **1968**, p. 163.
69R Rekalova, G.I., Shokov, A.A., Gavrushko, V.V.: Sov. Phys. Semicond. **2** (1969) 1452.
70C Cunningham, R.W., Gruber, J.B.: J. Appl. Phys. **41** (1970) 1804.
71D Dashevskii, M.Ya., Ivleva, V.S., Korl, L.Ya., Kurilenko, I.N., Litvak-Gorskaya, L.B., Mitrofanova, R.S., Fridlyand, E.Yu.: Sov. Phys. Semicond. (English Transl.) **5** (1971) 757; Fiz. Tekh. Poluprovodn. **5** (1971) 858.
71K Kosarev, V.V., Tamarin, P.V., Shalyt, S.S.: Phys. Status Solidi (b) **44** (1971) 525.
71P Price, D.L., Rowe, J.M., Nicklow, R.M.: Phys. Rev. **B3** (1971) 1268.
71R Rode, D.L.: Phys. Rev. **B3** (1971) 3287.
72M Murzin, V.N., Demishina, A.I., Umarov, L.M.: Sov. Phys. Semicond. (English Transl.) **6** (1972) 419; Fiz. Tekh. Poluprovodn. **6** (1972) 488.
73C Unpublished results by D.L. Kendall, quoted by Casey, H.C.: Atomic Diffusion in Semiconductors, Shaw, D. (ed.), New York: Plenum Press **1973**, p. 351.
73H Hultgren, R., Desai, P.D., Hawkins, D.T., Gleiser, M., Kelly, K.K., Wagman, D.D.: Selected Values of the Thermodynamic Properties of Binary Alloys, American Society of Metals, Metal Park, Ohio **1973**.
73K Kaplan, R.: Solid State Commun. **12** (1973) 191.
73L Lipari, N.O.: Ref. 6 in [73K].
73V1 Vinogradova, K.I., Ivleva, V.S., Il'menkov, G.V., Nasledov, D.N., Smetannikova, Yu.S., Tashkhodshaev, T.K.: Sov. Phys. Semicond. (English Transl.) **6** (1973) 1595; Fiz. Tekh. Poluprovodn. **6** (1973) 1845.
73V2 Vinogradova, K.I., Nasledov, D.N., Smetannikova, Yu.S., Tashkhodshaev, T.K.: Sov. Phys. Solid State (English Transl.) **15** (1973) 212; Fiz. Tverd. Tela **15** (1973) 295.
74L Ley, L., Pollak, R.A., McFeely, F.R., Kowalczyk, S.P., Shirley, D.A.: Phys. Rev. **B9** (1974) 600.
75F Filipchenko, A.S., Nasledov, D.N.: Phys. Status Solidi (a) **27** (1975) 11.
75W Wiley, J.D.: in "Semiconductors and Semimetals", Vol. 10, R.K. Willardson. A.C. Beer eds., Academic Press, New York and London, **1975**.
76C Chelikowski, J.R., Cohen, M.L.: Phys. Rev. **B14** (1976) 556.

77S Stillman, G.E., Wolfe, C.M., Dimmock, J.O.: in "Semiconductors and Semimetals", Vol. 12, R.K. Willardson, A.C. Beer eds., Academic Press, New York and London, **1977**.
78Y Yu, S.C., Spain, I.L., Skelton, E.F.: J. Appl. Phys. **49** (1978) 4741.
79B Blaut-Blachev, A.N., Ivleva, V.S., Selyanina, V.I.: Sov. Phys. Semicond. **13** (1979) 1342.
79K1 Kurilenko, I.N., Litvak-Gorskaya, L.B., Lugovaya, G.E.: Sov. Phys. Semicond. (English Transl.) **13** (1979) 906; Fiz. Tekh. Poluprovodn. **13** (1979) 1556.
79K2 Kaskaya, L.M., Kokhanovskii, S.I., Seisyan, R.P.,: Sov. Phys. Semicond. (English Transl.) **13** (1979) 234; Fiz. Tekh. Poluprovodn. **13** (1979) 2424.
79Z Zvonkov, B.N., Salashchenko, N.N., Filatov, O.N.: Sov. Phys. Solid State (English Transl.) **21** (1979) 777; Fiz. Tverd. Tela **21** (1979) 1344.
80D Dixon, J.R., Furdyna, J.K.: Solid State Commun. **35** (1980) 195.
80P Propov, V.V., Kosarev, V.V.: Phys. Status Solidi (a) **58** (1980) 231.
80S Seiler, D.G., Goodwin, M.W., Miller, A.: Phys. Rev. Lett. **44** (1980) 807.
81M Mattausch, H.J., Aspnes, D.E.: Phys. Rev. **B23** (1981) 1896.
82G Goodwin, M.W., Seiler, D.G., Weiler, M.H.: Phys. Rev. **B25** (1982) 6300.
83A Aspnes, D.E., Studna, A.A.: Phys. Rev. **B27** (1983) 985.
83G Goodwin, M.W., Seiler, D.G.: Phys. Rev. **B27** (1982) 3451.
83H Höchst, H., Hernández-Calderón, I.: Surf. Sci. **126** (1983) 25.
83K Kanskaya, L.M., Kokhanovskii, S.I., Seisyan, R.P., Efros, Al.L.: Phys. Status Solidi (b) **118** (1983) 447.
83L Littler, C.L., Seiler, D.G., Kaplan, R., Wagner, R.J.: Phys. Rev. **B27** (1983) 7473.
83Z Zengin, D.M.: J. Phys. **D16** (1983) 653.
84C Chelikowski, J.R., Cohen, M.L.: Phys. Rev. **B30** (1984) 4828.
84L Liarokapis, W., Anastassakis, E.: Phys. Rev. **B30** (1984) 2270.
85K Kopylov, A.A.: Solid State Commun. **56** (1985) 1.
85L1 Logothetidis, S., Vina, L., Cardona, M.: Phys. Rev. **B31** (1985) 947.
85L2 Littler, C.L., Seiler, D.G.: Appl. Phys. Lett. **46** (1985) 986.
85R Ram, R.K., Kushwara, S.S.: J. Phys. Soc. Jpn. **54** (1985) 617.
85W Warmenbol, P. Peeters, F.M., Devreese, J.T., Algebra, G.E., van Welzenis, R.G.: Phys. Rev. **B31** (1985) 5285.

Physical property	Numerical value	Experimental conditions	Experimental method, remarks	Ref.

2.16 Ternary and quaternary alloys between III–V compounds

Solid solutions between III–V compounds have become increasingly important for microelectronical applications, giving the possibility to choose the energy range e.g. for optoelectronic or laser applications more appropriate than with the binary compounds. The recent progress has mostly been achieved for epitaxial layers on substrates of III–V binary compounds. Fig. 1 shows the lattice parameter vs. the energy gap of various III–V compounds and their ternary and quaternary alloys. The alloys appropriate for lattice matching on GaSb, InP and GaAs and the energy gaps available with such alloys can easily be found. We discuss such alloys in the following sections.

2.16.1 Ternary alloys of the type III_x–III_{1-x}–V

Aluminum gallium nitride ($Al_xGa_{1-x}N$)

Both constituents of this pseudo-binary system are direct gap semiconductors, crystallizing in the same wurtzite structure. They are completely miscible. Most investigations have been made on thin films on sapphire or silicon.

Aluminum gallium phosphide ($Al_xGa_{1-x}P$)

Both components are indirect semiconductors with zincblende structure.

energy gap (in eV):

$E_{g,ind}$	$2.28 + 0.16\,x$	81B3

Aluminum gallium arsenide ($Al_xGa_{1-x}As$)

Electronic properties

The conduction band structure is characterized by a crossover from the sequence $\Gamma - L - X$ in GaAs to $X - L - \Gamma$ in AlAs. Thus $Al_xGa_{1-x}As$ is a direct gap semiconductor below a crossover concentration x_c and an indirect gap (X-conduction band) semiconductor at high x.

Physical property	Numerical value	Experimental conditions	Experimental method, remarks	Ref.

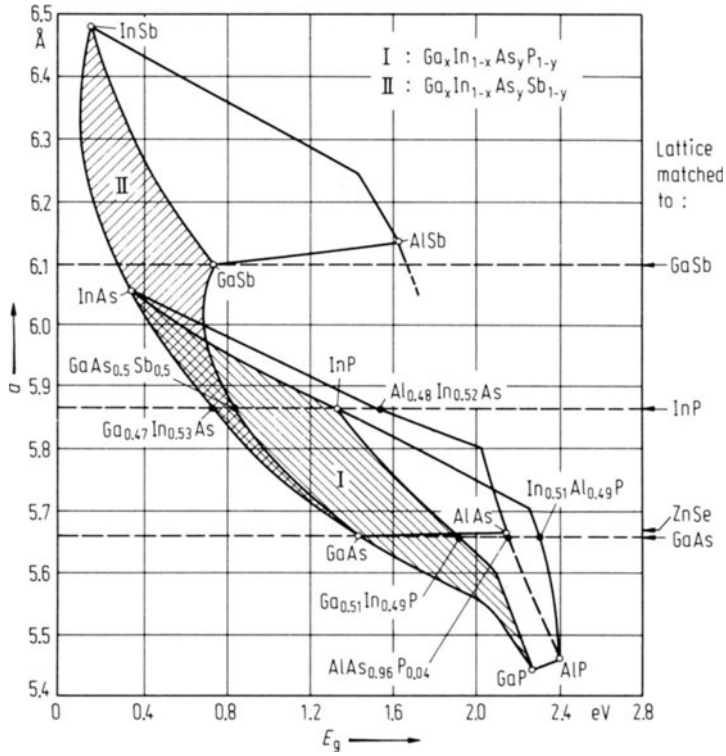

Fig. 1. Lattice parameter vs. energy gap (RT values) for various III-V compounds and their alloys.

energy gaps (energies of the Γ_{6c}, X_{6c} and L_{6c} conduction band minima relative to the top of the valence band Γ_{8v}, in eV):

$E_g(\Gamma)$	$1.420 + 1.087\,x + 0.438\,x^2$		81S
$E_g(X)$	$1.905 + 0.10\,x + 0.16\,x^2$		
$E_g(L)$	$1.705 + 0.695\,x$		
$x_c(L - X)$	0.35	crossover of X and L bands	
$x_c(\Gamma - X)$	0.43	crossover of Γ and X bands	
$x_c(\Gamma - L)$	0.47	crossover of Γ and L bands	

effective masses

According to [85A] a linear compositional dependence seems to be a good approximation.

Lattice properties

The lattice parameters of GaAs and AlAs are very similar. Thus $Al_xGa_{1-x}As$ layers on semiinsulating GaAs can be grown by MBE, LPE or VPE.

lattice parameter (in Å):

a	$5.6533 + 0.0078\,x$	85A

Physical property	Numerical value	Experimental conditions	Experimental method, remarks	Ref.
density (in $g\,cm^{-3}$):				
ϱ	$5.36 - 1.6\,x$			85A
melting point (in K):				
T_m	$1511 - 58\,x + 560\,x^2$		solidus curve	85A
	$1511 + 1082\,x - 580\,x^2$		liquidus curve	
phonon wavenumbers (in cm^{-1}):				
$\bar{\nu}_{LO}$(GaAs-type)	$292.2 - 52.8\,x + 14.4\,x^2$		best fit to experimental data of [79K]	
$\bar{\nu}_{LO}$(AlAs-type)	$359.7 + 70.8\,x - 26.8\,x^2$			
$\bar{\nu}_{TO}$(GaAs-type)	$268.3 - 5.2\,x - 9.3\,x^2$			
$\bar{\nu}_{TO}$(AlAs-type)	$359.7 + 4.4\,x - 2.4\,x^2$			
second order elastic moduli (in $10^{11}\,dyn\,cm^{-2}$):				
c_{11}	$11.88 + 0.14\,x$			85A
c_{12}	$5.38 + 0.32\,x$			
c_{44}	$5.94 - 0.05\,x$			

Transport properties

The transport properties in n-type samples with x around x_c are determined by the occurrence of electrons in all three subbands of the conduction band.

thermal resistivity (in $K\,cm\,W^{-1}$):				
κ^{-1}	$2.27 + 20.83\,x - 30\,x^2$			85A

Aluminum gallium antimonide ($Al_xGa_{1-x}Sb$)

The band structure of this compound is characterized by a double change of symmetry of the lowest conduction band minima from Γ to L and from L to X with increasing x [83A].

energy gaps (in eV):				
$E_0(\Gamma_{8v} - \Gamma_{6c})$	$0.813 + 1.097\,x + 0.40\,x^2$	4.2 K	photoluminescence	83B2
	$0.81 + 1.09\,x + 0.48\,x^2$	27 K	modulation spectroscopy	83A
	$0.73 + 1.10\,x + 0.47\,x^2$	300 K		
$E_x(\Gamma_{8v} - X_{6c})$	$1.11 + 0.577\,x$	4.2 K		83B2
	$1.12 + 0.56\,x$	27 K		83A
	$1.05 + 0.56\,x$	300 K		
$E_L(\Gamma_{8v} - L_{6c})$	$0.893 + 0.867\,x + 0.21\,x^2$	4.2 K		83B2

Aluminum indium phosphide ($Al_xIn_{1-x}P$)

According to [70L1, 70O] linear x-dependence of the energy gaps (relative to the top of the valence band at Γ) (in eV):

$E_g(\Gamma)$	$1.34 + 2.23\,x$
$E_g(X)$	$2.24 + 0.18\,x$
x_c	0.44

Physical property	Numerical value	Experimental conditions	Experimental method, remarks	Ref.
Aluminum indium arsenide ($Al_xIn_{1-x}As$)				
As in $Al_xIn_{1-x}P$ the band gap of $Al_xIn_{1-x}As$ changes from a direct gap in InAs to an indirect gap (at X) in AlAs [70L2].				
energy gaps (in eV, relative to the top of the valence band):				
$E_g(\Gamma)$	$0.37 + 1.91\,x + 0.74\,x^2$	300 K	extrapolation from data below for $x \approx 0.48$ and data for InAs and AlAs	84W
$E_g(X)$	$1.8 + 0.4\,x$			70L2
crossover concentration:				
$x_c(\Gamma - X)$	0.68	300 K	$E_g(x_c) = 2.05$ eV	70L2
$Al_{0.48}In_{0.52}As$ For $x = 0.48$ $Al_xIn_{1-x}P$ is lattice matched to InP.				
$E_g(x = 0.477)$	1.450	300 K	(see Fig. 1)	84D,
	1.508	4 K		84W
Aluminum indium antimonide ($Al_xIn_{1-x}Sb$)				
The band gap changes from direct to indirect as in $Al_xIn_{1-x}P$ and $Al_xIn_{1-x}As$.				
Gallium indium phosphide ($Ga_xIn_{1-x}P$)				
This series of alloys comprises large gap semiconductors with a direct gap for x up to about 0.7 and an indirect gap (at X) at higher values of x. An intermediate range with the L-minima as lowest conduction bands seems to exist. Of most interest are alloys with x around 0.55 lattice matched to GaAs (see Fig. 1).				
energy gaps (in eV, relative to the top of the valence band): From a compilation of various literature data in [83B3] the bowing parameters (in eV) and crossover concentrations lie in the following ranges:				
$c(\Gamma)$	0.44 ··· 0.88			
$c(X)$	0.15 ··· 0.20			
$c(L)$	0.34 ··· 0.86			
$x_c(\Gamma - L)$	0.63 ··· 0.68			
$x_c(L - X)$	0.74 ··· 0.77			
Data for lattice matched layers: Values for the compositional parameter at lattice match lie in the range 0.51 to 0.56.				
$E_g(\Gamma)$	1.903	x = 0.56, RT VPE-layer	photoluminescence	85Z
	$1.295 + 1.151\,x$	$0.50 \leqq x \leqq 0.53$ MBE-layer	photoluminescence	81R
	$1.469 + 0.511\,x + 0.6043\,x^2$	$0.49 \leqq x \leqq 0.55$ VPE-layer		78O
	1.902	x = 0.515, OMVPE layer	photoluminescence	85K
Gallium indium arsenide ($Ga_xIn_{1-x}As$)				
Both components, InAs and GaAs, are direct gap semiconductors. Being a member of the quaternary system $Ga_xIn_{1-x}As_yP_{1-y}$ ($y = 1$), $Ga_xIn_{1-x}As$ is an important material for many applications in microelectronics. $Ga_{0.47}In_{0.53}As$ has the same lattice parameter as InP (see Fig. 1).				

Physical property	Numerical value	Experimental conditions	Experimental method, remarks	Ref.
energy gap (in eV):				
$E_g(\Gamma)$	$0.422 + 0.7\,x + 0.4\,x^2$	2 K	photoluminescence	83B1
	$0.324 + 0.7\,x + 0.4\,x^2$	300 K		

$Ga_{0.47}In_{0.53}As$

As a member of the InP lattice matched quaternary $Ga_xIn_{1-x}As_yP_{1-y}$ alloys, $Ga_{0.47}In_{0.53}As$ has been investigated very intensively.

energy gap (in eV):				
$E_g(\Gamma)$	0.813	2 K	photoluminescence	83G
	0.75	300 K		
temperature dependence of energy gap:				
$E_g(T)$	$0.814 - 4.906 \cdot 10^{-4}\,T^2/(T + 301)$		photoluminescence, T in K	84Y
energy difference between Γ and L conduction bands:				
$E(L_{6c}) - E(\Gamma_{6c})$	0.55(5) eV	300 K	photoemission	82C
effective mass, electrons:				
m_n	$0.041\,m_0$	0 K, extrapol.	cyclotron resonance	85S
effective masses, holes (in units of m_0):				
$m_{p,h}$	0.465	‖[001]		80A
	0.56	‖[110]		
	0.60	‖[111]		
$m_{p,l}$	0.0503			
phonon wavenumbers (in cm^{-1}):				
$\bar{\nu}$	226	TO	Raman active modes	83P
	270.5	LO		
	235	LO, InAs-type	magnetophonon resonance	85S
	271	LO, GaAs-type		
electron mobility (in cm^2/Vs): typical values from papers on characterization of layers:				
μ_n	13 800	300 K	$n = 2 \cdot 10^{15}\,cm^{-3}$, LPE-layer	81O
	70 000	77 K		
	11 200	300 K	$n \approx 10^{15}\,cm^{-3}$, MOCVD-layer	85C
	64 000	77 K		

Gallium indium antimonide ($Ga_xIn_{1-x}Sb$)

The properties of this system are in many respect similar to those of $Ga_xIn_{1-x}As$. Both components are direct gap semiconductors.

energy gap (in eV):				
$E_g(x, 0)$	$0.235 + 0.1653\,x + 0.413\,x^2$	0 K	photovoltaic effect	80R

Physical property	Numerical value	Experimental conditions	Experimental method, remarks	Ref.
temperature dependence: $E_g(x, T) = E_g(x, 0) + a_1 T^2 x/(b_1 + T) + a_2 T^2(1-x)/(b_2 + T) - x(1-x)c_T T$				
a_1	$-6.2(1)\cdot 10^{-4}$ eV K^{-1}			80R
a_2	$-3.8(1)\cdot 10^{-4}$ eV K^{-1}			
b_1	260(20) K			
b_2	200(20) K			
c_T	$-5(2)\cdot 10^{-5}$ eV K^{-1}			

References for 2.16.1

70L1 Lucovski, G., Chen, M.F.: Solid State Commun. **8** (1970) 1397.
70L2 Lorenz, M.R., Onton, A.: Proc. 10th Int. Conf. Semicond. Phys., Cambridge/Mass., USAEC, New York 1970, p. 444.
70O Onton, A., Chicotka, R.J.: J. Appl. Phys. **41** (1970) 4305.
78O Olsen, G.H., Nuese, C.J., Smith, R.T.: J. Appl. Phys. **49** (1978) 5523.
79K Kano, H., Miyazawa, S., Sugiyama, K.: Jpn. J. Appl. Phys. **18** (1979) 2183.
80A Alavi, K., Aggarwal, R.L., Groves, S.H.: Phys. Rev. **B21** (1980) 1311.
80R Roth, A.P., Keeler, W.J., Fortin, E.: Can. J. Phys. **58** (1980) 560.
81O Oliver, J.D.: J. Cryst. Growth **54** (1981) 64.
81R Roberts, J.S., Scott, G.B., Gowers, J.P.: J. Appl. Phys. **52** (1981) 4018.
81S Saxena, A.K.: Phys. Status Solidi (b) **105** (1981) 777.
83A Alibert, C., Joullié, A., Joullié, A.M., Ance, C.: Phys. Rev. **B27** (1983) 4946.
83B1 Biryulin, Yu.F., Ganina, N.V., Mil'vidskii, M.G., Chaldychev, V.V., Shmartsev, Yu.V.: Sov. Phys. Semicond. (English Transl.) **17** (1983) 68; Fiz. Tekh. Poluprovodn. **17** (1983) 108.
83B2 Biryulin, Yu.F., Vul', S.P., Chaldychev, V.V., Shmartsev, Yu.V.: Sov. Phys. Semicond. (English Transl.) **17** (1983) 65; Fiz. Tekh. Poluprovodn. **17** (1983) 103.
83B3 Bugajski, M., Kontkiewicz, A.M., Mariette, H.: Phys. Rev. **B28** (1983) 7105.
83G Goetz, K.-H., Bimberg, D., Jürgensen, H., Selders, J., Solomonov, A.V., Glinskii, G.F., Razhegi, M.: J. Appl. Phys. **54** (1983) 4543.
83P Pearsall, T.P., Carles, R., Portal, J.C.: Appl. Phys. Lett. **42** (1983) 436.
84D Davies, G.J., Kerr, T., Tuppen, C.G., Wakefield, B., Andrews, D.A.: J. Vac. Sci. Technol. **B2** (1984) 219.
84W Wakefield, B., Halliwell, M.A.G., Kerr, T., Andrews, D.A., Davies, G.J., Wood, D.R.: Appl. Phys. Lett. **44** (1984) 341.
84Y Yu, P.W., Kuphal, E.: Solid State Commun. **49** (1984) 907.
85A Adachi, S.: J. Appl. Phys. **58** (1985) R1.
85C Chan, K.T., Zhu, L.D., Ballantyne, J.M.: Appl. Phys. Lett. **47** (1985) 44.
85K Kuo, C.P., Vong, S.K., Cohen, R.M., Stringfellow, G.B.: J. Appl. Phys. **57** (1985) 5428.
85S Sarkar, C.K., Nicholas, R.J., Portal, J.C., Razhegi, M., Chevrier, J., Massies, J.: J. Phys. **C18** (1985) 2667.
85Z Zarrabi, H.J., Alfano, R.R.: Phys. Rev. **B32** (1985) 3947.

2.16.2 Ternary alloys of the type III–V_{1-x}–V_x

Aluminum arsenide phosphide ($AlAs_{1-x}P_x$)

The only interest in this system up to now has been an improvement of the lattice match of AlAs on GaAs by adding a small amount of phosphorus. $AlAs_{0.96}P_{0.04}$ layers made by MOCVD lattice-match exactly on GaAs at RT (Fig. 1) [84K].

Gallium arsenide phosphide ($GaAs_{1-x}P_x$)

Alloys of this type are of technological interest when properties of GaAs should be combined with a higher direct energy gap material. Above $x = 0.45$ $GaAs_{1-x}P_x$ changes to an indirect gap semiconductor.

energy gaps (in eV, relative to the top of valence band):

$E_{gx}(\Gamma)$	$1.515 + 1.172\,x + 0.186\,x^2$	2 K	excitonic gap from photoluminescence	81C
$E_{gx}(X)$	$1.9715 + 0.144\,x + 0.211\,x^2$			

Physical property	Numerical value	Experimental conditions	Experimental method, remarks	Ref.

Gallium arsenide antimonide ($GaAs_{1-x}Sb_x$)

Both components are direct gap semiconductors. The system has a miscibility gap with a peritectic temperature of 751 °C [84C] limiting the range of composition which can be obtained by near equilibrium growth techniques at ordinary temperatures.

energy gap (in eV):

E_g	$1.43 - 1.9x + 1.2x^2$	RT	photoluminescence	77N

effective mass, electrons (in units of m_0):

m_n	$0.0634 - 0.0483x + 0.0252x^2$		$x \leqq 0.6$, Faraday rotation, plasma resonance	81D

Indium arsenide phosphide ($InAs_{1-x}P_x$)

This system has received considerable attention since the energy gaps cover the infrared spectrum. Both components are direct gap semiconductors.

energy gap (in eV):

E_g	$0.356 + 0.675x + 0.32x^2$	300 K	transmission	79N
	$0.414 + 0.64x + 0.36x^2$	77 K		

electron mobility:
Electron mobilities in epitaxial layers up to $3 \cdot 10^5$ cm^2/Vs at 77 K for $x = 0.87$ have been reported [84W].

Indium antimonide arsenide ($InSb_{1-x}As_x$)

Only a few papers on this system have been published.

Indium antimonide bismuthide ($InSb_{1-x}Bi_x$)

Since InBi is semimetallic with a tetragonal structure only a limited range of solid solutions show semiconducting behavior ($x < 0.03$). Metastable films have been investigated

References for 2.16.2

77N Nahory, R.L., Pollack, M.A., DeWinter, J.C., Williams, K.M.: J. Appl. Phys. **48** (1977) 513.
79N Nicholas, R.J., Stradling, R.A., Ramage, J.C.: J. Phys. **C12** (1979) 1641.
81C Capizzi, M., Modesti, S., Martelli, F., Frova, A.: Solid State Commun. **39** (1981) 333.
81D Devlin, P., Heravi, H.M., Woolley, J.C.: Can. J. Phys. **59** (1981) 939.
84K Kobayashi, N., Fukui, T.: J. Cryst. Growth **67** (1984) 513.
84C Cherng, M.J., Stringfellow, G.B., Cohen, R.M.: Appl. Phys. Lett. **44** (1984) 677.
84W Wang, P.J., Wessels, B.W.: Appl. Phys. Lett. **44** (1984) 766.

2.16.3 Quaternary alloys of the type III_x–III_{1-x}–V_y–V_{1-y}

Quaternary alloys provide the possibility to grow epitaxial layers with a broad range of energy gaps lattice matched to a suitable substrate.

The condition for lattice matching can easily be derived from the interpolation scheme for the determination of a material parameter $P(x, y)$ for an alloy $A_xB_{1-x}C_yD_{1-y}$ from the same parameters of the four constituents:

$$P(x, y) = (1 - x)yP(BC) + (1 - x)(1 - y)P(BD) + xyP(AC) + x(1 - y)P(AD).$$

Physical property	Numerical value	Experimental conditions	Experimental method, remarks	Ref.

For lattice matching on substrate BD (x = y = 0) the condition $a(x, y) = a(BD)$ leads to

$$x = \frac{[a(BC) - a(BD)]y}{[a(BD) - a(AD)] - [a(BC) + a(AD) - a(BD) - a(AC)]y}$$

or, in a linear approximation to this formula – exact at y = 0 and y = 1:

$$x/y = [a(BC) - a(BD)]/[a(BC) - a(AC)].$$

The main interest in quaternary III–V alloys stems from the possible applications in micro- and optoelectronic devices. Thus most of the data in the following sections refer to quaternary alloys lattice matched to GaSb, InP and GaAs (see Fig. 1 in section 2.16.1).

Several types of quaternary alloys are possible:

(a) III-III-V-V alloys. These materials will be discussed in the following subsections.

(b) III-III-III-V alloys. Several systems will be presented in section 2.16.4.

(c) III-V-V-V alloys. Here only one system seems to be of interest for applications: $InAs_{1-x-y}Sb_xP_y$.

Not much has been done in the field of *quintarnary alloys*. An example for such material is $(Al_xGa_{1-x})_{1-z}In_zP_yAs_{1-y}$ on GaAs [84M].

Gallium indium arsenide phosphide ($Ga_xIn_{1-x}As_yP_{1-y}$)

As shown in Fig. 1 of section 2.16.1 alloys of this system can be lattice matched on InP (E_g range: 0.73 ··· 1.35 eV), GaAs (E_g range: 1.42 ··· 1.90 eV) and ZnSe (slightly lower range). The matching conditions according to the formula above are ($0 \leqq y \leqq 1$):

x	0.1894 y/ (0.4184 − 0.013 y)	on InP substrate
	≈0.47 y	
	(1.00 + y)/2.08	on GaAs substrate
	(1.06 + y)/2.06	on ZnSe substrate

Most data have been obtained for InP lattice matched samples. All data in the following tables refer – if not stated otherwise – to InP lattice matched material.

direct energy gap (in eV):

$E_{g,dir}(x, y)$	$1.35 + 0.668\,x - 1.068\,y + 0.758\,x^2 + 0.078\,y^2 - 0.069\,xy - 0.322\,x^2y + 0.03\,xy^2$			84K1

from literature data for the constituents and interpolation formulas; for lattice match to InP this formula reduces to

$E_{g,dir}(y)$	$1.35 - 0.775\,y + 0.149\,y^2$	298 K	calculated, fitting photo-luminescence and electro-reflectance measurements,	82P
	$1.425 - 0.7668\,y + 0.149\,y^2$	4.2 K	calculated, fitting absorption and transmission measurements.	

bowing parameters for band gaps at L and X (in eV):

$c(\Gamma - L)$	0.10(5)	L-conduction band	84K2
$c(\Gamma - X)$	0.21(7)	X-conduction band from synchrotron radiation reflection spectroscopy	

higher interband transition energies (in eV):

E_1	$3.11 + 0.034\,x - 0.885\,y + 0.516\,x^2 + 0.275\,y^2 - 0.187\,xy + 0.017\,x^2y$			80L

Physical property	Numerical value	Experimental conditions	Experimental method, remarks	Ref.
at RT, from fitting of literature data: for InP lattice matched material this formula reduces to				
$E_1(y)$	$3.11 - 0.87\,y + 0.30\,y^2 + 0.007\,y^3$	RT		80L
spin-orbit splitting energies (in eV):				
$\Delta_0(y)$	$0.119 + 0.300\,y - 0.107\,y^2$	RT	electroreflectance,	80P
$\Delta_1(y)$	$0.145 + 0.173\,y - 0.064\,y^2$			80P
effective masses (in units of m_0):				
$m_n(x, y)$	$0.08 - 0.116\,x + 0.026\,y - 0.059\,xy + (0.064 - 0.02\,x)y^2 + (0.06 + 0.032\,y)x^2$			80R
interpolation formula; a relation for InP lattice matched material is				
$m_n(y)$	$0.077 - 0.050\,y + 0.014\,y^2$	RT	Shubnikov – de Haas effect	80P
lattice parameter (in Å):				
$a(x, y)$	$5.8688 - 0.4176x + 0.1896y + 0.0125y$		linear interpolation from lattice parameters of four constituents	82A1
density (in g cm^{-3}):				
d	$5.477 - 0.712y$			82A1
dielectric constant:				
$\varepsilon(0)$	$12.40 + 1.5y$			82A2
$\varepsilon(\infty)$	$9.55 + 2.2y$			

Gallium indium arsenide antimonide ($Ga_xIn_{1-x}As_ySb_{1-y}$)

This system is shown as shaded area in Fig. 1 of section 2.16.1. It is the only system applicable for the growth of low band gap epitaxial layers of GaSb substrate. In spite of interesting applications for optical sources and detectors in the 2···4 μm range only few reliable data on intrinsic properties have been published.

Aluminum gallium arsenide antimonide ($Al_xGa_{1-x}As_ySb_{1-y}$)

This system shows a broad miscibility gap. Epitaxial layer growth is possible
- *on GaSb* for small amounts of As; by adding small amounts of As the lattice matching of $Al_xGa_{1-x}Sb$ on GaSb can be improved (see Fig. 1 of section 2.16.1)
- *on GaAs* for small amounts of Sb; layers with y greater than 0.8 have been produced.

References for 2.16.3

80L Laufer, P.M., Pollack, M.A., Nahory, R.E.: Solid State Commun. **36** (1980) 419.
80P Perea, E.H., Mendez, E.E., Fonstad, C.G.: Appl. Phys. Lett. **36** (1980) 978.
80R Restorff, J.B., Houston, B., Allgaier, R.S.: J. Appl. Phys. **51** (1980) 2277.
82A1 Adachi, S.: J. Appl. Phys. **53** (1982} 8775.
82A2 Adachi, S.: J. Appl. Phys. **53** (1982) 5863.
82P Pearsall, T.P.: "GaInAsP Alloy Semiconductors", T.P. Pearsall ed., J. Wiley & Sons, New York **1982**, p. 295.
84K1 Kuphal, E.: J. Cryst. Growth **67** (1984) 441.
84K2 Kelso, S.M., Aspnes, D.E., Olson, C.G., Lynch, D.W., Bachmann, K.J.: Proc. SPIE Int. Soc. Opt. Eng. **452** (1984) 200.
84M Mukai, S., Yajima, H., Mitsuhashi, Y., Yanagisawa, S., Kutsuwada, N.: Appl. Phys. Lett. **44** (1984) 904.

Physical property	Numerical value	Experimental conditions	Experimental method, remarks	Ref.

2.16.4 Quaternary alloys of the type III_{1-x-y}–III_x–III_y–V

Indium aluminum gallium phosphide ($In_{1-x-y}Al_xGa_yP$)

The boundary alloys of the GaAs lattice matched series are $In_{0.49}Ga_{0.51}P$ and $In_{0.49}Al_{0.51}P$ (see Fig. 1 of section 2.16.1). Introducing the compositional parameter z by $x = 0.51\,z$ and the lattice matching condition $x + y = 0.51$ the series can be written as

$$In_{0.49}(Al_zGa_{1-z})_{0.51}P.$$

energy gap (in eV):

E_g	$1.9 + 0.6z$	RT		82A

electron effective mass (in units of m_0):

m_n	$0.0427(15) + 0.0328(7)z$			82O1, 82O2

Indium aluminum gallium arsenide ($In_{1-x-y}Al_xGa_yAs$)

The boundary alloys of the InP lattice matched series are $In_{0.53}Ga_{0.47}As$ and $In_{0.52}Al_{0.48}As$ (see Fig. 1 of section 2.16.1). Introducing the compositional parameter z by $x = 0.48\,z$ and the lattice matching condition $0.98x + y = 0.47$ the series can be written as

$$(In_{0.52}Al_{0.48})_z(In_{0.53}Ga_{0.47})_{1-z}As.$$

An often used approximation is

$$In_{0.53}(Al_zGa_{1-z})_{0.47}As \quad \text{with } x = 0.47z, \quad x + y = 0.47$$

energy gap (in eV):

$E_g(x, y)$	$0.36 + 2.093x + 0.629y + 0.577x^2 + 0.436y^2 + 1.013xy - 2.0xy(1 - x - y)$			82O1

For the lattice matching condition (given in [82O1] more exactly as $0.983x + y = 0.468$) using $z = x/0.48$ the experimental data obtained from photoluminescence at RT give:

$E_g(z)$	$0.76(4) + 0.49(5)z + 0.20(3)z^2$			82O1, 82O2

Indium aluminum gallium antimonide ($In_{1-x-y}Al_xGa_ySb$)

For material prepared by directional freezing and investigated by X-ray and optical methods the following relations have been obtained ($z = 1 - x - y$):

a[nm]	$0.64789 - 0.03433x - 0.03834y - xyz(0.025 + 0.325z)$			81Z
$E_{g,dir}$	$0.095 + 1.76x + 0.28y + 0.345(x^2 + y^2) + 0.085z^2 + xyz(23 - 28y)$			
$E_{g,ind}$	$1.0675 + 0.30x - 0.31y + 0.2625(x^2 + y^2 + z^2) + xyz(20x - 5.9)$			

References for 2.16.4

81Z Zbitnew, K., Woolley, J.C.: J. Appl. Phys. **52** (1981) 6611.
82A Asahi, H., Kawamura, Y., Nagai, H.: J. Appl. Phys. **53** (1982) 4928.
82O1 Olego, D., Chang, T.Y., Silberg, E., Caridi, E.A., Pinczuk, A.: Int. Phys. Conf. Ser. No. 65, Int. Symp. GaAs and Related Compounds, Albuquerque **1982**, p. 195.
82O2 Olego, D., Chang, T.Y., Silberg, E., Caridi, E.A., Pinczuk, A.: Appl. Phys. Lett. **41** (1982) 476.

Substance	Structure	Static and dynamical lattice parameters			Band structure parameters				Transport parameters	
		a [Å]	d [g cm^{-3}]	$\varepsilon(0)$, $\varepsilon(\infty)$	E_g [eV]	at T [K]	m [m_0]		μ [cm^2/Vs]	
		α	T_m [K]						σ [Ω^{-1}cm^{-1}]	
Boron	α-rhombohedral phase R $\bar{3}$m (12 atoms in unit cell)	a: 5.057	d: 2.45		$E_{g,ind\parallel}$: 1.97	300			μ:	120
		α: 58.06°	··· 2.46		$E_{g,ind\perp}$: 1.9	300			σ:	10^{-3}
			α-B transforms into β-B with increasing T via a series of intermediary phases		$E_{g,th}$: 2.0					··· $3\cdot10^{-2}$
	β-rhombohedral phase R $\bar{3}$m (105 atoms in unit cell)	a: 10.145	d: 2.326	$\varepsilon(0)_\parallel$: 10.24	$E_{g,ind\parallel}$: 1.635	300	m_n:	≅ 4.5	μ:	10^{-5}
		α: 65°17'	T_m: 2347	$\varepsilon(0)_\perp$: 11.55	$E_{g,ind\perp}$: 1.615	300	m_p:	≅ 1.8		··· $3\cdot10^{2}$
			··· 2392	$\varepsilon(\infty)_\parallel$: 8.41	$E_{g,th}$: 1.36				σ:	10^{-7}
				$\varepsilon(\infty)_\perp$: 9.12						··· 10^{-6}

3 Elements

3.1 Group III elements

Among the group III elements only the rhombohedral phases of boron show semiconducting properties. The main structure elements of its lattice are B_{12} icosahedra (Fig. 1, p. 247). Structure of rhombohedral phases: Figs. 2, 3 (p. 247); Brillouin zone: Fig. 4 (p. 247); band structure of α-boron: Fig. 5 (p. 248).

3.2 Group IV elements

See chapter 1.

Substance	Structure	Static and dynamical lattice parameters			Band structure parameters			Transport parameters	
		a, b, c [Å]	d [g cm^{-3}]	$\varepsilon(0), \varepsilon(\infty)$	E_g [eV]	at T [K]	m [m_0]	μ [cm^2/Vs]	
		α	T_m [K]	ν [THz]				σ [Ω^{-1}cm^{-1}]	

3.3 Group V elements

From the three modifications of phosphorus (white, black and red) the orthorhombic black phosphorus and the monoclinic red phosphorus shows semiconducting properties. Lattice structure of black P: Fig. 6 (p. 248); Brillouin zone and band structure: Figs. 7, 8 (p. 248).

Phosphorus	black phosphorus,	a :	3.3133	d :	2.70	ε :	6.1	$E_{g,th}$:	0.33	m_n : 0.34	μ_n : 220
	orthorhombic phase	b :	4.374	T_m :	1300				··· 0.35	m_p : 0.26	μ_p : 350
	D^{18}_{2h} - Bmab	c :	10.473							average values	σ : 0.7
	red phosphorus,			d:	2.34			$E_{g,th}$:	1.45		
	monoclinic phase			T_m :	590				··· 1.55		

The group V elements arsenic, antimony and bismuth crystallize at standard conditions in a rhombohedral structure. They are semimetals. Lattice structure of As, Sb and Bi: Fig. 9 (p. 259); Brillouin zone and band structures: Figs. 10 ··· 13 (p. 249,250).

Arsenic	rhombohedral	a :	4.1320	d :	5.720	ε_{33} :	50	$E_{g,ind}$:	- 0.54		complicated	μ_{n1} : 460
	D_{3d} - R $\bar{3}$m	α :	54.126°	T_m :	1090				··· - 0.36		effective mass	μ_{n2} : 40
								$E_{g,dir}$:	0.175		tensor	μ_{n3} : 550
												μ_{p1} : 1210
												μ_{p2} : 50
												μ_{p3} : 680
Antimony	rhombohedral	a :	4.5067	d :	6.69	ε :	80	$E_{g,ind}$:	- 0.160	300	complicated	μ_{n1} : 2.74
	D_{3d} - R $\bar{3}$m	α :	57.110°	T_m :	903		at 4.2K		- 0.204	4.5	effective mass	μ_{n2} : 0.11
						$\nu_{R,LO}$:	4.64	$E_{g,dir}$:	0.101	1.15	tensor	μ_{n3} : 1.95
						$\nu_{R,TO}$:	3.48					μ_{p1} : 3.63
												μ_{p2} : 0.18
												μ_{p3} : 3.22

Substance	Structure	Static and dynamical lattice parameters			Band structure parameters				Transport parameters
		a, b, c [Å]	d [g cm^{-3}]	$\varepsilon(0), \varepsilon(\infty)$	E_g [eV]	at T [K]	m [m_0]		μ [cm^2/Vs]
		α	T_m, T_{tr}[K]	ν [THz]					
Bismuth	rhombohedral	a : 4.7458	d : 9.8	ε_{xx} : 105	$E_{g,ind}$:	- 0.038	0	complicated	μ_{n1} : 35000
	D_{3d} - R $\bar{3}$m	α : 57.23°	T_m : 544.5	ε_{yy} : 105	$E_{g,dir}$:	0.0136	0	effective mass	μ_{n2} : 600
				ε_{zz} : 84				tensor	μ_{n3} : 14000
				ν_{TO} : 2.22					μ_{p1} : 5800
				ν_{LO} : 3.00					μ_{p2} : 5800
									μ_{p3} : 4500

3.4 Group VI elements

Nearly 50 allotropes of sulfur are known, based on differently bound molecular subunits with relatively weak intermolecular bonds. The most stable form under ambient conditions is the orthorhombic α-phase, consisting of crown like shaped S_8 molecules (Figs. 14, 15, p. 251).

Sulfur	orthorhombic	a : 10.46	d : 2.066	$\varepsilon(0)_{\parallel a}$: 3.65	$E_{g\parallel a}$:	3.8	300	$\mu_{n,dr}$:	1 ··· 4.5
	phase (α-S)	b : 12.88	·· 2.086	$\varepsilon(0)_{\parallel b}$: 3.85	$E_{g\parallel b}$:	4.1		$\mu_{p,dr}$:	1 ··· 10
	D^{24}_{2h} - Fddd	c : 24.48	T_{tr} : 368	$\varepsilon(0)_{\parallel c}$: 4.66	$E_{g\parallel c}$:	4.2			
			to β-phase	ν_R: 14.25					

Selenium crystallizes in at least five allotropes of trigonal, monoclinic and rhombohedral structure. The only modification stable under ambient conditions is the semiconducting trigonal phase. In this structure the atoms are arranged in right-handed (D^4_3) or left-handed (D^6_3) chains along the c-axis, a being the chain distance, c the period length and $r = ua$ the chain radius. Monoclinic and amorphous selenium are semicondutors, too. Monoclinic selenium occurs in three phases (α, β, γ). In these phases the atoms are arranged in puckered Se_8 rings. Almost all published data refer to a-monoclinic Se.

Lattice structure of the trigonal phase: Fig. 16 (p. 251); Brillouin zone and band structure: Figs. 17, 18 (p. 251). The direct energy gap is situated at the point H in the Brillouin zone. The top of the valence band is split into three levels (1, 2, 3, see data below). An indirect lower gap stems from R - H transitions.

Substance	Structure	Static and dynamical lattice parameters			Band structure parameters				Transport parameters
		a, b, c [Å]	d [g cm^{-3}]	$\varepsilon(0), \varepsilon(\infty)$	E_g [eV]	at T [K]		m [m_o]	μ [cm^2/Vs]
		u, β	T_m [K]						σ [Ω^{-1}cm^{-1}]
									n_i [cm^{-3}]
Selenium	trigonal phase	a : 4.36	d : 4.819	$\varepsilon(0)_{\parallel}$: 12.24	$E_{g,ind}$:	1.8525	1.4	$m_{p,ds}$: 1.4	$\mu_{p,H}$: 0.12
	$D^4_3(D^6_3)$ - $P3_121$	c : 4.95	T_m : 494.33	$\varepsilon(0)_{\perp}$: 7.43	$E_{g,dir}$ (1):	1.95	300	$m_{p\perp}/m_{p\parallel}$: 3.5	$\mu_{p\perp c}$: 26 ··· 260
		u : 0.225		$\varepsilon(\infty)_{\parallel}$: 11.62	$E_{g,dir}$ (2):	1.98	300		
				$\varepsilon(\infty)_{\perp}$: 6.97	$E_{g,dir}$ (3):	2.11	300		
	monoclinic phase	a : 9.05	d : 4.389	$\varepsilon(0)$: 7.39	$E_{g,opt}$:	2.48	5		$\mu_{n,dr}$: 1.5 ··· 3.6
	C^5_{2h} - $P2_1/n$	b : 9.08		$\varepsilon(\infty)$: 6.1		2.25			$\mu_{p,dr}$: 0.2 ··· 1.3
		c : 11.60				··· 2.53	300		
		β : 90.8°							

Tellurium crystallizes in the same trigonal structure as selenium.

Lattice structure: Fig. 16 (p. 251); Brillouin zone: Fig. 17 (p. 251); band structure: Fig. 19 (p. 252). The energy gap is direct (point H in the Brillouin zone). The top of the valence band is split as in selenium, but of more complicated structure.

Tellurium	trigonal	c : 5.95	d : 6.25	$\varepsilon(0)_{11}$: 30	$E_{g,opt}$:	0.335	300	$m_{n\parallel}$: 0.050	$\mu_{n\parallel c}$: 2380
	$D^4_3(D^6_3)$ - $P3_121$	u : 0.268	T_m : 723	$\varepsilon(0)_{33}$: 43	$E_{g,th}$:	0.333		$m_{n\perp}$: 0.060	$\mu_{n\perp}$: 1150
				$\varepsilon(\infty)_{11}$: 23				$m_{p\parallel}$: 0.109	$\mu_{p\parallel c}$: 1260
				$\varepsilon(\infty)_{33}$: 36				$m_{p\perp}$: 0.114	$\mu_{p\perp c}$: 650
									$\sigma_{i,11}$: 1.56
									$\sigma_{i,33}$: 3.04
									n_i : $5.6 \cdot 10^{15}$

Substance	Structure	Static and dynamical lattice parameters		Band structure parameters		Transport parameters
		a, b, c [Å]	d [g cm^{-3}]	E [eV]	at T [K]	μ [cm^2/Vs]
		β	T_m [K]			E_A [eV]

4 Binary compounds

4.1 IA-IB compounds

Among the alkali-noble metals Cu, Ag, Au intermetallic alloys several stable compounds with stoichiometric composition 1 : 1 have been observed. For cesium auride (CsAu) strong experimental evidence for semiconducting behavior exists, whereas for rubidium auride (RbAu) the experimental situation is less clear. Crystal structure: Fig. 20 (p. 252); Brillouin zone and band structures of CsAu and RbAu: Figs. 21 ··· 23 (p. 252).

CsAu	CsCl structure	a : 4.263	d : 7.065	E_g :	2.6	300	$\mu_{n,H}$:	$\cong 35$
	O^1_h - Pm3m		T_m : 863	$E_{g,dir}$:	$\cong 3$	calc.	$\mu_{p,H}$:	210
RbAu	CsCl structure	a : 4.105	T_m : 771	$E_{g,dir}$:	$\cong 3$	calc.		
	O^1_h - Pm3m							

4.2 I_x-V_y compounds

4.2.1 I-V compounds

The alkali-antimonide and -bismuthide compounds are of some technological interest due to the high photoelectric quantum efficiency in the visible region. NaSb and KSb crystallize in the monoclinic LiAs structure (Fig. 24, p. 253), CsSb in a orthorhombic structure (Fig. 25, p. 253).

NaSb	monoclinic	a : 6.80	T_m : 738	E_A :	0.82
	LiAs-structure	b : 6.34		from σ measured on	
	C^5_{2h} - $P2_1/c$	c : 12.48		evaporated films	
		β : 117.6°			

Substance	Structure	Static and dynamical lattice parameters a, b, c [Å] T_m, T_{tr} [K] β	Band structure parameters E_g [eV]	Transport parameters E_A [eV]
KSb	monoclinic LiAs-structure C^5_{2h} - $P2_1/c$	a : 7.18 T_m : 883 b : 6.97 c : 13.40 β : 115.1°		E_A : 0.88 from σ measured on evaporated films
CsSb	orthorhombic NaP structure D^4_2 - $P2_12_12_1$	a : 7.575 T_m : 859 b : 7.345 c : 13.273	$E_{g,opt}$: > 2	E_A : 0.61 ··· 0.63 from σ measured on evaporated films

4.2.2 I_3-V compounds

The I_3-V compounds crystallize in hexagonal and cubic phases (Figs. 26, 27, p. 253); Figs. 28 and 29 (p. 254) show the band structures of K_3Sb and Rb_3Sb.

Li_3Sb	hexagonal phase D^4_{6h} - $P6_3/mmc$	a : 4.710 T_m : 1420 c : 8.326 ··· 1570	E : 3.9 (photoemissive yield)	E_A : ≅ 1.0 in evaporated films
	cubic phase O^5_h - Fm3m	a : 6.572 T_{tr} : 923 to α-phase		
Li_3Bi	cubic O^5_h - Fm3m	a : 6.721 T_m : 1418	E : 3.6 (photoemissive yield)	E_A : 0.7 in evaporated films
Na_3Sb	hexagonal D^4_{6h} - $P6_3/mmc$	a : 5.335 T_m : 1132 c : 9.496	$E_{g,opt}$: 1.0	n-type conduction
K_3Sb	hexagonal phase D^4_{6h} - $P6_3/mmc$	a : 6.024 T_m : 1085 c : 10.693	$E_{g,opt}$: 1.1 ··· 1.3	E_A : 0.75 ··· 0.79

Substance	Structure	Static and dynamical lattice parameters a, c [Å]	T_m [K]	Band structure parameters E_g [eV]	Transport parameters μ [cm²/Vs] E_A [eV]
K_3Sb (cont.)	cubic phase O^5_h - Fm3m	a : 8.493		$E_{g,opt}$: 1.4	
Rb_3Sb	hexagonal phase D^4_{6h} - $P6_3/mmc$ cubic phase O^5_h - Fm3m	a : 6.29 c : 11.17 a : 8.84	T_m : 1006	$E_{g,opt}$: 1.0	E_A : ≅ 0.4 in thin films n- and p-conduction observed
Cs_3Sb	cubic O^7_h - Fd3m	a : 9.128	T_m : 998	$E_{g,opt}$: 1.6	μ_p : ≅ 10 E_A : 1.2
Cs_3Bi	cubic O^5_h - Fm3m	a : 9.31	T_m : 908	$E_{g,opt}$: ≤ 0.7	E_A : 0.04 ··· 0.4
Rb_3Bi	hexagonal phase D^4_{6h} - $P6_3/mmc$	a: 6.42 c: 11.46	T_m : 915	$E_{g,opt}$: ≤ 0.7	E_A: 0.04 ··· 0.4

4.2.3 I_2-I-V compounds

Several bialkali-antimonides are related to the alkali antimonides listed above. Fig. 30 (p. 254) shows the band structure of Na_2KSb.

Na_2KSb	BiF_3-structure	a : 7.74		$E_{g,opt}$: 1.0 ··· 1.1	$\mu_{p,H}$: 2.6 ··· 4.8
K_2CsSb	BiF_3-structure	a : 8.61		$E_{g,opt}$: 1.0 ··· 1.1	p-type conduction observed

For Na_2RbSb, Na_2CsSb, K_2RbSb and Rb_2CsSb energy gaps of 1.0, 0.8, 1.2 and 1.5 eV have been reported, respectively.

Substance	Structure	Static and dynamical lattice parameters			Band structure parameters			Transport parameters
		a, b, c [Å]	d [g cm^{-3}]	$\varepsilon(0), \varepsilon(\infty)$	E_g [eV]	at T [K]	m [m_o]	ρ [W cm]
		β	T_m [K]	ν [THz]				E_A [eV]
			c_{ik} [10^{11}dyn cm^{-2}]					

4.3 I_x-VI_y compounds

Stoichiometric cupric oxide (CuO) is difficult to prepare. Most data are obtained at thin films, oxidized at low temperature.

CuO	monoclinic	a :	4.652	d :	6.569	optical energy gap				E_A :	0.14
	C^6_{2h} - C2/c	b :	3.410			uncertain, as there is					0.3
		c :	5.108			no transparency gap in				ρ :	10^3 ··· 10^{-1}
		β :	99°29'			the visible and near					thin films
						infrared					

Cuprous oxide (Cu_2O) is one of the first known semiconductors. Its structure is responsible for its peculiar excitonic structure. It is metastable at room temperature. Fig. 31 (p. 255) shows the cuprite structure of Cu_2O, Fig. 32 (p. 255) its band structure.

Cu_2O	cubic	a :	4.2696	d :	5.746	$\varepsilon(0)$:	7.11	$E_{g,dir}$:	2.17	4.2	polaron masses :	ρ :	35
	T^2_h - Pn3 or				··· 6.14	$\varepsilon(\infty)$:	6.46		2.304		$m_{n,cr}$: 0.99	undoped sample	
	O^4_h - Pn3m			T_m :	1508	ν_R :	3.00		2.624		$m_{p,cr}$: 0.58	conductivity	
				c_{11} :	12.61		··· 3.30		2.755		band masses :	determined	
				c_{12} :	10.86	ν_{TO} :	4.39	limits of yellow, green,			m_n : 0.93	by deep levels	
				c_{44} :	1.36	ν_{LO} :	4.48	blue and violet excitonic			m_p : 0.56		
								series, respectively					

Copper sulfide (Cu_2S) is difficultly to prepare stoichiometrically. Cu_xS compounds with varying structure and properties can be prepared, x covering the range from 1.75 to 2.00.

Substance	Structure	Static and dynamical lattice parameters a, b, c [Å]	d [g cm^{-3}] T_m [K]	$\varepsilon(\infty)$	Band structure parameters E_g [eV]	at T [K]	m [m_0]	Transport parameters μ [cm^2/Vs], E_A [eV] ρ [Ωm] p [cm^{-3}]
Cu_xS	phases stable at room temperature :							
	x = 2 : chalcocite	a : 3.961	d : 5.8		$E_{g,ind}$: 1.05	300	m_p : 1.65	ρ : 0.06
	hexagonal	c : 6.722	T_m : 1373		··· 1.21		··· 1.82	··· 0.04
	D^4_{6h} - $P6_3/mmc$	at 425 K	depending		$E_{g,dir}$: 1.7	300		μ_p : 3.02
	(4 molecules in		strongly on					··· 4.75
	unit cell)		stoichiometry					p : $3.5 \cdot 10^{19}$
								··· $0.33 \cdot 10^{19}$
	x = 1.935 ··· 1.955	a : 29.92						
	djurleite	b : 15.71	d : 5.63		$E_{g,dir}$: 1.3		m_p : 1.65	
	orthorhombic	c : 13.56	··· 5.747				··· 1.82	
	(128 molecules in unit cell)							
	x = 1.765 ··· 1.79	a : 27.71	d : 5.6				m_p : 1.8	
	O^7_h-I4/mm	superstructure						

Copper selenide (Cu_2Se) also occurs in various compositions ranging from $Cu_{1.25}Se$ (Cu_5Se_4, athabascaite) to $Cu_{1.5}Se$ (Cu_3Se_2, umagite), $Cu_{1.9}Se$ (berzelianite) and Cu_2Se (crookesite).

Cu_xSe	x = 2, tetragonal	a : 10.40	d : 6.6 ··· 7.1	$\varepsilon(\infty)$: 11.0	E_g : 1.0 ··· 1.1	m_p :	≅ 0.5	ρ :	≅ 10^{-3}
	D^{17}_{4h} - I4/mm	c : 3.93	for x =	··· 11.6				p :	$1.9 \cdot 10^{20}$
			1.25 ··· 2.0					$\mu_{p,H}$:	20
									at 500 K
Cu_xTe	several structures		d : ≅ 7.4		$E_{g,opt}$: 0.50		m_p : 0.5	E_A:	0.24
	for x = 1.25 ··· 2.00						··· 0.85		

Substance	Structure	Static and dynamical lattice parameters			Band structure parameters				Transport parameters	
		a, b, c [Å]	d [g cm^{-3}]	ν [THz]	E_g [eV]	at T [K]	m [m_0]		μ [cm^2/Vs]	
		β	T_m [K]						ρ [Ωm]	
									n_i [cm^{-3}]	
									E_A [eV]	
Several oxides of silver are known (Ag_xO with x = 7/11, 2/3, 1, 4/3, 2). All compounds are metastable at RT and normal presure.										
Ag_2O	cubic cuprite	a : 4.72	d : 6.9	ν_{ir} : 2.55	$E_{g,dir}$:	1.571	4	m_n : 0.7	E_A :	0.75
	T^2_h - Pn3		T_m : 1088			1.2	293	m_p : 1.9	ρ :	10^8
Ag_2S is polymorphic. It occurs as the natural minerals acanthite (α-Ag_2S) and argenite (β-Ag_2S).										
Ag_2S	α-phase	a : 4.23	d : 7.234	ν_{ir} : 2.1,	$E_{g,ind}$:	0.85	300	m_n : 4.65	n_i :	$1.1 \cdot 10^{16}$
	monoclinic	b : 6.91	T_m : 1098	2.7 ...	$E_{g,dir}$:	1.0	300	m_p : 7.59	μ_n :	62.5
	C^5_{2h} - $P2_1/n$	c : 7.87		at 4.2K					μ_p :	18.4
		β : 99°35'								at 400 K
	β-phase	a : 4.88			E_g :	0.3		m_n : 0.23	n_i :	$4 \cdot 10^{19}$
	bbc sulfur sublattice							m_p : 0.23	μ_n :	160
	stable for T > 450 K									at 500K
Ag_2Se exists in two phases (α, β), the physical properties of both being very similar.										
Ag_2Se	α-phase: structure		d : 8.25		$E_{g,opt}$:	0.15	293	m_n : 0.20	n_i :	$3.2 \cdot 10^{19}$
	contradictory,		T_m : 1153		$E_{g,th}$:	0.046		··· 0.32	μ_n :	1990
	β-phase:	a : 4.99	··· 1170			··· 0.12		m_p : 0.54	μ_p :	523
	O^9_h - Im3m					at 349 K				at 349 K

Substance	Structure	Static and dynamical lattice parameters a, b, c [Å] d [g cm^{-3}] β T_m [K]	Band structure parameters E_g [eV] at T [K]	m [m_o]	Transport parameters μ [cm^2/Vs] E_A [eV]
In Ag_2Te three phases (α, β, γ) exist at room temperature.					
Ag_2Te	α-phase: monoclinic (rhombic ?) C^5_{2h} - $P2_1/c$	a : 6.593 d : 8.08 b : 6.2 ··· 8.41 c : 6.455 T_m: 1228 β : 88°30'	$E_{g,opt}$: ≅ 0.67	m_n : 0.026 ··· 0.034	E_A : 0.13 μ_n : 1000
	β-phase: fcc Te lattice, γ-phase: bcc Te lattice both with statistically distributed Ag ions	a : 6.58 a : 5.29	$E_{g,th}$: 0.20 500 ··· 650	m_n : 0.077 m_p : 1.5 at 438 K	μ_n : 1440 μ_p : 18 at 438 K

4.4 I-VII compounds

The I-VII compounds belong to the tetrahedrally coordinated isoelectronic series IV → III-V → II-VI → I-VII. Most of these compounds crystallize at normal conditions in the zincblende lattice (γ-phase) or wurtzite lattice (β-phase). Only in the large gap material AgF, AgCl and AgBr and in high-temperature phases of the other compounds the lattice turns to a cubic a-phase (NaCl lattice).
Figs. 33 ··· 37 (p. 256) show the lattice structures and Brillouin zones of the zincblende, wurtzite and NaCl lattices.

γ-CuF	zincblende T^2_d - F $\bar{4}$3m	chemical instable, no reliable data available.

All copper halides are direct gap semiconductors, the conduction band minimum and the two spin-orbit split valence band maxima being situated at the point Γ of the Brillouin zone. Figs. 38 (p. 257) and 39 (p. 258) show the band structures of CuCl, CuBr and CuI.

Substance	Structure	Static and dynamical lattice parameters				Band structure parameters			
		a [Å]	d [g cm^{-3}]	$\varepsilon(0)$, $\varepsilon(\infty)$		E_g, Δ [eV]	at T [K]		m [m_o]
			T_m [K]	ν [THz]					
			c_{ik} [10^{11}dyn cm^{-2}]						
γ-CuCl	zincblende	a : 5.4057	d :	4.136	$\varepsilon(0)$: 7.9	$E_{g,dir}$:	3.395	4.2	m_n : 0.415
	T^2_d - F $\bar{4}$3m		T_m :	695	$\varepsilon(\infty)$: 3.61		3.17	300	m_p : ≅ 20
			c_{11} :	4.70	ν_{TO} : 4.86	Δ_{so} :	0.0934	4.2	m^L_{ex} : 2.5
			c_{12} :	3.62	ν_{LO} : 6.06	E^L_{gx1} :	3.2080	4.2	m^T_{ex} : 2.5
			c^E_{44} :	1.45		E^T_{gx1} :	3.2025	4.2	all at 4.2 K
			c^D_{44} :	1.60		E^L_{gx2} :	3.290	1.9	
						E^T_{gx2} :	3.269	1.9	
γ-CuBr	zincblende	a : 0.569	d :	4.72	$\varepsilon(0)$: 7.9	$E_{g,dir}$:	3.077	4.2	m_n : > 0.21
	T^2_d - F $\bar{4}$3m		T_m :	760	$\varepsilon(\infty)$: 4.062		2.91	300	$m_{p,l}$: ≅ 1.1
			c_{11} :	4.35	ν_{TO} : 3.72	Δ_{so} :	0.154	4.2	$m_{p,h}$: ≅ 1.5
			c_{12} :	3.49	ν_{LO} : 4.89	E^T_{gx1} :	2.9644	4.2	m^L_{ex} : 11
			c_{44} :	1.47		E^L_{gx1} :	2.9766	4.2	all at low
						E_{gx2} :	3.116	4.2	temperatures
γ-CuI	zincblende	a : 6.0427	d :	5.667	$\varepsilon(0)$: 6.5	$E_{g,dir}$:	3.115	4.2	m_n : 0.33
	T^2_d - F $\bar{4}$3m		T_m :	875	$\varepsilon(\infty)$: 4.84		2.95	300	m_p : 1.4
			c_{11} :	4.51	ν_{TO} : 3.99	Δ_{so} :	0.690	4.2	··· 2.4
			c_{12} :	3.07	ν_{LO} : 4.84	E_{gx1} :	3.06	4.2	
			c^E_{44} :	1.82	at 80 K	$\Delta^{L\text{-}T}_{x1}$:	0.0061	4.2	
			c^D_{44} :	0.0185		E_{gx2} :	3.70	4.2	

The silver halogenides AgF, AgCl and AgBr crystallize in the cubic NaCl structure. These materials are light-sensitive at room temperature. For AgF only crystalline thin films have been prepared so far. Band structures of AgCl and AgBr: Fig. 38 (p. 257).

Substance	Structure	Static and dynamical lattice parameters			Band structure parameters				Transport parameters	
		a [Å]	d [g cm^{-3}]	$\varepsilon(0)$, $\varepsilon(\infty)$	E_g [eV]	at T [K]	m [m_o]		μ [cm^2/Vs]	
			T_m [K]	ν [THz]						
			c_{ik} [10^{11}dyn cm^{-2}]							
AgF, AgCl and AgBr are indirect gap semiconductors with the uppermost valence band located at L and the lowest conduction band at Γ.										
AgF	NaCl lattice	a : 4.936	d : 5.852	$\varepsilon(0)$: 10.6	$E_{gx,ind}$:	2.8	4.8			
	O^5_h - Tm3m		T_m : 708	$\varepsilon(\infty)$: 2.99	$E_{gx,dir}$:	4.63	4.8			
				ν_{TO} : 5.10						
				ν_{LO} : 9.60						
AgCl	NaCl lattice	a : 5.55023	d : 5.5667	$\varepsilon(0)$: 11.14	$E_{gx,ind}$:	3.2476	1.8	m_n : 0.302	$\mu_{n,H}$:	10^4
	O^5_h - Tm3m		T_m : 728	$\varepsilon(\infty)$: 3.92	$E_{gx,dir}$:	5.13	4.2	$m_{n,pol}$: 0.431		$\cdots 4\cdot10^4$
			c_{11} : 5.985	ν_{TO} : 3.18	$E_{g,dir}$:	5.15	4.2			at 4.2 K
			c_{12} : 3.611	ν_{LO} : 5.88						
			c_{44} : 0.624	ν_{TA} : ≅ 2						
				ν_{LA} : ≅ 3						
AgBr	NaCl lattice	a : 5.77475	d : 6.4753	$\varepsilon(0)$: 12.44	$E_{gx,ind}$:	2.6845	1.8	m_n : 0.215	μ_n :	60
	O^5_h - Tm3m		T_m : 703	$\varepsilon(\infty)$: 4.62	$E_{g,ind}$:	2.7125	1.8	$m_{p\parallel}$: 1.25	μ_p :	2
			c_{11} : 5.610	ν_{TO} : 2.37	$E_{gx,dir}$:	4.3 ··· 4.8	4.2	$m_{p\perp}$: 0.52		
			c_{12} : 3.270	ν_{LO} : 4.14		3.96	300		μ_n :	500 ··· 2000
			c_{44} : 0.724			··· 4.40			μ_p :	$3\cdot10^4$
					$E_{g,dir}$:	4.292	4.2			at 4.2 K
For silver iodide two phases coexist at room temperature : β-AgI and the metatable γ-AgI. Both are direct gap semiconductors with band extrema at the point Γ in the Brillouin zone. The band structures are shown in Figs. 40 and 41 (p. 258).										
AgI	γ-phase	a : 6.473	d : 6		$E_{g,dir}$:	2.91	4			
	zincblende					2.82	300			
	T^2_d - F 43m									

Substance	Structure	Static and dynamical lattice parameters			Band structure parameters			Transport parameters
		a, c [Å]	d [g cm^{-3}] T_m, T_{tr} [K] c_{ik} [10^{10} N cm^{-2}]	$\varepsilon(0)$, $\varepsilon(\infty)$ ν [THz]	E_g, Δ [eV]	at T [K]	m [m_o]	μ [cm^2/Vs] n_i [cm^{-3}]
AgI	β-phase	a : 4.580	d : 5.68	$\varepsilon(0)$: 7.0	$E_{g,dir}$: 3.023	4.5		
(cont.)	wurtzite	c : 7.494	T_{tr} : 420	$\varepsilon(\infty)$: 4.1	$E_{gx,dir}$: 2.95	4.5		
	C^4_{6v} - $P6_3mc$		to α-phase	··· 4.9	Δ_{so} : 0.840	4.2		
			T_m : 831	ν_{TO} : 3.24				
				ν_{LO} : 3.72				

4.5 II_x-IV_y compounds

4.5.1 II_2-IV compounds

In this group the compounds of magnesium with Si, Ge, Sn and Pb are of main interest as semiconductors. A few data on calcium compounds also are available.

In Mg_2Si, Mg_2Ge, Mg_2Sn and Mg_2Pb the two lowest sets of conduction bands have their minima at the point X in the Brillouin zone. The valence band is "germanium-like", i.e. the top of the valence band consists of a degenerate heavy hole band and a spin-orbit split light hole band. In Mg_2Pb conduction and valence bands overlap, so that this material is a semi-metal. Structure of the antifluorite lattice: Fig. 42 (p. 259); band structure of the four Mg compounds: Figs. 43 ··· 46 (p. 259,260).

Mg_2Si	antifluorite fcc	a : 6.338	d : 1.88	$\varepsilon(0)$: 18.8	$E_{g,ind}$: 0.77	0	m_n : 0.46	$\mu_{n,H}$: 370
	fcc lattice of		T_m : 1375	··· 20	0.60	90	··· 0.53	··· 550
	IV-atoms (a),		c_{11} : 12.1	$\varepsilon(\infty)$: 13.3	$E_{g,dir}$: 2.27	300	m_p : 0.87	$\mu_{p,H}$: 70
	sc sublattice of		c_{12} : 2.30	ν_{TO} : 8.0	Δ_{so} : 0.03		··· 2.6	n_i : 10^{14}
	Mg-atoms (a/2)		c_{44} : 4.64	ν_{LO} : 10.56	Δ_{cb} : 0.40			
	O^5_h - Fm3m			ν_R: 7.75				

Substance	Structure	Static and dynamical lattice parameters			Band structure parameters				Transport parameters	
		a, b, c [Å]	d [g cm^{-3}] T_m [K] c_{ik} [10^{10} N cm^{-2}]	$\varepsilon(0), \varepsilon(\infty)$ ν [THz]	E_g, Δ [eV]	at T [K]	m [m_o]		μ [cm^2/Vs] n, p, n_i [cm^{-3}]	
Mg_2Ge	as for Mg_2Si	a : 6.393	d : 3.09	$\varepsilon(0)$: 21.7	$E_{g,ind}$: 0.74	0	m_n : 0.18		μ_n : 280	
			T_m : 1388	$\varepsilon(\infty)$: 13.9	0.54	300	m_p : 0.31			··· 530
			c_{11} : 11.79	ν_{TO} : 6.2	$E_{g,dir}$: 1.64	300			μ_p : 110	
			c_{12} : 2.30	ν_{LO} : 7.7	Δ_{so} : 0.20	300			n_i : $2 \cdot 10^{14}$	
			c_{44} : 4.65		Δ_{cb} : 0.58					
Mg_2Sn	as for Mg_2Si	a : 6.762	d : 3.59	$\varepsilon(0)$: 23.75	$E_{g,ind}$: 0.36	0	m_n : 0.15		μ_n : 210	
			T_m : 1051	$\varepsilon(\infty)$: 15.5	0.18	300		··· 1.2		··· 320
			c_{11} : 8.24	ν_{TO} : 5.6	$E_{g,dir}$: 1.2	calc.	m_p : 0.10		μ_p : 150	
			c_{12} : 2.08	ν_{LO} : 6.6	Δ_{so} : 0.48	300		··· 1.3		··· 260
			c_{44} : 3.66		Δ_{cb} : 0.125	300			n_i : $3 \cdot 10^{17}$	
Mg_2Pb	as for Mg_2Si	a : 6.860	d : 5.54	ν_{LO} : 5.79	$E_{g,ind}$: - 0.15		$m_{p,h}$: 0.35		μ_n : 120000	
			T_m : 828	ν_R : 6.42				··· 0.45	$\mu_{p,h}$: 14000	
							depending on		$\mu_{p,l}$: 83000	
							direction		n : $3.5 \cdot 10^{19}$	
							$m_{p,l}$: 0.04		p_h : $3.6 \cdot 10^{19}$	
									p_l : $5.4 \cdot 10^{17}$	
									all at 4.2 K	
Ca_2Si	orthorhombic	a : 7.667			E_g : 1.9					
	(anti-$PbCl_2$	b : 9.002								
	lattice)	c : 4.799								
Ca_2Sn	orthorhombic	a : 7.975			E_g : 0.9					
	(anti-$PbCl_2$	b : 9.562								
	lattice)	c : 5.044								

Substance	Structure	Static and dynamical lattice parameters a, b, c [Å] T_m [K]	Band structure parameters E_g [eV]	Transport parameters μ [cm²/Vs] ρ [W cm]
Ca_2Pb	orthorhombic (anti-$PbCl_2$ lattice)	a : 8.072 b : 9.467 c : 5.100	E_g : 0.46	

3.5.2 II-IV$_2$ compounds

$BaSi_2$, $BaGe_2$ and $SrGe_2$ are known as semiconductors. They crystallize in an orthorhombic lattice (D^{16}_{2h} - Pnma). Energy gaps are given as 1.3, 1.0 and 0.9 eV, respectively. Lattice structure: Fig. 47 (p. 260).

4.6 II$_x$-V$_y$ compounds

More than 40 compounds are known in this group, several only as high temperature or pressure phases. The most important subgroups are II_3-V_2 , II_4-V_3 , II-V, II-V_2 and II-V_4 compounds, but other stoichiometric ratios (6/7, 7/10) also exist.

4.6.1 II$_3$-V$_2$ compounds

At room temperature magnesium arsenide Mg_3As_2 crystallizes in a cubic lattice with 16 molecules in its unit cell.

Mg_3As_2	α-phase anti-Mn_2O_3 lattice D^5_3	a : 12.33	T_m : 1073	$E_{g,th}$: 2.2	ρ : 10^5 $\mu_{n,H}$: 10 ··· 20 at 500 K

The phosphides of zinc and cadmium crystallize in an anti-CaF_2 lattice in which one quarter of the metal sites are vacant (Fig. 48, p. 260). The arsenides of both elements differ in its structure only by another arrangement of vacant sites (Fig. 49, p. 260). Valence and conduction bands have their extrema at the points Γ in the Brillouin zone. The valence band degeneracy is split by spin-orbit and crystal field interaction. Two conduction bands are degenerate or nearly coincident at Γ. Band structure of Cd_3P_2: Fig. 50 (p. 261).

Substance	Structure	Static and dynamical lattice parameters a, c [Å]	d [g cm^{-3}] T_m [K]	$\varepsilon(0)$, $\varepsilon(\infty)$	Band structure parameters E_g, Δ [eV]	at T [K]	m [m_o]	Transport parameters μ [cm^2/Vs] ρ [W cm] n, p, n_i [cm^{-3}]
Zn_3P_2	α-phase tetragonal D^{15}_{4h} - $P4_2/nmc$ (8 formula units in the unit cell)	a: 8.09 c: 11.45	d: 4.485 T_m: 1466	$\varepsilon(0)$: 11	$E_{g,th}$: 1.20 $E_{g,dir}$: 1.52 ··· 1.886 Δ_{so} 0.3 Δ_{cr}: 0.17	300 293 293		μ_p: 10 ··· 20 ρ: 10 ··· 10^5 n_i $3.56\cdot10^{14}$
Zn_3As_2	α-phase tetragonal b.c. D^{15}_{4v} - $I4_1cd$ (32 formula units in the unit cell)	a: 11.779 c: 23.643	d: 5.609 T_m: 1288	$\varepsilon(0)$: 10 ··· 11.8	$E_{g,th}$: 0.86 ··· 1.1 $E_{g,dir}$: 1.0 Δ_{so}: 0.35 Δ_{cr}: 0.07	300 300 calc.	m_n: 1.70 m_p: 0.66 at 600 K	μ_p: 10 ··· 17 ρ: 12 p $7.3\cdot10^{17}$
Cd_3P_2	as in Zn_3P_2	a: 8.754 c: 12.267	d: 5.64 T_m: 1012	$\varepsilon(0)$: 37 $\varepsilon(\infty)$: 14 ··· 17	E_g: 0.50 Δ_{so}: 0.067 ··· 0.16 Δ_{cr}: 0.04 Δ_{cb}: ≅ 0.1	300 calc. calc.	m_n: 0.05 $m_{p,h}$: 0.5	μ_n: 1500 ··· 4000 ρ: $9\cdot10^{-3}$ ··· $25\cdot10^{-3}$ n: $2\cdot10^{17}$ ··· $7\cdot10^{18}$
Cd_3As_2	as in Zn_3P_2	a: 12.64 c: 25.438	d: 6.29 T_m: 994	$\varepsilon(0)$: 42 $\varepsilon(\infty)$: 16	$E_{g,ind}$: - 0.05 - 0.19 Δ_{so} 0.21 ··· 0.31 Δ_{cr}: 0.04 ··· 0.07	4.2 300 300 300	m_n: 0.012 ··· 0.076 m_p: 0.12 ··· 0.5	μ_n: 1 ··· 2.5 ρ: ≅ 10^{-4} n: $6\cdot10^{16}$ ··· $1.2\cdot10^{19}$

Substance	Structure	Static and dynamical lattice parameters		Band structure parameters			Transport parameters
		a, b, c [Å]	d [g cm^{-3}]	E_g [eV]	at T [K]	m [m_o]	μ [cm^2/Vs]
			T_m [K]				ρ [W cm]
							p [cm^{-3}]

4.6.2 II_4-V_3 compounds

Zn_4Sb_3 and Cd_4Sb_3 are known in several modifications (orthorhombic, monoclinic, trigonal) (Fig. 51, p. 261). The number of phases as well as the temperature ranges of their existence are controversial. Thus, the few data on semiconductor properties cannot be assigned to special phases. Stable or metastable at room temperature are the α- and β-phases.

Zn_4Sb_3	β-phase	a : 10.877	d : 6.81	$E_{g,th}$: 1.0		m_p : 0.12	$\mu_{p,H}$: 998
	monoclinic	b : 12.231	T_m : 836				μ_n/μ_p : 0.3
	C^6_{2h} - C2/c	c : 8.186					ρ : $7.3\cdot10^{-3}$
							p : $8\cdot10^{17}$
Cd_4Sb_3	β-phase	a : 8.152	T_m : 703	$E_{g,th}$: 1.2 ··· 1.6			$\mu_{p,H}$: 53
	orthorhombic	b : 8.165					··· 110
	D^{13}_{2h} - Pmmn	c : 11.960					ρ : 10^{-2}
							p : $3\cdot10^{18}$
							··· 10^{19}

4.6.3 II-V compounds

Here only the two antimonides of zinc and cadmium are known as semiconductors. Crystal structure: Fig. 52 (p. 261).

ZnSb	primitive	a : 6.218	d : 6.36	$E_{g,ind}$: 0.5	300	$m_\perp$: 0.146	$\mu_{p\parallel c}$: 800
	orthorhombic	b : 7.741	T_m : 819	$E_{g,dir\parallel a}$: 1.11	4.2	$m_\parallel$: 0.175	$\mu_{p\parallel a}$: 200
	D^{15}_{2h} - Pbca	c : 8.115		$E_{g,dir\parallel b}$: 1.07	4.2	at Fermi surface	at 100 K
				$E_{g,dir\parallel c}$: 1.05	4.2	at 4.2 K	

Substance	Structure	Static and dynamical lattice parameters a, b, c [Å] β	 d [g cm^{-3}] T_m [K]	 $\varepsilon(0)$	Band structure parameters E_g [eV]	 at T [K]	 m [m_o]	Transport parameters μ [cm^2/Vs] ρ [Ωm] p, n_i [cm^{-3}]
CdSb	primitive	a : 6.471	d : 6.98	$\varepsilon(0)$: 16.4	$E_{g,ind \parallel a}$: 0.485	295	m_n : 0.6	μ_n : 100
	orthorhombic	b : 8.253	T_m : 729		$E_{g,ind \parallel b}$: 0.472	295	··· 0.7	··· 660
	D^{15}_{2h} - Pbca	c : 8.526			$E_{g,ind \parallel c}$: 0.459	295	$m_{p \parallel a}$: 1.07	μ_p : 300
					$E_{g,dir}$: 0.70			$\mu_{p \parallel b}$: 0.84 ··· 700
					··· 0.75	300		$\mu_{p \parallel c}$: 0.44

4.6.4 II-V_2 compounds

In this group several crystal structures occur. Figs. 53 ··· 56 (p. 261,262) show the structure of Zn and Cd phosphides and arsenides.

ZnP_2	α-phase	a : 5.08	d : 3.536		$E_{g,ind \parallel}$: 1.85	293		$\mu_{p,H}$: 1800
	tetragonal	c : 18.59	T_m : 1258		$E_{g,ind \perp}$: 1.65	293		p : $1.2 \cdot 10^{10}$
	D^4_4 - $P4_12_12$				$E_{g,dir}$: 2.18	293		ρ : $3 \cdot 10^7$
	or D^8_4 - $P4_32_12$				E_{gx} : 2.210	4.2		
	β-phase	a : 8.85	d : 3.55		$E_{g,th}$: 1.42			μ_n : 0.81
	primitive	b : 7.29	T_m: 1265		$E_{g \parallel}$: 1.33	293		μ_H : 1 ··· 3.5
	monoclinic	c : 7.56			$E_{g \perp}$: 1.37	293		ρ : 3 ··· 100
	C^5_{2h} - $P2_1/c$	β: 102.30°						
$ZnAs_2$	primitive	a : 9.21	d : 5	$\varepsilon(0)$: 14.5	$E_{g,th}$: 1.2			μ_n : 240
	monoclinic	b : 7.64	T_m : 1041	··· 15.5	$E_{g \parallel}$: 0.91			··· 500
	C^5_{2h} - $P2_1/c$	c : 7.985			$E_{g \perp}$: 0.93			μ_p : 50
		β: 102.28°						··· 100
								ρ : 10 ··· 10^5

Substance	Structure	Static and dynamical lattice parameters			Band structure parameters				Transport parameters	
		a, b, c [Å]	d [g cm^{-3}]	$\varepsilon(0), \varepsilon(\infty)$	E_g, Δ [eV]	at T [K]	m [m_o]		μ [cm^2/Vs]	
		β	T_m [K]						ρ [Ωm]	
CdP_2	β-phase	a: 5.283	d: 4.19		$E_{g,ind\parallel}$:	1.65 293				
	tetragonal	c: 19.808	T_m: 1057		$E_{g,ind\perp}$:	1.55 293				
	D^4_4 - $P4_12_12$				$E_{g,dir}$:	2.02 293				
	or D^8_4 - $P4_32_12$				E_{gx}:	2.135 63				
$CdAs_2$	orthorhombic	a: 7.954	d: 5.88	$\varepsilon(0)_\parallel$: 17.4	$E_{g,th}$:	1.13		$m_{n\parallel}$: 0.150	μ_n:	100
	D^{10}_4 - $I4_122$	c: 4.678	T_m: 894	$\varepsilon(0)_\perp$: 15.4		··· 1.14		$m_{n\perp}$: 0.58		··· 400
				$\varepsilon(\infty)_\parallel$: 13.8	$E_{g\parallel}$:	1.00 297		$m_{p\parallel}$: 0.094	ρ:	7 ··· 80
				$\varepsilon(\infty)_\perp$: 11.5	$E_{g\perp}$:	1.04 297		$m_{p\perp}$: 0.346		

4.6.5 II-V_4 compounds

Among the magnesium and cadmium arsenides and phosphides only data for semiconducting CdP_4 are available. Fig. 57 (p. 262) shows its lattice structure.

CdP_4	primitive	a: 5.27	d: 2.04		$E_{g\parallel}$:	0.90 293			ρ:	3.5 ··· 5.5
	monoclinic	b: 5.19			$E_{g\perp}$:	0.99 293			p:	$2\cdot10^{16}$
	C^5_{2h} - $P2_1/c$	c: 7.66			Δ_{cf}:	0.09 293				
		β: 80°32'								

4.6.6 Further II-V compounds

Cd_7P_{10}	orthorhombic	a: 23.0	d: 5.01		$E_{g,dir}$:	1.73				
	C^{19}_{2v} - Fdd2	b: 27.50	T_m: 1019							
	(8 formula units	c: 4.62								
	in unit cell)									

Substance	Structure	Static and dynamical lattice parameters a [Å] d [g cm^{-3}] T_m [K]	Band structure parameters E_g [eV] at T [K]	Transport parameters μ [cm^2/Vs] ρ [Ωm] n [cm^{-3}]
Cd_6P_7	cubic T^1_d - P $\bar{4}$3m (12 formula units in unit cell)	a : 10.567 d : 5.39 T_m : 1016	$E_{g,dir}$: 0.85	μ_n : 4200 ρ : 0.8 n : $1.5 \cdot 10^{17}$

4.7 II-VI compounds

As in the I-VII compounds the zincblende, wurtzite and NaCl lattices predominate in the II-VI compounds. The lattice structure and the Brillouin zones of these lattices are shown in Figs. 33 ··· 37 (p. 262).

4.7.1 IIA-VIB compounds

About beryllium chalcogenides little is known. BeO, crystallizing in a wurtzite lattice, is a pure ionic conductor.

BeS	zincblende T^2_d - F $\bar{4}$3m	a : 4.865	$E_{g,dir}$: 6.10 calc. $E_{g,ind}$: 4.17 calc. $E_{g,opt}$: < 5.5		
BeSe	zincblende T^2_d - F $\bar{4}$3m	a : 5.139	$E_{g,dir}$: 4.73 calc. $E_{g,ind}$: 3.61 calc. $E_{g,opt}$: 4 ··· 4.5		
BeTe	zincblende T^2_d - F $\bar{4}$3m	a : 5.625	$E_{g,dir}$: 1.45 calc. $E_{g,ind}$: 2.89 calc. $E_{g,opt}$: 2.7	μ_p : 6 ··· 30 p : 10^{14} ··· 10^{16}	

Substance	Structure	Static and dynamical lattice parameters			Band structure parameters				Transport parameters
		a [Å]	d [g cm^{-3}]	$\varepsilon(0)$, $\varepsilon(\infty)$	E_g [eV]	at T [K]	m [m_o]		μ [cm^2/Vs]
			T_m [K]	ν [THz]					
			c_{ik} [10^{11}dyn cm^{-2}]						
Many oxides of IIA elements show semiconducting properties. They all crystallize in a NaCl lattice. Band structures of MgO and CaO: Figs. 58 (p. 262) and 59 (p. 263).									
MgO	NaCl lattice	a : 4.216	d : 3.576	$\varepsilon(0)$: 9.83	$E_{g,th}$:	7.9			$\mu_{p,H}$: 2
	O_h^5 - Fm3m		T_m : 3073	$\varepsilon(\infty)$: 2.94	$E_{g,dir}$:	7.833	85		
			c_{11} : 29.71	ν_{LO} : 21.73	$E_{gx,dir}$:	7.672	85		
			c_{12} : 9.65	ν_{TO} : 12.02					
			c_{44} : 15.57						
CaO	NaCl lattice	a : 4.811	d : 3.335	$\varepsilon(0)$: 12.2	$E_{g,th}$:	7.8		m_n : 0.50	$\mu_{n,H}$: ≅ 8
	O_h^5 - Fm3m		T_m : 2853	$\varepsilon(\infty)$: 3.27	$E_{gx,dir}$:	6.931	85	m_{pol} : 0.68	at 700 K
			c_{11} : 22.189	··· 3.33	$E_{g,dir}$:	7.085	85		
			c_{12} : 5.781	ν_{LO} : 17.39					
			c_{44} : 8.032	ν_{TO} : 9.11					
SrO	NaCl lattice	a : 5.160	d : 4.75	$\varepsilon(0)$: 14.6	$E_{g,th}$:	6.4		m_n : 0.54	$\mu_{n,H}$: ≅ 5
	O_h^5 - Fm3m		T_m : 2533	$\varepsilon(\infty)$: 3.27	$E_{g,opt}$:	5.30	80	m_{pol} : 0.77	at 700 K
			c_{11} : 17.547	··· 3.71		5.22	300		
			c_{12} : 4.908	ν_{LO} : 14.39					
			c_{44} : 5.587	ν_{TO} : 7.02					
BaO	NaCl lattice	a : 5.5363	d : 5.68	$\varepsilon(0)$: 37.4	$E_{g,th}$:	4.4		m_n : 0.59	μ_n : ≅ 5
	O_h^5 - Fm3m		T_m : 2196	$\varepsilon(\infty)$: 3.56				m_{pol} : 0.86	at 600 K
			c_{11} : 12.614	··· 3.90					
			c_{12} : 5.003	ν_{LO} : 13.02					
			c_{44} : 3.368	ν_{TO} : 4.32					

Substance	Structure	Static and dynamical lattice parameters			Band structure parameters			Transport parameters
		a, c [Å]	d [g cm^{-3}]	$\varepsilon(0)$, $\varepsilon(\infty)$	E_g, E_b [eV]	at T [K]	m [m_o]	μ [cm^2/Vs]
			T_m [K]	ν [THz]				
			c_{ik} [10^{11}dyn cm^{-2}]					

4.7.2 Zinc chalcogenides

Zinc oxide is a direct gap semiconductor. The valence band maximum (at Γ) is split by crystal field and spin-orbit interactions into three spin-degenerate bands, usually designed by A, B and C. Band structure: Fig. 60 (p. 263).

ZnO	wurtzite	a : 3.253	d : 5.675	$\varepsilon(0)_{\parallel}$: 8.75	E_{gA} : 3.4376	1.6	m_n : 0.24	$\mu_{n,H}$: 200
	C^4_{6v} - $P6_3mc$	c : 5.213	T_m : ca. 2300	$\varepsilon(0)_{\perp}$: 7.8	E_{gB} : 3.4405	1.6	··· 0.28	
			cE_{11} : 20.7	$\varepsilon(\infty)_{\parallel}$: 3.75	E_{gC} : 3.4790	1.6	m_{pol} : 0.275	
			cE_{12} : 11.77	$\varepsilon(\infty)_{\perp}$: 3.70	$E_{b,ex}$ (A) : 0.0608	1.6	$m_{p\parallel}$ (A,B) : 0.59	
			cE_{13} : 10.61	ν_R : 2.94	$E_{b,ex}$ (B) : 0.0591	1.6	$m_{p\perp}$ (A,B) : 0.59	
			c_{33} : 20.95	$\nu_{TO\perp c}$: 12.29	$E_{b,ex}$ (C) : 0.059	4.2	$m_{p\parallel}$ (C) : 0.31	
			c_{55} : 4.48	$\nu_{TO\parallel c}$: 11.34			$m_{p\perp}$ (C) : 0.55	
			c_{66} : 0.446	$\nu_{LO\perp c}$: 17.64				
				$\nu_{LO\parallel c}$: 17.28				

Zinc sulfide crystallizes in two modifications, the cubic zincblende structure and the hexagonal wurtzite structure. ZnS is a direct gap semiconductor. For both modifications the valence band maximum is split into three levels A, B and C by crystal field and spin-orbit interaction. Band structure of both ZnS modifications: Figs. 61 and 62 (p. 264), of ZnSe: Fig. 63 (p. 265), of ZnTe: Fig. 64 (p. 265).

ZnS	cubic	a : 5.410	d : 4.075	$\varepsilon(0)$: 8.0	$E_{g,dir}$: 3.78	19	m_n : 0.34	$\mu_{n,dr\parallel}$: 165
	modification		T_m : under	··· 8.9	3.68	295	0.184	$\mu_{n,dr\perp}$: 280
	zincblende		normal pressure	$\varepsilon(\infty)$: 5.1	E_{gx} (A) : 3.783	80	$m_{p,h}$: 1.76	
	T^2_d - F $\bar{4}3m$		ZnS sublimes	··· 5.7	E_{gx} (B) : 3.7915	80	$m_{p,l}$: 0.23	
			before melting	ν_{LO} : 10.44	3.698	293	last 3 values	
			(under Ar pres-	ν_{TO} : 8.30	E_{gx} (C) : 3.859	80	calculated	
			sure T_m : 2103)		3.762	293		

Substance	Structure	Static and dynamical lattice parameters			Band structure parameters			Transport parameters
		a, b, c [Å]	d [g cm^{-3}] T_m, T_{tr} [K] c_{ik} [10^{11}dyn cm^{-2}]	$\varepsilon(0), \varepsilon(\infty)$ ν [THz]	E_g, Δ [eV]	at T [K]	m [m_o]	μ [cm^2/Vs]
ZnS (cont.)			c_{11} : 9.81 c_{12} : 6.27 c_{44} : 4.483					
	hexagonal modification wurtzite C^4_{6v} - $P6_3mc$	a : 3.822 c : 6.260	d : 4.087 T_{tr} : 1293 (cub. → hex.) c^E_{11} : 12.34 c^E_{12} : 5.85 c^E_{13} : 4.55 c^E_{33} : 2.885 c^E_{44} : 3.245 c^E_{66} : 13.96	$\varepsilon(0)$: 9.6 $\varepsilon(\infty)$: 5.13 ... 5.7	$E_{g,dir\parallel}$: 3.74 ... 3.78 300 $E_{g,dir\perp}$: 3.78 ... 3.87 300 Δ_{so} : 0.086 77 Δ_{cf} : 0.058 77 E_{gx} (A) : 3.8643 77 E_{gx} (B) : 3.8932 77 E_{gx} (C) : 3.9808 77		m_n : 0.28 $m_{p\parallel}$: 1.4 $m_{p\perp}$: 0.49	$\mu_{p,H}$: 100 ... 800
ZnSe	cubic modification zincblende T^2_d - $F\bar{4}3m$	a : 5.668	d : 5.27 T_m : 1793 c_{11} : 9.00 c_{12} : 5.34 c_{44} : 3.96	$\varepsilon(0)$: 7.6 $\varepsilon(\infty)$: 5.4 ν_{LO} : 7.59 ν_{TO} : 6.39	$E_{g,dir}$: 2.82 10 2.70 293 Δ_{so} : 0.40 293		m_n : 0.13 ... 0.17 m_p : 0.57 ... 0.75	$\mu_{n,H}$: 400 ... 600 $\mu_{p,H}$: 28
	hexagonal modification wurtzite C^4_{6v} - $P6_3mc$	a : 4.003 c : 6.540		ν_{LO} : 7.70 ν_{TO} : 6.20	$E_{g,dir}$: 2.874 4.2 2.834 300 $E_{g,dir\perp}$: 2.795 300 E_{gx} (A) : 2.860 15 E_{gx} (B) : 2.876 15 E_{gx} (C) : 2.926 15			

Substance	Structure	Static and dynamical lattice parameters			Band structure parameters				Transport parameters	
		a [Å]	d [g cm^{-3}] T_m [K] c_{ik} [10^{11}dyn cm^{-2}]	$\varepsilon(0)$, $\varepsilon(\infty)$ ν [THz]	E_g, Δ [eV]	at T [K]	m [m_o]		μ [cm^2/Vs]	
ZnTe	zincblende T^2_d - F $\bar{4}$3m	a : 6.10	d : 5.636 T_m : 1568 c_{11} : 7.13 c_{12} : 4.07 c_{44} : 3.12	$\varepsilon(0)$: 9.67 $\varepsilon(\infty)$: 7.28 ν_{LO} : 6.20 ν_{TO} : 5.30	$E_{g,dir}$: Δ_{so} :	2.3941 2.28 0.91	1.6 293 300	m_n : m_p :	0.13 0.6	μ_n : 330

4.7.3 Cadmium chalcogenides

Cadmium oxide possesses NaCl structure. The conduction band has its minimum at the point Γ of the Brillouin zone. The valence band consists of several branches with maxima at L and Σ. Band structure: Fig. 65 (p. 265).

CdO	NaCl structure O^5_h - Fm3m	a : 4.689	d : 8.15	$\varepsilon(0)$: 21.9 $\varepsilon(\infty)$: 5.3 ν_{LO} : 15.83 ν_{TO} : 7.85	$E_{g,ind}$: $E_{g,dir}$:	0.84 0.55 (L - Γ) 1.09 1.20 (Σ - Γ) 2.28	100 300 100 300 100	m_n :	0.11 ··· 0.31	$\mu_{n,H}$: ≅ 400 at 120 K

Cadmium sulfide crystallizes at room temperature in both modifications, cubic and hexagonal. In hexagonal CdS the conduction band (minimum at Γ) originates from the Cd 5s states. The valence band (A, B, C maxima at Γ split by crystal field and spin-orbit interaction) results from the S 3p states. In cubic CdS also the band gap is direct, both extrema being situated at Γ. Band structure for both modifications: Figs. 66 and 67 (p. 266).

Cadmium selenide resembles in its lattice and band structure CdS. Band structure: Fig. 68 (p. 267). Cadmium telluride is only known in the cubic zincblende structure. It is a wide gap semiconductor with band extrema at the midpoint of the Brillouin zone. Band structure: Fig. 69 (p. 267).

Substance	Structure	Static and dynamical lattice parameters			Band structure parameters				Transport parameters
		a, c [Å]	d [g cm^{-3}] T_m [K] c_{ik} [10^{11}dyn cm^{-2}]	$\varepsilon(0)$, $\varepsilon(\infty)$ ν [THz]	E_g, E_b, Δ [eV]	at T [K]	m [m_o]		μ [cm^2/Vs]
CdS	hexagonal modification wurtzite C^4_{6v} - $P6_3mc$	a : 4.136 c : 6.714	d : 4.82 T_m : 1750 c^E_{11} : 8.31 c^E_{12} : 5.04 c^E_{13} : 4.62 c^E_{33} : 9.48 c^E_{55} : 1.533 c^E_{66} : 1.63	$\varepsilon(0)_{\parallel}$: 9.12 $\varepsilon(0)_{\perp}$: 8.45 $\varepsilon(\infty)_{\parallel}$: 5.32 $\varepsilon(\infty)_{\perp}$: 5.32 $\nu_{LO\perp}$: 7.68 9.12 $\nu_{LO\parallel}$: 5.1 9.03 $\nu_{TO\perp}$: 1.26 6.0 7.26 $\nu_{TO\parallel}$: 6.3 7.14	E_g (A) : 2.573 2.485 E_g (B) : 2.589 2.500 E_g (C) : 2.643 2.554 Δ_{so} : 0.062 Δ_{cf} : 0.028 $E_{b,ex}$ (A) 0.03 $E_{b,ex}$ (B) 0.03	80 293 80 293 80 293 77 77 4.2 4.2	m_n : 0.20 ··· 0.25 $m_{p\perp}$ (A) : 0.7 $m_{p\parallel}$ (A) : ≅ 5	$\mu_{n,H}$: 300 $\mu_{p,H}$: 6 ··· 48
	cubic modification zincblende T^2_d - $F\bar{4}3m$	a : 5.825			$E_{g,dir}$: 2.50 ×××2.55		m_n : 0.14 m_p : 0.51 calc.		
CdSe	hexagonal modification C^4_{6v} - $P6_3mc$	a : 4.300 c : 7.011	d : 5.81 T_m : 1514 c_{11} : 7.490 c_{12} : 4.609 c_{13} : 3.926	$\varepsilon(0)_{\parallel}$: 10.16 $\varepsilon(0)_{\perp}$: 9.29 $\varepsilon(\infty)_{\parallel}$: 6.2 $\varepsilon(\infty)_{\perp}$: 6.3 $\nu_{LO\perp}$: 6.33 $\nu_{LO\parallel}$: 6.27 $\nu_{TO\perp}$: 1.02	E_g (A) : 1.829 1.751 E_g (B) : 1.855 1.771 E_g (C) : 2.258 2.176 Δ_{so} : 0.416	80 293 80 293 80 293 77	m_n : 0.12 $m_{p\perp}$ (A) : 0.45 $m_{p\parallel}$ (A) : > 1 $m_{p\perp}$ (B) : 0.9	$\mu_{n,H}$: 450 ··· 900 $\mu_{p,H}$: 10 ··· 50

Substance	Structure	Static and dynamical lattice parameters a [Å]	d [g cm^{-3}] T_m [K] c_{ik} [10^{11}dyn cm^{-2}]	$\varepsilon(0)$, $\varepsilon(\infty)$ ν [THz]	Band structure parameters E_g, E_b, Δ [eV]	at T [K]	m [m_o]	Transport parameters μ [cm^2/Vs]
CdSe (cont.)			c_{33} : 8.451 c_{44} : 1.315 c_{66} : 1.441	$\nu_{TO\parallel}$: 4.95	Δ_{cf} : 0.039 $E_{b,ex}$ (A) : 0.015 $E_{b,ex}$ (B) : 0.016	77 1.8 1.8		
	cubic modification zincblende T^2_d - F $\bar{4}$3m	a : 6.052			$E_{g,dir}$: 1.9	calc.	m_n : 0.11 m_p : 0.44 calc.	
CdTe	zincblende T^2_d - F $\bar{4}$3m	a : 6.482	d : 5.87 T_m : 1365 c_{11} : 5.33 c_{12} : 3.65 c_{44} : 2.04	$\varepsilon(0)$: 10.2 $\varepsilon(\infty)$: 7.1 ν_{LO} : 5.08 ν_{TO} : 4.20	$E_{g,dir}$: 1.606 1.49 Δ_{so} : 0.80	2 300 293	m_n : 0.090 $m_{p,h}$: 0.72 ··· 0.84 $m_{p,l}$: 0.12 at low T	$\mu_{p,H}$: 60 (1200 at 170 K)

4.7.4 Mercury chalcogenides

Only few results are available for HgO.

HgO	orthorhombic and rhombohedral phases		d : 11.046		$E_{g,opt}$: 2.19			

HgS (cinnabar) exists in two polymorphic modifications: the red α-HgS and the black β-HgS. α-HgS is a large-gap semiconductor, whereas β-HgS is a semi-metal. HgSe and HgTe, both crystallizing in the zincblende structure, are semi-metals. Fig. 70 (p. 268) shows the transition from semiconductor to semimetal in the system CdSe - HgSe; Fig. 71 (p. 268) presents the band structure of HgTe.

Substance	Structure	Static and dynamical lattice parameters			Band structure parameters				Transport parameters	
		a, c [Å]	d [g cm^{-3}] T_m [K] c_{ik} [10^{11}dyn cm^{-2}]	$\varepsilon(0), \varepsilon(\infty)$ ν [THz]	E_g, Δ [eV]	at T [K]	m [m_o]		μ [cm^2/Vs]	
HgS	α-phase trigonal point group : 32 - D_3	a : 4.149 c : 9.495	T_{tr} : 617 (α → β) c_{11} : 3.50 c_{33} : 4.86 c_{66} : 1.30	$\varepsilon(0)_{\parallel}$: 23.5 $\varepsilon(0)_{\perp}$: 18.2 $\varepsilon(\infty)_{\parallel}$: 7.9 $\varepsilon(\infty)_{\perp}$: 6.25	E_g :	2.275 2.10	4.2 300		$\mu_{\parallel}$: $\mu_{\perp}$:	30 ··· 45 10 ··· 13
	β-phase zincblende T^2_d - F $\bar{4}$3m	a : 5.851	d : 7.73 T_m : β-HgS dissociates into Hg and S vapor c_{11} : 8.13 c_{12} : 6.22 c_{44} : 2.64	$\varepsilon(0)$: 18.2 $\varepsilon(\infty)$: 11.36 ν_{LO} : 6.72 ν_{TO} : 5.31	E_g :	- 0.2 ··· - 0.5				
HgSe	zincblende T^2_d - F $\bar{4}$3m	a : 6.085	d : 8.25 T_m : 1072 c_{11} : 6.1 c_{12} : 4.4 c_{44} : 2.2	$\varepsilon(0)$: 25.6 $\varepsilon(\infty)$: 12 ··· 21 ν_{LO} : 4.9 ν_{TO} : 4.0	E_g : Δ_{so} :	- 0.205 - 0.061 0.396	80 300 10	m_n strongly dependent on n m_p : 0.78	μ_n :	≅ 1.5
HgTe	zincblende T^2_d - F $\bar{4}$3m	a : 6.46	d : 8.070 T_m : 943 c_{11} : 5.361 c_{12} : 3.660 c_{44} : 2.123	$\varepsilon(0)$: 21.0 $\varepsilon(\infty)$: 15.2 ν_{LO} : 4.14 ν_{TO} : 3.54	E_g :	- 0.3025 - 0.141	4.4 300	m_n : 0.03 m_p : 0.42	μ_n :	35 (800 at 4.2 K)

Substance	Structure	Static and dynamical lattice parameters			Band structure parameters	
		a, b, c [Å]	d [g cm^{-3}]	$\varepsilon(0), \varepsilon(\infty)$	E_g, Δ [eV]	at T [K]
		β	T_m [K]	ν [THz]		
			c_{ik} [10^{11}dyn cm^{-2}]			

4.8 II-VII$_2$ compounds

A considerable number of group II - dihalides crystallize in a layer structure. The metal ions are mostly octahedrally surrounded by halide ions. All halide ions are closely packed. The layers are held together by van der Waals forces. Several types of stacking are possible. Figs. 72 and 73 (p. 268) show two structure types: the lattices of $CdCl_2$ and CdI_2. Band structures of CdI_2 and HgI_2 are shown in Figs. 74 and 75 (p. 269).

$CdCl_2$	rhombohedral	a : 6.23	d : 4.047		E_g :	> 5.9	4.2
	D^5_{3d}	β : 36°02'	T_m : 841				
$CdBr_2$	rhombohedral	a : 6.63	d : 5.192		E_g :	> 4.9	4.2
	D^5_{3d}	β : 34°42'	T_m : 840				
CdI_2	hexagonal	various	d : 5.670	$\varepsilon(0)_{\parallel}$: 12.9	$E_{g,ind\perp}$:	3.473	2
	D^3_{3d}	polytypes	T_m : 660	$\varepsilon(0)_{\perp}$: 5.9	$E_{g,dir}$:	3.80	
			c_{11} : 4.91	$\varepsilon(\infty)_{\parallel}$: 4.6	Δ_{so} :	0.58	
			c_{12} : 2.04	$\varepsilon(\infty)_{\perp}$: 4.3			
			c_{13} : 0.89	$\nu_{TO\perp}$: 2.4			
			c_{14} : $\cong 0$	$\nu_{TO\parallel}$: 4.1			
			c_{33} : 2.25	$\nu_{LO\perp}$: 4.0			
			c_{44} : 0.55	$\nu_{LO\parallel}$: 4.6			
$HgCl_2$	orthorhombic	a : 4.325	d : 5.44	semiconducting properties proved, but no reliable data			
	V^{16}_h (D^{16}_{2h})	b : 12.735	T_m : 549				
		c : 5.963					

Substance	Structure	Static and dynamical lattice parameters			Band structure parameters			Transport parameters
		a, b, c [Å]	d [g cm^{-3}] T_m, T_{tr} [K] c_{ik} [10^{11}dyn cm^{-2}]	$\varepsilon(0), \varepsilon(\infty)$ ν [THz]	E_g, Δ [eV]	at T [K]	m [m_o]	μ [cm^2/Vs]
$HgBr_2$	orthorhombic $C^{12}{}_{2v}$	a : 4.624 b : 12.445 c : 6.798	d : 6.109 T_m : 509	semiconducting properties proved, but no reliable data				
HgI_2	α-phase tetragonal $D^{15}{}_{4h}$ (2 molecules in unit cell)	a : 4.357 c : 12.36	d : 6.36 T_{tr} : 400 (α → β) c_{11} : 3.16 c_{12} : 0.559 c_{13} : 1.168 c_{33} : 1.526 c_{44} : 0.727 c_{66} : 0.35	$\varepsilon(0)_{\parallel}$: 8.5 $\varepsilon(0)_{\perp}$: 25.9 $\varepsilon(\infty)_{\parallel}$: 6.8 $\varepsilon(\infty)_{\perp}$: 5.15 ν_R : 0.54 0.85 3.45 4.38 ν_{ir} : 3.15 3.75	$E_{g,dir}$: 2.3707 2.140 Δ_{so} : 1.012 Δ_{cf} : 0.199	4.2 300 4.2 4.2	$m_{n\parallel}$: 0.25 (0.31) $m_{n\perp}$: 0.29 (0.37) $m_{p\parallel}$: 1.72 (2.106) $m_{p\perp}$: 0.56 (1.03) values in brackets : polaron masses	$\mu_{dr,n\parallel}$: 50 ··· 100 $\mu_{n,dr\perp}$: 65
	β-phase orthorhombic (4 molecules in unit cell)	a : 4.674 b : 13.76 c : 7.32	d : 6.094 T_m : 532		E_g : 3.05	90		

4.9 III-V compounds

See chapter 2.

Substance	Structure	Static and dynamical lattice parameters			Band structure parameters			Transport parameters
		a, c [Å]	d [g cm^{-3}] T_m [K] c_{ik} [10^{11}dyn cm^{-2}]	$\varepsilon(0)$, $\varepsilon(\infty)$	E_g [eV]	at T [K]	m [m_o]	μ [cm^2/Vs]

4.10 III_x-VI_y compounds

4.10.1 III-VI compounds

GaS, GaSe and InSe crystallize in a hexagonal layer structure (Fig. 76, p. 270). The bonding is strongly covalent within the layers and weaker between them. Four basic polytypes are known (Fig. 77, p. 270). The GaTe lattice is a monoclinic distorted GaSe lattice (Fig. 78, p. 270). InS crystallizes in an orthorhombic structure (Fig. 79, p. 271), TlS, TlSe and InTe in the tetragonal TlSe structure (Fig. 80, p. 271).

Figs. 81 (p. 271) shows the Brillouin zone and Figs. 82 ··· 84 (p. 271, 272) the band structures for GaS, GaSe and InSe.

β-GaS	hexagonal layers	a : 3.587	d : 3.86	$\varepsilon(0)_{\parallel}$: 5.9	$E_{gx,ind}$:	2.593	1.5	m_n : 5	$\mu_{n,H}$:	12
	D^4_{6h} - $P6_3/mmc$	c : 15.492	T_m : 1233	$\varepsilon(0)_{\perp}$: 10.0		2.495	300		$\mu_{p,H}$:	16
				$\varepsilon(\infty)_{\parallel}$: 5.3	$E_{g,dir}$:	3.05	77		$\mu_{p,dr}$:	80
				$\varepsilon(\infty)_{\perp}$: 6.7	$E_{gx,dir}$:	3.028	77			
GaSe	hexagonal layers	a : 3.755	d : 5.03	$\varepsilon(0)_{\parallel}$: 6.18	$E_{g,dir}$:	2.1275	4.2	$m_{n\parallel}$: 1.6	$\mu_{n\parallel,dr}$:	80
(several	β : D^4_{6h} - $P6_3/mmc$	c : 16 ··· 34	T_m : 1211	$\varepsilon(0)_{\perp}$: 10.6		2.021	300	$m_{n\perp}$: 0.5	$\mu_{n\perp,dr}$:	3000
polytypes)	γ : C^5_{3v} - R3m	depending	c_{11} : 10.24	$\varepsilon(\infty)_{\parallel}$: 5.76	$E_{g,ind}$:	2.103	4.2	$m_{p\parallel}$: 0.2	$\mu_{p\parallel,dr}$:	210
	δ : C^4_{6v} - $P6_3mc$	on polytypes	c_{12} : 3.24	$\varepsilon(\infty)_{\perp}$: 7.44				$m_{p\perp}$: 0.8	$\mu_{p\perp,dr}$:	60
	ε : D^1_{3h} - P 6m2		c_{33} : 3.07						$\mu_{n,H}$:	250
			c_{55} : 0.70						$\mu_{p,H}$:	50
			c_{66} : 3.5							

Substance	Structure	Static and dynamical lattice parameters			Band structure parameters				Transport parameters
		a, b, c [Å]	d [g cm^{-3}]	$\varepsilon(0), \varepsilon(\infty)$	E_g [eV]	at T [K]	m [m_o]		μ [cm^2/Vs]
		γ	T_m [K]						
			c_{ik} [10^{11}dyn cm^{-2}]						
GaTe	monoclinic	a : 17.44	d : 5.44	$\varepsilon(0)_{\parallel}$: 10.58	$E_{g,dir}$:	1.799 1.6	$m_{p\parallel}$: 0.2		$\mu_{H,p\parallel}$: 0.1
	C^3_{2h} -B2/m	b : 10.456	T_m : 1097	$\varepsilon(0)_{\perp}$: 9.66		1.694 295	$m_{p\perp}$: 1.0		$\mu_{H,p\perp}$: 20
		c : 4.077		$\varepsilon(\infty)_{\parallel}$: 7.29	E_b :	0.0195 1.6	$m_{p,ds}$: 0.6		
		γ : 104.4°		$\varepsilon(\infty)_{\perp}$: 6.97		0.044 295			
InS	orthorhombic	a : 3.944	d : 5.18	$\varepsilon(\infty)$: 15.2	$E_{g,ind}$:	2.067 4.2	m_n : 0.4		$\mu_{n,H}$: 50
	D^{12}_{2h} - Pmnn	b : 4.447				1.896 300			
		c : 10.648			$E_{g,dir}$:	2.58 10			
						2.45 290			
InSe	hexagonal layers	a : 4.00	d : 5.55	$\varepsilon(0)_{\parallel}$: 5.4	$E_{g,ind}$:	1.32 30	$m_{n\parallel}$: 0.143		$\mu_{n\perp}$: 15 ··· 500
	space groups as	c : 25 ··· 74	T_m : 933	$\varepsilon(0)_{\perp}$: 8.6		1.172 300	$m_{n\perp}$: 0.156		
	for GaSe	depending	c_{11} : 11.81	$\varepsilon(\infty)_{\parallel}$: 4.9	$E_{g,dir}$:	1.3525 1.6	$m_{p\parallel}$: 0.54		
		on polytype	c_{13} : 3.2	$\varepsilon(\infty)_{\perp}$:6.2		1.2635 293	$m_{p\perp}$: 1.50		
			c_{33} : 3.82						
			c_{44} : 1.17						
			c_{66} : 3.53						
InTe	tetragonal	a : 8.454	d : 6.29	$\varepsilon(\infty)_{\parallel}$: 14.7	metallic as well as		$m_{n,ds}$: 0.09		μ_n : 112
	D^{18}_{4h} - I4/mcm	c : 7.152		$\varepsilon(\infty)_{\perp}$:14.0	semiconducting		$m_{p,ds}$: 0.26		μ_p : 150
	(14 formula units				characteristics have				
	in unit cell)				been reported				
TlS	tetragonal	a : 7.787	d : 7.60		$E_{g,ind\parallel}$:	1.37 300	$m_{n,ds}$: 0.07		μ_n : 8
	D^{18}_{4h} - I4/mcm	c : 6.807			$E_{g,ind\perp}$:	1.36 300	$m_{p,ds}$: 0.11		μ_p : 20
	(14 formula units				$E_{g,dir\parallel}$:	1.57 300			
	in unit cell)				$E_{g,dir\perp}$:	1.50 300			

Substance	Structure	Static and dynamical lattice parameters			Band structure parameters				Transport parameters	
		a, b, c [Å]	d [g cm^{-3}]	$\varepsilon(0), \varepsilon(\infty)$	E_g [eV]	at T [K]	m [m_o]		μ [cm^2/Vs]	
		β	T_m [K]							
			c_{ik} [10^{11}dyn cm^{-2}]							
TlSe	tetragonal	a : 8.02	d : 8.15	$\varepsilon(0)_{\parallel}$: 34 ··· 44	$E_{gx,dir}$:	0.790	90	$m_{n,ds}$: 0.30	μ_p :	15 ··· 150
	D^{18}_{4h} - I4/mcm	c : 7.00	T_m : 623	$\varepsilon(0)_{\perp}$: 15 ··· 20		0.745	300	$m_{p,ds}$: 0.60		
	(14 formula units		c_{11} : 4.5	$\varepsilon(\infty)_{\parallel}$: 12						
	in unit cell)		c_{12} : 0.3	$\varepsilon(\infty)_{\perp}$: 12						
			c_{13} : 1.7							
			c_{33} : 4.2							
			c_{44} : 3.2							
			c_{66} : 1.2							
TlTe	tetragonal	a : 12.954	d : 8.40					$m_{n,ds}$: 0.03	μ_p :	60
	D^{18}_{4h} - I4/mcm	c : 6.178						$m_{p,ds}$: 0.5		

4.10.2 III_2-VI_3 compounds

These compounds crystallize in a lattice containing ordered vacancies in the III-sublattice (vac), so that a designation vac-III_2-VI_3 is more appropriate. This group of quasi-binary (ternary) compounds is presented in Section 4.1.1.

4.10.3 Further III_x-VI_y compounds

Besides of the monochalcogenides (Section 3.10.1) and the sesquichalcogenides (Section 4.1.1) only few phases of the polychalcogenides of group III elements have been studied.

In_6S_7	monoclinic	a : 9.090	d : 5.08	$E_{g,ind}$:	0.7	300	
	C^2_2 - P^2_1	b : 3.887		$E_{g,dir}$:	0.945	77	
		c : 17.705			0.890	300	
		β : 108°20'					

Substance	Structure	Static and dynamical lattice parameters a, b, c [Å] β	d [g cm^{-3}] T_m [K]	$\varepsilon(0)$	Band structure parameters E_g [eV]	at T [K]	m [m_o]	Transport parameters μ [cm^2/Vs] σ [Ω^{-1}cm^{-1}]
In_4Se_3	orthorhombic D^{12}_{2h} - Pnnm	a : 15.297 b : 12.308 c : 4.081	d : 6.02		$E_{g,dir \parallel c}$: 0.64 $E_{g,dir \parallel a}$: 0.65	300		σ : 10-1
In_6Se_7	monoclinic C^2_2 - $P2_1$	a : 9.430 b : 4.063 c : 18.378 β : 109.84°	d : 6.21		$E_{g,ind \parallel c}$: 0.34 $E_{g,dir \parallel c}$: 0.86 $E_{g,dir \parallel b}$: 0.64		m_n : 0.45 m_p : 0.27	
In_4Te_3	orthorhombic D^{12}_{2h} - Pnnm	a : 15.630 b : 12.756 c : 4.441	d : 6.32		$E_{g,dir}$: 0.48 ··· 0.50	300		
TlS_2	liquid at RT		d : 5.498		E_g : 1.8			
Tl_5Te_3	tetragonal D^{18}_{4h} - I4/mcm	a : 8.929 c : 12.620						μ_p : 2

4.10.4 III-III-VI compounds

Most of the chalcogenides of this group are related to the TlSe structure. Fig. 85 (p. 273) shows the structure of $TlInSe_2$. Other structures occuring are shown in Figs. 86 and 87 (p. 273).

$TlGaS_2$	monoclinic space group controversial	controversial	d : 4.22 ··· 5.56 T_m : 1178	$\varepsilon(0)$: 26 ··· 31	$E_{g,ind}$: 2.46 $E_{g,dir}$: 2.544	293 293		

Substance	Structure	Static and dynamical lattice parameters			Band structure parameters				Transport parameters
		a, b, c [Å]	d [g cm^{-3}] T_m [K]	$\varepsilon(0), \varepsilon(\infty)$	E_g [eV]	at T [K]	m [m_o]		μ [cm^2/Vs]
$TlGaSe_2$	monoclinic space group controversial		d: 6.19 T_m: 1053	$\varepsilon(0)$: 20.4 $\varepsilon(\infty)$: 13.2	$E_{g,ind}$: 2.03 $E_{g,dir}$: 2.23	300 300	m_n: 0.37 m_p: 0.68		μ_n: 26 μ_p: 65
$TlGaTe_2$	TlSe structure tetragonal D^{18}_{4h} - I4/mcm	a: 8.429 b: 8.429 c: 6.865	d: 7.32 T_m: 1046	$\varepsilon(\infty)_{\parallel}$: 13.7 $\varepsilon(\infty)_{\perp}$: 14.8	$E_{g,ind}$: 1.2		m_n: 0.12 m_p: 0.23		μ_n: 66 μ_p: 96
$TlInS_2$	several modifications		d: 4.95 ··· 6.76 T_m: 870 ··· 1030 depending on modification	$\varepsilon(0)$: 26	$E_{g,ind}$: 1.14		$m_{n,ds}$: 0.34 $m_{p,ds}$: 0.784		μ_n: 68 μ_p: 170
$TlInSe_2$	tetragonal D^{18}_{4h} - I4/mcm	a: 8.075 c: 6.847	d: 7.06 T_m: 1081	$\varepsilon(\infty)_{\parallel}$: 8.0 $\varepsilon(\infty)_{\perp}$: 10.2	$E_{g,ind}$: 1.14		$m_{n,ds}$: 0.31 $m_{p,ds}$: 0.65		μ_n: 225 μ_p: 450
$TlInTe_2$	tetragonal D^{18}_{4h} - I4/mcm	a: 8.494 c: 7.181	d: 7.2 T_m: 1045	$\varepsilon(\infty)_{\parallel}$: 11.6 $\varepsilon(\infty)_{\perp}$: 14.2	E_g: 0.68		m_n: 0.08 m_p: 0.31		μ_n: 420 μ_p: 600

4.11 III-VII compounds

Thallous halides are characterized by the filled 6s shell, which exceeds the rare gas configuration. These cationic s-electrons are the reason for many peculiar properties of these compounds.

TlF crystallizes in a tetragonal and an orthorhombic modification (Fig. 88, p. 273). No quantitative data on semiconductor properties are available.

Substance	Structure	Static and dynamical lattice parameters			Band structure parameters			Transport parameters
		a, b, c [Å]	d [g cm^{-3}] T_m [K] c_{ik} [10^{11}dyn cm^{-2}]	$\varepsilon(0), \varepsilon(\infty)$ ν [THz]	E_g [eV]	at T [K]	m [m_o]	μ [cm^2/Vs]

TlCl, TlBr and TlI crystallize in a CsCl-type (I), an orthorhombic (II) and a NaCl-type (III) phase (Fig. 89, p. 274). The Brillouin zones and band structures for these three compounds are shown in Figs. 90 ··· 94 (p. 274, 275).

TlCl	I : CsCl-type O^1_h - Pm3m	a : 3.842	d : 7.018 T_m : 704 c_{11} : 4.066 c_{12} : 1.537 c_{44} : 0.77	$\varepsilon(0)$: 32.7 $\varepsilon(\infty)$: 4.76 ν_{TO} : 1.89 ν_{LO} : 5.19	$E_{gx,ind}$: $E_{g,ind}$: $E_{g,dir}$:	3.225 3.202 3.41 3.55	4.2 4.2 4.7 300	$m_{n,pol}$: 0.55 at R 0.7 at X $m_{p,pol\parallel}$: 0.58 at X $m_{p,pol\perp}$: 0.98 at X	$\mu_{n,dr}$: $\mu_{p,H}$:	20 15
	III : NaCl-type O^5_h -Fm3m	a : 6.34		ν_{LO} : 2.9	$E_{g,dir}$:	3.8	77			
TlBr	I : CsCl-type O^1_h - Pm3m	a : 3.986	d : 7.453 T_m : 733.2 c_{11} : 3.76 c_{12} : 1.458 c_{44} : 0.757	$\varepsilon(0)$: 30.6 $\varepsilon(\infty)$: 5.34 ν_{TO} : 1.44 ν_{LO} : 3.48	$E_{g,ind}$: $E_{g,dir}$:	2.665 3.013 3.12	2 4.7 300	$m_{n,pol}$: 0.52 at R 0.45 ··· 0.51 at X $m_{p,pol\parallel}$: 0.55 at X $m_{p,pol\perp}$: 0.74 at X	$\mu_{n,dr}$: $\mu_{p,dr}$:	30 7
	III : NaCl-type O^5_h - Pm3m	a : 6.58		ν_{LO} : 1.9	$E_{g,dir}$:	3.4	77			
TlI	I : CsCl-type	a : 4.21	T_m : 715.2	$\varepsilon(0)$: 29.6	$E_{g,ind}$: $E_{g,dir}$:	2.1 2.789	77 4			
	II : orthorhombic D^{17}_{2h} - Cmcm	a : 4.582 b : 12.92 c : 5.251	d : 7.088		$E_{g,dir}$:	2.8	80			

Substance	Structure	Static and dynamical lattice parameters			Band structure parameters			Transport parameters
		a, b, c [Å]	d [g cm^{-3}]	$\varepsilon(0), \varepsilon(\infty)$	E_g [eV]	at T [K]	m [m_0]	μ [cm^2/Vs]
		β	T_m [K]	ν [THz]				ρ [Ωm], p [cm^{-3}]
TlI (cont.)	III : NaCl-type O^5_h - Pm3m	a : 6.96 ··· 6.99		$\varepsilon(0)$: 21.2 $\varepsilon(\infty)$: 5.8 ··· 6.8 ν_{TO} : 1.53 ν_{LO} : 2.9	$E_{g,dir}$: 3			

4.12 IV_x-V_y compounds

4.12.1 IV-V compounds

SiP	orthorhombic	a : 20.85 b : 13.96 c : 3.54	d : 4.150		E_g : 2					
GeP	monoclinic C^3_{2h} - C2/m	a : 15.14 b : 3.638 c : 9.19 β : 101.1°	d : 2.37		E_g : 0.95					
SiAs	monoclinic C^3_{2h} - C2/m	a : 15.98 b : 3.668 c : 9.53 β : 106.0°	T_m : 1356	$\varepsilon(\infty)$: 9.6	$E_{g,ind \perp b}$: 1.45 $E_{g,dir \perp b}$: 1.57 $E_{g,dir \parallel b}$: 1.48 $E_{g,th}$: 2.18	300 300 300	$m_{p,ds}$: 0.8	μ_p : ρ : p :	24 28 $1.3 \cdot 10^{16}$
GeAs	monoclinic C^3_{2h} - C2/m	a : 15.59 b : 3.792 c : 9.49 β : 101.3°	T_m : 1010		$E_{g,ind \parallel b}$: 0.65 $E_{g,dir \parallel b}$: 1.65 $E_{g,dir \parallel a}$: 1.01	300 300 300			

Substance	Structure	Static and dynamical lattice parameters			Band structure parameters			Transport parameters
		a, b, c [Å]	d [g cm^{-3}]	$\varepsilon(0), \varepsilon(\infty)$	E_g [eV]	at T [K]	m [m_o]	μ [cm^2/Vs]
			T_m [K]					E_A [eV]

4.12.2 IV-V_2 compounds

SiP_2	pyrite-type	a : 5.7045	d : 2.7		$E_{g,opt}$: 1.89	300	m_p :	< 1	E_A :	≅ 0.9
$GeAs_2$	orthorhombic	a : 14.76	T_m : 1005		$E_{g,ind \parallel c}$: 1.06	300			μ_p :	60
	D^9_{2h} - Pbam	b : 10.16			$E_{g,dir \parallel b}$: 1.10	300				
		c : 3.728			$E_{g,dir \parallel c}$: 1.77	300				

4.13 IV_x-VI_y compounds

4.13.1 IV-VI compounds

The IV-VI compounds are isoelectronic to the group V elements. β-GeTe, β-SnTe, PbS, PbSe and PbTe crystallize in the NaCl structure. The structure of GeS, GeSe, γ-GeTe, SnS, SnSe and γ-SnTe is an orthorhombic distorted NaCl structure (Fig. 95, p. 275), the structure of α-GeTe and α-SnTe is As-like distorted (Fig. 96, p. 276). Brillouin zones and band structures for the Ge and Sn compounds are shown in Figs. 97 ··· 101 (p. 276 ··· 278).

GeS	orthorhombic	a : 10.44	d : 4.01	$\varepsilon(0)_{\parallel a}$: 25.1	$E_{g,dir \parallel a}$: 1.744	4.2	m_p :	0.3 ··· 0.7	μ_p :	90
	D^{16}_{2h} - Pnma	b : 3.65	T_m : 938	$\varepsilon(0)_{\parallel b}$: 29.5		1.65	300			
		c : 4.3		$\varepsilon(0)_{\parallel c}$: 30.0						
				$\varepsilon(\infty)_{\parallel a}$: 14.8						
				$\varepsilon(\infty)_{\parallel b}$: 12.0						
				$\varepsilon(\infty)_{\parallel c}$: 10.0						

Substance	Structure	Static and dynamical lattice parameters a, b, c [Å] α	 d [g cm^{-3}] T_m [K]	 $\varepsilon(0), \varepsilon(\infty)$ ν [THz]	Band structure parameters E_g [eV] at T [K]	 m [m_o]	Transport parameters μ [cm^2/Vs]
GeSe	orthorhombic D^{16}_{2h} - Pnma	a : 10.82 b : 3.85 c : 4.4	d : 5.52 T_m : 948	$\varepsilon(0)_{\parallel a}$: 21.9 $\varepsilon(0)_{\parallel b}$: 30.4 $\varepsilon(0)_{\parallel c}$: 25.8 $\varepsilon(\infty)_{\parallel a}$: 18.7 $\varepsilon(\infty)_{\parallel b}$: 21.9 $\varepsilon(\infty)_{\parallel c}$: 14.4	$E_{g,ind\parallel a}$: 1.075 300 $E_{g,ind\parallel b}$: 1.080 300		μ_p : ≅ 80
GeTe	rhombohedral C^5_{3v} - R3m	a : 5.97 α : 88°10'	d : 6.2	$\varepsilon(\infty)$: 36 ν_{TO} : 4.2 $\nu_{TO,LO}$: 2.94	E_g : 0.73 ··· 0.95 300	$m_{n,h}$: 0.48 ··· 0.78 $m_{p,h}$: 5 $m_{p,l}$: 1.15	μ : 15 ··· 120
SnS	orthorhombic D^{16}_{2h} - Pnma	a : 11.20 b : 3.99 c : 4.34	d : 5.08 T_m : 1153	$\varepsilon(0)_{\parallel a}$: 32 $\varepsilon(0)_{\parallel b}$: 48 $\varepsilon(0)_{\parallel c}$: 32 $\varepsilon(\infty)_{\parallel a}$: 14 $\varepsilon(\infty)_{\parallel b}$: 16 $\varepsilon(\infty)_{\parallel c}$: 16	$E_{g,ind\parallel a}$: 1.42 300 $E_{g,ind\parallel b}$: 1.095 300	$m_{n,ds}$: 0.45 $m_{p,ds}$: 0.95 $m_{p\parallel a}$: 0.2 $m_{p\parallel b}$: 0.2 $m_{p\parallel c}$: ≅ 1	$\mu_{p\perp c}$: ≅ 90
SnSe	orthorhombic D^{16}_{2h} - Pnma	a : 11.57 b : 4.19 c : 4.46	T_m : 1153	$\varepsilon(0)_{\parallel a}$: 45 $\varepsilon(0)_{\parallel b}$: 62 $\varepsilon(0)_{\parallel c}$: 42 $\varepsilon(\infty)_{\parallel a}$: 13 $\varepsilon(\infty)_{\parallel b}$: 17 $\varepsilon(\infty)_{\parallel c}$: 16	$E_{g,ind}$: 0.9 300	$m_{p\perp c}$: 0.15 ··· 0.5	$\mu_{p\perp c}$: < 7000 at 77 K

Substance	Structure	Static and dynamical lattice parameters			Band structure parameters			Transport parameters
		a, b, c [Å]	d [g cm^{-3}]	$\varepsilon(0), \varepsilon(\infty)$	E_g [eV]	at T [K]	m [m_o]	μ [cm^2/Vs]
			T_m [K]	ν [THz]				
			c_{ik} [10^{11}dyn cm^{-2}]					
SnTe	β-phase, NaCl	a : 6.3268	d : 6.445	$\varepsilon(0)$: 1200	$E_{g,opt}$: 0.19	300	m_p : 0.066	μ_p : 840
			c_{11} : 10.93	ν_{TO} : 0.78	depends strongly			
	pronounced dependence on		c_{12} : 0.21	ν_{LO} : 4.17	on carrier			
	devation from stoichiometry		c_{44} : 0.969		concentration			
Both the tetragonal (red) and the orthorhombic (yellow) forms of PbO are wide gap semiconductors. The energy gaps of both modifications are assumed to be indirect.								
PbO	tetragonal	a : 3.97	d : 9.53		$E_{g,ind}$: 1.9	300		$\mu_{n,H}$: 80
	D^7_{4h} - P4/nmm	c : 5.02	T_m : 1163		$E_{g,dir}$: 2.75			
					··· 3.18	300		
	orthorhombic	a : 5.489	d : 8.0		$E_{g,ind}$: 2.67	300		
	D^{11}_{2h} - Pbma	b : 4.755			$E_{g,dir}$: 2.8			
		c : 5.891			··· 3.36	300		
PbS, PbSe and PbTe are narrow gap semiconductors crystallizing in the NaCl structure. Band structures for these three compounds are shown in Fig. 102 ··· 104 (p. 279,280).								
PbS	NaCl (fcc)	a : 5.936	d : 7.6	$\varepsilon(0)$: 169	$E_{g,dir}$: 0.286	4.2	$m_{n\parallel}$: 0.105	μ_n : 700
	D^{16}_{2h} - Pnma		T_m : 1383	$\varepsilon(\infty)$: 17.2	0.41	300	$m_{n\perp}$: 0.080	
			c_{11} : 12.61	ν_{TO} : 1.96			$m_{p\parallel}$: 0.105	
			c_{12} : 1.624	ν_{LO} : 6.14			$m_{p\perp}$: 0.075	
			c_{44} : 1.709				all at 4 K	

Substance	Structure	Static and dynamical lattice parameters			Band structure parameters				Transport parameters
		a, b [Å]	d [g cm^{-3}]	$\varepsilon(0)$, $\varepsilon(\infty)$	E_g [eV]	at T [K]	m [m_o]		μ [cm^2/Vs]
		u	T_m [K]	ν [THz]					
			c_{ik} [10^{11}dyn cm^{-2}]						
PbSe	NaCl (fcc)	a : 6.117	d : 8.26	$\varepsilon(0)$: 210	$E_{g,dir}$:	0.145	4	$m_{n\parallel}$: 0.070	$\mu_{n,H}$: 300
	D^{16}_2 - Pnma		T_m : 1355	$\varepsilon(\infty)$: 22.9		0.278	300	$m_{n\perp}$: 0.040	$\mu_{p,H}$: 300
			c_{11} : 12.37	ν_{TO} : 3.99				$m_{p\parallel}$: 0.068	
			c_{12} : 1.93	ν_{LO} : 1.32				$m_{p\perp}$: 0.034	
			c_{44} : 1.591	at low T				all at 4 K	
PbTe	NaCl (fcc)	a : 6.462	d : 8.219	$\varepsilon(0)$: 414	$E_{g,dir}$:	0.187	4.2	$m_{n\parallel}$: 0.185	$\mu_{n,H}$: 1730
	D^{16}_{2h} - Pnma		T_m : 1197	$\varepsilon(\infty)$: 33		0.310	300	$m_{n\perp}$: 0.0223	$\mu_{p,H}$: 780
			c_{11} : 10.53	ν_{TO} : 0.965				$m_{p\parallel}$: 0.236	
			c_{12} : 0.70	ν_{LO} : 3.42				$m_{p\perp}$: 0.0246	
			c_{44} : 1.322					all at 4 K	

3.13.2 IV-VI_2 compounds

Within the IV-VI_2 compounds several crystal structures occur :
GeO_2, SnO_2, PbO_2 : rutile structure (Figs. 105 ··· 107, p. 280), SiS_2, $SiSe_2$: chain structure (Fig. 108, p. 280), GeS_2, $GeSe_2$: distorted orthorhombic layer structure (Fig.109, p. 281), SnS_2, $SnSe_2$: layer structure (Fig.110, p. 281).

Figs. 111 and 112 (p. 281) show the Brillouin zone for the rutile and the SnS_2 structures, Figs. 113 ··· 116 (p. 281 ··· 283) show the band structures of SnO_2, SnS_2 and $SnSe_2$. SiS_2 and $SiSe_2$ are called semiconductors in the literature but no detailed information is available.

GeO_2	rutile	a : 4.395	d : 6.24	$\varepsilon(0)_\parallel$: 12.2	$E_{g,dir\parallel}$:	≅ 6	300
	D^{14}_{4h} - $P4_2/nmm$	b : 2.859	T_m : 1359	$\varepsilon(0)_\perp$: 14.5	$E_{g,dir\perp}$:	5.35	300
		u : 0.307		$\varepsilon(\infty)_\parallel$: 4.1			
				$\varepsilon(\infty)_\perp$: 4.6			

Substance	Structure	Static and dynamical lattice parameters			Band structure parameters				Transport parameters
		a, b, c [Å]	d [g cm^{-3}]	$\varepsilon(0), \varepsilon(\infty)$	E_g [eV]	at T [K]	m [m_o]		μ [cm^2/Vs]
		u	T_m [K]						
GeS_2	orthorhombic	a : 11.66	T_m : 1113	$\varepsilon(0)_\perp$: 12	$E_{g,dir}$:	3.425	300		
	D^{13}_{2h} - Pmmn	b : 22.34		$\varepsilon(\infty)_\perp$: 6.8					
		c : 6.86							
$GeSe_2$	orthorhombic	a : 12.22	T_m : 1013	$\varepsilon(0)_{\parallel a}$: 9.5	$E_{g,dir}$:	2.485	300		
	D^{13}_{2h} - Pmmn	b : 23.036		$\varepsilon(0)_{\parallel b}$: 11.5	$E_{g,th}$:	2.3			
		c : 6.953		$\varepsilon(0)_{\parallel c}$: 11.8					
				$\varepsilon(\infty)_{\parallel a}$: 7					
				$\varepsilon(\infty)_{\parallel b}$: 8					
				$\varepsilon(\infty)_{\parallel c}$: 11					
SnO_2	rutile	a : 4.737	d : 6.99	$\varepsilon(0)_\parallel$: 9.58	$E_{g,dir\parallel}$:	3.99	4	$m_{n\parallel}$: 0.234	μ_n : 260
	D^{14}_{4h} - $P4_2/nmm$	c : 3.186	T_m : > 2200	$\varepsilon(0)_\perp$: 13.5		3.70	300	$m_{n\perp}$: 0.299	
		u : 0.307		$\varepsilon(\infty)_\parallel$: 4.17	$E_{g,dir\perp}$:	3.596	4		
				$\varepsilon(\infty)_\perp$: 3.78		3.47	300		
SnS_2	layer structure	a : 3.648	d : 4.47	$\varepsilon(0)_\parallel$: 17.7	$E_{g,ind}$:	2.29	273		$\mu_{n\perp}$: 51.5
(2H, if not	D^3_{3d}	c : 5.899	T_m : 1038	$\varepsilon(0)_\perp$: 6.19		2.15	(4H)		
stated		u : ≅ 0.25		$\varepsilon(\infty)_\parallel$: 7.57	$E_{g,dir}$:	2.44	273		
otherwise)				$\varepsilon(\infty)_\perp$: 5.65		2.34	(4H)		
					$E_{g,th}$:	2.18			
						1.89	(4H)		
						1.59	(6H)		

Substance	Structure	Static and dynamical lattice parameters			Band structure parameters			Transport parameters	
		a, b, c [Å] u	d [g cm^{-3}] T_m [K] c_{ik} [10^{11}dyn cm^{-2}]	$\varepsilon(0), \varepsilon(\infty)$	E_g [eV]	at T [K]	m [m_o]	μ [cm^2/Vs] n [cm^{-3}]	
$SnSe_2$ (2H, if not stated otherwise)	layer structure D^3_{3d}	a : 3.811 c : 6.137 u : ≅ 0.25	d : 6.01 T_m : 948 c_{11} : 10.32 c_{33} : 2.76 c_{44} : 1.35	$\varepsilon(0)_{\parallel}$: 9.97 $\varepsilon(0)_{\perp}$: 21.47 $\varepsilon(\infty)_{\parallel}$: 9.42 $\varepsilon(\infty)_{\perp}$: 10.7	$E_{g,ind}$: 0.97 1.16 $E_{g,dir}$: 1.62 1.28	300 (6H) 300 (6H)		$\mu_{n\perp}$: 30	
PbO_2	rutile D^{14}_{4h} - $P4_2/nmm$	a : 4.933 c : 3.360 u : ≅ 0.3			$E_{g,opt}$: 4.45	300		μ_n : ≅ 1 n : ≅ 10^{19} ··· 10^{21}	

4.13.3 IV_2-VI_3 compounds

For Si_2Te_3 two structures have been proposed (Fig. 117, p. 283). Sn_2S_3 and Pb_2S_3 crystallize in an orthorhombic lattice (Fig. 118, p. 283), $SnGeS_3$ and $PbGeS_3$ in a monoclinic structure (Fig. 119, p. 283).

Si_2Te_3	C^4_{3v} - P31c		d : 4.5 T_m : 1165		$E_{g,ind}$: 1.0 or 1.8 $E_{g,dir}$: 2.03 ··· 2.18		$m_{n,p\parallel}$: 5.4	$\mu_{p\parallel}$:	$2\cdot10^{-3}$
Sn_2S_3	D^{16}_{2h} - Pnam	a : 8.864 b : 14.020 c : 3.747	d : 4.87	$\varepsilon(0)_{\parallel a}$: 16.1 $\varepsilon(0)_{\parallel b}$: 17.7 $\varepsilon(0)_{\parallel c}$: 21.8 $\varepsilon(\infty)_{\parallel a}$: 8.8 $\varepsilon(\infty)_{\parallel b}$: 7.0 $\varepsilon(\infty)_{\parallel c}$: 8.5	$E_{g,opt}$: 0.95 $E_{g,th}$: 0.85	300			

Substance	Structure	Static and dynamical lattice parameters			Band structure parameters		
		a, b, c [Å]	d [g cm^{-3}]	$\varepsilon(0), \varepsilon(\infty)$	E_g [eV]	at T [K]	
		β	T_m [K]	ν [THz]			
			c_{ik} [10^{11}dyn cm^{-2}]				
$PbSnS_3$	D^{16}_{2h} - Pnam	a : 8.91	d : 5.64		$E_{g,opt}$:	1.05	300
		b : 14.18			$E_{g,th}$:	0.9	
		c : 3.88					
$SnGeS_3$	monoclinic	a : 7.269	d : 4.85		$E_{g,opt}$:	2.23	300
	C^5_{2h} - $P2_1/c$	b : 10.220					
		c : 6.873					
		β : 105.45°					
$PbGeS_3$	same structure	a : 7.27	d : 3.71		$E_{g,opt}$:	2.4	300
		b : 10.50					
		c : 6.88					
		β : 105.0°					

4.14 IV-VII$_2$ compounds

From the group IV dihalides only the Pb compounds are known as semiconductors. PbI crystallizes in the CdI_2 structure (Fig. 73, p. 268). Fig. 120 (p. 284) shows the band structure of PbI_2.

PbF_2	β-phase : cubic	a : 5.940	d : 7.659	$\varepsilon(0)$: 29.30	E_{gx} :	5.68	4.2
	O^5_h		T_m : 1128	$\varepsilon(\infty)$: 3.120		5.71	78
			c_{11} : 9.34	ν_{TO} : 3.06			
			c_{12} : 4.40	ν_{LO} : 10.11			
			c_{44} : 2.10				

Substance	Structure	Static and dynamical lattice parameters			Band structure parameters			Transport parameters
		a, b, c [Å]	d [g cm^{-3}] T_m [K] c_{ik} [10^{11}dyn cm^{-2}]	$\varepsilon(0), \varepsilon(\infty)$	E_g [eV] at T [K]	m [m_o]		μ [cm^2/Vs]
$PbCl_2$	orthorhombic V^{16}_{2h}	a : 9.030 b : 7.608 c : 4.525	d : 5.85 T_m : 874		$E_{gx,dir \parallel a}$: 4.690 78 $E_{gx,dir \parallel b}$: 4.710 78 $E_{gx,dir \parallel c}$: 4.650 78 E_b : 0.170 5			
$PbBr_2$	orthorhombic V^{16}_{2h}	a : 9.466 b : 8.068 c : 4.767	d : 6.66 T_m : 646		$E_{gx,dir \parallel a}$: 3.955 78 $E_{gx,dir \parallel b}$: 3.975 78 $E_{gx,dir \parallel c}$: 3.935 78			
PbI_2	hexagonal D^3_{3d}	2H : a : 4.557 c : 6.979 4H : a : 4.557 c : 13.958	d : 6.16 T_m : 675	$\varepsilon(0)_{\parallel}$: 9.3 $\varepsilon(0)_{\perp}$: 26.4 $\varepsilon(\infty)_{\parallel}$: 5.9 $\varepsilon(\infty)_{\perp}$: 6.1	$E_{g,dir \perp}$: 2.552 4.2 $E_{g,dir \perp}$: 2.562 4.2	$m_{n\parallel}$: 1.25 $m_{n\perp}$: 0.25 $m_{p\parallel}$: 1.1 $m_{p\perp}$: 1.1	$\mu_{n\parallel}$: 8 $\mu_{p\parallel}$: 2

4.15 V_x-VI_y compounds

Most semiconductors of this group have the composition V_2-VI_3. Only one other compound, As_4S_4 (realgar) is known as semiconductor.

The following structures are predominant:
tetradymite: Sb_2Te_3, Bi_2Se_3, Bi_2Te_3 (Fig. 121, p. 284), Sb_2S_3 structure: Sb_2S_3, Sb_2Se_3, Bi_2S_3 (Fig. 122, p. 284), claudetite: As_2O_3 (Fig. 123, p. 285), orpiment: As_2S_3, As_2Se_3 (Fig. 124, p. 285), orthorhombic valentinite: Sb_2O_3 (Fig. 125, p. 285), monoclinic : As_2Te_3 (Fig. 126, p. 286), tetragonal: β-Bi_2O_3 (Fig. 127, p. 286).

Substance	Structure	Static and dynamical lattice parameters			Band structure parameters				Transport parameters
		a, b, c [Å]	d [g cm^{-3}]	$\varepsilon(0), \varepsilon(\infty)$	E_g, Δ [eV]	at T [K]	m [m_o]		μ [cm^2/Vs]
		β	T_m [K]						ρ [Ωm]

Typical band structures are shown in Fig. 128 (As_2Se_3, p. 286), Fig. 129 (Sb_2S_3, p. 287) and Fig. 130 (Bi_2Te_3, p. 287).

Only some optical properties are known quantitatively for the high gap semiconductors As_2O_3 and Sb_2O_3.

As_2S_3	monoclinic	a: 11.475	T_m: 585	$\varepsilon(0)_{\parallel a}$: 12.1	$E_{g,dir}$: 2.6	300			$\mu_{n,dr}$: 1
	C^5_{2h} - $P2_1/n$	b: 9.577		$\varepsilon(0)_{\parallel b}$: 10.7	$E_{g,th}$: 2.78				$\rho_\perp$: $3 \cdot 10^{15}$
		c: 4.256		$\varepsilon(0)_{\parallel c}$: 5.9					
		β: 90°41'		$\varepsilon(\infty)_{\parallel a}$: 8.8					
				$\varepsilon(\infty)_{\parallel b}$: 7.0					
				$\varepsilon(\infty)_{\parallel c}$: 5.7					
As_2Se_3	monoclinic	a: 12.053	T_m: 650		$E_{g,dir}$: 1.85	300			$\mu_{n \parallel b}$: 20 ··· 80
	C^5_{2h} - $P2_1/n$	b: 9.890			$E_{g,th}$: 2.01				$\rho_{\parallel b}$: $\cong 10^{12}$
		c: 4.277			Δ_{cb}: $\cong$ 0.015				
		β: 90°28'			Δ_{so}: $\cong$ 0.040				
As_2Te_3	monoclinic	a: 14.339	T_m: 648		E_g: 0.9	> 500	m_n: 0.36		μ_n: 170
	C^3_{2h} - C2/m	b: 4.006					m_p: 0.50		μ_p: 80
		c: 9.873							
		β: 95.0°							
Sb_2S_3	orthorhombic	a: 11.299	d: 4.60	$\varepsilon(0)_{\parallel}$: 180	$E_{g,dir \parallel a}$: 1.88	300			
	D^{16}_{2h} - Pnam	b: 11.310	T_m: 823	$\varepsilon(0)_\perp$: 22					
	or C^9_{2v} - $Pna2_1$	c: 3.8389		$\varepsilon(\infty)_{\parallel}$: 9.5					
				$\varepsilon(\infty)_\perp$: 7.2					

Substance	Structure	Static and dynamical lattice parameters a, b, c [Å] β	 d [g cm^{-3}] T_m [K]	 $\varepsilon(0), \varepsilon(\infty)$	Band structure parameters E_g [eV]	 at T [K]	 m [m_o]	Transport parameters μ [cm^2/Vs] n [cm^{-3}]
Sb_2Se_3	orthorhombic D^{16}_{2h} - Pnam or C^9_{2v} - $Pna2_1$	a : 11.62 b : 11.77 c : 3.962	T_m : 885	$\varepsilon(0)_{\parallel}$: 133 $\varepsilon(\infty)_{\parallel}$: 15.1 $\varepsilon(\infty)_{\perp}$: 14.5	$E_{g,ind \parallel a}$: 1.11 $E_{g,ind \parallel c}$: 1.11 $E_{g,ind \perp c}$: 1.13 $E_{g,dir \perp b}$: $\cong$ 1 $E_{g,th}$: 1.08 ··· 1.32	293 293 293 300		μ_n : 15 μ_p : 42
Sb_2Te_3	trigonal D^5_{3d} - R 3m	a_{hex} : 4.25 c_{hex} : 30.35	d : 6.505 T_m : 894	$\varepsilon(0)_{\parallel}$: 36.5 $\varepsilon(0)_{\perp}$: 168 $\varepsilon(\infty)_{\parallel}$: 32.5 $\varepsilon(\infty)_{\perp}$: 51	$E_{g,opt \perp}$: 0.21 ··· 0.28	299		$\mu_{p \perp c}$: 270 $\mu_{p \parallel c}$: 31
Bi_2O_3	α-phase : monoclinic C^5_{2h} - $P2_1/c$	a : 5.848 b : 8.166 c : 7.510 β : 113.0°	d : 8.929 T_m : 1090		$E_{g,opt}$: 3.1 2.85 $E_{g,th}$: 1.6	77 300		
	β-phase : tetragonal D^4_{2d} - P 42_1c	a : 7.743 c : 5.631			$E_{g,opt}$: 2.8 2.6 $E_{g,th}$: 1.6	77 300		
Bi_2S_3	orthorhombic D^{16}_{2h} - Pnam or C^9_{2v} - $Pna2_1$	a : 11.150 b : 11.300 c : 3.981	d : 6.81 T_m : 1036	$\varepsilon(0)_{\parallel}$: 120 $\varepsilon(0)_{\perp}$: 38 $\varepsilon(\infty)_{\parallel}$: 13 $\varepsilon(\infty)_{\perp}$: 9	$E_{g,opt \parallel}$: 1.45 1.3 $E_{g,th}$: 1.0	77 300		μ_n : 200 n : $3 \cdot 10^{18}$

Substance	Structure	Static and dynamical lattice parameters			Band structure parameters			Transport parameters
		a, b, c [Å]	d [g cm^{-3}]	$\varepsilon(0), \varepsilon(\infty)$	E_g [eV]	at T [K]	m [m_o]	μ [cm^2/Vs]
		β	T_m [K]					
			c_{ik} [10^{11}dyn cm^{-2}]					
Bi_2Se_3	trigonal	a_{hex} : 4.138	d : 7.68	$\varepsilon(0)_\perp$: 113	$E_{g,dir\perp}$: 0.160	77	$m_{n,ds}$: 0.155	$\mu_{n,H}$: 690
	D^5_{3d} - R $\bar{3}$m	c_{hex} : 2.64	T_m : 979	$\varepsilon(\infty)_\perp$: 29	$E_{g,th}$: 0.160		m_p : 0.125	$\mu_{p,H}$: 42
Bi_2Te_3	trigonal	a_{hex} : 4.384	d : 7.86	$\varepsilon(0)_\parallel$: 75	$E_{g,ind\perp}$: 0.13	293	m_n : 0.32	$\mu_{n\perp}$: 18
	D^5_{3d} - R $\bar{3}$m	c_{hex} : 30.487	T_m : 858	$\varepsilon(0)_\perp$: 290	$E_{g,th}$: 0.16		m_p : 0.46	$\mu_{p\perp}$: 5.1
			c_{11} : 6.847	$\varepsilon(\infty)_\parallel$: 50				at 77 K
			c_{13} : 2.704	$\varepsilon(\infty)_\perp$: 85				
			c_{14} : 1.325					
			c_{33} : 4.768					
			c_{44} : 2.738					
			c_{66} : 2.335					
As_4S_4	molecular lattice	a : 9.325	d : 3.506		E_g : 2.40			$\mu_{n,dr}$: 0.02
	C^5_{2h} - $P2_1/n$	b : 13.571	T_m : 580					$\mu_{p,dr}$: 12
	(4 molecules in unit cell)	c : 6.587						
		β : 106°23'						

4.16 V-VII$_3$ compounds

AsI_3, SbI_3 and BiI_3 form layer lattices with octahedral coordination (Fig. 131, p. 288) similar to the CdI_2 lattice.

Fig. 132 (p. 288) shows the band structure of BiI_3.

Substance	Structure	Static and dynamical lattice parameters a, c [Å]	d [g cm^{-3}] T_m [K]	$\varepsilon(0), \varepsilon(\infty)$	Band structure parameters E_g [eV]	at T [K]	Transport parameters ρ [Ωm]
AsI_3	layer structure C^2_{3i} - R $\bar{3}$	a_{hex} : 7.20 c_{hex} : 21.43	d : 4.688 T_m : 414	$\varepsilon(0)_{\parallel}$: 4.7 $\varepsilon(0)_{\perp}$: 7.9 $\varepsilon(\infty)_{\parallel}$: 3.9 $\varepsilon(\infty)_{\perp}$: 4.8	$E_{g,dir}$: 2.47	90	
SbI_3	layer structure C^2_{3i} - R $\bar{3}$	a_{hex} : 7.48 c_{hex} : 20.90	d : 4.848 T_m : 443	$\varepsilon(0)_{\parallel}$: 8.9 $\varepsilon(0)_{\perp}$: 16.0 $\varepsilon(\infty)_{\parallel}$: 4.4 $\varepsilon(\infty)_{\perp}$: 5.3	$E_{g,dir}$: 2.41	90	$\rho_{\perp}$: $\cong 10^9$
BiI_3	layer structure D^5_{3d} - R $\bar{3}$m	a_{hex} : 7.51 c_{hex} : 20.71	d : 5.64 T_m : 673	$\varepsilon(0)_{\parallel}$: 8.6 $\varepsilon(0)_{\perp}$: 54 $\varepsilon(\infty)_{\parallel}$: 6.4 $\varepsilon(\infty)_{\perp}$: 7.1	$E_{g,dir}$: 2.00	90	$\rho_{\perp}$: $10^8 \ldots 10^9$

Substance	Structure	Static and dynamical lattice parameters			Band structure parameters	
		a, b, c [Å]	T_m [K]	ν [THz]	E_g [eV]	at T [K]
		γ				

5 Ternary compounds

In this chapter data on the most important groups of ternary (and a few quaternary) semiconductors will be presented. Ternary transition metal and rare earth compounds are dealt with in chapter 6. Chapter 4 already contains those ternary compounds, where two of the three partners belong to the same group (e. g. III-III-VI compounds are presented in the section on III_x-VI_y compounds).

5.1 Tetrahedrally bonded ternary and quasi-binary compounds

The compounds presented in this subchapter all obey the so-called Grimm-Sommerfeld rule: that the average number of valence electrons per atom is four in a tetrahedral structure. Compounds of this type generally adopt structures related to the zincblende or wurtzite structures (Figs. 33 and 34, p. 256). The most important crystal lattices occuring are the chalcopyrite lattice (Fig. 133, p. 289), the defect stannite and defect chalcopyrite lattices (Figs. 134 and 135, p. 289) and the spinel lattice (Fig. 136, p. 289). Since the unit cell of the chalcopyrite lattice is twice as large as the corresponding unit cell of the zincblende lattice, its Brillouin zone (Fig. 137, p. 289) has half the volume as that of the corresponding one (Fig. 36, p. 256).

5.1.1 III_2-VI_3 compounds

III_2-VI_3 compounds generally form tetrahedral structures since when vacancies are counted as zero valent atoms, they obey the Grimm-Sommerfeld rule: vac-III_2-VI_3 = $(1\times0 + 2\times3 + 3\times6)/6 = 4$. Important structures occuring in this group are shown in Fig. 138 (α-Ga_2S_3, p. 289), Fig. 139 (β-In_2S_3, p. 290) and Fig. 140 (α-In_2Te_3-II, p. 290).
No semiconducting properties have been reported for the sulfides, selenides and tellurides of Al and Tl, whereas the gallium and indium chalcogenides show at least in some modifications semiconducting behavior.

Ga_2S_3	α-phase :	a : 11.094	T_m : 1360	ν_{TO} :	9.72	$E_{g,opt}$:	3.438	1.6
	wurtzite-type	b : 9.578			10.44		3.424	77
	C^4_s - Bb	c : 6.395						
	ordered vacancies	γ : 141°15'						

Substance	Structure	Static and dynamical lattice parameters			Band structure parameters			Transport parameters	
		a, c [Å]	d [g cm^{-3}]	$\varepsilon(0), \varepsilon(\infty)$	E_g [eV]	at T [K]		μ [cm^2/Vs]	
			T_m [K]	ν [THz]				ρ [Ωm]	
Ga_2S_3 (cont.)	β-phase : wurtzite-type C^4_{6v} - $P6_3mc$ disordered vacancies	a : 3.678 c : 6.016			$E_{g,opt}$:	2.6 ··· 2.9 2.5 ··· 2.7	77.3 290		
Ga_2Se_3	β-phase : zincblende type D^{20}_{4h} - $I4_1/acd$ ordered vacancies	a : 23.235 c : 10.828	d : 4.91 T_m : 1005		$E_{g,dir}$: $E_{g,ind}$:	2.1 ··· 2.2 1.9 ··· 2.1 2.04 1.96	77.3 290 77 300		
Ga_2Te_3	zincblende type T^2_d - F 43m disordered vacancies	a : 5.899	d : 5.57 T_m : 1063		$E_{g,opt}$: $E_{g,th}$:	1.22 1.55	273	ρ :	10 ··· 10^7
In_2S_3	β-phase : ordered defect spinel D^{19}_{4h} - $I4_1/amd$	a : 7.618 c : 32.33	d : 4.613 T_m : 1363		$E_{g,ind}$: $E_{g,dir}$: $E_{g,th}$:	1.1 2.03 2.30	300 300	ρ :	10^3 ... 10^7
	γ-phase : layered structure S close packed In octahedral D^3_{3d} - P 3m1	a : 3.8 c : 9.04	d : 4.75 ··· 4.80 depending on As or Sb doping needed for RT stabilization	$\varepsilon(0)$: 13.5 $\varepsilon(\infty)$: 6.5	$E_{g,opt}$: $E_{g,th}$: $E_{g,opt}$: $E_{g,th}$:	1.88 1.38 1.44 1.42	300 (As-doped) 300 (Sb-doped)	ρ : ρ :	$9 \cdot 10^7$ $3 \cdot 10^4$
In_2Se_3	layered structure many phases α- and β-phases stable ar RT	a : 4.025 c : 9.6 ··· 28.5 depending on stacking order	T_m : 1163	$\varepsilon(0)$: 16.68 $\varepsilon(\infty)$: 9.53 ν_{TO} : 2.723 ν_{LO} : 2.835	$E_{g\perp}$: $E_{g,th}$:	1.2 ··· 1.5 1.41	300	μ_n :	10

Substance	Structure	Static and dynamical lattice parameters			Band structure parameters			Transport parameters
		a, b, c [Å]	d [g cm^{-3}]	$\varepsilon(0), \varepsilon(\infty)$	E_g, Δ [eV]	at T [K]	m [m_o]	μ [cm^2/Vs]
			T_m [K]	ν [THz]				ρ [Ωm]
								n_i [cm^{-3}]
In_2Te_3	α-phase :	I :						
	zincblende-type	a : 6.173	T_m : 940	$\varepsilon(0)$: 16	$E_{g,opt}$: 0.92 ··· 1.15		m_n : 0.70	μ_n : 5 ··· 70
	ordered vacancies	c : 12.438			$E_{g,th}$: 1.02 ··· 1.55		m_p : 1.23	n_i : ≅ 7·10^{12}
	I : D^{11}_{2d} - I 42m	II :						
	II : C^{20}_{2v} - Imm2	a : 4.358			no remarkable differences			
		b : 13.07			for α- and β-phases			
		c : 6.163						
	β-phase :	a : 6.163	d : 5.73					
	as Ga_2Te_3							

5.1.2 I-III-VI$_2$ compounds

Nearly all I-III-VI$_2$ compounds adopt at RT the chalcopyrite structure (Fig. 133, p. 289).

Fig. 137 (p. 289) and Fig. 141 (p. 290) show the Brillouin zone and general features of the band structure of chalcopyrite type compounds. Figs. 142 ··· 147 (p. 291) give examples of such band structures for six members of this group including crystal field splitting but neglecting spin-orbit splitting. The crystal field interaction leads to a splitting of the top of the valence band into two edges (Δ_{cf}), spin-orbit coupling to a further splitting (Δ_{so}) leading to three valence band edges. The energy gaps from these three edges to the conduction band edge are designed in the following by A, B and C.

$CuAlS_2$	chalcopyrite	a : 5.32	d : 3.45	ν_{TO} : 13.4	$E_{g,dir}$:	3.49	(A) 300		ρ :	10^2 ··· 10^8
	D^{12}_{2d} - I 42d	c : 10.430	T_m : 1570	ν_{LO} : 12.5		3.62	(B,C) 300			
					Δ_{cf} :	- 0.13	300			
					Δ_{so} :	0	300			

Substance	Structure	Static and dynamical lattice parameters			Band structure parameters			Transport parameters	
		a, c [Å]	d [g cm^{-3}]	$\varepsilon(0), \varepsilon(\infty)$	E_g, Δ [eV]	at T [K]	m [m_o]	μ [cm^2/Vs]	
			T_m [K]	ν [THz]				ρ [Ωm]	
								p [cm^{-3}]	
$CuAlSe_2$	chalcopyrite	a: 5.61	d: 4.69		$E_{g,dir}$:	2.72	(A) 78		
	D^{12}_{2d} - I 42d	c: 10.92	T_m: 1470			2.86	(B) 78		
						3.01	(C) 78		
					Δ_{cf}:	- 0.17	78		
					Δ_{so}:	0.18			
$CuAlTe_2$	chalcopyrite	a: 5.96	d: 5.47		$E_{g,dir}$:	2.06	(A) 300		
	D^{12}_{2d} - I 42d	c: 11.77							
$CuGaS_2$	chalcopyrite	a: 5.35	d: 4.38	$\varepsilon(0)_{\parallel}$: 7.6	$E_{g,dir}$:	2.43	(A) 300	m_n: 0.13	μ_p: 15
	D^{12}_{2d} - I 42d	c: 10.46	T_m: 1550	$\varepsilon(0)_{\perp}$: 8.9		2.502	(A) 77	m_p: 0.69	p: $4\cdot10^{17}$
				$\varepsilon(\infty)_{\parallel}$: 6.1		2.627	(B) 77		ρ: 1
				$\varepsilon(\infty)_{\perp}$: 6.2		2.638	(C) 77		
				ν_{TO}: 11.0	Δ_{cf}:	- 0.13	77		
				ν_{LO}: 11.8	Δ_{so}:	- 0.017	77		
$CuGaSe_2$	chalcopyrite	a: 5.61	d: 5.57	ν_{TO}: 7.62	$E_{g,dir}$:	1.68	(A) 300		μ_p: 60
	D^{12}_{2d} - I 42d	c: 11.00	T_m: 1310	ν_{LO}: 8.34		1.75	(B) 300		p: $3\cdot10^{17}$
			··· 1340			1.96	(C) 300		ρ: 0.4
					Δ_{cf}:	- 0.09	300		
					Δ_{so}:	0.231	300		
$CuGaTe_2$	chalcopyrite	a: 6.00	d: 5.95	ν: 6.27	$E_{g,dir}$:	1.227	(A) 300		μ_p: 50
	D^{12}_{2d} - I 42d	c: 11.93	T_m: 1140			1.280	(B) 300		p: 10^{18}
						1.97	(C) 300		
					Δ_{cf}:	- 0.08	300		
					Δ_{so}:	0.71	300		

Substance	Structure	Static and dynamical lattice parameters			Band structure parameters				Transport parameters
		a, c [Å]	d [g cm^{-3}]	$\varepsilon(0), \varepsilon(\infty)$	E_g, Δ [eV]	at T [K]		m [m_o]	μ [cm^2/Vs]
			T_m [K]	ν [THz]					n, p [cm^{-3}]
$CuInS_2$	chalcopyrite	a : 5.52	d : 4.74	ν_{TO} : 9.69	$E_{g,dir}$:	1.53	(A,B,C)	m_p : 1.3	μ_n : 1 ··· 240
	D^{12}_{2d} - I 42d	c : 11.08	T_m : 1270	ν_{LO} : 10.56			300		n : $4\cdot10^{12}$ ··· 10^{19}
			··· 1320		Δ_{cf} :	> - 0.005			μ_p : 0.2 ··· 95
					Δ_{so} :	- 0.02			p : 10^{13} ··· 10^{17}
					$E_{g,th}$:	1.62			
$CuInSe_2$	chalcopyrite	a : 5.78	d : 5.77	$\varepsilon(0)_{\parallel}$: 15.2	$E_{g,dir}$:	1.04	(A,B) 77	m_n : 0.09	μ_n : 1 ··· 1150
	D^{12}_{2d} - I 42d	c : 11.55	T_m : 1260	$\varepsilon(0)_{\perp}$: 16.0		1.27	(C) 77	m_p : 0.09	n : $2.6\cdot10^{15}$
				$\varepsilon(\infty)_{\parallel}$: 8.5	Δ_{cf} :	0.006	77		··· $3\cdot10^{17}$
				$\varepsilon(\infty)_{\perp}$: 9.5	Δ_{so} :	0.23	77		μ_p : 1 ··· 200
									p : 10^{16} ··· 10^{18}
$CuInTe_2$	chalcopyrite	a : 6.17	d : 6.10	$\varepsilon(0)_{\parallel}$: 12.9	$E_{g,dir}$:	1.064	(A,B) 290	$m_{p\parallel}$: 0.66	μ_p : 120 ··· 150
	D^{12}_{2d} - I 42d	c : 12.34	T_m : 1050	$\varepsilon(0)_{\perp}$: 10.5		1.67	(C) 290	$m_{p\perp}$: 0.85	ρ : $3.5\cdot10^{-3}$
				$\varepsilon(\infty)_{\parallel}$: 8.7	Δ_{cf} :	0	290		
				$\varepsilon(\infty)_{\perp}$: 11.0	Δ_{so} :	0.61	290		
				ν_{TO} : 5.0					
				ν_{LO} : 5.4					
$CuTlS_2$	chalcopyrite	a : 5.58	d : 6.13		E_g :	1.39	estimated		
	D^{12}_{2d} - I 42d	c : 11.16							
$AgAlTe_2$	chalcopyrite	a : 6.30	d : 6.15		$E_{g,dir}$:	2.27	(A) 300		
	D^{12}_{2d} - I 42d	c : 11.84							

Substance	Structure	Static and dynamical lattice parameters			Band structure parameters			Transport parameters
		a, b, c [Å]	d [g cm^{-3}]	$\varepsilon(0), \varepsilon(\infty)$	E_g, Δ [eV]	at T [K]		ρ [Ωm]
			T_m [K]	ν [THz]				
$AgGaS_2$	chalcopyrite	a: 5.75	d: 4.70	$\varepsilon(0)_{\parallel}$: 8.21	$E_{g,dir}$:	2.638	300	ρ: 10^8
	D^{12}_{2d} - I 42d	c: 10.29	T_m: 1220	$\varepsilon(0)_{\perp}$: 8.51		2.73	(A) 77	
			··· 1320	$\varepsilon(\infty)_{\parallel}$: 5.50		3.01	(B,C) 77	
				$\varepsilon(\infty)_{\perp}$: 5.90	Δ_{cf}:	- 0.28	77	
				ν_{TO}: 11.0	Δ_{so}:	0	77	
				ν_{LO}: 11.8				
$AgGaSe_2$	chalcopyrite	a: 5.98	d: 5.70	$\varepsilon(0)_{\parallel}$: 10.48	$E_{g,dir}$:	1.80	300	ρ: 10^5
	D^{12}_{2d} - I 42d	c: 10.88	T_m: 1130	$\varepsilon(0)_{\perp}$: 9.05		1.83	(A) 77	
				$\varepsilon(\infty)_{\parallel}$: 6.95		2.02	(B) 77	
				$\varepsilon(\infty)_{\perp}$: 6.80		2.29	(C) 77	
				ν_{TO}: 7.44	Δ_{cf}:	- 0.25	77	
				ν_{LO}: 8.22	Δ_{so}:	0.31	77	
$AgGaTe_2$	chalcopyrite	a: 6.29	d: 6.08	$\varepsilon(0)_{\parallel}$: 14.5	$E_{g,dir}$:	1.32	300	
	D^{12}_{2d} - I 42d	c: 11.95	T_m: 950	$\varepsilon(0)_{\perp}$: 15.0				
				$\varepsilon(\infty)_{\parallel}$: 11.0				
				$\varepsilon(\infty)_{\perp}$: 11.86				
				ν_{TO}: 6.12				
				ν_{LO}: 6.63				
$AgInS_2$	chalcopyrite	a: 5.82	d: 4.97		$E_{g,dir}$:	1.87	(A) 300	
	phase	c: 11.17	T_m: 1150			2.02	(B,C) 300	
	D^{12}_{2d} - I 42d				Δ_{cf}:	- 0.15	300	
	orthorhombic	a: 6.954			$E_{g,dir}$:	2.081	(A) 300	
	phase	b: 8.264				2.144	(B) 300	
	wurtzite-type	c: 6.683				2.168	(C) 300	

Substance	Structure	Static and dynamical lattice parameters			Band structure parameters			Transport parameters	
		a, c [Å]	d [g cm^{-3}]	$\varepsilon(0)$, $\varepsilon(\infty)$	E_g, Δ [eV]		at T [K]	μ [cm^2/Vs]	
			T_m [K]					σ [Ω^{-1}cm^{-1}]	
								n [cm^{-3}]	
$AgInSe_2$	chalcopyrite	a : 6.095	d : 5.82	$\varepsilon(0)_{\parallel}$: 10.73	$E_{g,dir}$:	1.24	(A) 300	μ_n :	750
	D^{12}_{2d} - I 42d	c : 11.69	T_m : 1055	$\varepsilon(0)_{\perp}$: 11.94		1.33	(B) 300	n :	$8 \cdot 10^{11}$
				$\varepsilon(\infty)_{\parallel}$: 7.16		1.60	(C) 300	σ :	10^{-4}
				$\varepsilon(\infty)_{\perp}$: 7.20	Δ_{cf} :	- 0.12	300		
					Δ_{so} :	0.30	300		
$AgInTe_2$	chalcopyrite	a : 6.43	d : 1.96	$\varepsilon(0)_{\parallel}$: 7.68	$E_{g,dir}$:	1.12	300		
	D^{12}_{2d} - I 42d	c : 12.59	T_m : 960	$\varepsilon(0)_{\perp}$: 8.10	$E_{g,ind}$:	0.99	300		
				$\varepsilon(\infty)_{\parallel}$: 6.38	$E_{g,th}$:	0.95			
				$\varepsilon(\infty)_{\perp}$: 6.48					
These are a few data available on the mineral chalcopyrite ($CuFeS_2$, band structure: Fig. 148, p. 293) and related compounds :									
$CuFeS_2$	chalcopyrite	a : 5.29	T_m : 1120					μ_p :	30
	D^{12}_{2d} - I 42d	c : 10.41	··· 1150					σ :	100
$CuFeSe_2$			T_m : 850					μ_p :	20
								σ :	700
$CuFeTe_2$			T_m : 1015					μ_p :	50
								σ :	400
$AgFeSe_2$	tetragonal	a : 6.58	T_m : 1009					μ_n :	250
		c : 8.96						σ :	1500
$AgFeTe_2$			T_m : 953					μ_n :	2000
								σ :	700

Substance	Structure	Static and dynamical lattice parameters			Band structure parameters			Transport parameters	
		a, c [Å]	d [g cm^{-3}]	$\varepsilon(0), \varepsilon(\infty)$	E_g, Δ [eV]	at T [K]	m [m_o]	μ [cm^2/Vs]	
			T_m [K]	ν [THz]				ρ [Ωm]	
								n, p [cm^{-3}]	

5.1.3 II-IV-V_2 compounds

Almost all II-IV-V_2 compounds take the chalcopyrite structure. In these compounds one pecularity of the band structure must be mentioned: By the folding of the zincblende Brillouin zone to the smaller chalcopyrite Brillouin zone (Fig. 137, p. 288) transitions, which are indirect in the band structure of the corresponding III-V compound (especially Γ - X transitions) become formally direct. Such transitions are called pseudodirect ($E_{g,pseu}$). Figs. 149 ··· 153 (p. 292 ··· 294) show band structures of some of the II-IV-V_2 compounds ($ZnSiAs_2$, $ZnGeP_2$, $CdSiP_2$, $CdSnP_2$, $CdSnAs_2$).

$MgSiP_2$	chalcopyrite	a: 5.72			$E_{g,pseu}$:	2.03	300			ρ:	$10 \cdots 10^4$
	D^{12}_{2d} - I 42d	c: 10.12			$E_{g,ind}$:	2.26	300				
					$E_{g,dir}$:	2.82	300				
					Δ_{cf}:	- 0.08					
					Δ_{so}:	0.16	300				
$ZnSiP_2$	chalcopyrite	a: 5.400	d: 3.35	$\varepsilon(0)_{\parallel}$: 11.15	$E_{g,pseu}$:	2.07	300	m_n:	0.11	μ_n:	$70 \cdots 100$
	D^{12}_{2d} - I 42d	c: 10.438	T_m: 1520	$\varepsilon(0)_{\perp}$: 11.7	$E_{g,dir}$:	2.96	300	m_p:	0.4	n:	10^{17}
			$\cdots$ 1640	$\varepsilon(\infty)_{\parallel}$: 9.68	Δ_{cf}:	- 0.12	300	m_p:	4 ··· 11		
				$\varepsilon(\infty)_{\perp}$: 9.26	Δ_{so}:	0.06	300			p:	$6 \cdot 10^{13}$
				ν_{TO}: 14.8							$\cdots 3 \cdot 10^{14}$
				ν_{LO}: 15.5							
$ZnSiAs_2$	chalcopyrite	a: 5.606	d: 4.69	ν_{TO}: 12.2	$E_{g,pseu}$:	1.74	300			μ_n:	40
	D^{12}_{2d} - I 42d	c: 10.886	T_m: 1370	ν_{LO}: 12.5	$E_{g,dir}$:	2.13	(A) 300			n:	10^9
						2.23	(B) 300			μ_p:	100
						2.69	(C) 300			p:	$8.2 \cdot 10^{14}$
					Δ_{cf}:	- 0.13	300				
					Δ_{so}:	0.286	300				

Substance	Structure	Static and dynamical lattice parameters			Band structure parameters				Transport parameters	
		a, b, c [Å]	d [g cm^{-3}]	$\varepsilon(0), \varepsilon(\infty)$	E_g, Δ [eV]	at T [K]	m [m_o]		μ [cm^2/Vs]	
		β	T_m, T_{perit} [K]	ν [THz]					n, p [cm^{-3}]	
$ZnGeN_2$	monoclinic	a : 3.167			$E_{g,opt}$:	2.67	300		μ_n :	0.5 ··· 5
	wurtzite-type	b : 5.194							n :	10^{18} ··· 10^{19}
		c : 3.167								
		β : 118°53'								
$ZnGeP_2$	chalcopyrite	a : 5.463	d : 4.04	ε_{11} : 15	$E_{g,pseu}$:	2.05	300		μ_p :	20
	D^{12}_{2d} - I 42d	c : 10.74	T_m : 1300	ε_{33} : 12	$E_{g,dir}$:	2.365	(A) 300		p :	≅ 10^{11}
				ν_{TO} : 11.97		2.43	(B) 300			
				ν_{LO} : 12.24		2.50	(C) 300			
					Δ_{cf} :	- 0.08	300			
					Δ_{so} :	0.09	300			
$ZnGeAs_2$	chalcopyrite	a : 5.671	d : 5.26		$E_{g,dir}$:	1.15	(A) 300		μ_p :	20 ··· 24
	D^{12}_{2d} - I 42d	c : 11.153	T_m : 1120			1.19	(B) 300		p :	$7 \cdot 10^{18}$
			×××1145			1.48	(C) 300			··· 10^{19}
					Δ_{cf} :	- 0.06	300			
					Δ_{so} :	0.31	300			
$ZnSnP_2$	chalcopyrite	a : 5.652	T_{perit} : 1200	$\varepsilon(0)$: 10.0	$E_{g,dir}$:	1.66	(A,B) 300		μ_p :	10 ··· 60
	D^{12}_{2d} - I 42d	c : 11.305		$\varepsilon(\infty)$: 8.08		1.75	(C) 300		p :	$3 \cdot 10^{16}$
										··· 10^{17}
				ν_{LO} : 9.8 ··· 9.9	Δ_{cf} :	0	300			
					Δ_{so} :	0.09	300			
$ZnSnAs_2$	chalcopyrite	a : 5.8515	d : 5.53	$\varepsilon(0)$: 15.6	$E_{g,dir}$:	0.745	(A,B) 300	m_p : 0.35	μ_p :	80 ···
	D^{12}_{2d} - I 42d	c : 11.703	T_m : 1048			1.185	(C) 300		p :	$5 \cdot 10^{17}$
					Δ_{cf} :	≅ 0	300			··· 10^{20}
					Δ_{so} :	0.34	300			

Substance	Structure	Static and dynamical lattice parameters			Band structure parameters			Transport parameters
		a, c [Å]	d [g cm^{-3}] T_m [K]	ν [THz]	E_g, Δ [eV]	at T [K]	m [m_o]	μ [cm^2/Vs] ρ [Ωm] n, p [cm^{-3}]
$ZnSnSb_2$	chalcopyrite	a: 6.273			$E_{g,opt}$: 0.4	77	m_n: 0.025	μ_p: 70
	D^{12}_{2d} - I 42d	c: 12.546			0.7	300	m_{p2}: 0.031	p: 10^{20}
							m_{p3}: 0.25	
$CdSiP_2$	chalcopyrite	a: 5.679	d: 3.97	ν_{TO}: 14.67	$E_{g,pseu}$: 2.2	300	$m_{n\parallel}$: 1.068	μ_n: 80 ··· 150
	D^{12}_{2d} - I 42d	c: 10.431	T_m: 1390	ν_{LO}: 15.36	$E_{g,dir}$: 2.75	300	$m_{n\perp}$: 0.124	n: 10^{14} ··· 10^{15}
					2.945	(A) 90		
					2.71	(B) 90		
					2.75	(C) 90		
					Δ_{cf}: 0.20	300		
					Δ_{so}: 0.07	300		
$CdSiAs_2$	chalcopyrite	a: 5.885	T_m: > 1120		$E_{g,dir}$: 1.55	(A) 300		μ_p: 300 ··· 500
	D^{12}_{2d} - I 42d	c: 10.881			1.74	(B) 300		p: $6 \cdot 10^{15}$
					1.99	(C) 300		
					Δ_{cf}: - 0.24	300		
					Δ_{so}: 0.297	300		
$CdGeP_2$	chalcopyrite	a: 5.740	T_m: 1073	ν_{TO}: 11.52	$E_{g,dir}$: 1.72	(A) 300		μ_n: 100
	D^{12}_{2d} - I 42d	c: 10.776		ν_{LO}: 12.0	1.90	(B) 300		n: 10^{12} ··· 10^{15}
					1.99	(C) 300		μ_p: 30 ··· 60
					Δ_{cf}: - 0.2	300		ρ: 10^7 ··· $2 \cdot 10^7$
					Δ_{so}: 0.11	300		

Substance	Structure	Static and dynamical lattice parameters			Band structure parameters				Transport parameters
		a, c [Å]	d [g cm^{-3}]	$\varepsilon(0), \varepsilon(\infty)$	E_g, Δ [eV]	at T [K]		m [m_o]	μ [cm^2/Vs]
			T_m [K]	ν [THz]					n, p [cm^{-3}]
$CdGeAs_2$	chalcopyrite	a : 5.943	d : 5.6	$\varepsilon(\infty)_{\parallel}$: 15.4	$E_{g,dir}$:	0.57	(A) 300	m_n : 0.26	μ_n : 1000
	D^{12}_{2d} - I 42d	c : 11.220	T_m : 943	$\varepsilon(\infty)_{\perp}$: 15.2		0.73	(B) 300	m_p : 0.035	··· 4000
				ν_{TO} : 8.16		1.02	(C) 300		n : $4\cdot10^{16}$ ··· 10^{18}
				ν_{LO} : 8.40	Δ_{cf} :	- 0.21	300		μ_p : 140 ··· 400
					Δ_{so} :	0.33	300		p : $7\cdot10^{15}$ ··· 10^{16}
$CdSnP_2$	chalcopyrite	a : 5.901	T_m : 840	$\varepsilon(0)$: 11.8	$E_{g,dir}$:	1.17	(A) 300		μ_n : 400 ··· 2000
	D^{12}_{2d} - I 42d	c : 11.514		$\varepsilon(\infty)$: 10.0		1.25	(B) 300		n : 10^{15} ··· 10^{18}
				ν_{TO} : 11.67		1.33	(C) 300		μ_p : 90 ··· 150
				ν_{LO} : 10.59	Δ_{cf} :	- 0.10	300		p : 10^{14}
					Δ_{so} :	0.48	300		
$CdSnAs_2$	chalcopyrite	a : 6.089	d : 5.71	$\varepsilon(0)$: 12.1	$E_{g,dir}$:	0.26	(A) 300	m_n : 0.05	μ_n : 11000
	D^{12}_{2d} - I 42d	c : 11.925	T_m : 868			0.30	(B) 300		··· 15000
						0.79	(C) 300		$\mu_{p,h}$: ≅ 36
					Δ_{cf} :	- 0.06	300		$\mu_{p,l}$: ≅ 540
					Δ_{so} :	0.48	300		

5.1.4 I_2-IV-V_3 compounds

The structures of the I_2-IV-V_3 compounds are not known in detail. They generally adopt a disordered zincblende-like lattice with the tendency of superstructure formation.

Cu_2GeS_3	tetragonal	a : 5.317	d : 4.45		$E_{g,th}$:	0.3			μ_n : 3
		c : 10.438	T_m : 1220						μ_p : 360
									p : $3\cdot10^{17}$

Substance	Structure	Static and dynamical lattice parameters a, c [Å]	T_m [K]	Band structure parameters E_g [eV]	at T [K]	Transport parameters μ [cm²/Vs] p [cm⁻³]	
Cu_2GeSe_3	tetragonal	a: 5.5913 c: 10.977	T_m: 2050	$E_{g,opt}$: 0.94	293	μ_p: p:	283 $1.5 \cdot 10^{17}$
Cu_2SnS_3	disordered cubic	a: 5.445	T_m: 1120	$E_{g,opt}$: 0.91 $E_{g,th}$: 0.59	293	μ_n: n: μ_p: p:	0.5 $1.2 \cdot 10^{20}$ 605 $6.1 \cdot 10^{17}$
Cu_2SnSe_3	disordered cubic	a: 5.6877	T_m: 970	$E_{g,opt}$: 0.96 $E_{g,th}$: 0.6 ··· 0.83	293	μ_p: p:	870 $5.1 \cdot 10^{17}$
Ag_2GeSe_3			T_m: 810	$E_{g,opt}$: 0.91 $E_{g,th}$: 0.9	77	μ_p: p:	850 $2 \cdot 10^{17}$
Ag_2GeTe_3			T_m: 600	$E_{g,th}$: 0.25		μ_p: p:	720 $8 \cdot 10^{17}$
Ag_2SnSe_3			T_m: 760	$E_{g,opt}$: 0.81 $E_{g,th}$: 0.7	293	μ_p: p:	910 10^{18}
Ag_2SnTe_3	zincblende-like		T_m: 590	$E_{g,th}$: 0.08		μ_p: p:	600 $5 \cdot 10^{17}$

5.1.5 I_2-V-VI_4 compounds

Little is known about the members of this group. Two structures are predominant the enargite structure (Fig. 154, p. 294) and the famatinite structure (Fig. 155, p. 294).

Substance	Structure	Static and dynamical lattice parameters a, b, c [Å]	T_m [K]	Band structure parameters E_g [eV]		m [m_o]		Transport parameters μ [cm²/Vs] n, p [cm⁻³]	
Cu_3PS_4	enargite wurtzite like C^7_{2v} - $Pmn2_1$	a : 7.296 b : 6.319 c : 6.072		$E_{g,th}$:	2				
Cu_3AsS_4	enargite wurtzite like C^7_{2v} - $Pmn2_1$	a : 7.407 b : 6.436 c : 6.154	T_m : 931	$E_{g,opt}$: $E_{g,th}$:	1.24 0.8			μ_n : n :	0.008 $8 \cdot 10^{19}$
Cu_3AsSe_4	famatinite zinkblende like D^{11}_{2d} - $I\bar{4}2m$	a : 5.570 c : 10.957	T_m : 733	$E_{g,opt}$: $E_{g,th}$:	0.88 0.76			μ_n : n :	505 $2.7 \cdot 10^{18}$
Cu_3SbS_4	famatinite zinkblende like D^{11}_{2d} - $I\bar{4}2m$	a : 5.385 c : 10.754	T_m : 830	$E_{g,th}$:	0.46				
Cu_3SbSe_4	famatinite zinkblende like D^{11}_{2d} - $I\bar{4}2m$	a : 5.645 c : 12.275	T_m : 700	$E_{g,opt}$: $E_{g,th}$:	0.31 0.13, 0.42	m_p :	0.73	μ_p : p :	50 ··· 60 10^{19}

5.1.6 II-III$_2$-VI$_4$ compounds

These compounds can be described as quaternary compounds including vacancies : vac-II-III$_2$-VI$_4$. They fulfill the Grimm-Sommerfeld rule: $(1\times0 + 1\times2 + 2\times3 + 4\times6)/8 = 4$. Almost all compounds of this group crystallize in one of the two structures, defect stannite (Fig. 134, p. 299) and defect chalcopyrite (Fig. 135, p. 299). The layer structure of $ZnIn_2S_4$ is shown in Fig. 156 (p. 294), the structure of $CdIn_2Se_4$ in Fig. 157 (p. 294).

Two typical band structures are shown in Fig. 158 ($ZnIn_2S_4$, p. 295) and Fig.159 ($CdIn_2S_4$, p. 295).

Substance	Structure	Static and dynamical lattice parameters			Band structure parameters			Transport parameters
		a, c [Å]	d [g cm^{-3}] T_m [K]	$\varepsilon(0)$, $\varepsilon(\infty)$	E_g, Δ [eV]	at T [K]		μ [cm^2/Vs]
$ZnIn_2S_4$	more than 20 polytypes hexagonal layers	a : 3.85 c : 12.34 ··· 296.16 depending on polytype		$\varepsilon(0)_\perp$: 6.0	$E_{g,opt}$:	2.87		$\mu_{n,H}$: 20
$ZnIn_2Se_4$	defect chalcopyrite S^2_4 - I $\bar{4}$	a : 5.69 c : 11.4	d : 5.36		$E_{g,dir}$:	2.0		
$ZnIn_2Te_4$	defect chalcopyrite S^2_4 - I $\bar{4}$	a : 6.11 c : 12.2			$E_{g,ind}$: $E_{g,dir}$:	1.35 1.87		
$CdGa_2S_4$	defect chalcopyrite S^2_4 - I $\bar{4}$	a : 5.56 c : 10.0	d : 3.97	$\varepsilon(0)_\parallel$: 9.6 $\varepsilon(0)_\perp$: 12.3 $\varepsilon(\infty)_\parallel$: 6.2	$E_{g,dir}$: $E_{g,ind}$: $E_{g,th}$:	3.44 or 3.25 3.05 2.92	 293 	μ_n : 34
$CdGa_2Se_4$	defect chalcopyrite S^2_4 - I $\bar{4}$	a : 5.73 c : 10.7	d : 6.28 T_m : 1250	$\varepsilon(0)_\parallel$: 8.2 $\varepsilon(0)_\perp$: 9.7 $\varepsilon(\infty)_\parallel$: 6.2 $\varepsilon(\infty)_\perp$: 6.7	$E_{g,dir\parallel}$: $E_{g,dir\perp}$: Δ_{cf} : Δ_{so} :	2.63 2.57 0.10 0.41	293 293 293 293	μ_n : 17
$CdGa_2Te_4$	defect chalcopyrite S^2_4 - I $\bar{4}$	a : 6.08 c : 11.7	d : 5.63		$E_{g,dir}$:	1.5		

Substance	Structure	Static and dynamical lattice parameters			Band structure parameters				Transport parameters	
		a, c [Å]	d [g cm^{-3}] T_m [K] c_{ik} [10^{11}dyn cm^{-2}]	$\varepsilon(0), \varepsilon(\infty)$	E_g [eV]	at T [K]	m [m_o]		μ [cm^2/Vs] n [cm^{-3}]	
$CdIn_2S_4$	spinel type T^2_d - F $\bar{4}$3m	a : 10.818	d : 5.0 T_m : 1378 c_{11} : 12.15 c_{12} : 2.46 c_{44} : 2.54	$\varepsilon(0)$: 17 $\varepsilon(\infty)$: 10	$E_{g,ind}$: 2.11 ··· 2.28 $E_{g,dir}$: 2.47 ··· 2.62	300 300	m_n : 0.18 m_p : 0.3		μ_n : 200 n : $\cong 2 \cdot 10^{15}$	
$CdIn_2Se_4$	a-phase : tetragonal (pseudocubic) D^1_{2d} - P $\bar{4}$2m	a : 5.81 c : 5.81	d : 5.54		$E_{g,ind}$: 1.51 $E_{g,dir}$: 1.65 ··· 1.73	300 300	m_n : 0.15			
	b-phase : defect chalcopyrite S^2_4 - I $\bar{4}$	a : 5.81 c : 11.62			$E_{g,ind}$: 1.30 $E_{g,dir}$: 1.49					
$CdIn_2Te_4$	defect chalcopyrite S^2_4 - I $\bar{4}$	a : 6.19 c : 12.3	d : 5.88		$E_{g,ind}$: 1.15 $E_{g,dir}$: 1.25				μ_n : 4000 n : 10^{14}	
$CdTl_2Se_4$	hexagonal	a : 4.28 c : 6.67	T_m : 1200		E_g : 0.8	calc.				
$HgGa_2S_4$	defect chalcopyrite S^2_4 - I $\bar{4}$	a : 5.49 c : 10.2	d : 4.95		$E_{g,ind}$: 2.79 $E_{g,dir}$: 2.84	300 300				
$HgGa_2Se_4$	defect chalcopyrite S^2_4 - I $\bar{4}$	a : 5.70 c : 10.7	d : 6.10		$E_{g,opt}$: 1.95					

Substance	Structure	Static and dynamical lattice parameters			Band structure parameters			Transport parameters	
		a, c [Å]	d [g cm^{-3}] T_m [K] c_{ik} [10^{11}dyn cm^{-2}]	$\varepsilon(0)$, $\varepsilon(\infty)$	E_g [eV]	at T [K]		μ [cm^2/Vs] ρ [Ωm] n, p [cm^{-3}]	
$HgIn_2Te_4$	defect chalcopyrite S^2_4 - I $\bar{4}$ or defect stannite D^{11}_{2d} - I $\bar{4}$2m	a: 6.17 c: 12.3	d: 6.34	$\varepsilon(0)_{\parallel}$: 9.64 $\varepsilon(0)_{\perp}$: 11.06 $\varepsilon(\infty)_{\parallel}$: 8.53 $\varepsilon(\infty)_{\perp}$: 8.57	$E_{g,dir\parallel}$: 0.94 $E_{g,dir\perp}$: 0.9	300 300		μ_n: 200 n: $3.5\cdot10^{15}$	

5.1.7 Other ordered vacancy compounds

$Zn_2In_2S_5$	layered hexagonal C^5_{3v} - R 3m	a: 3.85 c: 3.086×5n (for nH-polytype)			$E_{g,dir\perp}$: 2.5 ··· 2.7	300			
$Zn_3In_2S_6$	layered hexagonal D^3_{3d} - P $\bar{3}$m1	a: 3.85 c: 18.5			$E_{g,dir\perp}$: 2.8				

The structure of this compound is shown in Fig. 160 (p. 295).

$Hg_5Ga_2Te_8$	zincblende T^2_d - F $\bar{4}$3m	a: 12.472	T_m: 970 c_{11}: 4.97 c_{12}: 3.14 c_{44}: 2.18					μ_p: 90 ρ: 170	
$Hg_3In_2Te_6$	zincblende-like T^1_d - P $\bar{4}$3m	a: 18.870	c_{11}: 5.02 c_{12}: 3.33 c_{33}: 2.08		$E_{g,th}$: 0.71			μ_p: 210 p: $7\cdot10^{12}$	

Substance	Structure	Static and dynamical lattice parameters a, b, c [Å]	Band structure parameters E_g [eV] at T [K]	Transport parameters ρ [Ωm]

5.1.8 Quaternary compounds

There are 44 compounds of the type I_2-II-IV-VI_4, which adopt one of the two structures stannite or wurtz-stannite (Fig. 161, p. 296). We concentrate on the few where data for energy gaps are available.

Cu_2ZnSiS_4	wurtz-stannite	a : 7.435 b : 6.396 c : 6.135	$E_{g,opt}$:	3.25	300	
$Cu_2ZnSiSe_4$	wurtz-stannite	a : 7.823 b : 6.720 c : 6.440	$E_{g,opt}$: $E_{g,th}$:	2.33 0.3	300	ρ : $2 \cdot 10^3$
Cu_2ZnGeS_4	wurtz-stannite	a : 7.504 b : 6.474 c : 6.185	$E_{g,opt}$: $E_{g,th}$:	2.1 0.03	300	
$Cu_2ZnGeSe_4$	stannite	a : 5.622 c : 11.06	$E_{g,opt}$: $E_{g,th}$:	1.29 0.01	300	

Further compounds for which optical energy gaps are reported :

$AgAlGeSe_4$	$E_{g,opt}$:	2.02
$AgAlSnSe_4$		1.85
$AgGaGeSe_4$		1.85
$AgGaSnSe_4$		1.70
$AgInGeSe_4$		1.58

Substance	Structure	Static and dynamical lattice parameters a [Å] d [g cm^{-3}] T_m [K]	Band structure parameters E_g [eV] at T [K]	Transport parameters ρ [W cm]
$AgInSnSe_4$			$E_{g,opt}$: 0.94	
$CuAlGeSe_4$			2.25	
$CuAlSnSe_4$			1.90	
$CuGaGeSe_4$			1.87	
$CuGaSnSe_4$			1.42	
$CuInGeSe_4$			1.26	
$CuInSnSe_4$			0.71	

5.2 Further ternary compounds

5.2.1 I_x-IV_y-VI_z compounds

Ag_8GeS_6 argyrodite	I_8-IV-VI_6 compounds are isoelectronic analogues to the II_3-V_2 compounds; they crystallize at RT in several cubic or nearly cubic phases	a : 21.19	d : 6.21 T_m : 1228	$E_{g,opt}$:	1.41 ...1.48	295	ρ :	10^3
Ag_8SnS_6 canfieldite		a : 21.43	d : 6.28 T_m : 1112	$E_{g,opt}$:	1.28 ...1.39	295	ρ :	10^3
Ag_8SiSe_6		a : 10.87	d : 6.95 T_m : 1203	$E_{g,opt}$:	0.97	295		
Ag_8GeSe_6		a : 10.95	d : 7.07 T_m : 1175	$E_{g,opt}$:	0.84 ...0.88	300		
Ag_8SnSe_6		a : 11.07	d : 7.01 T_m : 1008	$E_{g,opt}$:	0.83	295	ρ :	0.015 ...50

Substance	Structure	Static and dynamical lattice parameters a, b, c [Å]	 d [g cm^{-3}] T_m, T_{perit} [K]	Band structure parameters E_g [eV]	 at T [K]	 	Transport parameters μ [cm^2/Vs] ρ [Ωm]
Ag_8GeTe_6			d : 5.01 T_{perit} : 918	$E_{g,opt}$:	0.43 ...0.47	295	
Cu_8GeS_6		a : 9.90	d : 9.97 T_m : 1253	$E_{g,opt}$:	0.10 0.04	β'-phase γ-phase	
$Cu_4Ge_3S_5$	tetragonal	a : 5.30 c : 10.48	T_m : 948				μ_H : 10...300
$Cu_4Ge_3Se_5$	fcc	a : 5.53	T_m : 888				μ_H : 10...300
$Cu_4Sn_3Se_5$	unknown		T_m : 873				μ_H : 10...300
Cu_4SnS_4	orthorhombic	a : 13.70 b : 7.750 c : 6.454		E_g :	0.03	300	μ_p : 3
5.2.2 I_x-V_y-VI_z compounds							
$AgAsS_2$ smithite	monoclinic C^6_{2h}	a : 14.02 c : 9.15	T_m : 692	$E_{g,ind}$: $E_{g,dir}$:	2.084 ...2.108 2.14	295 293	ρ : $9 \cdot 10^9$
$AgAsSe_2$			T_m : 663	E_g :	0.8...1.0		
$AgAsTe_2$			T_m : 598	E_g :	0.8...1.0		

Substance	Structure	Static and dynamical lattice parameters a, b, c [Å] d [g cm^{-3}] β T_m [K]	Band structure parameters E_g [eV] at T [K]	Transport parameters μ [cm^2/Vs] ρ [Ωm] E_A [eV]
$AgSbS_2$	monoclinic C^3_{2h}-A2/m or Aa	a : 13.2269 d_X : 5.42 b : 4.4112 T_m : 785 c : 12.8798 β : 98.48°	$E_{g,opt}$: 1.73 300	$\mu_{p,H}$: 0.24 E_A : 0.89
$AgSbSe_2$	NaCl structure	a : 5.786 d_X : 6.60 T_m : 909	$E_{g,th}$: 0.58..0.62	μ_p : 1500
$AgSbTe_2$	NaCl structure	a : 6.078 d_X : 7.12 T_m : 834		μ_p : 35..75 ρ : 0.006
$AgBiS_2$	NaCl structure	a : 5.648 d_X : 7.02 T_m : 1083	$E_{g,opt}$: 0.9	ρ : $2.5 \cdot 10^{-4}$
$AgBiSe_2$	NaCl structure	a : 5.832 d_X : 7.95 T_m : 1035		ρ : 0.005
$AgBiTe_2$	NaCl structure	a : 6.155 d_X : 8.14 T_m : 793	E_g : 0.16 300	ρ : $8 \cdot 10^{-4}$
$CuSbS_2$ chalcostibite	orthorhombic C^9_{2v}-Pna2$_1$	T_m : 808	ferro- and piezoelectric semiconductor	
$CuSbSe_2$	orthorhombic D^{16}_{2h}-Pnma	a : 6.40 d : 5.8 b : 3.95 T_m : 753 c : 15.33	$E_{g,th}$: 0.83	μ_p : 5 ρ : 0.25

Substance	Structure	Static and dynamical lattice parameters			Band structure parameters			Transport parameters	
		a, c [Å]	T_m [K]	$\varepsilon(0), \varepsilon(\infty)$	E_g [eV]	at T [K]		ρ [Ωm]	
$CuSbTe_2$	hexagonal Bi_2Te_3-type	a : 4.22 c : 29.9	T_m : 803					ρ :	$3 \cdot 10^{-4}$
$CuBiSe_2$	ffc	a : 5.69	T_m : 858					ρ :	$8 \cdot 10^{-4}$
$CuBiTe_2$	hexagonal Bi_2Te_3-type	a : 4.35 c : 30.1	T_m : 793					ρ :	$5 \cdot 10^{-4}$
$NaSbSe_2$	ffc	a : 5.96	T_m : 1013		E_g :	1.3			
Ag_3AsS_3 proustite	uniaxial structure C^6_{3v} - R3c	a : 10.80 c : 8.69	T_m : 753	$\varepsilon(0)_{\parallel}$: 21.4 $\varepsilon(0)_{\perp}$: 44.5 $\varepsilon(\infty)_{\parallel}$: 6.3 $\varepsilon(\infty)_{\perp}$: 7.45	$E_{g,ind\parallel}$: $E_{g,ind\perp}$: $E_{g,dir\parallel}$: $E_{g,dir\perp}$: $E_{g,th}$:	2.012 2.004 2.156 2.125 1.86	300 300 300 300	$\rho_{\parallel}$: $\rho_{\perp}$:	$2 \cdot 10^5$ 10^5
Figs. 162 and 163 (p. 296) show the Brillouin zone and the band structure of this compound.									
Ag_3SbS_3 pyrargite	uniaxial structure C^6_{3v} - R3c	a : 11.058 c : 8.698	T_m : 746	$\varepsilon(0)$: 27	$E_{g,th}$: $E_{g,opt}$:	1.77 1.93	 300	$\rho_{\parallel}$: $\rho_{\perp}$:	$3.3 \cdot 10^4$ $1.6 \cdot 10^4$
Cu_3AsS_3 tennanite			T_m : 913		called semiconductors in the literature				
Cu_3SbS_3 skinnerite			T_m : 828		called semiconductors in the literature				

Substance	Structure	Static and dynamical lattice parameters a, c [Å]	d [g cm^{-3}] T_m [K]	Band structure parameters E_g [eV]	at T [K]	m [m_0]	Transport parameters μ [cm^2/Vs]

5.2.3 II_x-III_y-VI_z compounds

For II-III_2-VI_4 compounds see section 4.1.6, for II_3-III_2-VI_6 compounds see section 4.1.7.

b-$CdInS_2$	tetragonal D^{17}_{4h}-I4/mmm (?)	a : 11.586 c : 6.522	d : 4.420	$E_{g,th}$:	1.70 ...1.74		m_n : 0.172 m_p : 0.44		
β-$CdInSe_2$	tetragonal D^{17}_{4h}-I4/mmm (?)	a : 12.152 c :7.14	d : 4.970	$E_{g,th}$:	1.40 1.42		m_p : 0.23		
β-$CdInTe_2$	tetragonal D^{17}_{4h}-I4/mmm (?)	a : 12.612 c : 7.434	d : 5.550	$E_{g,th}$:	1.10 ...1.12		m_n : 0.08 m_p : 0.18		
α-$CdTlS_2$	trigonal D^3_{3d}-P $\bar{3}$m1 or C^1_{3v}-P $\bar{3}$m1	a : 3.645 c : 6.825	d : 5.05 T_m : ≅ 870	$E_{g,th}$: $E_{g,opt}$:	1.46 ...1.52 1.56	 300	m_n : 0.19 m_p : 0.6	μ_p :	4200
α-$CdTlSe_2$	trigonal D^3_{3d}-P $\bar{3}$m1 or C^1_{3v}-P $\bar{3}$m1	a : 3.723 c : 7.073	d : 5.89	$E_{g,th}$:	0.40		m_n : 0.11 m_p : 0.65		
α-$CdTlTe_2$	trigonal D^3_{3d}-P $\bar{3}$m1 or C^1_{3v}-P $\bar{3}$m1	a : 3.890 c : 7.220	d : 6.40	$E_{g,th}$:	0.18				
β-$HgTlS_2$	tetragonal D^{17}_{4h}-I4/mmm(?)	a : 12.20 c : 6.60	d_X : 6.34	$E_{g,th}$: $E_{g,opt}$:	1.28 1.25				

Substance	Structure	Static and dynamical lattice parameters			Band structure parameters			Transport parameters	
		a, b, c [Å] α, β	d [g cm^{-3}] T_m [K]	$\varepsilon(0)$	E_g [eV]	at T [K]		μ [cm^2/Vs] ρ [Ωm]	

Also $HgTlSe_2$, $-Te_2$ and $ZnTlS_2$, $-Se_2$, $-Te_2$ have been synthesized and proved to display semiconducting properties.

5.2.4 III_x-V_y-VI_z compounds

$TlAsS_2$	monoclinic C^5_{2h}-$P2_1/c$	a: 6.11 b: 11.33 c: 12.27 β: 104.2°	d: 5.53 T_m: 533		E_g:	1.3	300		
$TlSbS_2$	disordered NaCl O^5_h-Fm3m	a: 5.87 ...5.94	d_X: 6.18 ...6.40 T_m: 757	$\varepsilon(0)$: 11.891	$E_{g,th}$: $E_{g,ind}$: $E_{g,dir}$:	1.42 ...1.7 1.54 1.69	 300 300	ρ:	10^9
$TlBiS_2$	rhombohedral D^5_{3d}-R $\bar{3}$m	a: 4.14 c: 10.91 in hexagonal description	T_m: 1013		E_g:	0.40			
$TlBiSe_2$	rhombohedral D^5_{3d}-R $\bar{3}$m	a: 4.24 c: 22.33 in hexagonal description	T_m: 993		E_g:	0.28			
$TlBiTe_2$	rhombohedral D^5_{3d}-R $\bar{3}$m	a: 8.137 α: 32°18'	d: 8.06 T_m: 808					μ_n:	64
Ga_6Sb_5Te					$E_{g,th}$: $E_{g,opt}$:	0.80 0.65	 300	μ_p: ρ:	9.5 3.8

Substance	Structure	Static and dynamical lattice parameters a, b, c [Å]	d [g cm^{-3}]	$\varepsilon(0)$	Band structure parameters E_g [eV]	at T [K]	m [m_o]	Transport parameters μ [cm^2/Vs] ρ [Ωm]
In_6Sb_5Te								μ_n: 1200 ρ: $0.7\cdot10^{-3}$
In_7SbTe_6								μ_p: 440 ρ: $2.5\cdot10^{-3}$
5.2.5 IV_x-V_y-VI_z compounds								
$Bi_{12}SiO_{20}$	cubic T^3-I23	a: 10.10433		$\varepsilon(0)$: 56	$E_{g,opt}$: 3.25	300	m_n: 14	$\mu_{n,dr}$: 0.029
$Bi_{12}GeO_{20}$	cubic T^3-I23	a: 10.1455	d_X: 9.222	$\varepsilon(0)$: 40	$E_{g,opt}$: 3.25			$\mu_{n,dr}$: 4.51 ρ: $8\cdot10^{10}$
$PbSb_2S_4$ zinkenite	orthorhomic $F5_6$	a: 12.29 b: 13.6 c: 8.66			$E_{g,opt}$: 1.13	300		ρ: $0.7\cdot10^7$
$GeSb_2Te_4$	hexagonal D^5_{3d}-R $\bar{3}$m	a: 4.21 c: 40.6		$\varepsilon(0)$: 39			m_n: 0.55	$\mu_{n,H}$: 30
$GeBi_2Te_4$	hexagonal D^5_{3d}-R $\bar{3}$m	a: 4.28 c: 39.2			$E_{g,opt}$: 0.23	300		
$GeSb_4Te_7$	layer structure D^3_{3d}-P $\bar{3}$m1	a: 4.21 c: 23.65		$\varepsilon(0)$: 35			m_p: 0.46	$\mu_{p,H}$: 39 $\rho_\parallel$: $0.3\cdot10^{-3}$ $\rho_\perp$: $0.5\cdot10^{-3}$

Substance	Structure	Static and dynamical lattice parameters a, b, c [Å]	d [g cm^{-3}] T_m [K]	$\varepsilon(0)$	Band structure parameters E_g [eV]	at T [K]	m [m_o]	Transport parameters μ [cm^2/Vs] ρ [Ωm]
$GeBi_4Te_7$	layer structure D^3_{3d}-P $\bar{3}$m1	a : 4.36 c : 24.11					m_n : 0.27	$\rho_{\parallel}$: 10^{-3} $\rho_{\perp}$: $0.5 \cdot 10^{-3}$
$PbBi_4Te_7$	layer structure D^3_{3d}-P $\bar{3}$m1	a : 4.42 c : 23.6		$\varepsilon(0)$: 44			m_n : 0.29	$\mu_{n\perp}$: 15

5.2.6 V-VI-VII compounds

AsSBr	chain structure D^{16}_{2h}-Pnam				$E_{g,th}$: 2.5			$\mu_{n,H}$: $< 10^{-1}$ ρ : $> 10^{12}$
SbSI	chain structure D^{16}_{2h}-Pnam	a : 8.52 b :10.13 c :4.10	d_X : 5.33 T_m : 670		$E_{g,dir\parallel}$: 1.88 $E_{g,dir\perp}$: 1.95	300		$\mu_{n,H}$: 50 ··· 100 $\rho_{\parallel}$: 10^8 ··· 10^9

Figs. 164 ··· 167 (p. 297,298) show the structure, the Brillouin zone and band structures for SbSI.

SbSBr	chain structure D^{16}_{2h}-Pnam	a :8.20 b : 9.70 c : 3.95	d_X : 4.94		$E_{g\perp}$: 2.26 $E_{g\parallel}$: 2.20			ρ : 10^6
SbSeBr	chain structure D^{16}_{2h}-Pnam	a : 8.30 b : 10.20 c : 3.95	d_X : 5.57		$E_{g\perp}$: 1.92 $E_{g\parallel}$: 1.88			
SbSeI	chain structure D^{16}_{2h}-Pnam	a : 8.65 b : 10.38 c : 4.12	d_X : 5.88		$E_{g\parallel}$: 1.66 $E_{g\perp}$: 1.68			$\rho_{\parallel}$: 10^7

Substance	Structure	Static and dynamical lattice parameters		Band structure parameters			Transport parameters	
		a, b, c [Å]	d [g cm^{-3}]	E_g [eV]	at T [K]		ρ [Ωm]	
SbTeI	chain structure	a : 9.18	d_X : 5.96	$E_{g\parallel}$:	1.25			
	D^{16}_{2h}-Pnam	b : 10.8		$E_{g\perp}$:	1.28			
		c : 4.23						
BiOCl	laminar tetragonal	a : 3.883		$E_{g,ind}$:	3.455	293		
	D^{7}_{4h}-P4/nmm	c : 7.347		$E_{g,dir}$:	3.50	293		
BiOBr	laminar tetragonal	a : 3.915		$E_{g,ind}$:	2.924	293		
	D^{7}_{4h}-P4/nmm	c : 8.076		$E_{g,dir}$:	3.00			
BiOI	laminar tetragonal	a : 3.984		$E_{g,ind}$:	1.890	293		
	D^{7}_{4h}-P4/nmm	c : 9.128		$E_{g,dir}$:	1.94	293		
BiSCl	chain structure	a : 7.70	d_X : 6.04	$E_{g\parallel}$:	1.89			
	D^{16}_{2h}-Pnam	b : 9.87		$E_{g\perp}$:	1.93			
		c : 4.02						
BiSBr	chain structure	a : 8.02	d_X : 6.83	$E_{g\parallel}$:	1.95		ρ :	$10^3 \cdots 10^4$
	D^{16}_{2h}-Pnam	b : 9.70		$E_{g\perp}$:	1.97			
		c : 4.01						
BiSI	chain structure	a : 8.46	d_X : 6.87	$E_{g\parallel}$:	1.56		ρ :	10^7
	D^{16}_{2h}-Pnam	b : 10.15		$E_{g\perp}$:	1.58			
		c : 4.14						
BiSeBr	chain structure	a : 8.18	d_X : 6.94	$E_{g\parallel}$:	1.50			
	D^{16}_{2h}-Pnam	b : 10.47		$E_{g\perp}$:	1.54			
		c : 4.11						

Substance	Structure	Static and dynamical lattice parameters a, c [Å]	d [g cm^{-3}] T_m [K]	$\varepsilon(0)$, $\varepsilon(\infty)$	Band structure parameters E_g [eV]	at T [K]	m [m_o]	Transport parameters μ [cm^2/Vs] ρ [Ωm]
BiSeI	chain structure D^{16}_{2h}-Pnam	a : 8.71 b : 10.54 c : 4.19	d_X : 7.16		$E_{g\parallel}$: 1.3 $E_{g\perp}$: 1.32			ρ : $10^2 \cdots 10^3$
BiTeBr	hexagonal layers D^3_{3d}-P $\bar{3}$m1	a : 4.23 c : 6.48	d : 6.65		$E_{g,ind}$: 0.472 $E_{g,dir}$: 0.501			
BiTeI	hexagonal layers D^3_{3d}-P $\bar{3}$m1	a : 4.30 c : 6.80	d : 6.91	$\varepsilon(0)$: 14.5 $\varepsilon(\infty)$: 19	$E_{g,opt}$: 0.39 $E_{g,ind}$: 0.448	295 295	m_n : 0.20 ...0.25	$\mu_{n,H}$: 280 ...445
5.2.7 Other ternary compounds								
$Cu_3In_5Se_9$	isostructural to In_2Se_3	a : 8.47 c : 17.41	d : 5.568 T_m : 1298		E_g : 1.10	300		
$Cu_3Ga_5Se_9$		a : 8.01 c : 16.46	d : 5.330 T_m : 1373		$E_{g,opt}$: 1.74	300		
$Ag_3In_5Se_9$			d : 5.668 T_m : 1098		$E_{g,opt}$: 1.22	300		
$Ag_3Ge_8Se_9$			d : 6.720 T_m : 1157		$E_{g,opt}$: 1.92	300		
$Cu_2Ga_4Te_7$	sphalerite	a : 5.93	d : 5.84 T_m : 1147		$E_{g,th}$: 1.08 $E_{g,opt}$: 1.04	 300		$\mu_{p,H}$: 120

Substance	Structure	Static and dynamical lattice parameters a, b, c [Å] d [g cm^{-3}] T_m [K]	Band structure parameters E_g [eV] at T [K]	Transport parameters μ [cm^2/Vs]
$Cu_2In_4Te_7$	sphalerite	a : 6.16 d : 5.93 T_m : 1067	$E_{g,th}$: 1.10	$\mu_{p,H}$: 0.27
$CuIn_3Te_5$	sphalerite	a : 6.16 d : 5.94 T_m : 1045	$E_{g,th}$: 1.20	$\mu_{p,H}$: 0.1
$AgIn_3Te_5$	sphalerite	a : 6.2476	E_g : 1.1	
$AgIn_5S_8$	spinel	a : 10.822 d : 4.85 T_m : 1348	$E_{g,opt}$: 1.7 300	$\mu_{n,H}$: 4
$AgIn_9Te_{14}$			E_g : 1.50	$\mu_{n,H}$: 40 at 600K
Cd_2SnO_4	D^9_{2h}-Pbam	a : 5.5674 b : 9.8871 c : 3.1923	$E_{g,opt}$: 2.06 293	μ_H : 35
$CdSnO_3$	ilmenite C^2_{31}-R $\bar{3}$	a : 5.4530 c : 14.960	E_g : 0.3	
Li_3CuO_3			E_g : 0.88	
Hg_3PS_3, Hg_3PS_4			E_g : around 2	
$Cd_4(P,As)_2(Cl,Br,I)_3$ cubic			E_g : 1.8...2.3	

Substance	Structure, space group	Energy gaps $E_{g,opt}$ [eV]	$E_{g,th}$ [eV]	Carrier mobilities μ_n [cm^2/Vs]	μ_p [cm^2/Vs]

6 Further compounds with semiconducting properties

Besides of the groups of semiconducting elements and compounds treated in Chapters 1 ··· 5 many compounds are described in the literature as having "semiconducting properties". Such substances show
- a high electrical resistivity,
- an optical energy gap (absorption edge) or thermal energy gap (activation energy of conductivity)
- a negative or positive Hall voltage caused by electrons or holes.

We present in this chapter data on three groups of compounds:
- boron compounds,
- binary and ternary transition metal compounds,
- binary and ternary rare earth compounds.

In these groups a large number of substances have semiconducting properties in the sense of the criteria stated above. We list in the following only such substances for which an optical or thermal energy gap or carrier (Hall) mobilities are given explicitly in the literature. Substances where only a high resistivity hints to semiconducting properties have not been included.

6.1 Boron compounds

The boron compounds and especially the borides show a wide variety of structures and compositions which include single atoms, connected pairs, multiple chains, planar networks and polyhedral groupings which are preferably based on octahedra, icosahedra or even more complex polyhedral structures. This variety is the consequence of the peculiar electronic structure of boron characterized by an unpaired electron in the $2s^2 2p^1$ configuration of the outer electron shell of the isolated boron atom, and leading to the various combinations of s^2p, sp, sp^2 and sp^3 electron configurations by the electron interchange between boron atoms or by the interaction with electrons of other atoms.

Among the more than hundred compounds investigated the most important group comprises the compounds of boron with group VB elements: BN, BP, and BAs. These compounds are explicitly described in chapter 2. In the following we present such compounds of boron with elements of other groups of the Periodic System for which reliable data are available. All these compounds have very complicated structures consisting of B_{12} icosahedra (see Section 3.1). The compound YB_{66} for instance has a unit cell with 104 icosahedra i.e. 1248 atoms.

$B_{1-x}H_x$	rhombohedral β-boron	1.10 ··· 1.7 for 9 ··· 24 at% H			
CuB_{24}	rhombohedral β-boron		0.54		
$LiAlB_{14}$	orthorhombic	1.82			
NaB_{15}	D^{28}_{2h} - Imam		0.32		
KB_6	cubic		0.29		
CaB_6	O^1_h - Pm3m		0.2 ··· 0.4		
SrB_6			0.45		
BaB_6			0.15		

Substance	Structure, space group	Energy gaps $E_{g,opt}$ [eV]	$E_{g,th}$ [eV]	Carrier mobilities μ_n [cm^2/Vs]	μ_p [cm^2/Vs]
α-AlB_{12}	tetragonal D^4_4 - $P4_12_12$	1.9			
β-AlB_{12}	orthorhombic O^1_h - Pm3m	2.5			
SmB_6	cubic		0.023	20	
EuB_6	O^1_h - Pm3m		0.30 ··· 0.38	100	
YbB_6			0.14		
YB_{66}	cubic		0.8		
SmB_{66}	O^6_h - Fm3c		0.80		15
GdB_{66}			0.73		15
YbB_{66}			1.27		5
B_4C	rhombohedral	0.48			0.2 ··· 1
B_6P	D^5_{3d} - R $\bar{3}$m	3.3			

6.2 Binary transition metal compounds

6.2.1 Compounds with elements of the IVth group

$Mn_{11}Si_{19}$ ($Mn_{26}Si_{45}$)	tetragonal D^8_{2d} - P $\bar{4}$n2 (D^2_{2d} - P $\bar{4}$c2)	0.66	0.5 ··· 1		230
$Mn_{15}Si_{26}$	tetragonal D^{12}_{2d} - I$\cdot\bar{4}$2d		0.702		6 ··· 30
Ru_2Si_3	orthorhombic		0.7		
Ru_2Ge_3	D^2_{2d} - P $\bar{4}$c2		0.52		
$CrSi_2$	hexagonal D^4_6 - $P6_222$		$\cong$ 0.30	0.27	0.8
$ReSi_2$	tetragonal D^{17}_{4h} - I4/mmm		0.13		
$FeSi_2$	orthorhombic D^{18}_{2h} - Cmca	1.0		0.26	2 ··· 10

6.2.2 Compounds with elements of the Vth group

$CrSb_2$	loellingite		0.16		
FeP_2	D^{12}_{2h} - Pnnm		0.37	80	
$FeAs_2$				0.22	
$FeSb_2$				$\cong$ 0.17	
RuP_2		0.8			
RuPAs		$\cong$ 0.8			
$RuAs_2$		$\cong$ 0.8			
$RuSb_2$			> 0.3		

Substance	Structure, space group	Energy gaps $E_{g,opt}$ [eV]	$E_{g,th}$ [eV]	Carrier mobilities μ_n [cm^2/Vs]	μ_p [cm^2/Vs]
OsP_2		≅ 0.2			
$OsAs_2$		≅ 0.9			
$OsSb_2$			> 0.3		
CoP_2	arsenopyrite		> 0.02		
$CoAs_2$	C^5_{2h} - $P2_1/c$		0.15 ··· 0.35		
$CoSb_2$			0.17		
RhP_2		≅ 1			
$RhAs_2$		1.15			
IrP_2			≅ 0.4		
$IrAs_2$		1.1			
IrAsSb			≅ 0.4		
NiP_2	C^6_{2h} - C2/c		0.5		
PdP_2			0.6 ··· 0.7		
PdPAs			0.45		
$NiAs_2$ (β)	marcasite D^{12}_{2h} - Pnnm		≅ 0.05		
PtP_2	pyrite		> 0.6		
PtPAs	T^6_h - Pa3		> 0.4		
$PtAs_2$			0.17 ··· 0.5		
$PtSb_2$		≅ 0.10 (ind.) > 0.4 (dir.)	0.05 ··· 0.11	420	830
CoP_3	skutterodite	0.45			
$CoAs_3$	T^5_h - Im3	< 0.4			
$CoSb_3$		< 0.4		290	
MnP_4 (8L)	monoclinic		0.28		
	C^6_{2h} - C2/c		0.54		
MnP_4 (6L)	triclinic		> 0.08		
MnP_4 (2L)	C^1_i - $P\bar{1}$				
FeP_4	monoclinic		0.32		
RuP_4	C^5_{2h} - $P2_1/c$		0.38		
OsP_4			0.40		

6.2.3 Oxides

There are many groups of transition metal oxides with "semiconducting properties". Important groups are:

TiO_2, Ti_2O_3, Ti_3O_5, Ti_4O_7, Ti_5O_9, Ti_6O_{11}, Ti_8O_{15},
V_3O_5, V_2O_3, VO_2, V_2O_5,
MnO, FeO, CoO, NiO, PdO,
Fe_3O_4, Co_3O_4, Mn_3O_4,
Cr_2O_3, Fe_2O_3, Rh_2O_3, Mn_2O_3, Nb_2O_3,
Ta_2O_5, WO_3.

Substance	Structure, space group	Energy gaps $E_{g,opt}$ [eV]	$E_{g,th}$ [eV]	Carrier mobilities μ_n [cm^2/Vs]	μ_p [cm^2/Vs]

In the most cases the electrical properties cannot be described by conduction via electrons and holes in conduction or valence bands. Parameters as optical or thermal energy gaps and carrier mobilities do not characterize the materials. Influences to be considered involve hopping processes, plasma effects, polaron coupling etc. Furthermore many properties of the transition metal oxides depend very sensitively on deviations from the stoichiometry.

A description of such properties affords a detailed discussion which cannot be given in the present context.

6.2.4 Chalcogenides

In the following formulae x means a small deviation from stoichiometry usually less than x = 0.1.

$Ti_{1+x}S_2$	C6	0.7		9.7	
$Ti_{1+x}Se_2$	D^3_{3d} - P $\bar{3}$m1	$\cong 0$			
ZrS_2		1.7		4.2	
$Zr_{1+x}Se_2$		1.2			
HfS_2		1.96			
$HfSe_2$		1.08			
TaS_2			0.04		
TiS_{3-x}	$ZrSe_3$-type	0.9			
ZrS_{3-x}	C^2_{2h} - $P2_1/m$	2.8			
$ZrSe_3$		1.25			
HfS_3		3.1			
Cr_2S_3	trigonal C^2_{3i} - R $\bar{3}$		1.1	4	
$Cr_{2+x}Se_3$	trigonal P $\bar{3}$1c		0.05		
Cr_3Se_4	monoclinic C^3_{2h} - I2/m		0.14		
$Cr_{1-x}Te$	hexagonal D^4_{6h} - $P6_3/mmc$		0.02		
2H-MoS_2	hexagonal	1.971	0.47	57	20
2H-$MoSe_2$	D^4_{6h} - $P6_3/mmc$	1.6	0.25		
2H-$MoTe_2$		1.1			
2H-WSe_2		1.78	0.17	100	
3R-MoS_2	trigonal	1.9	0.25		
3R-WS_2	C^5_{3v} - R3m	2.07			
α-MnS	cubic	2.8	0.62		
α-MnSe	O^5_h - Fm3m	2.5	0.48		
MnTe	hexagonal D^4_{6h} - $P6_3/mmc$	1.3		50	

Substance	Structure, space group	Energy gaps $E_{g,opt}$ [eV]	$E_{g,th}$ [eV]	Carrier mobilities μ_n [cm^2/Vs]	μ_p [cm^2/Vs]
TcS_2	triclinic,	1.0			
$TcSe_2$	primitive	0.88			
ReS_2	triclinic	1.33	0.4		
$ReSe_2$	$C1_i$ - P 1	1.15			
$Fe_{1-x}S$	hexagonal D^4_{3h} - P 62c				0.16
FeS_2	pyrite		0.4 ··· 0.95	230	
$FeSe_{2-x}$	T^6_h - Pa3		0.2 ··· 0.3		
RuS_2		1.8			
$RuSe_2$		1.0	> 0.6		
$RuTe_2$			0.25		
OsS_2		2.0			
$OsTe_2$			> 0.2		
RhS_3	defect pyrite T^6_h - Pa3	> 1.5			
Rh_2S_3	orthorhombic D^{14}_{2h} - Pbcn		0.8		
$RhSe_2$	orthorhombic	0.6			
IrS_2	D^{16}_{2h} - Pnam	0.9			
$IrSe_2$		≅ 1.0			
$RhSe_3$	C2	0.7			
IrS_3	trigonal distortion	2.0			
$IrSe_3$			> 0.45		
$Ni_{1-x}S$	hexagonal D^4_{6h} - $P6_3/mmc$			1 ··· 5	
NiS_2	pyrite T^6_h - Pa3	0.27	0.14		
PdS	tetragonal		0.5		
PdSe	C^2_{4h} - $P4_2/m$		0.2		
PdS_2	orthorhombic		0.7 ··· 0.8		
$PdSe_2$	D^{15}_{2h} - Pbca		0.4		
PtS	tetragonal $P4_2/mmc$	0.8		0.38 ··· 0.64	
$Pt_{0.97}S_2$	trigonal	0.95	0.4		
$PtSe_2$	D^3_{3d} - P $\bar{3}$m1		0.1		

Substance	Structure, space group	Energy gaps $E_{g,opt}$ [eV]	$E_{g,th}$ [eV]	Carrier mobilities μ_n [cm^2/Vs]	μ_p [cm^2/Vs]

6.3 Binary rare earth compounds

In rare earth compounds f- and d-bands play an important role. Optical energy gap data below are transitions between such bands or from f-bands into the conduction band. Instead of thermal gaps $E_{g,th}$ we list here activation energies E_A for conductivity.

SmS	cubic	$\cong$ 0.2	(4f-5d)	20 ··· 25
	$O5_h$ - Fm3m	2.3	(3p^6-5d)	
SmSe		0.46	(4f-5d)	
		1.4	(4p^6-5d)	
SmTe		0.63	(4f-5d)	
EuO		1.12	(4f-5d)	20 ··· 30
		3.9	(2p^6-5d)	
EuS		1.65	(4f-5d)	30
		2.3	(3p^6-5d)	
EuSe		1.80	(4f-5d)	0.5
EuTe		2.0	(4f-5d)	33 ··· 58
TmTe		0.22 ··· 0.35		
YbS		1 ··· 1.1		
YbSe		1.5		
YbTe		1.8 ··· 2.0		
β-La_2S_3	tetragonal	2.6		
β-$La_{10}S_{14}O$	D^{20}_{4h} - $I4_1/acd$	2.69		
Sm_3S_4	Th_3P_4-type		0.132 (E_A)	
Eu_3S_4	T_{6d} - $I\bar{4}3d$	1.7	0.22, 0.32 (E_A)	
γ-La_2S_3		2.9		
γ-La_2Te_3			0.43 (E_A)	
γ-Ce_2S_3			2.33 (E_A)	
γ-Nd_2S_3		2.0 ··· 2.3	2.7 ··· 3.8 (E_A)	
Eu_2Se_3		1.02		
γ-Gd_2S_3		3.4	1.6 ··· 1.9 (E_A)	
γ-Dy_2S_3		3 ··· 3.8	1.5 (E_A)	
δ-Dy_2S_3	monoclinic		0.34 (E_A)	
δ-Ho_2S_3	C^2_{2h} - $P2_1/m$		0.5 (E_A)	
ε-Yb_2S_3	rhombohedral		0.29 (E_A)	
	D^6_{3d} - $R\bar{3}c$			

Substance	Structure, space group	Energy gaps $E_{g,opt}$ [eV]	$E_{g,th}$ [eV]	Carrier mobilities μ_n [cm^2/Vs]	μ_p [cm^2/Vs]

6.4 Ternary transition metal compounds

6.4.1 Pnigochalcogenides

Most of the semiconducting compounds of transition metals with pnictides and chalcogenides (T-V-VI) are ternary analogs of the corresponding binary phases with the same cation d-electron configuration.

FePS	arsenopyrite-type		0.25		
FeAsS	C_{52h} - $P2_1/c$		0.3 ··· 0.5		
FeAsSe			0.6		
FeSbTe			0.04 (E_A)		
RuPS		> 1.4			
RuAsS		≅ 1.2			
RuSbSe		≅ 0.9	0.35		
RuSbTe			0.5		
OsPS		> 1.4			
OsAsS		≅ 1.3			
OsSbS			1.2		
OsPSe		≅ 1.4			
CoSbS	pararammelsbergite-type		0.5		
CoAsSe	D^{15}_{2h} - Pbca		0.2		
PdPS	PdPS-type		1.4		
PdPSe	D^{14}_{2h} - Pbcn	1.38	0.15 (E_A)		
CoPS	pyrite-type		0.4		
CoAsS	C^5_{2v} - $Pca2_1$		0.60 ··· 0.75		

6.4.2 Spinels and related compounds

$MnGa_2S_4$	monoclinic C^6_{4h} - C2/c		1.2		
$MnSb_2S_4$	spinel-type		1.0		
$CdCr_2S_4$	O^7_h - Fd3m	> 1.5	0.17 ··· 0.35 (E_A)		
$FeCr_2S_4$			0.02 (E_A)		0.3
$HgCr_2S_4$		1.42	0.36 (E_A)		
$CdCr_2Se_4$		1.2 ··· 1.7			
$CuCr_2S_3Se$			0.050 (E_A)		0.15
$CuCr_2S_{2.5}Se_{1.5}$			0.066		0.70
$HgCr_2Se_4$		0.84	0.36 (E_A)		
$ZnCr_2Se_4$		1.285		1 ··· 6	
$BaCr_2S_4$	hexagonal	1.0 ··· 1.5			

Substance	Structure, space group	Energy gaps $E_{g,opt}$ [eV]	$E_{g,th}$ [eV]	Carrier mobilities μ_n [cm^2/Vs]	μ_p [cm^2/Vs]

6.4.3 Oxides

Many of the semiconducting transition metal oxides are of interest as ferroelectrics. Reliable semiconductor data as optical energy gaps (mostly > 3 eV) or activation energies for conductivity are available only for a small number of compounds.

As examples of such ternary oxides we mention
$BaTiO_3$, $PbTiO_3$, $NaNbO_3$, $KNbO_3$, $KTaO_3$, $SrTiO_3$, $PbZrO_3$, $CaVO_3$, $LiVO_3$, $LaVO_3$, $MnVO_3$, $SbNbO_4$, $PbMoO_4$, $PbWO_4$,K_2CrO_4, $CuFe_2O_4$, $Co_3V_2O_8$, $Bi_2Pt_2O_7$.

5.4.4 Further chalcogenides

$Mn_{0.3}NbS_2$	hexagonal planes,	0.85	6.3	
$Fe_{0.3}NbS_2$	Mn,Fe,Co,Ni	1.05	4.4	
$Co_{0.3}NbS_2$	intercalated	0.90	5.1	
$Ni_{0.3}NbS_2$		0.85	4.3	
Tl_3VS_4	cubic T^3_d - I $\bar{4}$3m	1.76		

6.5 Ternary rare earth compounds

For a large number of ternary rare earth compounds data on energy gaps or activation energies for conductivity are published. We list only compounds where RT data are available.

$NdTiO_3$	orthorhombic		0.06 (E_A)	
$SmTiO_3$	D^{16}_{2h} - Pbnm		0.15 (E_A)	
$GdTiO_3$			0.19 (E_A)	
$TbTiO_3$			0.2 (E_A)	
$HoTiO_3$			0.2 (E_A)	
$ErTiO_3$			0.24 (E_A)	
$YbTiO_3$			0.24 (E_A)	
$LaVO_3$		≅ 1	0.16 (E_A)	0.15
$CeVO_3$			0.054 (E_A)	
$PrVO_3$			0.103 (E_A)	
$NdVO_3$			≅ 0 (E_A)	
$SmVO_3$			0.130 (E_A)	
$EuVO_3$			0.132 (E_A)	
$GdVO_3$			0.141 (E_A)	
$TbVO_3$			0.101 (E_A)	
$DyVO_3$			0.125 (E_A)	
$HoVO_3$			0.128 (E_A)	
$ErVO_3$			0.173 (E_A)	
$TmVO_3$			0.166 (E_A)	
$YbVO_3$			0.169 (E_A)	
$LaCrO_3$		4.7	0.18 ··· 0.6 (E_A)	0.005
$NdCrO_3$			0.29 (E_A)	
$SmCrO_3$		0.36		
$DyCrO_3$			0.27 (E_A)	

Substance	Structure, space group	Energy gaps $E_{g,opt}$ [eV]	$E_{g,th}$ [eV]	Carrier mobilities μ_n [cm^2/Vs]	μ_p [cm^2/Vs]
$HoCrO_3$			0.33 (E_A)		
$YbCrO_3$			0.37 (E_A)		
$LaMnO_3$			0.13 (E_A)		0.0002
$LaFeO_3$			0.39 (E_A)		
$GdFeO_3$			0.89 (E_A)		
$HoFeO_3$			1.10 (E_A)		
$HoMnO_3$	hexagonal		0.57 (E_A)		
$YbMnO_3$	C^3_{6v} - $P6_3cm$		0.73 (E_A)		
$LaCoO_3$	rhombohedral D^6_{3d} - $R\bar{3}c$		0.2 (E_A)		
Cu_3SmS_3	monoclinic		1.81		
Cu_3GdS_3	C^5_{2h} - $P2_1/b$		1.62		
Cu_3SmSe_3			0.15		
Cu_3TbS_3	trigonal		1.62		
Cu_3DyS_3	$P\bar{3}$		1.60		
Cu_3YS_3			1.78		
Cu_3HoS_3			1.65		
Cu_3YbS_3			1.56		
Cu_3LuS_3			1.50		
Cu_3ScS_3			1.86		
Cu_3GdSe_3			0.14		
Cu_3TbSe_3			0.16		
Cu_3DySe_3			0.20		
Cu_3YSe_3			0.88		
Cu_3HoSe_3			0.16		
Cu_3YbSe_3			0.20		
Cu_3ScSe_3			0.30		
Cu_3SmTe_3			0.23		
Cu_3GdTe_3			0.52		
Cu_3TbTe_3			0.46		
Cu_3DyTe_3			0.34		
Cu_3YTe_3			0.72		
Cu_3HoTe_3			0.26		
Cu_3ErTe_3			0.24		
Cu_3TmTe_3			0.14		
Cu_5HoS_4	hexagonal		0.53		
Cu_5LuS_4			0.50		
Cu_5GdSe_4			0.64		
Cu_5TbSe_4			1.04		
Cu_5YbSe_4			0.80		
Cu_5LuSe_4			1.00		
$ZnTm_2S_4$	orthorhombic	3.6			
$ZnYb_2S_4$		$\cong$ 2.5			
$ZnLu_2S_4$		3.7			
$ZnSc_2S_4$	spinel	2.1		3 ··· 40 doped with Ag,Cr,Ga	

Substance	Structure, space group	Energy gaps $E_{g,opt}$ [eV]	$E_{g,th}$ [eV]	Carrier mobilities μ_n [cm^2/Vs]	μ_p [cm^2/Vs]
$CdLa_2S_4$	cubic	≅ 2.6			
$CdPr_2S_4$	trigonal	≅ 2.1			
$CdDy_2S_4$		≅ 2.5			
$CdEr_2S_4$	spinel	≅ 1.8			
$CdTm_2S_4$		≅ 2.4			
$CdYb_2S_4$		≅ 2.5			
$CdSc_2S_4$		2.3		≅ 40 doped with Li,Cr	
La_2GeSe_5		1.7			
La_2SnSe_5		1.65			
Ce_2GeSe_5		1.55			
Ce_2SnSe_5		1.52			
Pr_2GeSe_5		1.82			
Pr_2SnSe_5		1.65			
Nd_2GeSe_5		1.90			
Nd_2SnSe_5		1.70			
Sm_2GeSe_5		2.00			
Sm_2SnSe_5		1.88			
Gd_2GeSe_5		1.90			
Gd_2SnSe_5		1.70			

7 Figures to chapters 3, 4 and 5

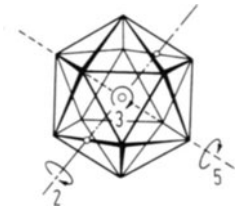

Fig.1. B. B_{12} icosahedron with examples of 2-fold, 3-fold and 5-fold rotation axes.

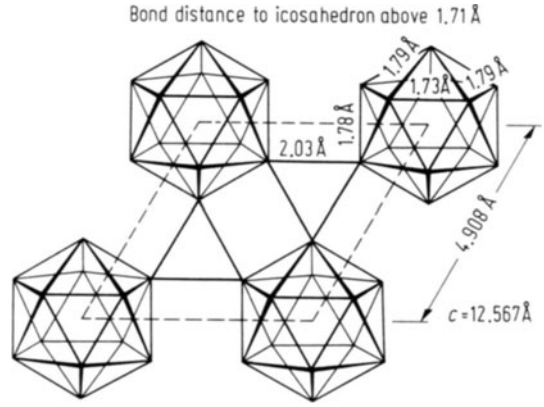

Fig.2. α-rhombohedral B. B_{12} icosahedra at the corners of the unit cell as viewed from above. Interatomic distances for the different types of bonds are indicated.

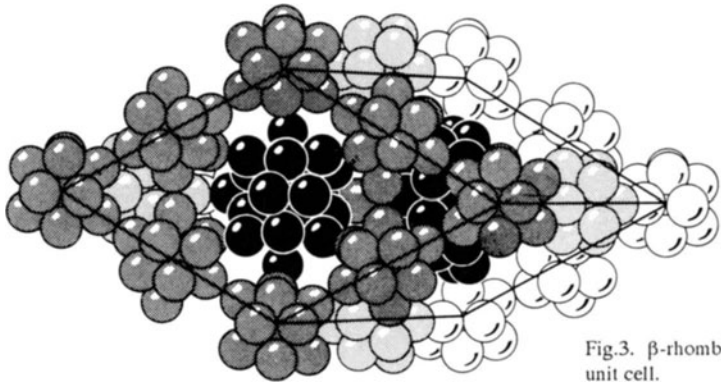

Fig.3. β-rhombohedral B. Model of the unit cell.

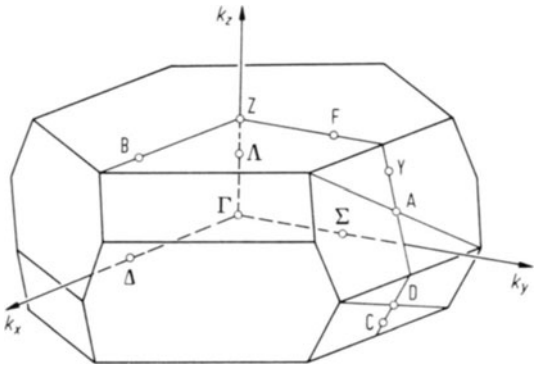

Fig.4. α- and β-rhombohedral B. Brillouin zone of the rhombohedral lattices.

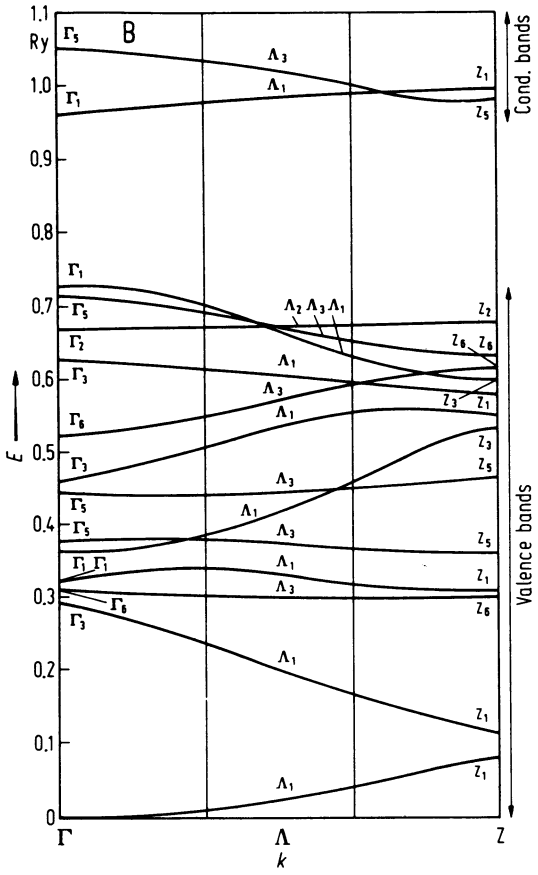

Fig.5. α-rhombohedral B. Band structure along the Γ - Z direction.

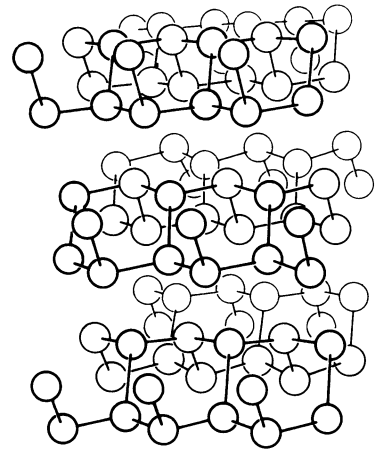

Fig.6. P. Perspective view of a portion of the black phosphorus structure; b-axis vertical and a-axis horizontal.

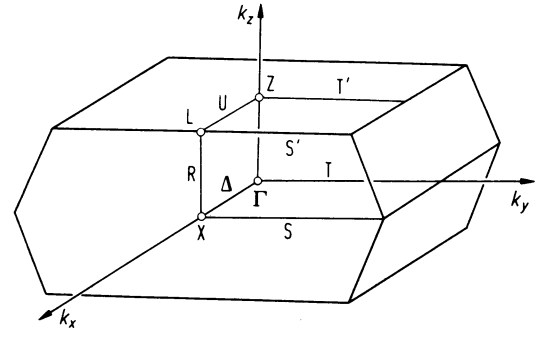

Fig.7. P. Brillouin zone of orthorhombic black phosphorus.

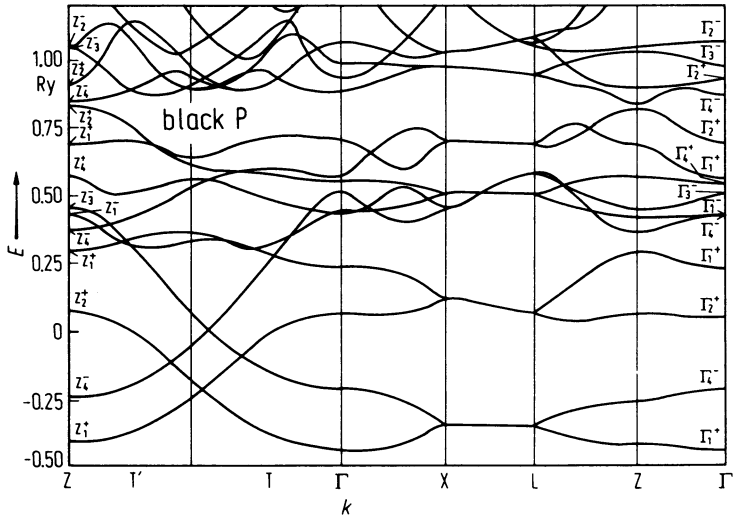

Fig.8. P (black). Band structure calculated with the self-consistent pseudopotential method.

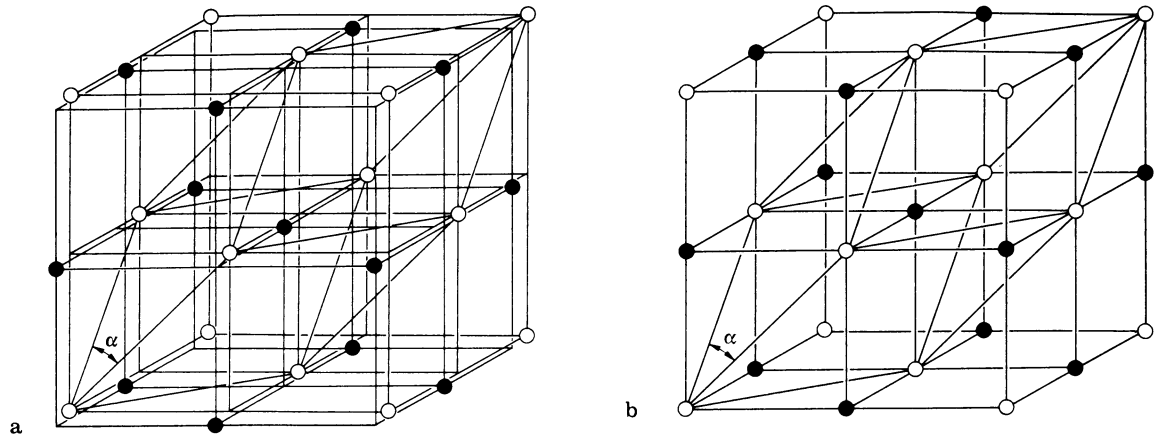

Fig.9. The A7 crystal structure (a) and the cubic NaCl structure (b) from which it can be derived. The rhombohedral angle α is indicated. Open circles represent sublattice one, solid circles sublattice two.

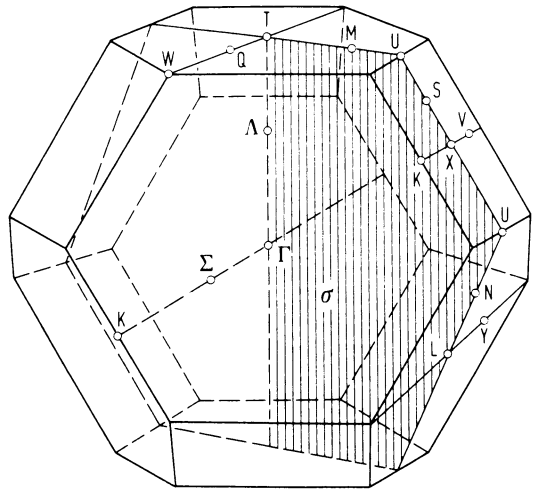

Fig.10. As, Sb, Bi. Brillouin zone of the rhombohedral lattice, showing points, lines and planes of symmetry. σ indicates the hatched plane.

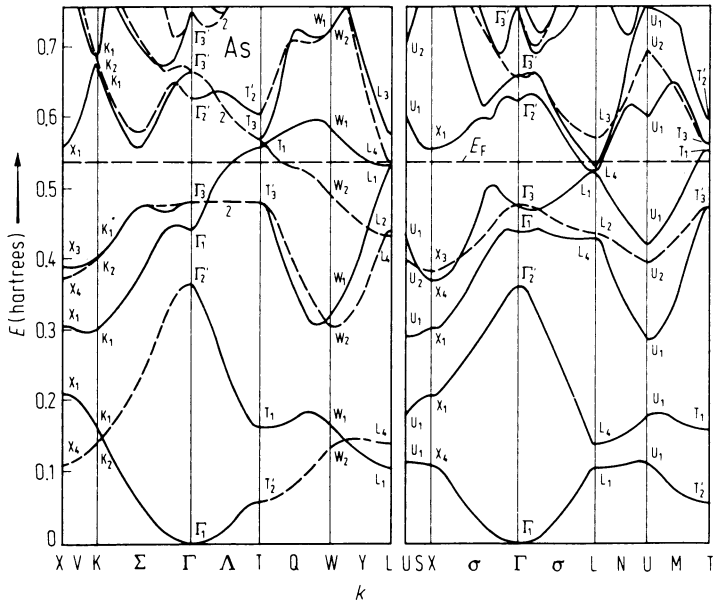

Fig.11. As. Band structure of rhombohedral As without spin along various symmetry lines, obtained from pseudopotential calculations. Solid lines and dashed lines indicate different symmetries.

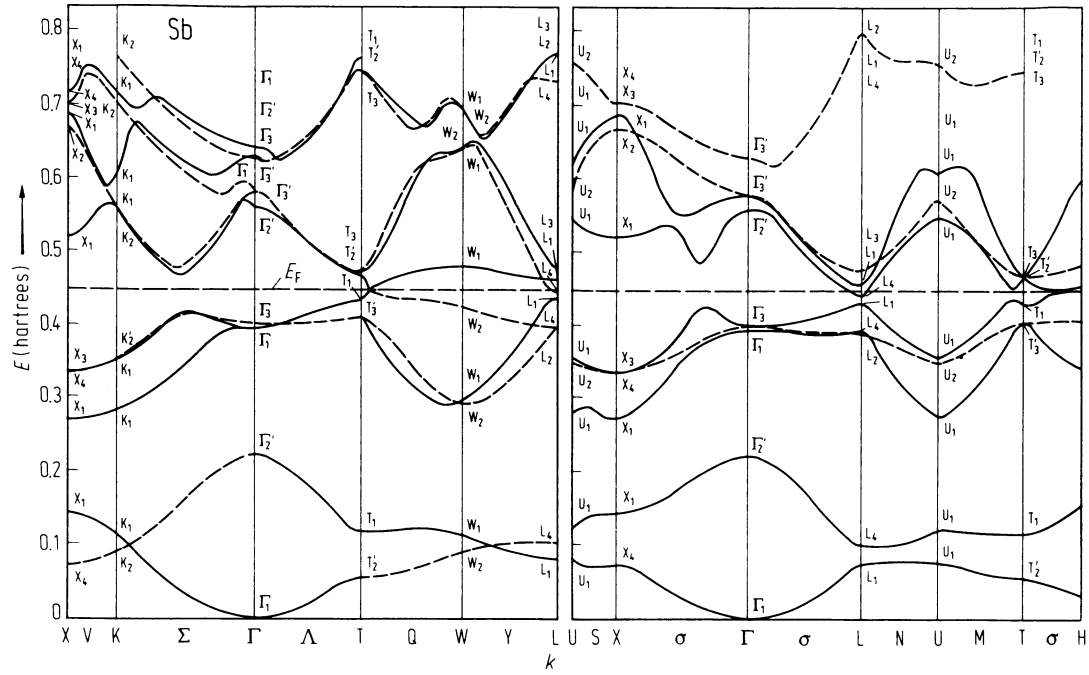
Sb
E (hartrees)
0.8
0.7
0.6
0.5
0.4
0.3
0.2
0.1
0
E_F
X V K Σ Γ Λ T Q W Y L U S X σ Γ σ L N U M T σ H
k

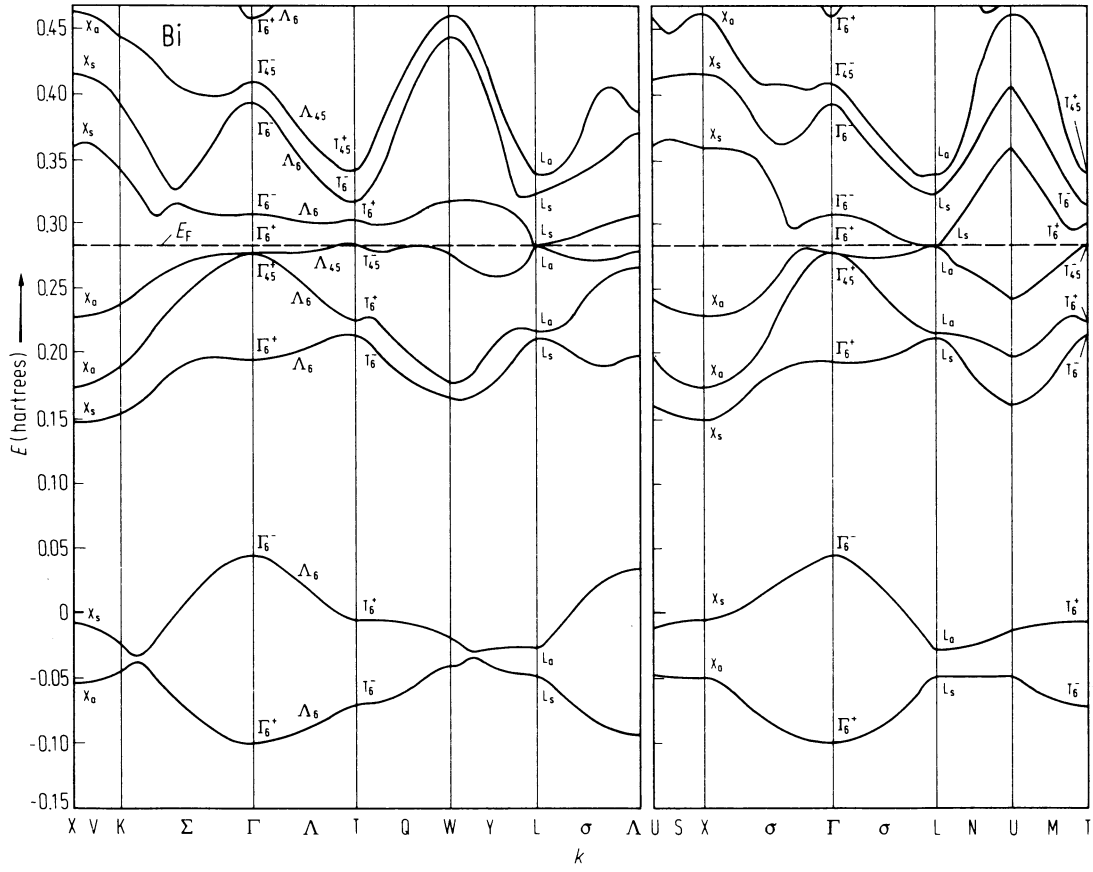
Bi
E (hartrees)
0.45
0.40
0.35
0.30
0.25
0.20
0.15
0.10
0.05
0
-0.05
-0.10
-0.15
E_F
X V K Σ Γ Λ T Q W Y L σ Λ U S X σ Γ σ L N U M T
k

◀ Left page:

upper figure:
Fig.12. Sb. Band structure of Sb without spin along various symmetry lines and planes. Solid lines and dashed lines indicate different symmetries.

lower figure:
Fig. 13. Bi. Band structure of bismuth along various symmetry lines and planes, obtained by a pseudopotential calculation.

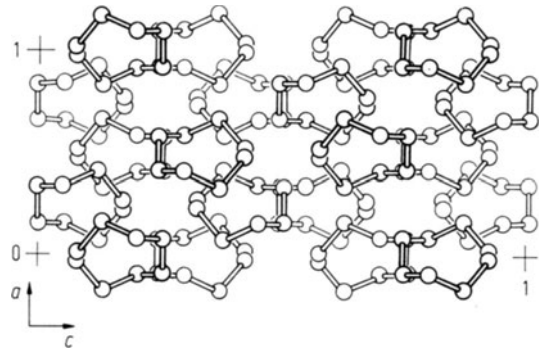

Fig.14. α-S. Projection of the orthorhombic sulfur structure along the b-axis.

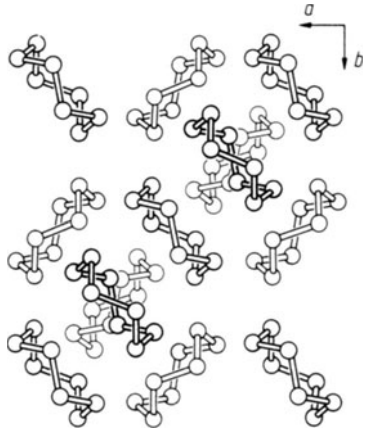

Fig.15. α-S. Projection of the orthorhombic structure along the c-axis.

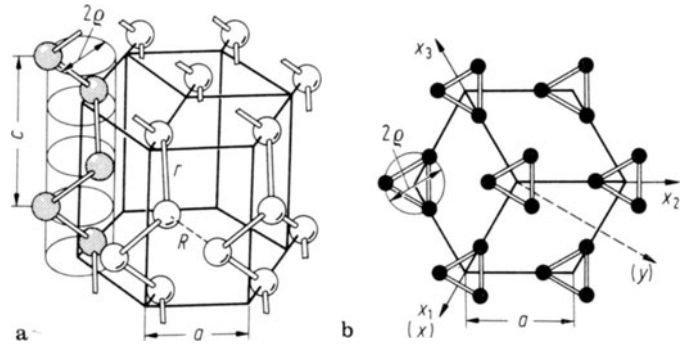

Fig.16. Se, Te (trigonal). (a) Lattice, (b) configuration of the chains with the polar axes x_i.

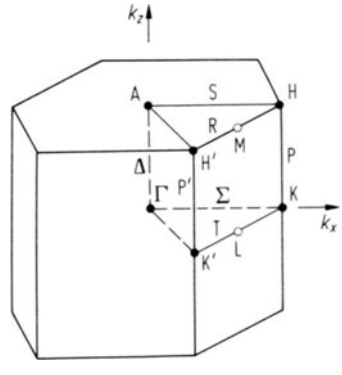

Fig.17. Se, Te (trigonal). Brillouin zone.

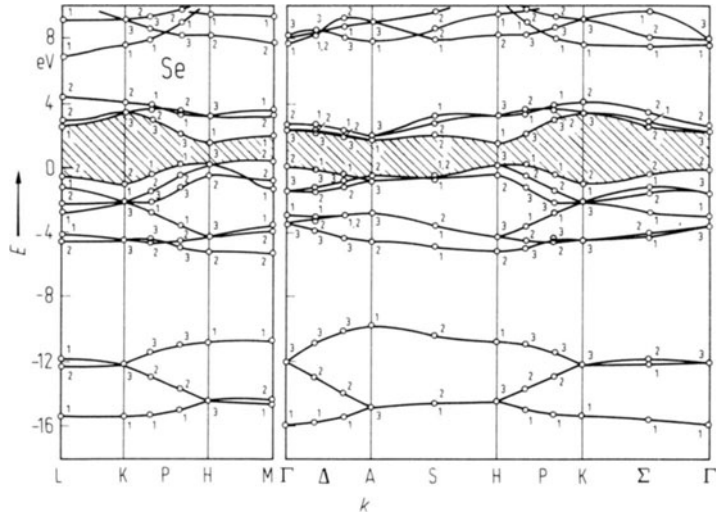

Fig.18. Se. Band structure calculated with a self-consistent symmetrized OPW method without spin-orbit interaction.

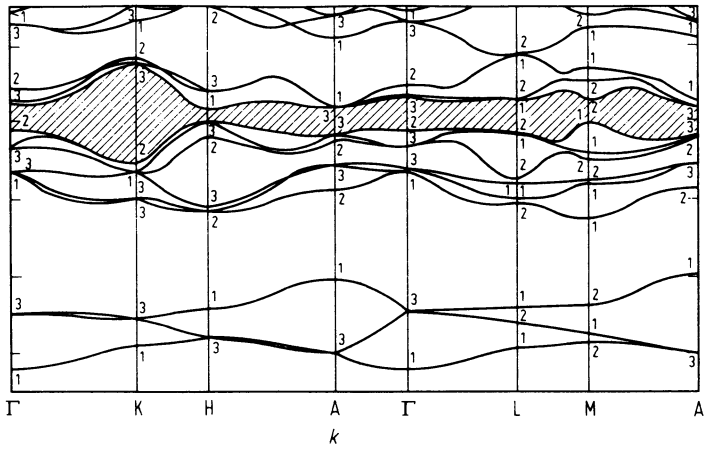

Fig.19. Te. Band structure.

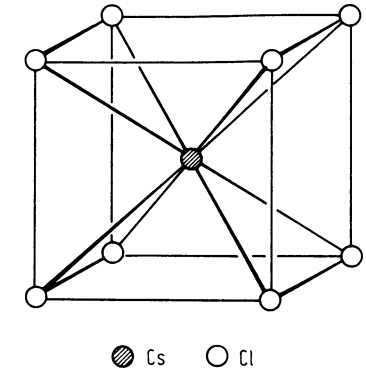

Fig.20. CsAu, RbAu. CsCl crystal structure.

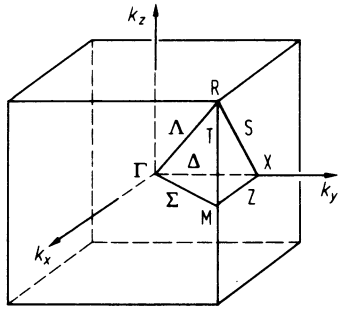

Fig.21. CsAu, RbAu. Brillouin zone for the simple cubic lattice.

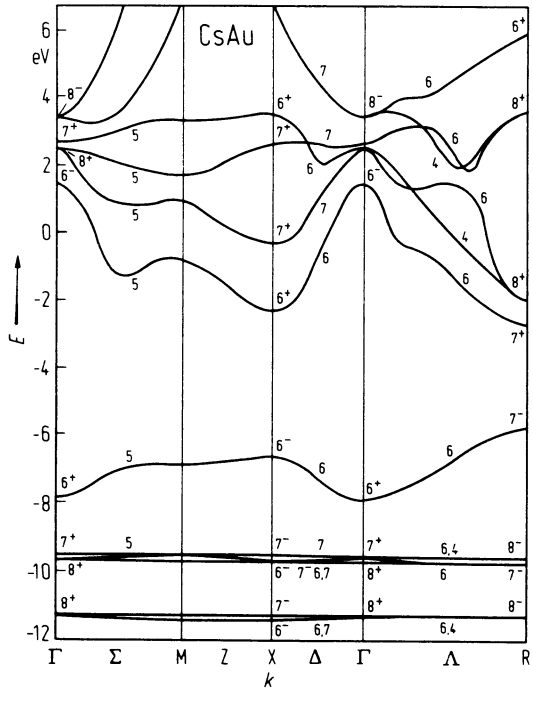

Fig.22. CsAu. Band structure according to a relativistic KKR calculation.

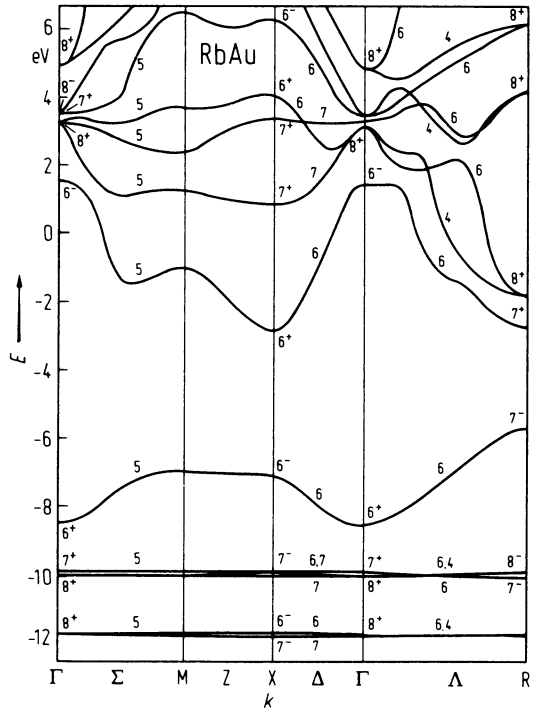

Fig.23. RbAu. Band structure according to a relativistic KKR calculation.

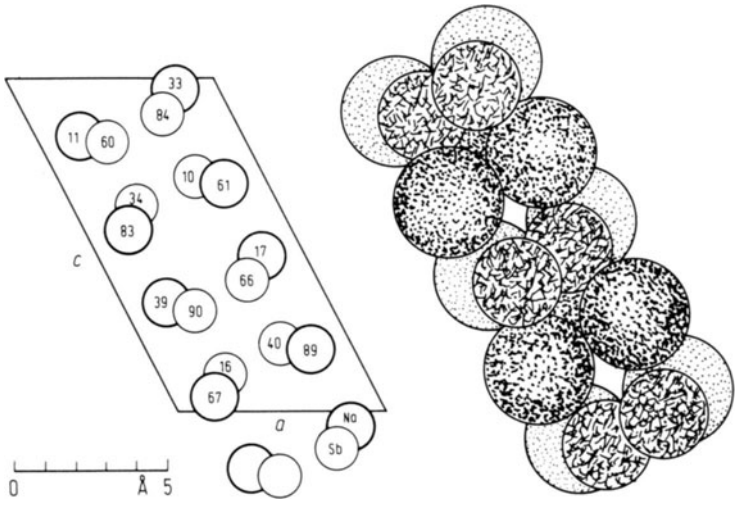

Fig.24. NaSb, KSb. Left: monoclinic structure projected along its b-axis; fractional y-parameters are inscribed in each atom. Right: packing of the NaSb arrangement seen along its b-axis.

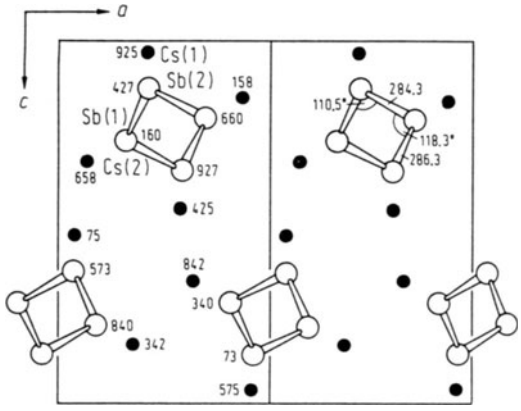

Fig.25. CsSb. Orthorhombic structure projected along the b-axis.

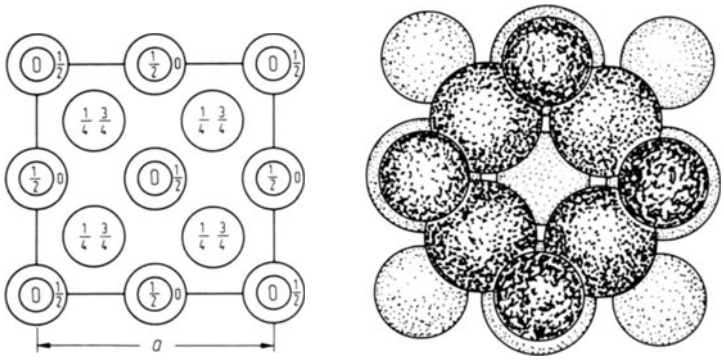

Fig.27. $(Li,Cs)_3Bi$, $(Li,K,Rb,Cs)_3Sb$. Cubic (BiF_3) structure. Left: projection on a cube face, the smaller circles are Bi atoms. Right: packing of half the atoms in the unit cube.

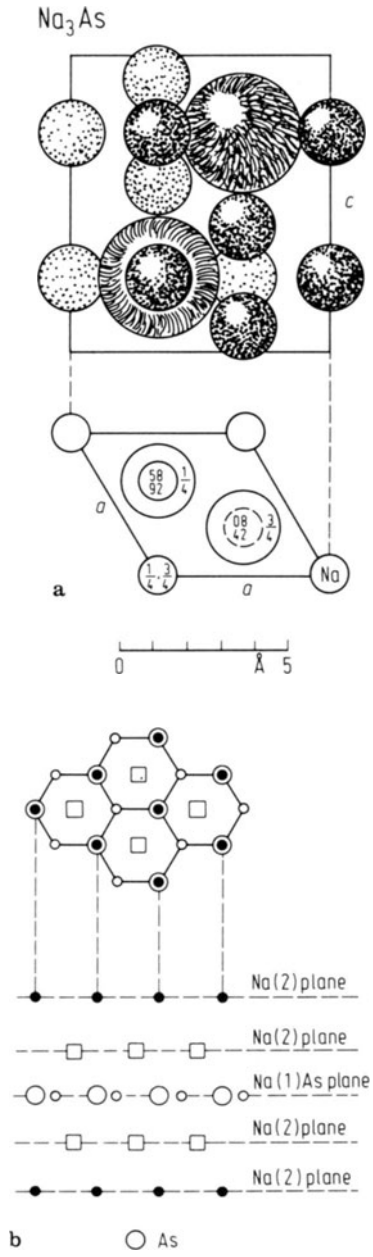

Fig.26. $(Li,Na,K,Rb)_3Sb$. Hexagonal (Na_3As) structure presented by two projections of (a) the hexagonal unit cell (As atoms line-shaded), (b) structure seen along the c- (upper part) and a-axes.

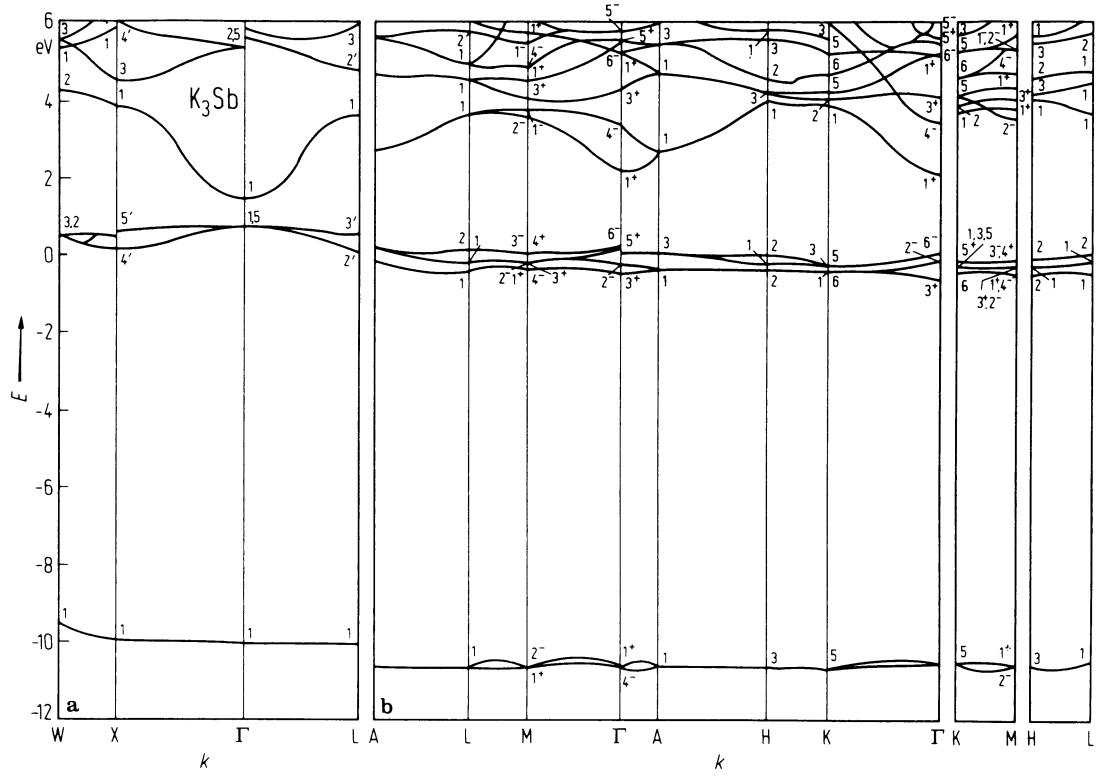

Fig.28. K_3Sb. Band structure (a) of hexagonal and (b) of cubic K_3Sb calculated by an empirical pseudopotential method without allowance for spin-orbit interaction.

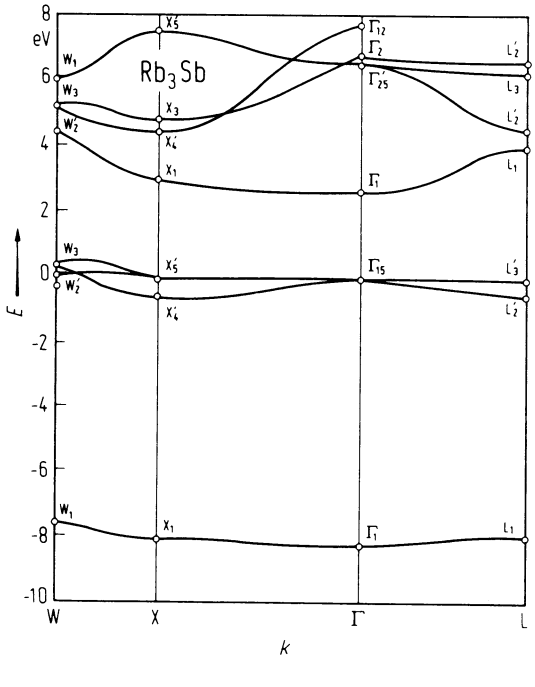

Fig.29. Rb_3Sb. Band structure calculated by an empirical pseudopotential method.

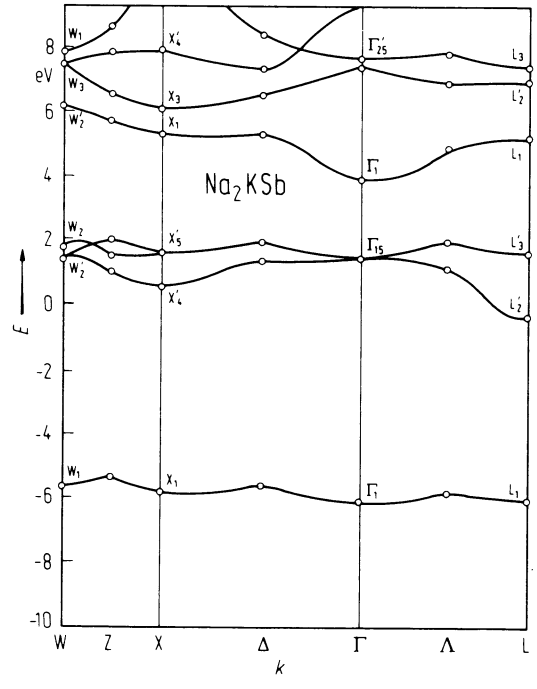

Fig.30. Na_2KSb. Band structure calculated by an empirical pseudopotential method.

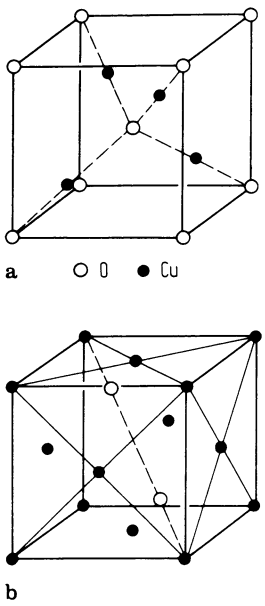

Fig.31. Cu_2O. Cuprite structure. (a) Origin on an O site; (b) origin on a Cu site.

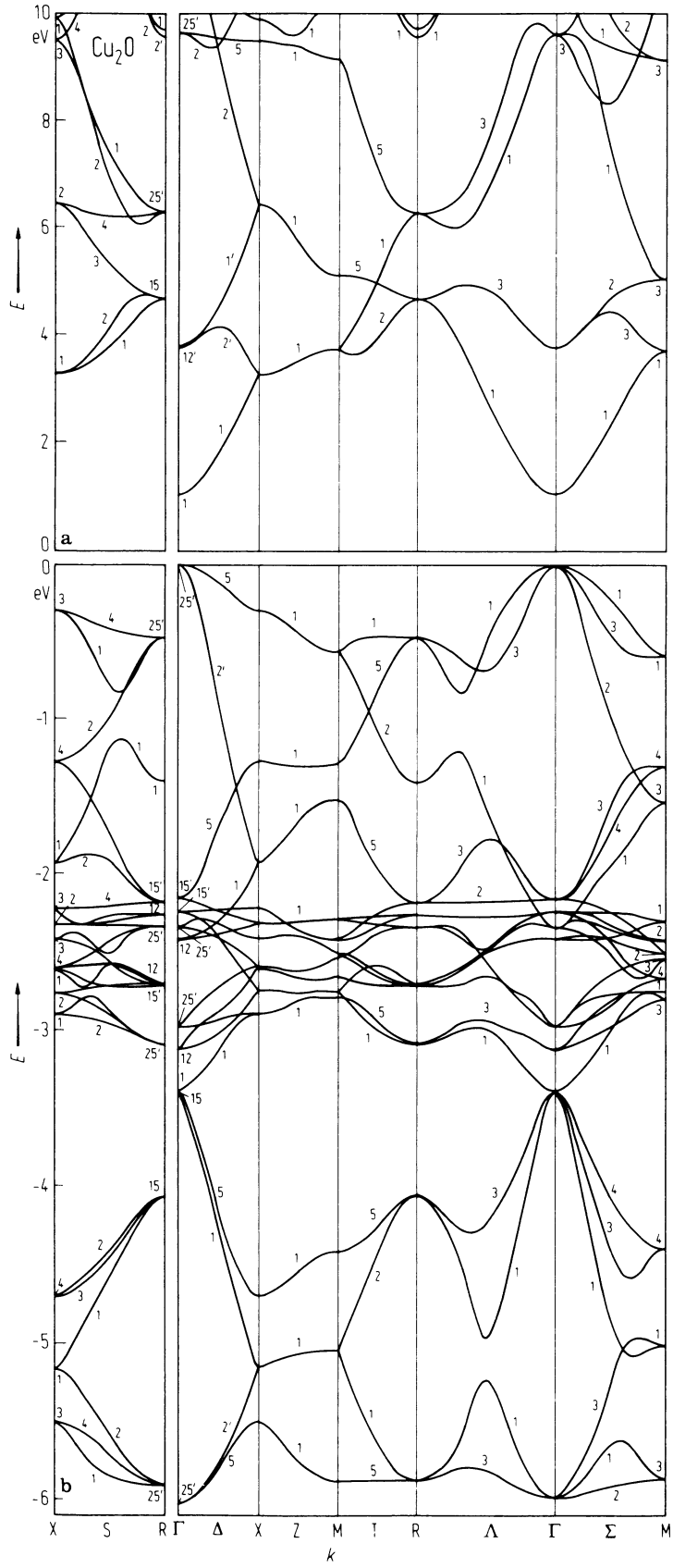

Fig.32. Cu_2O. Band structure for the (a) conduction bands and (b) valence bands.

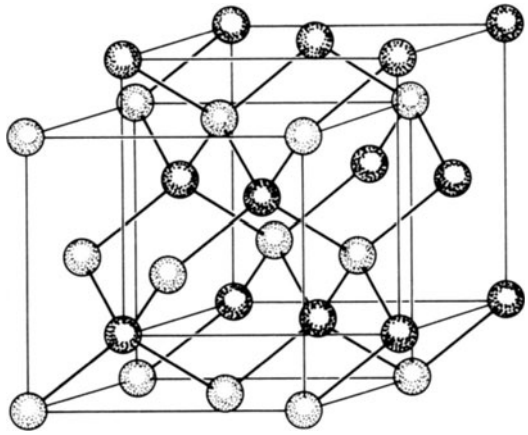

Fig.33. The zincblende lattice.

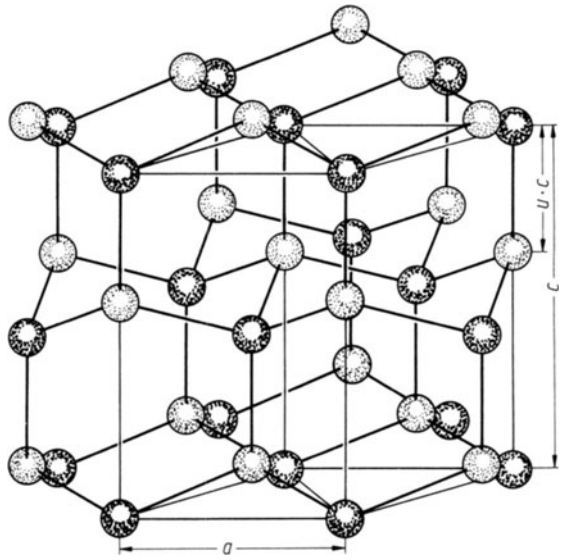

Fig.34. The wurtzite lattice.

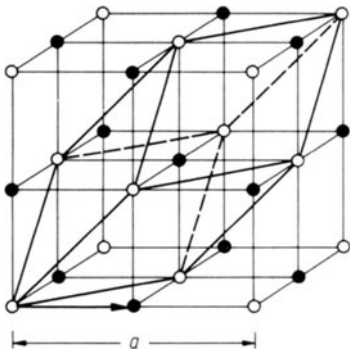

Fig.35. The NaCl lattice.

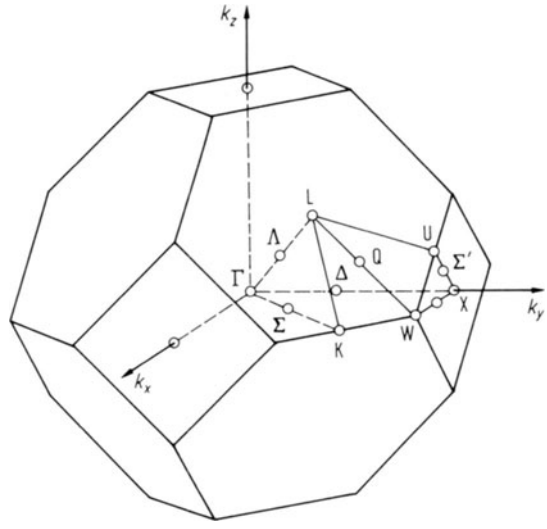

Fig.36. Brillouin zone of the zincblende and NaCl lattices.

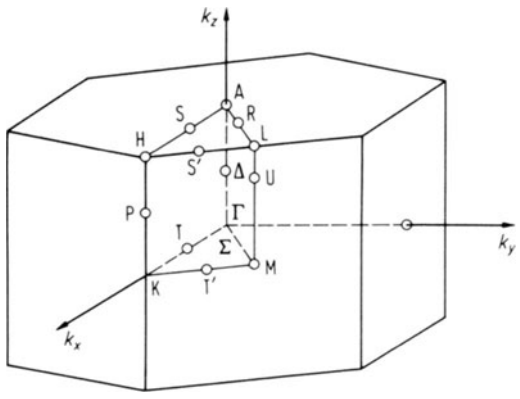

Fig.37. Brilloun zone of the wurtzite lattice.

Fig.38 (right). CuCl, CuBr, AgCl, AgBr. Band structures ▶ calculated with a relativistic KKR method.

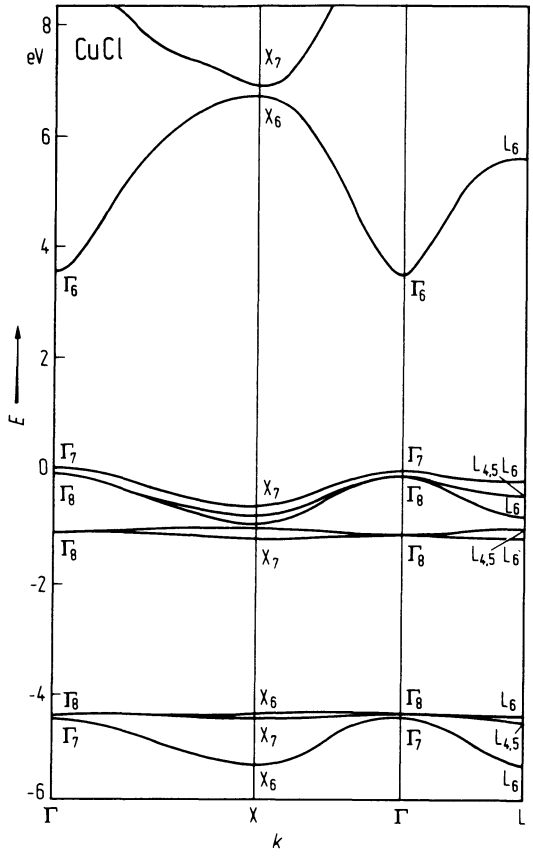
CuCl
eV
8
6
4
2
0
-2
-4
-6
E
Γ
X
Γ
L
k

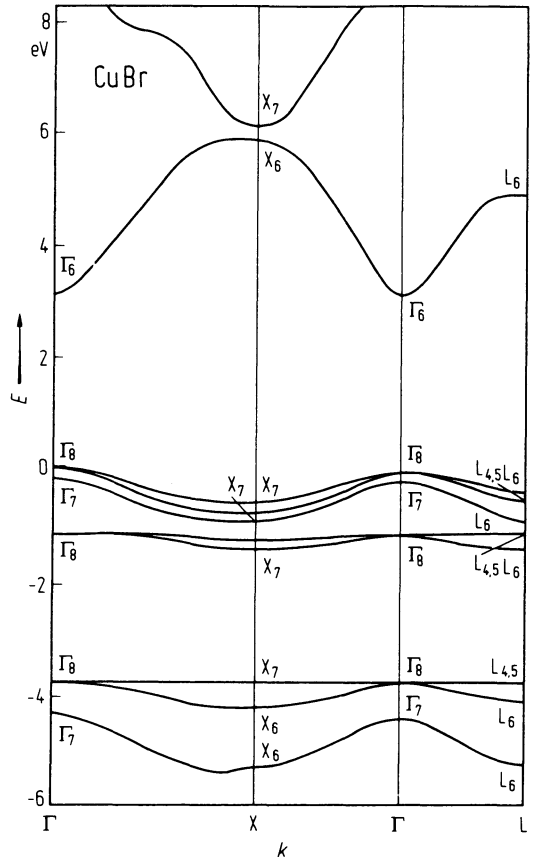
CuBr
eV
8
6
4
2
0
-2
-4
-6
E
Γ
X
Γ
L
k

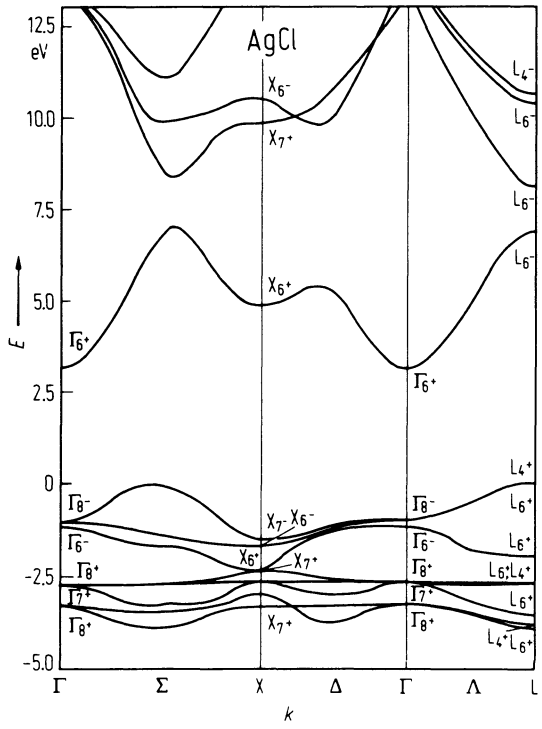
AgCl
eV
12.5
10.0
7.5
5.0
2.5
0
-2.5
-5.0
E
Γ
Σ
X
Δ
Γ
Λ
L
k

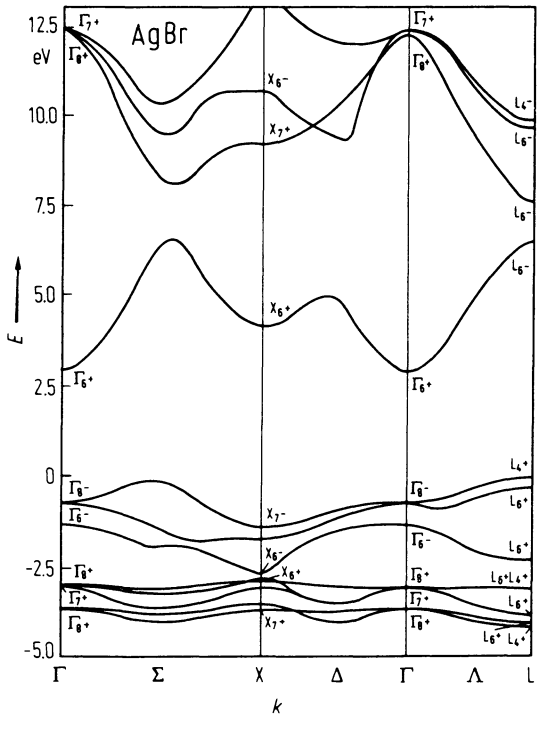
AgBr
eV
12.5
10.0
7.5
5.0
2.5
0
-2.5
-5.0
E
Γ
Σ
X
Δ
Γ
Λ
L
k

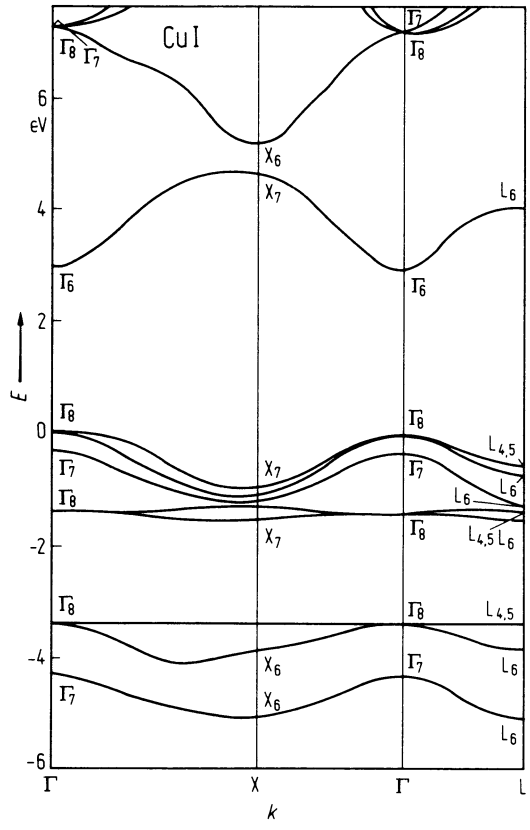

Fig.39. CuI. Band structure calculated with a relativistic KKR method.

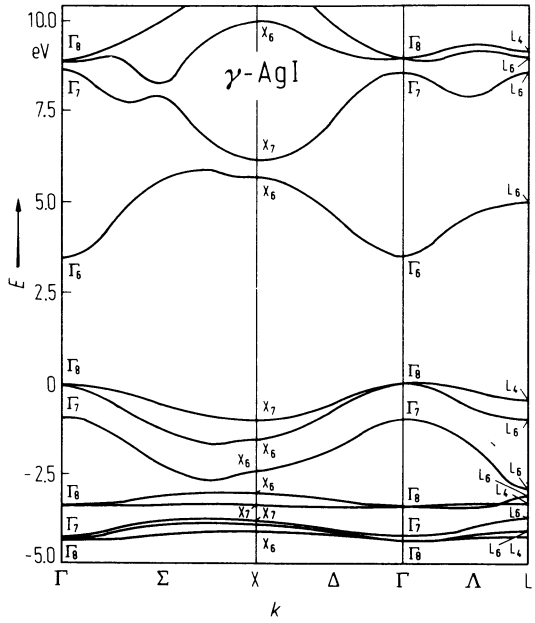

Fig.41. γ-AgI. Band structure calculated with a relativistic KKR method.

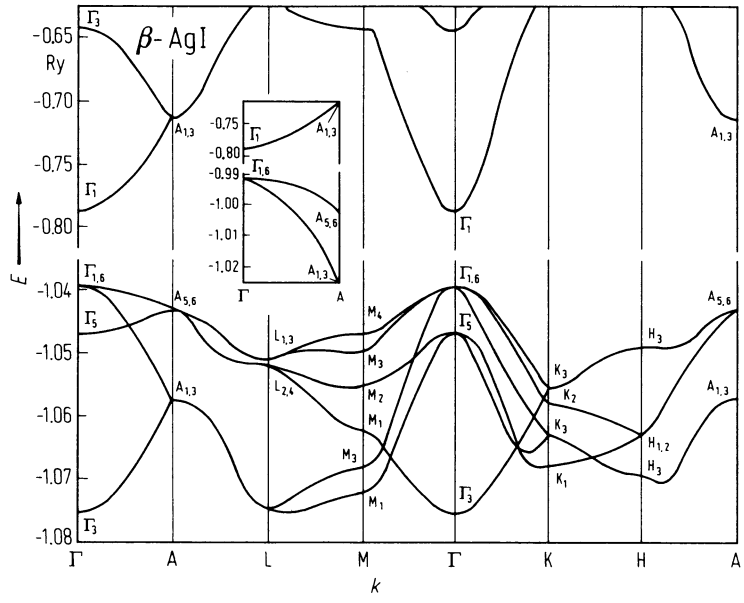

Fig.40. β-AgI. Band structure calculated by a tight-binding approach neglecting spin-orbit interaction.

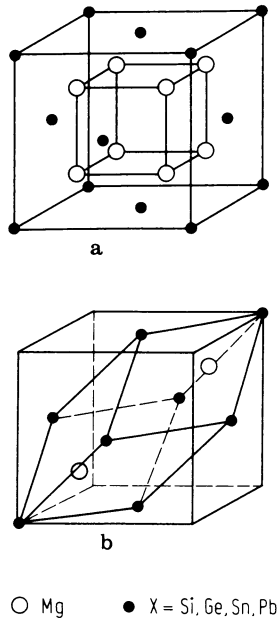

Fig.42. The antifluorite lattice of the Mg_2X-compounds. (a) Face centered sublattice of the X-atoms and simple cubic sublattice of the Mg-atoms, (b) primitive cell.

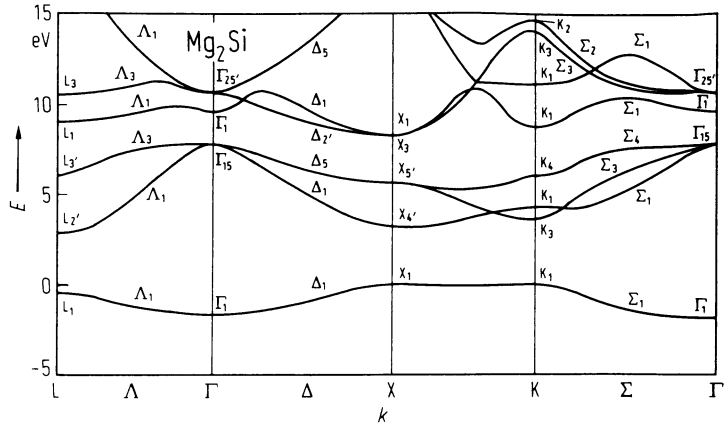

Fig.43. Mg_2Si. Band structure calculated by a non-relativistic pseudopotential method.

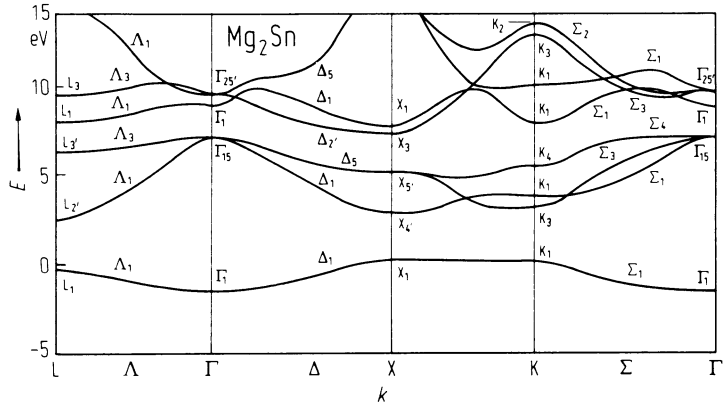

Fig.44. Mg_2Ge. Band structure calculated by a non-relativistic pseudopotential method.

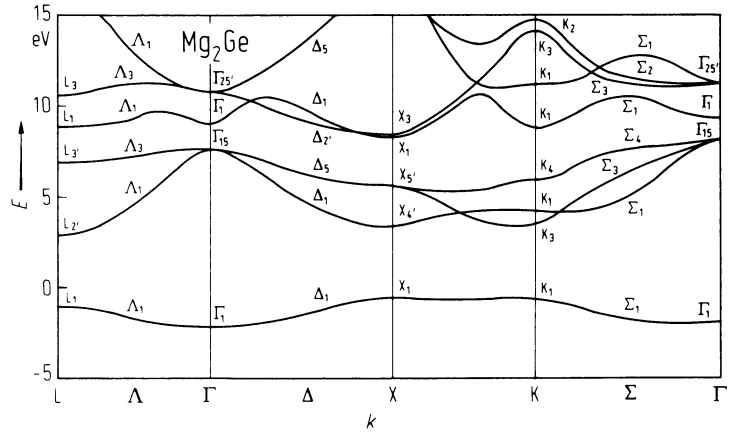

Fig.45. Mg_2Sn. Band structure calculated by a non-relativistic pseudopotential method.

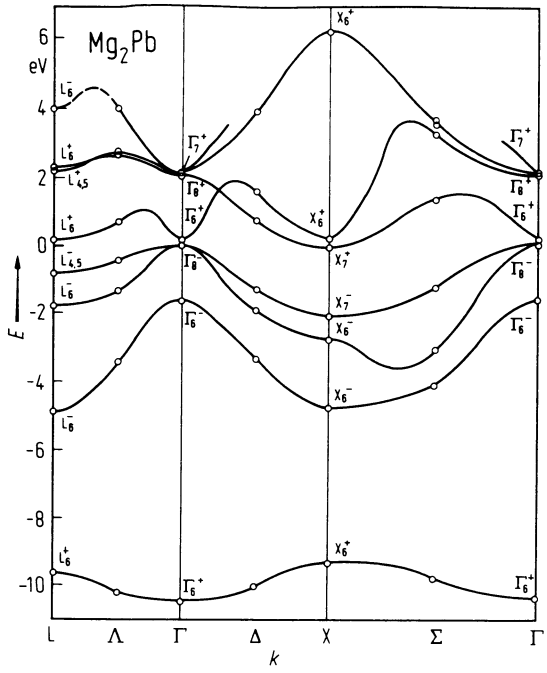

Fig.46. Mg_2Pb. Band structure calculated with a relativistic OPW method.

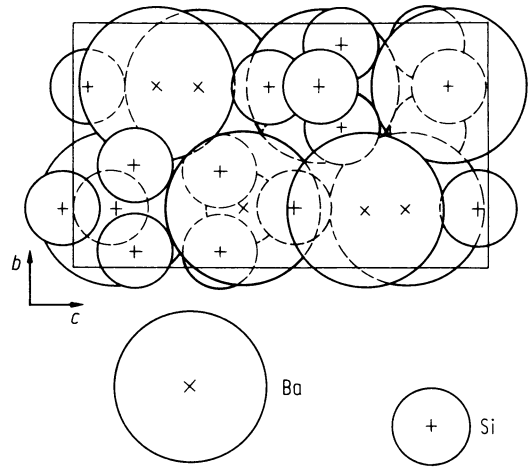

Fig.47. $BaSi_2$. Primitive cell containing eight Ba-atoms and four tetrahedra with four Si-atoms each.

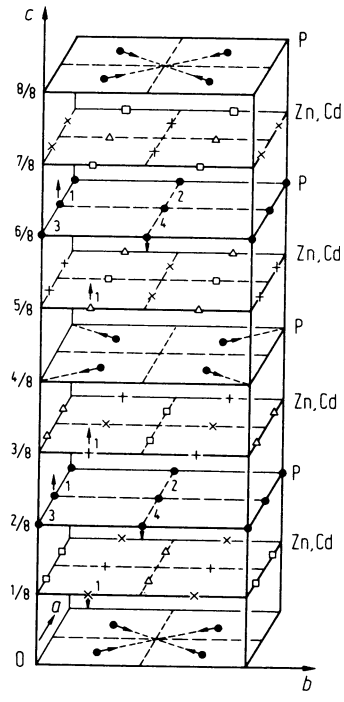

× Zn, Cd (1) site
+ Zn, Cd (2) site
△ Zn, Cd (3) site
□ vacant position on Zn sublattice
• P site

Fig.48. Zn_3P_2, Cd_3P_2. Unit cell stretched along the c-axis. Atoms at ideal positions.

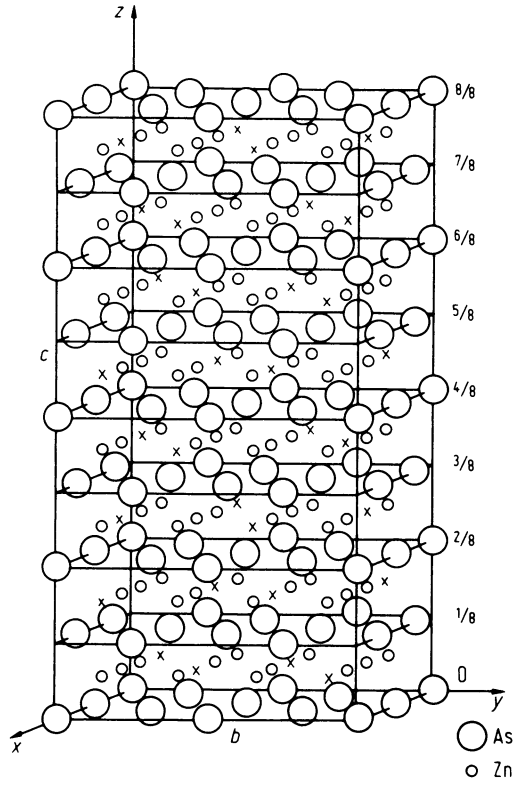

Fig.49. Zn_3As_2. Crystal structure of the α-phase.

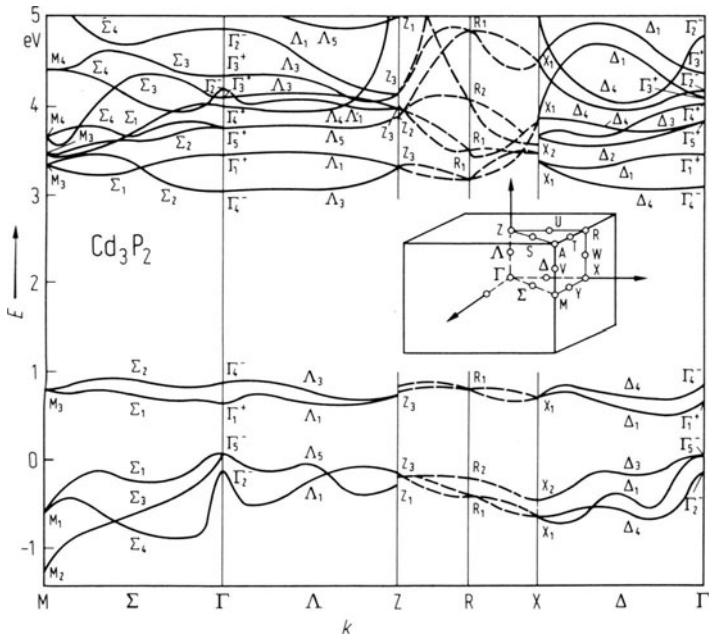

Fig.50. Cd_3P_2. Band structure calculated by the pseudopotential method.

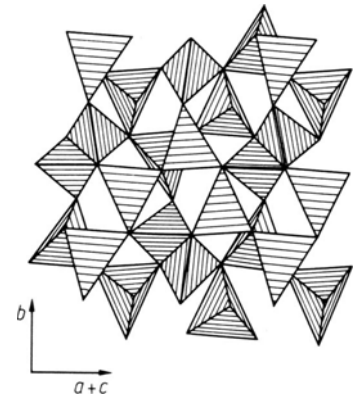

Fig.51. Zn_4Sb_3. Structure in coordination tetrahedrals.

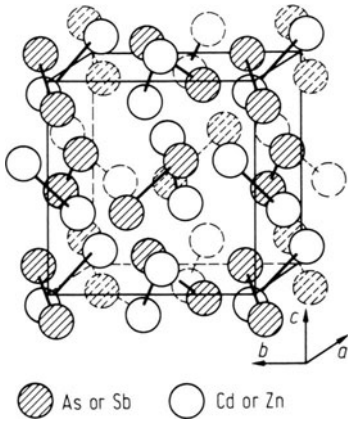

Fig.52. ZnSb, CdSb. Crystal structure.

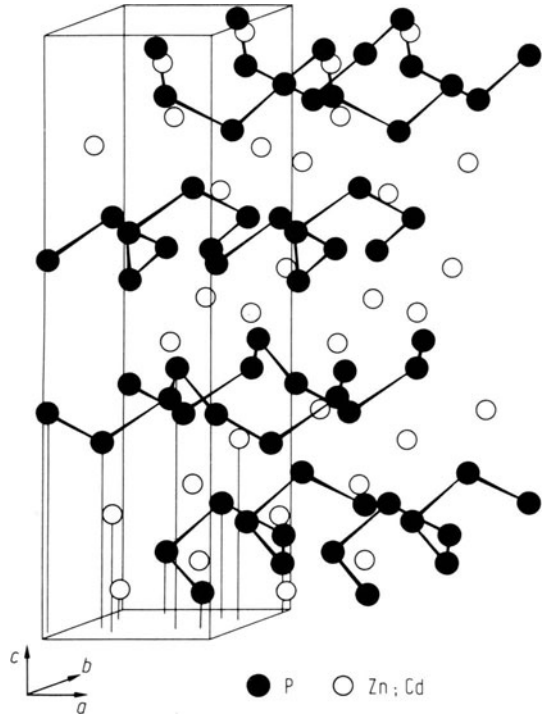

Fig.53. α-ZnP_2, β-CdP_2. Tetragonal unit cell.

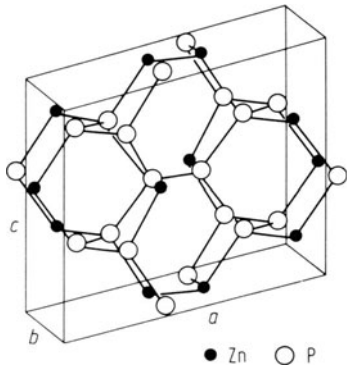

Fig.54. β-ZnP_2. Monoclinic unit cell.

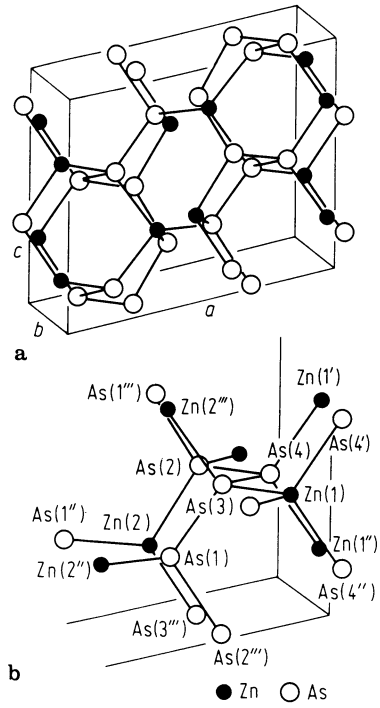

Fig.55. $ZnAs_2$. (a) Structure of the monoclinic lattice, (b) Zn and As environments.

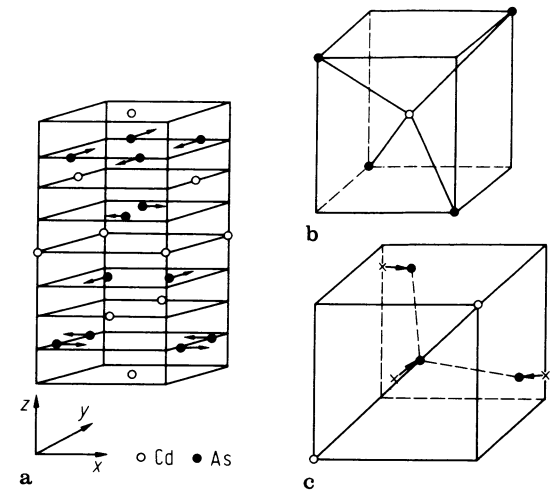

Fig.56. $CdAs_2$. The nearest environment of atoms in the $CdAs_2$-structure; (a) unit cell, (b) tetrahedral coordination of Cd, (c) tetrahedral coordination of As.

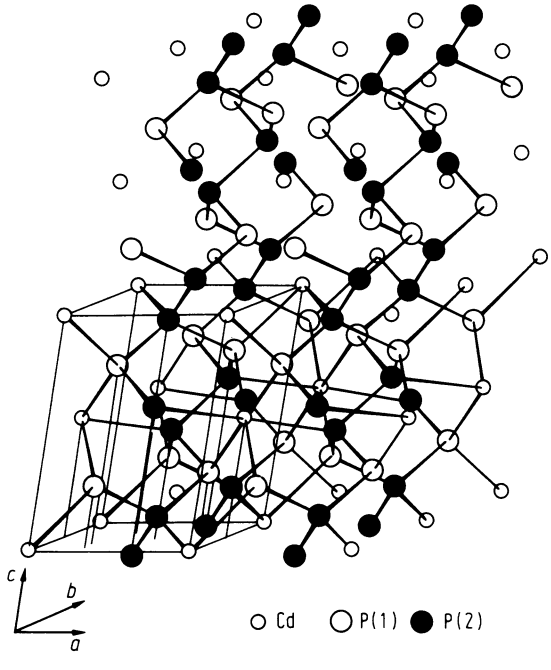

Fig.57. CdP_4. Monoclinic structure. Bonds between all atoms are shown in the lower part and the anion subarrays are emphasized in the upper part of the diagram.

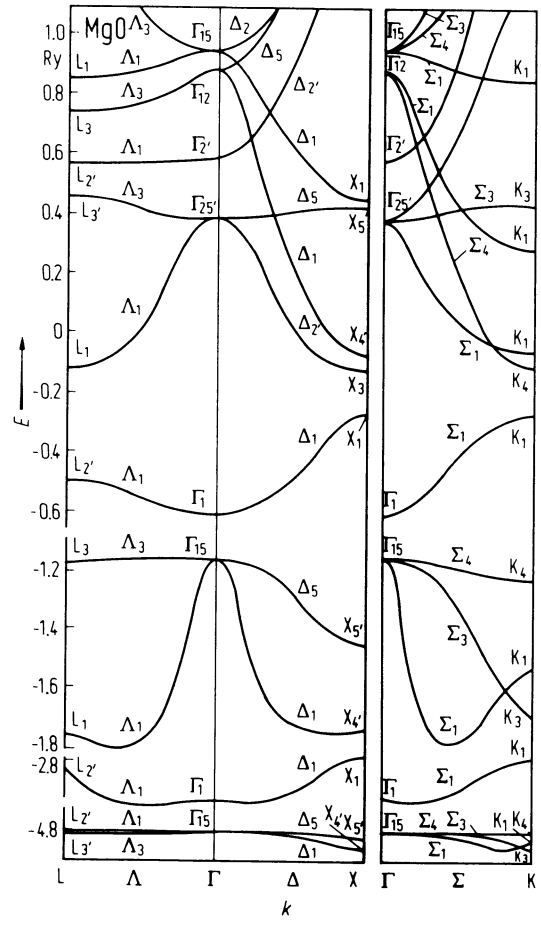

Fig.58. MgO. Band structure calculated with a combined tight-binding and pseudopotential method.

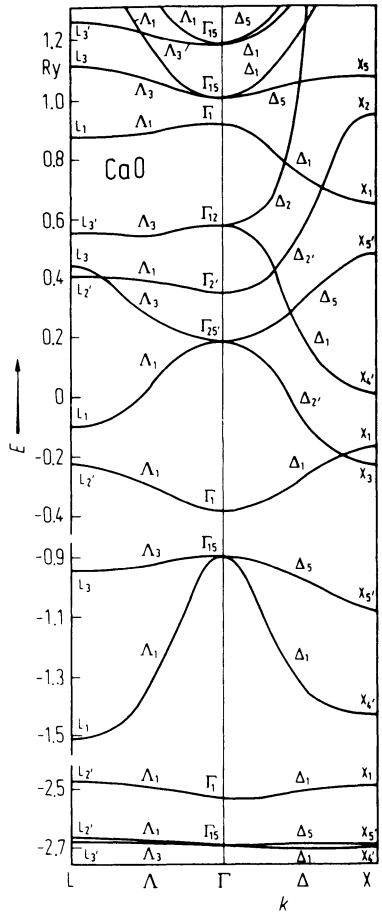

Fig.59. CaO. Band structure calculated with a combined tight-binding and pseudopotential method.

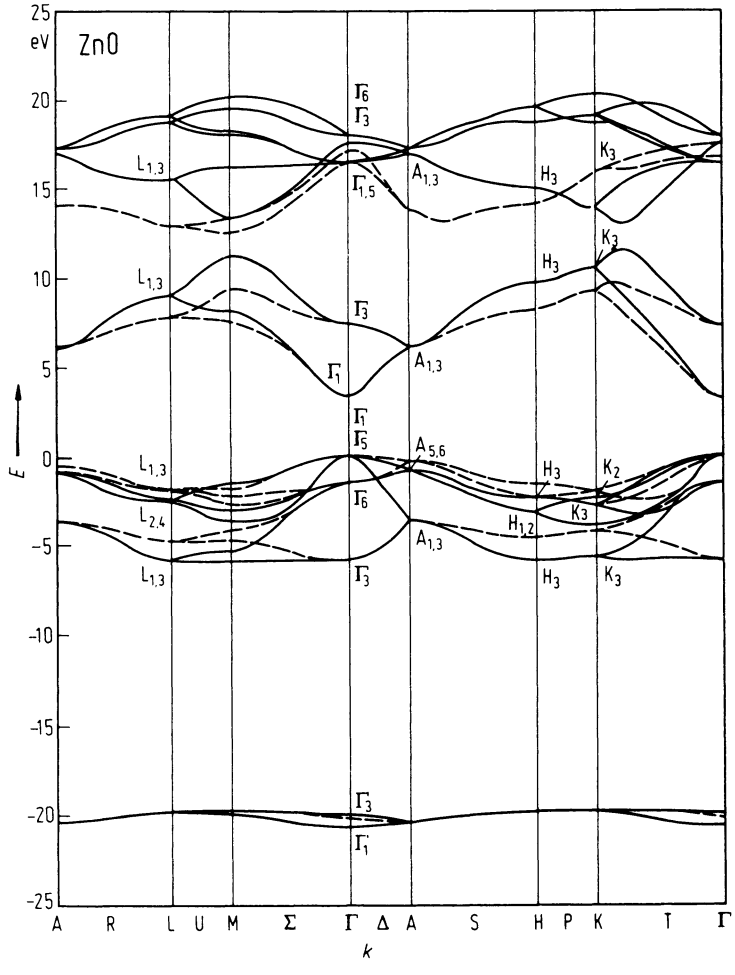

Fig.60. ZnO. Band structure calculated with an empirical tight-binding model. Energy bands corresponding to Zn 3d states are not included into the calculations.

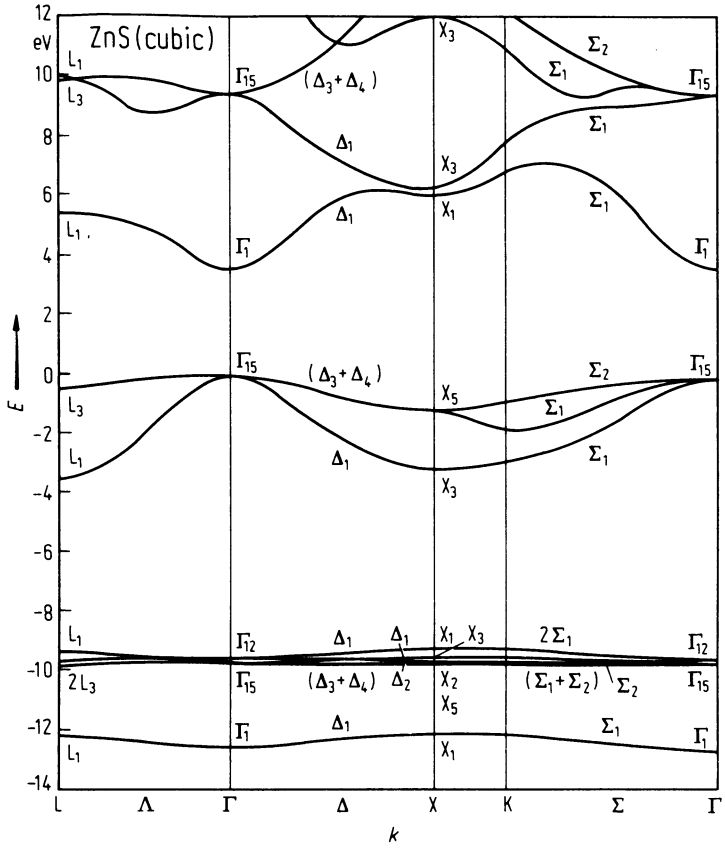

Fig.61. ZnS (cubic). Band structure from a first-principles OPW method.

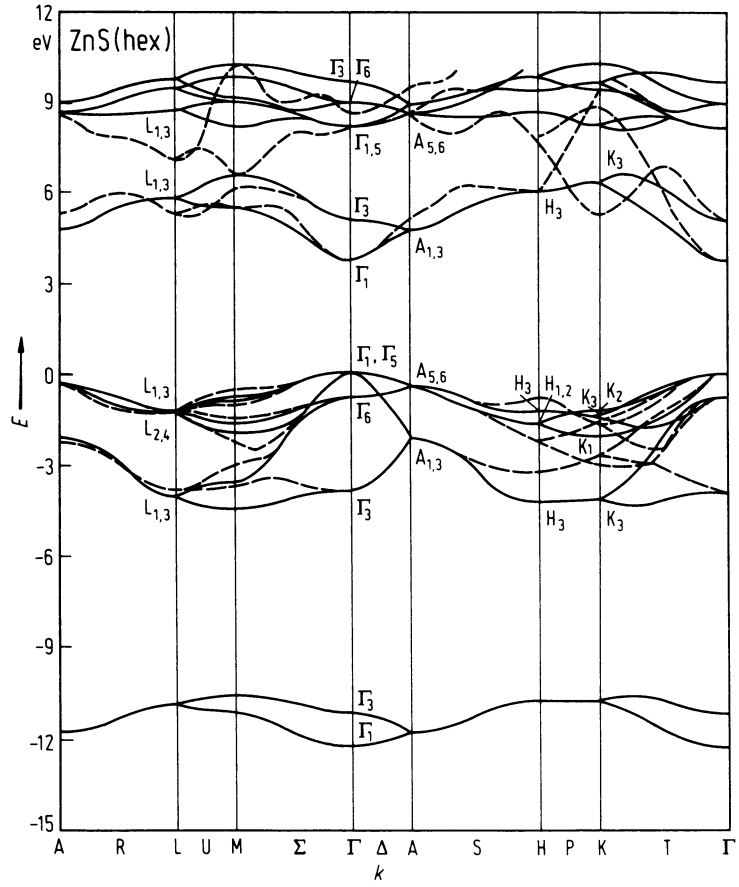

Fig.62. ZnS (hexagonal). Band structure from a semi-empirical tight-binding calculation. Energy bands corresponding to Zn 3d states and spin-orbit coupling are not included into the calculations.

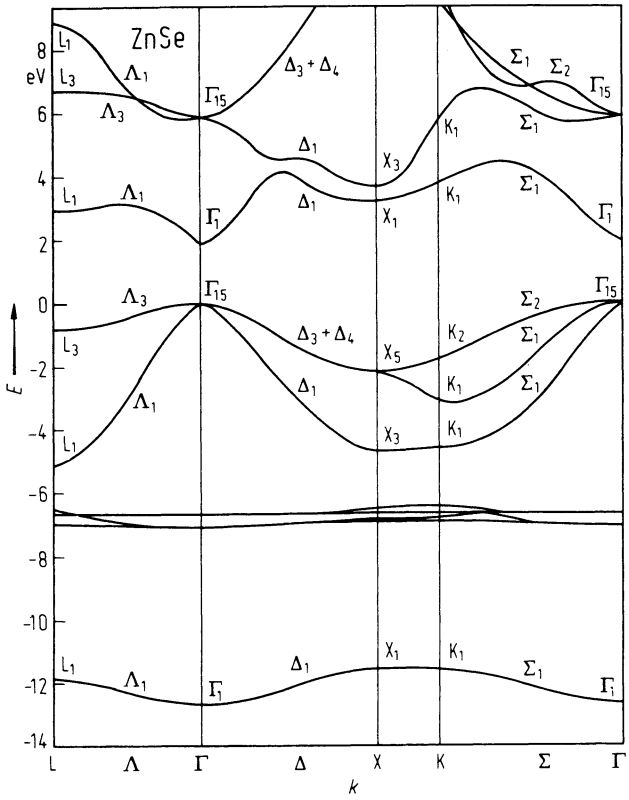

Fig.63. ZnSe. Band structure from a first-principles calculation. The calculation includes energy bands corresponding to Zn 3d states but does not consider spin-orbit coupling.

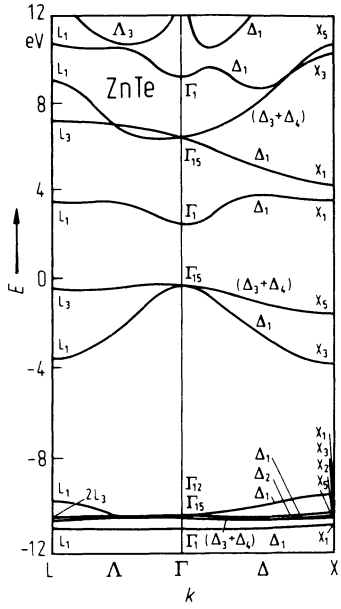

Fig.64. ZnTe. Band structure from an OPW calculation. The calculation includes Zn 3d states but not spin-orbit coupling.

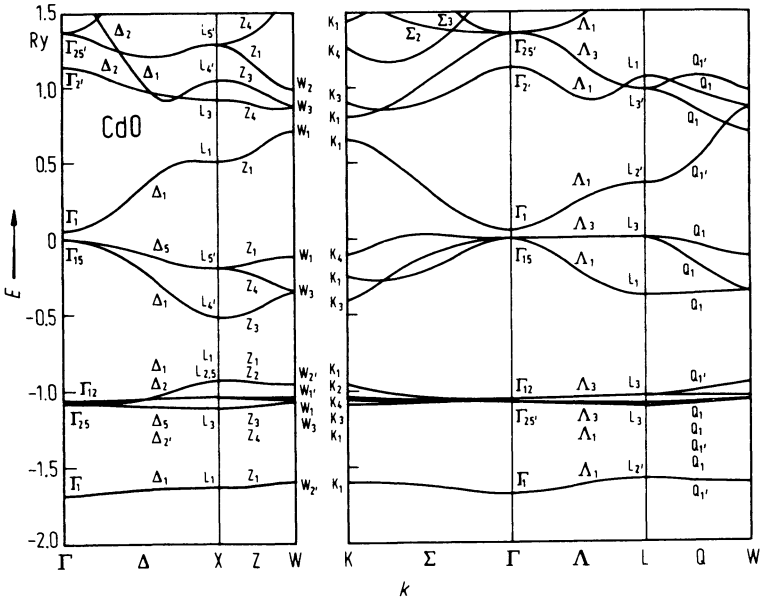

Fig.65. CdO. Band structure from an ab-initio calculation.

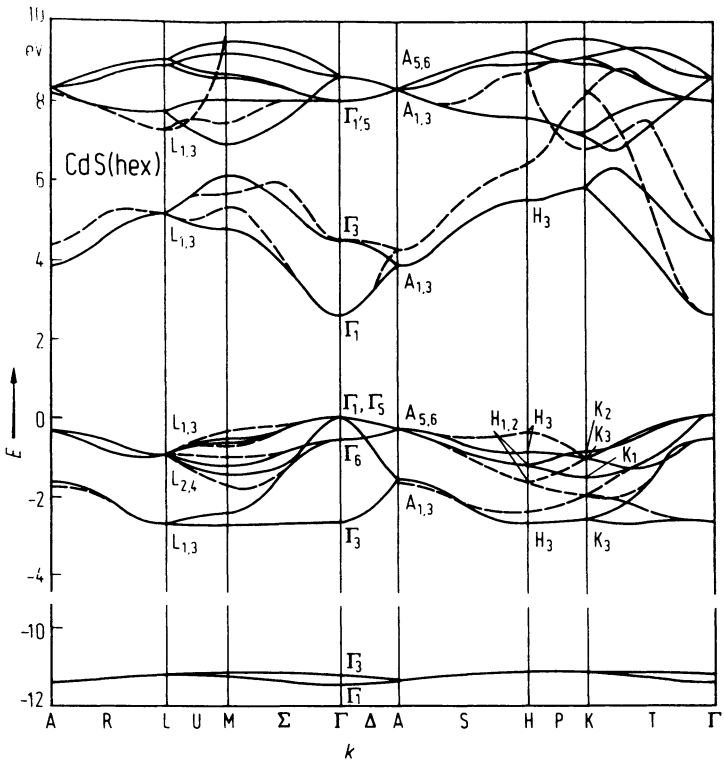

Fig.66. CdS (hexagonal). Band structure from an empirical tight-binding model (solid lines) compared with results from a pseudopotential calculation (dashed lines). Cd 4d states and spin-orbit coupling not considered.

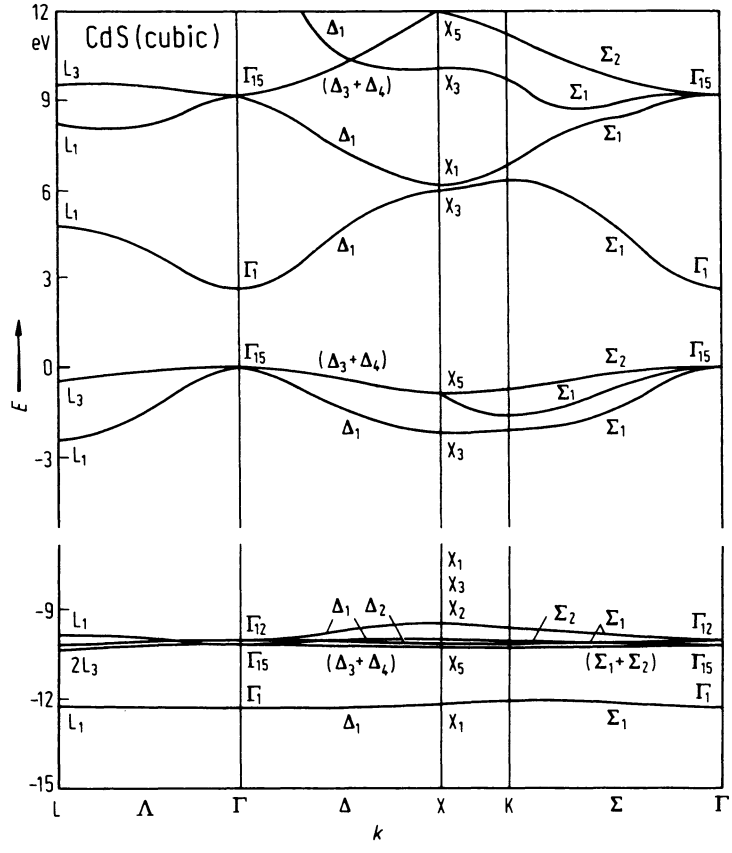

Fig.67. CdS (cubic). Band structure from a first principles calculation including Cd 4d states but not considering spin-orbit coupling.

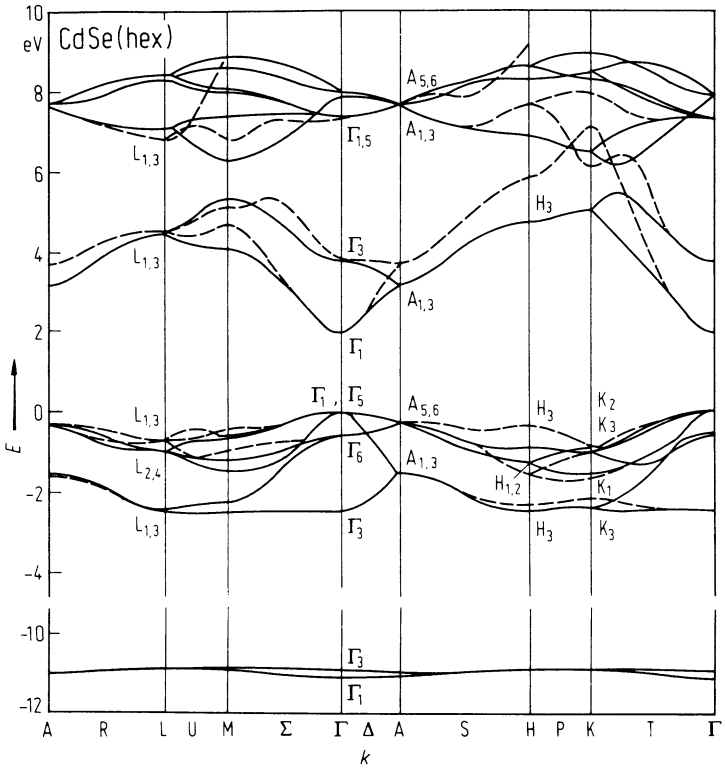

Fig.68. CdSe. Band structure from a semi-empirical tight-binding method. Cd 4d states and spin-orbit coupling not considered.

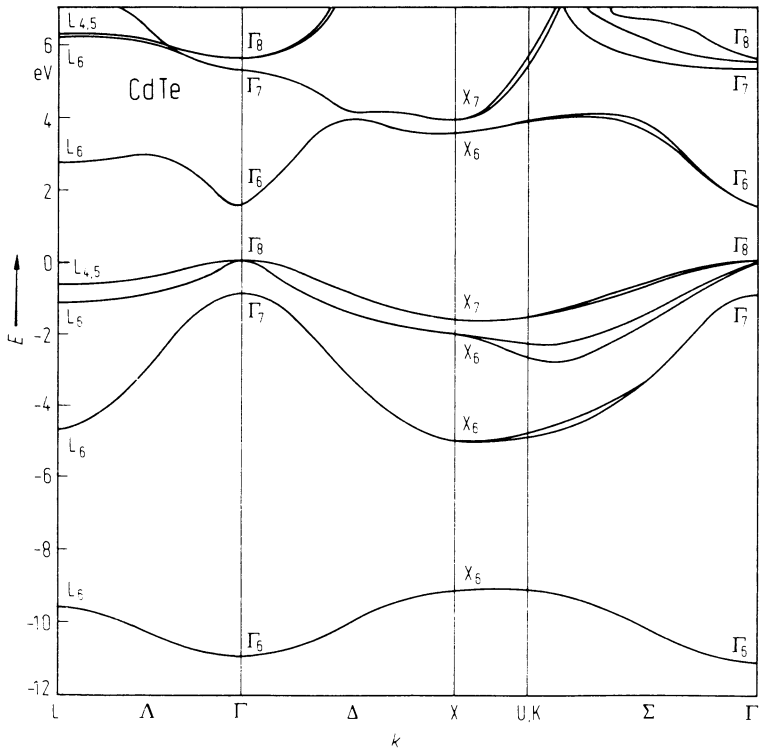

Fig.69. CdTe. Band structure from a non-local pseudopotential calculation.

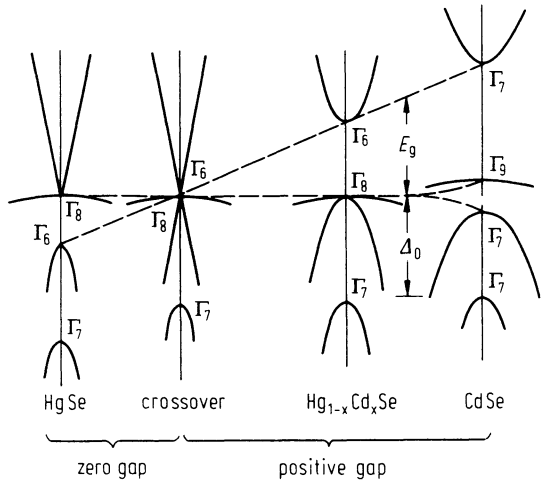

Fig.70. HgSe. Schematic band structure near the midpoint of the Brillouin zone for the Hg-Cd-Se system.

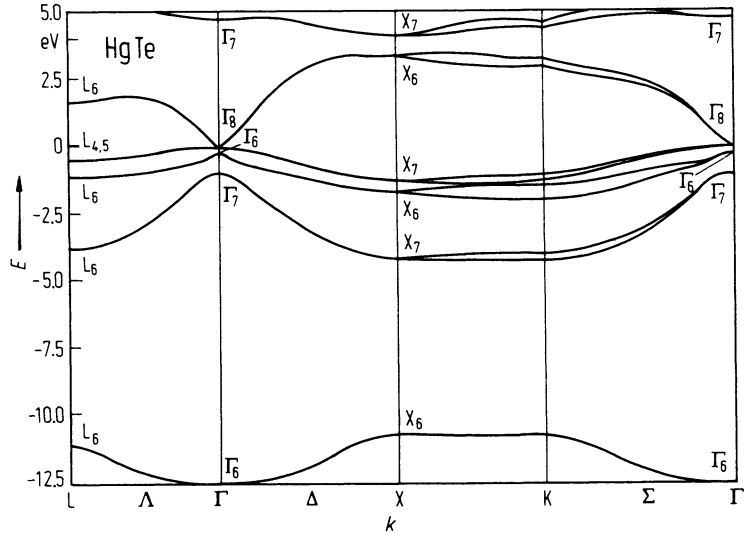

Fig.71. HgTe. Band structure from a tight-binding calculation.

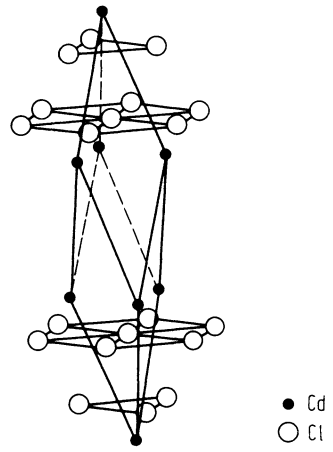

Fig.72. $CdCl_2$. Unit rhombohedron of the crystal lattice.

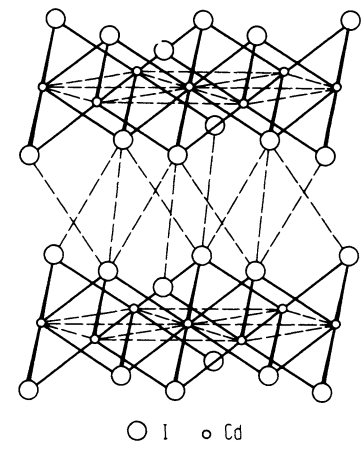

Fig.73. CdI_2. Crystal structure.

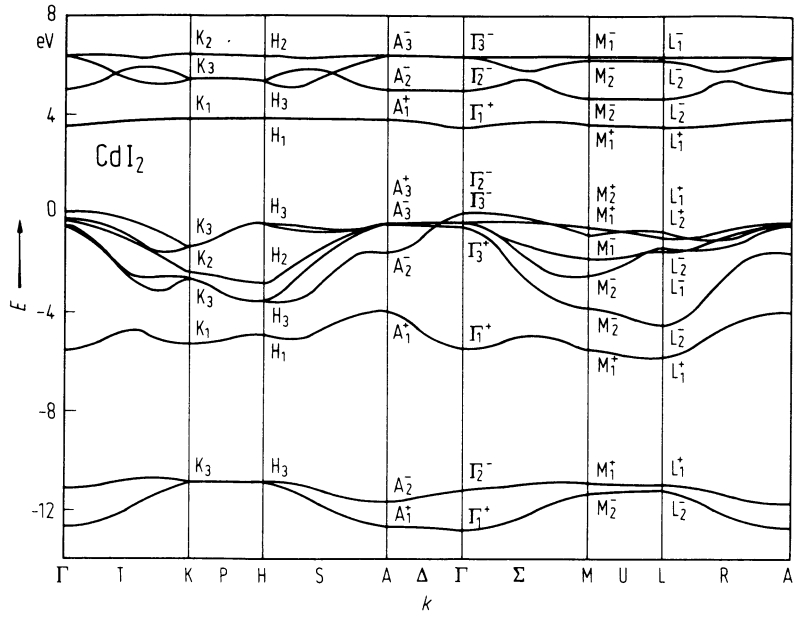

Fig.74. CdI_2. Band structure from a modified semi-empirical tight-binding calculation.

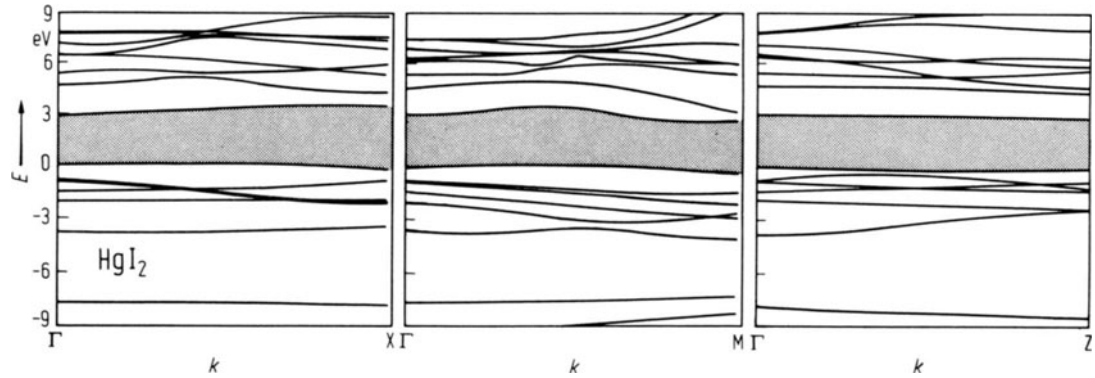

Fig.75. α-HgI_2. Pseudopotential band structure for three symmetry directions.

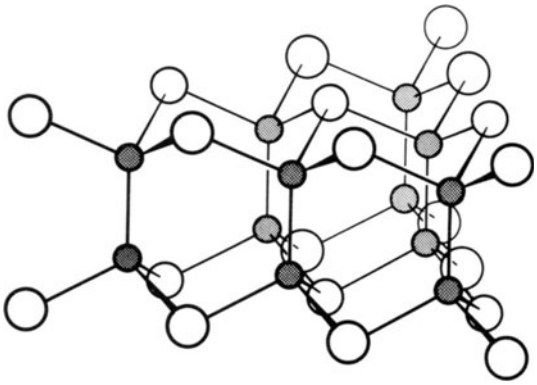

Fig.76. GaSe. The four-fold layer met in GaS, GaSe and InSe; cations: small shaded circles, anions: large open circles.

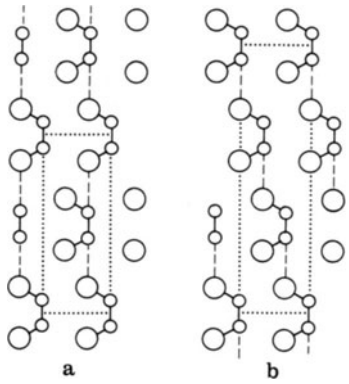

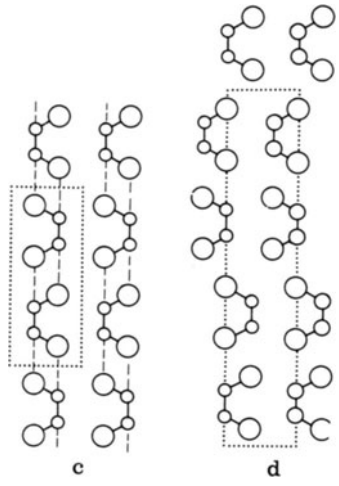

Fig.77. GaSe. Layer structure with cation pairs and tetrahedral cation coordination; (110) sections through the hexagonal cells. (a) ε-GaSe, (b) γ-GaSe, (c) β-GaSe, (d) δ-GaSe.

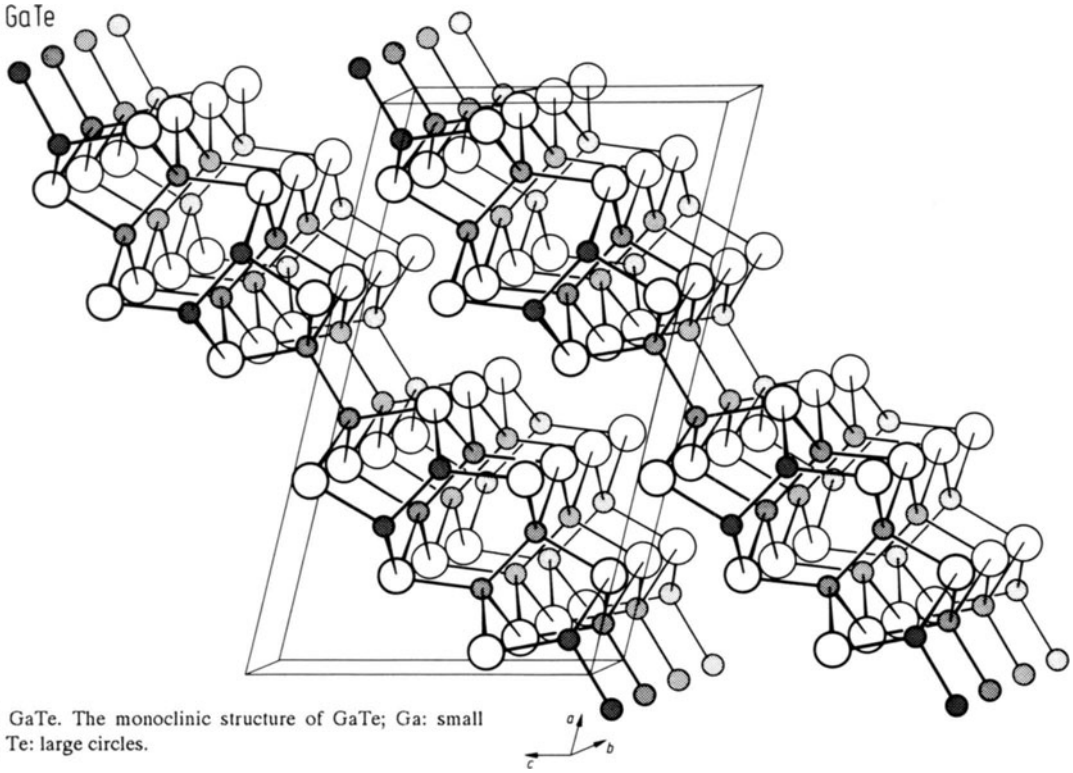

Fig.78. GaTe. The monoclinic structure of GaTe; Ga: small circles, Te: large circles.

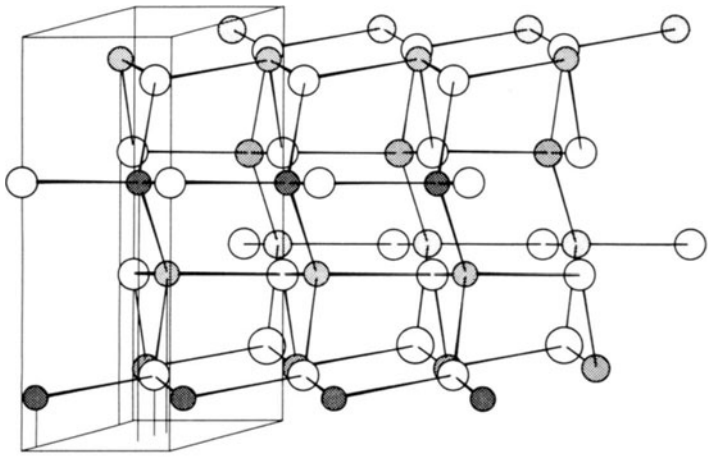

Fig.79. InS. The orthorhombic structure of β-InS. In: small shaded circles, S: large open circles.

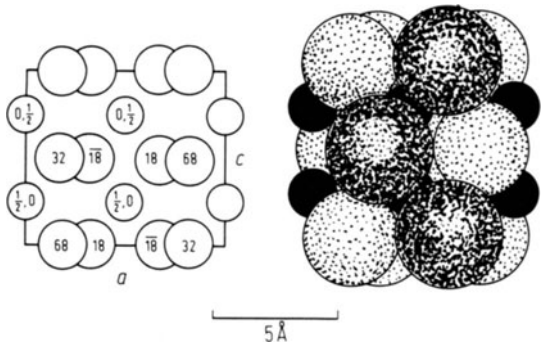

Fig.80. TlSe. The tetragonal structure of TlSe projected along the b-axis. Tl: small circles, Se: large circles. Integer numbers refer to fractional y coordinates.

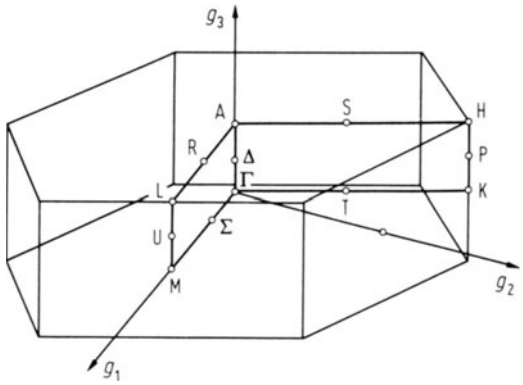

Fig.81. Brillouin zone for the hexagonal lattice.

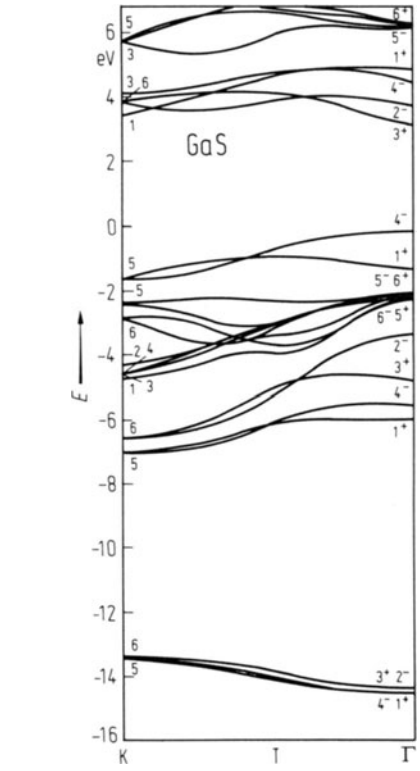

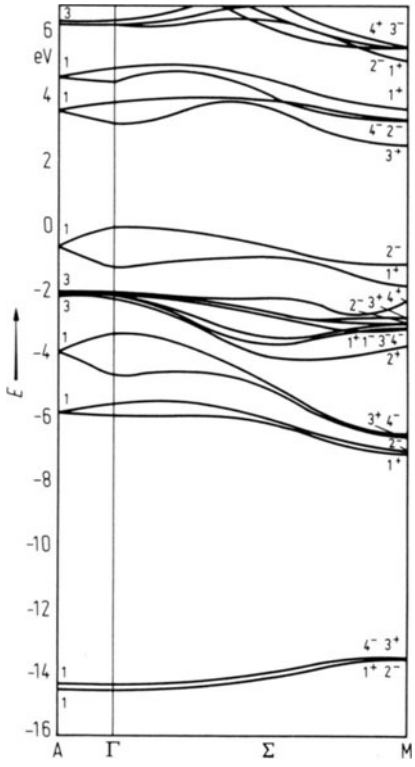

Fig.82. GaS. Empirical pseudopotential band structure for the β-polytype.

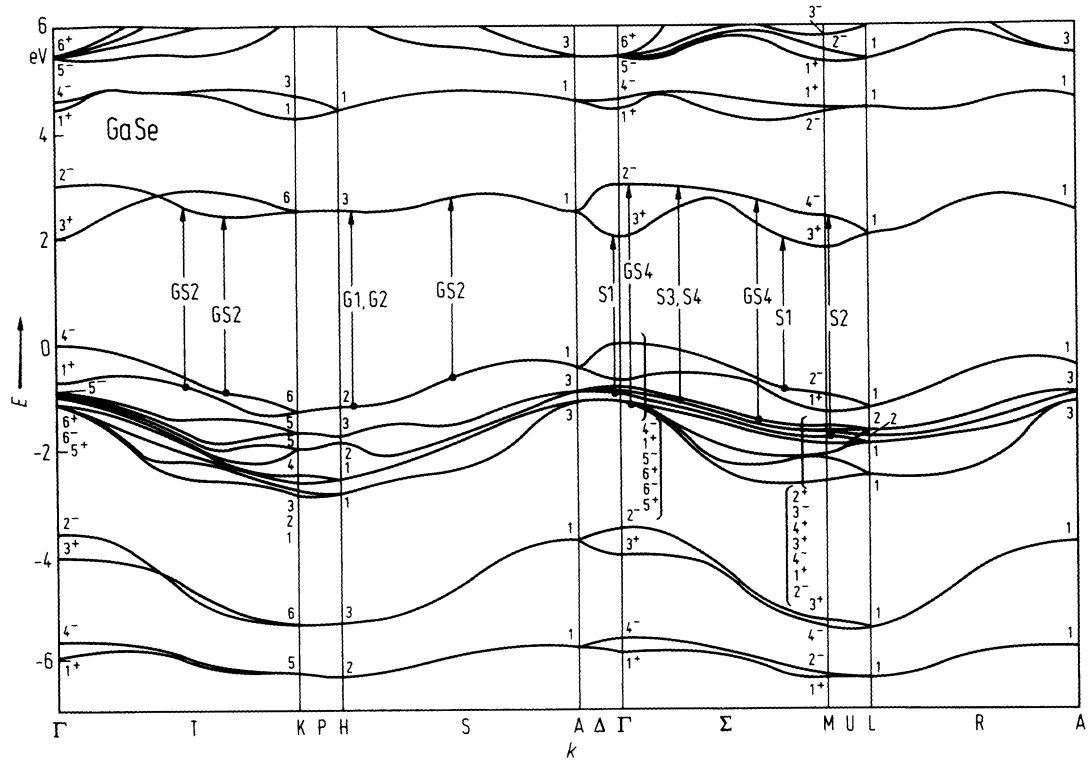

Fig.83. GaSe. Empirical pseudopotential band structure for the β-polytype.

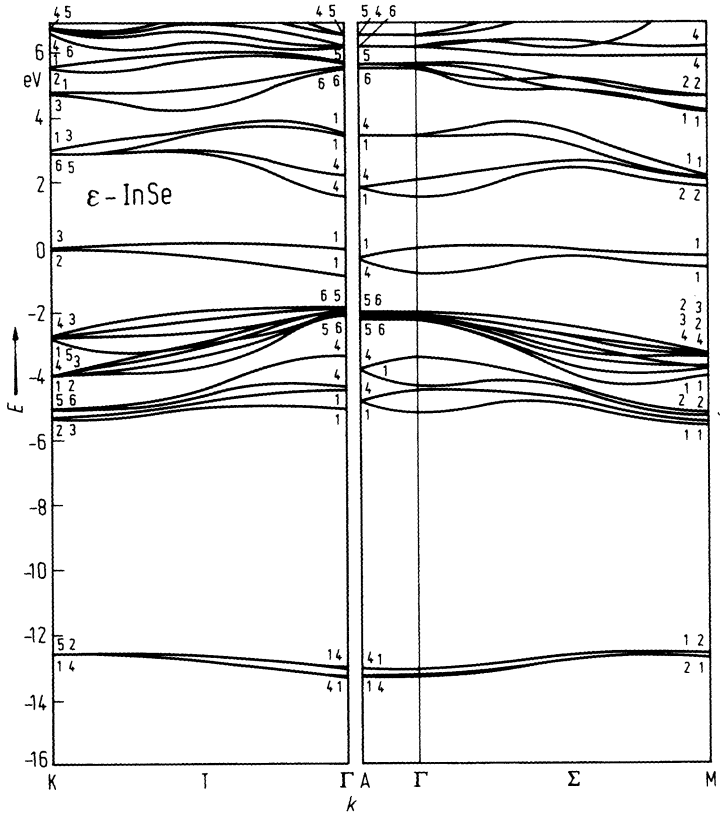

Fig.84. InSe. Empirical pseudopotential band structure for the ε-polytype.

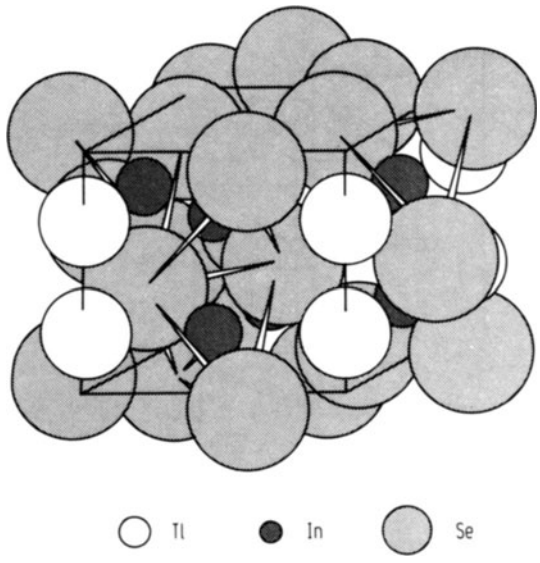

Fig.85. $TlInSe_2$. Crystal structure.

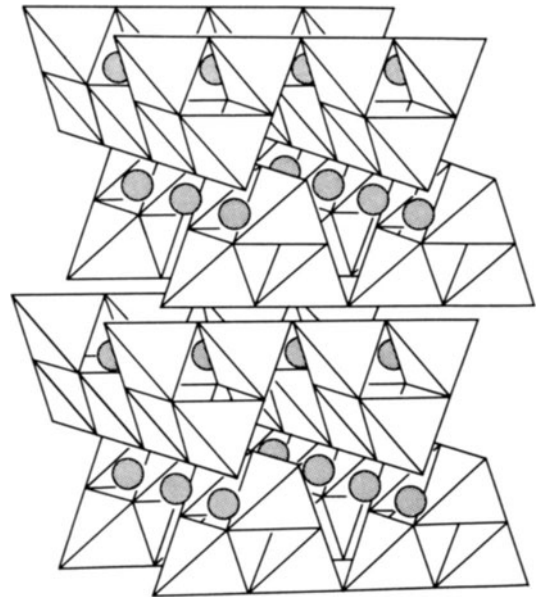

Fig.86. $TlGaSe_2$. Layered crystal structure of $TlGaSe_2$. The position of the Tl ions is shown between the stacking of the anion layers built of Ga_4Se_{10} polyhedra.

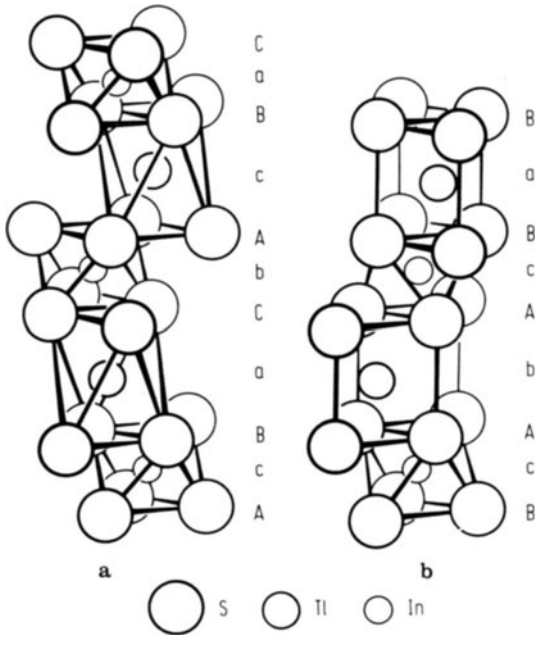

Fig.87. $TlInS_2$. Lattice structure, (a) type II, (b) type III. The stacking of the S ion layers and of the metal ion layers along the c-axis is indicated by small and large capitals, respectively.

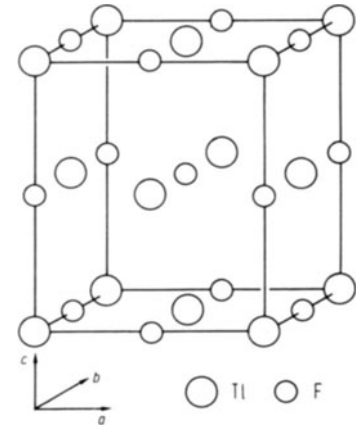

Fig.88. TlF(II). Unit cell of the orthorhombic TlF structure.

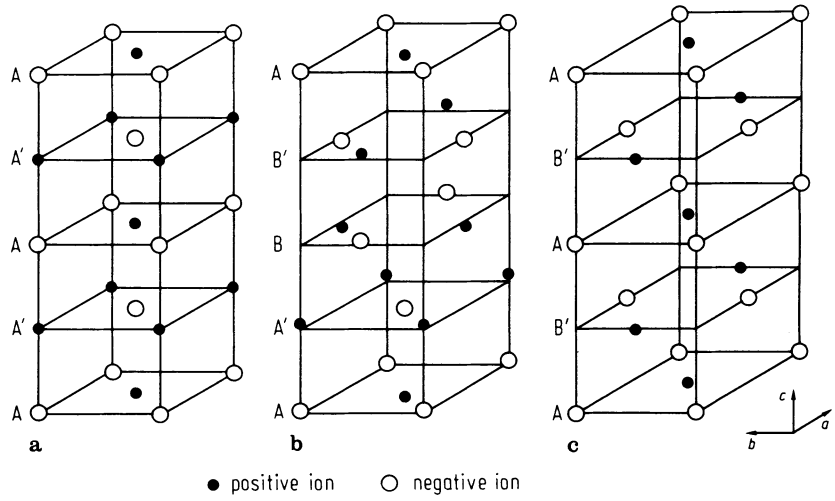

Fig.89. TlI. Enlarged unit cell of TlI: (a) NaCl-type, (b) orthorhombic TlI type, (c) CsCl-type.

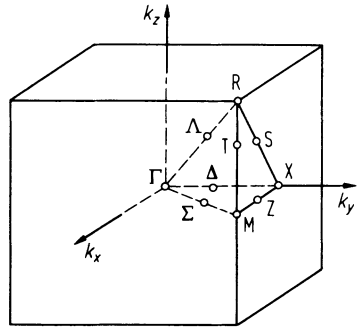

Fig.90. TlI(I). Brillouin zone of the CsCl lattice.

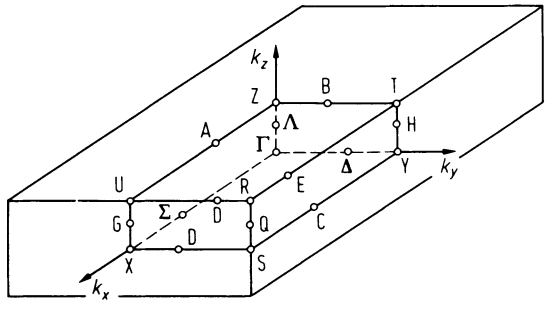

Fig.91. TlI(II). Brillouin zone for the orthorhombic TlI lattice.

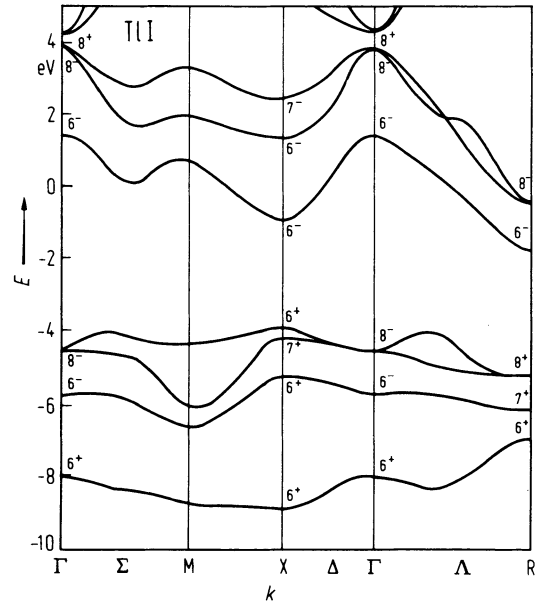

Fig.92. TlI(I). Band structure of ClCs-type TlI calculated with the relativistic KKR method.

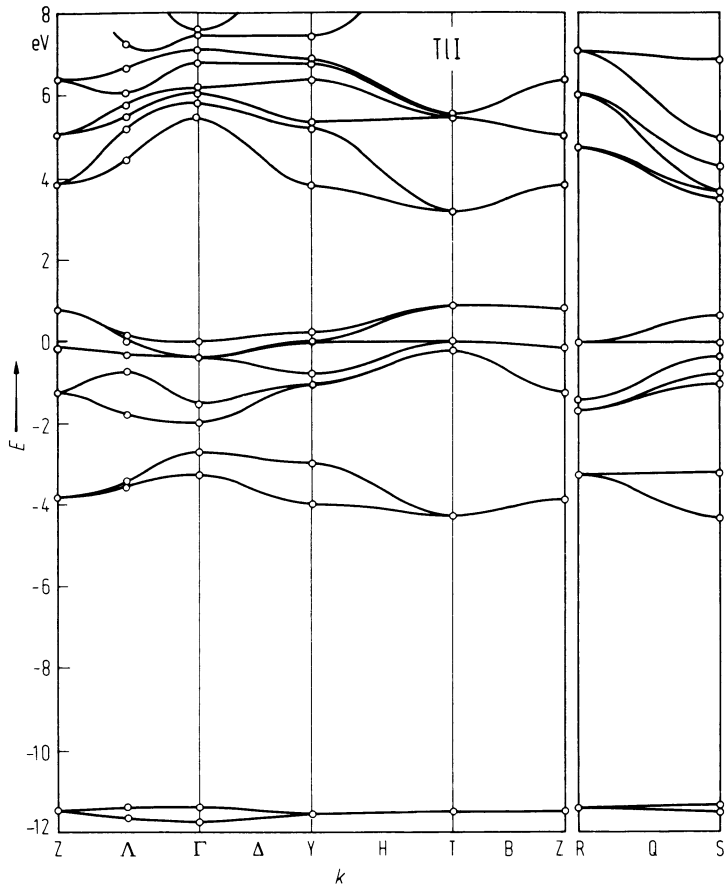

Fig.93. TlI(II). Band structure of orthorhombic TlI calculated with the OPW method neglecting spin-orbit interaction.

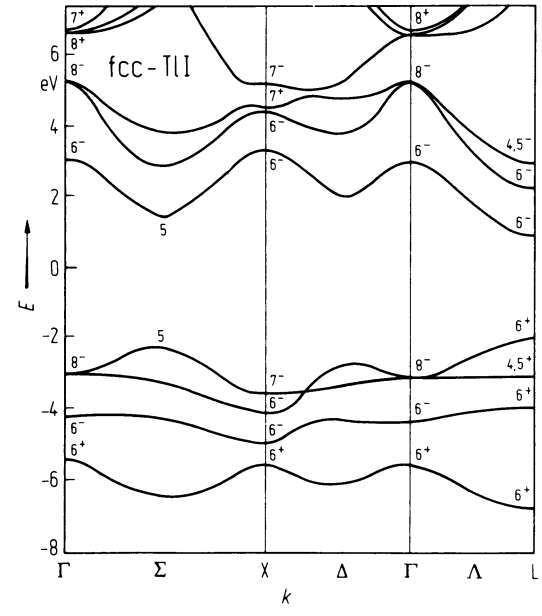

Fig.94. TlI(III). Band structure of fcc-TlI calculated with the relativistic KKR method.

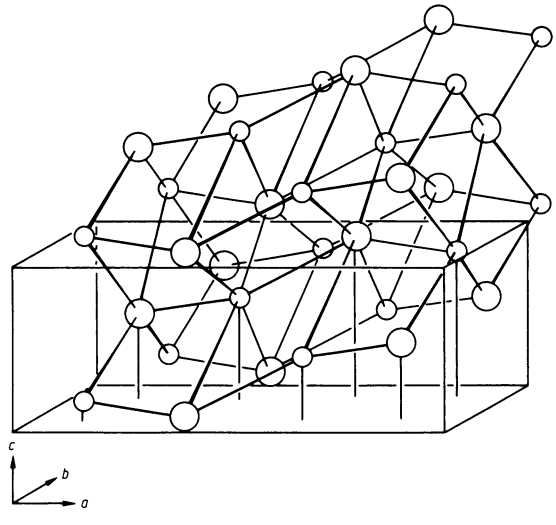

Fig.95. GeS. Lattice structure.

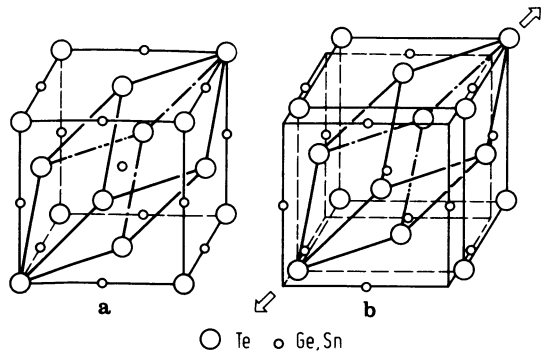

Fig.96. GeTe, SnTe. (a) Elementary cell of the NaCl-like structure, (b) the rhombohedral unit cell of the NaCl-type sublattice. A distortion along [111] direction combined with a sublattice shift causes the rhombohedral As-like B13 phase of GeTe and SnTe.

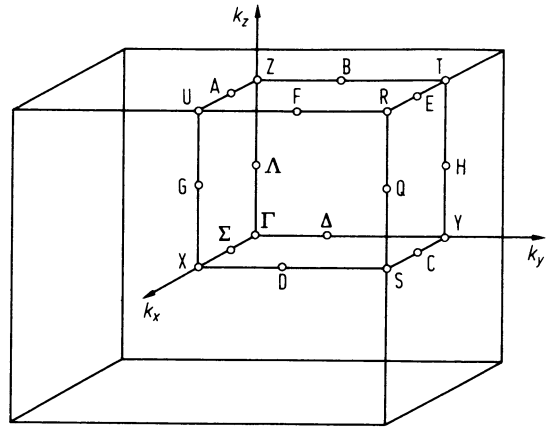

Fig.97. GeS. Brillouin zone for the simple orthorhombic GeS lattice.

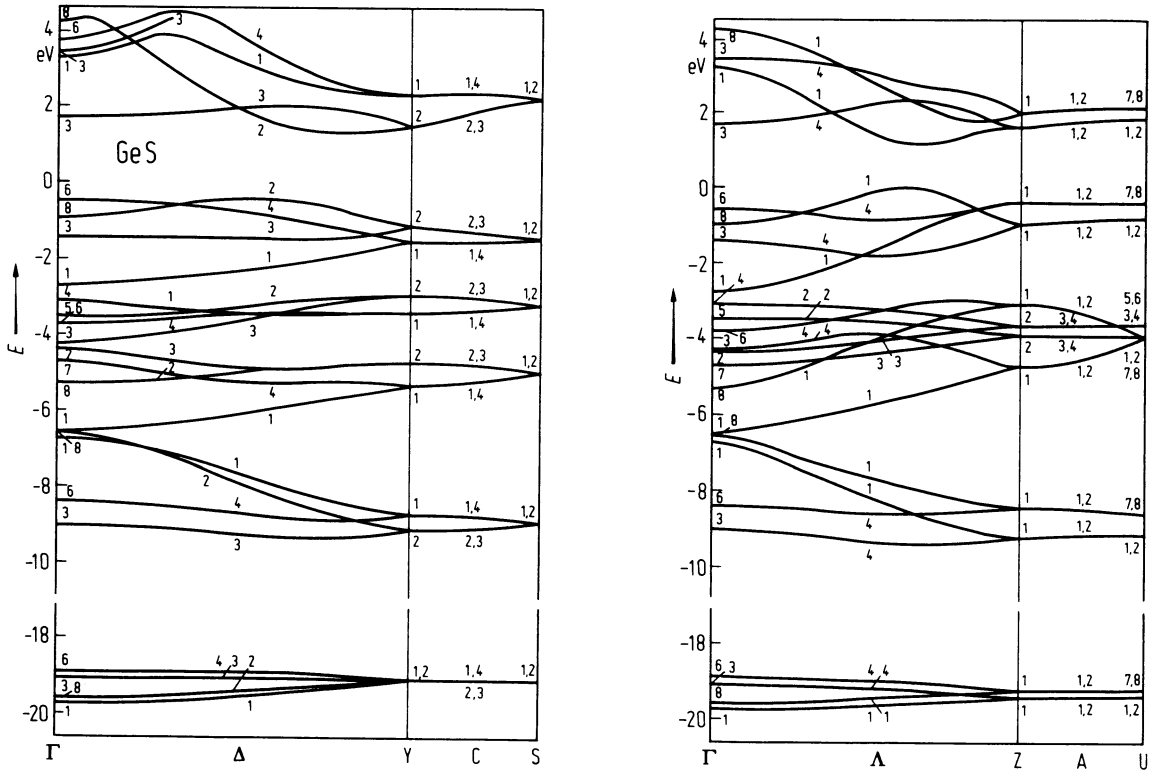

Fig.98. GeS. Band structure for different directions in the Brillouin zone calculated with an empirical pseudopotential method.

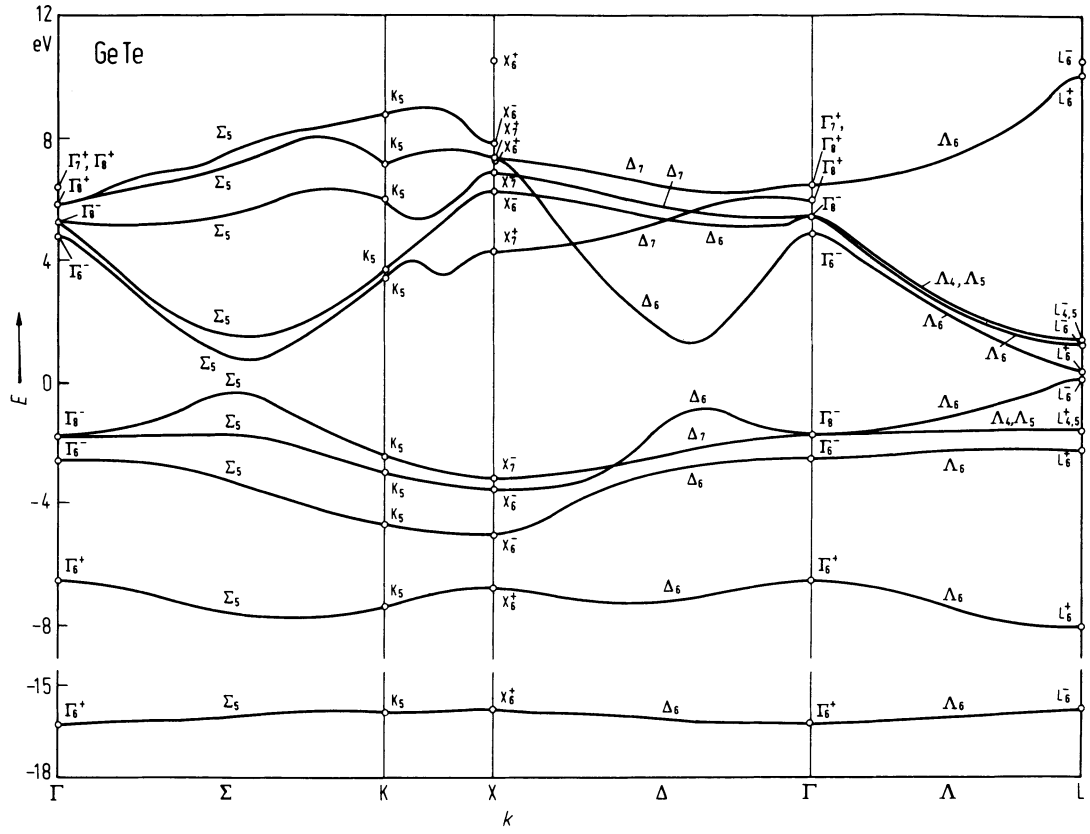

Fig.99. GeTe. Band structure.

Fig.100, next page

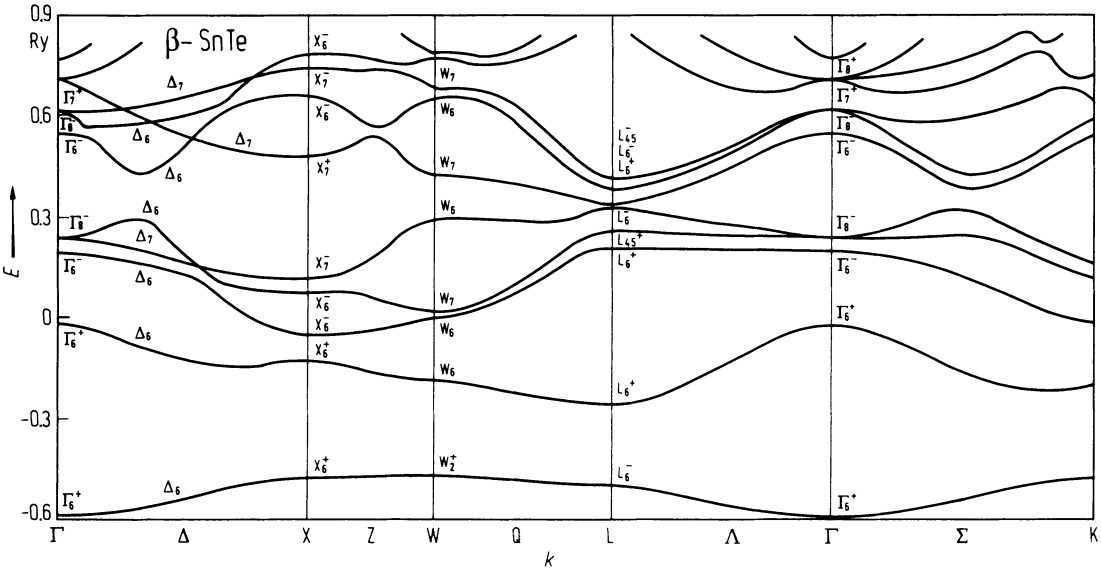

Fig.101. β-SnTe. Band structure obtained by a self-consistent relativistic calculation.

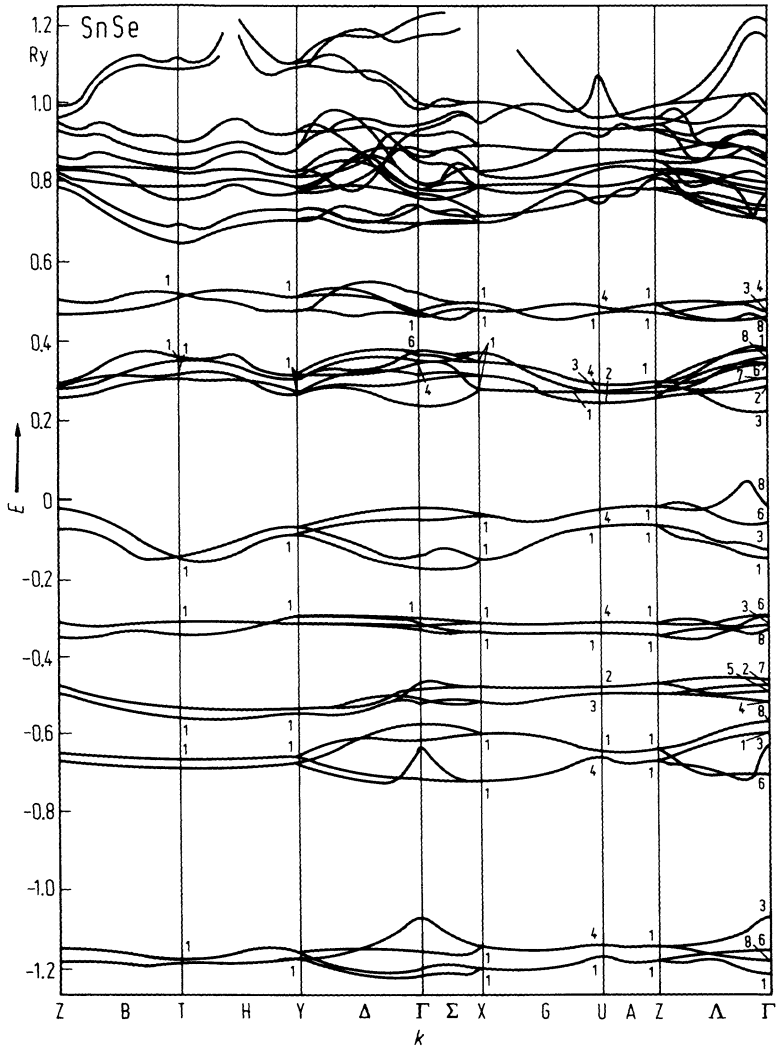

Fig.100. SnSe. Band structure calculated with the pseudopotential method.

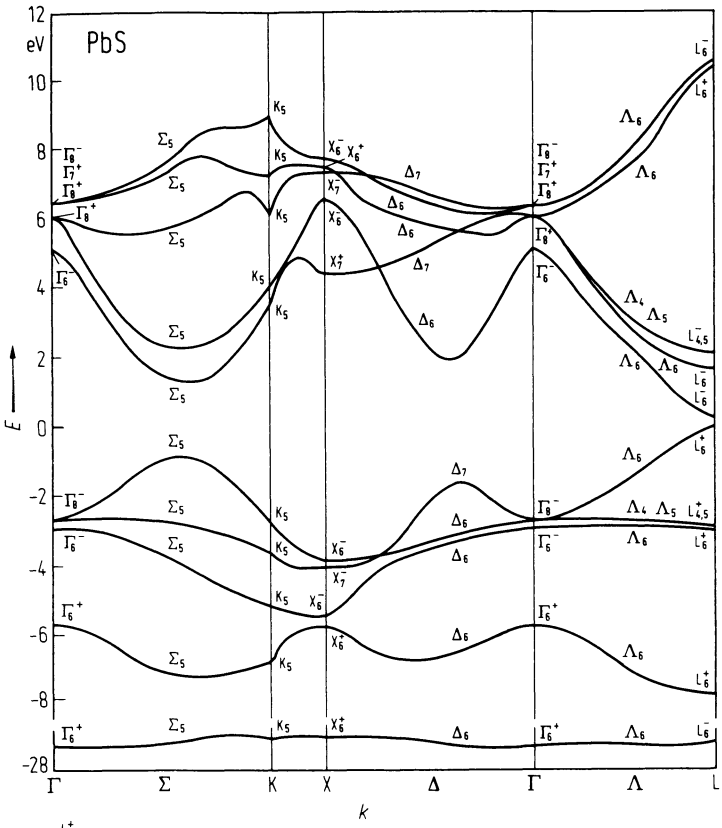

Fig.102. PbS. Band structure calculated by an empirical pseudopotential method.

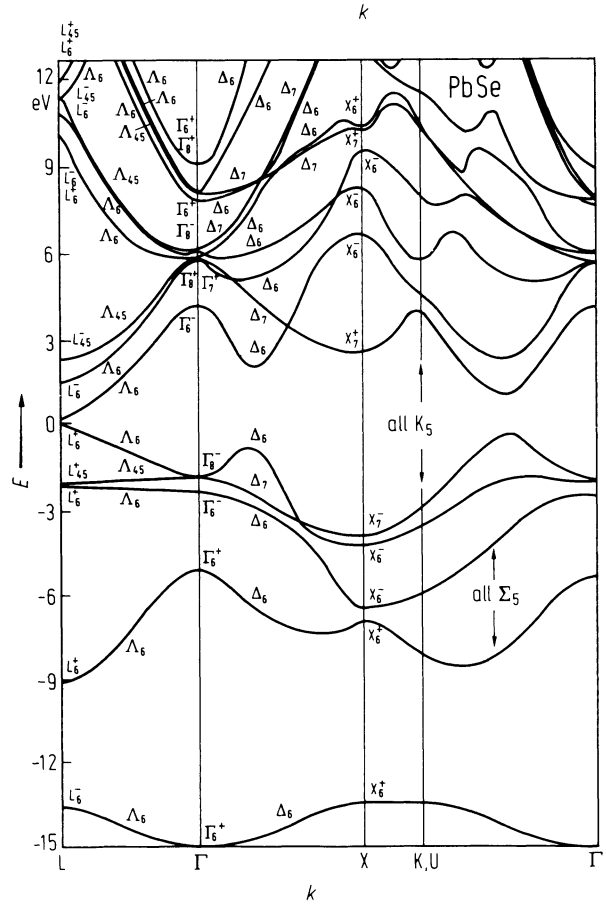

Fig.103. PbSe. Band structure calculated by an empirical pseudopotential method.

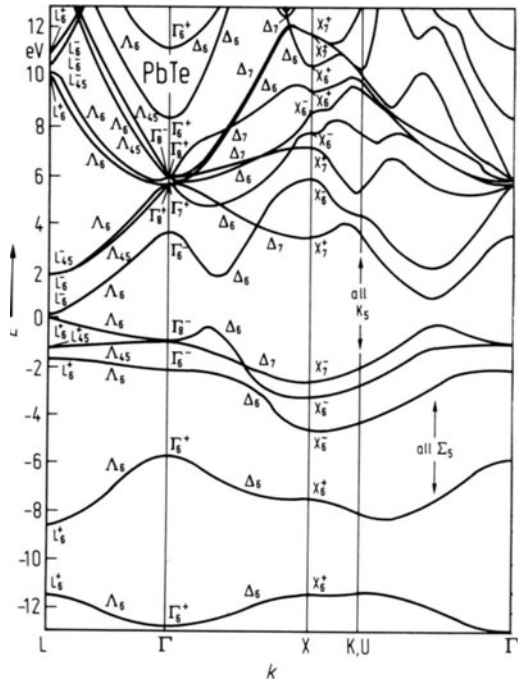

Fig.104. PbTe. Band structure calculated by an empirical pseudopotential method.

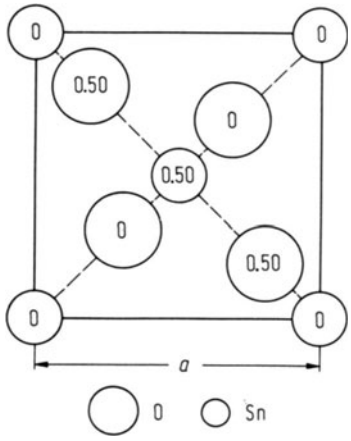

Fig.106. SnO_2. The atomic arrangement in the tetragonal unit cell projected on the basal c face. The small circles represent tin atoms.

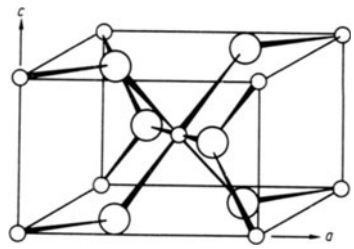

Fig.105. Rutile structure for the group IV dioxides. Small circles: metal atoms, large circles: oxygen atoms.

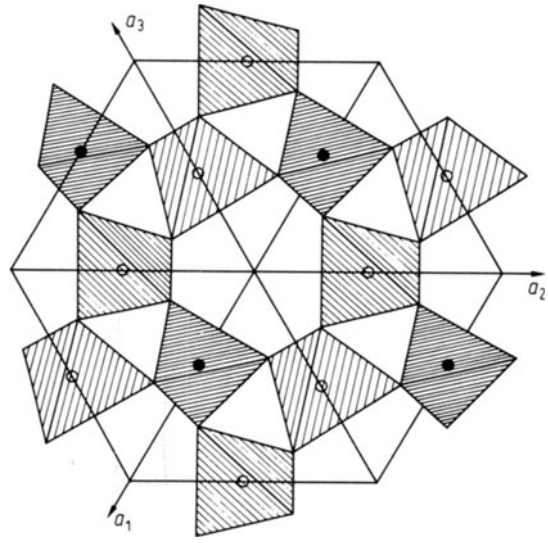

Fig.107. GeO_2. Projection of the α-quarz structure on the (0001)-plane.

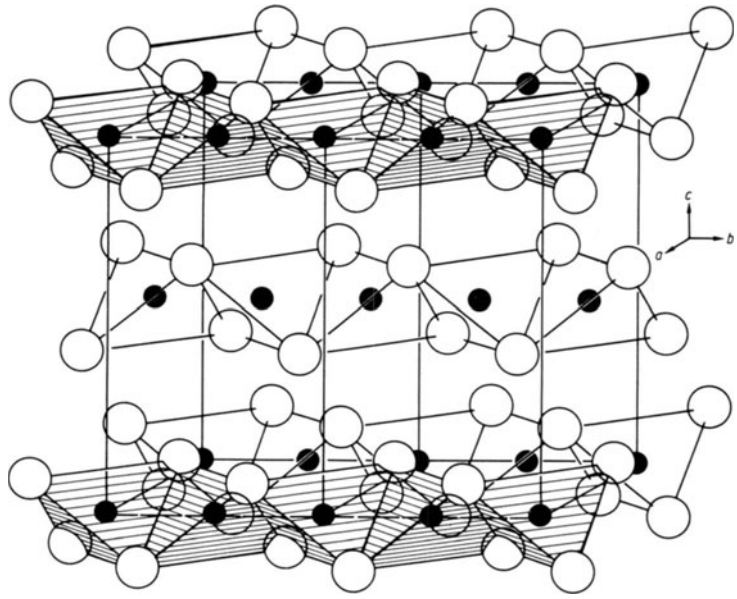

Fig.108. SiS_2. Lattice structure. The small circles represent the Si atoms.

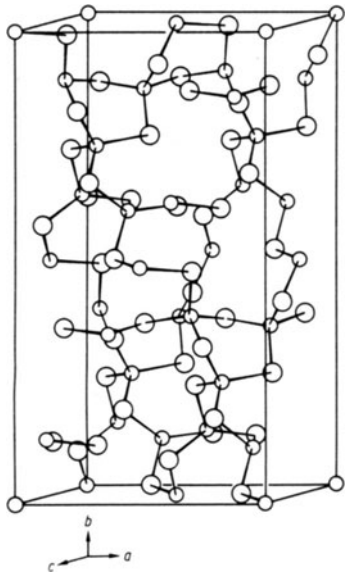

Fig.109. GeS_2, $GeSe_2$. Lattice structure.

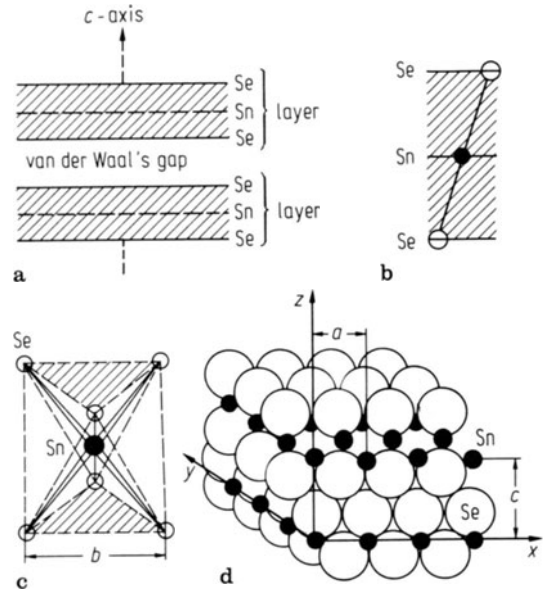

Fig.110. SnS_2, $SnSe_2$. (a) General form of the layer structure, (b) (1120)-section, (c) octahedral coordination in the layer, (d) packing of the atoms in $SnSe_2$.

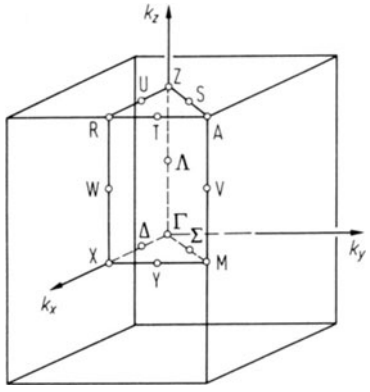

Fig.111. Brillouin zone of the rutile structure.

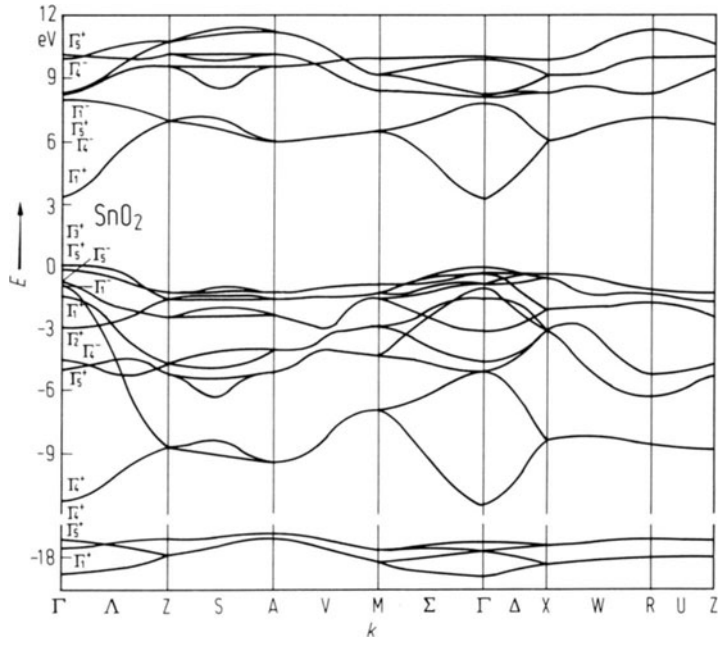

Fig.113. SnO_2. Band structure calculated with inclusion of Sn - O and O - O interactions.

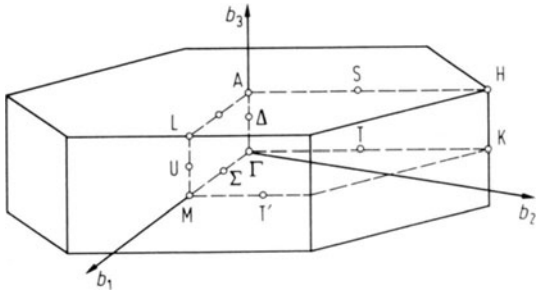

Fig.112. Brillouin zone of the SnS_2 structure.

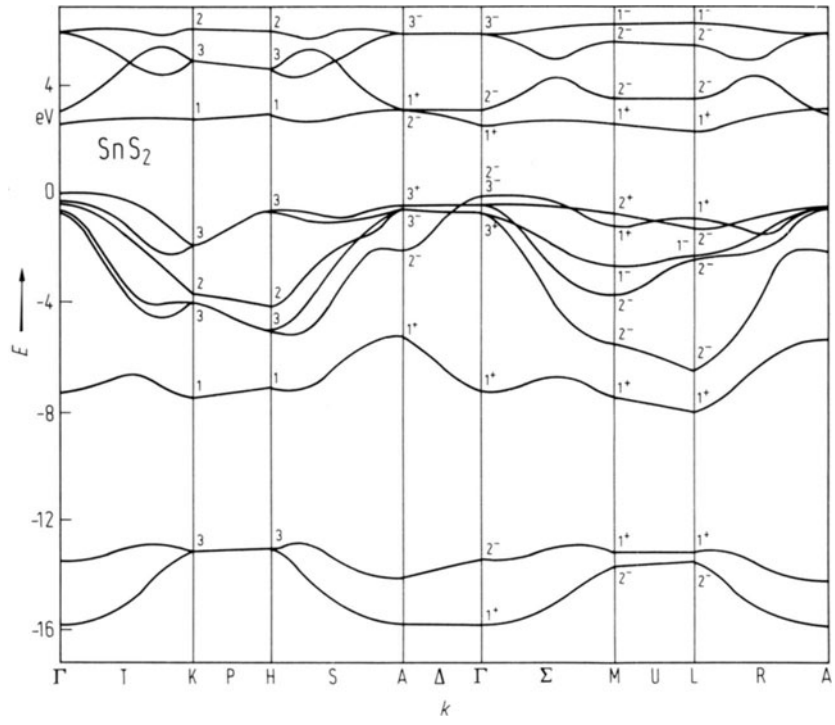

Fig.114. SnS_2. Band structure of the 2H polytype calculated by the tight binding method.

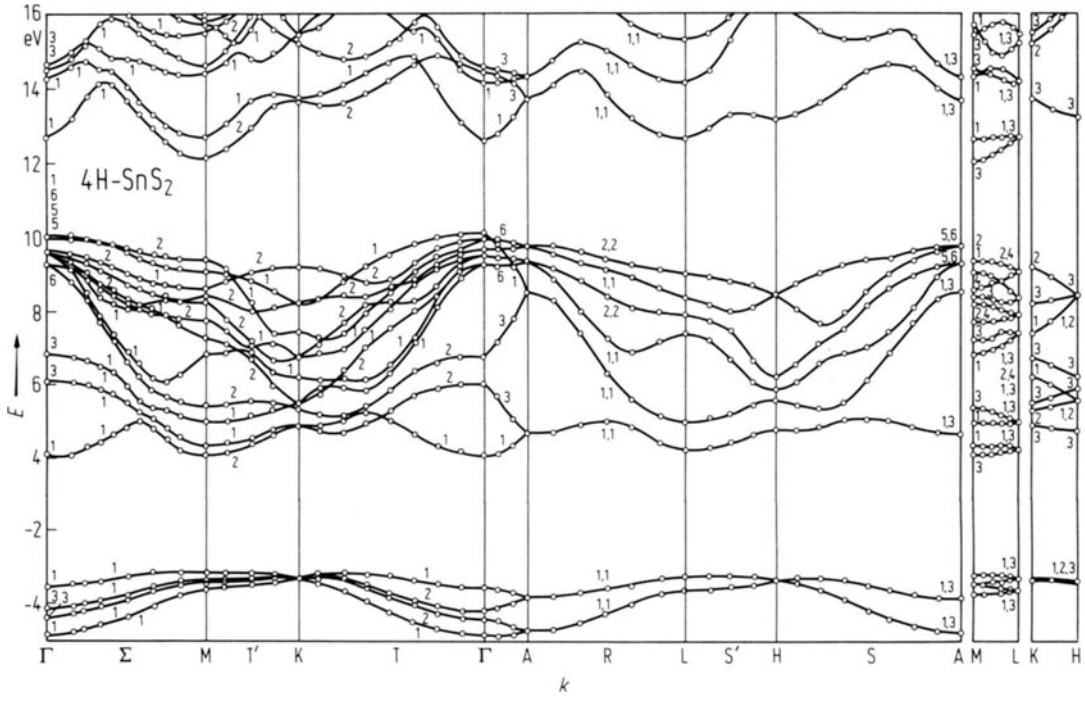

Fig.115. SnS_2. Band structure of the 4H polytype.

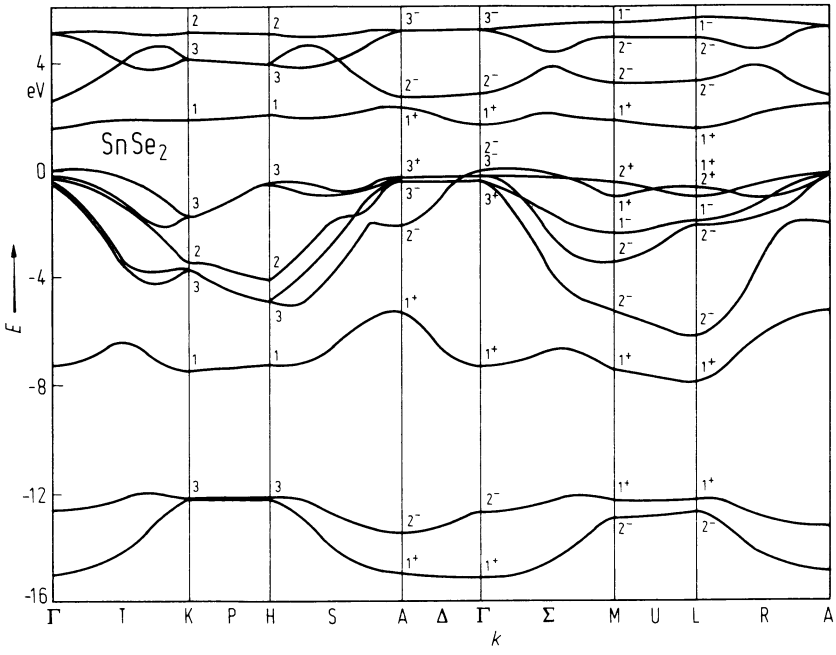

Fig.116. $SnSe_2$. Band structure calculated by the tight binding method.

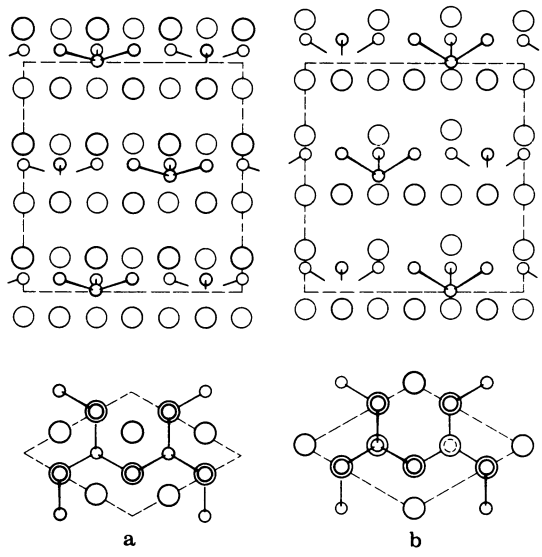

Fig.117. Si_2Te_3. (101) sections and projections along [001] of two models proposed. (a) One quarter of the Si atoms in octahedral interstices, (b) all Si atoms in tetrahedral interstices. Small circles: Si atoms.

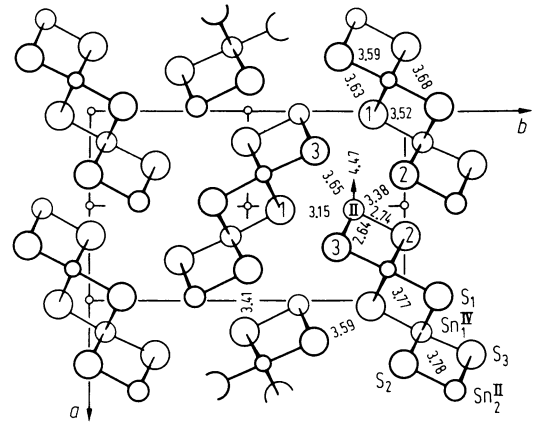

Fig.118. Sn_2S_3. Structure. The bold circles represent atoms with z = 3/4 and the light atoms with z = 1/4.

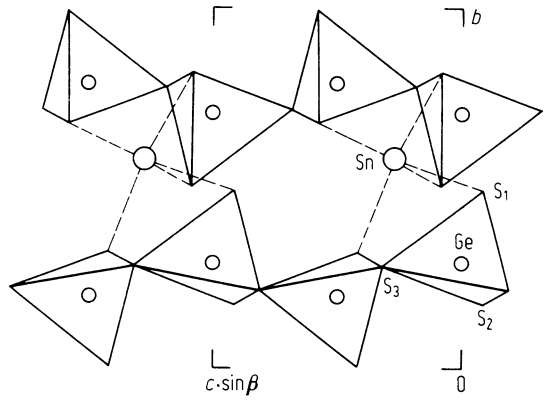

Fig.119. $SnGeS_3$. Part of the crystal structure.

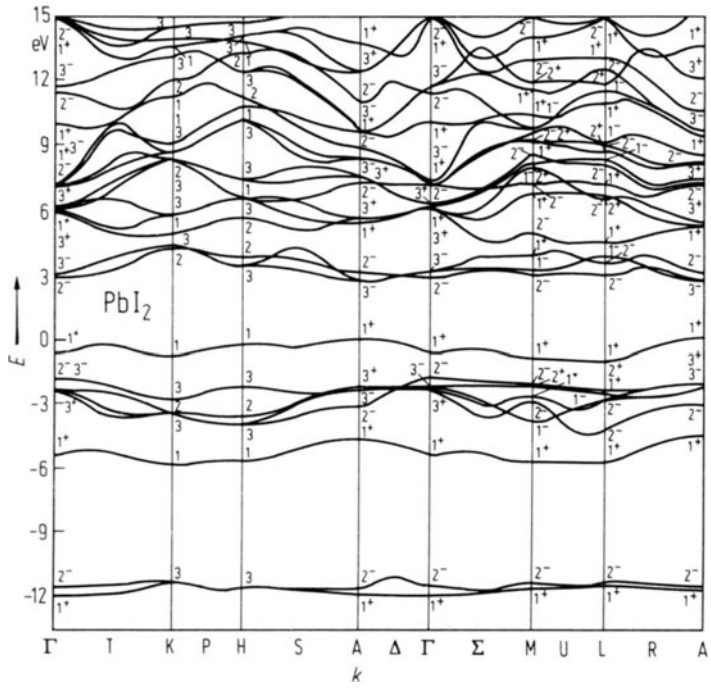

Fig.120. PbI_2. Band structure calculated by an empirical pseudopotential method.

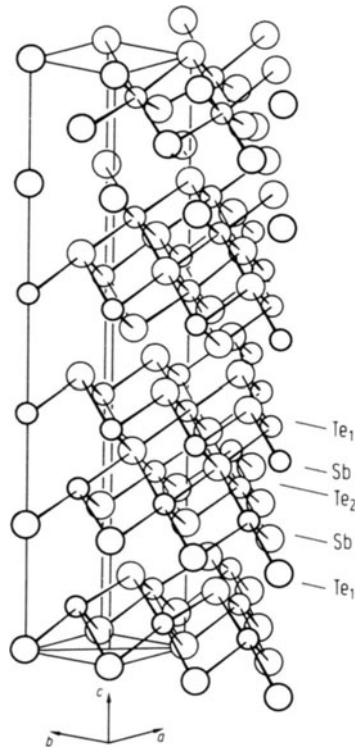

Fig.121. Crystal structure of the tetradymite-type M_2X_3 compounds. Se_2 (Te_2) atoms are nearly octahedrally coordinated to metal atoms. The bonding between adjacent Te_1-faces is relatively weak.

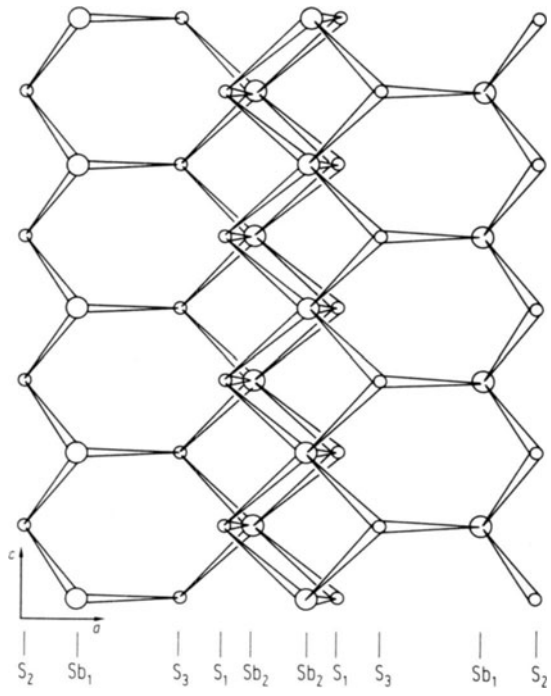

Fig.122. Sb_2S_3-type structure. Projection of one ribbon in the (010) plane along the [010] direction.

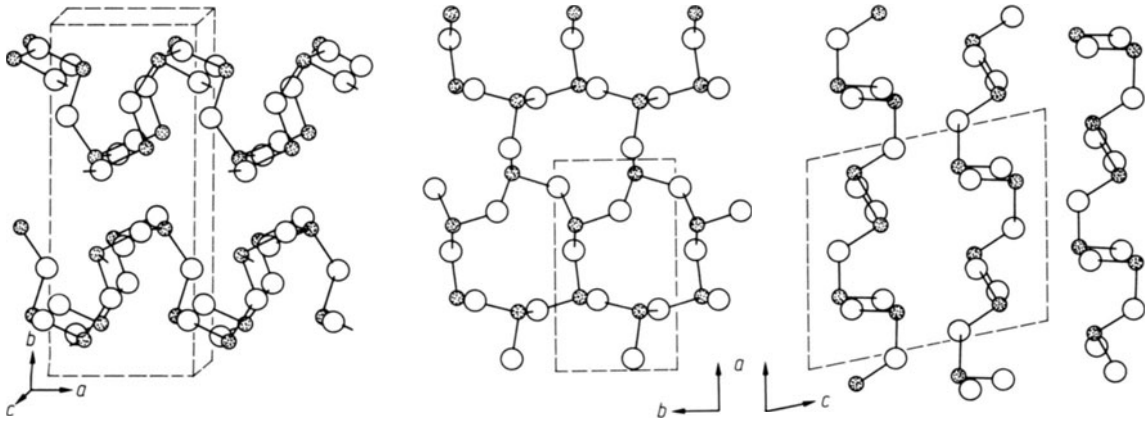

Fig.123. As_2O_3. Layer-type modification. Left: claudetite I, As atoms dotted; right: claudetite II, projection along [010] perpendicular to the layers, center: one layer projected onto the (a,b)-plane.

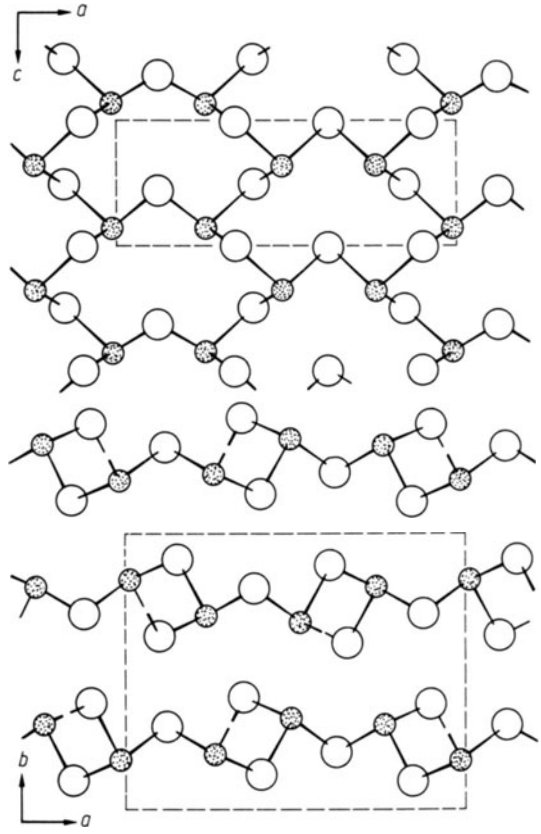

Fig.124. As_2S_3, As_2Se_3. Two projections of the structure; As atoms dotted.

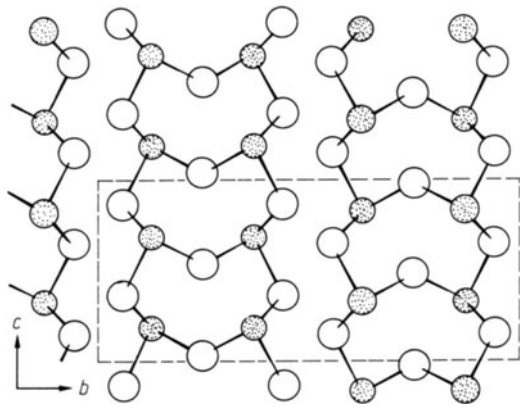

Fig.125. Sb_2O_3. The layered ribbons of the structure of valentinite projected along [100]. Small stippled spheres: Sb.

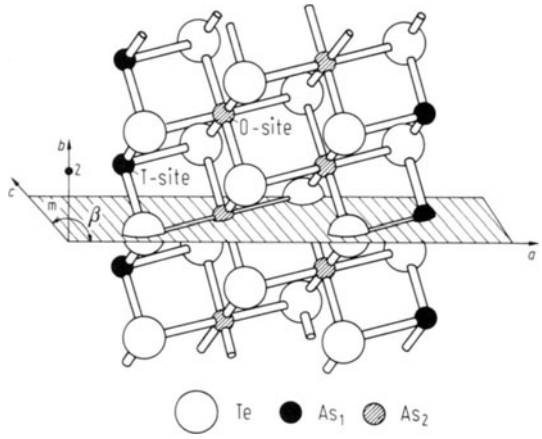

Fig.126. As_2Te_3. Schematic representation of the monoclinic structure. Crystalline As_2Te_3 is composed of complex chains parallel to the binary axis.

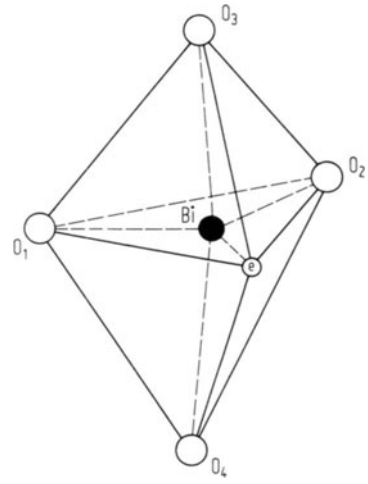

Fig.127. β-Bi_2O_3. Picture of a polyhedron showing the trigonal bipyramid.

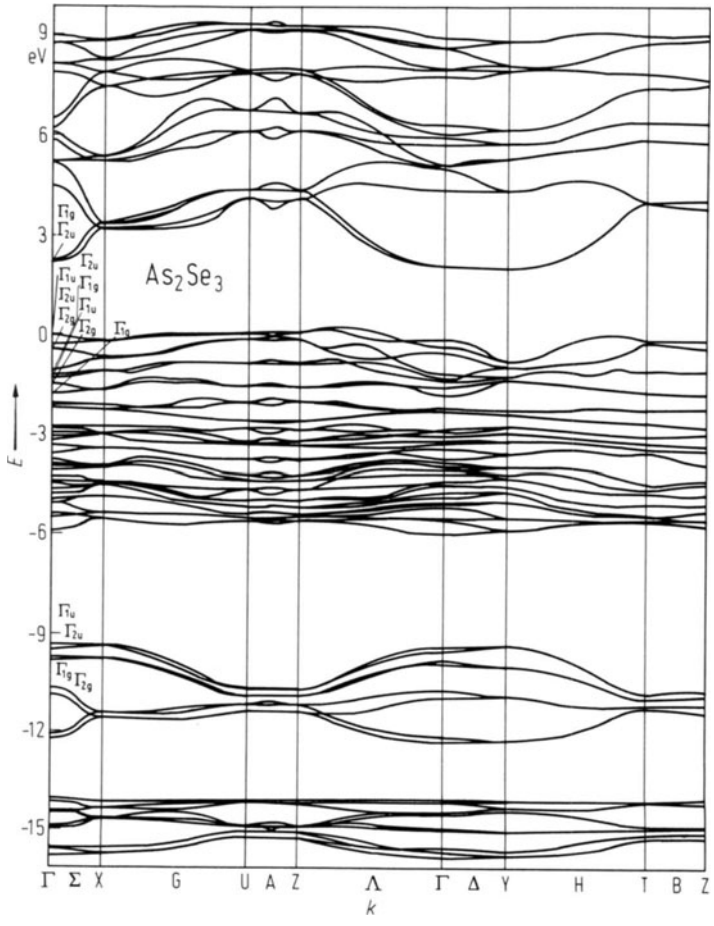

Fig.128. As_2Se_3. Band structure calculated by the LCAO method.

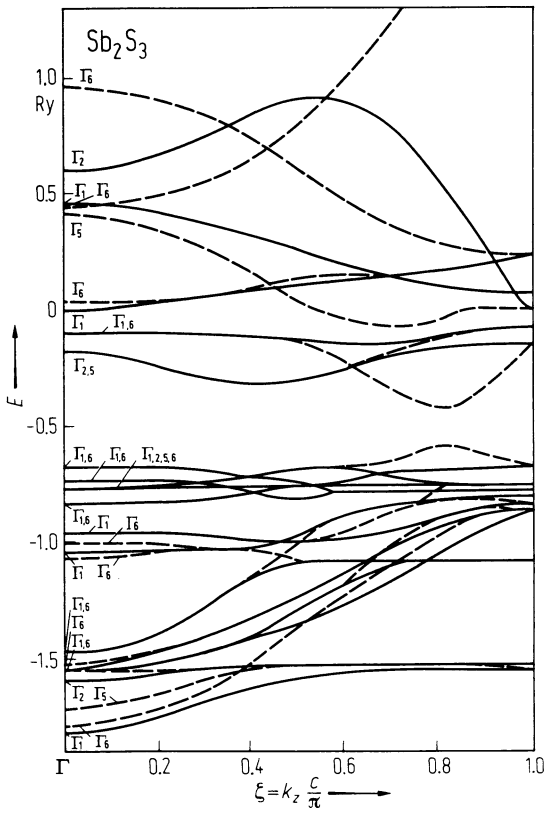

Fig.129. Sb_2S_3. Band structure along the Δ-axis.

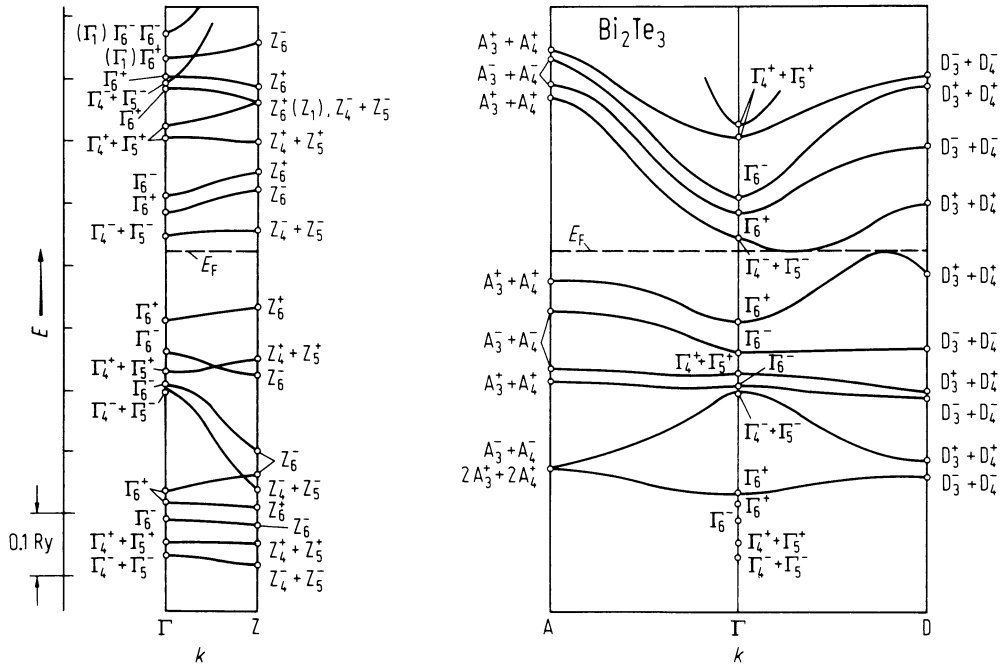

Fig.130. Bi_2Te_3. Band structure calculated with the empirical pseudopotential method including spin-orbit coupling.

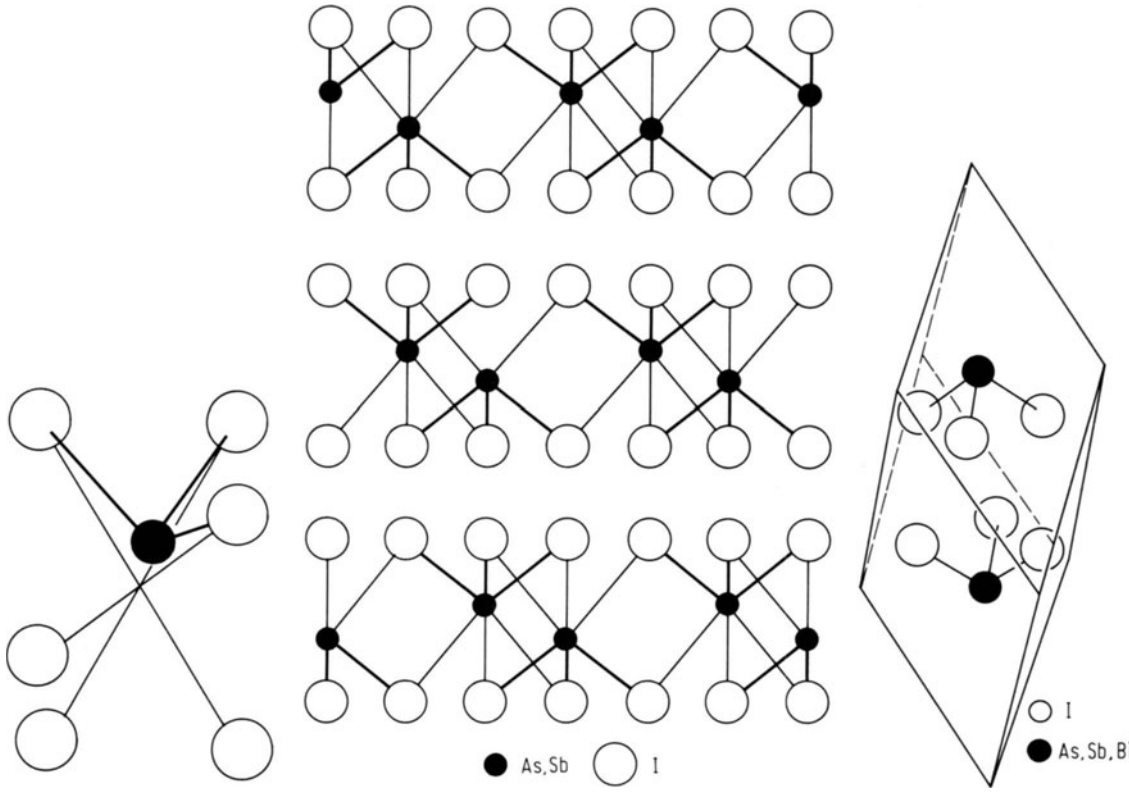

Fig.131. AsI_3, SbI_3, BiI_3. Left: Metal-iodine octahedron. Center: Schematic drawing of the layer lattice. Right: Rhombohedral elementary cell with two molecules.

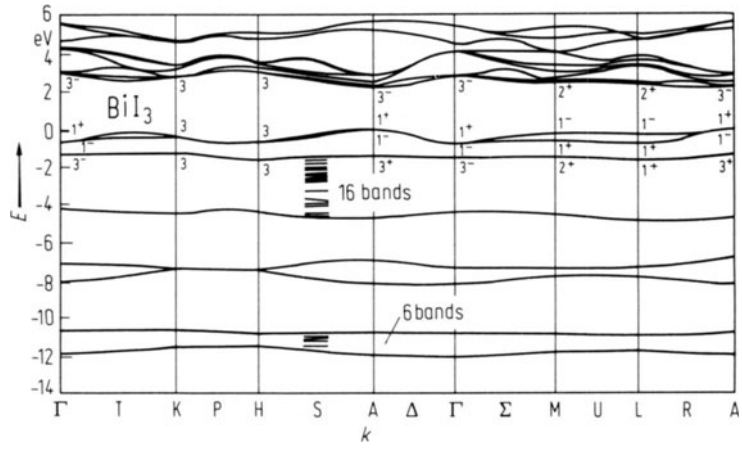

Fig.132. BiI_3. Band structure neglecting spin-orbit effects. For clarity, only the outermost bands are plotted.

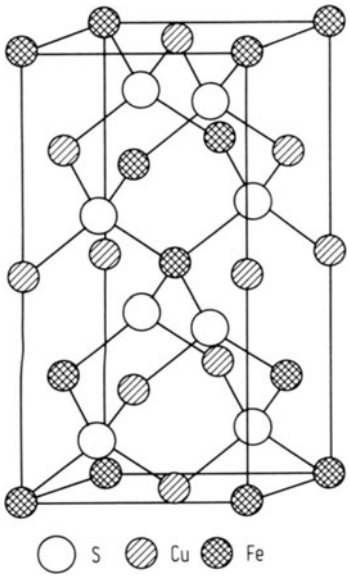

Fig.133. Structure of chalcopyrite.

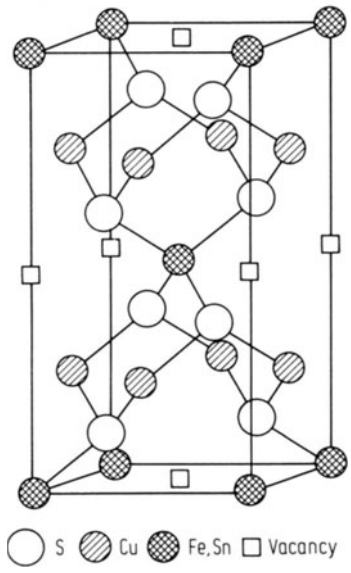

Fig.134. Structure of defect stannite.

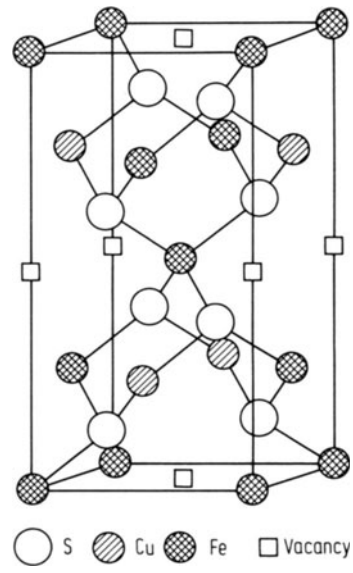

Fig.135. Structure of defect chalcopyrite (thiogallate).

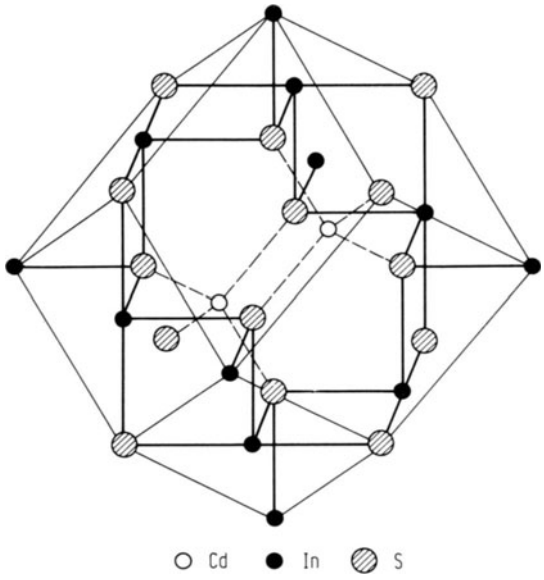

Fig.136. Structure of spinel.

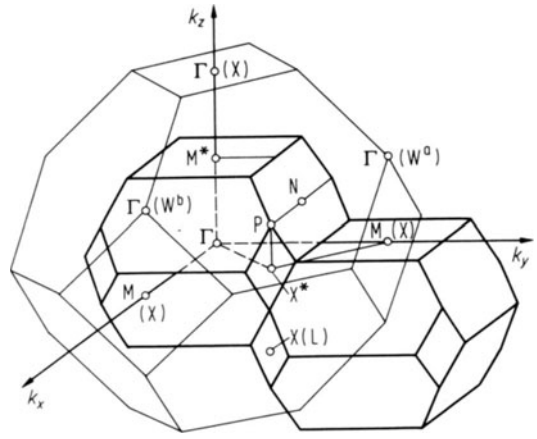

Fig.137. Brillouin zone of zincblende (narrow lines) and two Brillouin zones of chalcopyrite (broad lines).

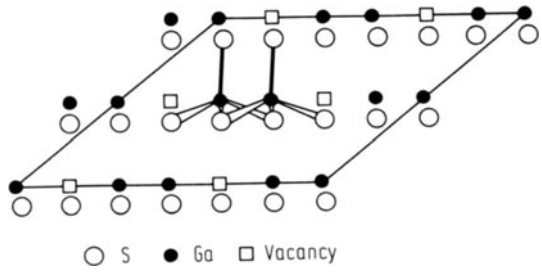

Fig.138. α-Ga_2S_3. Projection of the structure on the plane perpendicular to the c-axis.

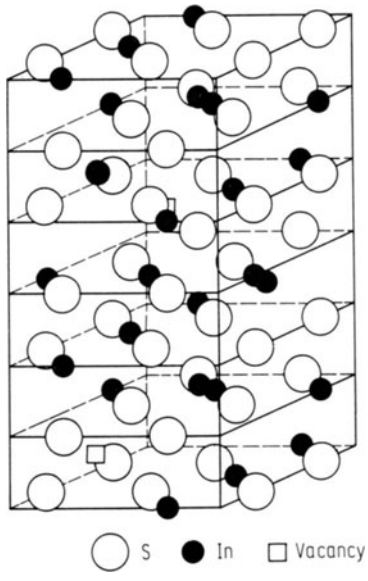

Fig.139. β-In_2S_3. Primitive unit cell.

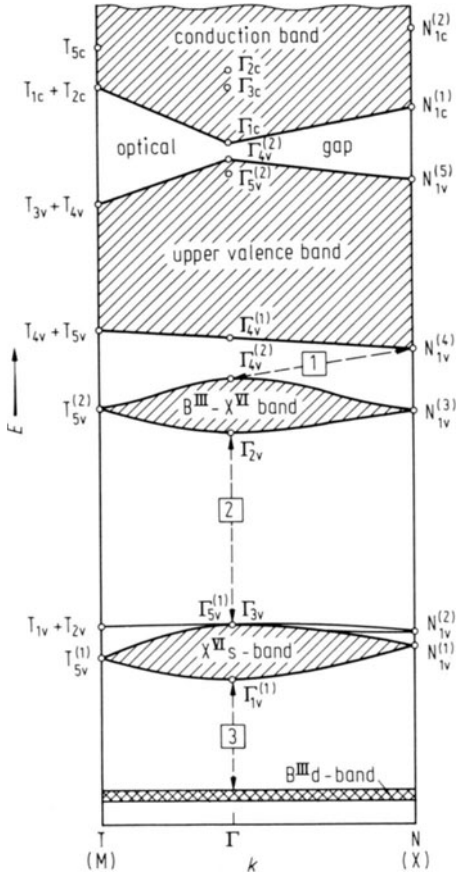

Fig.141. $A^{I}B^{III}X^{VI}_2$. General features of the band structure. Shaded and cross-hatched areas denote major subbands, and boxed numbers indicate the three internal gaps.

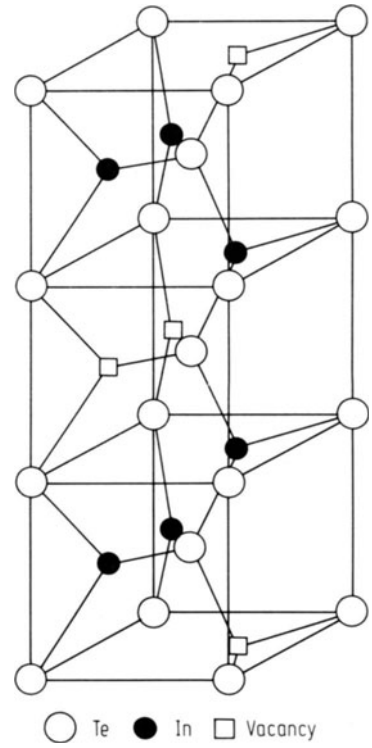

Fig.140.
α-In_2Te_3-II. Lattice structure.

▶

Figs.142···147: Self-consistent electronic band structures (from upper row left to lower row right):

Fig.142. $CuAlS_2$.
Fig.143. $CuAlSe_2$.
Fig.144. $CuGaS_2$.
Fig.145. $CuGaSe_2$.
Fig.146. $CuInS_2$.
Fig.147. $CuInSe_2$.

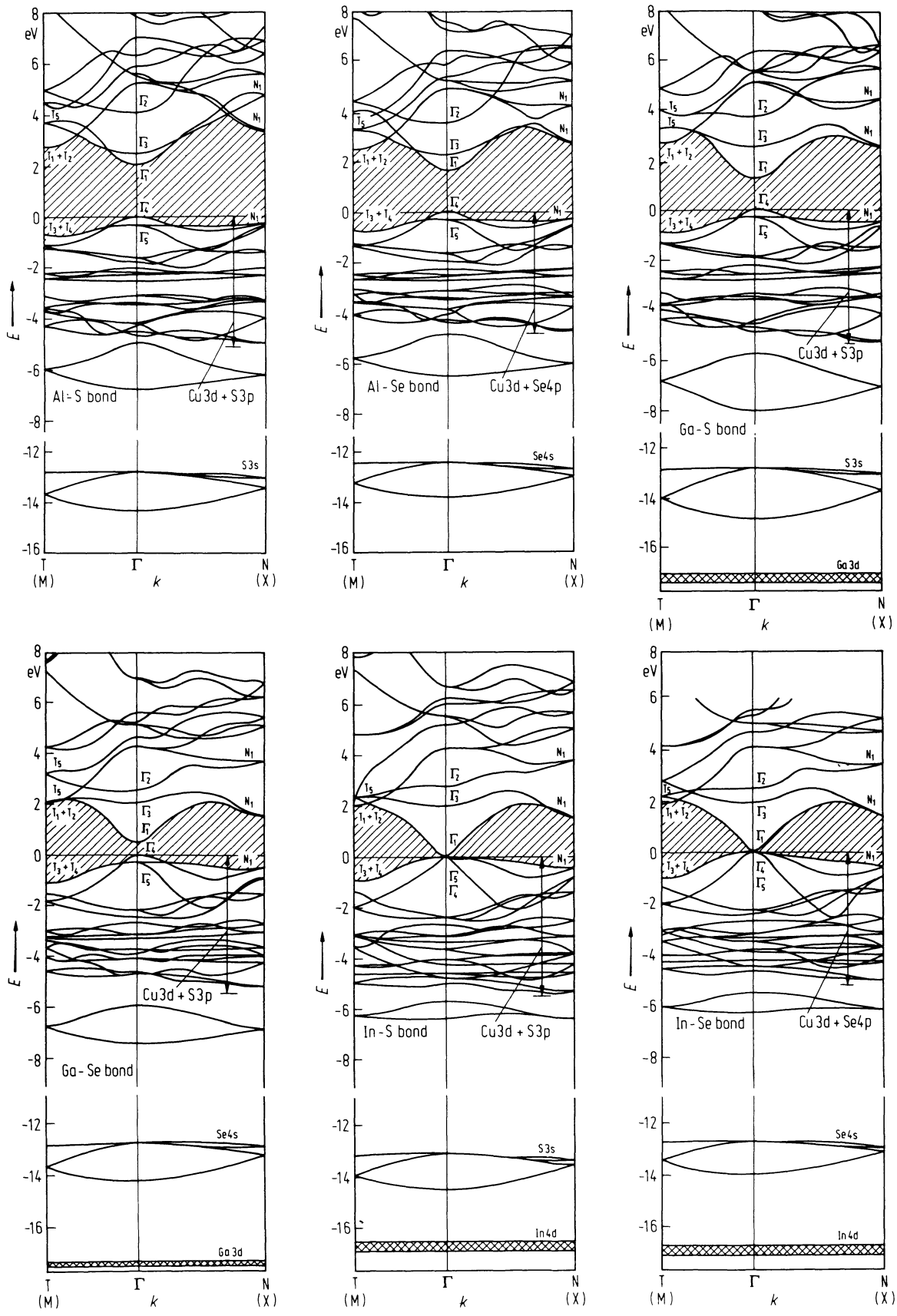
eV
E
Al-S bond
Cu3d + S3p
S3s
Al-Se bond
Cu3d + Se4p
Se4s
Ga-S bond
Ga3d
Ga-Se bond
In-S bond
In4d
In-Se bond
T
(M)
Γ
k
N
(X)

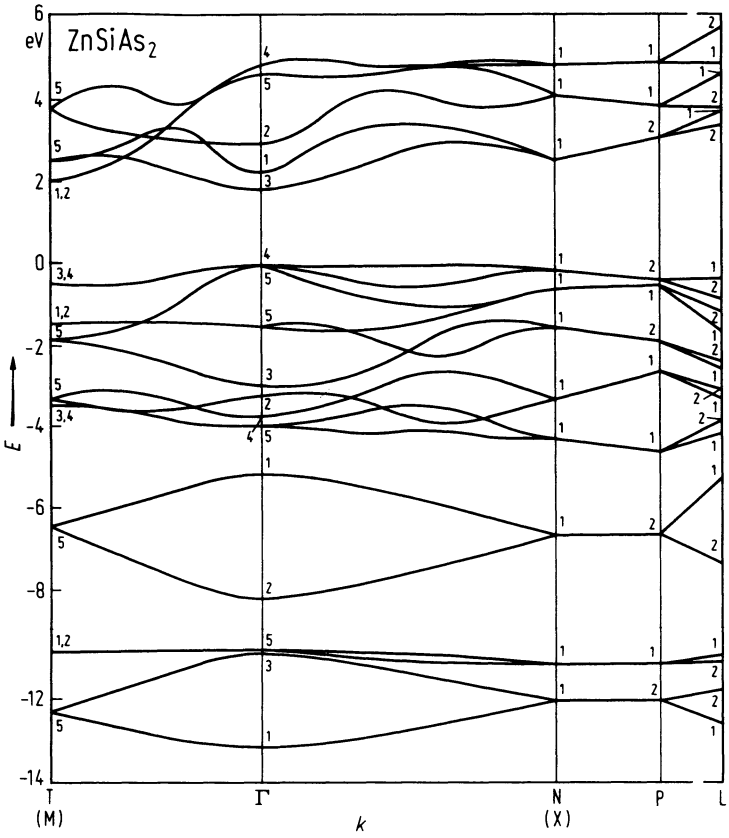

Fig.149. $ZnSiAs_2$. Band structure calculated by the empirical pseudopotential method.

Fig.148, next page

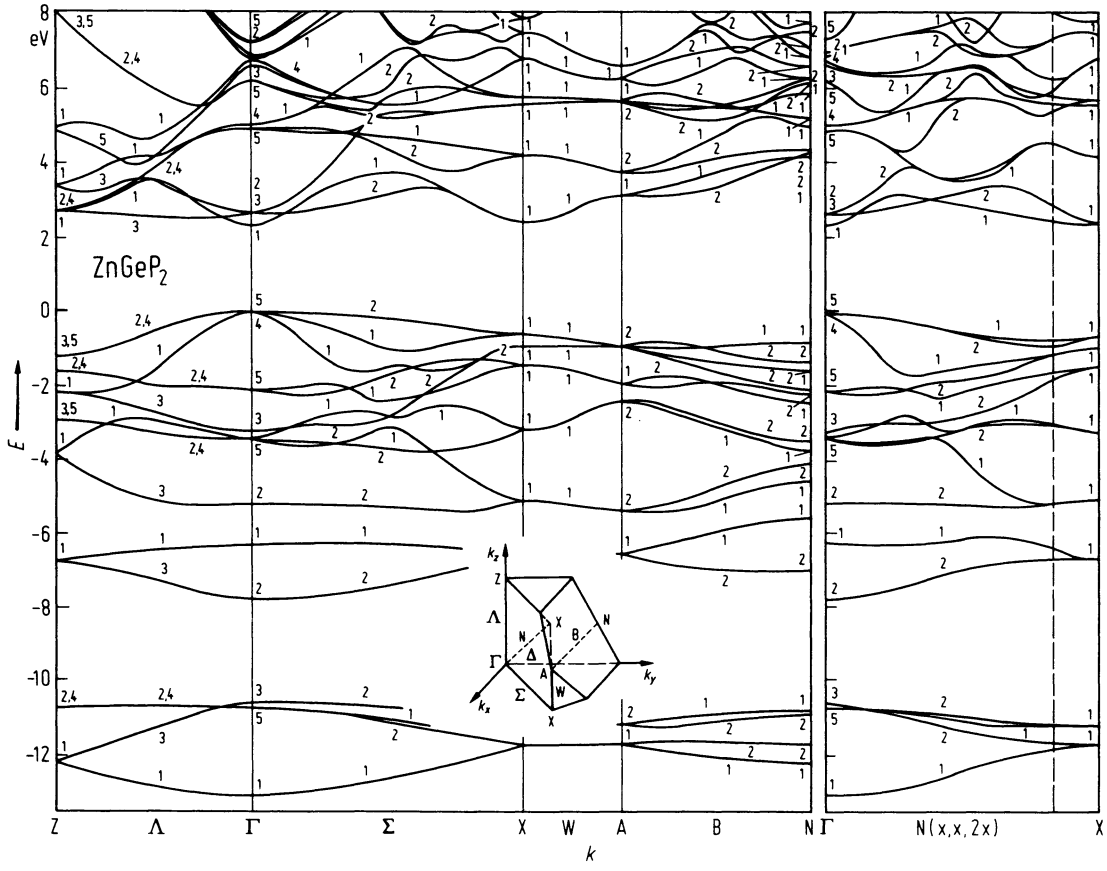

Fig.150. $ZnGeP_2$. Band structure and irreducible part of the Brillouin zone (insert). ▼

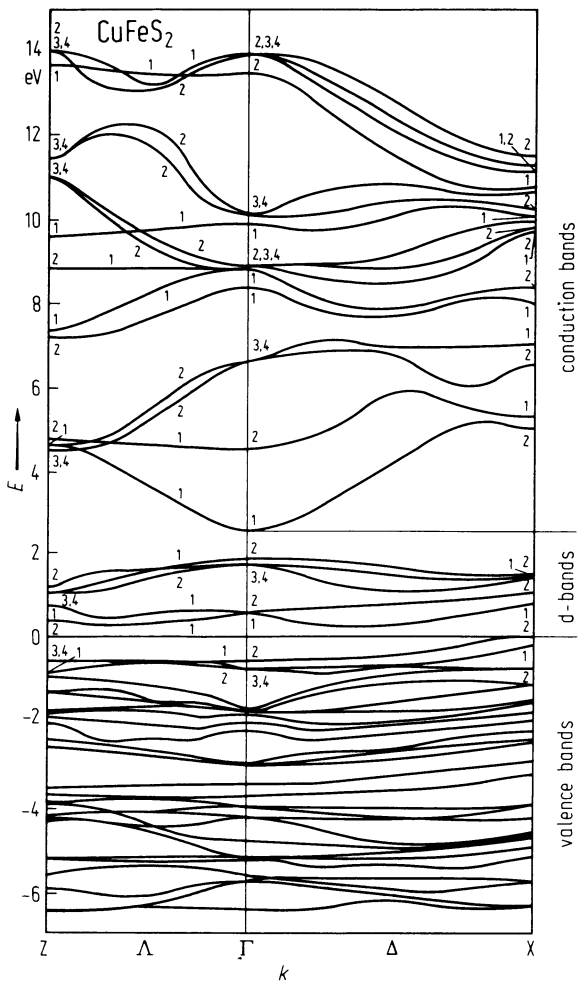

Fig.148. $CuFeS_2$. Band structure of the antiferromagnetic phase showing conduction and valence bands and d-bands in the fundamental gap.

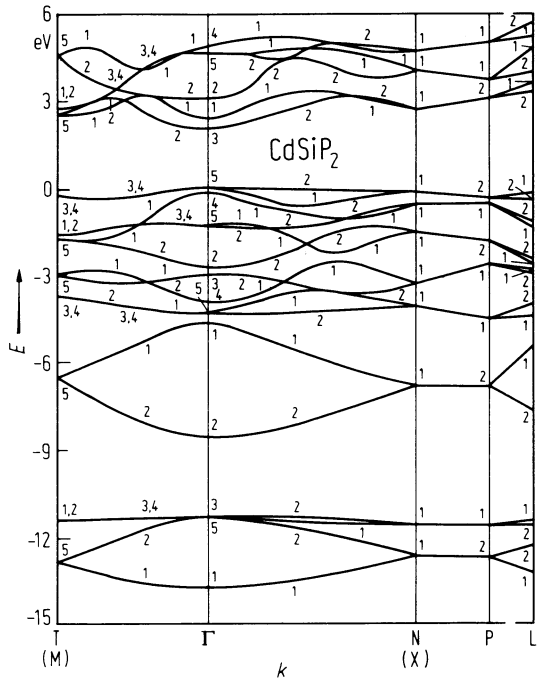

Fig.151. $CdSiP_2$. Band structure calculated with an empirical pseudopotential method.

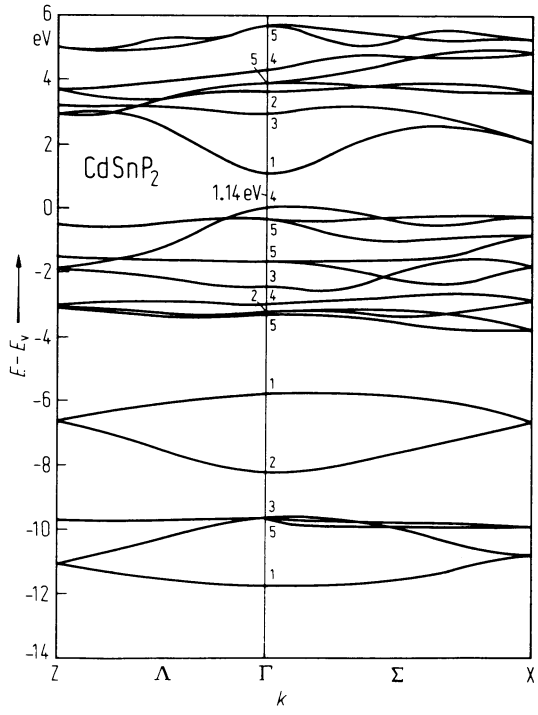

Fig.152. $CdSnP_2$. Band structure.

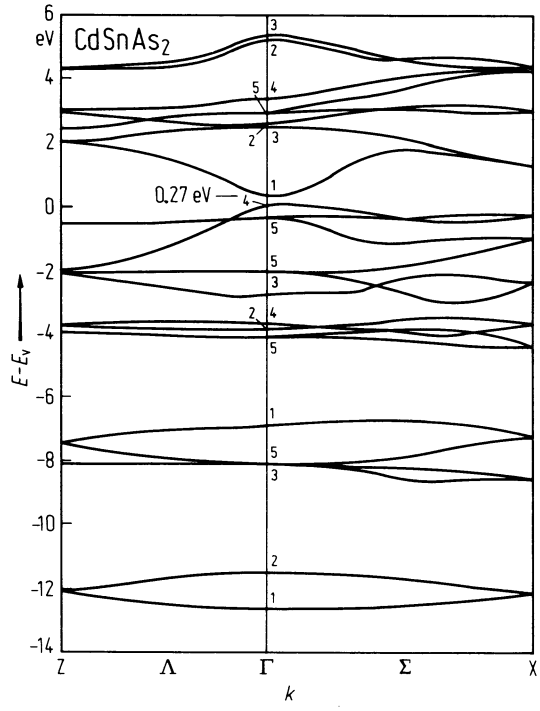

Fig.153. $CdSnAs_2$. Band structure.

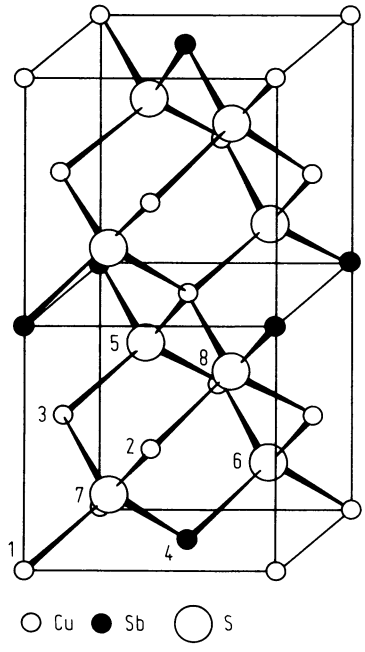

Fig.155. Cu_3SbS_4. Structure of famatinite.

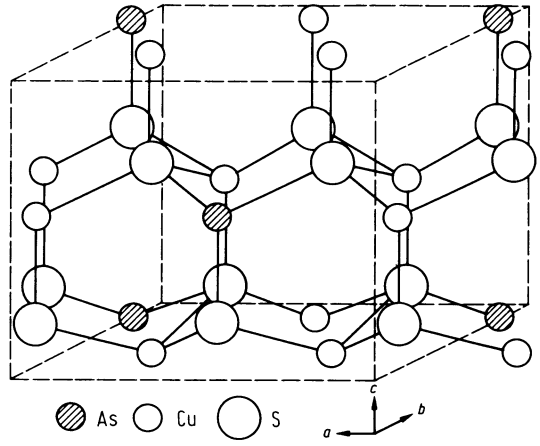

Fig.154. Cu_3AsS_4. Structure of enargite.

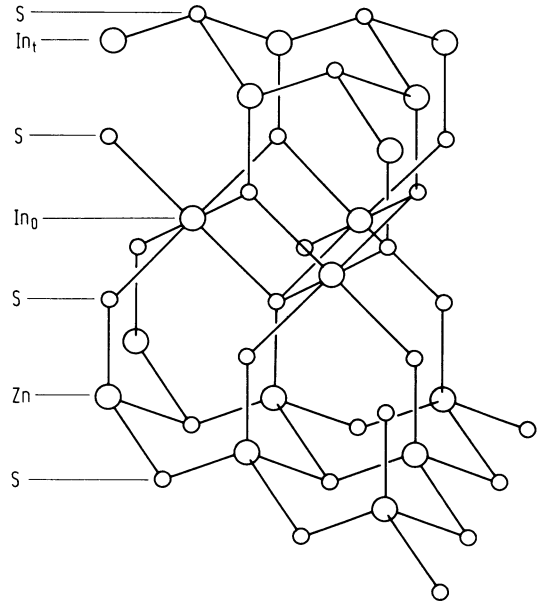

Fig.156. $ZnIn_2S_4$. Structure of one layer. In_t: tetrahedrally coordinated, In_o: octahedrally coordinated.

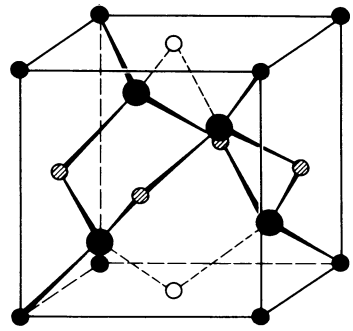

Fig.157. $CdIn_2Se_4$. Structure. Vacant site Se Cd In

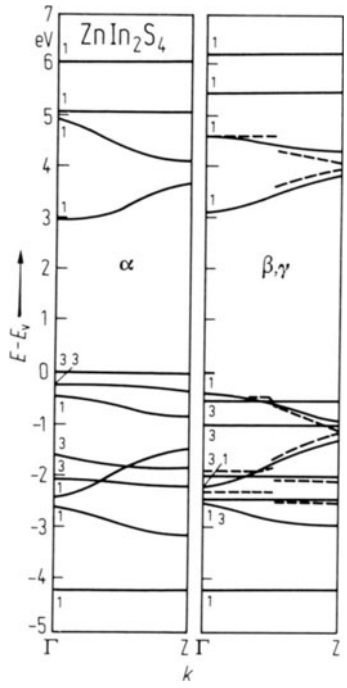

Fig.158. $ZnIn_2S_4$. Band structure of α, β and γ polytypes. Dashed lines: γ-phases, unfolded into BZ of β.

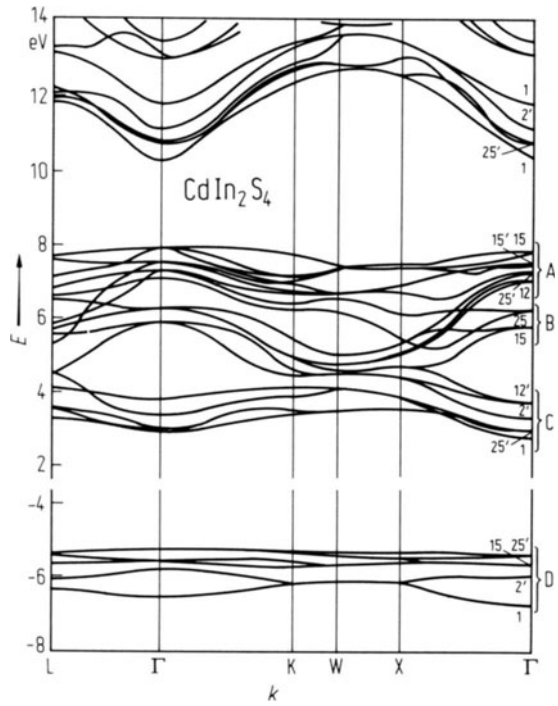

Fig.159. $CdIn_2S_4$. Band structure.

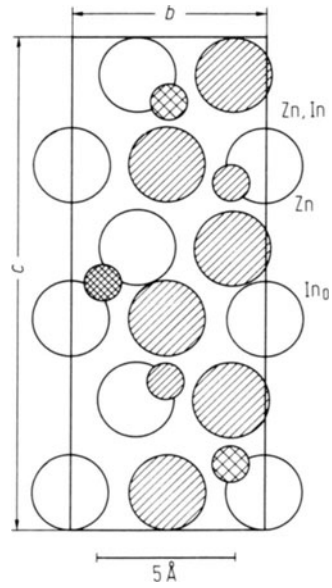

Fig.160. $Zn_3In_2S_6$. Cross section through [2110] plane. Atoms in plane are shaded.

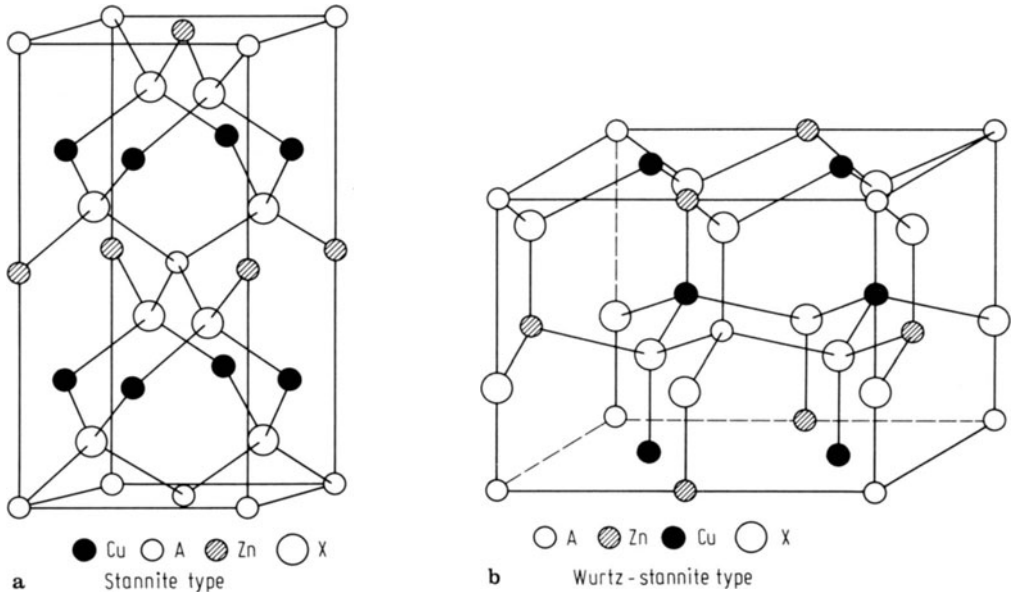

Fig.161. Cu_2ZnAX_4. (a) stannite-type structure, (b) wurtz-stannite-type structure.

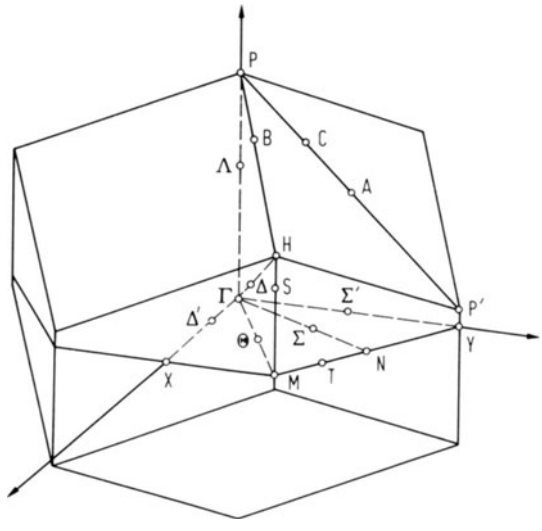

Fig.162. Ag_3AsS_3. Brillouin zone of the proustite structure.

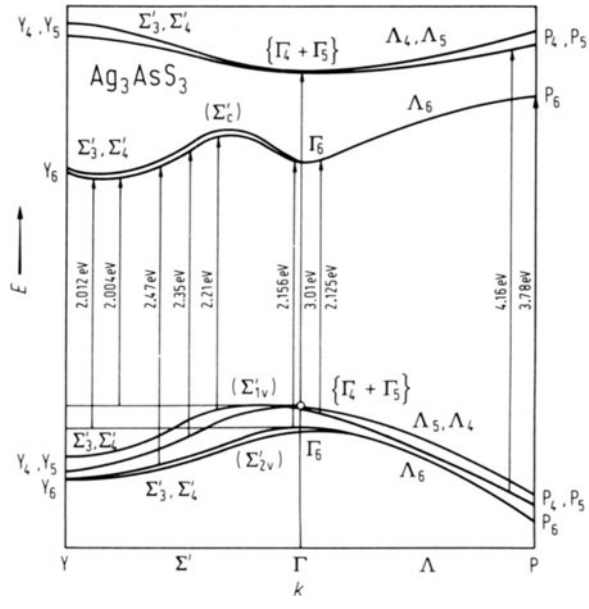

Fig.163. Ag_3AsS_3. Band structure along two principal axes in the Brillouin zone estimated by group theory and experimental results.

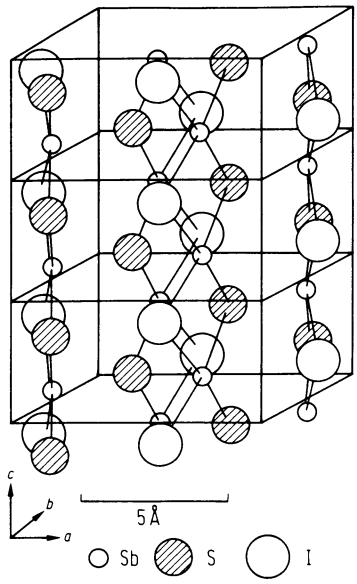

Fig.164. SbSI. Crystal structure in the paramagnetic phase as an example for the D^{16}_{2h} - Pnam lattice.

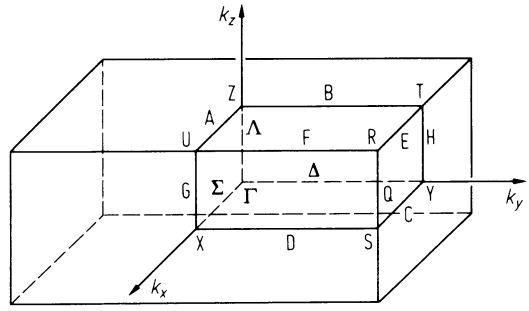

Fig.165. SbSI. Brillouin zone of the paraelectric and ferroelectric phases.

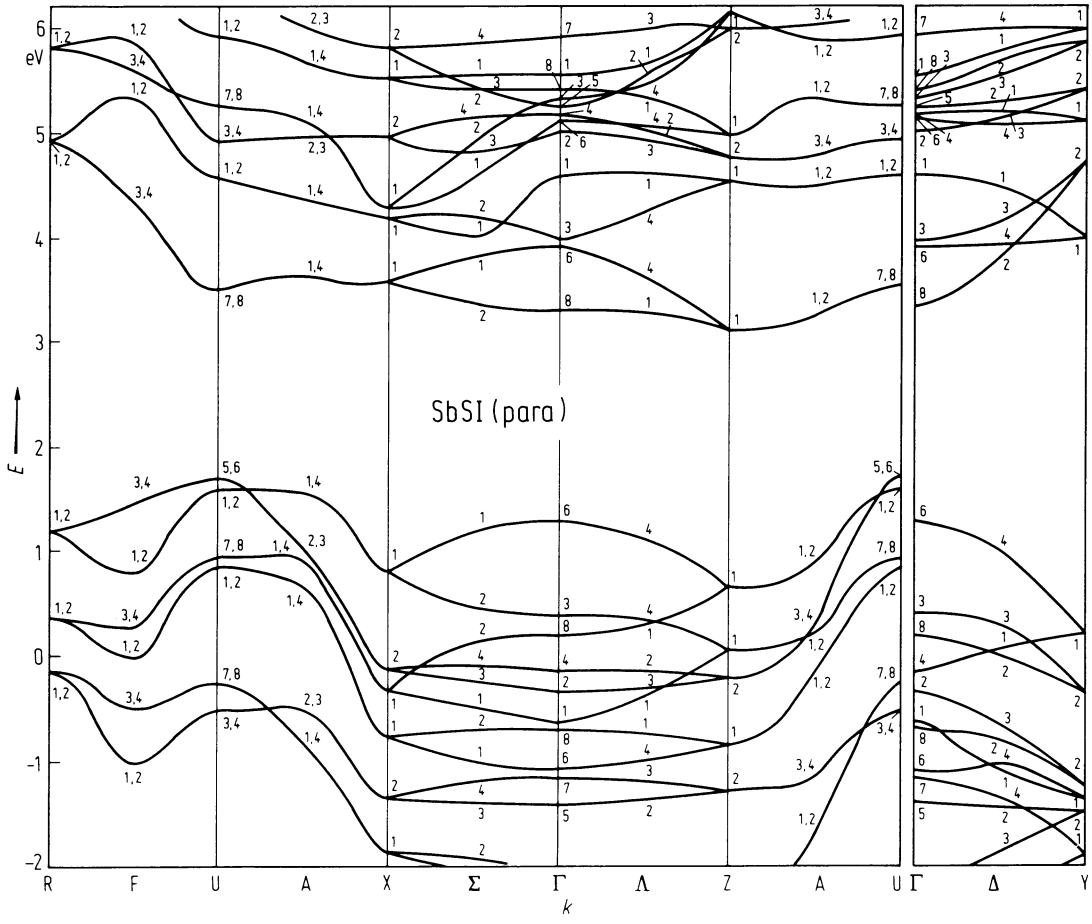

Fig.166. SbSI. Band structure in the paraelectric phase calculated with the pseudopotential method.

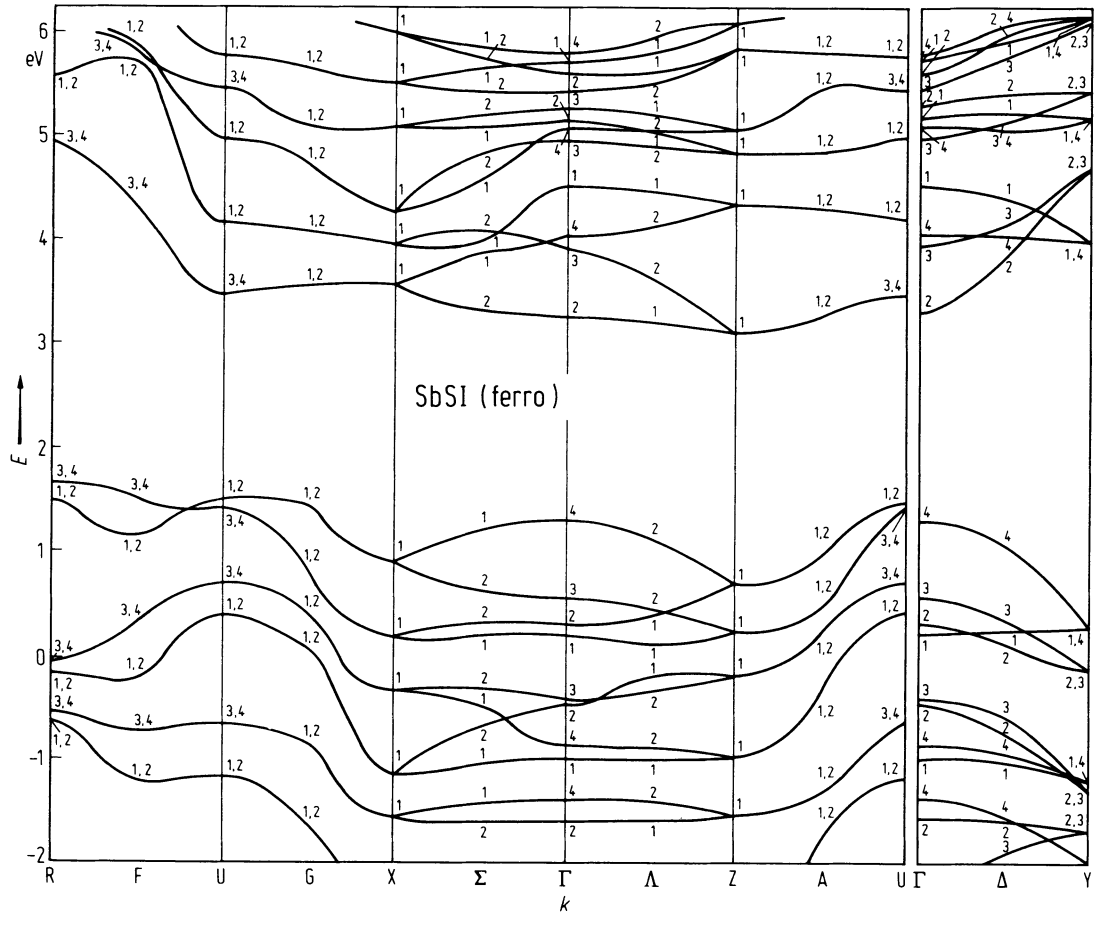

Fig.167. SbSI. Band structure in the ferroelectric phase calculated with the pseudopotential method.

Appendix

1 Index of Substances

In the following index all substances occuring in this volume are listed. In the first column the gross formulae of the substances are given in alphabetical order of their constituting elements. The second column lists the gross formulae in the order used in the literature and in the chapters of this volume.

Gross formula		Page
$AgAlGeSe_4$	$AgAlGeSe_4$	225
$AgAlSnSe_4$	$AgAlSnSe_4$	226
$AgAlTe_2$	$AgAlTe_2$	213
$AgAsS_2$	$AgAsS_2$	227
$AgAsSe_2$	$AgAsSe_2$	227
$AgAsTe_2$	$AgAsTe_2$	227
$AgBiS_2$	$AgBiS_2$	228
$AgBiSe_2$	$AgBiSe_2$	228
$AgBiTe_2$	$AgBiTe_2$	228
AgBr	AgBr	172
AgCl	AgCl	172
AgF	AgF	172
$AgFeSe_2$	$AgFeSe_2$	215
$AgFeTe_2$	$AgFeTe_2$	215
$AgGaGeSe_4$	$AgGaGeSe_4$	225
$AgGaS_2$	$AgGaS_2$	214
$AgGaSe_2$	$AgGaSe_2$	214
$AgGaSnSe_4$	$AgGaSnSe_4$	225
$AgGaTe_2$	$AgGaTe_2$	214
AgI	AgI	172
$AgIn_3Te_5$	$AgIn_3Te_5$	236
$AgIn_5S_8$	$AgIn_5S_8$	236
$AgIn_9Te_{14}$	$AgIn_9Te_{14}$	236
$AgInGeSe_4$	$AgInGeSe_4$	225
$AgInS_2$	$AgInS_2$	214
$AgInSe_2$	$AgInSe_2$	215
$AgInSe_4Sn$	$AgInSnSe_4$	226
$AgInTe_2$	$AgInTe_2$	215
AgS_2Sb	$AgSbS_2$	228
$AgSbSe_2$	$AgSbSe_2$	228
$AgSbTe_2$	$AgSbTe_2$	228
Ag_2GeSe_3	Ag_2GeSe_3	220
Ag_2GeTe_3	Ag_2GeTe_3	220
Ag_2O	Ag_2O	169
Ag_2S	Ag_2S	169
Ag_2Se	Ag_2Se	169

Gross formula		Page
Ag_2Se_3Sn	Ag_2SnSe_3	219
Ag_2SnTe_3	Ag_2SnTe_3	219
Ag_2Te	Ag_2Te	170
Ag_3AsS_3	Ag_3AsS_3	229
$Ag_3Ge_8Se_9$	$Ag_3Ge_8Se_9$	235
$Ag_3In_5Se_9$	$Ag_3In_5Se_9$	235
Ag_3SSb	Ag_3SbS	229
Ag_8GeS_6	Ag_8GeS_6	225
Ag_8GeSe_6	Ag_8GeSe_6	226
Ag_8GeTe_6	Ag_8GeTe_6	227
Ag_8S_6Sn	Ag_8SnS_6	226
Ag_8Se_6Si	Ag_8SiSe_6	226
Ag_8Se_6Sn	Ag_8SnSe_6	226
AlAs	AlAs	75
AlB_{12}	AlB_{12}	238
$AlB_{14}Li$	$LiAlB_{14}$	237
$AlCuGeSe_4$	$CuAlGeSe_4$	226
$AlCuS_2$	$CuAlS_2$	211
$AlCuSe_2$	$CuAlSe_2$	211
$AlCuSe_4Sn$	$CuAlSnSe_4$	226
$AlCuTe_2$	$CuAlTe_2$	211
AlN	AlN	69
AlP	AlP	72
AlSb	AlSb	80
As	As	161
AsB	BAs	68
AsBrS	AsSBr	233
AsCoS	CoAsS	243
AsCoSe	CoAsSe	243
$AsCu_3S_3$	Cu_3AsS_3	229
$AsCu_3S_4$	Cu_3AsS_4	221
$AsCu_3Se_4$	Cu_3AsSe_4	221
AsFeS	FeAsS	243
AsFeSe	FeAsSe	243
AsGa	GaAs	101
AsGe	GeAs	196

Gross formula		Page
AsI_3	AsI_3	208
AsIn	InAs	133
AsIrSb	IrAsSb	239
AsOsS	OsAsS	243
AsPPd	PdPAs	239
AsPPt	PtPAs	239
AsPRu	RuPAs	238
AsRuS	RuAsS	243
AsS_2Tl	$TlAsS_2$	231
AsSi	SiAs	196
$As_2Br_3Cd_4$	$Cd_4As_2Br_3$	236
As_2Cd	$CdAs_2$	179
As_2Cd_3	Cd_3As_2	177
$As_2Cd_4Cl_3$	$Cd_4As_2Cl_3$	236
$As_2Cd_4I_3$	$Cd_4As_2I_3$	236
As_2CdGd	$CdGeAs_2$	218
As_2CdSi	$CdSiAs_2$	218
As_2CdSn	$CdSnAs_2$	219
As_2Co	$CoAs_2$	239
As_2Fe	$FeAs_2$	238
As_2Ge	$GeAs_2$	197
As_2GeZn	$ZnGeAs_2$	217
As_2Ir	$IrAs_2$	239
As_2Mg_3	Mg_3As_2	175
As_2Ni	$NiAs_2$	239
As_2Os	$OsAs_2$	239
As_2Pt	$PtAs_2$	239
As_2Rh	$RhAs_2$	239
As_2Ru	$RuAs_2$	238
As_2S_3	As_2S_3	205
As_2Se_3	As_2Se_3	205
As_2SiZn	$ZnSiAs_2$	216
As_2SnZn	$ZnSnAs_2$	217
As_2Te_3	As_2Te_3	205
As_2Zn	$ZnAs_2$	178
As_2Zn_3	Zn_3As_2	176
As_3Co	$CoAs_3$	239
As_4S_4	As_4S_4	207
AuCs	CsAu	164
AuRb	RbAu	164
B	B	160
$B_{1-x}H_x$	$B_{1-x}H_x$	237
BN	BN	60
BP	BP	65
B_4C	B_4C	238
B_6Ba	BaB_6	237
B_6Ca	CaB_6	237
B_6Eu	EuB_6	238
B_6K	KB_6	237
B_6P	B_6P	238
B_6Sm	SmB_6	238
B_6Sr	SrB_6	237
B_6Yb	YbB_6	238
$B_{15}Na$	NaB_{15}	237
$B_{24}Cu$	CuB_{24}	237
$B_{66}Gd$	GdB_{66}	238
$B_{66}Sm$	SmB_{66}	238
$B_{66}Y$	YB_{66}	238
$B_{66}Yb$	YbB_{66}	238
$BaCr_2S_4$	$BaCr_2S_4$	243
$BaGe_2$	$BaGe_2$	175
BaO	BaO	181
BaO_3Ti	$BaTiO_3$	244
$BaSi_2$	$BaSi_2$	175
BeS	BeS	180
BeSe	BeSe	180
BeTe	BeTe	180
Bi	Bi	162
BiBrO	BiOBr	234
BiBrS	BiSBr	234
BiBrSe	BiSeBr	234
BiBrTe	BiTeBr	235
$BiCiTe_2$	$CuBiTe_2$	229
BiClO	BiOCl	234
BiClS	BiSCl	234
$BiCs_3$	Cs_3Bi	166
$BiCuSe_2$	$CuBiSe_2$	229
BiI_3	BiI_3	208
BiIO	BiOI	234
BiIS	BiSI	234
BiISe	BiSeI	235
BiITe	BiTeI	235
$BiLi_3$	Li_3Bi	155
$BiRb_3$	Rb_3Bi	166
BiS_2Tl	$TlBiS_2$	231
$BiSe_2Tl$	$TlBiSe_2$	231
$BiTe_2Tl$	$TlBiTe_2$	231
Bi_2GeTe_4	$GeBi_2Te_4$	232
Bi_2O_3	Bi_2O_3	206
$Bi_2O_7Pt_2$	$Bi_2Pt_2O_7$	244

Gross formula		Page
Bi_2S_3	Bi_2S_3	206
Bi_2Se_3	Bi_2Se_3	207
Bi_2Te_3	Bi_2Te_3	207
Bi_4GeTe_7	$GeBi_4Te_7$	233
Bi_4PbTe_7	$PbBi_4Te_7$	233
$Bi_{12}GeO_{20}$	$Bi_{12}GeO_{20}$	232
$Bi_{12}SiO_{20}$	$Bi_{12}SiO_{20}$	232
BrCu	CuBr	171
BrSbSe	SbSeBr	233
BrSSb	SbSBr	233
BrTl	TlBr	195
Br_2Cd	$CdBr_2$	188
Br_2Hg	$HgBr_2$	189
Br_2Pb	$PbBr_2$	204
$Br_3Cd_4P_2$	$Cd_4P_2Br_3$	236
C	C (Diamond)	5
CSi	SiC	47
CaO	CaO	181
CaO_3V	$CaVO_3$	244
Ca_2Pb	Ca_2Pb	175
Ca_2Si	Ca_2Si	174
Ca_2Sn	Ca_2Sn	174
$CdCl_2$	$CdCl_2$	188
$CdCr_2S_4$	$CdCr_2S_4$	244
$CdCr_2Se_4$	$CdCr_2Se_4$	243
$CdDy_2S_4$	$CdDy_2S_4$	246
$CdEr_2S_4$	$CdEr_2S_4$	246
$CdGa_2S_4$	$CdGa_2S_4$	222
$CdGa_2Se_4$	$CdGa_2Se_4$	222
$CdGa_2Te_4$	$CdGa_2Te_4$	222
$CdGeP_2$	$CdGeP_2$	218
CdI_2	CdI_2	188
$CdIn_2S_4$	$CdIn_2S_4$	223
$CdIn_2Se_4$	$CdIn_2Se_4$	223
$CdIn_2Te_4$	$CdIn_2Te_4$	223
$CdInS_2$	$CdInS_2$	230
$CdInSe_2$	$CdInSe_2$	230
$CdInTe_2$	$CdInTe_2$	230
$CdLa_2S_4$	$CdLa_2S_4$	246
CdO	CdO	184
CdO_3Sn	$CdSnO_3$	236
CdP_2	CdP_2	179
CdP_2Si	$CdSiP_2$	218
CdP_2Sn	$CdSnP_2$	219
CdP_4	CdP_4	179
$CdPr_2S_4$	$CdPr_2S_4$	246
CdS	CdS	185
CdS_2Tl	$CdTlS_2$	230
CdS_4Cd_2	$CdSc_2S_4$	246
CdS_4Tm_2	$CdTm_2S_4$	246
CdS_4Yb_2	$CdYb_2S_4$	246
CdSb	CdSb	178
CdSe	CdSe	185
$CdSe_2Tl$	$CdTlSe_2$	230
$CdSe_4Tl_2$	$CdTl_2Se_4$	223
CdTe	CdTe	186
$CdTe_2Tl$	$CdTlTe_2$	230
Cd_2O_4Sn	Cd_2SnO_4	236
Cd_3P_2	Cd_3P_2	177
$Cd_4Cl_3P_2$	$Cd_4P_2Cl_3$	236
$Cd_4I_3P_2$	$Cd_4P_2I_3$	236
Cd_4Sb_3	Cd_4Sb_3	177
Cd_6P_7	Cd_6P_7	180
Cd_7P_{10}	Cd_7P_{10}	179
CeO_3V	$CeVO_3$	244
Ce_2GeSe_5	Ce_2GeSe_5	246
Ce_2S_3	Ce_2S_3	242
Ce_2Se_5Sn	Ce_2SnSe_5	246
ClCu	CuCl	171
ClTl	TlCl	195
Cl_2Hg	$HgCl_2$	188
Cl_2Pb	$PbCl_2$	204
$Co_{0.3}NbS_2$	$Co_{0.3}NbS_2$	244
$CoLaO_3$	$LaCoO_3$	245
CoO	CoO	239
CoP_2	CoP_2	239
CoP_3	CoP_3	239
CoPS	CoPS	243
$CoSb_2$	$CoSb_2$	239
$CoSb_3$	$CoSb_3$	239
CoSSb	CoSbS	243
Co_3O_4	Co_3O_4	239
$Co_3O_8V_2$	$Co_3V_2O_8$	244
$Cr_{1-x}Te$	$Cr_{1-x}Te$	240
$CrDyO_3$	$DyCrO_3$	244
$CrHoO_3$	$HoCrO_3$	245
CrK_2O_4	K_2CrO_4	244
$CrLaO_3$	$LaCrO_3$	244
$CrNdO_3$	$NdCrO_3$	244
CrO_3Sm	$SmCrO_3$	244

Gross formula		Page
CrO_3Yb	$YbCrO_3$	245
$CrSb_2$	$CrSb_2$	238
$CrSi_2$	$CrSi_2$	238
Cr_2HgS_4	$HgCr_2S_4$	243
Cr_2HgSe_4	$HgCr_2Se_4$	243
Cr_2O_3	Cr_2O_3	239
Cr_2S_3	Cr_2S_3	240
Cr_2Se_4Zn	$ZnCr_2Se_4$	243
$Cr_{2+x}Se_3$	$Cr_{2+x}Se_3$	240
Cr_3Se_4	Cr_3Se_4	240
CsK_2Sb	K_2CsSb	166
$CsNa_2Sb$	Na_2CsSb	166
$CsRb_2Sb$	Rb_2CsSb	166
$CsSb$	$CsSb$	165
Cs_3Sb	Cs_3Sb	166
Cu_xS	Cu_xS	168
Cu_xSe	Cu_xSe	168
Cu_xTe	Cu_xTe	168
$CuCr_2S_{2.5}Se_{1.5}$	$CuCr_2S_{2.5}Se_{1.5}$	243
$CuCr_2S_3Se$	$CuCr_2S_3Se$	243
CuF	CuF	170
$CuFe_2O_4$	$CuFe_2O_4$	244
$CuFeS_2$	$CuFeS_2$	215
$CuFeSe_2$	$CuFeSe_2$	215
$CuFeTe_2$	$CuFeTe_2$	215
$CuGaGeSe_4$	$CuGaGeSe_4$	226
$CuGaS_2$	$CuGaS_2$	212
$CuGaSe_2$	$CuGaSe_2$	212
$CuGaSe_4Sn$	$CuGaSnSe_4$	226
$CuGaTe_2$	$CuGaTe_2$	222
$CuGeInSe_4$	$CuInGeSe_4$	226
CuI	CuI	171
$CuIn_3Te_5$	$CuIn_3Te_5$	236
$CuInS_2$	$CuInS_2$	215
$CuInSe_2$	$CuInSe_2$	215
$CuInSe_4Sn$	$CuInSnSe_4$	226
$CuInTe_2$	$CuInTe_2$	215
$CuLi_3O_3$	Li_3CuO_3	236
CuO	CuO	167
CuS_2Sb	$CuSbS_2$	228
CuS_2Tl	$CuTlS_2$	213
$CuSbSe_2$	$CuSbSe_2$	228
$CuSbTe_2$	$CuSbTe_2$	229
$Cu_2Ga_4Te_7$	$Cu_2Ga_4Te_7$	235
Cu_2GeS_3	Cu_2GeS_3	219
Cu_2GeS_4Zn	Cu_2ZnGeS_4	225
Cu_2GeSe_3	Cu_2GeSe_3	220
Cu_2GeSe_4Zn	$Cu_2ZnGeSe_4$	225
$Cu_2In_4Te_7$	$Cu_2In_4Te_7$	236
Cu_2O	Cu_2O	167
Cu_2S_3Sn	Cu_2SnS_3	220
Cu_2S_4SiZn	Cu_2ZnSiS_4	225
Cu_2Se_3Sn	Cu_2SnSe_3	220
Cu_2Se_4SiZn	$Cu_2ZnSiSe_4$	225
Cu_3DyS_3	Cu_3DyS_3	245
Cu_3DySe_3	Cu_3DySe_3	245
Cu_3DyTe_3	Cu_3DyTe_3	245
Cu_3ErTe_3	Cu_3ErTe_3	245
$Cu_3Ga_5Se_9$	$Cu_3Ga_5Se_9$	235
Cu_3GdS_3	Cu_3GdS_3	245
Cu_3GdSe_3	Cu_3GdSe_3	245
Cu_3GdTe_3	Cu_3GdTe_3	245
Cu_3HoS_3	Cu_3HoS_3	245
Cu_3HoSe_3	Cu_3HoSe_3	245
Cu_3HoTe_3	Cu_3HoTe_3	245
$Cu_3In_5Se_9$	$Cu_3In_5Se_9$	235
Cu_3LuS_3	Cu_3LuS_3	245
Cu_3PS_4	Cu_3PS_4	221
Cu_3S_3Sb	Cu_3SbS_3	228
Cu_3S_3Sc	Cu_3ScS_3	245
Cu_3S_3Sm	Cu_3SmS_3	245
Cu_3S_3Tb	Cu_3TbS_3	245
Cu_3S_3Y	Cu_3YS_3	245
Cu_3S_3Yb	Cu_3YbS_3	245
Cu_3S_4Sb	Cu_3SbS_4	221
Cu_3SbSe_4	Cu_3SbSe_4	221
Cu_3Se_3Sc	Cu_3ScSe_3	245
Cu_3Se_3Sm	Cu_3SmSe_3	245
Cu_3Se_3Tb	Cu_3TbSe_3	245
Cu_3Se_3Y	Cu_3YSe_3	245
Cu_3Se_3Yb	Cu_3YbSe_3	245
Cu_3SmTe_3	Cu_3SmTe_3	245
Cu_3TbTe_3	Cu_3TbTe_3	245
Cu_3Te_3Tm	Cu_3TmTe_3	245
Cu_3Te_3Y	Cu_3YTe_3	245
$Cu_4Ge_3S_5$	$Cu_4Ge_3S_5$	227
$Cu_4Ge_3Se_5$	$Cu_4Ge_3Se_5$	227
Cu_4S_4Sn	Cu_4SnS_4	227
$Cu_4Se_5Sn_3$	$Cu_4Sn_3Se_5$	227
Cu_5GdSe_4	Cu_5GdSe_4	245

Gross formula		Page
Cu_5HoS_4	Cu_5HoS_4	245
Cu_5LuS_4	Cu_5LuS_4	245
Cu_5LuSe_4	Cu_5LuSe_4	245
Cu_5Se_4Tb	Cu_5TbSe_4	245
Cu_5Se_4Yb	Cu_5YbSe_4	245
Cu_8GeS_6	Cu_8GeS_6	227
DyO_3V	$DyVO_3$	244
Dy_2S_3	Dy_2S_3	242
ErO_3Ti	$ErTiO_3$	244
ErO_3V	$ErVO_3$	244
EuO	EuO	242
EuO_3V	$EuVO_3$	242
EuS	EuS	242
EuSe	EuSe	242
EuTe	EuTe	242
Eu_2Se_3	Eu_2Se_3	242
Eu_3S_4	Eu_3S_4	242
F_2Pb	PbF_2	203
$Fe_{0.3}NbS_2$	$Fe_{0.3}NbS_2$	244
$Fe_{1-x}S$	$Fe_{1-x}S$	241
$FeCr_2S_4$	$FeCr_2S_4$	243
$FeHoO_3$	$HoFeO_3$	245
$FeLaO_3$	$LaFeO_3$	245
FeO	FeO	239
FeP_2	FeP_2	238
FeP_4	FeP_4	239
FePS	FePS	243
FeS_2	FeS_2	241
$FeSb_2$	$FeSb_2$	238
FeSbTe	FeSbTe	243
$FeSe_{2-x}$	$FeSe_{2-x}$	241
$FeSi_2$	$FeSi_2$	238
Fe_2O_3	Fe_2O_3	239
Fe_3O_4	Fe_3O_4	239
FTl	TlF	194
GaN	GaN	86
GaP	GaP	91
GaS	GaS	190
GaS_2Tl	$TlGaS_2$	193
GaSb	GaSb	116
GaSe	GaSe	186
$GaSe_2Tl$	$TlGaSe_2$	194
GaTe	GaTe	190
$GaTe_2Tl$	$TlGaTe_2$	194
$Ga_2Hg_5Te_8$	$Hg_5Ga_2Te_8$	224
Ga_2HgS_4	$HgGa_2S_4$	223
Ga_2HgSe_4	$HgGa_2Se_4$	223
Ga_2MnS_4	$MnGa_2S_4$	243
Ga_2S_3	Ga_2S_3	209
Ga_2Se_3	Ga_2Se_3	210
Ga_2Te_3	Ga_2Te_3	210
Ga_6Sb_5Te	Ga_6Sb_5Te	231
$GdFeO_3$	$GdFeO_3$	245
GdO_3Ti	$GdTiO_3$	244
GdO_3V	$GdVO_3$	244
Gd_2GeSe_5	Gd_2GeSe_5	246
Gd_2S_3	Gd_2S_3	242
Gd_2Se_5Sn	Gd_2SnSe_5	246
Ge	Ge	28
$GeMg_2$	Mg_2Ge	174
GeN_2Zn	$ZnGeN_2$	217
$GeNd_2Se_5$	Nd_2GeSe_5	246
GeO_2	GeO_2	200
GeP	GeP	196
GeP_2Zn	$ZnGeP_2$	217
$GePbS_3$	$PbGeS_3$	203
$GePr_2Se_5$	Pr_2GeSe_5	246
GeS	GeS	197
GeS_2	GeS_2	197
GeS_3Sn	$SnGeS_3$	203
$GeSb_2Te_4$	$GeSb_2Te_4$	232
$GeSb_4Te_7$	$GeSb_4Te_7$	232
GeSe	GeSe	198
$GeSe_2$	$GeSe_2$	201
$GeSe_5Sm_2$	Sm_2GeSe_5	246
GeTe	GeTe	198
Ge_2Sr	$SrGe_2$	175
Ge_3Ru_2	Ru_2Ge_3	238
HfS_2	HfS_2	240
HfS_3	HfS_3	240
$HfSe_2$	$HfSe_2$	240
HgI_2	HgI_2	189
$HgIn_2Te_4$	$HgIn_2Te_4$	224
HgO	HgO	186
HgS	HgS	187
HgS_2Tl	$HgTlS_2$	230
HgSe	HgSe	187
$HgSe_2Tl$	$HgTlSe_2$	231
HgTe	HgTe	187
$HgTe_2Tl$	$HgTlTe_2$	231
$Hg_3In_2Te_6$	$Hg_3In_2Te_6$	224
Hg_3PS_3	Hg_3PS_3	236

Gross formula		Page
Hg_3PS_4	Hg_3PS_4	236
$HoMnO_3$	$HoMnO_3$	245
HoO_3Ti	$HoTiO_3$	244
HoO_3V	$HoVO_3$	244
Ho_2S_3	Ho_2S_3	242
ISbSe	SbSeI	233
ISbTe	SbTeI	233
ISSb	SbSI	233
ITl	TlI	195
I_2Pb	PbI_2	204
I_3Sb	SbI_3	208
InN	InN	122
InP	InP	124
InS	InS	191
InS_2Tl	$TlInS_2$	194
InSb	InSb	141
InSe	InSe	191
$InSe_2Tl$	$TlInSe_2$	194
InTe	InTe	191
$InTe_2Tl$	$TlInTe_2$	194
In_2S_3	In_2S_3	210
In_2S_4Zn	$ZnIn_2S_4$	222
$In_2S_5Zn_2$	$Zn_2In_2S_5$	224
$In_2S_6Zn_3$	$Zn_3In_2S_6$	224
In_2Se_3	In_2Se_3	210
In_2Se_4Zn	$ZnIn_2Se_4$	222
In_2Te_3	In_2Te_3	210
In_2Te_4Zn	$ZnIn_2Te_4$	222
In_4Se_3	In_4Se_3	193
In_4Te_3	In_4Te_3	193
In_6S_7	In_6S_7	192
In_6Sb_5Te	In_6Sb_5Te	230
In_6Se_7	In_6Se_7	193
In_7SbTe_6	In_7SbTe_6	232
IrP_2	IrP_2	239
IrS_2	IrS_2	241
IrS_3	IrS_3	242
$IrSe_2$	$IrSe_2$	241
$IrSe_3$	$IrSe_3$	241
KNa_2Sb	Na_2KSb	166
$KNbO_3$	$KNbO_3$	244
KO_3Ta	$KTaO_3$	244
KSb	KSb	165
K_2RbSb	K_2RbSb	166
K_3Sb	K_3Sb	165
$LaMnO_3$	$LaMnO_3$	245
LaO_3V	$LaVO_3$	244
La_2GeSe_5	La_2GeSe_5	246
La_2S_3	La_2S_3	242
La_2Se_5Sn	La_2SnSe_5	246
La_2Te_3	La_2Te_3	242
$La_{10}OS_{14}$	$La_{10}S_{14}O$	242
LiO_3V	$LiVO_3$	244
Li_3Sb	Li_3Sb	155
Lu_2S_4Zn	$ZnLu_2S_4$	245
MgO	MgO	181
MgP_2Si	$MgSiP_2$	216
Mg_2Pb	Mg_2Pb	174
Mg_2Si	Mg_2Si	173
Mg_2Sn	Mg_2Sn	174
$Mn_{0.3}NbS_2$	$Mn_{0.3}NbS_2$	244
MnO	MnO	239
MnO_3V	$MnVO_3$	244
MnO_3Yb	$YbMnO_3$	245
MnP_4	MnP_4	241
MnS	MnS	240
MnS_4Sb_2	$MnSb_2S_4$	243
MnSe	MnSe	240
MnTe	MnTe	240
Mn_2O_3	Mn_2O_3	239
Mn_3O_4	Mn_3O_4	239
$Mn_{11}Si_{19}$	$Mn_{11}Si_{19}$	238
$Mn_{15}Si_{26}$	$Mn_{15}Si_{26}$	238
$Mn_{26}Si_{45}$	$Mn_{26}Si_{45}$	238
MoO_4Pb	$PbMoO_4$	244
MoS_2	MoS_2	240
$MoSe_2$	$MoSe_2$	240
$MoTe_2$	$MoTe_2$	240
$NaNbO_3$	$NaNbO_3$	244
NaSb	NaSb	164
$NaSSe_2$	$NaSSe_2$	229
Na_2RbSb	Na_2RbSb	166
Na_3Sb	Na_3Sb	165
$NbNi_{0.3}S_2$	$Ni_{0.3}NbS_2$	244
NbO_4Sb	$SbNbO_4$	244
Nb_2O_3	Nb_2O_3	249
NdO_3Ti	$NdTiO_3$	244
NdO_3V	$NdVO_3$	244
Nd_2S_3	Nd_2S_3	242
Nd_2Se_5Sn	Nd_2SnSe_5	246
$Ni_{1-x}S$	$Ni_{1-x}S$	241
NiO	NiO	239

Gross formula		Page
NiP_2	NiP_2	239
NiS_2	NiS_2	241
OPb	PbO	199
OPd	PdO	239
OSr	SrO	181
OZn	ZnO	182
O_2Pb	PbO_2	202
O_2Sn	SnO_2	201
O_2Ti	TiO_2	239
O_2V	VO_2	239
O_3PrV	$PrVO_3$	244
O_3Rh_2	Rh_2O_3	239
O_3SmTi	$SmTiO_3$	244
O_3SmV	$SmVO_3$	244
O_3SrTi	$SrTiO_3$	244
O_3TbTi	$TbTiO_3$	244
O_3TbV	$TbVO_3$	244
O_3Ti_2	Ti_2O_3	239
O_3TiYb	$YbTiO_3$	244
O_3TmV	$TmVO_3$	244
O_3V_2	V_2O_3	239
O_3VYb	$YbVO_3$	244
O_3W	WO_3	239
O_5Ta_2	Ta_2O_5	239
O_5Ti_3	Ti_3O_5	239
O_5V_2	V_2O_5	239
O_5V_3	V_3O_5	239
O_7Ti_4	Ti_4O_7	239
O_9Ti_5	Ti_5O_9	239
$O_{11}Ti_6$	Ti_6O_{11}	239
$O_{15}Ti_8$	Ti_8O_{15}	239
OsP_2	OsP_2	239
OsP_4	OsP_4	239
OsPS	OsPS	243
OsPSe	OsPSe	243
OsS_2	OsS_2	241
$OsSb_2$	$OsSb_2$	239
OsSSb	OsSbS	243
$OsTe_2$	$OsTe_2$	241
P	P	161
PPdS	PdPS	243
PPdSe	PdPSe	243
PRuS	RuPS	243
PSi	SiP	196
P_2Pd	PdP_2	239
P_2Pt	PtP_2	239
P_2Rh	RhP_2	239
P_2Ru	RuP_2	238
P_2Si	SiP_2	197
P_2SiZn	$ZnSiP_2$	216
P_2SnZn	$ZnSnP_2$	217
P_2Zn	ZnP_2	178
P_2Zn_3	Zn_3P_2	176
P_4Ru	RuP_4	239
PbO_3Ti	$PbTiO_3$	244
PbO_3Zr	$PbZrO_3$	244
PbO_4W	$PbWO_4$	244
PbS	PbS	199
PbS_3Sn	$PbSnS_3$	203
PbS_4Sb	$PbSb_2S_4$	232
PbSe	PbSe	200
PbTe	PbTe	200
PdS	PdS	241
PdS_2	PdS_2	241
PdSe	PdSe	241
$PdSe_2$	$PdSe_2$	241
Pr_2Se_5Sn	Pr_2SnSe_5	246
$Pt_{0.97}S_2$	$Pt_{0.97}S_2$	241
PtS	PtS	241
$PtSb_2$	$PtSb_2$	239
$PtSe_2$	$PtSe_2$	241
Rb_3Sb	Rb_3Sb	166
ReS_2	ReS_2	241
$ReSe_2$	$ReSe_2$	241
$ReSi_2$	$ReSi_2$	238
RhS_3	RhS_3	241
$RhSe_2$	$RhSe_2$	241
$RhSe_3$	$RhSe_3$	241
Rh_2S_3	Rh_2S_3	241
Ru_2Si_3	Ru_2Si_3	238
RuS_2	RuS_2	241
$RuSb_2$	$RuSb_2$	238
RuSbSe	RuSbSe	243
RuSbTe	RuSbTe	243
$RuSe_2$	$RuSe_2$	241
$RuTe_2$	$RuTe_2$	241
S	S	162
SSm	SmS	242
SSn	SnS	198
STl	TlS	191
SYb	YbS	242
SZn	ZnS	182

Gross formula		Page
S_2SbTl	$TlSbS_2$	231
S_2Sn	SnS_2	201
S_2Ta	TaS_2	240
S_2Tc	TcS_2	241
S_2Ti_{1+x}	$Ti_{1+x}S_2$	240
S_2Tl	TlS_2	193
S_2TlZn	$ZnTlS_2$	231
S_2W	WS_2	240
S_2Zr	ZrS_2	240
$S_{3-x}Ti$	TiS_{3-x}	240
$S_{3-x}Zr$	ZrS_{3-x}	240
S_3Sb_2	Sb_2S_3	205
S_3Sn_2	Sn_2S_3	202
S_3Yb_2	Yb_2S_3	242
S_4Sm_3	Sm_3S_4	242
S_4Tl_3V	Tl_3VS_4	244
S_4Tm_2Zn	$ZnTm_2S_4$	245
S_4Yb_2Zn	$ZnYb_2S_4$	245
Sb	Sb	161
SbZn	ZnSb	177
Sb_2Se_3	Sb_2Se_3	206
Sb_2SnZn	$ZnSnSb_2$	218
Sb_2Te_3	Sb_2Te_3	206
Sb_3Zn_4	Zn_4Sb_3	177
Sc_2S_4Zn	$ZnSc_2S_4$	245
Se	Se	163
SeSm	SmSe	242
SeSn	SnSe	198
SeTl	TlSe	192
SeYb	YbSe	242
SeZn	ZnSe	183
Se_2Sn	$SnSe_2$	202
Se_2Tc	$TcSe_2$	241
Se_2Ti_{1+x}	$Ti_{1+x}Se_2$	240
Se_2TlZn	$ZnTlSe_2$	231
Se_2W	WSe_2	240
Se_2Zr_{1+x}	$Zr_{1+x}Se_2$	240
Se_3Zr	$ZrSe_3$	240
Se_5Sm_2Sn	Sm_2SnSe_5	246
Si	Si	11
Si_2Te_3	Si_2Te_3	202
SmTe	SmTe	242
Sn	Sn (grey tin)	42
SnTe	SnTe	199
Te	Te	163
TeTl	TlTe	192
TeTm	TmTe	242
TeYb	YbTe	242
TeZn	ZnTe	183
Te_2TlZn	$ZnTlTe_2$	231
Te_3Tl_5	Tl_5Te_3	193

2 Synopsis of the sections of this book and the corresponding sections of volumes III/17, 22 and 23a of the New Series of Landolt-Börnstein

In this section we list all sections of this book and the corresponding sections of volumes III/17a ··· i, III/22a,b and III/23a of the New Series of Landolt-Börnstein for further information about the various groups of semiconductors.

At the end of this section topics of volumes III/17 are listed which have been not included into this volume.

Sections in this volume		Sections in III/17, III/22 and III/23a	
1 Elements of the IVth group and IV-IV compounds			
1.1	Diamond	III17a	36 ··· 42, 352 ··· 358
		III/22a	9 ··· 13, 261 ··· 263
		III/22b	173 ··· 206
		III/23a	12 ··· 15
1.2	Silicon	III17a	43 ··· 87, 359 ··· 400
		III/22a	14 ··· 28, 263 ··· 275
		III/22b	207 ··· 438
		III/23a	15 ··· 20
1.3	Germanium	III17a	87 ··· 127, 400 ··· 434
		III/22a	28 ··· 38, 275 ··· 282
		III/22b	439 ··· 489
		III/23a	20 ··· 24
1.4	Grey tin	III17a	127 ··· 132, 434 ··· 441
		III/22a	39 ··· 43, 283 ··· 286
		III/23a	24 ··· 27
1.5	Silicon carbide	III17a	132 ··· 142, 442 ··· 449
		III/22a	43 ··· 50, 286 ··· 289
		III/22b	490 ··· 498
		III/23a	27 ··· 30
1.6	Silicon germanium alloys	III17a	142, 449 ··· 454
		III/22a	50 ··· 51, 289 ··· 291
2 III-V compounds			
2.1	Boron nitride	III17a	148 ··· 153, 460 ··· 464
		III/22a	52 ··· 55, 291 ··· 295
		III/22b	719
		III/23a	30 ··· 34
2.2	Boron phosphide	III17a	153 ··· 156, 464 ··· 467
		III/22a	55 ··· 57, 291 ··· 293
		III/22b	720
		III/23a	34 ··· 35
2.3	Boron arsenide	III17a	156 ··· 157, 468
2.4	Aluminium nitride	III17a	158 ··· 161, 469 ··· 472
		III/22a	58 ··· 60, 297
		III/23a	36
2.5	Aluminium phosphide	III17a	161 ··· 164, 473 ··· 476
		III/22a	60 ··· 63, 298
		III/23a	37

2.6 Aluminium arsenide	III17a	164 ··· 168, 476 ··· 479
	III/22a	63 ··· 67, 299 ··· 300
	III/23a	38 ··· 41
2.7 Aluminium antimonide	III17a	169 ··· 178, 479 ··· 487
	III/22a	67 ··· 71, 300 ··· 303
	III/23a	41 ··· 43
2.8 Gallium nitride	III17a	178 ··· 185, 487 ··· 494
	III/22a	72
	III/22b	499 ··· 503
2.9 Gallium phosphide	III17a	185 ··· 218, 494 ··· 511
	III/22a	72 ··· 82, 304 ··· 310
	III/22b	504 ··· 565
	III/23a	43 ··· 47
2.10 Gallium arsenide	III17a	218 ··· 258, 512 ··· 545
	III/22a	82 ··· 97, 310 ··· 321
	III/22b	566 ··· 658
	III/23a	47 ··· 55
2.11 Gallium antimonide	III17a	258 ··· 278, 546 ··· 557
	III/22a	97 ··· 106, 321 ··· 325
	III/22b	659 ··· 666
	III/23a	55 ··· 59
2.12 Indium nitride	III17a	278 ··· 280, 558
	III/22a	106, 326 ··· 327
	III/23a	59 ··· 60
2.13 Indium phosphide	III17a	281 ··· 297, 559 ··· 572
	III/22a	107 ··· 116, 327 ··· 335
	III/22b	667 ··· 705
	III/23a	60 ··· 65
2.14 Indium arsenide	III17a	297 ··· 310, 572 ··· 584
	III/22a	117 ··· 123, 335 ··· 338
	III/22b	706 ··· 709
	III/23a	65 ··· 68
2.15 Indium antimonide	III17a	310 ··· 333, 584 ··· 602
	III/22a	123 ··· 135, 338 ··· 342
	III/22b	710 ··· 718
	III/23a	69 ··· 74
2.16 Ternary and quaternary alloys between III-V compounds	III17a	333 ··· 348, 603 ··· 642
	III/22a	135 ··· 159, 343 ··· 368
	III/22b	721 ··· 749
3 Elements		
3.1 Group III elements	III/17e	9 ··· 27, 263 ··· 285
3.2 Group IV elements	see chapter 1	
3.3 Group V elements	III/17e	27 ··· 63, 285 ··· 322
3.4 Group VI elements	III/17e	63 ··· 122, 322 ··· 378
4 Binary compounds		
4.1 IA-IB compounds	III/17e	123 ··· 125, 379 ··· 381
4.2 I_x-V_y compounds	III/17e	126 ··· 136, 382 ··· 394
4.2.1 I-V compounds	III/17e	129, 382 ··· 384
4.2.2 I_3-V compounds	III/17e	129 ··· 135, 384 ··· 393
4.2.3 I_2-I-V compounds	III/17e	135, 393 ··· 395
4.3 I_x-VI_y compounds	III/17e	137 ··· 163, 395 ··· 432
4.4 I-VII compounds	III/17b	253 ··· 302, 489 ··· 527
	III/22a	235 ··· 260, 440 ··· 451
4.5 II_x-IV_y compounds	III/17e	163 ··· 177, 432 ··· 455
4.5.1 II_2-IV compounds	III/17e	164 ··· 176, 433 ··· 455
4.5.2 II-IV_2 compounds	III/17e	176

4.6 II_x-V_y compounds	III/17e	178 ··· 249, 455 ··· 518
4.6.1 II_3-V_2 compounds	III/17e	183 ··· 213, 463 ··· 499
4.6.2 II_4-V_3 compounds	III/17e	235 ··· 237, 517 ··· 518
4.6.3 II-V compounds	III/17e	229 ··· 235, 514 ··· 517
3.6.4 II-V_2 compounds	III/17e	213 ··· 228, 499 ··· 512
3.6.5 II-V_4 compounds	III/17e	228 ··· 229, 513 ··· 514
3.6.6 Further II-V compounds	III/17e	237 ··· 238, 518
4.7 II-VI compounds	III/17b	10 ··· 252, 319 ··· 488
	III/22a	160 ··· 234, 370 ··· 439
4.7.1 IIA-VIB compounds	III/17b	13 ··· 34, 321 ··· 335
4.7.2 Zinc chalcogenides	III/17b	35 ··· 161, 335 ··· 405
	III/22a	160 ··· 192, 370 ··· 399
	III/23a	74 ··· 87
4.7.3 Cadmium chalcogenides	III/17b	161 ··· 230, 405 ··· 459
	III/22a	192 ··· 216, 399 ··· 415
	III/23a	87 ··· 103
4.7.4 Mercury chalcogenides	III/17b	230 ··· 252, 460 ··· 488
	III/22a	217 ··· 227, 415 ··· 424
4.8 II-VII_2 compounds	III/17e	250 ··· 262, 519 ··· 533
4.9 III-V compounds	see chapter 2	
4.10 III_x-VI_y compounds	III/17f	9 ··· 102, 289 ··· 339
4.10.1 III-VI compounds	III/17f	9 ··· 74, 289 ··· 327
4.10.2 III_2-VI_3 compounds	see section 5.1.1	
4.10.3 Further III_x-VI_y compounds	III/17f	74 ··· 83, 327 ··· 329
4.10.4 III-III-VI compounds	III/17f	84 ··· 102, 330 ··· 339
4.11 III-VII compounds	III/17f	103 ··· 122, 340 ··· 356
4.12 IV_x-V_y compounds	III/17f	123 ··· 126, 356 ··· 360
4.12.1 IV-V compounds	III/17f	123 ··· 125, 356 ··· 360
4.12.2 IV-V_2 compounds	III/17f	125
4.13 IV_x-VI_y compounds	III/17f	126 ··· 219, 361 ··· 473
4.13.1 IV-VI compounds	III/17f	126 ··· 190, 363 ··· 443
4.13.2 IV-VI_2 compounds	III/17f	191 ··· 213, 444 ··· 468
4.13.3 IV_2-VI_3 compounds	III/17f	214 ··· 218, 469 ··· 473
4.14 IV-VII compounds	III/17f	219 ··· 234, 474 ··· 485
4.15 V_x-VI_y compounds	III/17f	234 ··· 280, 486 ··· 559
4.16 V-VII_3 compounds	III/17f	280 ··· 288, 559 ··· 562
5 Ternary compounds		
5.1 Tetrahedrally bonded ternary and quasi-binary compounds	III/17h	9 ··· 156. 329 ··· 381
5.1.1 III_2-VI_3 compounds	III/17h	12 ··· 26, 330 ··· 338
5.1.2 I-III-VI_2 compounds	III/17h	26 ··· 67, 339 ··· 352
5.1.3 II-IV-V_2 compounds	III/17h	68 ··· 111, 353 ··· 367
5.1.4 I_2-IV-V_3 compounds	III/17h	111 ··· 118, 367 ··· 370
5.1.5 I_2-V-VI_4 compounds	III/17h	118 ··· 123, 370 ··· 373
5.1.6 II-III_2-VI_4 compounds	III/17h	124 ··· 149, 373 ··· 379
5.1.7 Other ordered vacancy compounds	III/17h	150 ··· 153, 380
5.1.8 Quaternary compounds	III/17h	153 ··· 156, 381
5.2 Further ternary compounds	III/17h	292 ··· 328, 523 ··· 565
5.2.1 I_x-IV_y-VI_z compounds	III/17h	292 ··· 296, 523 ··· 528
5.2.2 I_x-V_y-VI_z compounds	III/17h	296 ··· 304, 528 ··· 534
5.2.3 II_x-III_y-VI_z compounds	III/17h	304 ··· 306, 534 ··· 538
5.2.4 III_x-V_y-VI_z compounds	III/17h	306 ··· 309, 538 ··· 542
5.2.5 IV_x-V_y-VI_z compounds	III/17h	310 ··· 313, 542 ··· 545
5.2.6 V-VI-VII compounds	III/17h	313 ··· 325, 545 ··· 562
5.2.7 Other ternary compounds	III/17h	326 ··· 328, 562 ··· 565

6 Further compounds with semiconducting properties

6.1	Boron compounds	III/17g	9 ··· 62, 345 ··· 381
6.2	Binary transition metal compounds	III/17g	63 ··· 344, 381 ··· 666
6.2.1	Compounds with elements of the IVth group	III/17g	63 ··· 79, 381 ··· 397
6.2.2	Compounds with elements of the Vth group	III/17g	80 ··· 116, 398 ··· 412
6.2.3	Oxides	III/17g	129 ··· 291, 413 ··· 595
6.2.4	Chalcogenides	III/17g	291 ··· 316, 595 ··· 620
6.3	Binary rare earth compounds	III/17g	317 ··· 344, 621 ··· 666
6.4	Ternary transition metal compounds	III/17g	117 ··· 128
		III/17h	157 ··· 226, 382 ··· 493
6.4.1	Pnigochalcogenides	III/17g	117 ··· 128
6.4.2	Spinels and related compounds	III/17h	157 ··· 187, 382 ··· 435
6.4.3	Oxides	III/17h	187 ··· 220, 435 ··· 487
6.4.4	Further chalcogenides	III/17h	220 ··· 225, 488 ··· 493
6.5	Ternary rare earth compounds	III/17h	225 ··· 291. 494 ··· 522

Topics of volumes III/17 and III/22 not included into the present volume:

Semimagnetic semiconductors	III/17b	302 ··· 318, 528 ··· 543
Technology of semiconductors	III/17c	1 ··· 651
	III/17d	1 ··· 429
Amorphous semiconductors	III/17i	1 ··· 105
Organic semiconductors	III/17i	106 ··· 218
Space charge layers and interfaces	III/17i	219 ··· 255
Hot electrons	III/17i	256 ··· 296
Electron hole liquids	III/17i	297 ··· 312

3 Contents of the volumes of the New Series of Landolt-Börnstein dealing with semiconductors

In this appendix some informations are given about the 12 volumes of the New Series of Landolt-Börnstein dealing with semiconductors. The information is restricted to the bibliographical data, the names of the editors and the authors of the volumes and to shortened Lists of Contents containing for each volume the titles of the main chapters and sections and the respective authors.

Volume III/17: Semiconductors

Editors: O. MADELUNG (a,b,e ... h), M. SCHULZ, H. WEISS (c,d), O. MADELUNG, M. SCHULZ, H. WEISS (i)
Subvolume a:1982. 1316 figs., XI, 642 pages. ISBN 3-540-10610-3
Subvolume b: 1982. 891 figs., XI, 543 pages. ISBN 3-540-11308-8
Subvolume c: 1984. 738 figs., XIII, 651 pages. ISBN 3-540-11474-2
Subvolume d: 1984. 461 figs., XIV, 429 pages. ISBN 3-540-11779-2
Subvolume e: 1983. 1020 figs., XIII, 533 pages. ISBN 3-540-11780-6
Subvolume f: 1983. 1061 figs., XII, 562 pages. ISBN 3-540-12160-9
Subvolume g: 1984. 1164 figs., XI, 666 pages. ISBN 3-540-12744-5
Subvolume h: 1985. 913 figs., XI, 565 pages. ISBN 3-540-13507-3
Subvolume i: 1985. 675 figs., XI, 385 pages. ISBN 3-540-15072-2

Contents

Subvolume a: Physics of Group IV Elements and III-V Compounds
A Introduction (O. MADELUNG)
1 General remarks on the contents and the structure of subvolumes 17a ... 17e 1
2 Semiconductor properties, their definition and methods for their determination 3
2.1 Basic properties of semiconductors 3
2.2 Experimental methods useful for the determination of semiconductor properties 8
2.3 Impurities and defects 16
2.4 Properties of tetrahedrally bonded semiconductors 19
3 Frequently used symbols, abbreviations, conversion tables 26
B Physical data of semiconductors I
1 Elements of the IVth group and IV-IV compounds (R. BLACHNIK, M. CARDONA, TH. GRAVE, G. HARBEKE, K. HÜBNER, W. KRESS, O. MADELUNG, W. v. MÜNCH, U. RÖSSLER, M. SCHULZ, M.S. SKOLNICK) 33
2 III-V compounds (D. BIMBERG, R. BLACHNIK, M. CARDONA, P.J. DEAN, TH. GRAVE, G. HARBEKE, K. HÜBNER, U. KAUFMANN, W. KRESS, O. MADELUNG, U. RÖSSLER, J. SCHNEIDER) 144

Subvolume b: Physics of II-VI and I-VII Compounds, Semimagnetic Semiconductors
A Introduction (O. MADELUNG)
B Physical data of semiconductors II
3 II-VI compounds 10
3.0 Structure, chemical bond (I. BROSER, H. FINKENRATH, H.E. GUMLICH, E. MOLLWO, H. NELKOWSKI, G. NIMTZ) 10
3.1 Magnesium oxide (MgO) (H. FINKENRATH, under assistance of N. UHLE) 13
3.2 Calcium oxide (CaO) (H. FINKENRATH, under assistance of N. UHLE) 22
3.3 Strontium oxide (SrO) (H. FINKENRATH, under assistance of N. UHLE) 27
3.4 Barium oxide (BaO) (H. FINKENRATH, under assistance of N. UHLE) 31
3.5 Zinc oxide (ZnO) (E. MOLLWO) 35
3.6 Zinc sulfide (ZnS) (H. NELKOWSKI, H. J. SCHULZ, under assistance of B. DIKO, K. PETERMANN, H. PRADELLA, G. ROUSSOS, W. SCHLAAK) 61

3.7 Zinc selenide (ZnSe) (H. E. GUMLICH, D. THEIS, D. TSCHIERSE) 126
3.8 Zinc telluride (ZnTe) (G. NIMTZ) 157
3.9 Cadmium oxide (CdO) (H. FINKENRATH, under assistance of N. UHLE) 161
3.10 Cadmium sulfide (CdS) (I. BROSER, R. BROSER, M. ROSENZWEIG, under assistance of R. BAUMERT, A. HOFFMANN, A. ROUSSEL) 166
3.11 Cadmium selenide (CdSe) (I. BROSER, R. BROSER, A. HOFFMANN, under assistance of R. BAUMERT, M. ROSENZWEIG, A. ROUSSEL) 202
3.12 Cadmium telluride (CdTe) (G. NIMTZ) 225
3.13 Mercury oxide (HgO) (G. NIMTZ) 230
3.14 Mercury sulfide (HgS) (G. NIMTZ) 231
3.15 Mercury selenide (HgSe) (G. NIMTZ) 236
3.16 Mercury telluride (HgTe) (G. NIMTZ) 239
3.17 Solid solutions 244
3.17.1. IIA-VIB compounds (H. FINKENRATH) 244
3.17.2. IIB-VIB compounds (I. BROSER, H. NELKOWSKI, G. NIMTZ) 244
4 I-VII compounds (W. VON DER OSTEN) 253
5 Semimagnetic semiconductors (R.R. GALATZKA, J. KOSSUT) 302

Subvolume c: Technology of Si, Ge, and SiC

A Introduction (M. SCHULZ)
1 General remarks 1
2 Frequently used symbols 2
3 Conversion of units 5
4 Abbreviations frequently used in semiconductor technology 6
B Technology of semiconductors
6 Tetrahedrally bonded semiconductors 12
6.1 Silicon and germanium 12
6.1.1 Technological data (A. MÜHLBAUER) 12
6.1.2 Crystal growth 23
6.1.2.1 Deposition of polycrystalline silicon (W. DIETZE) 23
6.1.2.2 Preparation and purification methods of Ge (W. DIETZE) 28
6.1.2.3 Czochralski growth of Si and Ge (W. ZULEHNER) 28
6.1.2.4 Zone melting (A. MÜHLBAUER, subsection 6.1.2.4.6 P. GLASOW). 41
6.1.2.5 Unconventional Si crystallization techniques (M. SCHULZ, E. SIRTL) 50
6.1.2.6 Wafer preparation (W. ZULEHNER) 54
6.1.3 Characterization of crystal properties 62
6.1.3.1 Properties of polycrystalline silicon (W. DIETZE) 62
6.1.3.2 Properties of Czochralski silicon (W. ZULEHNER) 62
6.1.3.3 Properties of float-zone silicon (A. MÜHLBAUER) 69
6.1.3.4 Properties of high purity germanium (P. GLASOW) 73
6.1.3.5 Diagnostic techniques (A. MÜHLBAUER, subsection 6.1.3.5.3 P. GLASOW) 77
6.1.4 Device technology 90
6.1.4.0 Basic device structures (H. MADER, subsection 6.1.4.0.9, P. GAMOW) 90
6.1.4.1 Diffusion (W. LANGHEINRICH under assistance of K. HABERLE) 118
6.1.4.2 Ion implantation (H. RUNGE) 150
6.1.4.3 Nuclear transmutation doping (M. SCHNÖLLER) 185
6.1.4.4 Silicon epitaxy (A. LUDSTECK) 192
6.1.4.5 Fabrication of layers (subsections 6.1.4.5.0 ... 7: E. DOERING, 6.1.4.5.8 ... 12: L. SCHLEICHER) 213
6.1.4.6 Litography (H. MADER) 250
6.1.4.7 Etching processes (H. MADER) 280
6.1.4.8 Final device preparation (E. UDEN) 367
6.2 Silicon carbide (W. v. MÜNCH) 403

Subvolume d: Technology of III-V, II-VI and Non-Tetrahedrally Bonded Compounds

A Introduction (M. SCHULZ)
B Technology of semiconductors
6 Tetrahedrally bonded semiconductors (continued) 12
6.3 III-V compounds 12
6.3.0 Introduction 12
6.3.1 Technological data (H. JACOB, G. MÜLLER) 12
6.3.2 Crystal growth (H. JACOB, G. MÜLLER) 34
6.3.3 Characterization of crystal properties (H. JACOB, G. MÜLLER) 52
6.3.4 Device technology 68
6.3.4.0 Basic device structures (C. WEYRICH) 68
6.3.4.0.1 Light emitting devices (C. WEYRICH) 68
6.3.4.0.2 Photodetectors (C. WEYRICH, R. TROMMER) 76
6.3.4.0.3 Solar cells (C. WEYRICH) 78
6.3.4.0.4 Photocathodes and cold cathodes (C. WEYRICH) 79
6.3.4.0.5 Microwave devices (C. WEYRICH, J.E. MÜLLER) 80
6.3.4.0.6 Integrated circuits (C. WEYRICH, J.E. MÜLLER) . 83
6.3.4.0.7 Magnetic field devices (C. WEYRICH) 83
6.3.4.1 Diffusion of dopants (C. WEYRICH, C. CLEMEN, P. ECKSTEIN) 88
6.3.4.2 Ion implantation (H. RUNGE) 92
6.3.4.3 Epitaxy 105
6.3.4.3.1 General aspects of epitaxy (C. WEYRICH, M. PLIHAL) 105
6.3.4.3.2 Lattice matching (C. WEYRICH, M. PLIHAL) 106
6.3.4.3.3 Vapour phase epitaxy (C. WEYRICH, M. DRUMINSKI, S. GISDAKIS, K. SCHWARZMICHEL) 108
6.3.4.3.4 Liquid phase epitaxy (C. WEYRICH, S. LEIBENZEDER, M. PLIHAL) 115
6.3.4.3.5 Molecular beam epitaxy (C. WEYRICH, F. RAISCH) 121
6.3.4.4 Etching processes (C. WEYRICH, H. HUBER) 131
6.3.4.5 Contact fabrication (C. WEYRICH, J. HEINEN) 134
6.3.4.5.1 Ohmic contacts (C. WEYRICH, J. HEINEN) 135
6.3.4.5.2 Schottky contacts (C. WEYRICH, H. ALBRECHT) 136
6.3.4.6 Pattern definition (C. WEYRICH) 142
6.3.4.7 Final device preparation (C. WEYRICH) 142
6.4 II-VI compounds (Wide gap semiconductors) (R. HELBIG) 145
6.5 II-VI compounds (Zero gap and narrow gap semiconductors) (H. MAIER) 211
7 Non-tetrahedrally bonded semiconductors 245
7.1 IV-VI compounds (J. BAARS) 245
7.2 Mercury iodide (P. GLASOW, E. TOMZIG) 292
7.3 Selenium (K. KASSEL) 308

Subvolume e: Physics of Non-Tetrahedrally Bonded Elements and Binary Compounds I

A Introduction (O. MADELUNG)
B Physical data of semiconductors III
8 Non-tetrahedrally bonded elements
8.1 Elements of the IIId group: Boron (B) (H. WERHEIT) 9
8.2 Elements of the Vth group: P, As, Sb, Bi, $Bi_{1-x}Sb_x$ (H. LEHMANN) 27
8.3 Elements of the IVth group: S, Se, Te, Se_xTe_{1-x} 63
8.3.0 Structure, chemical bond (P. GROSSE, G. WEISER) 63
8.3.1 Sulfur (S) (G. WEISER) 69
8.3.2 Selenium (Se) (G. WEISER) 86
8.3.3 Tellurium (Te) (P. GROSSE, W. RICHTER) 106
8.3.4 Se_xTe_{1-x} (G. WEISER) 118
9 Non-tetrahedrally bonded binary compounds 123
9.1 IA-IB compounds (W. FREYLAND) 123
9.2 I_X-V_Y compounds (W. FREYLAND) 126
9.3 I-VI compounds (A. GOLZENÉ, C. SCHWAB) 137

9.4 II-IV compounds (O. MADELUNG) 163
9.5 II_X-V_Y compounds (W. ZDANOWICZ, sections 9.5.7 and 9.5.9 under assistance of J. WESZKA, sections 9.5.14, 9.5,15 and 9.5.17 under assistance of V. YA. SHEVCHENKO) 178
9.6 II-VII_2 compounds (G. HARBEKE) 250

Subvolume f: Physics of Non-Tetrahedrally Bonded Binary Compounds II
A Introduction (O. MADELUNG)
B Physical data of semiconductors IV
9.7 III-VI compounds (K. MASCHKE, F. LÉVY) 9
9.8 III-VII compounds (J. TREUSCH) 103
9.9 IV_X-V_Y compounds (O. MADELUNG) 123
9.10 IV_X-VI_Y compounds 126
9.10.1 IV-VI compounds (G. NIMTZ, F.J. SCHMITTE) 126
9.10.2 IV-VI_2 compounds (F. J. SCHMITTE) 191
9.10.3 IV_2-VI_3 compounds (F. J. SCHMITTE) 214
9.11 IV-VII_2 compounds (G. HARBEKE) 219
9.12 V_X-VI_Y compounds (A. KROST) 234
9.13 V-VII_3 compounds (R. CLASEN) 280

Subvolume g: Physics of Non-Tetrahedrally Bonded Binary Compounds III
A Introduction (O. MADELUNG)
B Physical data of semiconductors V
9.14 Boron compounds (H. WERHEIT) 9
9.15 Binary transition-metal compounds 63
9.15.1 Compounds with elements of the IIId and IVth groups (F. HULLIGER) 63
9.15.2 Binary transition-metal oxides (J.B. GOODENOUGH, A. HAMNETT) 129
9.15.3 Binary transition-metal chalcogenides (J.B. GOODENOUGH, S.K. RAMASESHA) 291
9.16 Binary rare earth compounds (G. HUBER, M. LEISS) 317

Subvolume h: Physics of Ternary Compounds
A Introduction (O. MADELUNG)
B Physical data of semiconductors VI
10 Ternary compounds
10.1 Tetrahedrally bonded ternary and quasi-binary compounds (A. MACKINNON) 9
10.1.0 Introduction, general remarks on structure and properties 9
10.1.1 III_2-VI_3 compounds 11
10.1.2 I-III-VI_2 compounds 26
10.1.3 II-IV-V_2 compounds 68
10.1.4 I_2-IV-VI_3 compounds 111
10.1.5 I_3-V-VI_4 compounds 118
10.1.6 vacancy-II-III_2-VI_4 compounds 124
10.1.7 Other ordered vacancy compounds 150
10.1.8 Quaternary compounds 153
10.2 Ternary transition-metal compounds (M. BÖHM, A. SCHARMANN) 157
10.3 Ternary rare earth compounds (G. HUBER, E.-G. SCHARMER) 226
10.4 Further ternary compounds (O. MADELUNG) 292

Subvolume i: Special Systems and Topics. Comprehensive Index for III/17 a ... i
A. Special systems
11 Amorphous semiconductors (W. FUHS) 1
11.0 Lists of frequently used symbols and abbreviations 1
11.1 Silicon (a-Si) 3
11.2 Germanium (a-Ge) 13
11.3 III-V compounds 20

12 Organic semiconductors (N. KARL) 106
12.0 Introduction 106
12.1 Photoconductive wide band gap organic semiconductors 112
12.2 Dark-conductive narrow band gap organic semiconductors 144
12.3 Comparative representation of some general properties of selected compounds 151
Figures for 12 159
References for 12 206
B Special topics (edited by M. SCHULZ)
13 Space charge layers at surfaces and interfaces (I. EISELE) 219
13.0 List of symbols 219
13.1 General remarks 220
13.2 Experimental methods 223
13.3 Surface data for various semiconductor layers 223
14 Hot electrons (H. KAHLERT) 256
14.0 Introduction .256
14.1 Carrier heating by electronic fields 258
15 Electron-hole liquids (D. BIMBERG) .297
Comprehensive index for III/17a ... i (O. MADELUNG, M. SCHULZ))
1. Index of substances for subvolumes 17a, b, e ... i (except organic semiconductors) 314
2. Index of binary and quasi-binary phase diagrams for subvolumes 17a, b, e ... i 333
3. Index of mineral and common names 335
4. Index of organic semiconductors (Chap. 12 of subvolume i) 335
5. Subject index for subvolumes 17c, d 338

Volume III/22: Semiconductors

(Supplements and extensions to volume III/17)

Editors: O. MADELUNG (a), M. SCHULZ (b)
Subvolume a: 1987. 681 figs., XII, 451 pages. ISBN 3-540-16609-2
Subvolume b: 1989. 812 figs., XX, 776 pages. ISBN 3-540-17917-8

Contents

Subvolume a: Intrinsic Properties of Group IV Elements and III-V, II-VI and I-VII Compounds

A Introduction (O. MADELUNG) 1
B Physical data
1 Elements of the IVth group and IV-IV compounds (O. MADELUNG) 9
2 III-V compounds (O. MADELUNG) 52
2.1 ... 2.15 Compunds 52
2.16 Ternary and quaternary alloys between III-V compounds and with other semiconductors 135
2.16.1 Ternary alloys of the type III_x-III_{1-x}-V 135
2.16.2 Ternary alloys of the type III-V_{1-x}-V_x 148
2.16.3 Quaternary alloys of the type III_x-III_{1-x}-V_y-V_{1-y} 151
2.16.4 Quaternary alloys of the type III_{1-x-y}-III_x-III_y-V 156
2.16.5 Alloys of III-V compounds with elements of the IVth group 158
3 II-VI compounds (U. RÖSSLER) 160
4 I-VII compounds (W. VON DER OSTEN) 235

Subvolume b: Impurities and Defects in Group IV Elements and III-V Compounds

1 Introduction (M. SCHULZ) 1
2 Trends of impurity and defect properties (P. VOGL) 12
2.0 Outline of the theoretical chapters 12
2.1 Introduction 12
2.2 Theoretical predictions of impurity properties 14
Figures for 2 29
References for 2 49

3 Measurement methods 51
3.1 Electrical methods (G. PENSL) 51
3.2 Optical methods 105
3.2.1 Absorption (R. MURRAY, R.C. NEWMAN) 105
3.2.2 Luminescence (R. SAUER) 118
3.3 Magnetie resonance methods (J. SCHNEIDER) 123
3.4 Analysis of extended defeets (W. BERGHOLZ) 126
3.5 Chemical analysis (H.-J. RATH) 159
4 Impurity and defect properties in group IV elements 173
4.1 Diamond (C) 173
4.1.1 Impurities (W. v. MÜNCH) 173
4.1.2 Defects (W. v. MÜNCH) 174
4.1.3 Paramagnetic centers (C.A.J. AMMERLAAN) 177
4.2 Silicon (Si) 207
4.2.1 Solubility and segregation of impurities (M. SCHULZ) 207
4.2.2 Diffusion of impurities (M. SCHULZ) 230
4.2.3 Impurity levels (M. SCHULZ) 270
4.2.4 Excited bound states of acceptors and donors (R. SAUER) 325
4.2.5 Photoluminescence properties of impurities and defects (R. SAUER) 338
4.2.6 Paramagnetic centers in silicon (C.A.J. AMMERLAAN) 365
4.2.7 Vibrational modes of impurities and defects (R. MURRAY, R.C. NEWMAN) 382
4.2.8 Oxygen-related defects and microdefects (W. ZULEHNER) 391
4.3 Germanium (Ge) 439
4.3.1 Solubility and segregation of impurities (N.A. STOLWIJK) 439
4.3.2 Diffusion of impurities (N.A. STOLWIJK) 451
4.3.3 Impurity levels (M.S. SKOLNICK) 466
4.3.4 Capture cross sections (M.S. SKOLNICK) 476
4.3.5 Photoionization cross sections (M.S. SKOLNICK) 477
4.3.6 Deformation potential (M.S. SKOLNICK) 477
4.3.7 Luminescence of bound excitions (M.S. SKOLNICK) 478
4.3.8 Electron paramagnetic resonance (EPR) (M.S. SKOLNICK) 479
4.3.9 Local vibrational modes (M.S. SKOLNICK) 479
4.4 Silicon carbide (SiC) (W. V. MÜNCH) 490
5 Impurity and defect properties in group III-V compounds 499
5.1 Gallium nitride (GaN) 499
5.1.1 Shallow impurities (after D. BIMBERG, Vol. III/17a) 499
5.1.2 Deep defect states (A.R. PEAKER) 502
5.2 Gallium phosphide (GaP) 504
5.2.1 Solubility and diffusion of impurities (A.F.W. WILLOUGHBY) 504
5.2.2 Vibrational modes of impurities and defects (R. MURRAY, R.C. NEWMAN) 505
5.2.3 Shallow impurities (after P.J. DEAN, Volume III/17a) 510
5.2.4 Deep defects 525
5.2.5 Transition metal impurities (B. CLERJAUD) 537
5.2.6 Rare earth impurities (H. ENNEN) 561
5.3 Gallium arsenide (GaAs) 566
5.3.1 Solubility of impurities (A.F.W. WILLOUGHBY) 566
5.3.2 Diffusion of impurities and defects (A.F.W. WILLOUGHBY) 568
5.3.3 Vibrational modes of impurities and defects (R. MURRAY, R.C. NEWMAN) 576
5.3.4 Shallow impurities and defects (B. HAMILTON) 583
5.3.5 Deep defects 594
5.3.5.1 Defect levels (A.R. PEAKER) 594
5.3.5.2 Optical properties of deep defects (U. KAUFMANN) 603
5.3.5.3 ESR, ENDOR, and ODMR data (J. SCHNEIDER) 620
5.3.6 Transition metal impurities (B. CLERJAUD) 627
5.3.7 Rare earth impurities (H. ENNEN) 654

5.4 Gallium antimonide (GaSb) 659
5.4.1 Diffusion of impurities and defects (A.F.W. WILLOUGHBY) 659
5.4.2 Vibrational modes of impurities (R. MURRAY, R.C. NEWMAN) 661
5.4.3 Shallow impurities and defects (after D. BIMBERG, Vol. III/17a) 662
5.4.4 Deep defects (A.R. PEAKER) 665
5.5 Indium phosphide (InP) 667
5.5.1 Diffusion of impurities and defects (A.F.W. WILLOUGHBY) 667
5.5.2 Vibrational modes of impurities (R. MURRAY, R.C. NEWMAN) 669
5.5.3 Shallow impurities and defects (B. HAMILTON) 670
5.5.4 Deep impurities 677
5.5.4.1 Deep defect states (H. GRIMMEISS) 677
5.5.4.2 Photoluminescence (U. KAUFMANN) 681
5.5.4.3 ESR and ODMR data (J. SCHNEIDFR) 683
5.5.5 Transition metal impurities (B. CLERJAUD) 685
5.5.6 Rare earth impurities (H. ENNEN) 698
5.6 Indium arsenide (InAs) 706
5.6.1 Solubility of impurities (A.F.W. WILLOUGHBY) 706
5.6.2 Diffusion of impurities and defects (A.F.W. WILLOUGHBY) 706
5.6.3 Vibrational modes of impurities (R. MURRAY, R.C. NEWMAN) 708
5.6.4 Shallow impurities (after D. BIMBFRG, VOI. III/17a) 708
5.6.5 Deep defect states (H. GRIMMEISS) 709
5.6.6 Transition metal impurities (B. CLERJAUD) 709
5.7 Indium antimonide (InSb) 710
5.7.1 Diffusion of impurities and defects (A.F.W. WILLOUGHBY) 710
5.7.2 Vibrational modes of impurities and defects (R. MURRAY, R.C. NEWMAN) 713
5.7.3 Shallow impurities (after D. BIMBERG, Vol. III/17a) 713
5.7.4 Deep impurities (H. GRIMMEISS) 717
5.7.5 Transition metal impurities (B. CLERJAUD) 718
5.8 Boron nitride (BN) 719
5.8.1 Deep defect states (H. GRIMMEISS) 719
5.9 Boron phosphide (BP) 720
5.9.1 Deep defect states (H. GRIMMEISS) 720
6 Impurity and defect properties in ternary compounds 721
6.1 Gallium arsenide phosphide ($GaAs_{1-x}P_x$) 721
6.1.1 Solubility and diffusion of impurities (A.F.W. WILLOUGHBY) 721
6.1.2 Deep defect states (H. GRIMMEISS) 723
6.1.3 Transition metal impurities (B. CLERJAUD) 729
6.2 Gallium arsenide antimonide ($GaAs_{1-x}Sb_x$) 731
6.2.1 Deep defect states (H. GRIMMEISS) 731
6.3 Indium arsenide phosphide ($InAs_{1-x}P_x$) 733
6.3.1 Solubility and diffusion of impurities (A.F.W. WILLOUGHBY) 733
6.3.2 Optical and electronic properties (B. CLERJAUD) 734
6.4 Gallium aluminum arsenide ($Ga_{1-x}Al_xAs$) 735
6.4.1 Solubility and diffusion of impurities (A.F.W. WILLOUGHBY) 735
6.4.2 Defect levels (A.R. PEAKER) 736
6.4.3 Transition metal impurities (B. CLERJAUD) 742
6.5 Gallium aluminum antimonide ($Ga_{1-x}Al_xSb$) 744
6.5.1 Deep defect states (A.R. PEAKER) 744
6.6 Gallium indium arsenide ($Ga_{1-x}In_xAs$) 744
6.6.1 Solubility and diffusion of impurities (A.F.W. WILLOUGHBY) 744
6.6.2 Defect levels (B. CLERJAUD) 746
6.6.3 Optical properties (B. CLERJAUD) 746
6.7 Gallium indium phosphide ($Ga_xIn_{1-x}P$) (B. CLERJAUD) 747
7 Impurity and defect properties of quaternary compounds 749
7.1 Gallium indium arsenide phosphide($Ga_xIn_{1-x}As_yP_{1-y}$) 749
7.1.1 Energy levels (B. CLERJAUD) 749
7.1.2 Optical properties (B. CLERJAUD) 749
8 Subject index 750

Springer-Verlag and the Environment

We at Springer-Verlag firmly believe that an international science publisher has a special obligation to the environment, and our corporate policies consistently reflect this conviction.

We also expect our business partners – paper mills, printers, packaging manufacturers, etc. – to commit themselves to using environmentally friendly materials and production processes.

The paper in this book is made from low- or no-chlorine pulp and is acid free, in conformance with international standards for paper permanency.